

FLOOR DIAPHRAGMS IN MULTI-STOREY TIMBER BUILDINGS

Daniel Moroder

A thesis presented for the degree of
Doctor of Philosophy In Civil Engineering

at the

University of Canterbury

Christchurch, New Zealand

March 2016

“Unless you try to do something beyond what you have already mastered, you will never grow.”

— Ronald E. Osborn

Abstract

This thesis studies the behaviour of diaphragms in multi-storey timber buildings by providing methods for the estimation of the diaphragm force demand, developing an Equivalent Truss Method for the analysis of timber diaphragms, and experimentally investigating the effects of displacement incompatibilities between the diaphragm and the lateral load resisting system and developing methods for their mitigation.

The need to better understand the behaviour of diaphragms in timber buildings was highlighted by the recent 2010-2011 Canterbury Earthquake series, where a number of diaphragms in traditional concrete buildings performed poorly, compromising the lateral load resistance of the structure. Although shortcomings in the estimation of force demand, and in the analysis and design of concrete floor diaphragms have already been partially addressed by other researchers, the behaviour of diaphragms in modern multi-storey timber buildings in general, and in low damage Pres-Lam buildings (consisting of post-tensioned timber members) in particular is still unknown. The recent demand of mid-rise commercial timber buildings of ten storeys and beyond has further highlighted the lack of appropriate methods to analyse timber diaphragms with irregular floor geometries and large spans made of both light timber framing and massive timber panels.

Due to the lower stiffness of timber lateral load resisting systems, compared with traditional construction materials, and the addition of in-plane flexible diaphragms, the effect of higher modes on the global dynamic behaviour of a structure becomes more critical. The results from a parametric non-linear time-history analysis on a series of timber frame and wall structures showed increased storey shear and moment demands even for four storey structures when compared to simplistic equivalent static analysis. This effect could successfully be predicted with methods available in literature. The presence of diaphragm flexibility increased diaphragm inter-storey drifts and the peak diaphragm demand in stiff wall structures, but had less influence on the storey shears and moments. Diaphragm force demands proved to be significantly higher than the forces derived from equivalent static analysis, leading to potentially unsafe designs. It is suggested to design all diaphragms for the same peak demand; a simplified approach to estimate these diaphragm forces is proposed for both frame and wall structures.

Modern architecture often requires complex floor geometries with long spans leading to stress concentrations, high force demands and potentially large deformations in the diaphragms. There is a lack of guidance and regulation regarding the analysis and design of timber diaphragms and a practical alternative to the simplistic equivalent deep beam analysis or costly finite element modelling is required. An Equivalent Truss Method for the analysis of both light timber framed and massive timber diaphragms is proposed, based on analytical formulations and verified against finite element models. With this method the panel unit shear forces (shear flow) and therefore the fastener demand, chord forces and reaction forces can be evaluated. Because the panel stiffness and fastener stiffness are accounted for, diaphragm deflection, torsional effects and transfer forces can also be assessed. The proposed analysis method is intuitive and can be used with basic analysis software. If required, it can easily be adapted for the use with diaphragms working in the non-linear range.

Damage to floor diaphragms resulting from displacement incompatibilities due to frame elongation or out-of plane deformation of walls can compromise the transfer of inertial forces

to the lateral load resisting system as well as the stability of other structural elements. Two post-tensioned timber frame structures under quasi-static cyclic and dynamic load, respectively, were tested with different diaphragm panel layouts and connections investigating their ability to accommodate frame elongations. Additionally, a post-tensioned timber wall was loaded under horizontal cyclic loads through two pairs of collector beams. Several different connection details between the wall and the beams were tested, and no damage to the collector beams or connections was observed in any of the tests. To evaluate the increased strength and stiffness due to the wall-beam interaction an analytical procedure is presented. Finally, a timber staircase core was tested under bi-directional loading. Different connection details were used to study the effect of displacement incompatibilities between the orthogonal collector beams. These experiments showed that floor damage due to displacement incompatibilities can be prevented, even with high levels of lateral drift, by the flexibility of well-designed connections and the flexibility of the timber elements.

It can be concluded that the flexibility of timber members and the flexibility of their connections play a major role in the behaviour of timber buildings in general and of diaphragms specifically under seismic loads. The increased flexibility enhances higher mode effects and alters the diaphragm force demand. Simple methods are provided to account for this effect on the storey shear, moment and drift demands as well as the diaphragm force demands. The analysis of light timber framing and massive timber diaphragms can be successfully analysed with an Equivalent Truss Method, which is calibrated by accounting for the panel shear and fastener stiffnesses. Finally, displacement incompatibilities in frame and wall structures can be accommodated by the flexibilities of the diaphragm panels and relative connections. A design recommendations chapter summarizes all findings and allows a designer to estimate diaphragm forces, to analyse the force path in timber diaphragms and to detail the connections to allow for displacement incompatibilities in multi-storey timber buildings.

Acknowledgements

Carrying out research for all these years and writing such a thesis would not have been possible without the help and the support from many people. In the next paragraphs I would like to acknowledge the people who guided, helped and accompanied me during these last years and made this work possible in a way or the other.

First and foremost I would like to thank my supervisors Professor Andy Buchanan and Professor Stefano Pampanin. Your technical and financial support as well as your guidance and immense thrust were essential in the outcome of this thesis. At this stage I would like to recall the three basic principles to success I was told by Andy, and they don't just apply to the challenge of writing a doctoral thesis:

- Work hard - play hard (nothing better than to recover from a long week in the office on a peak in the Southern Alps);
- Teamwork (working with my colleagues in the timber team not only encouraged the exchange of ideas, but allowed the best use of everybody's expertise and has united us for the next common adventure as design engineers);
- When in doubt, do it (without this motto I would have never moved to New Zealand, one of the best decisions in my life).

I also would like to acknowledge Associate Professor Alessandro Palermo and Dr Minghao Li for their advice and discussions on my research. Special thanks also go to Professor Felice Ponzio, Dr Antonio di Cesare, Dr Michele Simonetti and Domenico Nigro from the University of Basilicata for not only sharing experimental data and knowledge, but also for the excellent hospitality I experienced on my visits.

Further, I also would like to acknowledge Russell McConchie, Gavin Keats and Mosese Fifita as well as all other technical staff for their help, advice and technical skills necessary to get the different experimental campaigns underway. A big thank-you also goes to Elizabeth Ackermann, who solved quite some bureaucratic hurdles and organized most conference travels.

The financial support from the Structural Timber Innovation Company for the experimental test campaigns and from the University of Canterbury for the Doctoral Scholarship is highly acknowledged.

To my partner Johanna, not only were you part of this New Zealand journey from almost day one, but your love, empathy and patience were essential for the accomplishment of this work. Nobody else has been so closely through all the ups and downs and you always cheered me up when in need.

To my parents for giving me your continuous support, especially when being so far away from home. Over so many years you have allowed and encouraged me to explore, study and work all over the world. Because you always believed in me, this young boy in the last row is now an expert on his way to success.

To my sister Magda, we share the same passions, values and fears, thank you for supporting my choices and actions and being there when I needed you.

My acknowledgements also go to all my colleagues and friends at the 3rd level of the Civil Engineering building: Dr Tobias Smith, Dr Francesco Sarti, Chris Watson, Harry Johnston, Tom Armstrong, Dr Wouter van Beerschoten, Andrew Dunbar, Maxim Millen, Michael Hobbs, Dr Sahin Tasligedik, Dr Andrew Baird, Dr Denis Pau, Gareth Morris, Zeinab Chegini, Audsley Jones, Dr James O'Neil, Sam MacHattie, Jeff Tuck, Ethan Thomson, Royce Liu, Gabrielle Granello, Claudio Cappellaro, Lisa Ottenhaus, Jan Dormanns and all other members of the Grizzly Bairds, our technical and less technical discussions, beer o'clocks and BYO were of great value and often a welcome distraction to the daily research.

Finally, the last years and this thesis would not have been the same without all my friends I spend my spare time with. Thank you bros and sis for all the adventures, tramps, BBQs and theme dinners, you really made this journey a very special and enjoyable one.

Table of Contents

Abstract.....	ii
Acknowledgements	iv
Table of Contents.....	vi
1 Introduction, motivation and scope.....	1
1.1 Introduction.....	1
1.2 Research motivation.....	2
1.3 Objectives	3
1.4 Scope	5
1.5 Research methodology.....	6
1.6 Chapter summary	6
2 The importance of diaphragms.....	8
2.1 Introduction.....	8
2.1.1 Background.....	8
2.2 The role of diaphragms.....	9
2.3 Definition of diaphragms and their components	10
2.4 Complexities in the design of diaphragms	12
2.4.1 Higher modes effects	12
2.4.2 Transfer forces	13
2.4.3 Load path.....	13
2.4.4 Displacement incompatibilities.....	13
2.5 Type of diaphragms	14
2.6 Timber diaphragm materials	15
2.6.1 New developments in timber diaphragm systems	16
2.7 Literature review	16
2.8 Past Performance of timber diaphragms	17
2.9 Recent buildings with enhanced diaphragm connections	18
3 State-of-the-art in diaphragm analysis design	21
3.1 Introduction.....	21
3.1.1 Background.....	21
3.2 Code provisions for design of timber diaphragms	22
3.2.1 Code provisions for the design of timber diaphragms.....	22
3.2.2 Code provisions for the seismic design of timber diaphragms	24
3.2.3 Flexible and rigid diaphragms	26
3.2.4 Provisions for overstrength factors in codes and recent literature	27
3.3 Determination of diaphragm forces	30
3.3.1 Deep beam/girder analogy	30
3.3.2 Shear field analogy	34

3.3.3	Strut-and-tie method	36
3.3.4	Equivalent truss method	39
3.3.5	Finite element modelling	41
3.3.6	Synopsis of proposed diaphragm analysis methods	43
3.4	Determination of diaphragm components capacity	44
3.4.1	Component capacity in LTF timber diaphragms	44
3.4.2	Component capacity in massive timber diaphragms	46
3.4.3	Timber-concrete-composite (TCC) and concrete diaphragms	47
3.5	Discussion	47
3.6	Conclusions.....	48
4	The influence of diaphragm stiffness on the dynamic behaviour of multi-storey timber buildings	50
4.1	Introduction.....	50
4.1.1	Background.....	50
4.2	Review of available research regarding the influence of diaphragm stiffness on the behaviour of buildings	51
4.2.1	Literature review	52
4.2.2	Conclusions from the literature review	55
4.3	General information on the parametric analysis	55
4.3.1	Design of sample diaphragms for the parametric study.....	56
4.3.2	Diaphragm stiffness.....	58
4.3.3	Earthquake selection.....	61
4.4	Parametric analysis on the dynamic performance of post-tensioned timber frames.....	62
4.4.1	Numerical model for the frame structures	62
4.4.2	Design of the sample frame structures.....	64
4.4.3	Diaphragm design for the frame structures.....	68
4.4.4	Results of the analysis of the post-tensioned timber frames	69
4.5	Parametric analysis of the dynamic performance of post-tensioned timber walls.....	76
4.5.1	Numerical model for the wall structure.....	76
4.5.2	Design of the sample wall structures	78
4.5.3	Diaphragm design for the wall structures.....	80
4.5.4	Results of the analysis of the post-tensioned timber walls	82
4.6	Discussion	91
4.7	Conclusions.....	94
5	Determination of shear forces, moments and diaphragm forces.....	95
5.1	Introduction.....	95
5.1.1	Background.....	95
5.2	Discussion of the available methods for the determination of floor forces	96
5.2.1	Analysis methods	96
5.2.2	Design standards and codes.....	100
5.2.3	Methods from current research.....	102
5.3	Transfer forces.....	106
5.4	Elastic versus ductile diaphragm design.....	109
5.5	Determination of shears and moments	111

5.5.1	Dynamic amplification according to the New Zealand Concrete Standard NZS 3101	112
5.5.2	Priestley et al. (2007) and further modifications	113
5.5.3	Dynamic amplification of shear forces, moments and diaphragm forces in frame structures	115
5.5.4	Dynamic amplification of shear forces, moments and diaphragm forces in wall structures	120
5.6	Discussion	123
5.7	Conclusions.....	126
6	Diaphragm loads, massive timber diaphragms and deformation estimation	127
6.1	Introduction.....	127
6.1.1	Load application	127
6.1.2	Massive timber diaphragms	127
6.1.3	Diaphragm deformation and stiffness	128
6.2	Types of load application and their influence on the load path	128
6.2.1	Load application types, example diaphragms and analysis method.....	129
6.2.2	Results and discussion for regular LTF diaphragms	131
6.2.3	Results and discussion for regular massive timber diaphragms	132
6.2.4	Results and discussion for irregular LTF diaphragms	134
6.2.5	Results and discussion for irregular massive timber diaphragms.....	136
6.2.6	Load introduction through the chord beam	140
6.3	Massive timber diaphragms	141
6.4	Deformation of timber diaphragms	144
6.4.1	Current knowledge in the calculation of diaphragm deflection	145
6.4.2	Deflection of unblocked diaphragms	147
6.4.3	Deflection of diaphragms with non-uniform fasteners	148
6.4.4	Deflection of irregular diaphragms	148
6.4.5	Floor stiffness in historic buildings and retrofit solutions.....	149
6.4.6	Parameters influencing the diaphragm deflection	149
6.4.7	Flexibility of the connections between the diaphragm and the lateral load resisting system.....	151
6.4.8	Deflection equation for diaphragms with solid timber panels	152
6.4.9	Limitations of the deflection equation.....	154
6.5	Discussion	154
6.5.1	Load application	154
6.5.2	Massive timber diaphragms	154
6.5.3	Diaphragm deformation and stiffness	155
6.6	Conclusions.....	156
7	Equivalent Truss Method for timber diaphragms	157
7.1	Introduction.....	157
7.1.1	Strut-and-Tie Method	157
7.1.2	Equivalent Truss Method for timber diaphragms	158
7.1.3	Proposed enhancements to the Equivalent Truss Method for timber diaphragms.....	158
7.2	The general principles of the truss analogy for timber diaphragms	159
7.3	The Truss Analogy for LTF diaphragms.....	161

7.4	Example of the truss analogy on a cantilevered LTF diaphragm.....	164
7.5	The Equivalent truss Method for massive timber diaphragms	168
7.6	Multiple diagonals per sheathing panel	169
7.7	Comparison of different truss model geometries	172
7.8	Verification of the truss model.....	176
7.8.1	LTF diaphragm loaded in -y direction.....	178
7.8.2	Massive timber diaphragm loaded in -y direction	179
7.8.3	Massive timber diaphragm loaded in x and y direction.....	181
7.9	Non-linear diaphragm behaviour	183
7.10	Limitations of the equivalent Truss Method	185
7.11	Discussion	185
7.12	Conclusions.....	187
8	Displacement incompatibilities between diaphragms and frame structures.....	188
8.1	Introduction.....	188
8.1.1	Background.....	188
8.2	Displacement incompatibilities in frame structures	189
8.3	Review of current design approaches to avoid diaphragm damage in frame structures	190
8.3.1	Connections in multi-storey concrete frame buildings.....	190
8.3.2	Connections in multi-storey steel frame buildings	192
8.3.3	Connections in multi-storey timber frame buildings	194
8.4	Findings from a post-tensioned two bay frame	196
8.4.1	Experimental setup	196
8.4.2	Test results	198
8.4.3	Design recommendations	201
8.4.4	Concrete diaphragms	203
8.5	Findings from a three storey post-tensioned frame structure under dynamic loads.....	203
8.5.1	Experimental setup	204
8.5.2	Test results	206
8.5.3	Design recommendations	209
8.6	Discussion	210
8.7	Conclusions.....	211
9	Displacement incompatibilities between diaphragms and wall structures.....	212
9.1	Introduction.....	212
9.1.1	Background.....	212
9.2	Displacement incompatibilities in wall structures	213
9.3	Review of current design approaches to avoid damage in diaphragms in wall structures	214
9.3.1	Connections in multi-storey concrete wall buildings.....	214
9.3.2	Connections in multi-storey steel wall buildings	215
9.3.3	Connections in multi-storey timber wall buildings	216
9.4	Conceptual design solution	218
9.5	Findings from a post-tensioned wall	220
9.5.1	Experimental setup	220

9.5.2	Test results	223
9.5.3	Cost analysis	226
9.5.4	Design recommendations	227
9.6	Findings from a post-tensioned CLT core-wall structure	228
9.6.1	Experimental setup	228
9.6.2	Test results	231
9.6.3	Design recommendations	236
9.7	Discussion	237
9.8	Conclusions.....	238
10	Analytical modelling of a post-tensioned wall with collector beams	239
10.1	Introduction.....	239
10.1.1	Background.....	239
10.2	Analytical procedures.....	240
10.2.1	Iterative moment-curvature procedure.....	241
10.2.2	Compatibility forces and moments.....	246
10.2.3	Force-displacement curve.....	250
10.3	Comparison with experimental values.....	251
10.3.1	Validation on the bare wall	252
10.3.2	Comparison for the wall-beam system	254
10.4	Parametric analysis.....	256
10.4.1	Influence of the beam length and the number of fasteners.....	257
10.4.2	Influence of the connection position on the collector beam.....	257
10.4.3	Influence of the beam height.....	258
10.4.4	Connections placed at a distance from the mid-span of the collector beam.....	259
10.5	Discussion	260
10.6	Conclusions.....	262
11	Recommendations for the design of diaphragms in multi-storey timber buildings.....	263
11.1	Determination of the diaphragm force demand.....	263
11.1.1	Fundamental period of vibration	263
11.1.2	Diaphragm stiffness in frame structures.....	264
11.1.3	Force demand in frame structures.....	264
11.1.4	Diaphragm stiffness in wall structures.....	265
11.1.5	Force demand in wall structures.....	265
11.1.6	Transfer forces	266
11.2	Diaphragm analysis and load paths.....	267
11.2.1	Girder analogy	267
11.2.2	Strut-and-Tie Method – concrete diaphragms	269
11.2.3	Equivalent Truss Method – timber diaphragms.....	269
11.2.4	Diaphragm deflection.....	276
11.3	Diaphragm connections and displacement incompatibilities	277
11.3.1	Connections between single timber floor elements.....	277
11.3.2	Chord beams	278
11.3.3	Collector and strut beams.....	279
11.3.4	Connections between diaphragms and frames	280

11.3.5	Connections between diaphragms and walls	289
12	Conclusions and recommendations for future research	297
12.1	Conclusions.....	297
12.2	Answers to the research questions	301
12.3	Recommendations for further research.....	309
	References.....	311
A	Appendix – Derivation of the diaphragm deformation equations	325
A.1	Deformation equations for light timber framing diaphragms	325
A.1.1	Bending deformation	325
A.1.2	Shear deformation	326
A.1.3	Fastener slip	327
A.1.4	Chord beam splice slip	330
A.1.5	Diaphragm deflection for LTF diaphragms.....	331
A.1.6	Code implementation of the deflection equation	331
A.2	Deformation equation of a quadrilateral system with a diagonal	333
A.3	Deformation equations for massive timber diaphragms	334
B	Appendix – Finite element modelling of timber diaphragms.....	336
B.1.1	Definition of the finite element diaphragm models	336
B.1.2	Definition of the stiffness values for the link elements	338
C	Appendix – Experimental setups.....	340
C.1	Experimental setup of a post-tensioned two bay frame under quasi static loads	340
C.1.1	Test setup.....	340
C.1.2	Loading protocol and instrumentation	343
C.1.3	Results	344
C.2	Experimental setup of a three storey post-tensioned frame structure tested under dynamic loads	348
C.2.1	Test setup.....	348
C.2.2	Loading protocol and instrumentation	351
C.2.3	Results	353
C.3	Experimental setup of a post-tensioned wall under quasi static loads.....	356
C.3.1	Test setup.....	357
C.3.2	Loading protocol and instrumentation	362
C.3.3	Results	363
C.3.4	Cost analysis	367
C.4	Experimental setup of a 1/2 scale post-tensioned CLT staircase core under quasi static loads	369
C.4.1	Test setup.....	369
C.4.2	Loading protocol and instrumentation	374
C.4.3	Results	376

D	Appendix – Derivation of the stiffness formulae for wall-beam assemblies.....	386
D.1	Derivation of the stiffness Relationship between a rocking wall and a collector beam.....	386
D.1.1	Beam stiffness	386
D.1.2	System stiffness.....	387
D.2	Additional demand in the wall-to-beam connection due to displacement incompatibilities	393
D.3	Fastener demand and stiffness of bolted connections	398
D.3.1	Calculation of the fastener demand.....	398
D.3.2	Connection with moment and forces	399
D.3.3	Connection stiffness.....	402
E	Appendix – Design example.....	403
E.1	Diaphragm design.....	403
E.2	Errata corrige.....	405

1 Introduction, motivation and scope

1.1 INTRODUCTION

Timber structures are gaining recognition in providing a sustainable, energy efficient, durable, affordable and resilient answer to the growing demand of multi-storey residential and commercial buildings. Although timber has been largely neglected as a construction material over the last few decades, booming material costs for steel and concrete, need for pre-fabrication of structures or part thereof, request for eco-friendly materials, good performance of wooden buildings in recent earthquakes and the availability of new engineered timber products are leading to a worldwide renaissance of timber structures.

The recent construction of a number of engineered multi-storey timber buildings has attracted growing interest from developers, researchers, engineers and the timber industry. As part of this push for taller timber buildings, several feasibility studies on high-rise timber buildings were published (Waugh et al. 2010; CEIArchitecture 2011; Van De Kuilen et al. 2011; mgb 2012; C.F. Møller 2013; FPIinnovations 2013; SOM 2013). More high rise timber buildings are to be built in Canada (Canadian Wood Council and Natural Resources Canada 2013), Norway (The Norwegian Barents Secretariat 2009) and Austria (Holzbau Austria 2015), some with government subsidies promoting innovation.

This new interest in medium to high-rise multi-storey timber buildings creates the need for a more rigorous approach in design. The presence of some of these structures in seismically active countries has highlighted knowledge gaps surrounding their performance under earthquake loading, with special focus on the design of diaphragms.

The recent 2010 and 2011 Canterbury earthquake series in New Zealand has shown the vulnerability of historic and also recent building fabric. The huge economic loss due to business interruption and forced demolition of thousands of buildings due to extensive damage suggested a new definition of seismic performance targets in designing structures. The distrust in current design practice called for new technologies to improve the performance of buildings (Canterbury Earthquake Royal Commission 2012). One of the answers to these requests was the already ongoing development of jointed ductile Prestressed Laminated timber structures (Pres-Lam) developed at the University of Canterbury, New Zealand (Palermo et al. 2005; Buchanan et al. 2011). The rocking nature of these structures however raised concern on the

behaviour of the diaphragms, since these have the potential to undergo substantial damage due to displacement incompatibilities caused by beam elongation in frame buildings, and uplift and rotation in wall structures. Further, poor performance of diaphragms in reinforced concrete buildings (Canterbury Earthquake Royal Commission 2012; Bull and Henry 2014) raised concerns about the appropriateness of current code provision and analysis tools for the design of diaphragms in general.

The increasing availability of engineered timber products like Laminated Veneered Lumber (LVL), glued laminated timber (glulam) and Cross-Laminated Timber (CLT) not only provides a more reliable and strong construction material, but also allows for taller structures with fewer lateral load resisting elements and more complex floor geometries. Common timber diaphragm analysis methods, developed for regular Light Timber Frames (LTF) structures, do not allow for the design of modern diaphragms with a high degree of geometric irregularities. Although improved tools have been made available for the design of concrete diaphragms, little is available for irregular LTF and massive timber diaphragms.

Most international codes do not specifically address the determination of diaphragm demand under seismic actions. Although definitions for rigid and flexible diaphragms are provided in codes, diaphragms are commonly modelled as rigid elements, leading to inaccurate results. Capacity design principles are normally required to protect diaphragms, but most timber material codes fail to provide the required overstrength values. Recent research concerning the design of cast-in-situ and pre-cast concrete diaphragms is currently being implemented in loading codes (Fleischman 2014; Standards New Zealand 2015), but similar work on timber diaphragms is still missing.

1.2 RESEARCH MOTIVATION

A number of Pres-Lam timber frame and wall structures have been designed and erected in New Zealand since 2008 (Devereux et al. 2011; Brown et al. 2012; Dekker and Chung 2012; MPI 2014). This low-damage technology, based on previous research on the PREcast Seismic Structural Systems (PRESS System) in San Diego, California (Priestley 1991), has been extensively tested at the University of Canterbury (Palermo et al. 2005; Smith 2008; Iqbal 2011; Newcombe 2011; Pino 2011; Armstrong et al. 2014; Dunbar 2014; Smith 2014; Sarti 2015), but a significant knowledge gap regarding the design of diaphragms in such buildings was highlighted by the designers. In the aftermath of the Canterbury earthquakes, severe concerns regarding the displacement incompatibilities in diaphragms were raised. Even though these concerns were based on observed damage in concrete buildings with concrete

diaphragms, such behaviour was also expected in multi-storey Pres-Lam timber buildings, especially because of the occurrence of seismic rocking at beam-column interfaces. This has led to the perception of potential diaphragm damage in Pres-Lam structures, leading some architects and engineers to use other structural systems in their designs.

In the initial phase of this research, aimed primarily to solve the displacement incompatibility issue in timber buildings by experimental testing, it was soon realized that the knowledge gap behind the poor design of timber diaphragms was of larger scale. Diaphragm analysis methods available in literature and implemented in design codes are based on regular LTF diaphragms only. Common floor layouts with openings, off-sets, multiple supports and concentrated load applications cannot be analysed with such methods. Further, is it unknown whether such methods are appropriate for diaphragms made of massive timber panels. In the past the lack of appropriate design tools has led to increased design fees, non-economical solutions, inadequate designs or in the worst case, the move to another construction material. A report by the TDA (2015) relates the lack of diaphragms analysis methods to the limited uptake of modern timber buildings.

Another shortcoming which required further investigation was the determination of the diaphragm demand in timber buildings. Structural failures from the Northridge 1994 earthquake showed that diaphragm demand could not be properly estimated with available code provisions (Nakaki 2000; Fleischman and Farrow 2001; Rodriguez et al. 2002). Research findings showed increased force demand due to higher mode effects, over-strength and diaphragm flexibility. Little information is available on such effects in timber buildings and practical guidance is required.

The research findings of this work may be used in the revision of the New Zealand Timber Standard NZS 3603 (Standards New Zealand 1993) and in a future New Zealand guideline for the design of timber diaphragms in traditional light timber framing, modern massive timber and Pres-Lam buildings.

1.3 OBJECTIVES

The objectives of this thesis are to provide simple design methods to:

1. establish the force demand on diaphragms in multi-storey timber buildings;
2. analyse the load path and determine the deflections of timber diaphragms; and
3. transfer the forces into the lateral load resisting system under the consideration of displacement incompatibilities.

These three main objectives are shown schematically in Figure 1.1. To make this research as practical as possible, a number of design related questions have been asked and the answers will be found in the individual sections of this thesis.

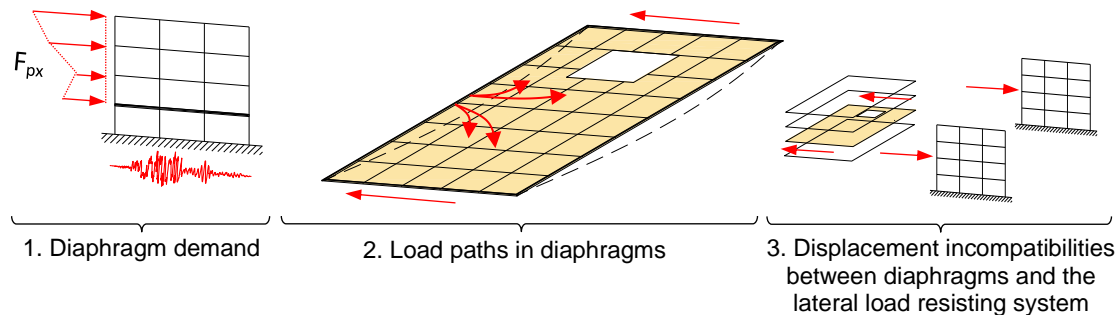


Figure 1.1 Schematic display of the three main objectives of this research

Determination of the seismic demand in multi-storey timber buildings

1. *Can current seismic analysis methods predict the seismic demand in multi-storey timber buildings?*
2. *What is the effect of diaphragm flexibility on the seismic behaviour of timber structures?*
3. *Is the definition of flexible diaphragms according to current codes adequate to evaluate the dynamic behaviour of a timber structure?*
4. *Are current capacity design principles adequate to protect timber diaphragms under seismic loading?*
5. *How can the diaphragm force demand in timber structures be evaluated?*

Load path and deflections in diaphragms

6. *Are current diaphragm analysis methods adequate to design timber diaphragms and to determine the component demand?*
7. *Can the principles of such methods be applied to massive timber diaphragms?*
8. *Can a strut-and-tie or truss analysis be used to analyse timber diaphragms?*
9. *How can diaphragm stiffness be assessed?*
10. *How can the force distribution into the lateral load resisting system be determined?*

Connection of the floor diaphragms to the lateral load resisting systems and displacement incompatibilities

11. *What displacement incompatibilities can occur in timber buildings?*
12. *How can displacement incompatibilities be allowed for in frame structures?*
13. *How can displacement incompatibilities be allowed for in wall structures?*
14. *How can the wall-to-diaphragm interaction be quantified for design purposes?*

A number of these questions have already been asked by US practitioners and researchers in a timber diaphragm workshop held in 1979 (ATC 1979), and a number of them have not been yet answered or implemented in design practice. It is hoped that the conclusions from this thesis, together with findings from other authors on the behaviour of diaphragms, are soon implemented in code provisions or guidelines.

1.4 SCOPE

The main scope of this thesis is the evaluation of forces, load paths and displacement incompatibility issues of timber diaphragms in multi-storey timber buildings. The emphasis is on post-tensioned Pres-Lam timber frame, wall and core-wall buildings, but the results are also applicable to other forms of multi-storey timber buildings. Since the use of timber-only diaphragms is promoted in such buildings, little focus is put herein on design solutions for concrete diaphragms, whose behaviour is beyond the scope of this research. Available analysis tools will be summarized and discussed for diaphragms independently from the material used, but design methods will be proposed only for diaphragms of light timber frame and massive timber panels.

The influence of higher modes and diaphragm flexibility on the dynamic behaviour of timber structures is based on the numerical analysis of Pres-Lam structures. Diaphragm peak inertial force demand is determined from the same analysis. Since similar trends are expected in other modern multi-storey timber structures, such structures are not analysed in detail. Transfer forces in diaphragms will be discussed in principle, but their determination in timber buildings are not covered in this research, because it only focusses on structures which are regular in geometry and stiffness up the building height.

Since the force transfer mechanism in diaphragms is independent from the type of horizontal load applied, the complexities in the determination of the force demand and the nature of displacement incompatibilities are unique to seismic actions. This is due to the distinct dynamic behaviour of structures and the desired non-linear behaviour of the lateral load resisting systems. The main observations and conclusions drawn in this thesis are therefore relevant to seismic loading, although most of them are also applicable for non-seismic loading.

1.5 RESEARCH METHODOLOGY

The research findings presented herein were based on the following numerical and analytical investigations:

- A parametric study with varying structure height, dissipative reinforcement level and diaphragm stiffness carried out with non-linear time history analyses based on lumped plasticity frame and wall models;
- Truss analyses for the development of the Equivalent Truss Method;
- Linear and non-linear finite element analyses of light timber frame and massive timber diaphragms to determine the implications of different load types and to validate the Equivalent Truss Method;
- An iterative analytical procedure to determine the moment-rotation and force displacement curves of post-tensioned wall systems connected to collector beams.

In addition to the mathematical tools, a series of experimental tests have been carried out:

- Quasi-static testing of a two bay post-tensioned timber frame with floor diaphragms;
- Unidirectional dynamic testing of a three storey post-tensioned timber frame structure with massive timber diaphragms;
- Quasi-static testing of a post-tensioned timber wall with and without end columns loaded through collector beams;
- Unidirectional and bidirectional testing of a core-wall structure loaded through orthogonal collector beams.

1.6 CHAPTER SUMMARY

Chapter 2 of this thesis introduces the importance and role of diaphragms as well as their development and performance over the years.

Since the design community lacks simple and reliable analysis tools to analyse and design diaphragms in general, Chapter 3 provides a summary of the code provisions regarding capacity design principles for the determination of the floor force demand in diaphragms in general, and the design of timber diaphragms in particular. Available diaphragm analysis methods are discussed and their limitations are highlighted.

Chapters 4 and 5 investigate the behaviour of multi-storey timber structures under earthquake loading with varying level of diaphragm flexibilities. Chapter 4 first introduces the models studied in the analysis and then discusses the shear force and moment distribution as well as interstorey drifts. Chapter 5 compares the results from the analysis with methods which account for higher mode effects. Further tools for the determination of peak floor inertial forces are introduced.

Chapter 6 studies the implications of different load types on the load distribution and in-plane deflection behaviour of different diaphragm types. The applicability of current design methods on massive timber diaphragms is then investigated on the basis of finite element analysis. Finally, diaphragm deflection equations are discussed and adapted for massive timber diaphragms.

Based on the shortcomings of most simplified analysis methods discussed in Chapter 3, Chapter 7 introduces an Equivalent Truss Model for light timber frame diaphragms and its enhancements for use with massive timber diaphragms. Results are validated against finite element analysis.

As an answer to the concerns raised regarding the potential damage to diaphragms from displacement incompatibilities, Chapters 8 and 9 study the interaction of diaphragms with frame and wall structures respectively. Results based on four experimental setups with different connection details are presented and design recommendations given. For wall connections a cost comparison is also presented.

In order to account for the interaction between the diaphragms and the walls, a simple tool to evaluate the increased pushover response is required by practitioners. Based on the results from the experimental setup, Chapter 10 introduces a modified analytical iterative procedure to evaluate the increased strength and stiffness of walls connected to collector beams.

Chapter 11 provides recommendations for the design of diaphragms in timber buildings, covering all aspects from the determination of the diaphragm demand, the load paths in the diaphragm and the connections to the lateral load resisting system.

Chapter 12 summarizes the main conclusions of this work by answering the research questions from Chapter 1. Recommendations for future research are also provided.

2 The importance of diaphragms

2.1 INTRODUCTION

This chapter defines the roles and individual components of floor diaphragms. Commonly encountered complexities in the design of diaphragms are summarized. Traditional as well as modern timber diaphragm materials are briefly described together with a literature review on their development over the years. Further, the performance of some timber diaphragms under extreme events is shown. The chapter is concluded with the description of some recent buildings with special diaphragm connections to mitigate displacement incompatibilities.

2.1.1 Background

Diaphragms have a fundamental role in the framework of a structure, independent of the material used and the type of external action. Diaphragms not only transfer any horizontal load to the lateral load resisting system, but they also tie all structural and non-structural elements together providing the building's integrity.

Floors and roofs are mainly designed to carry gravity loads by providing out-of-plane strength and stiffness. Most floors also possess some in-plane strength and stiffness, which allow for some diaphragm action. These intrinsic in-plane properties have often led to the misconception that all diaphragms are rigid and strong and therefore can withstand arbitrary loads and deformations without damage. This fallacy can partially be attributed to shortcomings in design codes, literature and designer's education, where the design of diaphragms is often neglected (Scarry 2015).

Concrete and timber diaphragms are normally analysed according to the deep beam or girder analogy (shown schematically in Figure 2.1a and discussed further in Chapter 3). Such simplified analysis methods provide satisfactory results, as long as the floor is rectangular and does not contain substantial irregularities. Irregularities, such as floor openings, re-entrant corners, and concentrated force, influence the load path, leading to stress concentrations and therefore require specific designs. Although it is well known to engineers that steel and timber beams with openings, cut outs, concentrated forces etc. (see Figure 2.1b and c) need local reinforcement because of stress concentrations, such effects in the design of irregular diaphragms are often neglected. Like irregular beams, diaphragms need collector and strut beams to redistribute stresses to other parts of the diaphragms as shown in Figure 2.1d. In

addition, such diaphragms are weakened and are therefore more flexible, another effect often neglected in design.

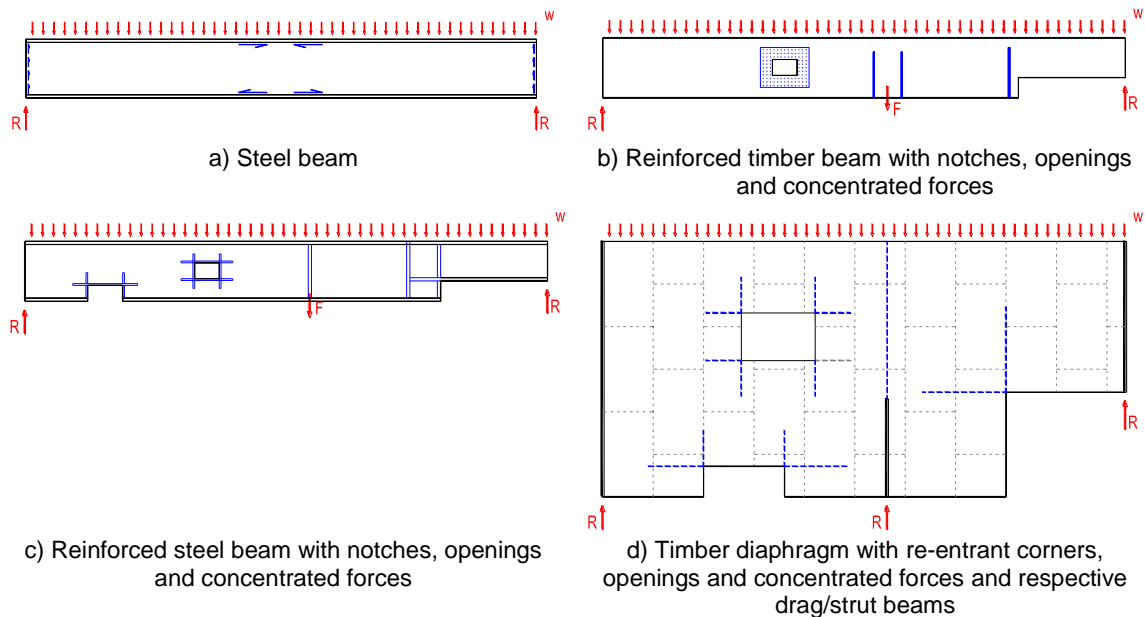


Figure 2.1 Beam analogy (modified and adapted from Scarry (2015))

2.2 THE ROLE OF DIAPHRAGMS

Floor diaphragms are critical components of all buildings. A loss of diaphragm action could lead to partial or total collapse of a building due to instabilities of vertical load carrying elements or due to the missing horizontal load distribution into the lateral load resisting system.

The roles of diaphragms can be summarized in the following list (Moehle et al. 2010; Standards New Zealand 2015) which is graphically shown in Figure 2.2. The role of diaphragms is to:

- **Transfer horizontal forces to the lateral load resisting system** - such forces can be generated by wind actions or the seismic acceleration of the floor masses or other elements connected to the floors;
- **Provide lateral support for vertical elements** to prevent buckling of columns running over several stories and to prevent torsional buckling of gravity beams;
- **Resist wall and façade out-of-plane forces** from the inertial forces generated by the mass within the elements as well as wind pressures acting on the façade and other components attached to it;
- **Resist horizontal thrust** from inclined columns, ramps and stairs;
- **Resist transfer forces** from displacement incompatibilities in the lateral load resisting system or because of changes in the vertical geometry of the structure like set-backs or podiums as well as concentrated forces;

- **Provide pull-back forces** to gravity and lateral load resisting elements on earthquake reversal;
- **Resist soil loads** from walls bearing against slopes, or levels below grade.

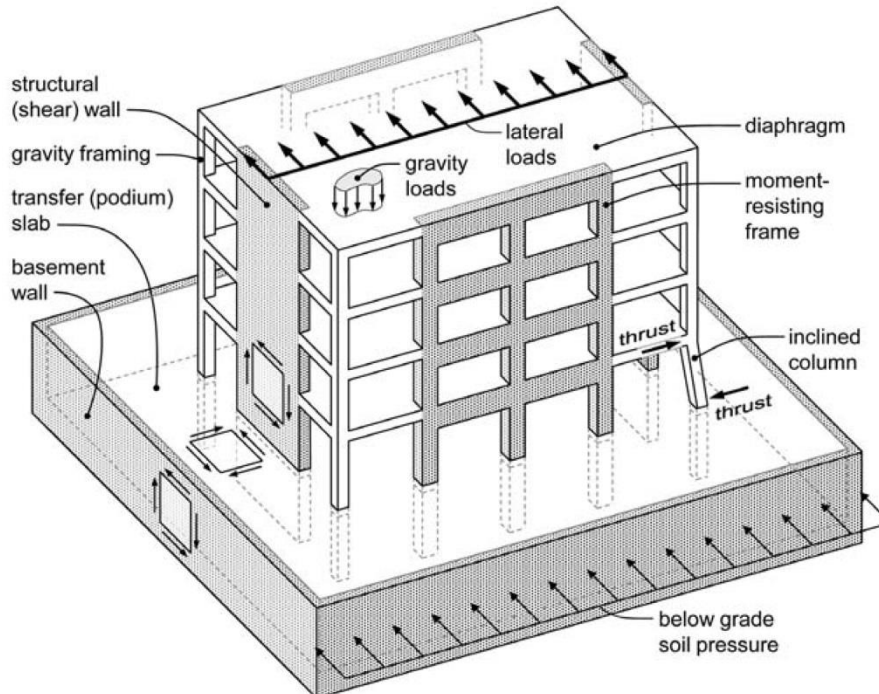


Figure 2.2 Roles of diaphragms (Moehle et al. 2010)

2.3 DEFINITION OF DIAPHRAGMS AND THEIR COMPONENTS

Whereas diaphragms can be made from many different materials like cast-in-situ concrete, pre-cast concrete panels, timber-concrete-composite floors, concrete composite steel decks, light timber framing and massive timber panels – their main components can be grouped as follows (see Figures 2.3 and 2.4):

- plate element;
- chord beams;
- collectors;
- drag/strut beams;
- connections to the lateral load resisting system.

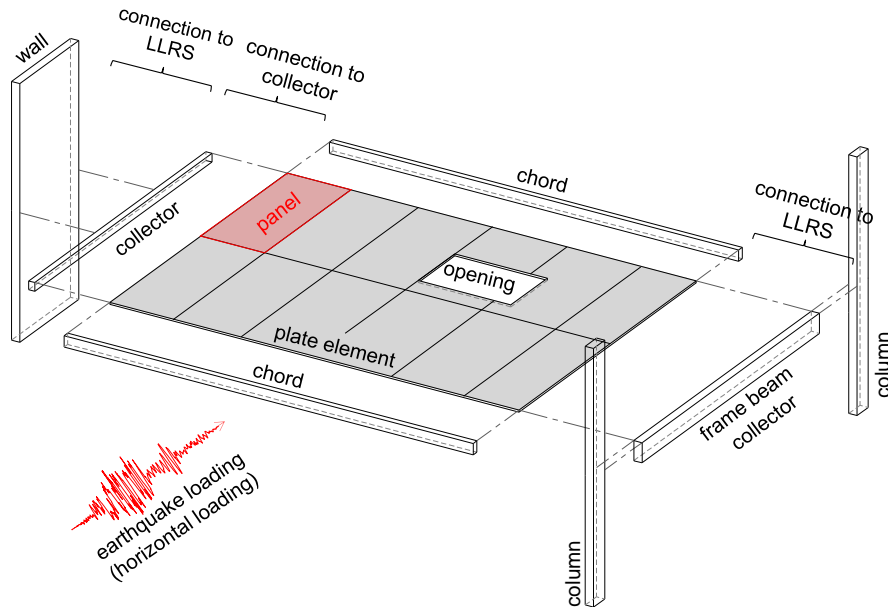


Figure 2.3 Definitions of diaphragm components

The diaphragm components are best explained on the basis of the girder analogy, where the web is made of the plate element and the flanges consist of the chord beams. The *plate element* with possible openings transfers the unit shear forces (forces per unit length) and the *chord beams* resist the diaphragm bending via compression and tension forces. For diaphragms made of a number of single panel elements, these need to be connected by fasteners in order to guarantee the force transfer. Around openings and re-entrant corners, *strut or drag beams* collect the shear forces from the disturbed area and anchor them into adjacent parts of the diaphragm. These parts are commonly referred to as sub or transfer diaphragms (Diekmann 1995; Malone and Rice 2012) (not to be confused with diaphragms which resist transfer forces from displacement incompatibilities). Often reduced fastener spacing, increased reinforcement or thicker framing members are adopted around irregularities, but the sub-diaphragms are essentially designed as regular diaphragms. The resultant shear forces in the diaphragm have to be collected and conveyed to the lateral load resisting system via the *collectors* (i.e. collector regions or beams). The *connection of the collector to the lateral load resisting system* has to be designed properly, as it is an essential part of the load path into the foundations.

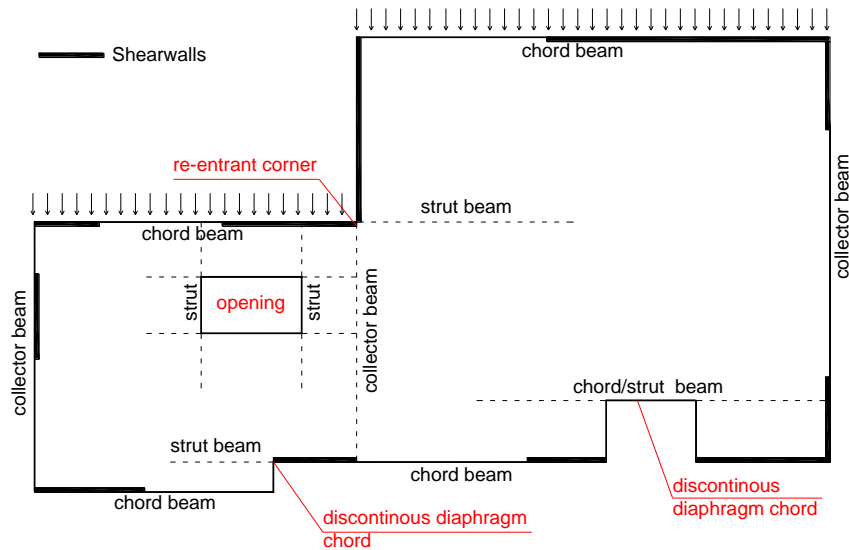


Figure 2.4 Irregular floor geometry with typical diaphragm components

2.4 COMPLEXITIES IN THE DESIGN OF DIAPHRAGMS

In the last two decades a number of researchers have raised concerns regarding the appropriateness of current diaphragm designs in seismic resisting buildings. Research on this area was mainly carried out in New Zealand (Park et al. 1997; CAE 1999; Bull 2004; Fenwick et al. 2010) and the US (fib 2003; Fleischman et al. 2008; Cleland et al. 2012) but was mainly concerned with cast-in-situ and pre-cast concrete diaphragms, with elastic or inelastic concrete lateral load resisting systems. Most of these findings are discussed and referred to in other sections of this thesis and only a general summary is given here.

The main issues for design include the estimation of diaphragm force demand, the determination of the load path in the diaphragms and diaphragm damage due to displacement incompatibilities. These three points of concern are on the basis of the research objectives of this thesis, answered in the context of timber structures.

2.4.1 Higher modes effects

The difficulties in determining the inertial force demand in diaphragms include the fact that static methods are based on a first mode response, and therefore ignore the influence of higher modes. Higher mode effects are often ignored, or in the best case, accounted for with amplification factors providing peak responses along the building height (Rodriguez et al. 2002; Standards New Zealand 2006; Priestley et al. 2007). In order to prevent brittle failure of diaphragms, capacity design principles need to be applied when determining the inertial diaphragm demand. Overstrength factors are not always readily available, their calculation is often difficult and the resulting values often vary notably in magnitude.

2.4.2 Transfer forces

Inertial forces are not the only action to be considered in diaphragms. Structures with non-uniform lateral load resisting systems up the building height can generate large transfer forces in diaphragms. These are caused by the force redistribution and displacement incompatibility between lateral load resisting systems with different stiffnesses. This effect can be observed in podium structures, structures with dual lateral load resisting systems with wall and frames, structures with walls of different lengths at different levels, or in structures where walls are horizontally offset or missing between one floor and the next.

Transfer forces cannot be determined from peak inertial forces from a modal response spectrum or time history analysis, since the obtained forces are not in equilibrium and do not maintain their sign. Until now, no generally accepted design methods exist for the design of diaphragms which considers all the factors mentioned above. The few existing methods have yet to be validated for timber structures.

2.4.3 Load path

The load path in diaphragms can easily be determined with sufficient accuracy in regular, squat or compact floor geometries. Deep beam or steel girder analogies provide the force demand in the single diaphragm elements and fasteners and forces are distributed according to either perfectly rigid or flexible diaphragm assumptions. However, real floor diaphragms are often irregular in plan with semi-rigid behaviour. Over recent years, strut-and-tie methods (Schlaich et al. 1987) have been used to determine the load paths in concrete diaphragms (McSaveney 1997; Bull 2004). A similar approach to the strut-and-tie method for timber diaphragms is a subject of this research.

2.4.4 Displacement incompatibilities

Researchers at the University of Canterbury in New Zealand have been investigating the effects of displacement incompatibilities between the lateral load resisting systems and concrete diaphragms for many years (Fenwick and Fong 1979; Matthews et al. 2003; Bull 2004; Fenwick et al. 2010). Sources of such incompatibilities can be of multiple nature: double curvature deflection of frame beams versus the simply supported beam deflection of the floors, beam elongation in frame beams, uplift and rocking of walls, torsion of frame beams etc. These incompatibilities could potentially lead to severe damage to the floors including column separation or column push-out and hence loss of support, wide cracks along the diaphragm perimeters, diaphragm topping delamination and failure of diaphragm reinforcement.

For pre-cast concrete diaphragms it was observed that design of discrete fasteners between the individual panels not only had to resist shear, but also tension and flexure. Solutions have been proposed in the forms of increased seating, exclusion of non-ductile wire mesh as diaphragm reinforcement, link slabs (Lindsay et al. 2004), articulated floors (Amaris et al. 2008; Vides and Pampanin 2015), slotted beam connections (Au 2010; Muir et al. 2012), and diaphragm ties located away from corner columns (Bull and Henry 2014) etc.

2.5 TYPE OF DIAPHRAGMS

Diaphragms can typically be categorised by their construction materials as shown in Table 2.1 and Figure 2.5.

Table 2.1 Diaphragms categorized by materials

Concrete diaphragms	Steel diaphragms	Timber diaphragms
<ul style="list-style-type: none"> - cast-in-situ diaphragms; - pre-cast concrete diaphragms; 	<ul style="list-style-type: none"> - steel deck diaphragms (mostly roofs); - steel-concrete composite deck diaphragms; 	<ul style="list-style-type: none"> - diaphragms with wooden boards; - Light Timber Frame (LTF) diaphragms with (thin) wooden sheathing panels; - massive timber diaphragms; - Timber-Concrete-Composite (TCC) diaphragms.

For all type of diaphragms, chord and collector actions are resisted by dedicated beam or reinforcing elements which are integrated in the body of the diaphragm plate or sit under the diaphragm. For cast-in-situ concrete diaphragms the shear transfer occurs via aggregate interlock and reinforcing bars in dowel action. For diaphragms built from single panels (precast concrete, steel or wooden panels) the shear transfer needs to be guaranteed via continuous or discrete connections between panels.



a) Cast-in-situ concrete diaphragm (Moehle et al. 2010)



b) Composite steel deck diaphragm (Sabelli et al. 2011)



c) LTF diaphragm (Cobeen et al. 2014)

Figure 2.5 Floor diaphragms in concrete, steel and timber

Diaphragms are also often categorized by the presence of a concrete topping and its contribution to the diaphragm action as shown in Table 2.2.

Table 2.2 Diaphragms categorized by concrete topping

Un-topped diaphragms	Topped diaphragms	
	Non-structural topping	Structural topping
Sometimes used in pre-cast concrete and TCC diaphragms in conjunction with discrete connectors. All timber-only and steel-only diaphragms fall under this category.	The concrete topping does not provide any diaphragm action and is merely used to add mass (i.e. to increase the acoustic and vibration performance), to incorporate services or to provide a level and even surface.	The diaphragm action is resisted by the concrete topping. Normally the presence of concrete is used with composite action to resist gravity forces.

2.6 TIMBER DIAPHRAGM MATERIALS

Timber diaphragm panels can be made of massive wood (CLT), plywood, oriented strand board (OSB) or other wood based materials. Framing elements can be made of solid wood, glulam or LVL, as well as built-up members like I-beams, trusses etc. Individual panels are connected by metallic fasteners like nails, screws or staples or by adhesives or a combination of both.

Over the years, better understanding of the diaphragm behaviour as well as new materials strongly influenced the way timber diaphragms were built. The following provides a list of past and actual timber diaphragm types:

- **Transverse single boards:** boards are running perpendicular to the framing members and are fixed with at least two nails at each crossing;
- **Diagonal boards:** same as above, but the boards are inclined at 45° in respect to the framing elements. The board orientation and the use of two or more nails make this kind of diaphragm stronger and stiffer;
- **Double diagonal boards:** boards are placed in two layers, where the second runs 90° to the first one. This layout provides much higher stiffness and strength compared to single diagonal boards;
- **Panel sheathing:** large size plywood panels or OSB panels made of other wood materials nailed to framing elements (commonly known as Light Timber Framing, LTF).
- **Massive timber panels:** engineered wood panels like glued laminated timber (gluelam), Laminated Veneer Lumber (LVL), Cross Laminated Timber (CLT). Larger element dimensions and high strength values make these diaphragms well suited for multi-storey timber buildings.

More information regarding the performance of single boards and LTF diaphragms can be found in Elliott (1979), the design principles are derived and discussed in Jephcott and Dewdney (1979) and Dean (1982).

2.6.1 New developments in timber diaphragm systems

The recent availability of massive engineered timber products has led to new floor diaphragm systems, in the following called ‘massive timber’ diaphragms. Individual boards or sheeting panels nailed to framing elements (Figure 2.6a) have been replaced by large solid timber panels (Figure 2.6b). These elements carry both gravity and horizontal loads and do not require framing elements to resist vertical loads, to transfer the unit shear forces between panels or to introduce axial loads into the diaphragm. For the diaphragm action, panels can be connected to each other with a myriad of connection details available (Gagnon et al. 2011; STIC 2013). The larger available sizes of massive timber panels, as well their increased strength and stiffness, open the possibility to build larger and taller timber buildings.



Figure 2.6 Light timber frame and massive timber diaphragm examples, with schematic cross sections

2.7 LITERATURE REVIEW

An exhaustive literature review regarding the development of timber diaphragms can be found in Carney (1975) and Peterson (1983). Lack of uniform diaphragm design led to a workshop in 1979 where design engineers reported about timber diaphragm performance and best-practice examples (ATC 1979). During the workshop a list of research questions and objectives regarding diaphragm design were asked; some of these have been addressed in this thesis. As a follow up from the workshop, a guideline for the design of horizontal wood diaphragms was published (ATC 1981). Major contributions on the understanding of timber diaphragm behaviour can be attributed to research carried out by the *Douglas Fir Plywood Association* in the US. The diaphragm in-plane deflection equations first presented by Countryman (1952) are

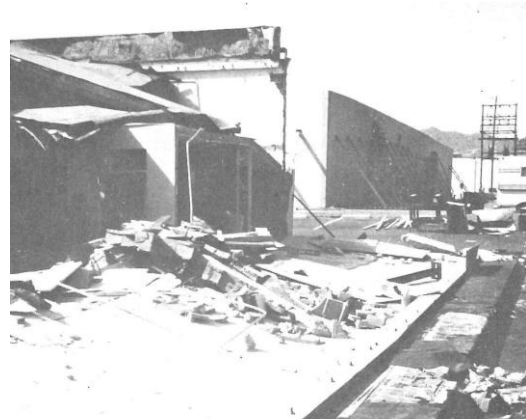
still in use in modern design codes. This association later changed its name to the *American Plywood Association* and later again to *APA The Engineered Wood Association*, which still continues to produce reports and guidelines for the design of timber diaphragms and shear walls (Tissell and Elliott 2004; APA 2007). Other leading research work, especially focusing on the analysis of diaphragms openings, was published by Diekmann et al. (1997). Only recently a manual on the design of irregular light timber frame diaphragms with a wide range of design examples has been published by Malone and Rice (2012). The current New Zealand Timber Standard (Standards New Zealand 1993) contains little guidance on the design of diaphragms and refers to publications by Dean (1982) and Smith et al. (1986). Their work provides guidance on the analysis and design of different timber diaphragms including openings. Major contributions to the design of timber diaphragms can be attributed to Kessel (Kessel 2001; Kessel and Schönhoff 2001), whose work on the 'shear field theory' has been implemented in a number of current design standards (SIA 2003; Eurocode 5 2008; Eurocode 5 DIN NA 2010).

2.8 PAST PERFORMANCE OF TIMBER DIAPHRAGMS

Earthquake performance has shown that wood frame houses generally withstood seismic action in terms of life safety but the economic loss due to the damage of these structures was very significant, given the volume of buildings involved (Rainer and Karacabeyli 2000; Buchanan et al. 2011a). The weakness of LTF structures as summarized by Graf (2008) consists of brittle shear wall sheathing, poorly braced walls, limited shear strength in straight and diagonal sheathing diaphragms and soft or weak storey mechanisms. Most of the reported damage related to diaphragms is located in the connection to the lateral load resisting system. Evidence from the San Fernando earthquake in 1971 (Gray 1979) showed that nails pulled through plywood sheathing or out of the collector beams. Some of the collectors split along the bolts which were supposed to transfer the forces from the diaphragm into the wall (see Figure 2.7a). In other cases the connections between the diaphragm and the masonry walls failed, leading to out-of-plane movement of the walls and a partial collapse of the building.



a) Vector Electronics Building, Sylmar, CA
Collapsed roof due to failure of support



b) M&L Machine Shop, Sylmar, CA
Collapsed roof area and wall

Figure 2.7 Damaged timber diaphragms due to the San Fernando, California 1971 Earthquake (Gray 1979)

Other cases of inadequate diaphragm connections were reported after heavy winds or tornados in the US, such an example is shown in Figure 2.8, where an entire roof was lifted of the building.

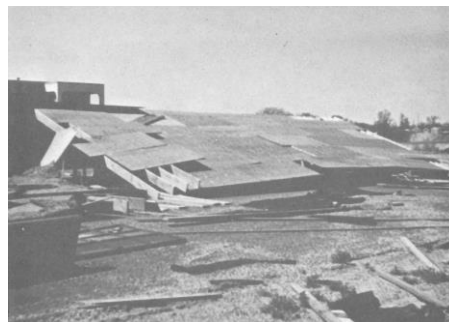


Figure 2.8 a) Wood diaphragm separated from supporting structure by extreme winds (Spangler 1979)

2.9 RECENT BUILDINGS WITH ENHANCED DIAPHRAGM CONNECTIONS

Very little information on the behaviour of recently constructed multi-storey timber structures under larger seismic events has been reported. This is mainly because many countries with higher seismic risk do not have many engineered timber structures. A report by Buchanan et al. (2011b) highlights good performance of engineered timber structures. No damage of diaphragms or diaphragm connections was reported.

The Nelson Marlborough Institute of Technology (NMIT) (Devereux et al. 2011) shown in Figure 2.9 was built in 2008 and has since been through a number of minor earthquakes, including the 2013 Seddon earthquake. No visible damage was reported; measured data from accelerometers and other instrumentations is currently being analysed (Morris et al. 2011). In the structure, diaphragm action is provided by the Timber-Concrete-Composite (TCC) floor.

The diaphragm-to-wall connection is provided by a large diameter pin to minimize displacement incompatibilities.



Figure 2.9 NMIT Building in Nelson with the diaphragm connection detail made of a large diameter pin

The Trimble Navigation Building in Christchurch (Brown et al. 2012) shown in Figure 2.10 was built after the 2011 Canterbury earthquake. Because the diaphragm is made of a rigid TCC floor, the diaphragm-to-wall connections are made of steel-to-steel connections with slotted holes to avoid displacement incompatibilities from both wall uplift and rotation. Steel plates were connected to the walls and beams with inclined fully threaded screws and rivets respectively. Two round pins transfer the loads, while allowing for uplift and rotation in case of an earthquake. In the orthogonal directions of the walls, seismic frames resist the lateral loads, pre-cracks in the concrete slab and unbonded rebars allow for the beam-column-gap opening.



Figure 2.10 Connection of the collector beams to walls via steel-to-steel connection with slotted holes for the Trimble Navigation Building in Christchurch

The Kaikoura District Council Building shown in Figure 2.11, which is still under construction, is made of a timber only floor made of stressed-skin-panels. Because of the relatively flexible

floor (compared to TCC), an economic connection detail between the collector beams and the walls was chosen, using a ring or group of bolts to provide the transfer of vertical and horizontal forces, while allowing for some rotation between the two elements.



Figure 2.11 Kaikoura District Council Building under construction; wall-to-beam connection with a ring of bolts

In the Richmond Warehouse, the diaphragms are connected to the walls by a large diameter pin which transfers both the vertical and horizontal loads while allowing for differential rotations (see Figure 2.12).



Figure 2.12 The Warehouse building in Richmond with wall-to-beam connection via a large diameter pin

More information on the displacement incompatibilities in frame and wall structures can be found in Chapters 8 and 9.

3 State-of-the-art in diaphragm analysis design

3.1 INTRODUCTION

This chapter summarizes and discusses current code provisions and analysis methods for the design of timber diaphragms. Emphasis is also put on the seismic design of timber structures considering capacity design principles and overstrength factors. A limited number of analysis approaches for concrete diaphragms are also mentioned, referring interested readers to specialized literature on this topic.

3.1.1 Background

In the design of buildings, designers historically put their main focus on the gravity supporting system, giving the lateral load resisting system less importance. This attitude has been slowly changing since the 1970s when better detailing rules were introduced, after a number of collapsed buildings as a result of different seismic events. By now, literature and codes provide sufficient guidance for the design of walls, frames and other (vertical) bracing systems, but cover the design of diaphragms only superficially. For the design of timber diaphragms this might be explained by the lack of large or complex engineered timber buildings in areas with high seismic risk.

This chapter summarizes and highlights current knowledge, and methods for the analysis and design of diaphragms with an emphasis on timber diaphragms. Timber-concrete-composite floors can be designed in the same way as concrete diaphragms, which are not studied specifically here.

A number of international codes are summarized regarding their provisions for the design of timber diaphragms in general and the capacity design principles of timber buildings with a special focus on overstrength factors. Available diaphragm analysis methods, ranging from simple hand calculations to equivalent trusses and finite element analysis are discussed in more detail, highlighting advantages and limitations of each method, providing an overview on the state-of-the art of past and current design methods. Principles for the determination of capacity of the individual diaphragm components are discussed.

3.2 CODE PROVISIONS FOR DESIGN OF TIMBER DIAPHRAGMS

3.2.1 Code provisions for the design of timber diaphragms

A comparative study of six international timber design codes listed in Table 3.1 shows that only limited guidance on the design of timber diaphragms is available. All referenced codes are limited to Light Timber Framing (LTF) diaphragms and shear walls. The recently revised Australian Timber Structures Standard AS 1720.1:2010 (Standards Australia 2012) does not mention the design of diaphragms at all and is therefore not included in the table.

For the comparison, emphasis was put on admissible diaphragm aspect ratios, the requirement of blocking (i.e. all edges of the sheathing panels are connected to each other via framing members or blocking elements), the assumed load application, the required design verifications, the evaluation of diaphragm deformation and the presence of openings.

Although the New Zealand and the North American codes base their design on the girder analogy (see Dean (1982), Smith et al. (1986) and (ATC 1981) respectively), the European codes are based on the '*shear field analogy*' (Kessel and Schönhoff 2001; Blaß et al. 2004; Jung 2009). To prevent very flexible diaphragms, designs are normally limited to an aspect ratio of 4 and 6 in Europe and the US respectively. Unblocked diaphragms, where not all panel edges are connected to each other, are only allowed in Germany in cases where certain additional geometric conditions and load limitations are satisfied, and in North America where such configurations have been tested.

Most codes specify the assumed load application type, but only the German National Appendix to Eurocode 5 (Eurocode 5 DIN NA 2010) considers the difference between area loads and loads applied to the diaphragm edges. Numerical analysis presented in Chapter 6 shows that the type of load application influences the demand on the panel fasteners and the degree of participation of the whole diaphragm. Blaß et al. (2004) suggest designing diaphragms as simply supported beams, even if the diaphragm is continuous, and this assumption is backed up by a clause in Eurocode 5. The Swiss SIA 265 (SIA 2003b) suggests calculating the diaphragms with their real statical system, in accordance with recommendations found in Cobeen et al. (2014)

All codes equally require the strength verification of the fasteners, chords and panel elements. Although this is done in Europe via a mechanical approach based on first principles, fasteners and panels are verified against tabulated values in North American codes. Because of the

resulting limitation on available design options, Ni et al. (2010) proposed a mechanics based approach to design of diaphragms for different timber species and connection options.

The requirement for diaphragm deflection checks varies for all analysed codes and only the New Zealand, the US and the Canadian codes provide equations to estimate such deformations. In Europe, diaphragm deflection equations can only be found in accompanying documents to the codes (Blaß et al. 2004; Brunner et al. 2010). The presence of openings is mentioned only in the German and New Zealand codes, where the German code allows small openings without any further restrictions and the New Zealand Code refers to the *Shear Transfer Method* (Dean et al. 1984) to account for the stress concentrations. The Swiss code requires the specific design for openings, without providing any further guidance.

The use of massive timber elements for diaphragms is not mentioned in any of the codes.

Table 3.1 Comparison of six design codes in regards to timber diaphragm design

	Europe EN1995-1-1:2008 (Eurocode 5 2008)	Germany DIN EN1995-1-1/NA:2010 (Eurocode 5 DIN NA 2010)	Switzerland SIA 265:2003 (SIA 2003b)	New Zealand NZ3603:1993 (Standards New Zealand 1993)	Canada O86-14 (Standards Council of Canada 2014)	USA ANSI/AF&PA SDPWS-2008 (AF&PA American Wood Council 2008)
Diaphragm construction	Timber framing and sheathing panels (LTF diaphragms)					
Aspect ratio (L/H)	2-6	≤ 6	No information provided			≤ 3 (unblocked), ≤ 4 (blocked)
Blocked/unblocked ¹⁾	Blocked only	Blocked and unblocked	Blocked only		Blocked and unblocked	
Load	Uniformly Distributed Load along edge	UDL along edge or area load	UDL along edge	No information provided		UDL along edge or area load
Statical system	Simply supported beam	Continuous beams as simply supported beams	Continuous beam on supports	No information provided		
Verifications	Chords, shear in panels and fasteners (mechanical approach)					Tabulated capacity values for shear for nails/staples and panels.
Deformation	No information provided	Can be omitted under certain conditions	Required	Equation provided for blocked simply supported diaphragms		
Openings	No information provided	Can be ignored if of very limited size	Need to be considered		Transfer elements to be designed with 20% force increase	Need to be designed for

¹⁾ In blocked diaphragms all panel edges are connected to each other via faming elements or special blocking elements allowing for the direct transfer of the unit shear forces

3.2.2 Code provisions for the seismic design of timber diaphragms

3.2.2.1 Capacity design philosophy

Structures in areas with moderate to high seismic hazard are normally designed to behave in a ductile manner to mitigate the force demand on the building. Such buildings need to be designed according to *capacity design principles*. The idea behind the capacity design of structures was first introduced by Hollings (1968) and later defined and published by Paulay and Park (1975). New Zealand’s design standards have since then been some of the leading codes for the design of ductile concrete structures.

The capacity design procedure outlined in Figure 3.1 requires the selection of a mechanism with designated ductile regions or ductile connections. These ductile components must be designed to withstand large cyclic deformations, and all other (less ductile or brittle) elements must be designed with proper overstrength. This principle can be best explained with a chain analogy shown in Figure 3.2, where the maximum capacity is dictated by the weakest link and when the weakest link is ductile, the overall chain is ductile.

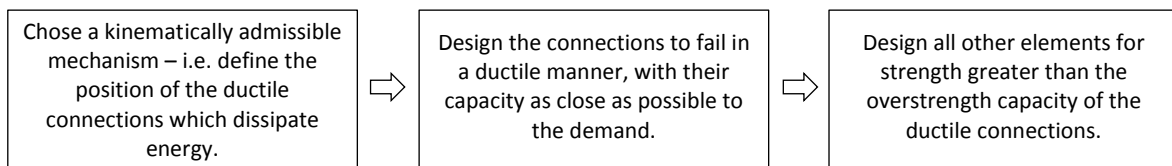


Figure 3.1 Capacity design procedure

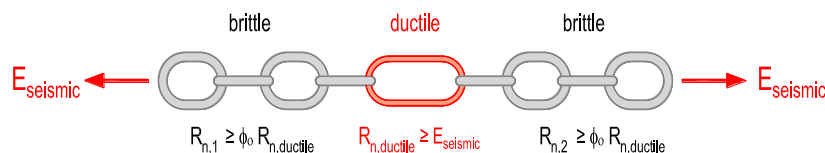


Figure 3.2 Capacity design and chain analogy ($E_{seismic}$ seismic demand, $R_{n,ductile}$ strength of ductile element, ϕ_o overstrength factor of ductile element, $R_{n,i}$ strength of brittle element i) (modified from Paulay and Park (1975))

Capacity design principles have been implemented in most international loading codes as well as in material specific concrete or steel standards. For the design of timber structures little guidance has been given so far, with overstrength factors often left to the designer’s judgement. This is thought to be linked to the fact that leading research bodies on timber structures are situated in low seismic areas like Germany, Switzerland or Austria. Places like New Zealand, California, Japan and British Columbia have a long history in the construction of LTF residential housing; the most common typology of one- and two storey houses are however mostly designed based on prescriptive rules. The fact that most such buildings have

shown very satisfactory behaviour under past earthquakes, explains the little effort in the understanding of the seismic behaviour of timber buildings given in the past.

3.2.2.2 Seismic design of timber buildings

The recent global interest in tall wood buildings in seismic active areas has finally attracted research on the seismic design of timber buildings. A number of scientific articles, guidelines and books have been published over the last two decades, but comprehensive code provisions on the seismic and capacity design of timber structures and their diaphragms are still poor or missing.

Table 3.2 summarizes the three key aspects regarding the seismic design of timber diaphragms according to loading codes and timber design standards for six countries.

Table 3.2 Comparison of design codes in regards to the seismic design of timber diaphragms

	Europe	Italy	Switzerland	New Zealand	Canada	USA
	EN 1995:2008, EN 1998:2010 (ECs 5 and 8) (Eurocode 8 2004; Eurocode 5 2008)	NTC2008 (Consiglio Superiore dei Lavori Pubblici 2008)	SIA 265:2003, SIA 261:2003 (SIA 2003b, a)	NZS3603:1993, NZS1170.5: 2004 (Standards New Zealand 1993, 2004)	O86-14 and NBC 2010 (Canadian Commission of Building and Fire Codes 2010; Standards Council of Canada 2014)	ASCE 7-10, IBC 2012 and SDPWS 2008 (AF&PA American Wood Council 2008; ASCE 2010; International Code Council 2011)
Elastic/ yielding diaphragms	No explicit provisions are given.			Elastic only	Elastic and yielding	Elastic only
Flexible diaphragm definition ¹⁾	$\Delta_{\text{diaphragm}} \geq 1.1 \Delta_{\text{LLRS}}$		No information provided	$\Delta_{\text{diaphragm}} \geq 2 \Delta_{\text{LLRS}}$	No information provided	$\Delta_{\text{diaphragm}} \geq 2 \Delta_{\text{LLRS}}$
Capacity design provisions	Overstrength factors mentioned, no values for timber provided	Overstrength factors mentioned, no values for timber provided; diaphragm loads need to be increased by 30% ²⁾	Overstrength factor of 1.2 provided	Overstrength factor of 2.0 provided	Overstrength factors provided	Overstrength factors provided for collector beams ³⁾ ; special provisions for the anchorage details provided
Spectral reduction factor for LTF walls ⁴⁾	5	5	3	-	5.1	6.5

1) $\Delta_{\text{diaphragm}}$ = deformation of the diaphragm at the storey of interest;

Δ_{LLRS} = interstorey deformation of the Lateral Load Resisting System (LLRS) of at the storey of interest;

2) The draft version of the new NTC (Consiglio Superiore dei Lavori Pubblici 2013) provides specific overstrength values for different structures. For the design of timber structures the application of the overstrength values is specifically addressed.

3) Structures with light-frame shear walls are exempt from this rule, i.e. collector beams are designed with the standard load combination.

4) Given values are the response modification factor R for ASCE 7-10; force modification factors R_d , R_o for NBCC, behaviour factor q for Eurocode 8 and SIA 261.

Although diaphragms are only supposed to work in the elastic range in New Zealand and the US, designers in Canada can also opt for yielding diaphragms. European codes do not provide

any guidance on this regard. All studied codes and standards require the application of capacity design principles for the design of seismic resistant buildings, but specific overstrength factors are not always provided. The Eurocodes and the Italian Building Code (Consiglio Superiore dei Lavori Pubblici 2008) do not provide any overstrength factors for timber structures, suggesting factors for brittle and ductile concrete structures only. Independently from the material, the Italian code requires an additional increase of the diaphragm demand by 30%. New Zealand provides an overstrength factor of 2.0 for nailed connections of wooden sheathing panels, with Switzerland defining a general factor of 1.2 independently from the fasteners or structural system adopted. Only the North American codes provide a series of overstrength factors for different lateral load resisting systems.

In addition it was also found that the reduction factors for timber structures necessary to determine the design spectra vary in the different codes. This is due the fact that these values are defined and calibrated in different ways in different codes.

Another discrepancy was found in the provided strength values under wind and seismic action. In the US the tabulated shear capacities of diaphragms and shearwalls for wind are 40% higher than for seismic loading. According to Eurocode 8 the design strengths for seismic loads are in average increased by 60% in respect to values for wind loads and in Switzerland the strength properties are increased by 40% for seismic loading conditions.

3.2.3 Flexible and rigid diaphragms

The definition of flexible and rigid floor diaphragm behaviour has always been a point of discussion, especially for light timber frame construction. The flexibility of the floor diaphragm has the potential to change the dynamic response of the whole building as will be shown in Chapter 4 and impacts on the distribution of lateral forces into the lateral load resisting system as known from first principles. The standard assumption is that flexible diaphragms distribute loads in proportion to tributary areas, whereas rigid diaphragms distribute loads to the lateral load resisting elements in proportion to their stiffness. For the latter, torsional effects because of mass eccentricities also need to be considered.

Definitions of 'flexible' diaphragms vary widely (see Table 3.2 and Figure 3.3), and the rationale behind the limits are mostly unknown (Sadashiva et al. 2012). Since the inter-storey drifts and the individual diaphragm deflections vary up the building height, diaphragms could be defined as flexible for some storeys and rigid for others. This will cause some complexity in designing

taller structures and its actual application by practitioners is questionable. It is also unclear for which force demand the diaphragm deflections are to be calculated, considering that the values from the equivalent static analysis normally under-predict the values determined from a NLTHA.

Code provisions seem to be applicable to single storey structures, with taller structures to be analysed by more sophisticated analysis methods. As an alternative, a global diaphragm stiffness definition based on the diaphragm deflection and an inter-storey drift measured at the mid-height of the structure could be considered as suggested by Fleischman and Farrow (2001). This value provides an average value of flexibility which could be used for design.

Some timber design codes provide prescriptive detailing rules for rigid diaphragms, but their application is questionable for modern floor materials and panel layouts.

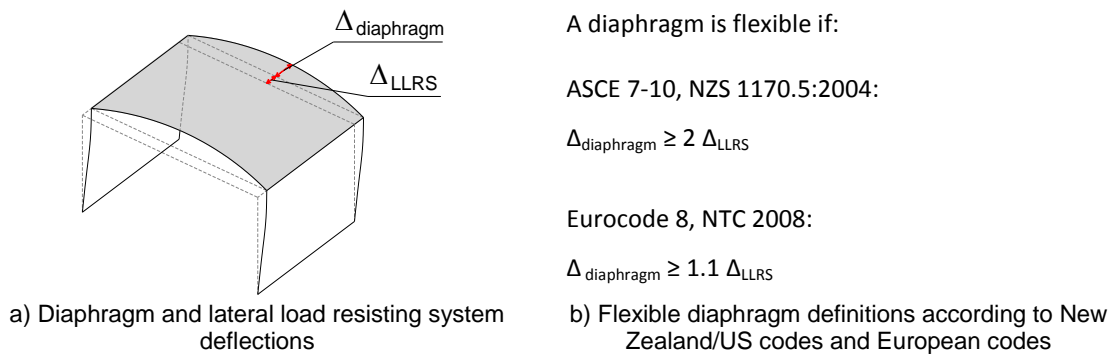


Figure 3.3 Diaphragm flexibility according to international seismic codes

Since the force distribution in the diaphragm and the lateral load resisting system is affected by the diaphragm flexibility, both stiffnesses need to be assessed and forces distributed as mentioned before. Timber diaphragms normally behave in a semi-rigid manner and can be designed by either an envelope method (Gagnon et al. 2011; FPInnovations 2013) or through a specific analysis. For such an approach the Equivalent Truss Method, as will be introduced in Chapter 7, is recommended.

3.2.4 Provisions for overstrength factors in codes and recent literature

In order to ensure that the ductile link in the system is indeed the weakest component along any given load path, an 'overstrength' factor is defined for ductile links. It comprises all sources of additional strength a ductile link can have above its design strength. According to the capacity design principles mentioned above, all other elements of the building then need to be designed for a demand corresponding to the overstrength of the ductile link. In this way the strength hierarchy is guaranteed and brittle failure modes are prevented. Paulay and Park

(1975) defined the overstrength factor for concrete structures to account for higher-than-specified material strength, strain hardening at large deformations and sections sizes larger than assumed.

A different definition of the term overstrength is based on the structure's higher strength in resisting earthquakes as a whole. This building overstrength is not coming only from additional resources in the lateral load resisting system, but also from the contribution of non-structural elements. ASCE 7-10 and NBC specify such overstrength factors which are required to derive the design spectra from the elastic spectra. NZS 1170.5 (Standards New Zealand 2004) defines a structural performance factor S_p which amongst other factors considers higher building strengths from observations. The structural behaviour factor q in Eurocode 8 and SIA 261 (SIA 2003a) already includes the building overstrength.

Most codes specifically try to protect diaphragms from higher than expected loads and define overstrength factors to achieve this. ASCE 7-10 requires a specific load combination including the building overstrength factor Ω_o . NBC provides different factors to amplify diaphragm loads, depending on their expected working range (elastic or yielding). Eurocode 8, SIA 261 and NZS 1170.5 require the application of overstrength factors based on the effective strength of the ductile links to protect brittle elements and diaphragms in particular; but only the latter two provide values for timber structures.

Concept of overstrength

$$R_{b,k} \geq \gamma_{Rd} R_{c,k}$$

with

$$\gamma_{Rd} \geq \gamma_{sc} \gamma_{an} \gamma_M$$

where

$$\gamma_{sc} = \frac{R_{c,0.95}}{R_{c,0.05}}$$

considers the reliability of the connection (statistical scatter);

$$\gamma_{an} = \frac{R_{c,0.05}}{R_{c,k}}$$

considers the approximation from the analytical formulations when compared to experimental values;

$$\gamma_M = \frac{R_{c,k}}{R_{c,d}}$$

considers material safety factor (difference between nominal and factored strength).

$R_{c,d}$ is the analytical prediction of the connection design strength;

$R_{c,k}$ is the analytical prediction of the connection characteristic strength;

$R_{c,0.05}$ is the 5th percentile of the connection strength capacity;

$R_{c,0.95}$ is the 95th percentile of the connection strength capacity;

$R_{b,d}$ is the design strength of the brittle element (beam);

$R_{b,k}$ is the characteristic strength of the brittle element (beam).

Graphical representation

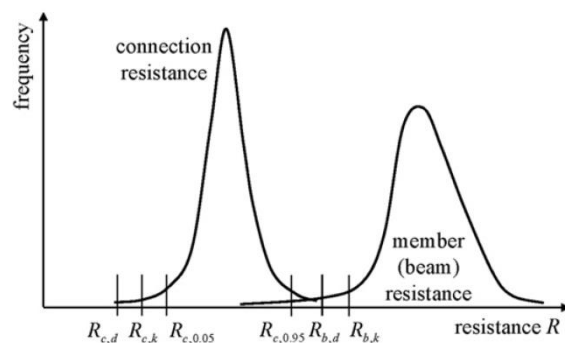


Figure 3.4 Concept of overstrength: the ductile connection resistance must be smaller than the brittle member (beam) resistance with sufficient probability (Jorissen and Fragiaco 2011)

Recently a number of researchers (BRANZ 1999; Mitchell et al. 2003; Popovski and Karacabeyli 2005; Jorissen and Fragiaco 2011; Sustersic and Dujic 2011; Schick et al. 2013; Brühl et al.

2014) have started testing and deriving overstrength factors for different fasteners or whole lateral load resisting systems in timber. Unfortunately there is no consensus on a common approach of how to determine overstrength values and what factors (i.e. statistical scatter, approximation of analytical expressions, over-capacity, hidden reserves from mechanical effects etc.) should be included. Figure 3.4 shows the graphical representation of one approach to determine the overstrength for a timber connection. Jorissen and Fragiacomò (2011) defined 3 partial factors considering statistical scatter, approximation in the analytical formulation and material safety factors. Sustersic and Dujic (2011) used the same approach but included an additional partial factor to consider the actual capacity of the ductile link in respect to the demand. This was necessary to account for rounding or limited available sizes for the chosen connectors. Schick et al. (2013) included also a term to account for hidden reserves, like friction and pull-out resistance of the fasteners. This value is a function of the whole wall-frame assembly under consideration. Brühl et al. (2014) used the same concept as shown in Figure 3.4 and extended it by running a Monte Carlo simulation to account for the variability of material properties (steel strength, timber density and strength), connection geometry and model uncertainty.

The research described above provides a good basis for the determination of overstrength factors in timber structures, but a unified method will be necessary, before values can be adopted in design codes.

3.3 DETERMINATION OF DIAPHRAGM FORCES

In literature several analysis methods to determine the load path in diaphragms are available; the most common are the deep beam analogy, the truss analogy, the Vierendeel truss analogy, the strut-and-tie method and finite element analysis. Not all analysis methods can be equally applied to both concrete and timber diaphragms. A list of available analysis methods with their reference to the relevant section in this chapter are shown in Table 3.3.

Table 3.3 Application of different analysis methods to concrete and timber diaphragms and reference to relevant sections

Analysis method	Concrete diaphragm	Timber diaphragm
Deep beam analogy	Commonly used for regular diaphragms (see section 3.3.1.2)	Commonly used for regular diaphragms (see section 3.3.1.1)
Vierendeel truss analogy	Not applicable	Used for unblocked diaphragms and diaphragms with straight boards (not discussed)
Shear field analogy	Used in the form of the 'stringer-panel method' (Blaauwendraad and Hoogenboom 1996) (not discussed)	Commonly used for regular and to a limited extent to irregular diaphragms (see section 3.3.2)
Strut-and-tie method	Used for regular and irregular diaphragms (see section 3.3.3)	Not applicable
Truss analogy	Applicable, not widely used (see section 3.3.4.1)	Applicable, not widely used (see section 3.3.4.2)
Finite element analysis	Applicable, used for special studies (see section 3.3.5.1)	Applicable, used for special studies (see section 3.3.5.2)

3.3.1 Deep beam/girder analogy

Timber and concrete diaphragms with regular geometries are commonly analysed with the deep beam or girder analogy. In this approach flexural tension and compression forces are resisted by the chord beams which are running along the diaphragm edges perpendicular to the load direction, and shear forces are resisted by the diaphragm panels as shown in Figure 3.5.

The number, nature and size of diaphragm irregularities, which would make this simplified method non-conservative, are seldom mentioned. In general, the diaphragm must be free of re-entrant corners, concentrated loads, big openings and other irregularities causing stress concentrations. In spite of this, the girder analogy is commonly applied to irregular

diaphragms, leading to local or global diaphragm damage due to stress concentrations and excessive diaphragm deformations.

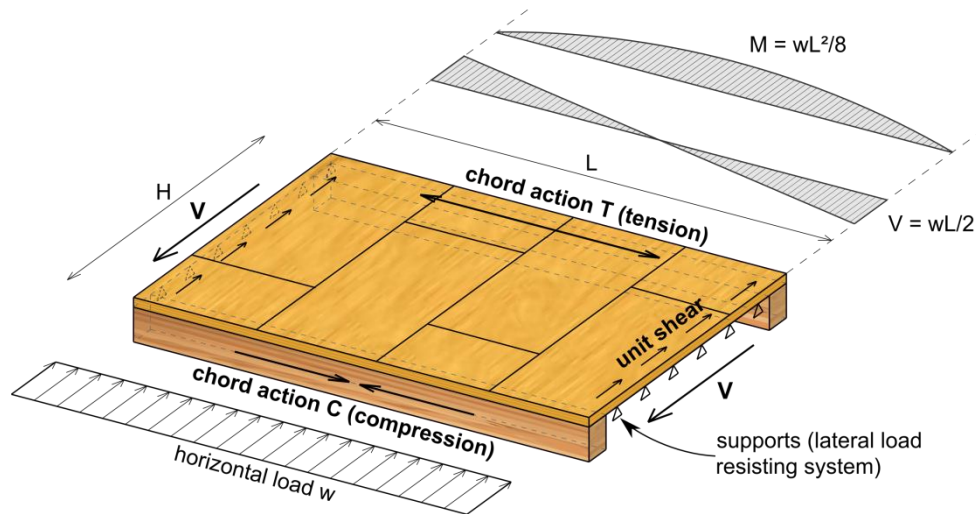


Figure 3.5 Girder analogy

To obtain the tension and compression forces in the chord beams, the following equations can be used:

$$T = C = \frac{M}{H} = \frac{wL^2}{8H}, \quad (3.1)$$

where

- T is the tension force in the chord beam;
- C is the compression force in the chord beam;
- w is the uniform distributed load;
- L is the diaphragm span;
- H is the diaphragm depth;
- M is the moment from uniform distributed load.

The unit shear force, defined as the shear force per unit length (or shear flow), can be calculated as

$$v = \frac{V}{H} = \frac{wL}{2H}; \quad (3.2)$$

where

- v is the unit shear force;
- V is the shear force at diaphragm supports.

These equations can be modified to account for loads different from the uniform distributed load.

3.3.1.1 *The girder analogy in timber diaphragms*

Especially for timber diaphragms the girder analogy has found wide acceptance. Usual timber floor assemblies consist of joists supported by main beams, which are then covered with wooden panels. Under diaphragm action, bending is taken by the chord beams acting as *flanges* and shear is resisted by the panels (diaphragm sheathing acting as *webs*). Experimental evidence showed that the assumed constant shear distribution along the diaphragm depth, as opposed to a parabolic constant shear distribution found by first principles, is appropriate for the design of timber diaphragms (ATC 1981; Smith et al. 1986). To guarantee that the sheathing panels work as a splicing plate as in steel girders, all panel edges need to be connected to each other (blocked diaphragm). Unblocked diaphragms withstand loads with a completely different mechanism like the '*moment couple series*' normally used to design diaphragms made of transverse boards based on a Vierendeel Truss Analogy.

Diaphragm aspect ratios are normally limited to values from 1 to 5. For aspect ratios smaller than 1, sheathing panels and joists substantially contribute to the bending resistance. Because of the high diaphragm depth however, the resulting tension and compression forces will be relatively small, yielding to a conservative design (Prion 2003). The upper limit of the aspect ratio is normally intended to limit flexible diaphragm designs, rather than setting a limit to the analysis method itself.

3.3.1.2 *Deep beam analogy in concrete diaphragms*

Concrete diaphragms are either designed according to the classical beam theory, where plane sections remain plane or to the deep beam theory. In either case, chord beams, which consist in either gravity beams or specially reinforced strips in the slab itself, are designed using equation (3.1) to resist tension and compression forces. The shear stress is considered to be constant over the diaphragm depth and can be calculated according to equation (3.2).

For usual diaphragm sizes the concrete can resist most of the shear force, and the reinforcement required to resist gravity loads or for crack control additionally contributes to the shear strength. For tension chords it is paramount to guarantee that the axial force can be resisted by the reinforcement provided, this requires appropriate curtailment in case of splices. Frame beams should not be used as chord beams in diaphragms, due to the potential presence of plastic hinges and the inability to transfer large tension forces.

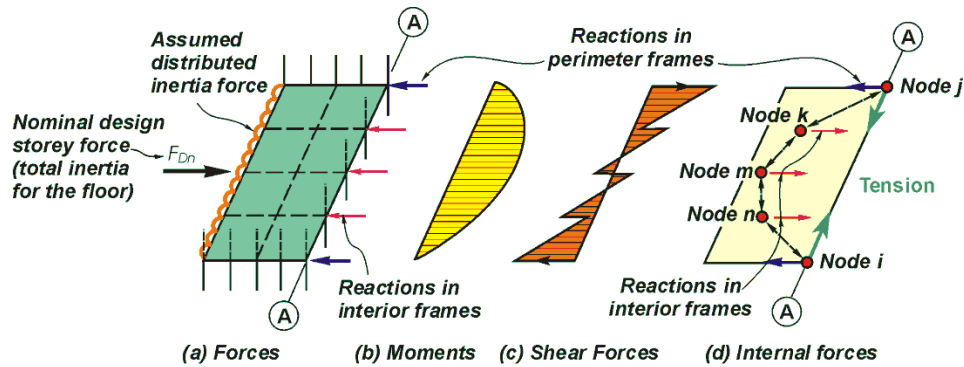


Figure 3.6 Deep beam analogy for a typical concrete diaphragm with a frame structure (modified from Park et al. (1997) by Des Bull)

3.3.1.3 Limitations of the Deep Beam Analogy

The big majority of structures require floor geometries which are far from being regular. Set-backs, openings, re-entrant corners, concentrated force introduction etc. limit the use of the deep beam analogy. Because of the lack of (simple) analysis methods and the little attention many designers give to diaphragms, this procedure is still applied to most diaphragm designs, ignoring the presence of stress concentrations.

Openings and other irregularities can be accounted for by additional calculations based on first principles. A number of publications (Elliott 1979; Jephcott and Dewdney 1979; Diekmann 1982; Dean et al. 1984; Kessel and Schönhoff 2001; Prion 2003; Tissell and Elliott 2004) provide the theory and the methods for openings in timber diaphragms. Not all methods have been verified against experimental evidence and a number of the approaches can soon become complex considering the number of equations involved (for a design example see Appendix E).

For diaphragms in high seismic areas, where transfer forces and other displacement incompatibilities are likely to occur, it is recommended not to use the deep beam analogy. This is because not all diaphragm forces can be accurately predicted and the assumed load distributions might not be compatible with the general building behaviour (Bull 2004).

It has been shown that for topped and untopped precast diaphragms the girder analogy requires a certain degree of plastic redistribution. For the flexural reinforcement in the chords to be activated, the shear reinforcement (or connectors) in the web may need to undergo tensile stresses. This force combination in the shear reinforcement cannot be predicted with the deep beam analogy and might cause premature failure in the diaphragm (fib 2003).

3.3.2 Shear field analogy

The shear field analogy has its origin in the aeronautical engineering and has been subsequently introduced into applications of civil engineering. Nielsen introduced the method 1979 for the use with concrete walls (Kærn 1979), Schulze and Schönhoff (1989) further applied the principles to the calculation of LTF diaphragms. Eurocode 5 (Eurocode 5 2008), its German National Appendix (Eurocode 5 DIN NA 2010) and the Swiss Timber Code SIA 265 (SIA 2003b) are all explicitly based on the shear field analogy. Both the report by Kessel and Schönhoff (2001) and the Commentary to the former German Timber Standard DIN1052:2004 (Blaß et al. 2004) explain the method with its advantages and provide some practical examples.

The shear field analogy overcomes the disadvantages of the ‘*diagonal analogy*’ referred to in the former German Timber Standard DIN1052:1988 (DIN 1988) and the strut-and-tie methods (Schlaich et al. 1987). Timber diaphragms are not capable of providing node force transfer as assumed by these methods (see section 3.3.4). It also derives the constant unit shear force along the diaphragm depth and the linear force distribution along the frame and boundary beams, not explained by the girder analogy.

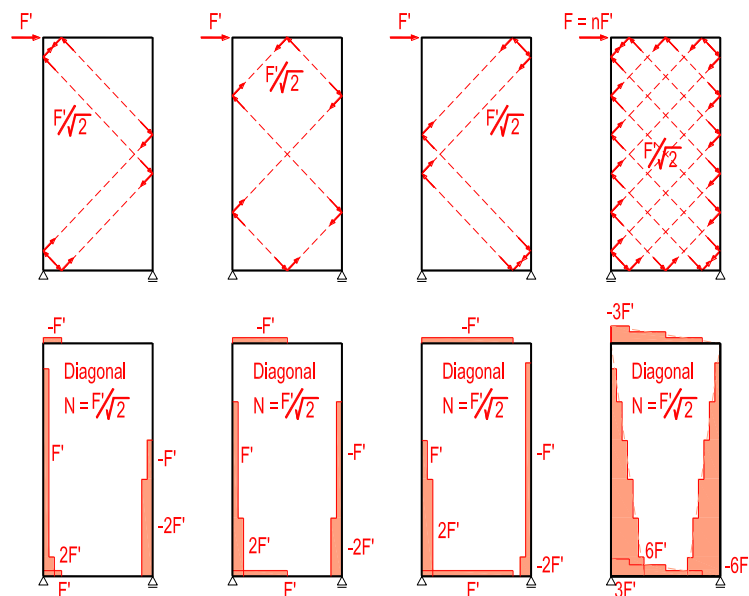


Figure 3.7 Derivation of the shear field analogy as a superposition of truss models (modified from Kessel and Schönhoff (2001))

Figure 3.7 shows the derivation of the shear field analogy from the superposition of a number of equivalent trusses. All diagonals inclined in one direction have the same force in tension, and the diagonals inclined in the other direction have the same force in compression. Consequently the resultant forces along the panel edge are constant and parallel to it. The

framing elements therefore only transfer axial loads, which are linearly distributed in the ideal case of an infinite number of equivalent diagonals. Since the fasteners are only loaded by shear forces parallel to the panel edge, the minimum nailing distances for unloaded edges can be used (see Figure 3.8).

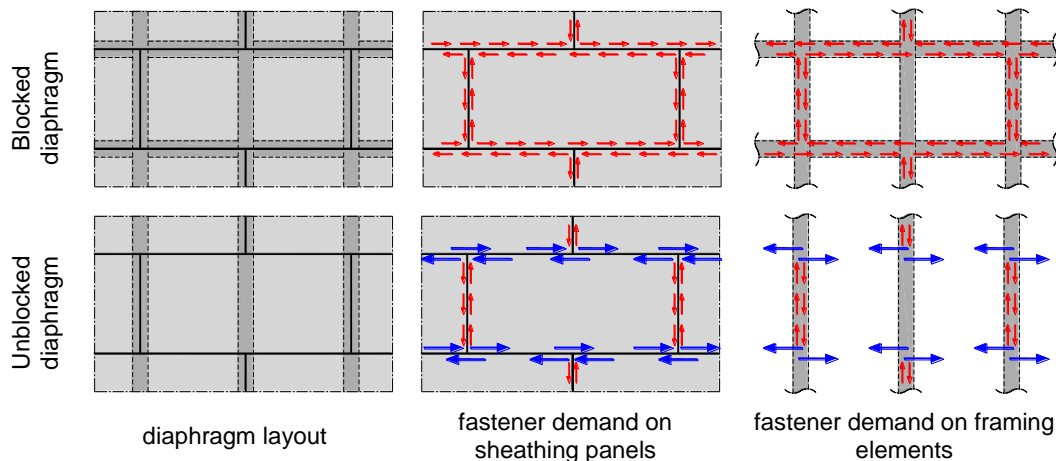


Figure 3.8 Blocked (top) and unblocked (bottom) diaphragms, fastener demands on sheathing panels and framing elements (modified from Kessel and Schönhoff (2001))

The requirements and basic assumptions of the shear field analogy can be summarized as:

- 1) The diaphragm must consist of sheathing panels fixed with metallic fasteners to framing elements along all edges (blocked LTF diaphragm);
- 2) Loads can only be introduced along the framing elements running in the load direction (see Chapter 6 for other loads introductions);
- 3) The fastener stiffness is smaller than the shear stiffness of the sheathing panels and the axial stiffness of the framing elements.
- 4) The capacity of the diaphragms is dictated by the (ductile) failure of the connections.

3.3.2.1 Limitations of the shear field theory

The shear field analogy provides a reasonably easy method to analyse LTF diaphragms including irregularities like openings or re-entrant corners. With increasing number of irregularities this method based on hand calculations, however, soon becomes too complex.

The assumptions of the shear field analogy very often are violated in real structures. Loads not applied via the framing elements in their axial direction and displacement incompatibilities cause inconsistencies in the method. A number of such incongruencies are:

- The actual axial and shear stiffness of the framing elements and sheathing panels respectively is not considered;

- Because of floor irregularities and load applications perpendicular to framing elements, fasteners are activated perpendicularly to the panel edge. Because fasteners normally provide strength and stiffness in this direction, framing elements are activated in bending and sheathing panels resist axial stresses;
- Framing elements and especially chord beams are continuous over several panels and are activated in bending because of the relative displacement to adjacent panels;
- Connections between framing elements are activated under the deformation of the panels, providing additional stiffness;
- Framing elements are not continuous over the whole diaphragm because of limited commercially available lengths or because they are interrupted by orthogonal elements. The stiffness of splices is not taken into consideration in the analogy;
- Under larger deformations, panel edges can touch each other, thus a wedging effect is provided which makes the diaphragm notably stiffer.

Construction economy often dictates that not all panel edges are connected to each other and are therefore not able to transfer the shear forces. This causes an additional force demand in the remaining fasteners and causes force components perpendicular to the framing elements as shown in Figure 3.8 (blue arrows). Research by Meyer (2006) showed that concentrated fasteners can partially solve this problem. The fastener spacing however has to be increased accordingly and torsional shear of the framing element needs to be taken into account.

The German National Appendix to Eurocode 5 (Eurocode 5 DIN NA 2010) allows for unblocked diaphragms under certain geometric conditions and load limitations by reducing its nominal strength by 33%.

For concrete diaphragms, a very similar method known as panel-stringer-method has been developed (Blaauwendraad and Hoogenboom 1996). The method is not well known and has therefore found little application so far and is not discussed herein.

3.3.3 Strut-and-tie method

The strut-and-tie method has been developed for concrete members and relies on the compression strength of concrete and the tensile strength of reinforcement bars.

The strut-and-tie method has found wide application after its formal definition by Schlaich et al. (1987), even though it has found earlier use in the truss analogy for concrete beams (Ritter 1899; Mörsch 1912). The method is especially suited for the study and detailing of disturbed

regions (D-regions) in reinforced concrete structures. D-regions are areas or sections in a reinforced concrete element where the Bernoulli hypothesis of plane sections (beam theory) is not valid anymore. The strut-and-tie method can also be used to design entire members where both disturbed and Bernoulli regions exist.

The method guarantees equilibrium at each node and provides an admissible force path in the structural element by setting up a truss-like system. Compression struts and tension ties are assigned in a way to guarantee the shortest possible load path with the minimum strain energy required (fib 2011). The tension strength of concrete is normally neglected and concrete struts do not intersect except at nodes. For tension ties enough steel reinforcement needs to be provided, for compression struts the cross section is verified taking into consideration possible transverse tensile strains (i.e. for bottle struts, struts in tension regions). The verification of nodes depends on the number of ties and/or struts connected and is the most delicate part of the procedure. Coefficients normally provide reduced concrete strengths in case of tensile stresses in the nodal area. Most international concrete codes (Eurocode 2 2005; Standards New Zealand 2006; Standards Australia 2009; ACI 2014) provide guidelines and provision for the use of strut-and-tie models.

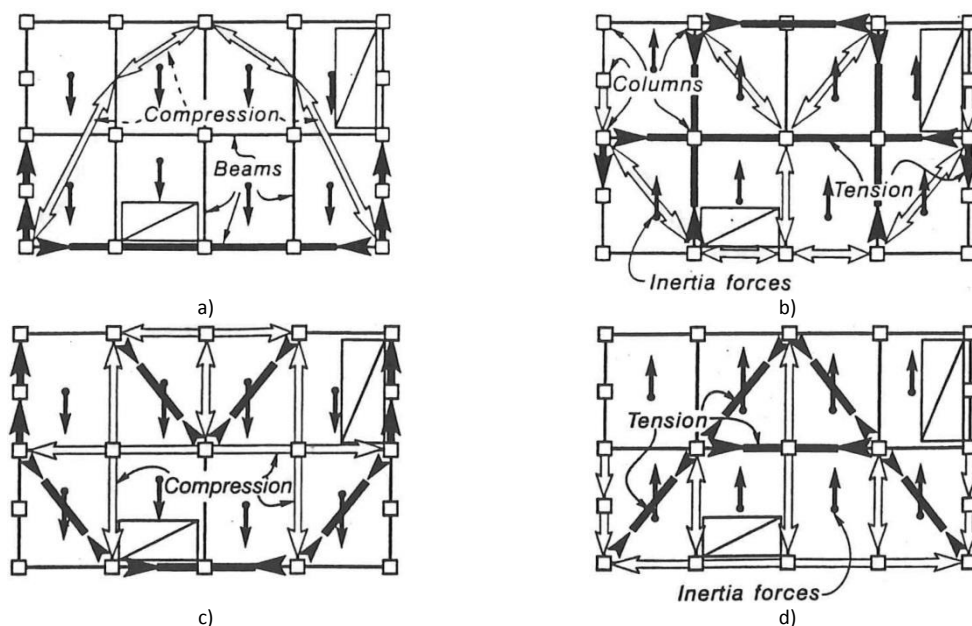


Figure 3.9 Strut-and-tie models for a floor diaphragm with openings; a) and b) using compression fields, c) and d) using tension fields (Paulay ; Park et al. 1997)

In New Zealand the strut-and-tie model has been the preferred method for the design of concrete diaphragms over the last two decades (Paulay 1996; Park et al. 1997; Bull 2004) and

has since then been included in the Concrete Structures Standard (Standards New Zealand 1995).

Figure 3.9a is a representation of the force flow in a diaphragm as assumed in the deep beam analogy. For the load reversal in b) struts and ties are similar as for typical truss models. The models shown in c) and d) assume diagonal tension fields, achieved by the rebars in the floor.

Tension ties often correspond to be the tension chords or specially designed internal beams with continuous reinforcement. Small tension forces are normally resisted by reinforcement meshes required by gravity or crack control. If the tension force becomes too big, for example around floor openings, it might be necessary to provide some additional ties in form of drag bars.

3.3.3.1 Limitations of the strut-and-tie method

The choice of the strut-and-tie model geometry is not unique. Although forces prefer the load path with the biggest stiffness, designer sometimes choose scenarios with a quite tortuous load path. Even though statically admissible, such load paths imply force redistribution, which is often accompanied by extensive cracking. This may lead to excessive diaphragm damage and failure of other structural elements attached to the diaphragm. The choice of the most appropriate and adequate strut-and-tie model should therefore be determined based on stress trajectories from an elastic FEM analysis or should be based on design experience.

The localized ties in the analysis method require concentrated reinforcement in specific positions. Diaphragm reinforcement however is normally made of steel mesh or a grillage of reinforcement bars, providing a distributed reinforcement instead. This can influence the load path and in extreme cases lead to bar yielding before drag ties or chords are activated.

One of the mayor disadvantages of the strut-and-tie method is the dependency of the chosen model geometry to a specific applied load. A different loading condition or even a load reversal might require a new analysis with a completely different load path. This can result in a number of analysis cases for irregular floor geometries with a number of loading conditions.

Because the strut-and-tie method is based on force equilibrium at the nodes, it is not able to distribute the horizontal loads as a function of the stiffness of the diaphragm and the lateral load resisting system. Designers therefore need to decide beforehand on a force distribution according to a flexible or rigid diaphragm assumption. This assumption always needs to be verified and the load path adjusted accordingly.

3.3.4 Equivalent truss method

3.3.4.1 Equivalent truss method for concrete diaphragms

Lattice models in their earliest form have been used by Ritter (1899) and Morsch (1912) in their truss analogy of concrete beams and have found also application in the 'Framework Method' by Hrennikoff (1941). The elastic continuum was described as a framework of bars arranged in a specific pattern so that deformation, stresses and unit shears could be successfully represented. At that time, design software for such models was not readily available and the verification of the method only became available with the development of finite element methods. The framework method therefore remained purely theoretical for many years and practitioners preferred simpler approaches like the strut-and-tie method.

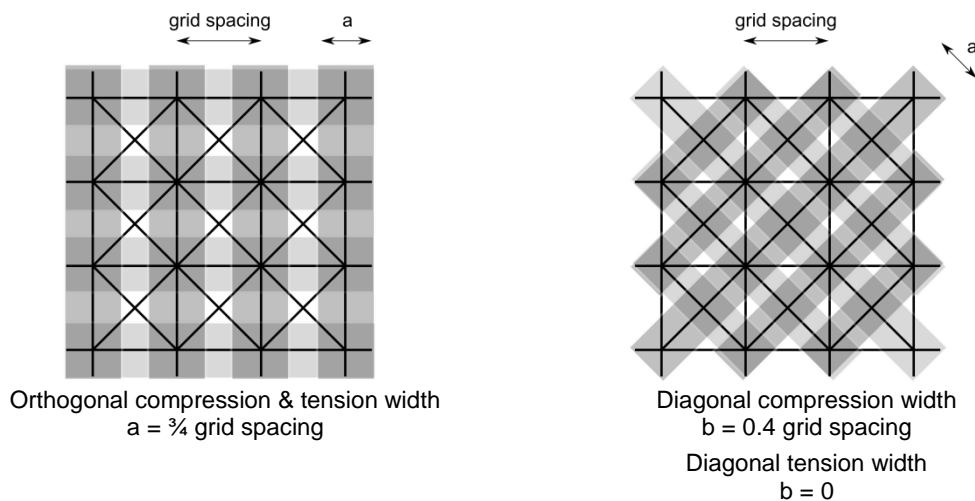


Figure 3.10 Width of truss elements in concrete diaphragms (modified from Bull and Henry (2014), based on Hrennikoff (1940))

Several authors have used lattice models based on beam or truss elements to represent concrete elements on a micro or macro scale. A comprehensive summary and study on such models with various levels of complexity including compression non-linearity, tensile fracture, interaction with concrete steel, concrete cracking and loading complexities can be found in Ilgadi (2013).

The use of equivalent trusses (sometimes also described as grillages, meshes etc.) has found a wider acceptance over the last decades in New Zealand. Based on Hrennikoff's work, Gardiner (2011) shows the applicability of equivalent trusses for the design of irregular concrete diaphragms. Bull and Henry (2014) and Scarry (2014) are further disseminating the use of equivalent trusses for the analysis of diaphragms. Figure 3.10 shows a possibility of the definition of compression and tension elements, which can be implemented in any structural

analysis program capable to solve trusses. The truss not only provides tension and compression forces for any possible loading conditions, but also considers the load distribution according to the diaphragm stiffness, and if modelled, the stiffness of the lateral load resisting system. The struts and ties as well as the nodal areas can be designed in the same way as for the strut-and-tie method.

3.3.4.2 Equivalent truss method for timber diaphragms

The former German Timber Standard DIN1052:1988 (DIN 1988) allowed for the design of LTF walls and diaphragms by using equivalent tension diagonals. In this initial form of an equivalent truss, the sheathing panel was verified by assuming a relatively narrow strip of the panel as shown in Figure 3.11. The connection of the tension force into the surrounding framing elements was carried out along the full length of the panel edges. The fastener capacity was verified considering the force components parallel to the framing members. Not only was the fastener check not compatible with the statical model chosen, but the principles of the 'tension-field theory' were not admissible for LTF diaphragms (Colling 2011). This theory, introduced by Wagner (1929), does only apply to thin webbed members after buckling occurs, which generally does not occur for common panels thicknesses and spacing of framing elements. Furthermore, the force demand in a panel joint as shown in Figure 3.11 b) is very difficult to design. The shear field analogy discussed previously could show that such force transfer does not occur in LTF diaphragms.

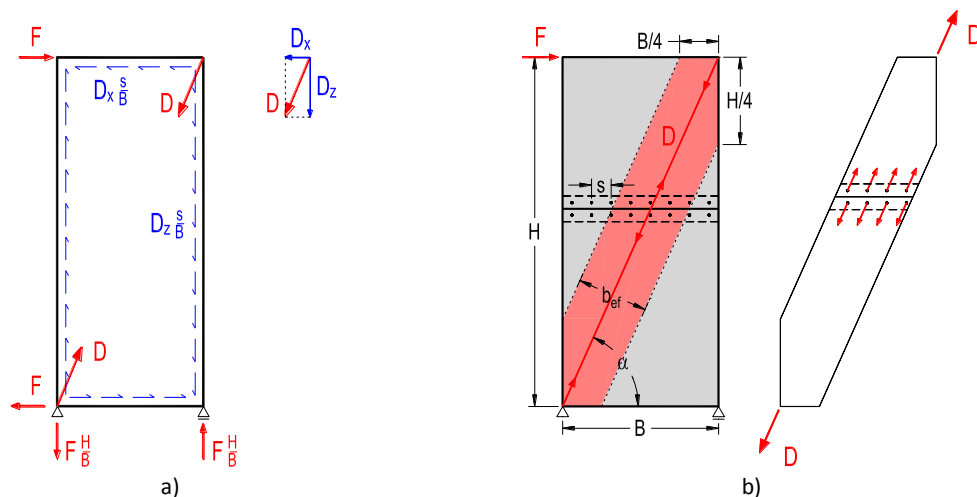


Figure 3.11 Basic truss model for walls according to DIN 1052:1988 (DIN 1988) (modified from Kessel and Schönhoff (2001))

By using the same basic assumptions as for the shear field analogy, Kamiya (1990) derived the stiffness of an equivalent diagonal to reproduce the membrane effect of LTF walls. This idea

was then later further elaborated and explained by Kessel et al. (2001). In this analogy the stiffness of the equivalent diagonal represents both the sheathing panel stiffness and the fastener stiffness and can therefore represent the actual stiffness of the diaphragm. The comparison of the deflections of a tested LTF diaphragm with the truss analysis can be found in Kamiya and Itani (1998), where an error of 28% was observed.

The derivation of the equivalent truss model for LTF diaphragms with its refinement and adaptation for massive timber diaphragms can be found in Chapter 7.

3.3.4.3 Limitations of the truss analogy

The truss analogy can be seen as a compromise between a simple approach like the girder analogy and a sophisticated finite element analysis. It allows for irregular geometries and provides a clear force path through all involved members. For complex geometries a refined mesh might be necessary, resulting in a number of different diagonals. Because the forces are introduced as concentrated loads in the nodes, some calculated results (like the axial force in framing members) require some post-processing in order to account for the real force distribution along the members' length.

For timber diaphragms the diagonal stiffness depends on fastener stiffness and spacing. These values need to be iterated on an initial assumption. To obtain shear stresses and axial forces in framing members, some additional calculations are necessary.

3.3.5 Finite element modelling

Finite element analysis is arguably the most accurate way to analyse diaphragms, since it allows for the continuous nature of the element. The load paths including tension, compression and shear stresses can be accurately predicted as well as the diaphragm deflections.

3.3.5.1 Finite element modelling for concrete diaphragms

For simplified analyses, a concrete floor can be modelled as a linear elastic and isotropic shell element, meshed in smaller elements to guarantee accurate details. Principal stresses can be obtained and maximum compression stresses can be verified against code values. Reinforcement needs to be provided to account for tension forces. Since floor diaphragms should be designed to remain elastic, this approach often provides satisfactory results for simple designs. It has to be noted that displacement incompatibilities from the ductile

behaviour of the lateral load resisting system and load redistribution because of cracking around floor openings cannot be accounted for in this simple approach.

For a more comprehensive approach, both concrete and reinforcing steel need to be modelled with their relative constitutive laws, so to account for concrete cracking, tension stiffening, non-linear response of concrete in compression and non-linear behaviour of the reinforcement including strain hardening. This can result in a complex model if pre-defined reinforced concrete elements are not provided in the analysis software.

3.3.5.2 Finite element modelling for timber diaphragms

To describe the behaviour of timber framed structural elements loaded in-plane, finite element analysis can provide a very powerful tool. Stresses in the sheathing panels and in the framing members, as well as forces in the connections and the deformation of all involved elements can be determined under monotonic and cyclic loading. However the accuracy of the results is in proportion to the model complexity, which again is in proportion to the knowledge and time required in setting up the model and post-processing the results.

Pioneering work in the use of computer analysis for panelised structures can be accredited to Foschi (1977) and Falk and Itani (1989). A series of stand-alone analysis programs or sub-routines for commercial software have been developed over time to solve timber diaphragms. A non-exhaustive list of specialized software for the analysis of LTF systems is summarized in Table 3.4.

Aside from above mentioned specialized tools, commercially available software like *SAP2000* (CSI 2004) or *Abaqus* (Dassault Systèmes HQ 2011) and research software like *OpenSEES* (McKenna et al. 2000) and *Ruaumoko* (Carr 2006) can be used to model timber framed structures. Although panel and frame elements can be modelled with membrane and beam elements respectively, fasteners are still the weak point in the model definition. Commonly each fastener is modelled with a linear or non-linear link element with stiffnesses obtained by code provisions or fitted from experimental data. Research by Judd and Fonseca (2005) and Winkel (2006) further show that uncoupled spring pairs overestimate the model stiffness. To overcome this, oriented springs which follow the orientation of the resultant force in the element should be considered, which are however not available in most software.

Table 3.4 Specialized FEM models or routines for the analysis of LTF shear walls and diaphragms

Name	Description	Author
<i>DAP-3D</i>	Diaphragm analysis program for wooden houses subjected to wind loads, later extended by including pinching effects of nails.	Foschi (1999)
<i>HYST</i>	Studies the hysteretic behaviour of connections in light-frame wood construction.	Foschi (2000), expanded by Li et al. (2012)
<i>CASHEW</i>	Cyclic analysis of shear walls.	Folz and Filiatrault (2000a)
<i>SAWS</i>	Seismic analysis of LTF structures.	Folz and Filiatrault (2000b)
<i>LightFrame3D</i>	Nonlinear finite-element model to study 3D timber light-frame buildings under static loading conditions.	He et al. (2001)
<i>FLOOR2D</i>	Analysis of light wood-frame diaphragms under static cyclic loading with smeared connections.	Li and Foschi (2004)
<i>WoodFrameMesh, WoodFrameSolver</i>	Meshes and solves wood frame structures.	Pathak (2008)
<i>M-Cashew2</i>	Extended version of <i>CASHEW</i> (Matlab routine).	Pang and Hassanzadeh (2010)
<i>SAPWood</i>	Nonlinear seismic structural analysis and loss analysis of LTF structures.	Lindt et al. (2010)

3.3.5.3 Limitations of the finite element method

Even though the finite element method is the most powerful approach in modelling diaphragms and structural elements in general, it tends to be quite time intensive. With increasing complexity of the model also the source of errors is likely to increase.

3.3.6 Synopsis of proposed diaphragm analysis methods

From the analysis methods and approaches listed above none can be categorized as wrong or correct. Designers need to decide which approach suits the given problem best and which level of accuracy is required. Because of its capabilities and still easy applicability to real structures, the truss analogy will be used for further development in this study.

Error! Reference source not found. provides a quick overview of which method can be applied to timber diaphragms and which features can be accounted for.

Because of its capabilities and easy applicability to real structures, the truss analogy will be used for further development in this study.

Table 3.5 Requirements, allowed irregularities and deformation estimation of the different methods

Analysis method	Continuous chord beams	Unsupported edges	Concentrated loads	Openings/re-entrant corners	Deformations
Deep beam/girder analogy	Required	Allowed for tabulated capacities	Not allowed	Not allowed	Not determined
Shear field analogy	Required	Allowed under certain circumstances	Not allowed	Allowed	Not determined
Truss analogy	Required	Allowed under certain circumstances	Allowed	Allowed	Determined
Finite element analysis	Not required	Allowed	Allowed	Allowed	Determined

3.4 DETERMINATION OF DIAPHRAGM COMPONENTS CAPACITY

Once the diaphragm force demand, in form of floor forces including overstrength and higher mode amplifications (see Chapter 5), is determined and the resulting load path in the diaphragm is analysed by one of the methods discussed above, the capacities of the individual diaphragm components need to be verified. The first two steps can be achieved with a number of different available approaches, but capacity checks are normally well defined in design codes.

The following sections summarize the required verifications of the individual diaphragm components, specific design equations and factors involved should be taken from the relevant design codes.

3.4.1 Component capacity in LTF timber diaphragms

All diaphragm elements like sheathing panels, fasteners, frame elements, chord/collector/strut beams need to be verified, together with the connection of the collector beam to the lateral load resisting system. The latter must also allow for displacement incompatibilities between the lateral load resisting system and the floor (see Chapters 8 and 9 for frame and wall structure respectively).

3.4.1.1 Sheathing panels, panel connections and framing elements

Sheathing panels need to resist the unit shear force in the diaphragm, which is a function of the panel thickness and the shear strength. Even though the panel is continuously fixed to

framing members, panel shear buckling should also be considered. From all codes listed in the previous sections, panel buckling is only considered in the German National Appendix to Eurocode 5 (Eurocode 5 DIN NA 2010), with its derivation found in Blaß et al. (2004). North American codes provide tabulated values derived from experimental testing, and therefore implicitly account for eventual buckling failures for the given geometries.

The panel connection needs to be checked for the fastener capacity and spacing. For load components perpendicular to the panel edge, not only the resultant force needs to be verified against the fastener capacity, but also the minimum distance to the loaded edge force needs to be respected.

Frame elements normally do not need to be verified, since their axial load is generally relatively small. In cases where large concentrated forces are introduced into the diaphragm by framing elements (for example large wind loads from the façade), compression or tension checks might be required. Buckling can normally be ignored since lateral displacements are prevented by the sheathing panels.

The German National Appendix to Eurocode 5 provides the most comprehensive guidance for the design of panelised systems. Reduction factors account for the eccentricities between the centre of the framing elements and the mid-height of the panels, as well as for concentrated forces applied perpendicularly to framing elements. Another reduction factor is provided for unblocked diaphragms to consider the additional fastener demand and increased flexibility. It also provides a number of prescriptive rules in order to prevent lateral buckling of framing elements for both single and double sheathed diaphragm assemblies.

3.4.1.2 Chord and collectors beams

Tension and compression forces in chord beams need to be verified in accordance with code equations. Similar to the frame elements, compression chords are normally not subjected to buckling, since the diaphragm is restraining any lateral displacements. For chord splices a conservative design should be adopted, since a loss in chord capacity could compromise the whole building's behaviour. Flexible splices can also significantly increase the diaphragm deflection and should therefore be avoided. Blaß et al. (2004) suggest designing the splice for a chord force equal to 1.5 times the actual demand.

Collector and strut beams collect all shear forces and transfer them either to the lateral load resisting system or re-distribute them into other parts of the diaphragm. As such they carry tension and compression forces and need to be designed accordingly.

The load demand from both gravity and horizontal forces must be used with the appropriate load combination in order to verify any beam element.

3.4.1.3 Connection of the diaphragm to the LLRS

Forces from the collector beams need to be introduced by appropriate connection details into the lateral load resisting system. These details obviously depend on the material and the structural system adopted. In addition to the horizontal force transfer, also possible displacement incompatibilities (frame beam elongation, wall uplift and rotation etc.) must be considered in the design as will be discussed in Chapters 8 and 9.

3.4.1.4 Dependency of the design capacity and the load direction

It is common practice to consider horizontal loads along the two principal directions of the building. For certain analysis methods or expected structural ductility levels, some codes require the application of a full load in one direction together with 30% of the load in the orthogonal direction (Eurocode 8 2004; Standards New Zealand 2004; Consiglio Superiore dei Lavori Pubblici 2008). Considering also the reversal action of wind and seismic loads, as well as the natural and accidental torsional eccentricities of structures, a number of load combinations need to be considered when designing the lateral load resisting system.

Panels and panel fasteners must be designed for the maximum unit shear force from all combinations. Depending on the loading direction considered, the functions of chord and collector beams are interchanged. For load applications in an arbitrary direction, boundary beams need to resist both chord or collector actions.

3.4.2 Component capacity in massive timber diaphragms

The same design verifications as for LTF diaphragms need to be carried out for massive timber diaphragms with some additional considerations. Panel shear buckling can normally be ignored because of the increased panel thickness. Because of the missing framing elements, longitudinal forces are carried only by the massive timber panels and their connections. Axial buckling should therefore be checked.

Because of the presence of both shear forces and axial forces, massive timber panels should be verified for this combined load. As an example, the Norris criterion can be used as it allows for the verification of a generic stress state in a timber element (Thelandersson and Larsen 2003). Stress levels are normally relatively small, making such verifications redundant. Brittle failures in tension perpendicular to the grain must be avoided independently from the approach taken. Connectors must be designed for the forces parallel and perpendicular to the panel edges and increased minimum distances to the loaded edge must be respected.

3.4.3 Timber-concrete-composite (TCC) and concrete diaphragms

The design of the individual components of concrete slab diaphragms is strongly influenced by the structural system considered. Chord and collector beams can be made of timber elements connected to the concrete slab or can be integrated in the concrete slab itself. Depending on the solution adopted, the beams should be verified following the relevant material code. The concrete slab must be designed to carry the unit shear forces (deep beam analogy) or the tension and compression forces in the ties and struts respectively (strut-and-tie-method). If latter method is used, nodal zones need to be designed carefully, with special attention to reinforcement anchoring.

3.5 DISCUSSION

Considering the limited amount of information available, the summary of code provisions, analysis methods and design verifications given in this chapter aims to provide a comprehensive status-quo of the design of timber diaphragms. Not only does it provide a general overview on the current possibilities in the design of diaphragms, but it also highlights gaps or possible revivals of less known approaches.

International design codes and guidelines are becoming more sophisticated and detailed, with timber standards following this trend. The review carried out in this chapter however highlights a mayor gap regarding the seismic design of timber buildings. It was found that the general knowledge on diaphragm analysis methods is often limited to either very basic hand calculations or very sophisticated finite element analysis. The most common analysis method for the design of timber diaphragms is found in the girder analogy. The approach provides reasonable estimates regarding forces in chord beams and panel elements, but it is mostly limited to regular diaphragms. Although simple methods exist to account for openings or other

irregularities, these methods soon reach their limits because of time consuming and complex calculations. The strut-and-tie method, which is gaining more popularity in the design of concrete diaphragms, has not yet found its counterpart for timber diaphragms. More general truss methods, available for both concrete and timber diaphragms, provide a simple yet exhaustive approach in determining both loads and deflections in diaphragms. Given its potential, a truss analogy for timber diaphragms will be further studied and extended for massive timber panels in Chapter 7. The use of finite elements for the analysis of timber diaphragms provides the most sophisticated approach in analysing diaphragms, providing the greatest detail. Because of its complexity it is however not suitable for every-day use in design offices. For this research it will be used in several occasions to proof certain assumptions and to verify the accuracy of the truss analogy.

The review also revealed that only regular diaphragms build with sheathed panels on framing elements are regulated. No guidance is provided on massive timber panels, which are currently revolutionizing the design of multi-storey timber buildings. Openings and other floor irregularities are either allowed with very restrictive dimensional limitations, or not mentioned at all. Deflection and stiffness considerations are only covered in a limited number of codes and definitions for flexible diaphragms vary notably. Diaphragms are generally required to work in the elastic range, but capacity design principles to achieve this are very limited, with overstrength values left to the designer's judgement. The definition of these overstrength factors is furthermore not unique; it is therefore recommended to define a common approach for future code revisions.

The design of the single diaphragm components normally does not require any special provisions, since all elements can be verified with common codified rules for axial, compression and shear strength. Effects like panel shear buckling, frame buckling, additional demand from eccentricities however are normally not considered except for a very limited number of standards or experimentally determined capacities.

3.6 CONCLUSIONS

To promote and assure proper diaphragm design in timber buildings, it is recommended that more sophisticated analysis and design methods such as the truss analogy are used for the analysis and design of complex and irregular diaphragms. More guidance for the analysis and design of massive timber panels is needed. Capacity design principles and especially

overstrength factors for commonly used connections and lateral load resisting systems need to be provided to designers.

4 The influence of diaphragm stiffness on the dynamic behaviour of multi-storey timber buildings

4.1 INTRODUCTION

In order to study the influence of diaphragm stiffness in multi-storey timber structures, a parametric analysis on 6 frame and 6 wall structures has been carried out in this chapter. The structures were analysed by Non Linear Time History (NLTH) analyses assuming a perfectly rigid diaphragm. Subsequently, the structures have been analysed considering the stiffness of a real timber diaphragm. Finally, a flexible diaphragm has also been considered as the opposite extreme case to the rigid diaphragm. Key parameters like fundamental period, storey shear, storey moment, interstorey drift and floor accelerations are compared in order to discuss the influence of diaphragm stiffness. In Chapter 5 the outcomes are used in order to estimate the diaphragm demand.

4.1.1 Background

Considerable research has recently been carried out on the seismic behaviour of timber buildings under horizontal loading including traditional (James 1984; Deam 1996; CUREE 2000; Christovasilis et al. 2007; Pang and Rosowsky 2007; Källsner and Girhammar 2009; Fragiaco et al. 2010; van de Lindt et al. 2010) and innovative timber structures (Palermo et al. 2005a; Ceccotti et al. 2006; Newcombe 2011; Sustersic and Dujic 2011; Fragiaco et al. 2012; Schick et al. 2013; Wrzesniak et al. 2013; Loo et al. 2014; Jamil et al. 2015). Most work however only focusses on the behaviour of an isolated lateral load resisting system, assuming a perfect force introduction through a rigid diaphragm. Timber diaphragms tend to be more flexible than concrete diaphragms, and this flexibility has the potential to alter the dynamic behaviour of a structure as well as the force distribution into the lateral load resisting system. This chapter studies the effect of the diaphragm flexibility on multi-storey post-tensioned timber Pres-Lam frame and wall structures. Based on the PRESSS technology (PREcast Seismic Structural System), developed at the University of California at San Diego (Priestley et al. 1999), Pres-Lam structures are made of engineered timber walls, beams and columns connected to each other by post-tensioning strands, cables or bars (Palermo et al. 2005; STIC 2013). In case of large seismic events, these structures will rock and lead to geometric gap opening at the wall-

foundation or beam-column interfaces. This is accompanied by elastic elongation of the post-tensioning elements which re-centre the structure to its original position, leaving the structure undamaged. Sacrificial mild steel dissipation devices can be placed in correspondence of the gapping elements to achieve hysteretic dissipation. Since the force-displacement hysteretic behaviour of Pres-Lam structures is very similar to other modern timber frame and wall structures and timber structures are normally deflection governed, the general findings and trends can be extended to timber frame and wall structures in general.

Current design codes and literature provide a number of methods to analyse structures under seismic actions. These methods allow for the determination of forces acting on the lateral load resisting systems such as the walls, frames or other bracing elements. For structures where higher mode effects are expected to be significant, simpler methods like the equivalent static analysis are either not allowed (Eurocode 8 2004) or allowed with a slight increase in the top storey shear force (Standards New Zealand 2004). The New Zealand Concrete Standard NZS 3101 (Standards New Zealand 2006) provides dynamic amplification factors to account specifically for such effects if only an equivalent static analysis is carried out. Alternatively, higher mode effects can be accounted for with more complex analysis methods like time history analysis and, to a certain extent, with modal spectrum analysis. Little attention is, however, given in design codes to the influence of diaphragm flexibility, which has the potential to alter mode shapes in buildings. The New Zealand Loading Standard for Earthquake Action NZS 1170.5 (Standards New Zealand 2004) requires that flexible diaphragms are modelled as such, leaving it to the designer's judgement of which method to apply.

4.2 REVIEW OF AVAILABLE RESEARCH REGARDING THE INFLUENCE OF DIAPHRAGM STIFFNESS ON THE BEHAVIOUR OF BUILDINGS

Several researchers investigated the influence of diaphragm stiffness on the global dynamic behaviour of structures. In most cases parametric analysis with varying diaphragm stiffness, number of storeys and different lateral load resisting systems were carried out. Almost all available research is based on concrete and steel structures, providing little information regarding the behaviour of timber structures. Since timber has a lower modulus of elasticity and timber diaphragms tend to be more flexible than concrete diaphragms, the influence of higher mode effects is expected to be of more concern than in other type of structures.

4.2.1 Literature review

Jain and Jennings (1985) developed an analytical model to determine the fundamental period and base shear for one and two storey structures with flexible diaphragms spanning between end walls. The outcome of the analysis clearly showed that the flexible diaphragm influences the dynamic behaviour of the structure which is dominated by the first mode of vibration of the diaphragm. Higher diaphragm modes did not influence the base shear of structures.

Kunnath et al. (1991) studied reinforced concrete buildings with dual lateral load resisting systems with perimeter walls and internal frames. The key finding was that diaphragm deformations, especially in the inelastic range, increased the strength demand and ductility demand of internal frames. This can be mainly attributed to the fact that the frame's tributary area increased with diaphragm flexibility. Diaphragm flexibility further increased both the structure's fundamental period and floor displacements.

Saffarini and Qudaimat (1992) studied 37 reinforced concrete buildings in order to evaluate the error in assuming rigid diaphragms, by varying the number of stories, the storey height, the slab type and the size and spacing of columns or shear walls. The study focuses mostly on the distribution of the shear forces into the lateral load resisting system consisting of either walls, frames or a combination of these. With increasing diaphragm flexibility, shear forces in the internal walls increased. This is due to the fact that the force distribution becomes closer to the tributary area approach rather than being proportional to the wall stiffness. For higher structures or for slender walls this effect decreased, showing that not the absolute diaphragm flexibility, but rather the ratio between the flexibilities of the lateral load resisting system and the diaphragm should be considered. For frame buildings, which tend to be more flexible, the diaphragm flexibility had less influence on the dynamic behaviour of the structures. Even if not explicitly mentioned, also the magnitude of transfer forces in dual systems was considered in the study. For lower floors the shears in the frames were higher because of the displacement incompatibility with the walls, an effect which decreased with flexible diaphragms. Finally it was also observed that for all cases the structures' displacements increased in presence of flexible diaphragms.

Moon and Lee (1994) stated that floor flexibility alters the seismic response of the building in the case of high floor aspect ratios and a low number of storeys. It was shown that especially for low rise buildings diaphragm flexibility causes the elongation of the fundamental period

and a change in the mode shapes. It was shown that high diaphragm flexibility decreased the base shear in structures, but the force distribution in internal bracing elements increased.

Tremblay and Stiemer (1996) studied the dynamic behaviour of one storey steel structures with flexible diaphragms. The diaphragms were designed based on a capacity design approach and therefore worked in the elastic range; all inelastic behaviour was concentrated in the lateral load resisting system. The authors therefore suggested that only the displacements of the vertical bracing elements need to be amplified because of inelasticity. It was recommended that the in-plane forces and deformation of the diaphragms as obtained from a static analysis need to be modified to account for the dynamic effects. An amplification factor was proposed in order to amplify the diaphragm in-plane moments and displacements. The fundamental period of the structure was underestimated when compared with code values; this, however, normally leads to conservative base shear forces and is therefore not of big concern.

Based on three case studies, Tena-Colunga and Abrams (1996) compared the results of analytical studies with measured values from reference buildings exposed to the 1989 *Loma Prieta Earthquake*. With increasing diaphragm flexibility, the floor accelerations and the fundamental period increased, whereas forces due to torsional effects of the building decreased. The authors came to the conclusion that since diaphragm and shear wall accelerations can increase in the presence of flexible diaphragms, designs based on a rigid diaphragm assumption can be non-conservative.

Ju and Lin (1999) concluded in their study based on the response spectrum analysis of regular and irregular buildings, that the floor flexibility can be neglected even for irregular shaped floor geometries, in the case of frame structures. This confirms the findings of Saffarini and Qudaimat (1992) as mentioned above. For wall structures, however, they recommended that the floor flexibility be considered, since the moments due to ground acceleration differed substantially from the values obtained with a rigid diaphragm assumption. This was explained by the fact that the diaphragm flexibility is much higher than the flexibility of the walls. In such cases a number of low modes have been found, all with nearly identical frequencies corresponding to the vibration of the diaphragms at different levels.

Fleischman and Farrow (2001) studied the dynamic behaviour of 3 and 6 storey structures with diaphragms with high aspect ratios and perimeter walls. A critical diaphragm flexibility ratio was defined, above which the masses of the diaphragm and the lateral load resisting system

act independently. Flexible diaphragms designed on a storey by storey basis with strength demands from an equivalent static analysis vibrated out of phase to the structure, inducing large drifts in in the mid and upper storeys. Elastic structures with diaphragms designed uniformly for the highest force demand had reduced interstorey drifts. Increased force demand for elastic structures and increased deformations were observed for ductile structures at lower levels.

Lee et al. (2007) investigated the effect of floor flexibility on 3 and 6 storey structures with end walls by means of a NLTH analysis. It was stated that because of closely spaced diaphragm modes, the estimation of peak response with the root of the sum of squares from modal spectrum analyses is not accurate in the presence of flexible diaphragms. By using an equivalent static analysis, the higher mode contributions to interstorey drifts in structures with flexible diaphragms also cannot be accounted for. It was shown that this shortcoming may lead to the design of diaphragms with inadequate low stiffness at lower levels. For structures with equal diaphragm properties along the height of the structure, the interstorey drift at lower floors increased with increasing diaphragm flexibility. This was explained by the presence of higher mode contributions in structures with a higher number of flexible diaphragms. A simple method based on a lumped mass model was presented in order to predict inter-storey drifts in wall structures.

Sadashiva et al. (2012) used elastic and inelastic time history analysis on a set of different buildings with a range of different diaphragm stiffnesses. General findings were that the fundamental natural period of structures with flexible diaphragms was always greater than those with rigid diaphragms. For elastic structures, the presence of flexible diaphragms decreased the storey forces but increased the displacements. Such effects were shown to be biggest for one storey structures and reduced with increasing structure height. Equations to estimate the fundamental period and displacement of structures with flexible diaphragms were proposed.

Humar and Popovski (2013) studied the elastic and inelastic behaviour of one-storey structures. The diaphragms were supposed to work only in the elastic range, concentrating the non-linear behaviour of the structure in the lateral load resisting system. In the presence of flexible diaphragms the fundamental period of the structure increased notably. It was also shown that the forces acting on the diaphragm were not distributed uniformly, with higher forces at the mid-span of the diaphragm. Furthermore also the displacement of the lateral load

resisting system increased, therefore increasing also its ductility demand. A simple expression to obtain the appropriate force reduction factor in order to determine the appropriate ductility demand was proposed.

van Beerschoten and Newcombe (2010) studied the influence of diaphragm flexibility in a multi-storey Pres-Lam frame case study building. Because of the typically very flexible lateral load resisting system, it was concluded that diaphragm flexibility does not affect the dynamic behaviour of frame structures. It was however recommended to account for in-plane floor flexibilities in wall structures.

4.2.2 Conclusions from the literature review

From the literature review it can be concluded that the presence of flexible diaphragms changes the dynamic behaviour of concrete and steel structures. Such effects were more pronounced in structures with a low number of storeys, and in wall structures. Flexible diaphragms increased the structure's fundamental period, and resulted in higher displacement demands. The force distribution from the diaphragm into the lateral load resisting system was also influenced by the diaphragm stiffness; confirming the tributary area approach for flexible diaphragms.

Little information on the effect of diaphragm flexibility in timber structures is available; this chapter investigates such effects on a number of timber frame and wall structures.

4.3 GENERAL INFORMATION ON THE PARAMETRIC ANALYSIS

A total of 6 post-tensioned timber frame and 6 post-tensioned timber wall structures with varying number of storeys have been considered in a parametric analysis. The structures have been first analysed with rigid diaphragms to provide benchmark values. Successively the structures were analysed considering semi-rigid and flexible diaphragms respectively. This resulted in 18 frame and 18 wall structures total.

The design of these structures has been carried out independently from the diaphragm stiffness based on the Displacement Based Design (DBD) approach (Priestley et al. 2007) and the STIC Design Guideline for Post-Tensioned Timber Buildings (STIC 2013) as summarized in Figure 4.1.

The sample structures have been modelled and analysed in OpenSEES (McKenna et al. 2000) with a non-linear time history analysis and a set of 10 earthquake records. The records have been selected and scaled in order to fit the design spectrum in accordance with the New Zealand Earthquake Actions Standards NZS 1170.5 (Standards New Zealand 2004). The averages of the maximum values from the single earthquake records have been used for the discussion on the effects of diaphragm stiffness on post-tensioned timber structures.

Whereas this study is carried out on a set of post-tensioned timber frame and wall structures, the general trend regarding the influence of diaphragm flexibility is deemed to be extendible to modern timber frame and wall structures in general.

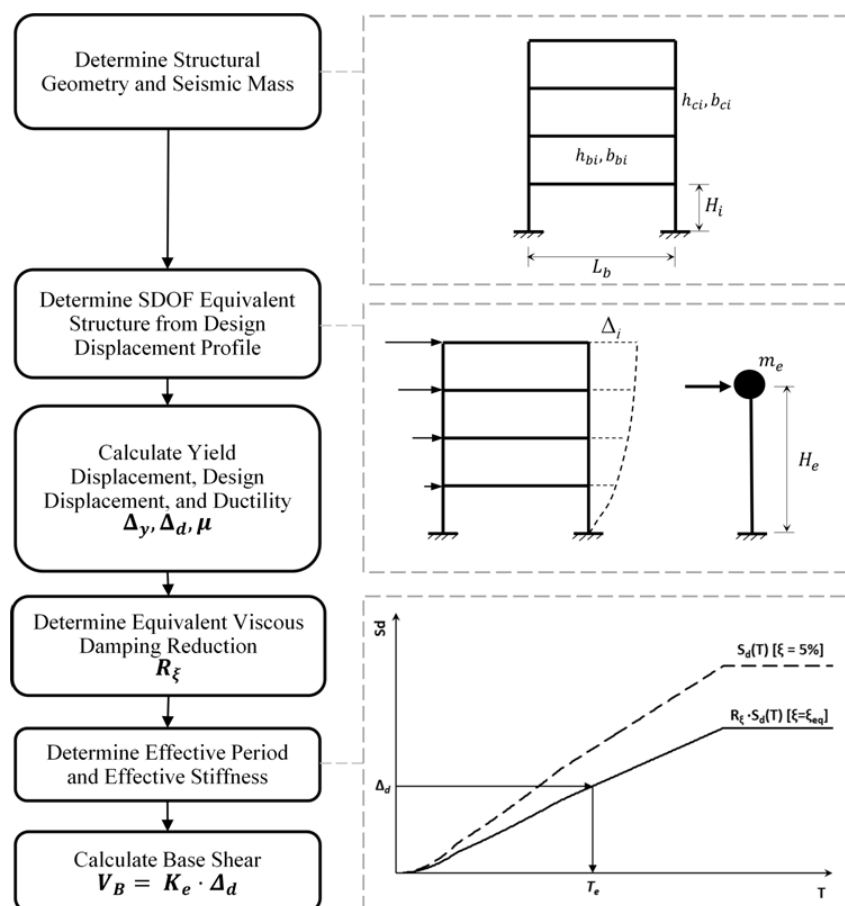


Figure 4.1 Principles and steps involved in the Direct Displacement Based Design of structures (STIC (2013), modified from Priestley et al. (2007))

4.3.1 Design of sample diaphragms for the parametric study

The floor layout in Figure 4.2 has been used for all parametric studies. For the frame structures, five identical post-tensioned frames resisted both the gravity and lateral loads. For the wall structures, the internal frames were considered to resist only gravity loads and the two shear walls positioned at the East and West edges resisted all the seismic loads.

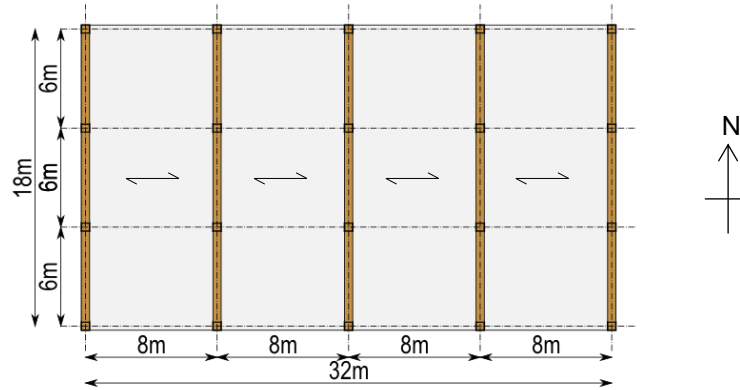


Figure 4.2 Sample building plan view

The floor was assumed to be made out of 100 mm thick Cross Laminated Timber (CLT) panels spanning 8 m between the frames. CLT panel dimensions were 1.2 m x 8 m with a shear modulus of 600 MPa. Two chord beams were placed along the building length having a cross section of 200 mm x 400 mm and a modulus of elasticity of 11 GPa.

The panels were connected to each other with screws over on a lap joint as shown in Figure 4.3. Each connector had a capacity of 4.5 kN and a slip modulus of 3,000 kN/m.

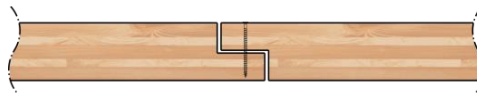


Figure 4.3 Cross section of the CLT floor with the lap joint and screw connection

For the wall structures the diaphragms were fixed to gravity beams, acting as collector beams. The connection between the wall and these collector beams introduced an additional source of flexibility to the diaphragm. Bolted connections with diameter 16 fasteners with a capacity of 15 kN and a slip modulus of 7800 kN/m were assumed.

A separate diaphragm design was carried out for each of the 12 buildings (6 frame and 6 wall structures). The design was carried out according to the following steps:

- Determination of the storey shears following the DBD approach;
- Amplification of the top storey shear force with an assumed diaphragm dynamic amplification factor;
- Design of the diaphragms by selecting an appropriate fastener spacing;
- Determination of the diaphragm stiffness to be used in the parametric analysis.

The determination of floor forces for the design of the diaphragms and the therefore required number of fasteners was based on the top storey amplified shear values as per Priestley et al. (2007). More information on the determination of diaphragm forces can be found in Chapter

5. For the *frame structures* the provided amplification for the column shears at the top of the structure V_N has been used to determine the force in the diaphragms. For the *wall structures* the top storey amplified shear force V_n^o (see equation (5.17) in Chapter 5) has been considered as the maximum diaphragm force.

In this study, the dynamic amplification factor ω_D is taken as the ratio between the maximum force acting on the lateral load resisting system obtained from the design procedure (from the DBD analysis in this case) and the diaphragm force

$$\omega_D = \frac{F_{diap}}{F_{LLRS}} \quad (4.1)$$

where

- ω_D is the diaphragm dynamic amplification factor.
- F_{diap} is the peak force in diaphragm;
- F_{LLRS} is the top storey force in the lateral load resisting system.

Since the numerical model has been based on the exact moment-curvature behaviour of the frames and walls, no source of overstrength other than the material safety factor $\phi = 0.9$ and dimension rounding is present. To estimate the diaphragm demand, an overstrength of $\phi^o = 1.2$ has therefore been applied.

For the different diaphragm designs for the sample structures, only the panel fastener spacing and the number of bolts for the wall-beam connection had to be determined to achieve the required diaphragm capacity. This was based on the assumption that the panel shear capacity and the tension/compression capacities of the chord beams were always larger than the imposed demand.

4.3.2 Diaphragm stiffness

The flexible behaviour of the diaphragms, including their connection to the lateral load resisting system, can be idealized as a single degree of freedom oscillator with an equivalent stiffness as shown in Figure 4.4. This SDOF system can then be added at each floor level of a structure to simulate the flexible diaphragms.

This method has been shown to provide sufficient accuracy to model diaphragms in multi-storey structures (Lee et al. 2007; Brignola et al. 2008). The connection to the lateral load resisting system can be considered as two springs K_C in parallel. The total stiffness $K_{eq,c+d}$ can be found by combining the stiffness of the lateral load resisting system with the diaphragm

stiffness $K_{eq,d}$ in series. The obtained diaphragm stiffnesses for the frame and wall structures are provided in sections 4.4.3 and 4.5.3, respectively.

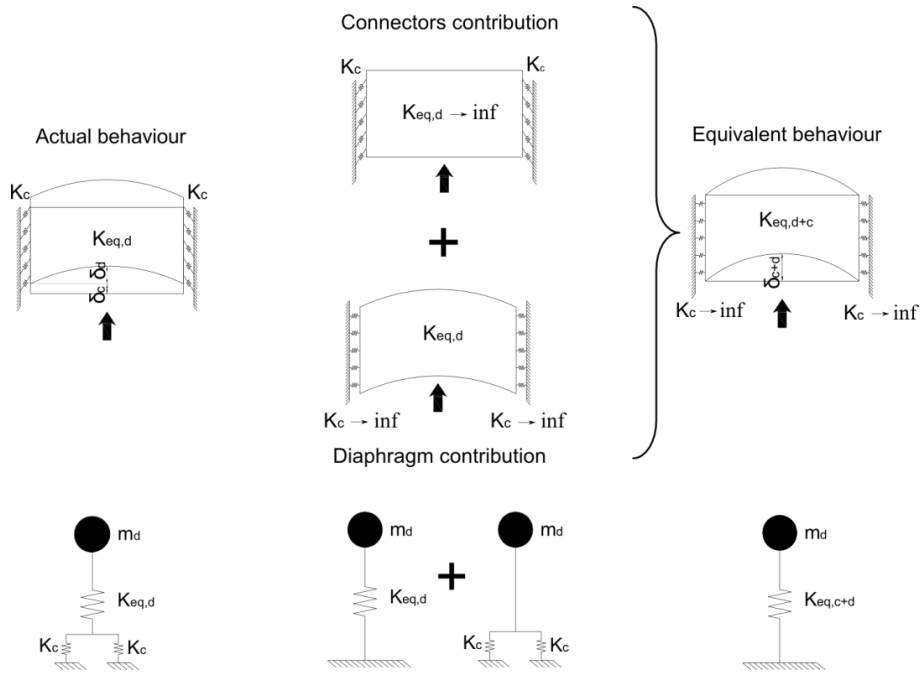


Figure 4.4 Schematic contributions of connectors and diaphragm stiffness to the overall stiffness (Brignola et al. 2008)

The diaphragm stiffness $K_{eq,d}$ was evaluated with the diaphragm deflection equation presented in Chapter 6. The equation considers diaphragm deformation due to chord deformation, shear deformation of the panels and fastener slip. To obtain the diaphragm stiffness, the applied diaphragm force was divided by the relative diaphragm deflection at mid-span. The diaphragm, connection and total system stiffnesses were evaluated with the following equations

$$K_{eq,d} = K_{diap} = \frac{F_{diap}}{u_{diap}}; \quad (4.2)$$

$$K_{eq,c} = K_{con} = \frac{V_{diap}}{u_{con}} = \frac{F_{diap}}{2 u_{con}}; \quad (4.3)$$

$$K_{eq} = K_{eq,d+c} = \left(\frac{1}{K_{diap}} + \frac{1}{K_{con}} \right)^{-1}; \quad (4.4)$$

where

- K_{diap} diaphragm stiffness;
- K_{con} connection stiffness;
- K_{eq} diaphragm and connection stiffness (total stiffness);
- F_{diap} force applied to the diaphragm;
- V_{diap} maximum diaphragm shear;
- u_{diap} diaphragm deflection at mid-span;
- u_{con} beam-wall connection slip.

The fundamental period of the diaphragm can be estimated as

$$T_{diap} = 2\pi \sqrt{\frac{M}{K_{eq}}}; \quad (4.5)$$

where

- T_{diap} fundamental period of vibration of the diaphragm [seconds];
- M mass applied on the diaphragm [kg];
- K_{eq} diaphragm and connection stiffness [N/m].

An Equivalent Truss Model of the diaphragm as presented in Chapter 7 has also been analysed by a modal analysis in SAP2000 (CSI 2004) as shown in Figure 4.5. The chord and collector beam properties were assigned with their real values and the beam-to-wall connection stiffness was assigned with two linear springs. For the diaphragm of sample structure W-6-70 as defined later, the modal analysis provided a first fundamental period of 0.41 seconds. This values matches exactly the period calculated with the single degree of freedom model as shown in Table 4.8. Based on this result and based on the findings of Spooner (2008) and van Beerschoten and Newcombe (2010), the flexible diaphragm was modelled as an equivalent single degree of freedom substructure attached to the lateral load resisting system of the building.

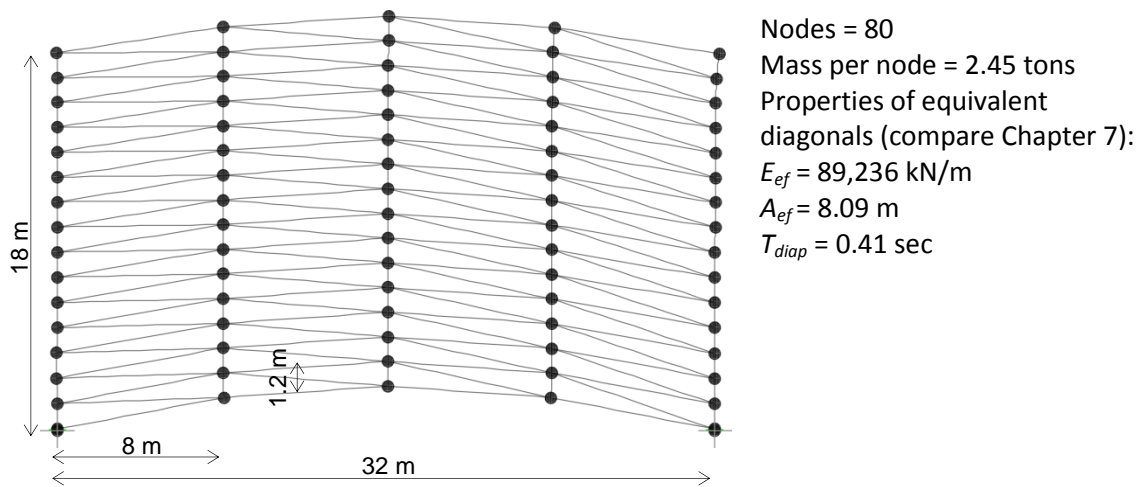


Figure 4.5 Modal analysis on the semi-rigid diaphragm of wall structure W-6-70 with SAP2000

To evaluate the sensitivity of the diaphragm stiffness in regards to the panel orientation, a second floor layout with panels spanning 6 m between additional secondary beams running between the frames was evaluated as well. The difference in diaphragm stiffness was less than 5% and therefore only the first floor layout was considered in the parametric analysis.

4.3.3 Earthquake selection

The selection of the earthquake records for the NLTH analysis was based on the New Zealand Earthquake Actions Standards NZS 1170.5 (Standards New Zealand 2004), assuming the following parameters:

- Importance level: IL2;
- Return period factor: $R = 1.0$ (500 years return period);
- Location: Wellington;
- Hazard factor: $Z = 0.4$;
- Soil type C;
- Near-fault factor: $D = 1$;
- Structural performance factor $S_p = 0.7$.

10 strong motion records as summarized in Table 4.1 obtained from the Pacific Earthquake Engineering Research Center (PEER) Next-Generation Attenuation (NGA) database (Chiou et al. 2008) have been selected. The records were scaled in accordance with NZS 1170.5 to match the design spectrum. The procedure requires the scaling of each record to fit the design spectra on a defined period interval around the structure's fundamental period. Therefore the 10 records were scaled for each of the 18 structures with the relative diaphragm configuration considered.

Table 4.1. Information regarding the 10 input earthquakes

ID	Location	Station	Year	M_w	PGA [g]	Epicentral distance [km]
NGA0183	Imperial Valley-06	El Centro Array #8	1979	6.53	0.54	28
NGA0292	Irpinia, Italy-01	Sturno	1980	6.90	0.29	30
NGA0725	Superstition Hills-02	Poe Road (temp)	1987	6.54	0.36	11
NGA0767	Loma Prieta	Gilroy Array #3	1989	6.93	0.46	31
NGA0995	Northridge-01	LA - Hollywood Stor FF	1994	6.69	0.34	24
NGA1012	Northridge-01	LA 00	1994	6.69	0.32	14
NGA1081	Northridge-01	Stone Canyon	1994	6.69	0.34	14
NGA1107	Kobe, Japan	Kakogawa	1995	6.90	0.27	24
NGA1487	Chi-Chi, Taiwan	TCU047	1999	7.62	0.36	86
NGA1512	Chi-Chi, Taiwan	TCU078	1999	7.62	0.39	5

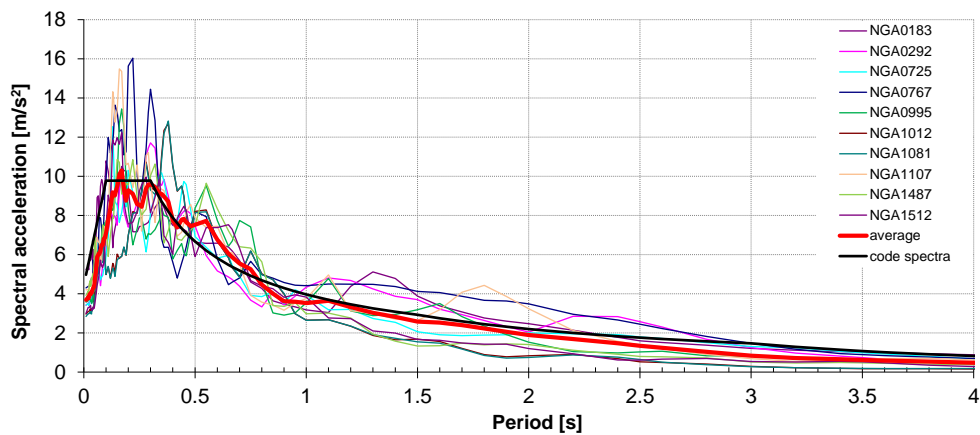


Figure 4.6 Code spectra and selected earthquake input for testing

4.4 PARAMETRIC ANALYSIS ON THE DYNAMIC PERFORMANCE OF POST-TENSIONED TIMBER FRAMES

4.4.1 Numerical model for the frame structures

Six benchmark post-tensioned Pres-Lam frame structures have been used in the parametric analysis. Two, four and six storey frames were designed with and without additional dissipation. The structures consisted of elastic timber beam and columns elements with concentrated ductility at the beam-column-joints and at the column base. The self-centering capability of the frame is provided by post-tensioning bars running through the box beams.

The model definition, schematically shown in Figure 4.7 has been initially developed by Smith (2014) for implementation into a Ruaumoko (Carr 2006) routine. For the analyses presented herein, the frames have been modelled in OpenSEES (McKenna et al. 2000) with a similar routine as used for the wall structures.

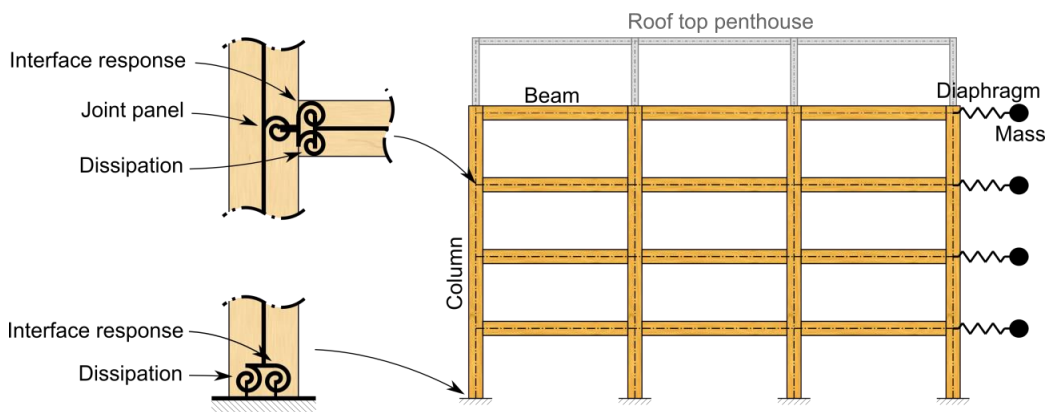


Figure 4.7 Numerical model of the frame structures for the OpenSEES analysis (the figure shows the sample structure F-4-070 with four storeys)

Because of the jointed ductile nature of post-tensioned structures with a controlled rocking mechanism, Pres-Lam frames can be successfully modelled with the use of a lumped plasticity approach (Palermo et al. 2005b; Newcombe 2011; Smith 2014). In this approach elastic beam elements are used in combination with non-linear elastic springs which simulate the gap opening at the beam-column joints. Since the Euler–Bernoulli theory is not verified at these interfaces, the Modified Monolithic Beam Analogy (MMBA) (Palermo 2004) is applied to define the rotational behaviour in timber rocking elements.

Two different approaches can be used to model post-tensioned timber elements, either an advanced multi-spring formulation (Spieth et al. 2004) or a number of parallel rotational springs. With the former also secondary effects like beam elongation and localized timber crushing can be captured, in addition the neutral axis depth and the strains and stresses in the post-tensioning and mild steel elements are provided. The simpler rotational springs only simulate the correct moment-curvature behaviour at the joint, but provide sufficiently accurate results in building deformation and force demand (Newcombe et al. 2010). The use of the rotational springs implies that the beam members are not subjected to the axial forces introduced by the post-tensioning.

For the frame analysis presented in this chapter the approach with rotational springs has been used. As shown in Figure 4.7, for each beam-column joint a linear joint-panel rotational spring, a non-linear interface rotational spring and a non-linear steel dissipation spring were used. The interface rotational spring, which considers the gap opening behaviour in presence of the post-tensioning and also includes the interface compression stiffness caused by the column compression deformation perpendicular to the grain, was modelled as a multi-linear elastic spring as shown in Figure 4.8a. The mild steel dissipaters, when present, were modelled as uniaxial elasto-plastic springs as shown in Figure 4.8b. At the column base, moment capacity is provided by steel reinforcement and gravity. The gravity forces produce a re-centering moment, the relative spring is therefore modelled similarly to the beam-column-joint, except that no interface stiffness needs to be taken into account. All springs had zero length and were placed at the beam-column or column-foundation interface.

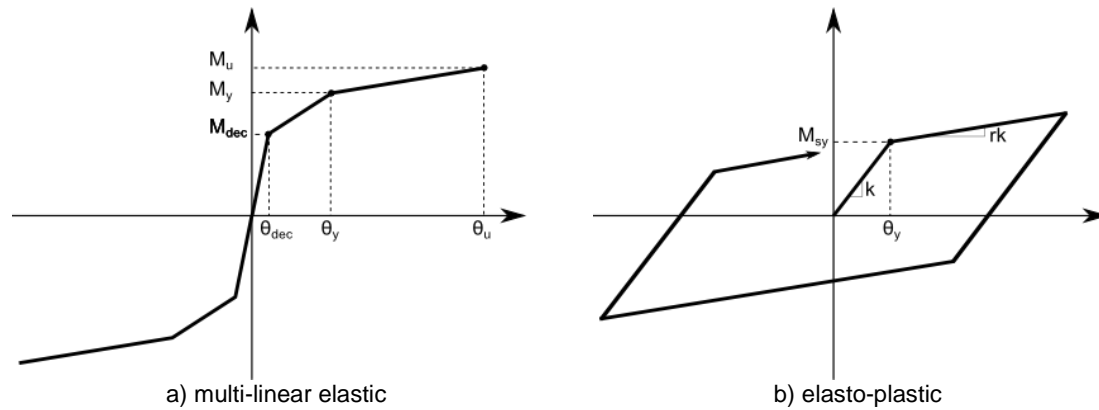


Figure 4.8 Rotational spring model calibration

Even though the beams and columns were working in the elastic range, they were modelled as non-linear beam elements in order to include shear deformations. The material properties used in the model are summarized in Table 4.2.

Table 4.2 Material properties of the frame structures

Timber		Mild steel reinforcement	
Elastic modulus parallel to grain	$E_0 = 13$ GPa	Yield stress	$f_y = 300$ MPa
Elastic modulus perpendicular to grain	$E_{90} = 660$ MPa	Post-yield stiffness	$r = 0.08$
Shear modulus	$G = 660$ MPa	Elastic modulus	$E_s = 200$ GPa
Post-tensioning bars			
Yield stress	$f_y = 835$ MPa		
Elastic modulus	$E_{pt} = 157$ GPa		
Threaded bar diameter	$D_{pt} = 26.5$ mm		
Threaded bar area	$A_{pt} = 552$ mm ²		

For the benchmark structures with rigid diaphragms, the floor masses were slaved to the storey nodes of the frames. The semi-rigid and flexible diaphragms were simulated as elastic springs at each storey with the storey mass attached to them. The diaphragm stiffness has been evaluated as shown in section 4.3 with respective values determined later in section 4.4.3.

For the OpenSEES analysis a tangent stiffness proportional Rayleigh damping model was used. The elastic damping contribution has been assumed to be 3% in accordance with research on the dynamic behaviour of post-tensioned timber frame structures (Smith 2014). The critical damping was assigned to the 1st and 3rd modes.

4.4.2 Design of the sample frame structures

Two different re-centering ratios β (defined as the ratio of the moment resistance provided by the post-tensioning to the total moment resistance, see STIC (2013)) of 1.0 (100% re-centering

contribution from the post-tensioning, 0% dissipative contribution) and 0.7 (70% re-centering contribution, 30% dissipative contribution) were used to design the frame structures. For the structures without any dissipation at the beam column-joints, the system was relying on the equivalent yielding point in the non-linear elastic behaviour provided by the change of stiffness due to gap opening. For structures with re-centering ratios β of 0.7, energy dissipation was provided by means of internal mild steel reinforcement, resulting in a flag-shaped hysteresis behaviour of the system as shown schematically in Figure 4.9.

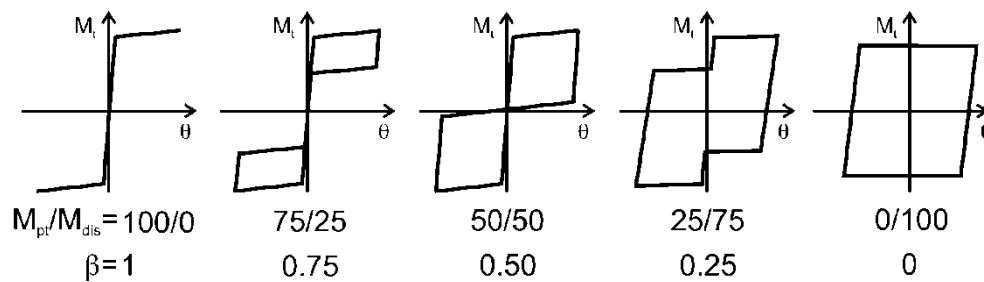


Figure 4.9 Moment response with varying levels of the re-centering parameter (STIC 2013)

The sample building as shown in Figure 4.10 had a footprint of 18 x 32 m² with an approximate floor area of 600 m² (STIC 2013). Five frames with three 6 meters bays each resisted the horizontal actions and carried the gravity loads.

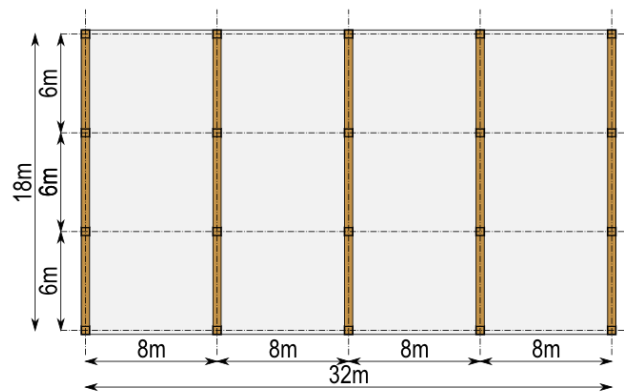


Figure 4.10 Sample building plan view with 5 seismic and gravity frames

For the analysis three different building heights as shown in Figure 4.11 were considered, all structures had a constant inter-storey height of 3.6 m. A seismic load of 4.0 kPa was considered for all floor levels, this was based on an office type loading and a timber only floor slab. The top floor consisted of a penthouse with a lightweight roof structure as shown in Figure 4.7; assuming a residential type loading and by lumping the weight of the lightweight roof structure to roof level, the seismic mass equalled the one from the lower stories. Since the floor diaphragm could be classified as rigid as discussed later, all frames were assumed to

equally resist the imposed horizontal action. The relative storey mass for each frame therefore resulted in 47 tons.

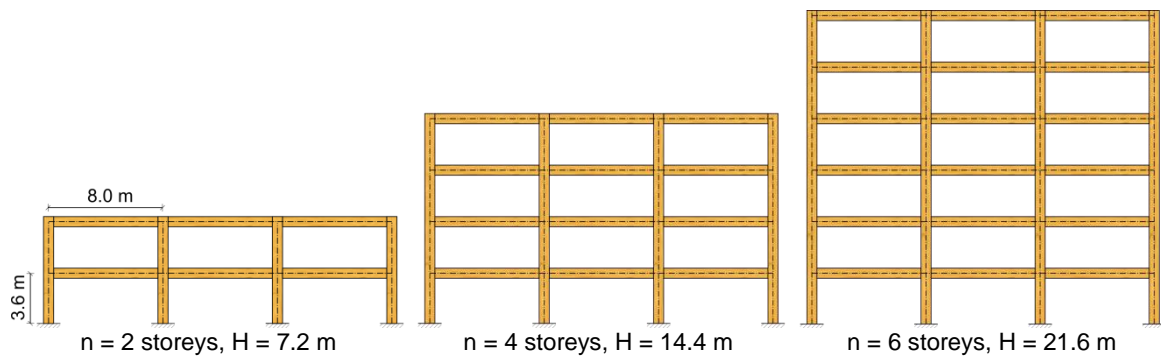


Figure 4.11 Selection of frames used for the parametric analysis

The frame structures were designed according to the Displacement Based Design (DBD) philosophy developed by Priestley et al. (2007) and adapted for post-tensioned rocking frames by Newcombe (2011) and Smith (2014). A step by step explanation of the design of Pres-Lam timber frames using DBD can be found in the Design Guide for Post-Tensioned Timber Buildings (STIC 2013). A design target drift of 1.8% and a ductility of 2 have been selected. The beam and column section sizes were chosen in order to obtain elastic rotations (beam, column and joint rotations) of about 0.8%. This meant that aside from the interface rotation given by the compression deformation at the column, the gap opening at the beam-column-interface was around 1%. The post-tensioning was made of 26.5 mm diameter bars which were placed in the centre of the box beams. The void in the beams was constant for all structures and had a size of 200 x 65 mm². The unbonded length of the mild steel reinforcement was chosen in order to have a strain of 0.03 at the target drift. The same amount of reinforcement was considered in tension and compression; all bars were placed at a distance of 100 mm from the beam edges.

The section properties for the design of the 2, 4 and 6 storey structures with and without mild steel dissipators are summarized in Table 4.3. The name of the individual sample structures consisted of the structural type (*F* for frames), the number of storeys (2, 4 and 6 respectively) and the re-centering ratio (70 for a 70% re-centering contribution and 100 for a full re-centering contribution).

Table 4.3 Section properties of the frame structures

ID	n_{storey}	T_e [s]	β	h_b [m]	b_b [m]	h_c [m]	b_c [m]	$D_{s,b}$ [mm]	$n_{s,b}$	$l'_{ub,b}$ [mm]	$D_{s,c}$ [mm]	$n_{s,c}$	$l'_{ub,c}$ [mm]	D_{PT} [mm]	n_{pt} [m]	l_{ub} [m]	$T_{PT,0}$ [kN]	
1	F-2-70	2	1.06	0.7	0.45	0.325	0.45	0.325	8	2	112	19	3	130	26.5	1	18.950	290
2	F-4-70	4	1.46	0.7	0.550	0.375	0.550	0.375	11	2	100	3	17	160	26.5	2	19.050	520
					0.500	0.325	0.550	0.375	9	2	120				26.5	2	19.050	320
3	F-6-70	6	1.97	0.7	0.650	0.450	0.650	0.450	14	2	100	16	4	230	26.5	3	19.150	810
					0.600	0.400	0.650	0.450	11	2	170				26.5	2	19.150	420
4	F-2-100	2	0.81	1.0	0.550	0.350	0.550	0.350	0	0	0	24	3	175	26.5	2	19.050	560
5	F-4-100	4	1.11	1.0	0.675	0.425	0.675	0.425	0	0	0	23	3	225	26.5	2	19.175	1000
					0.575	0.400	0.675	0.425	0	0	0				26.5	3	19.175	650
6	F-6-100	6	1.48	1.0	0.800	0.525	0.800	0.525	0	0	0	22	4	300	26.5	4	19.300	1350
					0.725	0.475	0.800	0.525	0	0	0				26.5	3	19.300	660

Note: for the 4 and 6 storey structures two different beam sections for the lower and upper half of the building respectively were considered

where

- n_{storey} number of storeys;
- T_e effective (secant) period of the equivalent single degree of freedom system;
- β re-centering ratio;
- h_b beam depth;
- b_b beam width;
- h_c column depth;
- b_c column width;
- $D_{s,b}$ mild steel reinforcement diameter for the beam connections;
- $n_{s,b}$ number of mild steel reinforcement bars for the beam connections;
- $l'_{ub,b}$ unbonded length of mild steel reinforcement for the beam connections;
- $D_{s,c}$ mild steel reinforcement diameter for the column base connections;
- $n_{s,c}$ number of mild steel reinforcement bars for the column base connections;
- $l'_{ub,c}$ unbonded length of mild steel reinforcement for the column base connections;
- D_{PT} diameter of the post-tensioning bars;
- n_{pt} number of the post-tensioning bars;
- l_{ub} unbonded length of the post-tensioning bars;
- $T_{PT,0}$ initial post-tensioning force.

Figure 4.12 shows the Acceleration-Displacement Response Spectra (ADRS) (Chopra and Goel 1999) relative to the chosen design spectrum for frame structure F-4-070. This curve is obtained by plotting the spectral acceleration in function of the spectral demand. The latter can be obtained by twice integrating the acceleration in respect to the period. In addition also the capacity curve (push-over curve) of the frame is shown. The intersection of the two curves provides the performance point of the structure under the expected earthquake excitation. Instead of showing the displacement of the structure, the drift at the effective height as defined by the DBD procedure is used.

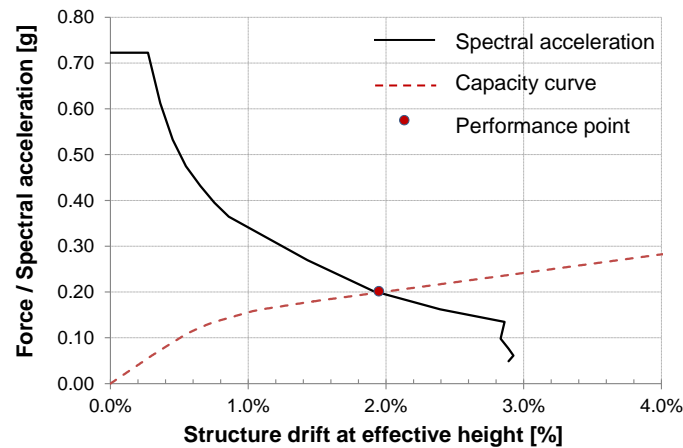


Figure 4.12 Acceleration-displacement response spectra and capacity curve in g of frame structure F-4-70

4.4.3 Diaphragm design for the frame structures

The general procedure for the determination of diaphragm forces and the therefore resulting diaphragm design and stiffness has already been presented in section 4.3.

For the 6 frame structures the diaphragm forces, diaphragm connection configuration and therefore resulting diaphragm stiffness are shown in Table 4.4. Based on the common flexible diaphragm definition, where a diaphragm is considered flexible if its deflection is larger than twice the average storey displacement at that level (Standards New Zealand 2004; ASCE 2010), all designed diaphragms can be considered as rigid (called semi-rigid in this dissertation to differentiate them from the perfectly rigid diaphragms). This is based on the design drift of 1.8% resulting in an interstorey displacement of 64.8 mm.

For the parametric analysis an additional diaphragm stiffness has been introduced, which is taken as 1/10 of the real semi-rigid diaphragm stiffness. Even with this artificially lower stiffness, none of the designed diaphragms can be classified as flexible according to the code definition from NZS1170.5. This is due to the very short diaphragm span in the frame structures. Even though these diaphragms cannot be classified as flexible, they are called flexible in this dissertation in order to distinguish them from the rigid and semi-rigid (real) diaphragm cases.

The ratio between the design floor forces F_{LLRS} from the DBD analysis and the assumed diaphragm forces F_{diap} (taken as the amplified top storey shear force as per Priestley et al. (2007)) is denominated as ω_D in Table 4.4. More on the determination of the diaphragm forces can be found in Chapter 5.

Table 4.4 Diaphragm forces, stiffness and fundamental period for the frame structures

ID	F_{diap} kN	v kN/m	ω_D	Semi-rigid			Flexible		
				K_{eq} kN/m	Δ_{diap} mm	T_{diap} sec	K_{eq} kN/m	Δ_{diap} mm	T_{diap} sec
F-2-070	210	12	1.4	45,000	5	0.20	4,500	48	0.64
F-4-070	221	12	1.6	53,000	4	0.19	5,300	43	0.59
F-6-070	287	16	1.8	67,000	4	0.17	6,700	45	0.53
F-2-100	322	18	1.3	77,000	5	0.16	7,700	48	0.49
F-4-100	321	18	1.4	90,000	4	0.14	9,000	44	0.45
F-6-100	413	23	1.5	110,000	5	0.13	11,000	48	0.41

where

- F_{diap} assumed force in diaphragm;
- v unit shear force in diaphragm;
- ω_D diaphragm force amplification factor;
- K_{eq} equivalent diaphragm stiffness;
- Δ_{diap} diaphragm mid-span deflection;
- T_{diap} fundamental period of the diaphragm.

4.4.4 Results of the analysis of the post-tensioned timber frames

A number of key parameters like the fundamental period, the storey shear forces and moments, as well as the structure's drift and displacements are compared for each of the 6 frame structures with the rigid, semi-rigid and flexible diaphragms. It is reminded that the 'flexible' diaphragm for the frame structures did not fall in the classical flexible diaphragm definition found in codes, and was defined as ten times more flexible than the real, semi-rigid diaphragm.

If not other ways stated, all values are taken as the average of the maximum values from each of the ten earthquake records.

4.4.4.1 Structural period of vibration

The outcomes of the modal analysis of the frame structures in terms of periods of vibrations are summarized in Table 4.5. The fundamental period is only marginally affected by the diaphragm flexibility in case of semi-rigid diaphragms. Only for the flexible diaphragms a more substantial increase can be observed. This increment is more pronounced in structures with a low number of levels. The reason for this behaviour is that frames already lead to relatively flexible structures and the additional diaphragm flexibility does not alter the dynamic behaviour substantially, also because the diaphragm period is normally much smaller than the structure's period. This is in contrast with wall structures as will be discussed later.

The presence of non-rigid diaphragms increases the structures' higher mode periods, which all approach the diaphragm's period. This is because the diaphragm vibration governs over the higher modes of the structures. In simplified terms, the structure remains in its undeformed state and the floor masses vibrate in the diaphragm's period following the typical mode shapes known from the dynamics of multiple degree of freedom systems. Further explanation is given for wall structures.

Table 4.5 Periods in seconds of the different frame sample structures for all three diaphragm flexibilities (numbers in parenthesis are the variation in respect to the rigid values)

Mode		T_{rigid}	$T_{semi-rigid}$		$T_{flexible}$	
1	F-2-070	0.80	0.82	(103%)	1.02	(128%)
		0.20	0.29	(142%)	0.67	(333%)
1	F-4-070	1.22	1.24	(101%)	1.36	(111%)
		0.36	0.40	(113%)	0.69	(194%)
		0.17	0.25	(150%)	0.61	(369%)
		0.11	0.21	(203%)	0.60	(568%)
1	F-6-070	1.41	1.42	(101%)	1.50	(107%)
		0.43	0.46	(107%)	0.68	(157%)
		0.21	0.27	(127%)	0.57	(267%)
		0.13	0.21	(163%)	0.54	(419%)
		0.09	0.19	(209%)	0.53	(590%)
		0.07	0.18	(249%)	0.53	(729%)
1	F-2-100	0.64	0.66	(103%)	0.81	(126%)
		0.15	0.22	(142%)	0.51	(333%)
1	F-4-100	0.98	0.99	(101%)	1.08	(110%)
		0.27	0.31	(113%)	0.53	(193%)
		0.12	0.19	(153%)	0.47	(378%)
		0.08	0.16	(208%)	0.46	(585%)
1	F-6-100	1.13	1.13	(101%)	1.20	(106%)
		0.33	0.36	(107%)	0.53	(159%)
		0.16	0.20	(129%)	0.44	(278%)
		0.09	0.16	(170%)	0.42	(445%)
		0.07	0.15	(219%)	0.42	(625%)
		0.05	0.14	(260%)	0.41	(767%)

The increased structure's fundamental period due to diaphragm flexibility can be calculated by the following equations, defined previously by Nakaki (2000) in the case where all diaphragms have the same flexibility

$$T' = T_{rigid} \sqrt{\frac{1 + \alpha^2}{\alpha^2}}; \quad (4.6)$$

$$\alpha = \frac{T_{rigid}}{T_{diap}}; \quad (4.7)$$

where

- T' is the structure's fundamental period including diaphragm flexibility;
- T_{rigid} is the structure's fundamental period with rigid diaphragms;
- T_{diap} is the diaphragm's period.

The values determined with this equation perfectly fit the values obtained from the numerical analysis.

4.4.4.1 Shear forces from NLTHA

Little influence from the diaphragm flexibility on the shear force distribution for frame structures can be observed. Influence from a second mode can be observed in taller structures, especially in the 6 storey structures. These effects seem to be less pronounced for flexible diaphragms.

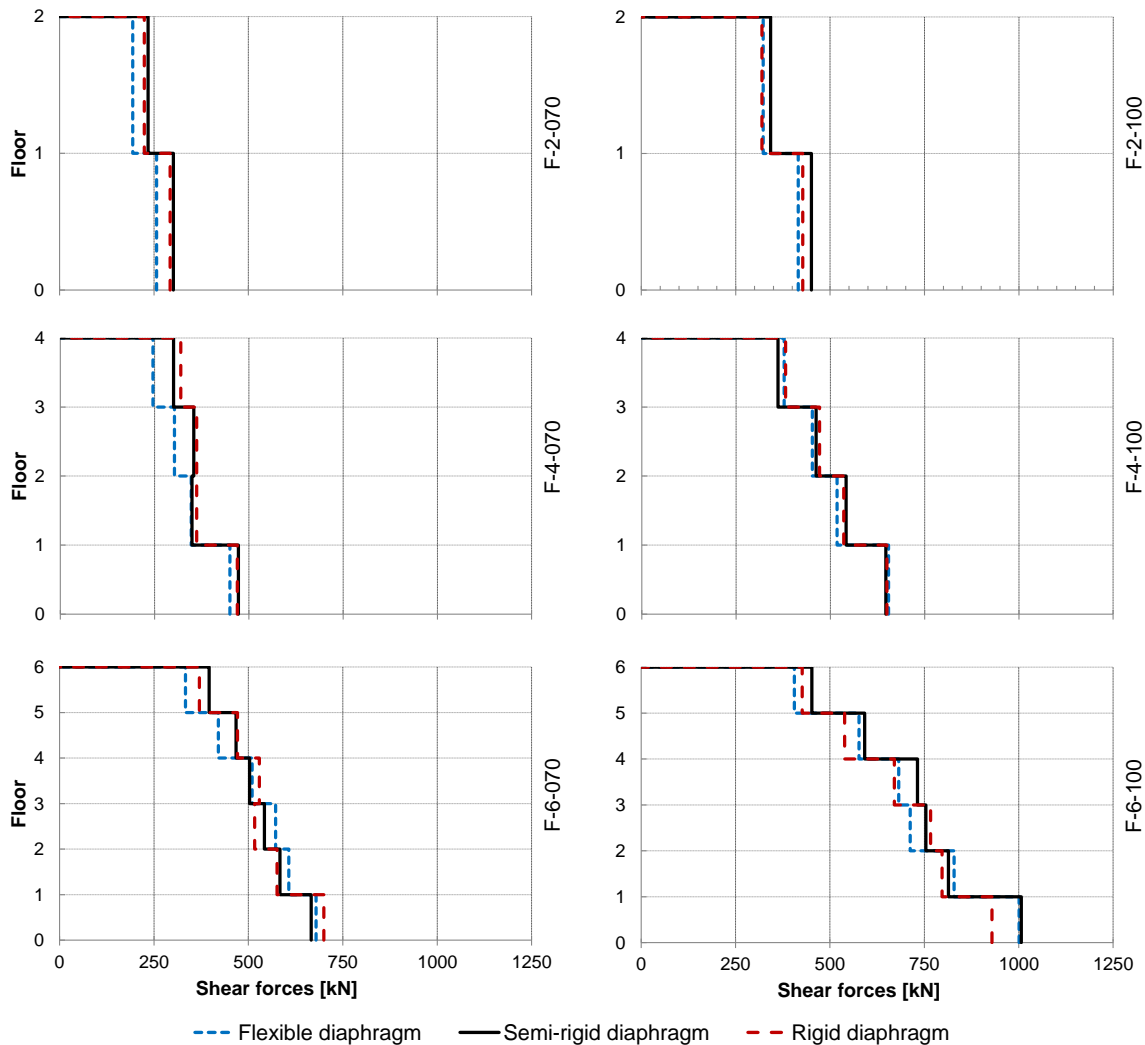


Figure 4.13 Shear forces in the 6 sample frame structures

4.4.4.2 Column moments from NLTHA

Figure 4.14 shows the storey moments as a sum of all column moments along the structure plotted as absolute values. It can be seen that the diaphragm flexibility does not significantly influence the moment distribution. Influence from higher modes can again be observed in taller structures, with a convex shaped moment envelope on the middle storeys.

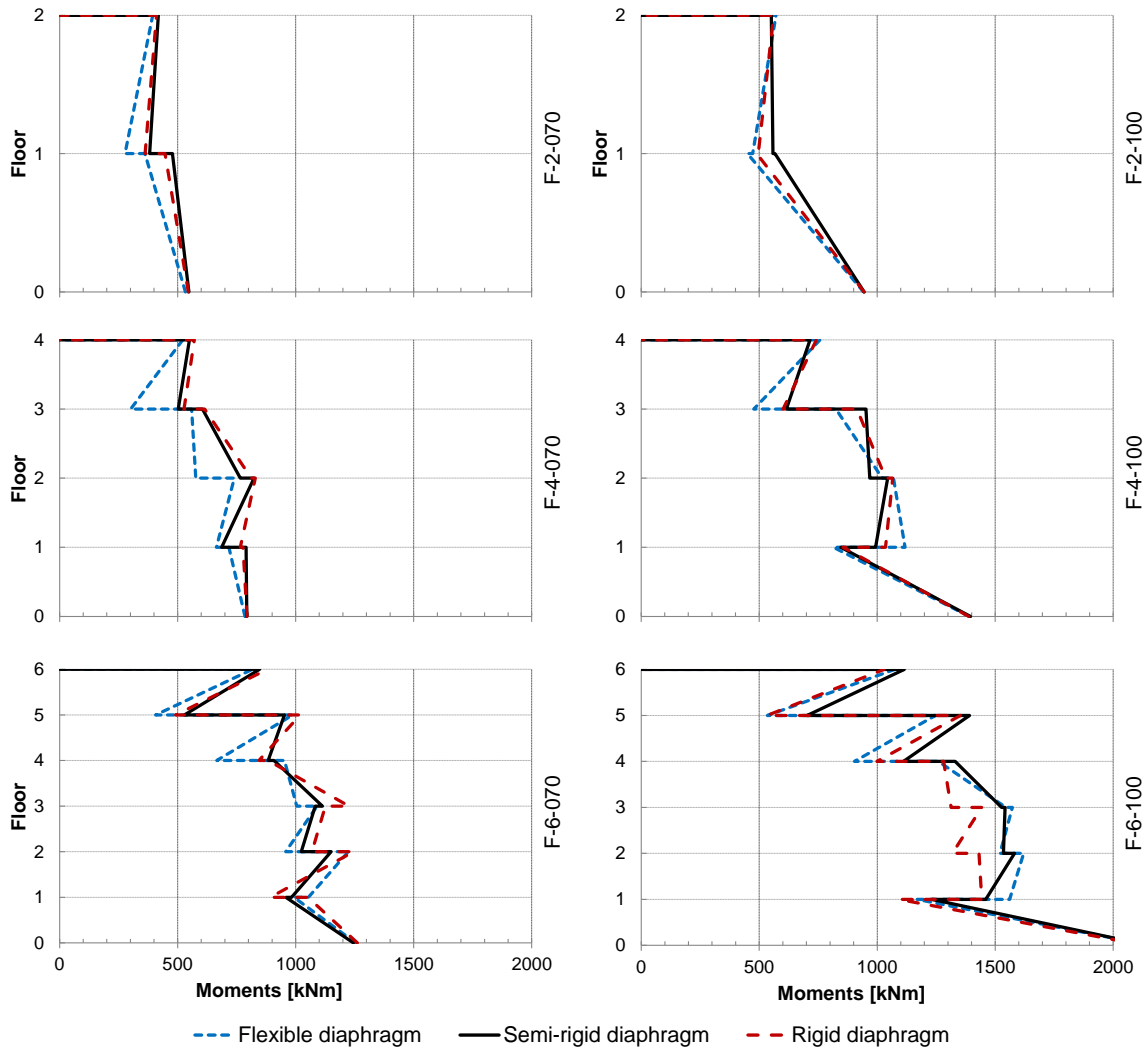


Figure 4.14 Column moments in the 6 sample frame structures

4.4.4.3 Frame interstorey drift from NLTHA

Post-tensioned frames designed with the currently proposed design procedure found in (STIC 2013) lead to reduced drift values when compared to the design target values (dotted line in Figure 4.15). This can be explained by a number of factors and assumptions, like the influence of the material strength reduction factor ϕ of 0.9, the design for an average beam moment demand over a number of storeys, the design for an average base column moment and the assumption of point of flexure in the base storey at 0.6 of the height.

Especially in the hybrid structures with additional dissipation devices, higher modes are leading to excessive drifts in upper stories; on the other hand the drifts at lower stories are reduced because of a pull-back effect. Diaphragm flexibility does not change the column moment envelope significantly, further no proportional relation between flexibility and amount of drift can be observed.

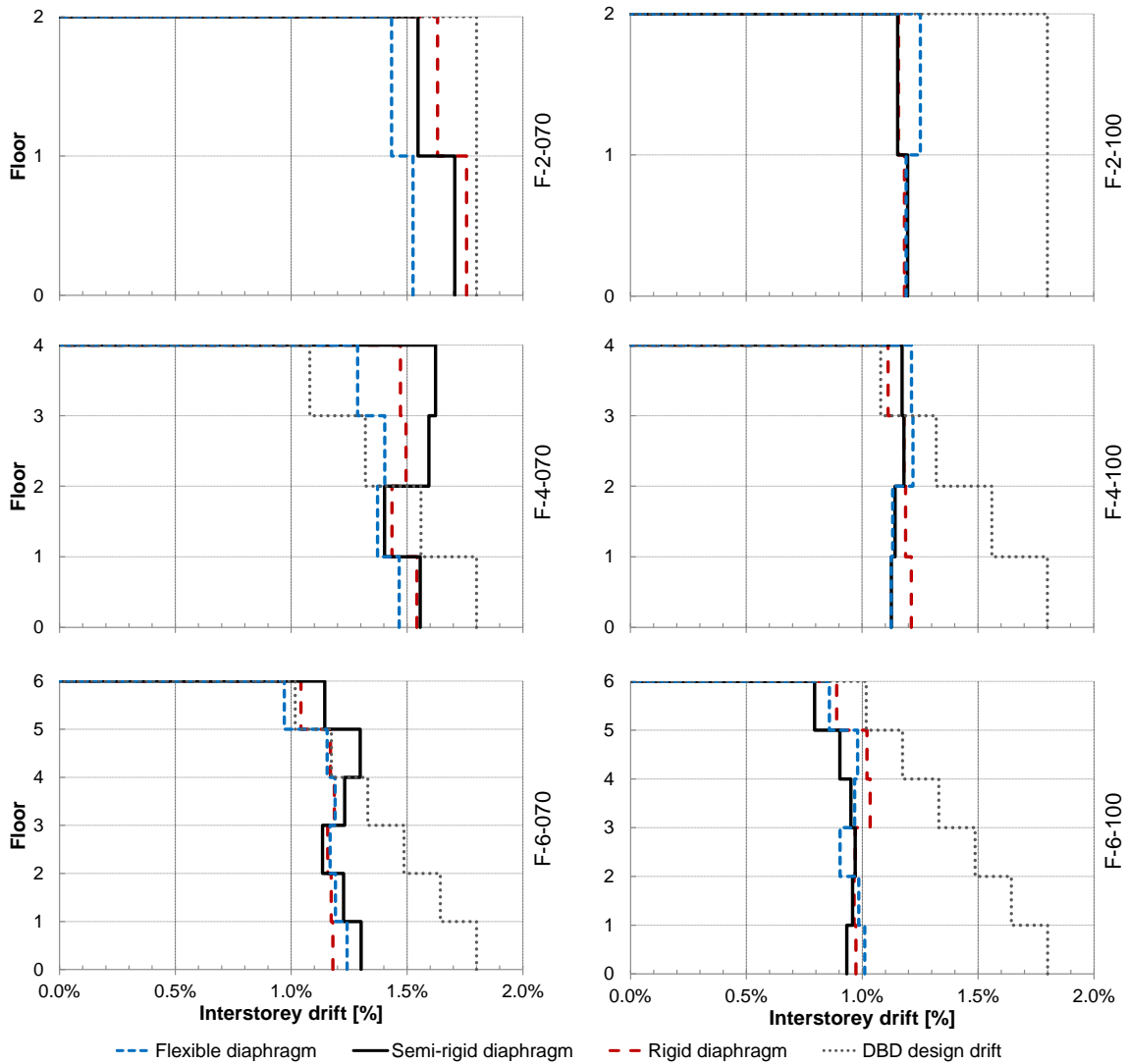


Figure 4.15 Interstorey drift of the 6 sample frame structures

4.4.4.4 Total displacement from NLTHA

Figure 4.16 shows the maximum relative displacement values of the sample structures for both the frames and at the mid-span of the diaphragms respectively. Maximum values of the two displacements can occur at different moments during the earthquake, so plots are an approximation only.

Except for very high diaphragm flexibilities the frames' displacements are not sensitive to the diaphragm flexibility and can be neglected. Diaphragm displacements are also not notably bigger, indicating that diaphragm deflections are only minimal.

In the case of flexible diaphragms, frame displacements are decreased for some structures and diaphragm deflections always increased. Since the chosen stiffness for the flexible diaphragm is fictitious and not-realistic in real frame structures, this behaviour is not further discussed.

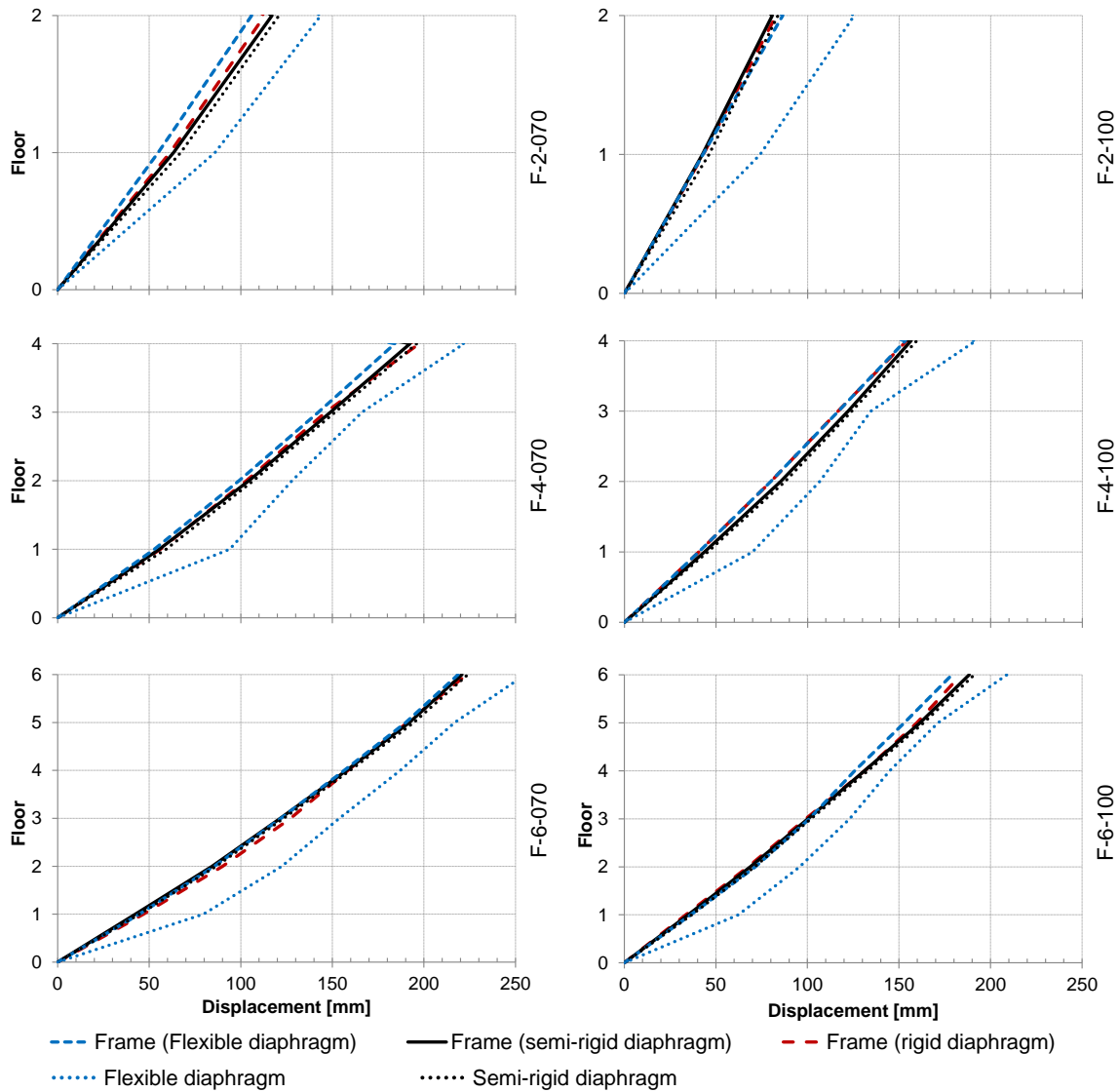


Figure 4.16 Frame and diaphragm displacements for the 6 sample structures

4.4.4.1 Floor acceleration magnification from NLTHA

A good indicator on the influence of higher modes and the distribution of forces along the building height is the Floor Acceleration Magnification (FAM), defined as the ratio between the Peak Floor Accelerations (PFA) and the Peak Ground Acceleration (PGA). In Figure 4.17 the structures' acceleration distributions for a single earthquake record at the peak floor acceleration at the individual floor levels are shown together with their respective time of occurrence.

For the two storey structures first mode responses are responsible for the peak accelerations at both stories. For structure F-4-100 peak accelerations at levels 2-4 are caused by a first mode response, whereas the peak acceleration at level 1 is generated by a second mode. For

the four storey dissipative structure most peak accelerations have a strong influence from a 2nd mode. For the six storey structures mostly higher modes are governing the acceleration distributions. It is also shown in the pictures that the maximum storey accelerations, and therefore floor forces, don't occur simultaneously. Further it is evident that high accelerations at the lower levels of taller structures are governed by higher modes.

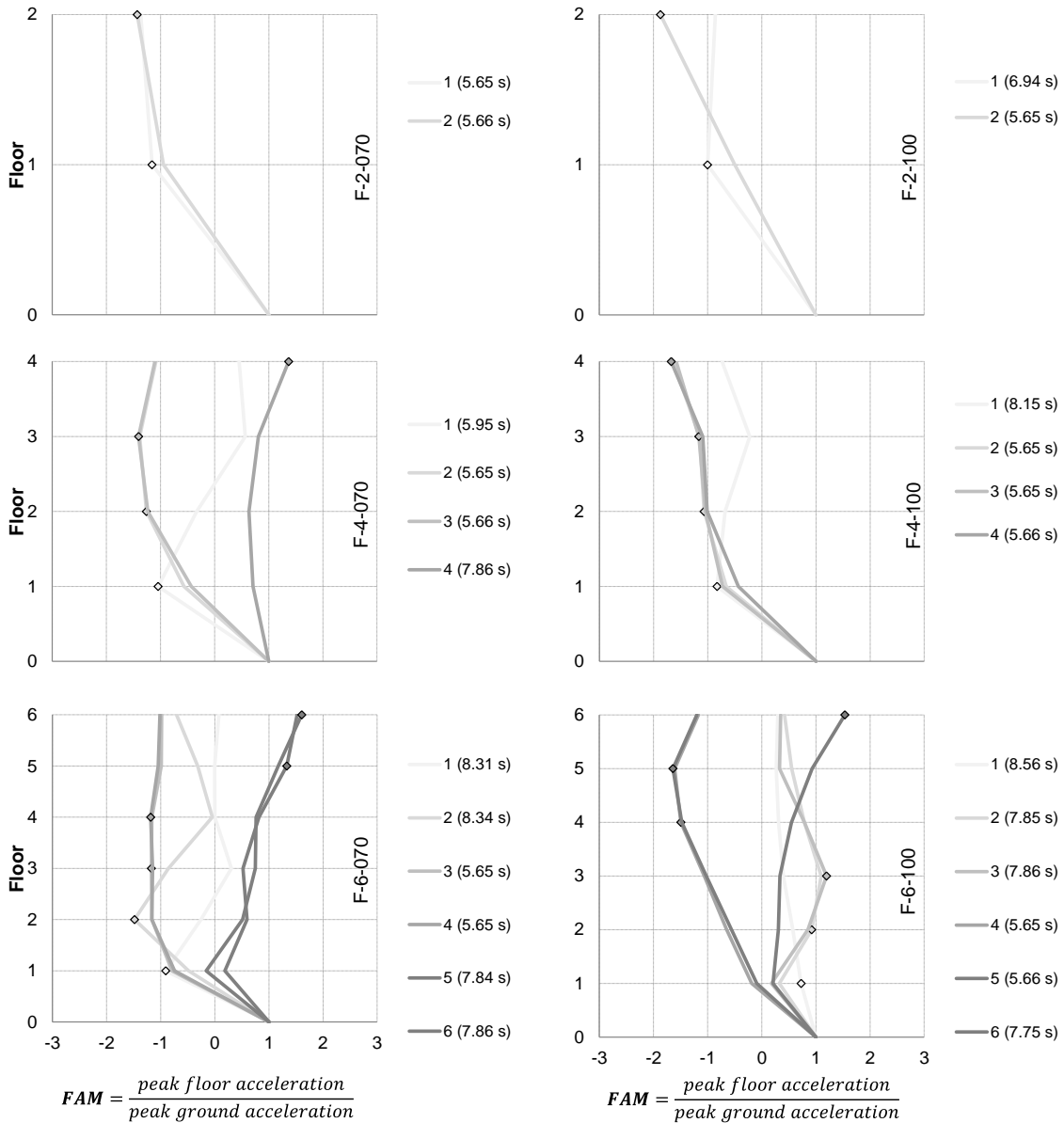


Figure 4.17 Acceleration distribution for peak floor accelerations occurring at the individual floor levels with the corresponding times for the frame structures with rigid diaphragms for the NGA0183 Imperial Valley-06 earthquake

4.4.4.2 Statistical scatter of results

Figure 4.18 shows the storey shear forces, storey moments, displacement and inter-storey drifts of frame structure F-4-070 in terms of mean value and standard deviation obtained from

the results with the 10 different earthquake records. It can be seen that the statistical scatter of the shear forces and the moments is within an acceptable margin. The displacements and therefore also drifts are more subjective to the different earthquake records and care should be taken when evaluating this values. The same trend could be observed for all other frame structures, independently from the diaphragm stiffness.

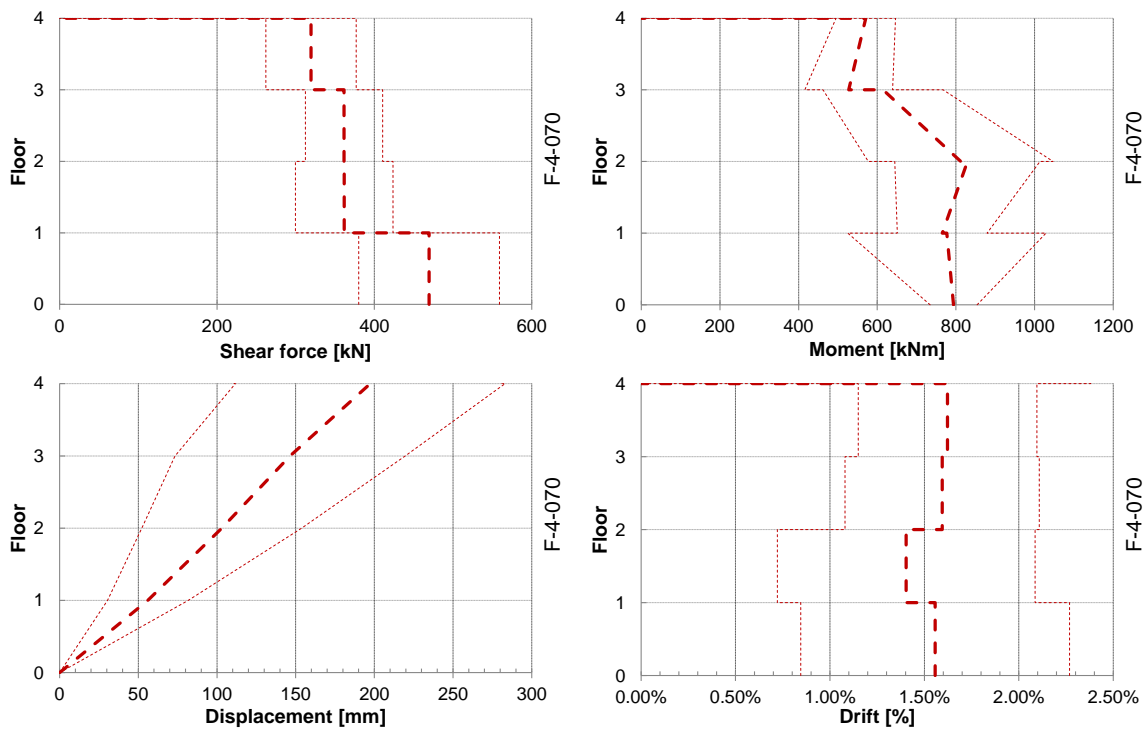


Figure 4.18 Shear force, moment, displacement and drift plots of frame structure F-4-070 with rigid diaphragms with mean value (dark dashed line) and the standard deviation (light dashed line)

4.5 PARAMETRIC ANALYSIS OF THE DYNAMIC PERFORMANCE OF POST-TENSIONED TIMBER WALLS

4.5.1 Numerical model for the wall structure

In the following paragraphs the numerical model of the 6 post-tensioned Pres-Lam timber wall structures is briefly presented. The model definition, schematically shown in Figure 4.19, as well as the OpenSEES (McKenna et al. 2000) routine, are based on the work of Sarti (2015). The structures consist of an elastic timber wall with a lumped ductility at the base with a self-centering capability provided by post-tensioning bars.

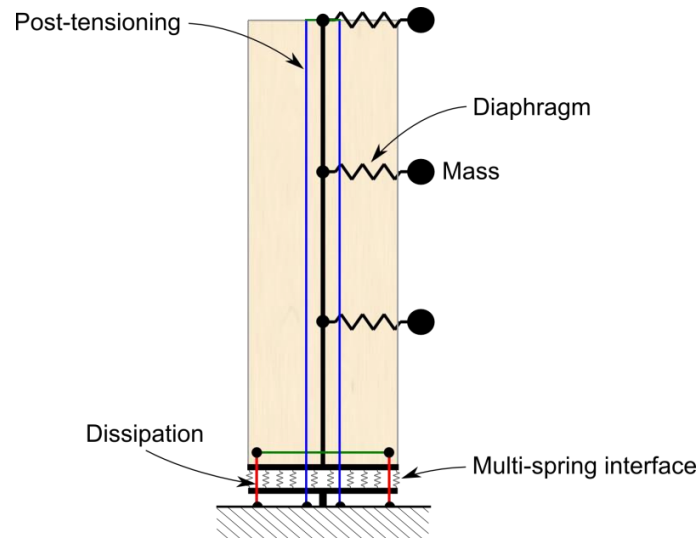


Figure 4.19 Numerical model of the wall for the OpenSEES analysis (the figure shows the sample structure W-3-70 with three storeys)

The modelling of the rocking wall is based on a multi-spring element at the wall-foundation interface, which simulates gap opening and neutral axis position. The multi-spring element was calibrated against the iterative moment-curvature approach based on the Modified Monolithic Beam Analogy (MMBA) (Palermo 2004). The post-tensioning bars and the mild steel dissipators are simulated as truss elements based on their material properties using a Menegotto-Pinto hysteresis rule (Menegotto and Pinto). These elements were connected via rigid links to the wall at their anchorage height, so to model their unbonded length and therefore real stiffness.

The wall itself was modelled as a non-linear beam-column element which also included shear deformations. Like in real buildings, first the post-tensioning forces were applied to the wall as a pre-load and then the mild steel elements were applied to the model. This was necessary to avoid initial compression of the dissipators. The material properties used in the model are summarized in Table 4.6.

Table 4.6 Material properties of the wall structures

Timber		Mild steel reinforcement	
Elastic modulus parallel to grain	$E_o = 13$ GPa	Yield stress	$f_y = 346$ MPa
Shear modulus	$G = 0.66$ GPa	Elastic modulus	$E_s = 200$ GPa
		Curvature factor	$R = 20$
		Post-yield stiffness	$r = 0.08$
Post-tensioning tendons		Isotropic hardening parameters	$a_1 = 0.05$
Yield stress	$f_y = 835$ MPa		$a_2 = 1.0$
Elastic modulus	$E_{pt} = 170$ GPa		$a_3 = 0.0$
Curvature factor	$R = 10$		$a_4 = 1.0$
Post-yield stiffness	$r = 0.09$		

For the benchmark structures with rigid diaphragms, the floor masses are slaved to the storey nodes of the wall. The semi-rigid and flexible diaphragms were simulated by means of elastic springs at each storey with the storey mass attached to them. The diaphragm stiffness has been evaluated as discussed in section 4.3 with respective values determined later in section 4.5.3.

An alternative method to model a rocking wall can be achieved by using rotational springs at the base as used for the frame structures. Whereas this approach is computationally more efficient, it does not provide information about the neutral axis depth, reinforcement elongation and uplift of the wall. Latter is especially of interest when studying displacement incompatibilities of the wall and the floor diaphragms. Whereas this information is not relevant for the contents of this chapter, the approach based on the multi-spring analysis was used.

For the OpenSEES analysis a tangent stiffness proportional Rayleigh damping model was used. The elastic damping contribution has been assumed to be 3%, in accordance with research on the dynamic behaviour of post-tensioned timber structures (Marriott 2009; Smith 2014). The critical damping was assigned to the 1st and 3rd modes.

4.5.2 Design of the sample wall structures

Two different re-centering ratios β of 1.0 (100% re-centering contribution, 0% dissipative contribution) and 0.7 (70% re-centering contribution, 30% dissipative contribution) were used to design the wall structures. For the former no dissipation was provided to the system and the system is relying on the apparent ductility provided from the change of stiffness due to gap opening. For the latter, energy dissipation was provided by means of mild steel reinforcement, creating a flag-shaped hysteresis behaviour of the system.

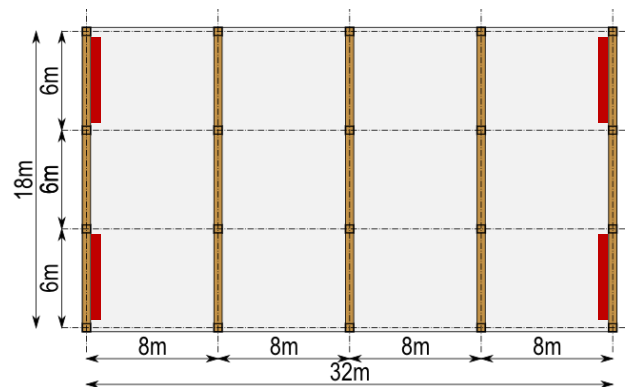


Figure 4.20 Sample building plane view with four walls

The sample building as shown in Figure 4.20 has a footprint of $18 \times 32 \text{ m}^2$ with an approximate floor area of 600 m^2 (STIC 2013). Five three bay frames carry the gravity loads and the post-tensioning shear walls are connected to the outer two frames whose beams act as collectors beams.

For the analysis three different building heights as shown in Figure 4.21 were considered, all structures had a constant inter-storey height of 3.6 m. A seismic load of 3.4 kPa was assumed for all floor levels, this was based on an office type loading and a timber only floor slab. The storey mass of the whole structure resulted therefore in 196 tons.

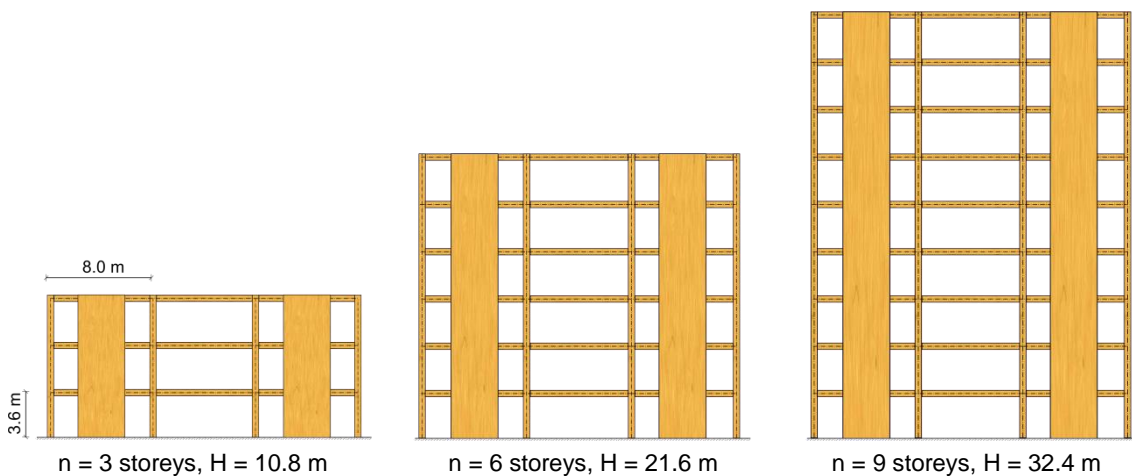


Figure 4.21 Selection of walls used for the parametric analysis

The wall structures were designed according to the Displacement Based Design (DBD) philosophy developed by Priestley et al. (2007) and adapted for post-tensioned rocking walls by Newcombe (2011) and Sarti (2015). A step by step explanation of the design of timber walls using DBD can be found in the Design Guide for Post-Tensioned Timber Buildings (STIC 2013). A design drift for the wall of 1.2% and a ductility of 3 have been selected.

The section properties for the design of the 3, 6 and 9 storey structures with and without mild steel dissipators are summarized in Table 4.7. The name of the individual sample structures consists of the structural type (W for walls), the number of storeys (3, 6 and 9 respectively) and the re-centering ratio (70 for a 70% re-centering contribution and 100% for a full re-centering contribution).

Table 4.7 Section properties of the wall structures

ID		n_{storey}	T_e [s]	h [m]	b [m]	β	n_{wall}	d_s [m]	D_s [mm]	n_s	l'_{ub} [m]	D_{PT} [mm]	n_{pt} [m]	l_{ub} [m]	$T_{PT,0}$ [kN]
1	W-3-70	3	1.08	3.6	0.36	0.7	2	0.72	22	6	0.55	60	2	7.2	1800
2	W-6-70	6	1.58	3.6	0.36	0.7	4	0.72	22	8	0.5	50	4	18	3005
3	W-9-70	9	2.29	3.6	0.36	0.7	4	0.72	23	10	0.33	60	4	28.8	4844
4	W-3-100	3	0.77	3.6	0.36	1.0	4	0	0	0	0.33	50	4	7.2	2517
5	W-6-100	6	1.11	4.8	0.45	1.0	4	0	0	0	0.33	50	6	18	6499
6	W-9-100	9	1.50	4.8	0.45	1.0	6	0	0	0	0.33	60	6	28.8	7711

where:

- n_{storey} number of storeys;
- T_e effective (secant) period of the equivalent single degree of freedom system;
- h wall depth;
- b wall width;
- β re-centering ratio;
- n_{wall} number of walls in the structure;
- d_s centroid of mild steel reinforcement measured from wall edge;
- D_s mild steel reinforcement diameter;
- n_s number of mild steel reinforcement bars;
- l'_{ub} unbonded length of mild steel reinforcement;
- D_{PT} diameter of the post-tensioning bars;
- n_{PT} number of the post-tensioning bars;
- l_{ub} unbonded length of the post-tensioning bars;
- $T_{PT,0}$ initial post-tensioning force.

Figure 4.22 shows the Acceleration-Displacement Response Spectra (ADRS) relative to the chosen design spectrum for wall structure W-6-070. In addition also the capacity curve of the wall is shown. The intersection of the two curves provides the performance point of the structure under the expected earthquake excitation. The drift is measured at the effective height as defined by the DBD procedure.

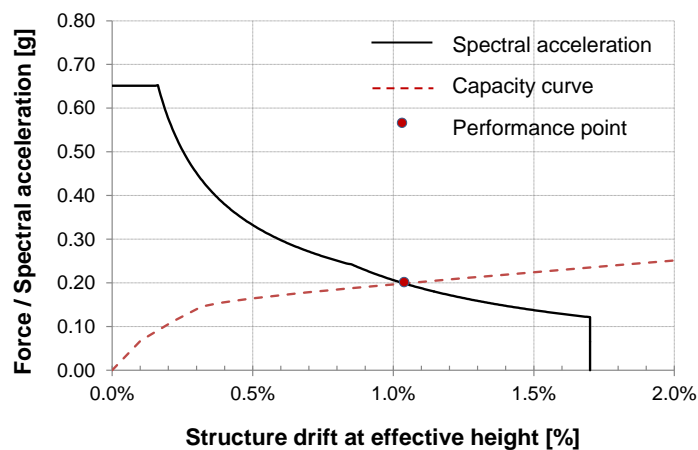


Figure 4.22 Acceleration-displacement response spectra and push-over curve of wall structures W-6-70

4.5.3 Diaphragm design for the wall structures

The general procedure for the determination of diaphragm forces and the therefore resulting diaphragm design and stiffness has already been presented in section 4.3.

For the 6 wall structures the diaphragm forces, diaphragm connection configuration and therefore resulting diaphragm stiffness are shown in Table 4.8. Based on the common flexible diaphragm definition, where a diaphragm is considered flexible if its deflection is larger than twice the average storey displacement at that level (Standards New Zealand 2004; ASCE 2010), all designed diaphragms are to be considered as rigid (called semi-rigid in this dissertation to differentiate them from the perfectly rigid diaphragm). This is based on the design drift of 1.2% resulting in an interstorey displacement of 43.2 mm.

For the parametric analysis an additional diaphragm stiffness has been introduced, which is taken as 1/3 of the real diaphragm stiffness. Based on these new values the diaphragms can be classified as flexible. These values represent commonly designed light timber frame diaphragms without any dynamic amplification factors (only designed based on capacity design principles).

Table 4.8 Diaphragm forces, stiffness and fundamental period for the wall structures

ID	F_{diap} kN	v kN/m	ω_D	Semi-rigid			Flexible		
				K_{eq} kN/m	Δ_{diap} mm	T_{diap} sec	K_{eq} kN/m	Δ_{diap} mm	T_{diap} sec
W-3-070	1244	35	2.1	30,000	47	0.51	10,000	142	0.88
W-6-070	1866	52	3.8	45,000	49	0.41	15,000	146	0.72
W-9-070	1865	52	5.4	50,000	45	0.39	16,667	134	0.68
W-3-100	2102	58	1.8	48,000	49	0.40	16,000	146	0.70
W-6-100	2792	78	2.8	62,000	51	0.35	20,667	152	0.61
W-9-100	2915	81	3.6	65,000	51	0.34	21,667	154	0.60

where:

- F_{diap} assumed force in diaphragm;
- v unit shear force in diaphragm;
- ω_D diaphragm force amplification factor;
- K_{eq} equivalent diaphragm stiffness;
- Δ_{diap} diaphragm mid-span deflection;
- T_{diap} fundamental period of the diaphragm.

The ratio between the design floor forces F_{LLRS} from the DBD analysis and the assumed diaphragm forces F_{diap} (assumed as the amplified top storey shear force V_n^o (see equation (5.17) in Chapter 5) according to Priestley et al. (2007)) is denominated as ω_D in Table 4.8. More on the determination of the diaphragm forces can be found in Chapter 5. For the dissipative 9 storey structure a very high diaphragm amplification factor of approximately 5 has been determined, this reflects the expected large contribution of higher modes in a very flexible timber structure.

4.5.4 Results of the analysis of the post-tensioned timber walls

A number of key parameters like the fundamental period, the storey shear forces and moments, as well as the structure’s drift and displacements are compared for each of the 6 frame structures with the rigid, semi-rigid and flexible diaphragms. If not otherwise stated, all values are taken as the average of the maximum values from each of the ten earthquake records.

4.5.4.1 Structural period of vibration

Results from the modal analysis of the wall structures with and without flexible diaphragms are shown in Table 4.9. As already found by other researches as stated in section 4.2, the introduction of the diaphragm flexibility lengthens the structures’ fundamental period. This effect is very pronounced for the three storey structures and becomes smaller for the nine storey structures.

Table 4.9 Periods in seconds of the different sample wall structures for all three diaphragm flexibilities (numbers in parenthesis are the variation in respect to the rigid values)

Mode		T_{rigid}	$T_{semi-rigid}$		$T_{flexible}$		T_{rigid}	$T_{semi-rigid}$		$T_{flexible}$		
1	W-3-070	0.59	0.78	(132%)	1.06	(179%)	W-3-100	0.42	0.58	(139%)	0.81	(194%)
2		0.15	0.53	(355%)	0.89	(598%)		0.11	0.41	(394%)	0.70	(667%)
3		0.09	0.52	(573%)	0.88	(982%)		0.06	0.41	(639%)	0.70	(1097%)
1	W-6-070	1.27	1.33	(105%)	1.45	(115%)	W-6-100	0.77	0.85	(110%)	0.98	(128%)
2		0.24	0.48	(201%)	0.76	(318%)		0.16	0.39	(238%)	0.63	(388%)
3		0.11	0.43	(377%)	0.73	(638%)		0.08	0.36	(436%)	0.62	(741%)
4		0.08	0.42	(532%)	0.72	(910%)		0.06	0.36	(598%)	0.61	(1027%)
5		0.06	0.42	(648%)	0.72	(1114%)		0.05	0.36	(722%)	0.61	(1242%)
6		0.06	0.42	(720%)	0.72	(1240%)		0.04	0.36	(798%)	0.61	(1375%)
1	W-9-070	2.14	2.15	(101%)	2.19	(102%)	W-9-100	1.27	1.31	(103%)	1.39	(109%)
2		0.35	0.45	(126%)	0.59	(167%)		0.23	0.40	(173%)	0.61	(264%)
3		0.15	0.31	(207%)	0.50	(329%)		0.11	0.34	(323%)	0.57	(542%)
4		0.10	0.29	(300%)	0.48	(500%)		0.07	0.33	(472%)	0.57	(804%)
5		0.07	0.28	(388%)	0.48	(657%)		0.05	0.33	(605%)	0.57	(1038%)
6		0.06	0.28	(463%)	0.48	(790%)		0.05	0.33	(718%)	0.57	(1235%)
7		0.05	0.28	(524%)	0.48	(896%)		0.04	0.33	(808%)	0.56	(1393%)
8		0.05	0.28	(568%)	0.48	(974%)		0.04	0.33	(874%)	0.56	(1508%)
9		0.05	0.28	(595%)	0.48	(1021%)		0.04	0.33	(915%)	0.56	(1578%)

For structures with flexible diaphragms it can be seen that whereas the first period of vibration increases to a new value, almost all periods of the higher modes tend to a constant value. These values correspond to the period of the diaphragm considered. This is in line with the

findings of Ju and Lin (1999), Fleischman and Farrow (2001) and Lee et al. (2007) who also observed a number of closely spaced modes.

This behaviour can be explained with Figure 4.23, where the extreme cases of the mode shapes of the structure with rigid diaphragms and of the modes shapes of flexible diaphragm on a rigid structure are shown. In the case of rigid diaphragms the structure deforms in the typical modal shapes known from dynamics as in Figure 4.23a. For an almost perfectly rigid structure with flexible diaphragms, the structure remains in its undeformed shape and the diaphragm springs deform following the mode shapes as in Figure 4.23b. All of these modes have the same period which corresponds to the period of the diaphragm. The analysed sample structures behave somewhere in between these two extreme cases as shown in Figure 4.23c. For modes 2 and 3 the walls are deforming only marginally. For the first mode the structure deforms with the diaphragm springs also elongating in the same direction. The combination of the two deformations made the system more flexible and therefore increased the fundamental period. For the higher modes the structure remained almost still and only the diaphragms followed the mode shapes, all vibrating at the same period.

For all structures with a low number of storeys all modes higher than the first correspond to the vibration of the diaphragms. For taller structures also the second and third modes correspond to the vibration of both the structure and the diaphragms; all higher modes again correspond to the modes of the diaphragms.

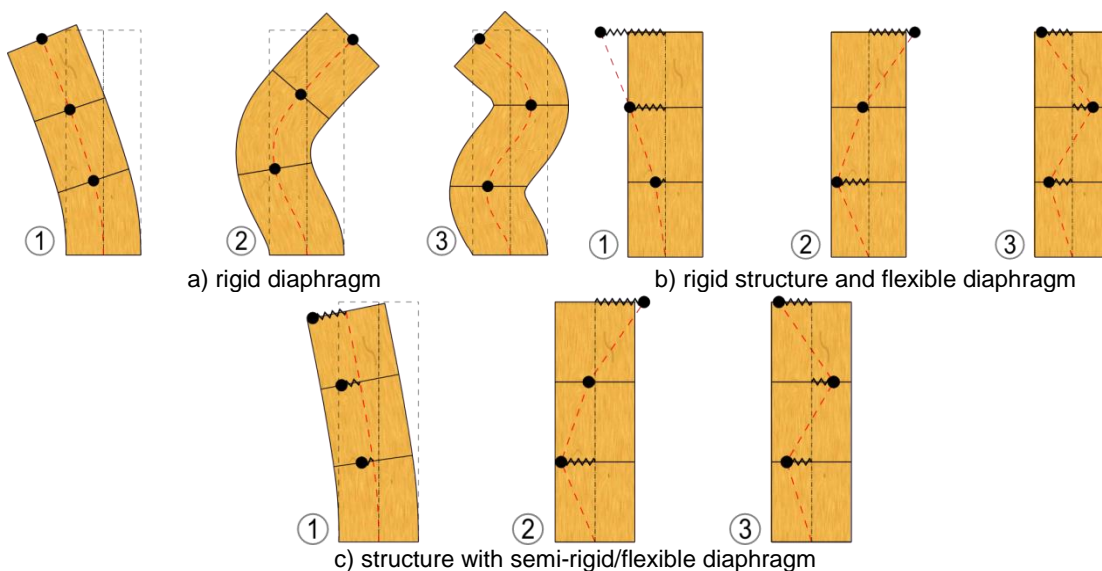


Figure 4.23 Mode shapes of the wall structure and the diaphragms

As for the frame structures, the structure's fundamental period including diaphragm flexibility can be evaluated with Equations (4.6) and (4.7).

4.5.4.2 Shear forces from NLTHA

For the base shear of the structures no general trend regarding the influence of diaphragm flexibility can be made. Only for both nine storey structures the semi-rigid diaphragms leads to slightly higher shears. Whereas the base shear of structures with non-rigid diaphragms becomes smaller with increasing fundamental periods, this reduction seems to be counteracted by the effect of diaphragm modes.

A clear trend, which is independent from the diaphragm flexibility, is the increasing influence of higher modes on the distribution of the shear forces along the structure's height. On the two nine storey structures the second mode increases the shear forces at the top storeys. For structures with high diaphragm flexibility this behaviour is less pronounced.

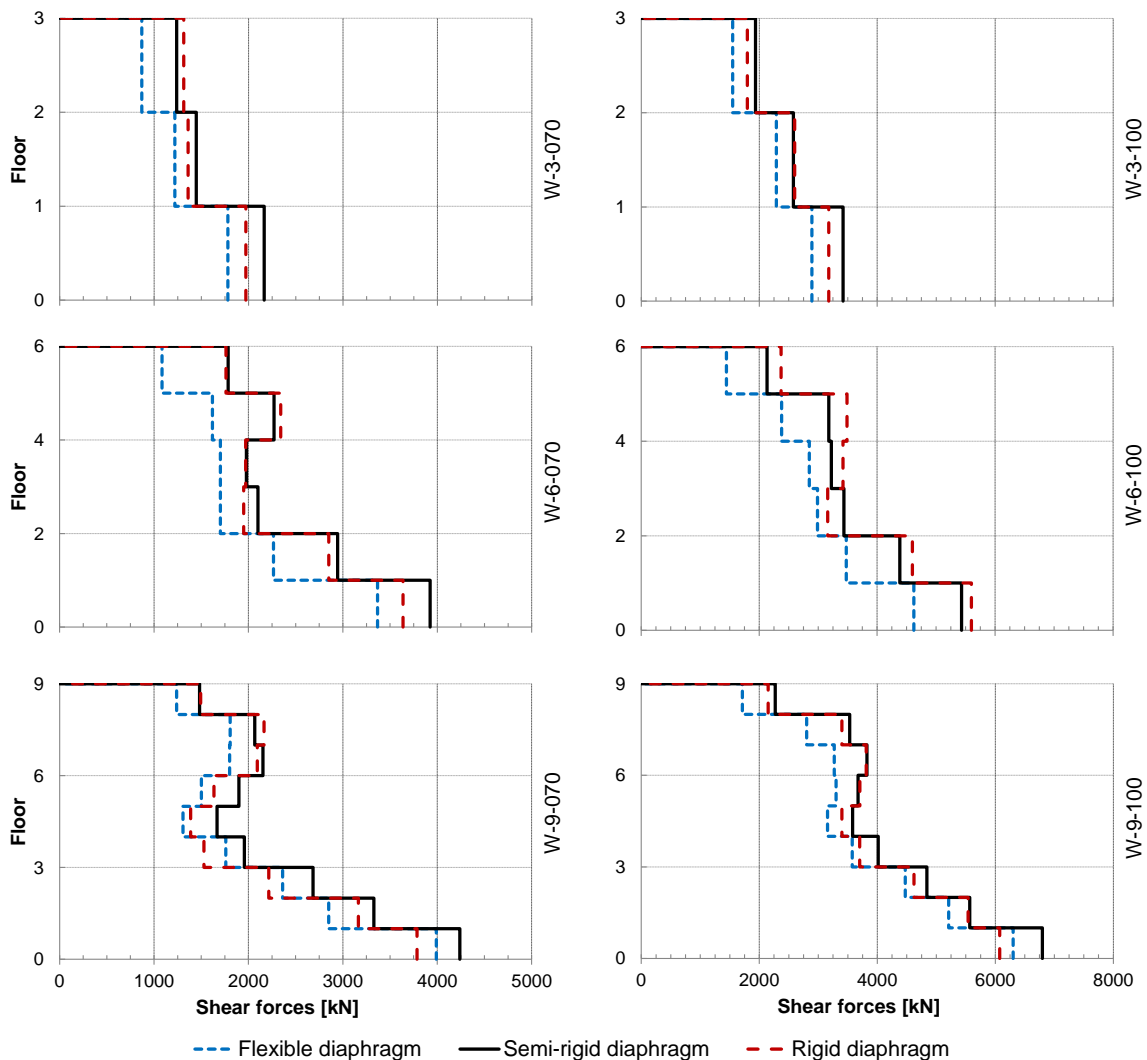


Figure 4.24 Shear forces in the 6 sample wall structures

4.5.4.3 Wall moments from NLTHA

The base moment proved to be almost independent from the diaphragm flexibility. Only for very flexible diaphragms can a small reduction from the base and along the structure be observed.

Higher mode effects can be noticed for both 9 storey structures, with an extreme found in the dissipative W-90-070 sample structure, which had very slender walls.

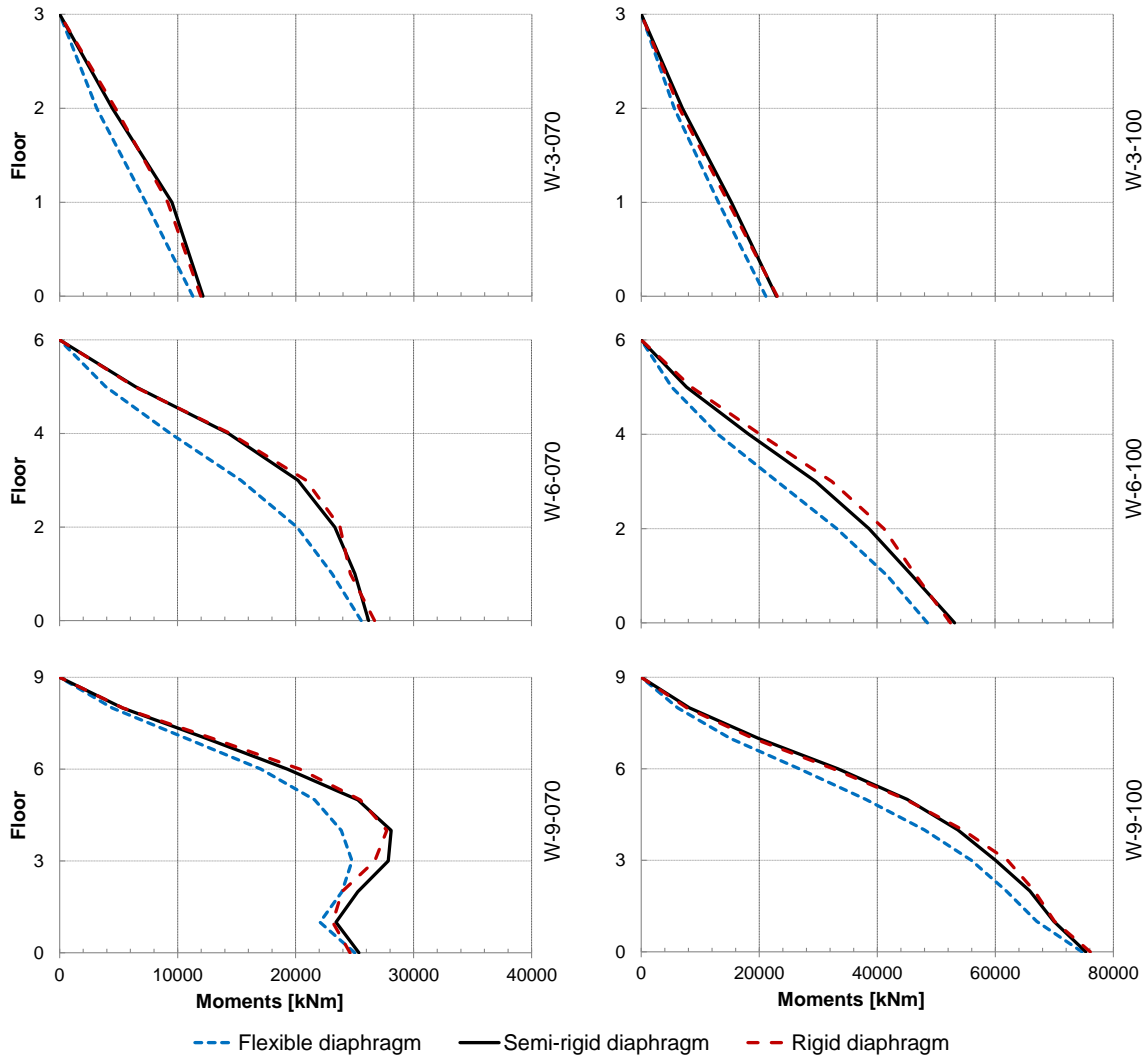


Figure 4.25 Moments in the 6 sample wall structures

4.5.4.4 Wall interstorey drift from NLTHA

Also for the wall interstorey drifts no clear trend regarding the influence of diaphragm flexibility can be seen. For almost all cases the drifts of the structures with rigid and with semi-rigid diaphragms are very similar. Only the structures with very flexible diaphragms smaller

drift values become evident. The drift values in general closely follow the target drift values from the DBD design at the bottom storeys and tend to be smaller at higher storeys.

An exception to this behaviour is structure W-90-070, where the structures with rigid and flexible diaphragms are very close to each other and follow the target design drifts. The wall with semi-rigid diaphragms shows higher drift values both at the bottom and top storeys.

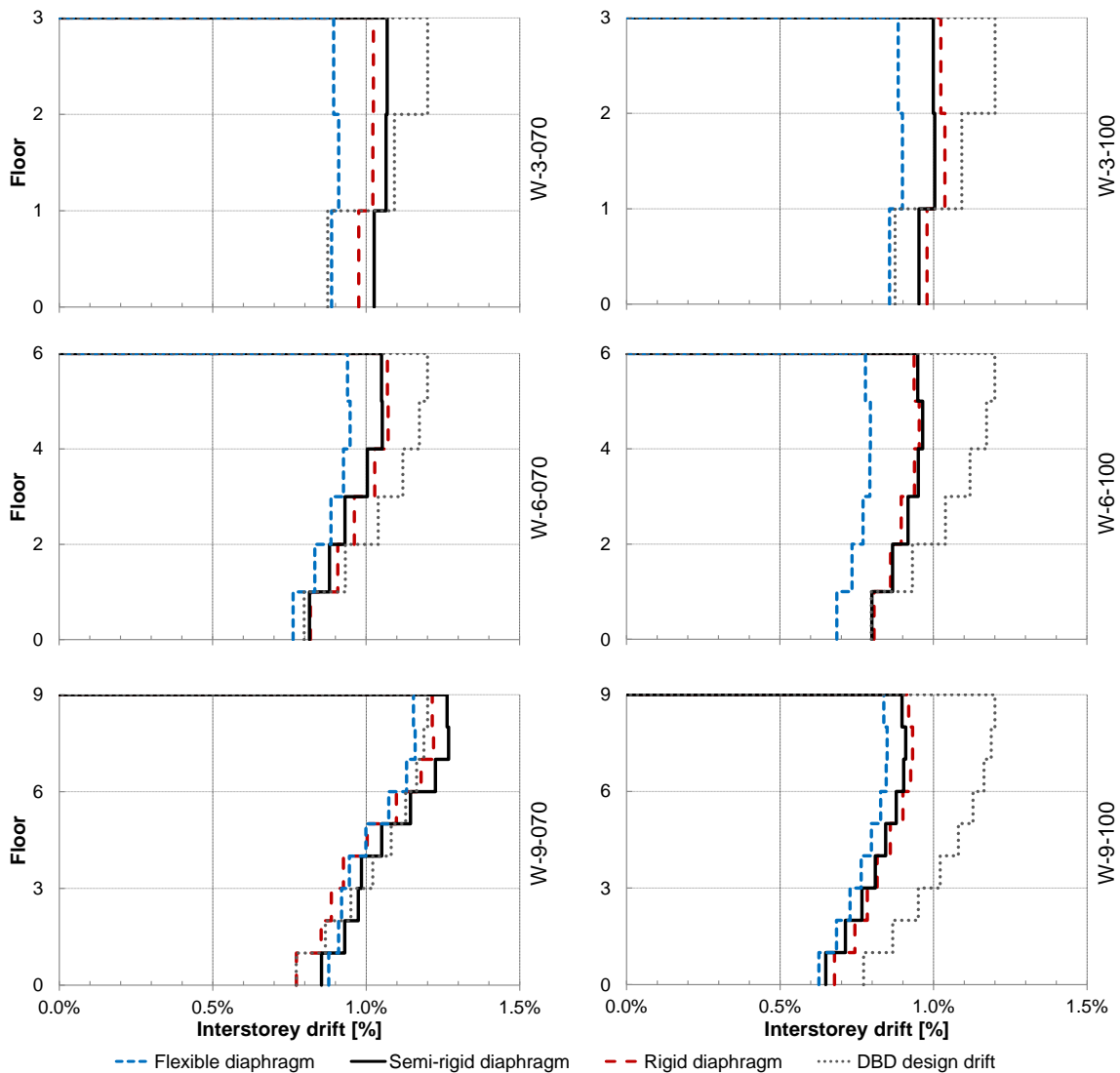


Figure 4.26 Interstorey drift of the 6 sample wall structures

4.5.4.5 Diaphragm interstorey drift from NLTHA

Unlike the wall interstorey drifts, which more or less follow the target drift values, the interstorey drift ratios related to the mid-span of the diaphragm are much higher. The largest values can be observed for the dissipative 3 and 6 storey structures with more than 3% interstorey drift at the base levels. For taller structures the diaphragm drift at the bottom storey is also very increased in the presence of non-rigid diaphragms. This is explained by the

strong influence of higher modes at the first storey compared to the stiff wall. This effect becomes more pronounced with increasing diaphragm flexibility.

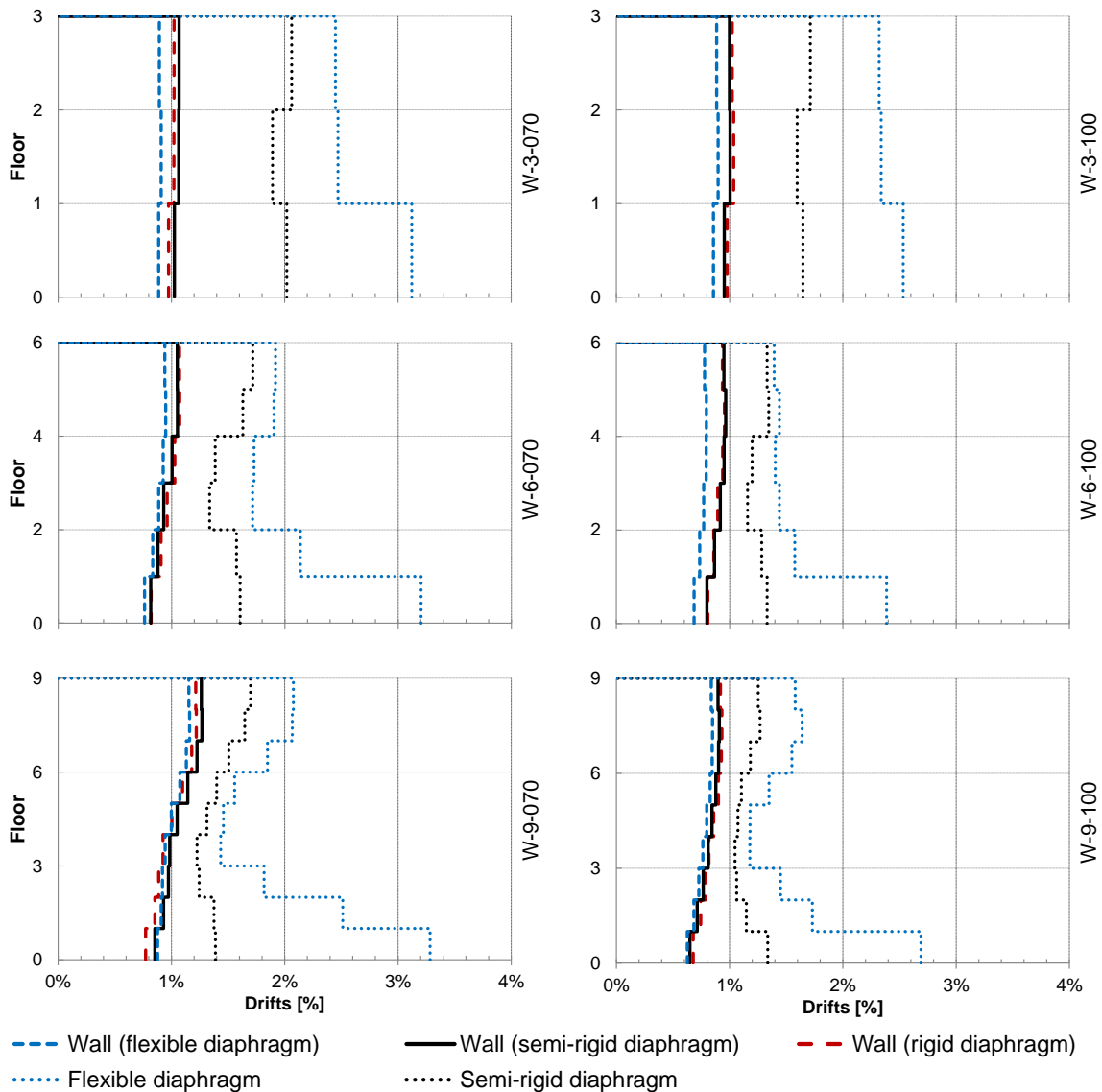


Figure 4.27 Wall and diaphragm drifts for the 6 sample structures

4.5.4.6 Total displacement from NLTHA

Figure 4.28 shows the maximum relative displacement values of the sample structures for both the walls and at the mid-span of the diaphragms. Maximum values of the two displacements can occur at different moments during the earthquake, therefore the plots are an approximation only.

As already found by Fleischman and Farrow (2001) it can be seen that high diaphragm flexibility tends to somewhat decrease the wall displacements. Inversely, the relative diaphragm deflections tend to increase with increasing flexibility. It can also be noted that the

largest diaphragm displacement occur at the lower storeys and again at the top storeys. This behaviour is clearly visible for structure W-6-070 in Figure 4.29, where the middle storeys have the smallest diaphragm displacement.

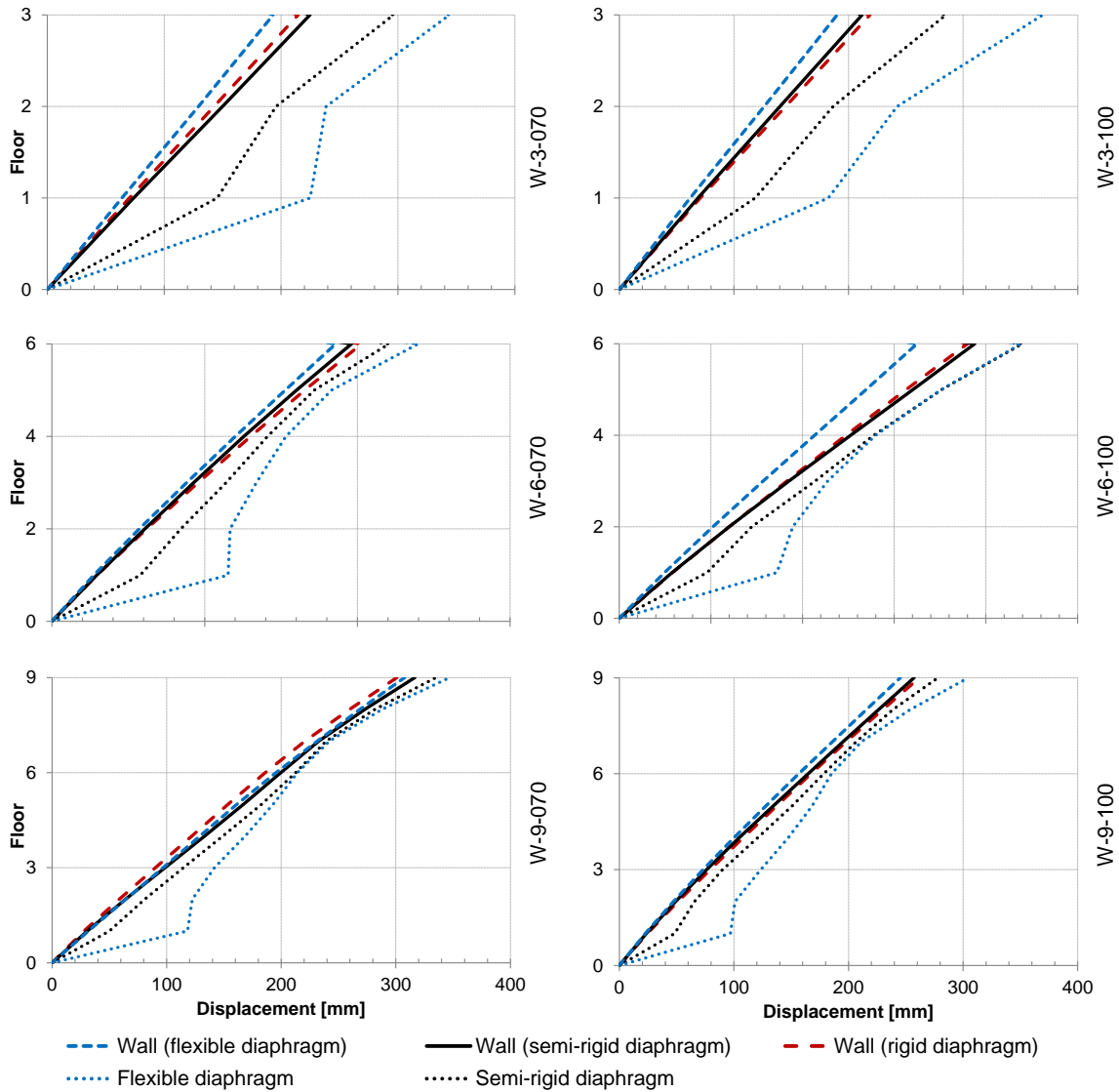


Figure 4.28 Wall and diaphragm displacements for the 6 sample structures

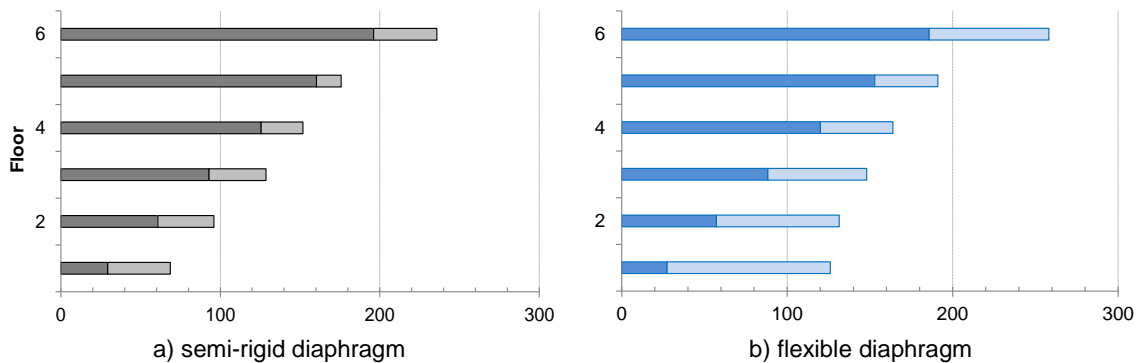


Figure 4.29 Wall deflection (dark shaded) and relative diaphragm deflection (light shaded) for wall W-6-070

4.5.4.7 Floor acceleration magnification from NLTHA

Figure 4.30 shows the Floor Acceleration Magnification (FAM) defined as the ratio between the Peak Floor Accelerations (PFA) for the individual levels at the Peak Ground Acceleration (PGA) together with their time of occurrence for the Imperial Valley-06 earthquake. For the definition of the FAM please refer to section 4.4.4.1.

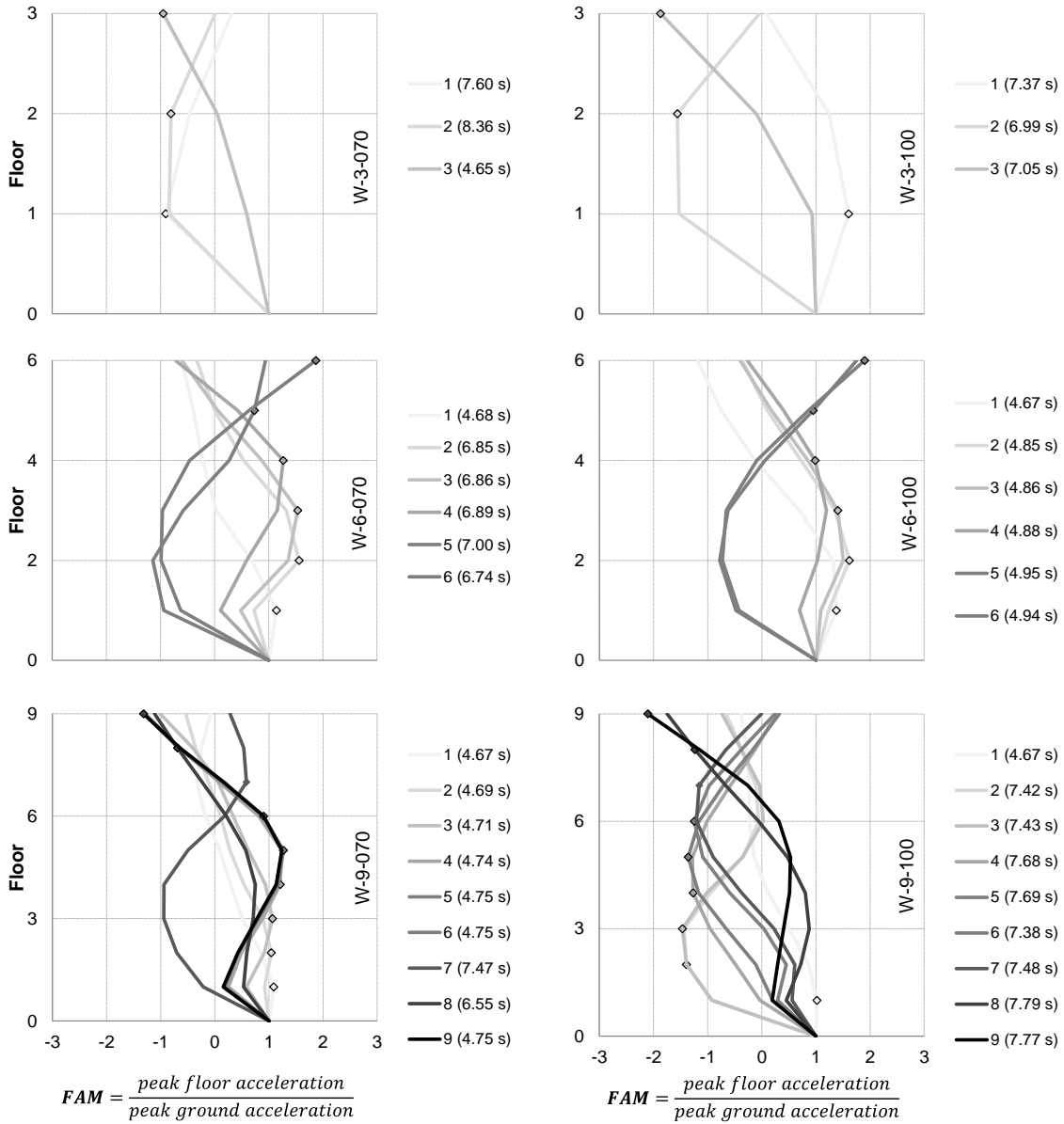


Figure 4.30 Acceleration distribution for peak floor accelerations occurring at the individual floor levels with corresponding time for the wall structures with rigid diaphragms for the NGA0183 Imperial Valley-06 earthquake

For the three storey structures peak accelerations at the first and second level are generated by second modes, only the top storey peak acceleration is due to a first mode. Inversely, for the 6 and 9 storey structures, the top storey accelerations are generated by a second and third

mode respectively. Other peak accelerations at other levels are created by combinations of the first and higher modes.

In general it can be stated that floor accelerations don't follow a first mode distribution and that high accelerations at lower storeys are created by higher modes. These convex shaped distribution at the bottom storeys, also been found by Fleischman and Farrow (2001), is not significantly influenced by diaphragm flexibility.

Figure 4.31 shows the measured floor accelerations at the wall from earthquake record NGA0725 (Superstition Hills-02). For both cases with rigid and semi-rigid diaphragms it can be seen that the structures tend to vibrate along the 2nd, 3rd or higher mode while following the oscillations from the fundamental period.

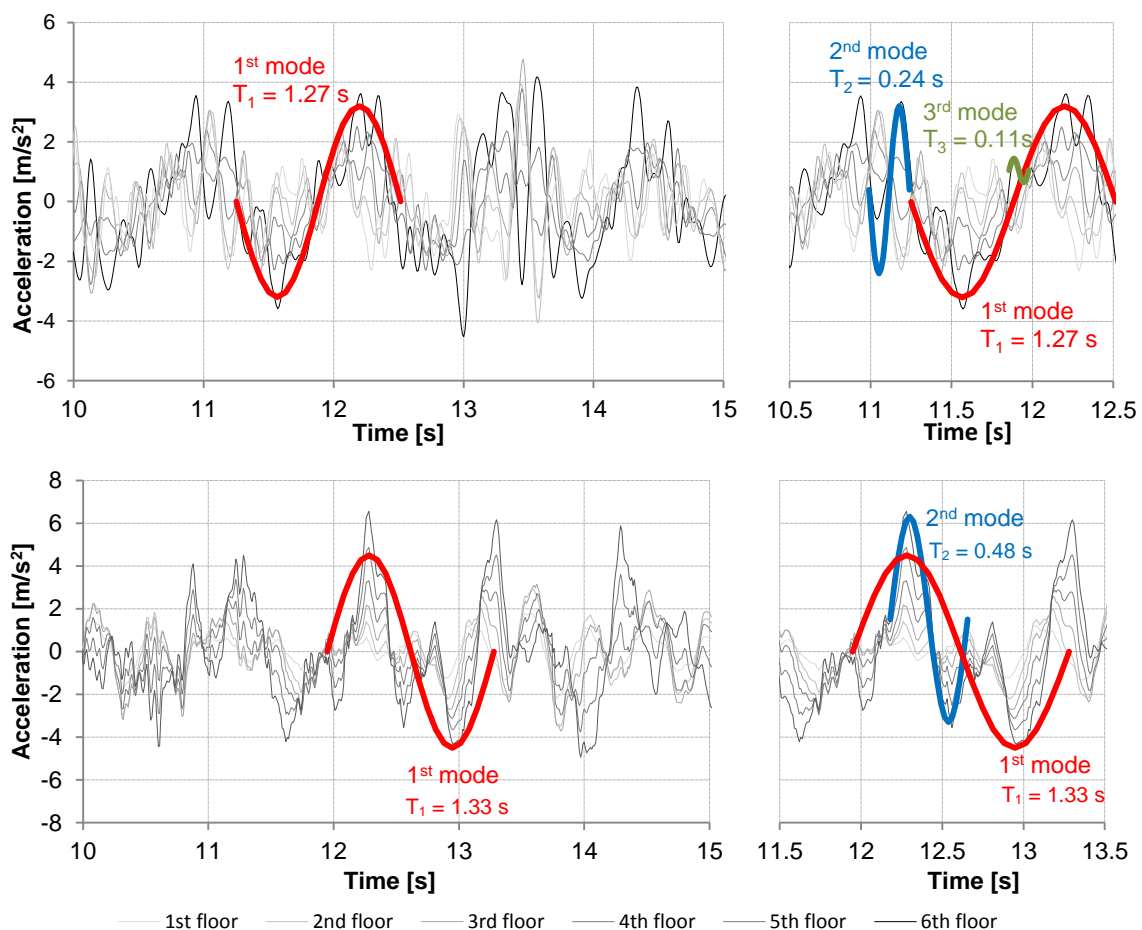


Figure 4.31 Floor acceleration response of all six storeys of the sample structure W-6-070 with rigid diaphragms (top) and semi-rigid diaphragms (bottom)

4.5.4.8 Statistical scatter of results

Figure 4.32 shows the storey shear forces, storey moments, displacement and inter-storey drifts of wall structure W-6-070 in terms of mean value and standard deviation from the 10

different earthquake records. Similarly as observed in the frame structures, it can be seen that the statistical scatter of the shear forces and the moments is within an acceptable margin, considering the scatter of the ten earthquake records used in the analyses.

The scatter in the shear force distribution is larger at the top and bottom stories and smaller at the mid-height of the structure. The displacements and therefore also drifts are very subjective to the different earthquake records and care should be taken when evaluating these values. The same could be observed for all other wall structures, independently from the diaphragm stiffness.

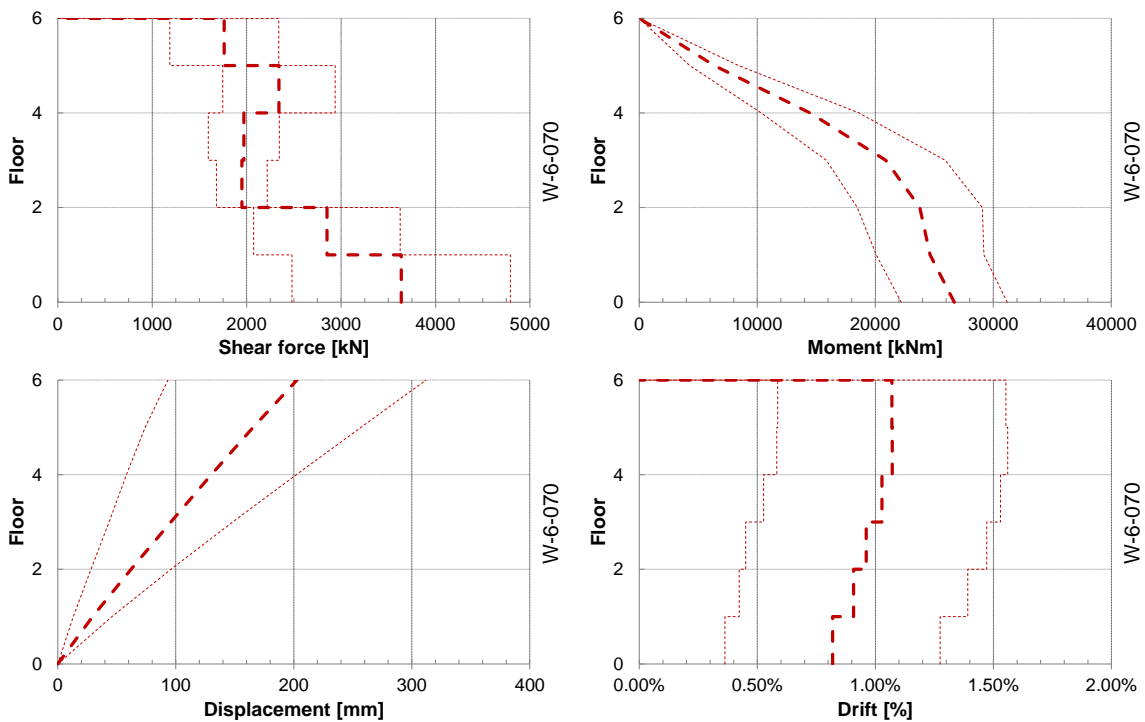


Figure 4.32 Shear force, moment, displacement and drift plots of wall structure W-6-070 with rigid diaphragms with mean value (dark dashed line) and the standard deviation (light dashed line)

4.6 DISCUSSION

In this chapter the dynamic behaviour of multi-storey post-tensioned timber Pres-Lam frame and wall structures was analysed using non-linear time history analyses. Along with varying the number of storeys and amount of hysteretic damping, the influence of diaphragm flexibility was investigated. The structures were analysed with perfectly rigid, semi-rigid and flexible diaphragms. The semi-rigid diaphragm corresponded to a real timber diaphragm made of light timber framing or massive timber panels. The flexible diaphragm did not necessarily

correspond to a realistic floor setup, and was used to provide the other extreme case to the rigid diaphragms.

The diaphragm flexibility was defined as the combination of the diaphragm flexibility considering panel shear, flexural deflection of the chords and fastener slip contributions as well as the stiffness of the diaphragm-to-lateral load resisting system connection.

In the analysis the storey shear and moment distribution, total displacement and interstorey drift as well as the Floor Magnification Amplification (FAM), equated as the ratio between the maximum storey acceleration to the Peak Ground Acceleration (PGA), were compared. For both frame and wall structures higher modes heavily dictated the dynamic response. The results were found from the analysis of post-tensioned Pres-Lam frame and wall structures. Because timber structures are normally deflection governed (i.e. the member sections are dictated by Serviceability Limit States) similar trends can be expected for all modern multi-storey buildings built with engineered timber materials. The general trends for both frame and wall structures are briefly summarized.

Frame structures:

- Because of the typically relatively small distance between gravity frames, typical diaphragms behave as rigid in accordance to code definitions. For the analysis an additional, artificially high, flexible diaphragm was considered.
- Period elongation because of diaphragm flexibility was almost absent for the semi-rigid diaphragm cases. This was explained by the relatively flexible structural system and the stiff diaphragms. Only for the very flexible diaphragms was a substantial increase observed. The structure's higher mode periods corresponded to the diaphragm period.
- Base shears were not significantly influenced by the diaphragm stiffness. For tall structures the storey shears were influenced by higher modes.
- Moments within the frame were essentially independent from the diaphragm flexibility. Higher modes influenced the moment distribution in the middle stories, creating a convex shaped envelope.
- For most structures drift values exceeded the targeted values in the top stories. In the lower stories a 'pull back' effect from higher modes reduced the drift values. The structure's drift values were not significantly influenced by the diaphragm stiffness.

- Total structure displacements were almost equal for rigid and semi-rigid diaphragms, diaphragm deflection can therefore be normally ignored. Only for very high diaphragm flexibility were frame displacements reduced and diaphragm deflections relevant.
- Storey accelerations were governed by the first mode distribution for the two storey structures. Higher modes were more dominant on the distribution of floor accelerations with increasing number of storeys. These caused high accelerations at lower stories in taller structures. Peak floor accelerations at different levels occurred at different instances in time. These findings will be used in Chapter 5 to determine the diaphragm demand.

Wall structures:

- For both non-rigid diaphragms, period elongation was observed. The structure's higher modes periods converged to the diaphragm period.
- Base shear values were not influenced by diaphragm flexibility. Tall structures had a shear force distribution influenced by higher modes, resulting in higher shears in the walls at the upper stories when compared to a typical first mode distribution.
- Wall moments were independent from the diaphragm flexibility and were influenced by higher modes in case of taller structures.
- Wall drifts were equal to or smaller than design target drifts, except for very tall and slender structures. The structure's interstorey drifts decreased slightly with increasing diaphragm flexibility.
- Drift values measured at the diaphragm mid-span increased notably in respect to the design target drifts. For short structures increased drift was observed everywhere, while for tall structures peak drift values were observed in the bottom stories. High diaphragm interstorey drift increased the displacement demand in gravity columns, façade and non-structural elements, and need to be considered in the design. The high diaphragm interstorey drift values for the real diaphragms show that the code definition of diaphragm flexibility (see Chapter 3) is not appropriate, since it would have been classified as rigid.
- The displacement of the lateral load resisting system was reduced with increasing diaphragm flexibility. Higher relative diaphragm displacements at the bottom and top storeys were observed.
- Floor accelerations were governed by higher modes for all taller structures. High acceleration at lower stories was observed for all structures, these values clearly

deviated from a first mode distribution. Peak floor accelerations at different levels occurred at different instances in time. These findings will be used in Chapter 5 to determine the diaphragm demand.

The results of the analysis will be further used in Chapter 5 in order to determine maximum diaphragm inertial forces.

4.7 CONCLUSIONS

The following conclusions can be drawn for timber frame and wall structures

- Diaphragm flexibility elongates the fundamental period of stiff structures (short frame and short to mid-rise wall structures), while in the case of flexible structures (tall frame and wall structures) the effect is negligible;
- Higher mode periods converge to the period of vibration of the diaphragms (closely spaced modes);
- Shear and moment distribution for both frame and wall structures are not significantly influenced by diaphragm flexibility;
- Higher mode effects have a strong influence on shear and moment distribution for frame structures with 4 or more storeys and for wall structures with 6 or more storeys;
- Frame displacements are the same for rigid and non-rigid diaphragms, while for wall structures the total displacements decrease slightly with increasing diaphragm flexibility;
- Diaphragm interstorey drift values are not influenced significantly by diaphragm flexibility in frame structures;
- Diaphragm interstorey drift values are notably higher for semi-rigid and flexible diaphragms in wall structures; diaphragm drifts are multiple times higher than the target wall drifts and diaphragm deflections and therefore need to be considered in design even for diaphragms defined as “rigid” according to current code provisions;
- Maximum floor accelerations occur at different instances in time and can be substantial at lower storeys because of higher mode effects. The expected first mode force distribution on the lateral load resisting system is therefore unlikely to be appropriate for the determination of floor forces, as will be discussed in Chapter 5.

5 Determination of shear forces, moments and diaphragm forces

5.1 INTRODUCTION

This chapter discusses code provisions and methods from literature for the determination of the diaphragm demand. Further, the design of diaphragms in regards to capacity design principles and transfer forces is discussed. Most attention is given to the estimation of the inertia floor forces for the multi-storey timber structures studied in Chapter 4. The results from the Non-Linear Time History (NLTH) analyses are compared with some available simplified methods to determine storey forces. A simple procedure is proposed to estimate the maximum expected diaphragm forces in multi-storey timber buildings.

5.1.1 Background

Diaphragms have multiple roles in resisting horizontal lateral forces in buildings as highlighted in Chapter 2. Since diaphragms are interacting with the lateral load resisting system, determining diaphragm forces can become quite a complex endeavour. In case of earthquake loading, diaphragms distribute inertial forces created within the floor slab to the lateral load resisting system. This force distribution is dependent on the relative stiffness of the lateral load resisting system and the diaphragms. Transfer forces can be created within diaphragms in the following cases:

- in dual lateral load resisting systems (i.e. frames and walls in the same structure); or
- in systems with elements of different stiffness (i.e. walls with different stiffnesses at the same level); or
- in lateral load resisting systems with varying stiffness up the building's height (such as podium structures); or
- in structures with discontinuous lateral load resisting elements up the building's height.

Finally, it is generally required that diaphragms are kept elastic (Standards New Zealand 2004a), requiring the application of capacity design principles and dynamic amplifications due to higher mode effects.

Current design practice does not normally differentiate between the forces acting on the lateral load resisting system and the floor diaphragm forces. It is normally accurate enough to design frames or walls according to a force distribution resulting from a Force Based Design (FBD) analysis like the Equivalent Static Analyses (Standards New Zealand 2004a) or a Displacement Based Design (DBD) procedure (Priestley et al. 2007). This is because it is very unlikely to have all maximum storey forces occurring at all levels at the same time, and a first mode approximation is normally satisfactory. Diaphragms, however, will be exposed to the maximum forces occurring at any instant during an earthquake, resulting in much higher floor forces than in the lateral load resisting system. These peak actions are heavily influenced by higher mode effects resulting from the fact that the structure has multiple degrees of freedom. Chapter 4 showed that higher modes do affect the shear force distribution in Pres-Lam multi-storey timber wall and frame buildings, and such influence needs to be considered when determining the diaphragm forces. Even though the numerical analyses were carried out on post-tensioned timber buildings only, similar trends regarding the dynamic behaviour can be expected for modern timber buildings with engineered timber materials. This is because most timber buildings are stiffness governed and the timber lateral load resisting systems are all normally designed for the same drift limits.

5.2 DISCUSSION OF THE AVAILABLE METHODS FOR THE DETERMINATION OF FLOOR FORCES

5.2.1 Analysis methods

Design codes allow for a number of different methods to determine the actions induced by earthquakes on a structure. These methods are extensively covered in literature and are briefly discussed hereafter.

5.2.1.1 Force Based Equivalent Static Analysis (ESA)

The Equivalent Static Analysis (ESA) is based on the assumption that the structure behaves like a Single Degree Of Freedom (SDOF) system. The deflected shape corresponds to the first mode shape of the structure and it is assumed that all masses are activated by this mode only. Once a seismic base shear is determined, the storey forces are distributed along the structure's

height based on an inverted triangular distribution. This distribution again reflects the first mode deflected shape of the structure.

To determine the seismic base shear, traditionally a Force Based Design (FBD) method is applied. Based on the fundamental period of the SDOF, the acceleration of the structure's mass can be determined on the basis of a design acceleration spectrum. This spectrum is defined on the basis of a number of code parameters like the seismic hazard factor, soil class type, near fault factor, importance factor, ductility, overstrength and others. By multiplying the structure's mass times the spectral acceleration, the base shear can be determined.

Although this method provides a very simple and intuitive tool, it should not be used for irregular structures in height and plan and in cases where significant higher mode effects are expected. If higher modes become more pronounced, only a part of the total mass will be activated in the first mode, with other modes of vibration influencing the force distribution and deflection along the structure's height.

The Force Based Design (FBD) method is strongly dependent on the fundamental period of the structure and the ductility factor μ (or force reduction factor R or behaviour factor q) which is based on the equal displacement approximation or the equal energy approximation for structures with medium to long and short periods respectively. It is apparent that the determination of the fundamental period is of paramount importance in FBD. Even if sometimes ignored in design, once the period is initially estimated based on a preliminary design, the seismic forces are determined and the structural elements designed, it might be necessary to recalculate the period to account for the real structures' dimensions and connections.

5.2.1.2 Displacement Based Design

The dependency of the estimated initial period of the FBD approach together with other inconsistencies as discussed in Priestley (2003) and Priestley et al. (2007) have led to development of the Displacement Based Design (DBD) method. Aside from overcoming some shortcomings found in the FBD, the DBD method also recognizes the fact that displacements are the main cause of structural and non-structural damage.

The DBD is based on the choice of a target displacement which the structure needs to withstand under an earthquake. The structure therefore needs to be characterized by the

effective stiffness (secant to the structure's target displacement). Therefore, instead of estimating the initial stiffness, the deflected shape of the structure needs to be determined.

Based on the deflected shape, the Multiple Degree Of Freedom (MOD) system is converted into an equivalent SDOF. The elastic pseudo-displacement spectrum is derived from the acceleration spectrum and is then reduced to account for the elastic and hysteretic damping. Knowing the target displacement, the effective (secant) period can be obtained directly from the reduced pseudo-displacement spectrum and the secant stiffness can be calculated. The base shear is finally determined as the stiffness times the pseudo-displacement.

The storey forces on the lateral load resisting system can be determined based on the ESA as outlined before, the internal actions are normally determined by the equilibrium method (Priestley et al. 2007). Similarly as above, peak floor forces cannot be directly estimated.

5.2.1.3 Response spectrum analysis

Modal response spectrum analysis is generally required for irregular structures and in cases where higher mode effects are expected to be significant.

By solving for the eigenvalues and eigenvectors of the structure of interest, the fundamental periods, modal shapes, modal masses and participation factors can be obtained. Because of the orthogonality of the single modes, the equation of motion of a MDOF structure can be decoupled in the equations of motion of a number of independent SDOF.

Similarly to the ESA used in force based design, for each SDOF the spectral acceleration is then found. The actions from the single modes need to be combined based on their relative contribution to the global behaviour. Different design codes prescribe the minimum number of modes to be considered which is normally based on the sum of SDOF masses participating in the motion.

Peak actions from different modes however occur at different instances during an earthquake, which can also be of opposite sign to each other. Methods like the Square Root of the Sum of the Squares (SRSS) rule or the Complete Quadratic Combination (CQC) rule are used to determine the envelope maxima for a given structure. Forces acting on the lateral load resisting system can therefore be estimated satisfactorily, but actions are not in equilibrium and peak floor forces cannot be determined accurately.

5.2.1.4 Time history analysis

Time History Analysis (THA) allows for the integration of the complete equation of motion of a structure under arbitrary ground motions for each chosen time step. Stiffness values of the individual elements can be updated for each calculation step and therefore account for non-linearity.

Non-linear Time History (NLTH) is the most sophisticated method available to study the dynamic behaviour of a structure considering potential ductile elements with their own hysteresis. Complex material properties like stiffness and material degradation, strain hardening etc. can be accounted for. Outcomes of the integration are based on complex iteration procedures and can be very sensitive to certain parameters like damping, time step and the ground motion input.

For the determination of design actions the choice of the ground motion record is crucial as it needs to represent the code design spectra, accounting for the type of soil, near or far fault rupture, frequency content and other considerations. Design standards normally provide guidance on the selection of ground motions and might require scaling in order to fit the design spectra. Online databases provide a variety of real earthquake records as well as synthetic records derived specifically for certain design spectra.

Because the method provides force and displacement values for each time step, it accounts for maximum diaphragm forces as well as the interaction with the remainder of the structure. Setting up a model and interpreting the outcomes, however, is a delicate and time consuming matter and should only be carried out by trained engineers.

5.2.1.5 Parts and components

The 'parts and components' method is a force based design method used to determine the design actions of non-structural elements attached to a structure. It is based on the assumption that a part or component is acting as a SDOF element attached at a certain height to the structure. Once the weight and period of the part or component is known, the spectral acceleration can be obtained from a specially determined accelerations spectrum.

The method allows for the determination of the maximum force acting on the part or component, without considering its influence or interaction with the remaining structure. In the past this method has also been used to determine diaphragm forces, leading to very

conservative loads and unrealistic high displacements of the structure, overestimating transfer forces.

5.2.2 Design standards and codes

5.2.2.1 New Zealand Earthquake Loading Code NZS 1170.5

The New Zealand Earthquake Loading Code NZS 1170.5 (Standards New Zealand 2004a) allows for the use of the ESA if at least either one of the following criteria are satisfied:

- Structure's height is smaller than 10 m;
- Fundamental period is less than 0.4 seconds;
- Horizontal and vertical regular structures and a fundamental period less than 2 seconds.

By requiring that 92% of the base shear is distributed along the building height and the remaining 8% are applied at the top, some allowance for higher mode effects is made.

Further, it is required that specific modelling of the diaphragm with three-dimensional modal or time history analysis in case of irregular structures with more than 15 meters height is carried out. In general, diaphragm actions need to account for overstrength and higher mode effects. The commentary of the code (Standards New Zealand 2004b) recommends the pseudo Equivalent Static Analysis (pESA) discussed later. Further information on this method will be provided in the upcoming amendment of the commentary.

The commentary of the former New Zealand Loading Standard NZS 4203 (Standards New Zealand 1992) implied that in-plane forces in diaphragms can be evaluated using the provision for part and components. These approach, however, was not intended for the determination of the diaphragm force demand (Park et al. 1997) and is no longer allowed.

5.2.2.2 New Zealand Concrete Structures Standard NZS 3101

The former New Zealand Concrete Structures Standard NZS 3101 (Standards New Zealand 1995) implied that diaphragm forces are derived by applying an overstrength factor to the forces derived from an equivalent static analysis. In the current version of NZS 3101 (Standards New Zealand 2006), this has been removed and no provisions regarding diaphragm actions are given. In the appendix amplification factors to account for higher modes and overstrength for the determination of wall shears and frame column shears are provided. The suitability of

these factors for the determination of floor forces in multi-storey timber buildings will be discussed later in this chapter.

5.2.2.3 Eurocode 8 - EN1998-1-1

Eurocode 8 (Eurocode 8 2004) allows for the use of the ESA in order to determine the structure's base shear and floor forces for cases where higher mode effects are not expected to alter the dynamic behaviour of the structure. If such effects are considered substantial, a tri-dimensional modal response spectrum analysis is required.

The code prescribes the application of overstrength factors when determining diaphragm forces. Provided values however are not normative and are valid for concrete diaphragms only.

5.2.2.4 Minimum design loads for buildings and other structures ASCE 7-10

ASCE 7-10 (ASCE 2010) allows for different type of analysis methods based on the structure's height, the seismic design category, the structural system and the structure's regularity. Independently if an equivalent static or a response spectrum analysis is used to determine the forces in the lateral load resisting system, the diaphragm demand needs to be evaluated with specifically provided equations. The procedure accounts for the fact that the single diaphragm can be exposed to higher forces than the lateral load resisting system (see Figure 5.1). Upper and lower limits to the equation are independent from the ductility and the type of lateral load resisting system. The lower bound considers effects from higher modes which do not contribute in the base shear which are often the governing factor for structures with a high period or a high ductility. The upper bound normally governs structures with a short period or with limited ductility and represents nearly elastic response. For the design of the collector beams and the diaphragm connections to the lateral load resisting system special load combinations including overstrength factors are provided.

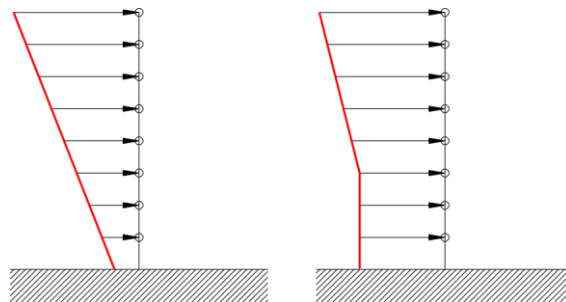


Figure 5.1 Force distribution in the lateral load resisting system (left) and on floor diaphragms (right) (Sabelli et al. 2009)

5.2.3 Methods from current research

5.2.3.1 New Zealand Concrete Society Technical Report No 20

The diaphragm chapter of the New Zealand Concrete Society Technical Report No 20 (Park et al. 1997) written by Bull requires that diaphragms are designed for the overstrength of the lateral load resisting system when designed for ductile behaviour. To avoid inelastic deformation demand in the diaphragms, capacity design principles need to be applied to the diaphragms. This conservative approach was justified since very large peak forces at a certain level of the structure can occur because of higher mode effects.

Because this method does not account for higher mode effects, but only consider capacity design principles, Fleischman (2014) considers this approach as not conservative.

5.2.3.2 Pseudo Equivalent Static Analysis

Bull (2004) and Gardiner et al. (2008) extended the above mentioned procedure in conjunction with the use of the ESA. This new procedure, the pseudo Equivalent Static Analysis (pESA), is based on the static forces from the ESA, which are amplified by the overstrength factor of the structure. Since the ESA however under-predicts the diaphragm forces at lower storeys, an effect also found in the parametric analysis in Chapter 4 of this thesis, forces based on the peak ground accelerations are to be considered as shown in Figure 5.2.

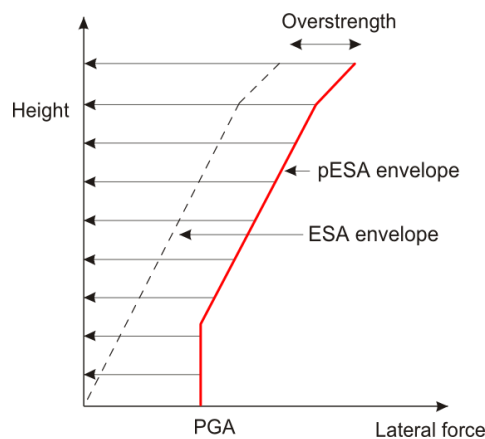


Figure 5.2 Static forces for ESA and pESA envelopes (modified from Gardiner et al. (2008))

The pESA was developed as a desktop method, able to predict both inertia and transfer forces in diaphragms. The approach provides equilibrium and allows the definition of clear load paths, enabling the design of all involved elements and connections. Gardiner et al. (2008) compared results of the pESA with NLTH analysis results of regular concrete perimeter frame

structures. It was shown that the diaphragm forces at lower storeys are reasonably well predicted for frame structures with less than 9 storeys. For taller structures the method over-predicted the floor forces. The method has recently been included in the 2015 Draft Amendment for the Commentary of New Zealand Earthquake Loading Code (Standards New Zealand 2015) as a simple tool for the determination of concrete diaphragm forces.

5.2.3.3 Pseudo Equivalent Static Analysis

The pESA introduced above was further extended and tested by Gardiner (2011) in order to determine floor forces in multi-storey structures with frames developing beam sway mechanisms as well as in dual systems with frames and walls. Corrected displacements determined with the pESA can be applied to the structure to determine transfer forces.

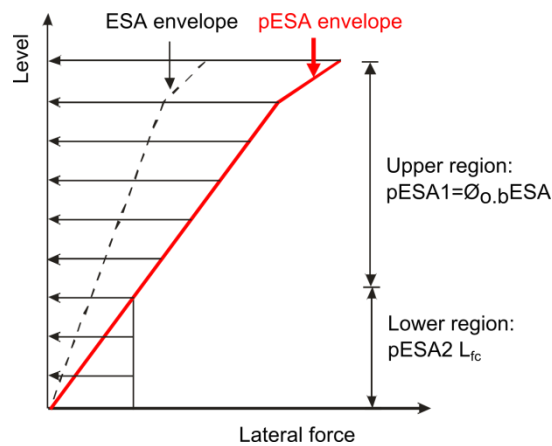


Figure 5.3 Static forces for ESA and pESA envelopes (modified from Gardiner (2011))

For the extended pESA method the forces in the upper region are found by amplifying the forces from the ESA by the overstrength factor of the lateral load resisting system. In the lower region the floor forces are determined by multiplying the floor weight by a factor depended on the PGA, the soil type, the fundamental period and the type of lateral load resisting system (frame or dual structure).

Unfortunately, no information on the applicability of the pESA has been given for structures made of other materials than reinforced concrete. Higher mode effects tend to be higher in such cases as shown in later sections and the sole application of the overstrength factor might not be sufficient to include dynamic effects (Fleischman 2014).

5.2.3.4 First mode reduced method

The first mode reduced method (Rodriguez et al. 2002) was developed based on parametric numerical investigations of cantilevered wall structures and allows for the determination of floor forces in the case of rigid diaphragms. The method is based on the assumption that only the accelerations associated with the first mode of vibration are affected by the ductility of the structure. The acceleration at an arbitrary floor can be derived under the consideration of the modal participating factors, the mode shapes, periods of vibration, damping ratios and the design spectrum. In order to avoid a full modal analysis, the method has been further simplified by accounting that higher mode effects are almost independent from the level of ductility, that all modes have the same damping ratio and that all higher modes have periods corresponding to the maximum spectrum ordinate.

5.2.3.5 Modified part and component

This proposed method by Cowie et al. (2014) is based on the ‘part and component’ method of NZS 1170.5 (Standards New Zealand 2004a) and findings from Uma et al. (2009). In the latter the part and component coefficient has been found to be overly conservative and therefore a constant factor for all storeys of 1.6 was proposed. The method is deemed to provide good estimates for inertia forces acting on diaphragm where transfer forces are not expected. The diaphragm force F_{diap} at a level i can be calculated as

$$F_{diap} = C_{diap}W_i; \quad (5.1)$$

$$C_{diap} = C_{h\ modal}(T_1 = 0)ZRS_pC_{h\ diap}; \quad (5.2)$$

where

W_i	diaphragm mass at level i ;
$C_{h\ modal}(T_1 = 0)$	spectral shape factor at $T = 0$ s for the modal response spectrum analysis;
Z	hazard factor;
R	return period factor;
S_p	structural performance factor;
$C_{h\ diap}$	= 1.6.

For transfer diaphragms the storey forces derived from the overstrength of the lateral load resisting system are added by means of a SRSS rule to the force demand determined with the modified part and component method.

5.2.3.6 *Modified response spectrum analysis*

For regular tall buildings without significant irregularities, Scarry (2015) suggested to carry out response spectrum analysis. Results are to be linearly increased so that the obtained base shear corresponds to the values obtained by the ESA. From the storey shears, the floor forces and therefore floor accelerations can be obtained. These values are then amplified by the building overstrength factor. The obtained forces consider higher mode effects as well as increased demand at lower storeys. This method avoids the potentially higher inertia forces at upper levels, caused by applying the 8% of the base shear at the top storey.

5.2.3.7 *Design procedure for perimeter lateral-system structures with highly flexible diaphragms*

Due to the failure of a number of parking structures made of precast concrete diaphragms and perimeter lateral load resisting system during the 1994 Northridge Earthquake, Fleischman et al. (2002) investigated the behaviour of such structures with flexible diaphragms designed under current design provisions. Analytical results showed that diaphragm flexibility caused very large drifts which could potentially damage gravity elements. Further, it was shown that large ductility demands in diaphragms could occur and that floor forces in wall structures were much larger than predicted by design methods.

Based on this preliminary analysis, the authors provide the following design recommendations:

- all diaphragms shall be designed in order to have the same strength;
- in the case of wall structures, provided overstrength values guarantee elastic diaphragm behaviour for Design Based Earthquakes (DBE); for Maximum Credible Earthquakes (MCE) the diaphragm's ductility level is reached;
- For frame structures, diaphragms are to be designed based on the top storey force demand;
- The contribution of the diaphragm flexibility shall be included in the structure's drift calculations.

5.2.3.8 *Seismic Design Methodology for Precast Concrete Diaphragms*

The work by Fleischman et al. (2002) has been further advanced together with other universities to develop a new design methodology for precast concrete diaphragms to be implemented in future code provisions. The Diaphragm Seismic Design Methodology (DSDM) (Fleischman et al. 2005; Fleischman et al. 2013; Fleischman 2014) research consortium carried

out multiple degree of freedom dynamic analysis, finite element pushover tests, shake table tests, component test and model calibrations. The provided performance based design methodology intends to provide diaphragm designs which have a measure of deformation capacity so to avoid uneconomic elastic designs. The approach does not intend to create diaphragms contributing to the structures' dissipation.

The developed performance based design philosophy allows for different diaphragm seismic design levels and three different design options ranging from an elastic design (elastic behaviour for a MCE), a basic design (elastic behaviour for a DBE) to a reduced design option (inelastic behaviour for a DBE). The choice of the design option depends on the connector classification which can be of limited, medium or high ductility. The diaphragm demand is considered maximum at the upper and lower storeys with some reduction in the middle storeys of the structure. For the different design options, diaphragm force amplification factors are provided. These are based on the diaphragm length, floor aspect ratio and number of storeys. Further are shear overstrength factors and drift amplification factors provided. Based on the determined demand, diaphragm internal forces and respective reinforcement can be determined and the diaphragm stiffness checked in order to avoid excessive drifts.

The design procedure has been further simplified in order to be applicable to the proposal IT06-001 for the 2014 version of the ASCE 7 provisions. It is interesting to note that the results from the First Mode Reduced Method (Rodriguez et al. 2002) are equal to the basic design option presented in this methodology.

5.2.3.9 Elastic design of precast and cast-in-place concrete diaphragms

The report by Nakaki (2000) shows that current code provisions in terms of floor diaphragm forces and floor aspect ratio limitations are not able to guarantee elastic diaphragm designs. A simplified method was proposed which accounts for diaphragm flexibility in the dynamic behaviour of the structure. It is suggested that the structure's overstrength needs to be accounted when determining diaphragm forces. When checking the lateral deformation of a structure, the elastic deformation of the diaphragm needs to be added to the inelastic deformations of the lateral load resisting system.

5.3 TRANSFER FORCES

Aside from the floor inertia forces, which result from the acceleration of the floor masses, transfer forces can arise in buildings as a cause of deformation incompatibility between the

different lateral load resisting systems. As can be seen in Figure 5.4 for a dual system with a frame and a wall, a sort of ‘fighting’ occurs by the linking action of the diaphragm as it connects frames and walls, which deform in a shear and a flexural mode respectively (Paulay and Priestley 1992). The walls govern the structural behaviour at the lower levels and the frames govern at the upper levels, causing negative forces (opposite the inertia forces) at the upper levels.

These transfer forces, sometimes also denominated compatibility forces, can be substantial in the case of dual systems where frame and walls are of similar stiffness and the structure has more than 3 storeys (Gardiner 2011). For structures where one or both lateral load resisting systems have a low stiffness, transfer forces are significantly reduced. According to Bull (2004), that transfer forces will develop in every diaphragm to a certain extent; this is because lateral load resisting systems seldom are symmetric in geometry and stiffness. This can be the case of walls with different lengths and therefore different stiffnesses.

Another very common form of transfer forces can be found in podium structures, where an upper structure with a smaller footprint sits on a larger, stiffer structure. All lateral forces from the tower need to be transferred through the top diaphragm of the podium to the lateral load resisting system of the podium. The diaphragm therefore needs to resist very large forces.

Large transfer forces can also result from set-backs up the height of the structure, or other vertical irregularities, such as offset or missing walls.

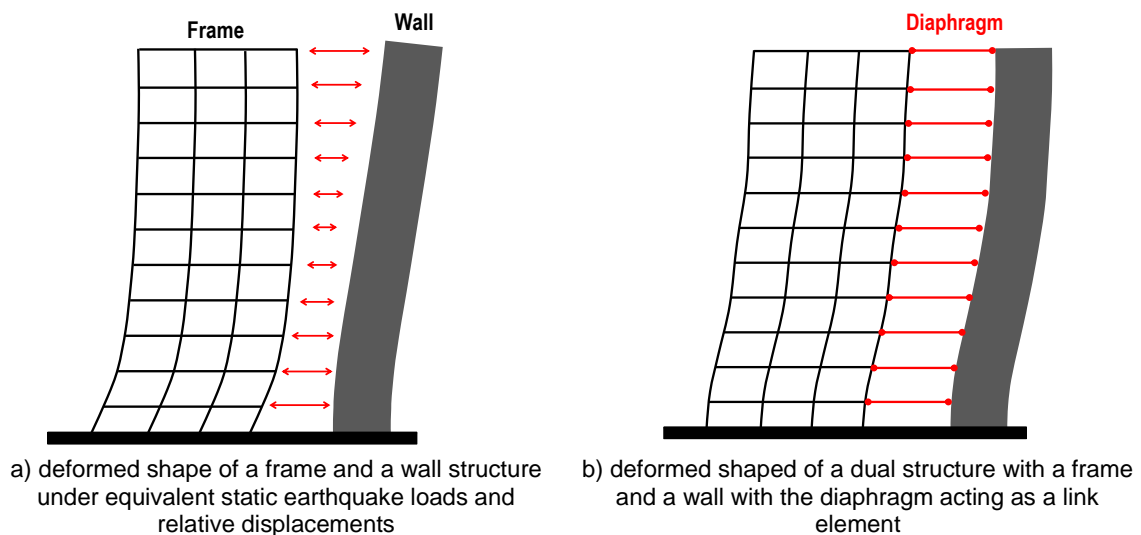


Figure 5.4: Deformation pattern for frame and wall elements

Time history analysis by Gardiner et al. (2008) showed that transfer forces can also be many times higher than inertial forces. The most accurate way to determine transfer forces is by

non-linear time history analysis and by modelling the real stiffness of the lateral load resisting system and the diaphragms. The stiffer the diaphragm, the higher the transfer forces, as displacement incompatibilities are not ‘attenuated’ by the deformation capability of the diaphragms and connectors.

As stated by Bull (2004) and confirmed by Gardiner (2011), inertia and transfer are related. Once storey masses are accelerated, the structure deforms and displacement incompatibilities create transfer forces. The maximum values of these forces however can occur at different instances during an earthquake. It is therefore not correct to apply the maximum inertia forces from a response spectrum analysis or as an envelope of a time history analysis to the whole structure. It has been shown that the forces obtained by the pseudo Equivalent Static Analysis developed by Bull (2004) and Gardiner (2011) can be applied to the lateral load resisting system in order to determine transfer forces.

Another method employed by Sabelli et al. (2011) in order to determine both inertia and transfer forces is to carry out a separate analysis for each floor level. First the forces from the ESA are applied to the lateral load resisting system, then for each level under consideration the lateral force is replaced by the diaphragm force as calculated by the ASCE 7-10 code (ASCE 2010) as shown in Figure 5.5c-f. A similar method which also considers force redistribution can be found in Sabelli et al. (2009).

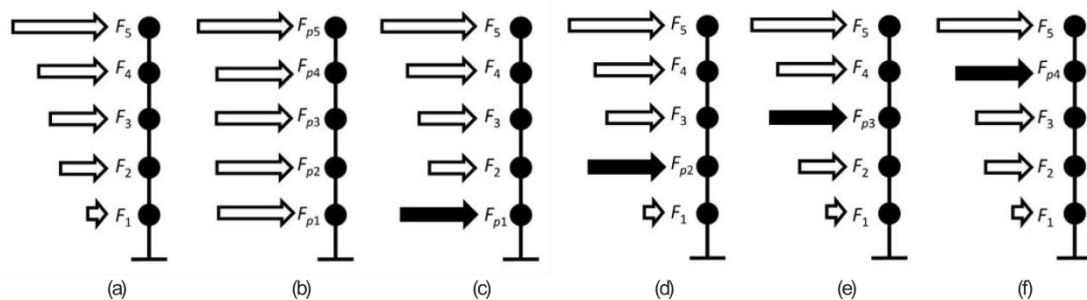


Figure 5.5: Vertical force distribution with diaphragm forces with a) lateral load distribution from ESA, b) diaphragm forces according to ASCE 7-10, c-f) force combinations in order to obtain diaphragm inertia and transfer forces (Sabelli et al. 2011)

As mentioned above, Cowie et al. (2014) suggested to account for transfer forces by combining the diaphragm forces from the modified part and components formulation with the diaphragm forces obtained from the overstrength of the lateral load resisting system with the SRSS rule.

Because of the inherent flexibility of timber diaphragms, as will be discussed in the next chapters, smaller transfer forces are expected to develop. Cobeen et al. (2014) therefore also state that transfer forces due to smaller changes in wall stiffness can be neglected in design.

Currently no design method for dual timber structures is available and therefore the transfer forces in such system could not be evaluated by time history analyses. In the case of multi-storey structures where substantial transfer forces are expected, the use of Sabelli's method together with the peak diaphragm forces as discussed later in this chapter could be used. Clearly more research on this topic is necessary.

5.4 ELASTIC versus DUCTILE DIAPHRAGM DESIGN

Diaphragms are a primary element in resisting lateral loads in structures and as such must be designed to withstand all actions and displacements potentially occurring during a seismic event. If diaphragms are to be design to work in the elastic range, overstrength and dynamic amplification factors as discussed in section 5.2.3 need to be applied. If diaphragms are allowed to yield, their force demand can be decreased as discussed in Fleischman (2014) and dynamic amplification factors can be reduced. Since no general design procedure for ductile timber diaphragms exist, conservative force demands based on overstrength and dynamic amplification should be considered as discussed next. As an exception, the Canadian timber design code (Standards Council of Canada 2014) allows yielding diaphragms in case of lateral load resisting system made of materials other than timber. For the determination of the diaphragm forces demand no reduction is applied but the overstrength or overcapacity factors from the lateral load resisting system can be taken as unity.

Since inelastic deformations in a diaphragm can compromise not only the diaphragm performance but also all other structural elements attached to it, it is recommended that diaphragms are designed to perform in the elastic range. Such recommendation can also be found in other specific literature (Smith et al. 1986; Tremblay and Stierner 1996; Prion 2003) and is implemented in design codes like the New Zealand Earthquake Loading Code NZS1170.5 (Standards New Zealand 2004a). Limited ductility is only allowed in confined areas and shall not compromise the force path in the diaphragms. The inelastic behaviour of the diaphragm shall not be considered as a source of additional structural damping. This can be explained by the fact that highest diaphragm forces can be measured close to the supports with decreasing values at mid-span. To achieve a uniform fastener yielding and a stable damping, a staggered fastener setup along the diaphragm length would be necessary, a solution seldom adopted in construction practice. If only the fasteners at the supports yield, a potential 'soft diaphragm' mechanism could develop, where the diaphragm would fail similarly as in a soft storey mechanism.

Capacity design principles have already been proposed in the past (Park et al. 1997) in order to achieve elastic diaphragm designs. After the 1994 Northridge Earthquake effort was put to provide prescriptive design procedures in order to guarantee the elastic behaviour of concrete diaphragms based on capacity design principles and code provisions (Nakaki 2000). It was however shown by several other researchers (Fleischman and Farrow 2001; Rodriguez et al. 2002; Lee et al. 2007) that forces at individual floor levels can be much higher than predicted by such an approach. This behaviour due to higher mode effects could be observed in the frame and wall structures analysed in Chapter 4. Finally it has been shown that large floor forces can also develop after the yielding of the lateral load resisting system, where the dynamic properties of the structure can significantly change (Fleischman and Farrow 2001; Fleischman 2014).

For timber structures such studies are still missing and the findings from Chapter 4 are limited to only a small number of structures, design ductility levels, structural systems and diaphragm flexibilities. For the elastic design of diaphragms it is suggested to consider the overstrength of the lateral load resisting system and in case of taller structures a dynamic amplification due to higher mode effects. An approach to determine diaphragm forces including higher mode effects based on Priestley et al. (2007) is shown later in this chapter. A discussion on available overstrength values for timber structures can be found in Chapter 3. A clear and complete definition of such factors for a wider range of structural timber systems is still missing.

In cases where elastic diaphragm design is considered as either uneconomical or cannot be carried out, a design procedure for precast concrete diaphragms by Fleischman (2014) allows for inelastic diaphragm behaviour. A similar proposal with fuse type connections was proposed by Vides and Pampanin (2015). To achieve the expected diaphragm behaviour, panel connections need to possess a well-defined deformation capacity. Such approach could also be employed for timber diaphragms, considering the yielding behaviour of common timber fasteners. Further research including static and big scale dynamic testing would be required to develop an equivalent method for timber diaphragms.

In spite of the requirement for elastic design, the diaphragm as a whole should have sufficient ductility and ultimate deformation capacity to adhere to the basic requirement of collapse prevention under higher-than-expected seismic loading, either through non-linear behaviour of the connections to the lateral load resisting system or between panels. Similarly, when special buildings of high importance level are designed for a maximum considered earthquake

(MCE, 2500 years return period), some diaphragm yielding can be allowed, with designated ductile connections and prevention of brittle failures. Special analysis needs to be carried out if large portions of diaphragms are ever required to work in the inelastic range.

5.5 DETERMINATION OF SHEARS AND MOMENTS

The results from the time history analysis carried out in Chapter 4 have shown that the distribution of floor forces is greatly influenced by the effects of higher modes. The presence of diaphragm flexibility does affect the fundamental frequencies of the structure as well as the storey drifts, but the shear and moment distribution is less influenced and can be neglected for the structures analysed.

The methods by Nakaki (2000), Rodriguez et al. (2002), Fleischman et al. (2002), Bull (2004), Fleischman (2014) are all calibrated against concrete frame and wall structures and can therefore not directly be applied to timber structures. Results from the NLTH in Chapter 4 show that higher modes have a very large effect on timber buildings. This is due to the fact that the onset of yielding in timber structures is delayed because of large elastic displacements, influencing its non-linear behaviour (Buchanan and Smith 2015).

Pres-Lam structures, like the ones analysed in Chapter 4, are normally designed following a Displacement Based Design approach. Since the behaviour of the structure needs to be determined as exactly as possible, material properties are modelled as close as possible to reality, and therefore reducing sources of overstrength. Methods to determine diaphragm force demand based on overstrength factors only (Nakaki 2000; Bull 2004) therefore do not consider the amplification from higher mode effects and therefore potentially under-predict the force demand for flexible buildings.

In this chapter the storey forces from Chapter 4 are compared to the provisions for frame column and wall shear forces from the New Zealand Concrete Standard NZS 3101 (Standards New Zealand 2006), the approach proposed by Priestley et al. (2007), the modified parts and components method by Cowie et al. (2014) and the pESA (Bull 2004; Gardiner et al. 2008). Their applicability will be investigated to predict the force demand in multi-storey timber buildings. The concrete code approach has been suggested for implementation in the soon to be released new version of the New Zealand Timber Design Standard. The second approach was specifically developed for structures designed on the basis of the DBD approach and has

been modified and tested by Newcombe (2011) and Sarti (2015) for the use on Pres-Lam frame and wall structures respectively. Following these methods are introduced briefly.

Since the analyses were carried out using the same material specifications and moment-rotation behaviour as adopted in the design procedure, the overstrength factor is limited to rounding of section sizes and reinforcing dimensions, as well as the material reduction factor used in the design ($\phi = 0.9$). An overstrength factor of $\phi^o = 1.2$ has therefore been used.

5.5.1 Dynamic amplification according to the New Zealand Concrete Standard NZS 3101

Appendix D of the New Zealand Concrete Standard 3101 (Standards New Zealand 2006) provides methods for the determination of the amplified storey moments and shears in ductile frame and wall structures due to overstrength and higher mode effects. These methods are not specifically developed to estimate diaphragm forces, but the amplified top storey shear provides a measure of the maximum force to be expected in a diaphragm.

For frame structures the dynamic magnification factor for the column shear at the top storey is given by either

$$V_{col}^* = 1.15 \frac{(M_{oc,bottom} + M_{oc,top})}{H} \quad (5.3)$$

in case a plastic hinge forms in the top storey columns or by

$$V_{col}^* = 1.3\phi_o V_E ; \quad (5.4)$$

where

- V_{col}^* is the amplified column shear demand;
- $M_{oc,bottom}$ and $M_{oc,top}$ are the overstrength bending moments at the bottom and top of the column;
- H storey height;
- V_E shear in the column from ESA of first mode analysis;
- ϕ_o average overstrength factor in the beam-column-joint.

In the case of uniform wall structures the shear forces above the primary plastic hinge region can be calculated as

$$V_{col}^* = \omega_V \phi_o V_E ; \quad (5.5)$$

where

- ω_V is the dynamic shear magnification factor:
 $\omega_V = 0.9 + n/10$ for buildings up to 6 storeys, and
 $\omega_V = 1.3 + n/30 \leq 1.8$ for buildings over 6 storeys;
- n number of storeys;

ϕ_o	overstrength factor related to flexural actions $\phi_o = \frac{M_o}{M_{ESA}}$;
M_o	overstrength moment;
M_{ESA}	moment demand from ESA.

5.5.2 Priestley et al. (2007) and further modifications

With the Displacement Based Design (DBD) procedure moments and shears throughout the building can be determined based on the first mode of vibration. This is adequate to design the potential ductile elements like plastic hinges or the rocking behaviour of jointed ductile elements since their forces are defined and governed by the first mode values, reduced by the expected ductility and damping. Remaining elements are subjected to effects deriving from higher modes and need to be protected according to capacity design principles. Under inelastic behaviour, overstrength and overcapacity will be developed in the potential ductile elements and all moments throughout the structure will increase in proportion. This form of capacity design can conventionally be written as

$$\phi_s S_D = S_R = \phi^o \omega S_E ; \quad (5.6)$$

where

ϕ_s	is the strength reduction factor;
S_R	is the required dependable strength;
ϕ^o	is the overstrength factor to account of the flexural overcapacity in the potential plastic hinge region;
ω	is the dynamic amplification factor.

Amplification for concrete frame structures:

The required column flexural strength for concrete frame structures can be estimated by

$$\phi_f M_N \geq \phi^o \omega_f M_E ; \quad (5.7)$$

where ω_f depends on the structure's height and ductility μ and is

$$\omega_f = 1.15 + 0.13 \left(\frac{\mu}{\phi^o} - 1 \right) \quad (5.8)$$

from the first storey to $\frac{3}{4}$ of the total height of the structure and 1 at the base and the top storey.

The frame column shear can be obtained by

$$\phi_s V_N \geq \phi^o V_E + 0.1 \mu V_{E,base}; \quad (5.9)$$

where

V_E	is the shear value found from the lateral force distribution;
$V_{E,base}$	is the base shear value from the DBD process.

Modification of the amplifications formulation for Pres-Lam frame structures

Previous equations have been altered by Newcombe (2011) based on non-linear time history analysis of Pres-Lam frames. Equation (5.8) was modified to

$$\omega_f = 1.15 + 0.25 \left(\frac{\mu}{\phi^o} - 1 \right) \quad (5.10)$$

and Equation (5.9) is written in function of the moment demand as

$$\phi_s V_N \geq \phi^o V_E + (\omega_f - 1) \frac{M_E}{H}; \quad (5.11)$$

where

H is the interstorey height; and
 M_E is the average of the interstorey moment at the bottom and top of each column.

Amplification for concrete wall structures

For cantilevered concrete wall structures, Priestley et al. (2007) suggest a bilinear capacity design envelope for the storey moments. The envelope is defined by the overstrength moment $\phi^o M_B$ at the base, the moment $M_{0.5H}^o$ at mid-height and zero at the top of the wall. The mid-height moment is defined as

$$M_{0.5H}^o = C_{1,T} \phi^o M_B; \quad (5.12)$$

$$C_{1,T} = 0.4 + 0.075 T_i \left(\frac{\mu}{\phi^o} - 1 \right) \geq 0.4; \quad (5.13)$$

where

T_i is the elastic fundamental period of the wall.

The shear force capacity design envelope is defined by the amplified base shear force as

$$V_B^o = \phi^o \omega_V V_{E,base}; \quad (5.14)$$

$$\omega_V = 1 + \frac{\mu}{\phi^o} C_{2,T}. \quad (5.15)$$

$$C_{2,T} = 0.067 + 0.4(T_i - 0.5) \leq 1.1; \quad (5.16)$$

And the shear force at the top of the wall as

$$V_n^o = C_{3,T} V_B^o; \quad (5.17)$$

$$C_{3,T} = 0.9 - 0.3 T_i \geq 0.3. \quad (5.18)$$

Modification of the amplification formulation for Pres-Lam wall structures

Based on a series of a parametric non-linear time history analysis of Pres-Lam walls, Sarti (2015) refined above equations. In order to determine the moment capacity design envelope Equation (5.13) is modified to

$$C_{1,T} = 0.4 + 0.2(T_i - 0.4) + 0.1(T_i - 0.4) \left(\frac{\mu}{\phi^o} - 1 \right) \geq 0.4 . \quad (5.19)$$

The shear envelope found by Priestley et al. (2007) was found to be appropriate for timber Pres-Lam walls.

5.5.3 Dynamic amplification of shear forces, moments and diaphragm forces in frame structures

The shear force and moment envelopes defined from the equations above are compared to the maximum values from frame and wall structures analysed in Chapter 4. Since the diaphragm flexibility did not substantially alter the shear force and moment distribution, only the maximum values between the rigid, semi-rigid and flexible diaphragm options are considered below.

5.5.3.1 Prediction of shear forces in frame structures

Figure 5.6 shows the peak shear forces from the non-linear time history analysis. These values are compared to the ESA values and the envelopes according to Priestley et al. (2007) and Newcombe (2011). The envelopes according to Priestley et al. (2007) predict the moment shears relatively well for lower storeys, for upper storeys values are however slightly underpredicted. This shortcoming is taken into account in the proposed formulation for the estimation of the diaphragm forces as discussed later. The envelopes by Newcombe (2011) tend to underpredict the shear values.

For the determination of the envelope, the ductility factor μ is only of influence if damping is added to the structure. The pure change of stiffness is not influencing the effects of higher modes on the structure. For the non-dissipative frame structures, the ductility factor μ is therefore taken as 1.

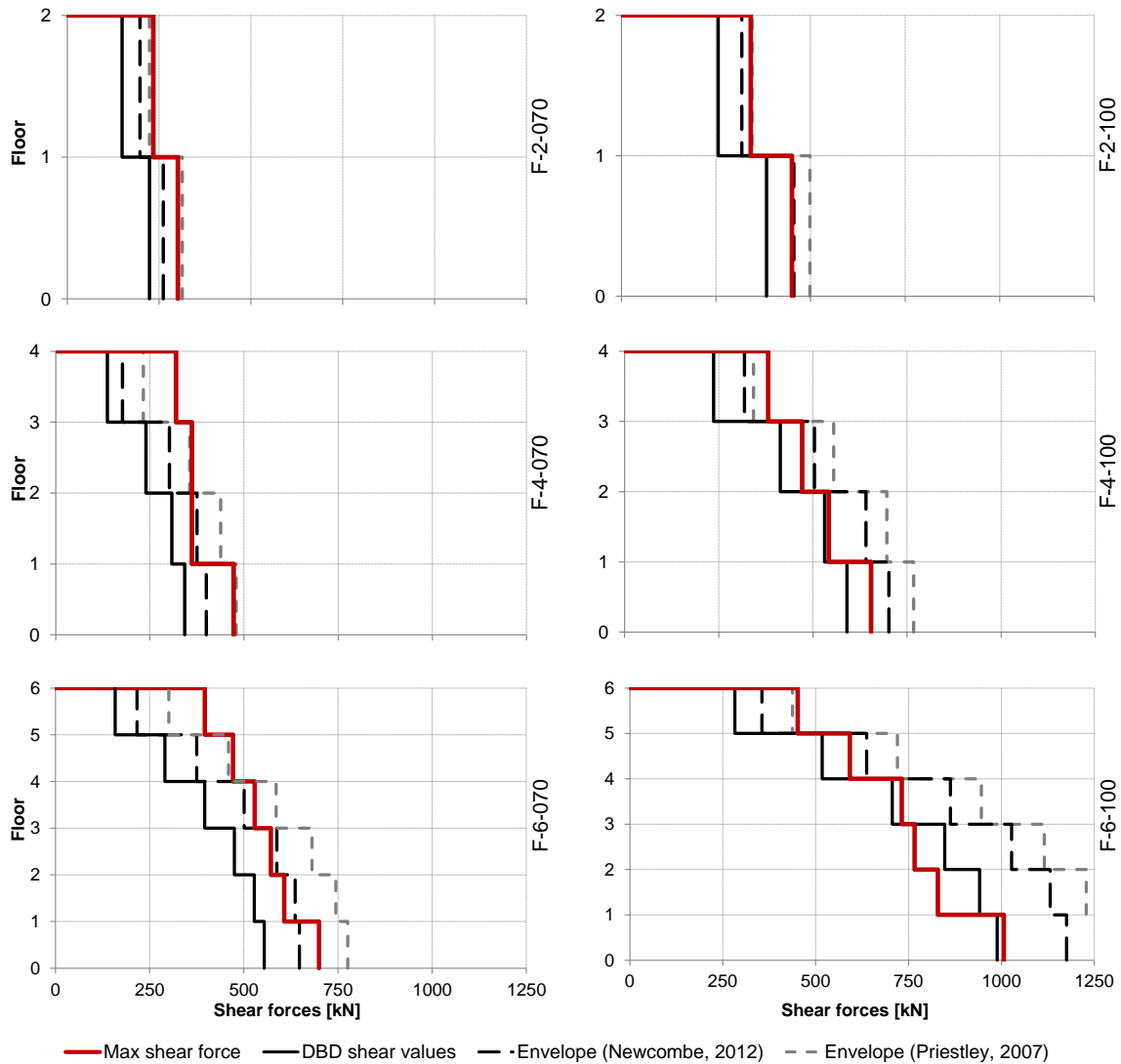


Figure 5.6 Maximum storey shear forces from the NLTH and suggested envelopes for frame structures

5.5.3.2 Prediction of moments in frame structures

Measured and calculated column base moments show good agreement; this is because there is no amplification at the base of the structure since it is controlled by the moment capacity. The increased moment demand and middle storeys because of higher modes is well captured by the envelopes for taller structures, only for frame F-6-100 suggested values are somewhat conservative. Top storey column moments are slightly underpredicted for taller structures.

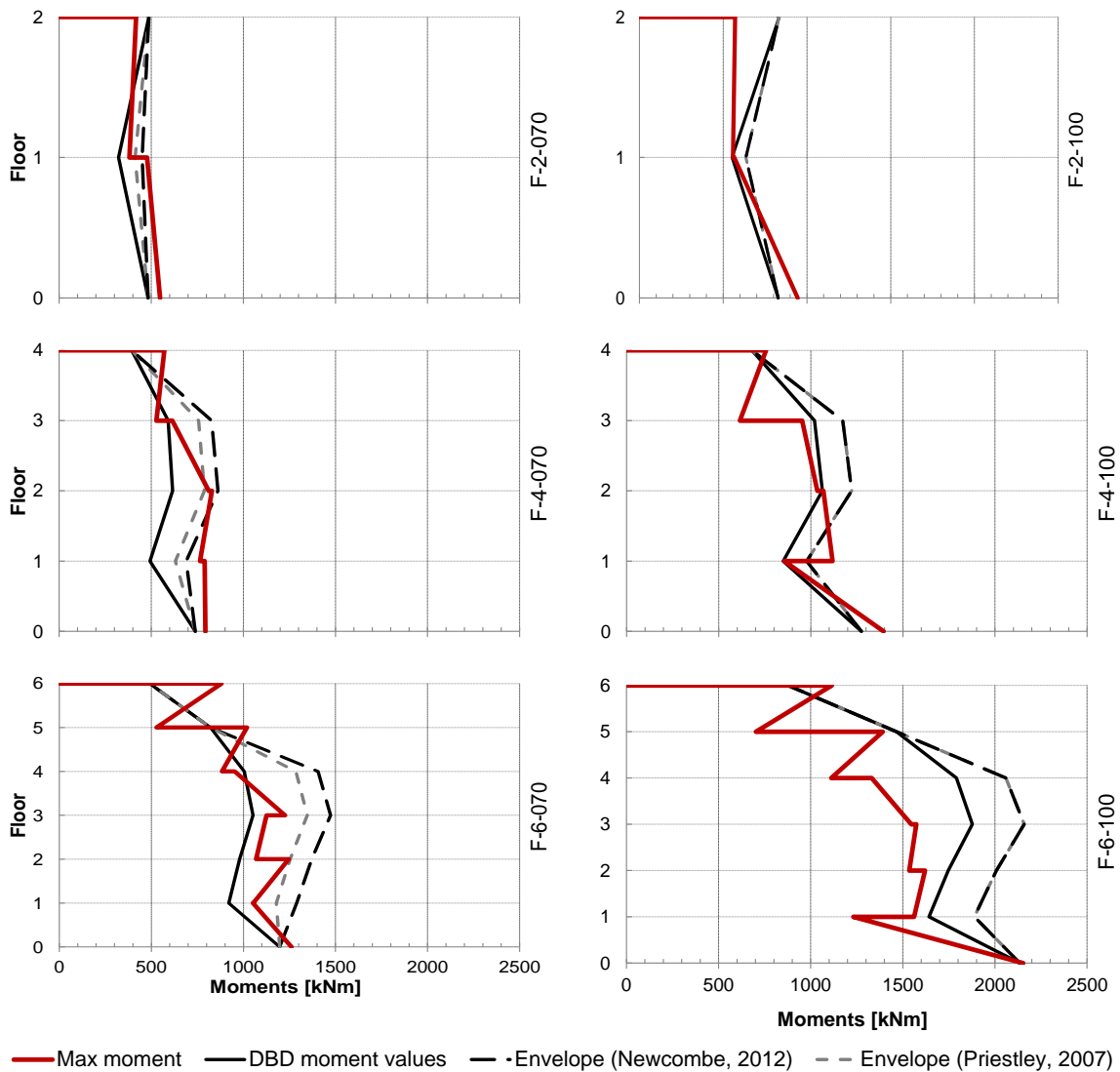


Figure 5.7 Maximum moments from the NLTH and suggested envelopes for frame structures

5.5.3.3 Prediction of floor forces in frame structures

Figure 5.8 shows the peak floor forces at the individual floor levels. As discussed in Chapter 4, these are maximum values and do not occur at the same instant in time during a ground motion. These results are only to be used to determine the largest force in any of the diaphragms in the structure when subjected to a design earthquake.

It can be seen that the diaphragm flexibility is not significantly influencing the maximum diaphragm demand. It is also clearly visible that the force distribution does not follow the expected first mode distribution. The almost constant force pattern along the structure's height can be attributed to higher mode effects, which mostly affect the lower half of the structures.

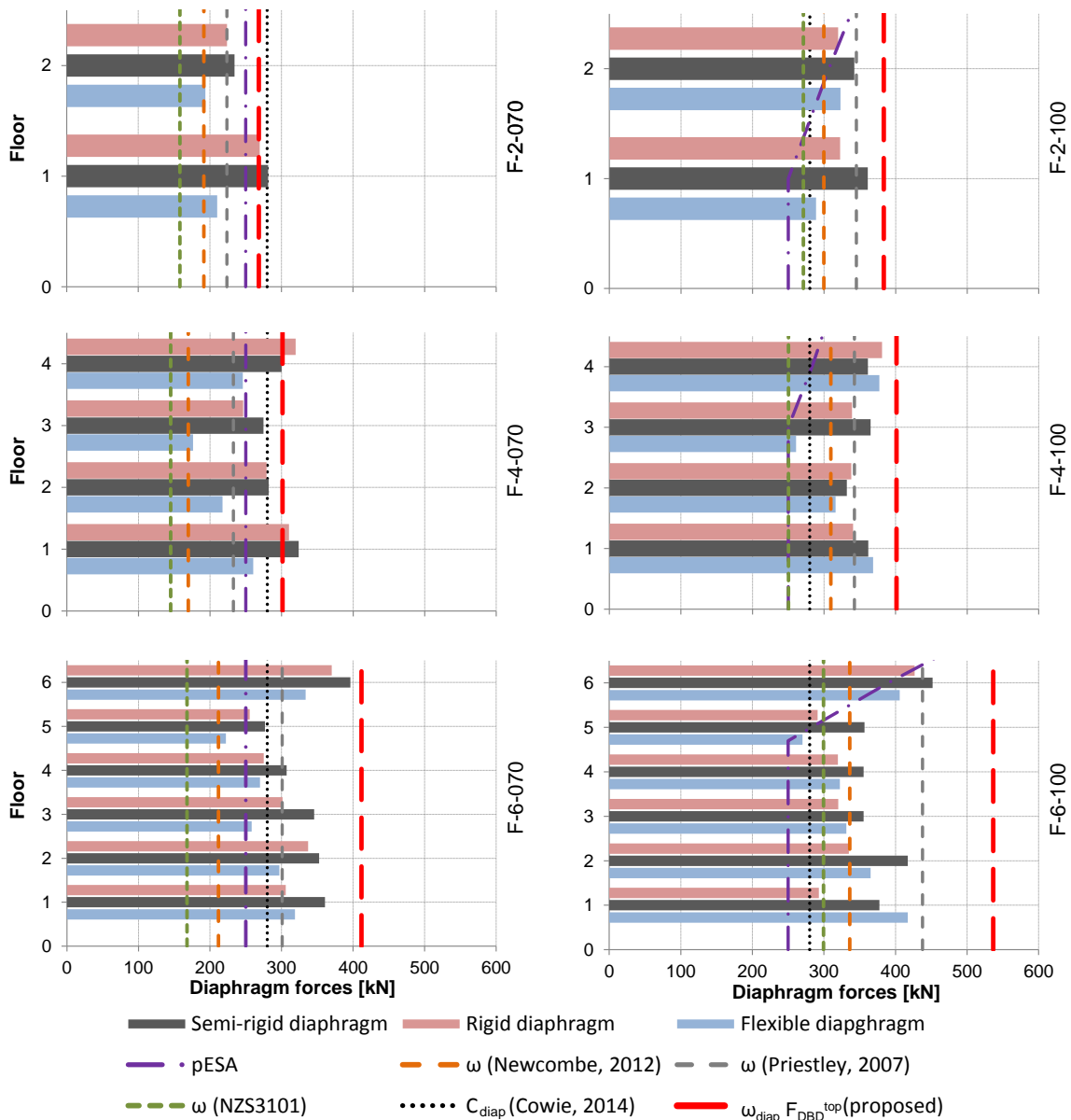


Figure 5.8 Diaphragm forces from the NLTH and suggested design values for frame structures

Figure 5.8 shows that the forces obtained by the New Zealand Concrete Code provisions for frame structures are not able to capture the dynamic amplification and are not suggested for timber frame structures. The original equations by Priestley et al. (2007) and the modified equations by Newcombe (2011) underpredict the diaphragm forces for most structures, only for the non-dissipative frame structure can former predict maximum values accurately. Similarly are diaphragm demands determined by the pseudo Equivalent Static Analysis and the method according to Cowie et al. (2014) underestimating the peak values as determined by the time history analysis.

For frame structures it is therefore suggested to design all floor diaphragms with the same strength considering a maximum estimated force demand. It is suggested to determine this demand by the following equation

$$E_{diap}^* = \phi^o V_{E,top} + 0.2\mu V_{E,base} ; \quad (5.20)$$

where

- E_{diap}^* is the diaphragm force demand;
- ϕ^o is the overstrength factor of the lateral load resisting system;
- μ ductility of the structure;
- $V_{E,top}$ is the shear value at the top storey found from the ESA;
- $V_{E,base}$ is the base shear value from the DBD procedure.

Equation (5.20) has been modified from Equation (5.9) as defined in Priestley et al. (2007) by increasing the multiplier of the base shear value from 0.1μ to 0.2μ . It is reminded that for the non-damped structures the ductility needs to be taken as 1.

Table 5.1 shows the measured and proposed diaphragm amplification factors ω_D defined as the ratio between the maximum measured floor force from the numerical analysis and the top storey force from the ESA. For the slender F-6-070 frame structure the diaphragm demand can be up to 2.5 times the top storey equivalent static force. The proposed values derived by Equation (5.20) predict the diaphragm force amplification very well, with some minimal non-conservatism for dissipative structures F-2-070 and F-4-070.

Table 5.1 Diaphragm amplification factors for the frame structures with varying diaphragm flexibilities

ID	measured ω_D			Average	proposed ω_D
	Rigid	Semi-rigid	Flexible		
F-2-07	1.8	1.9	1.4	1.7	1.8
F-4-07	2.3	2.4	1.9	2.2	2.2
F-6-07	2.3	2.5	2.1	2.3	2.7
F-2-100	1.3	1.4	1.3	1.3	1.4
F-4-100	1.6	1.5	1.6	1.6	1.7
F-6-100	1.5	1.6	1.5	1.5	1.9

5.5.4 Dynamic amplification of shear forces, moments and diaphragm forces in wall structures

5.5.4.1 Prediction of shear forces in wall structures

Figure 5.9 shows the wall shear forces from the numerical analysis along with the ESA distribution according to the DBD design base shear and the envelopes according to Priestley et al. (2007).

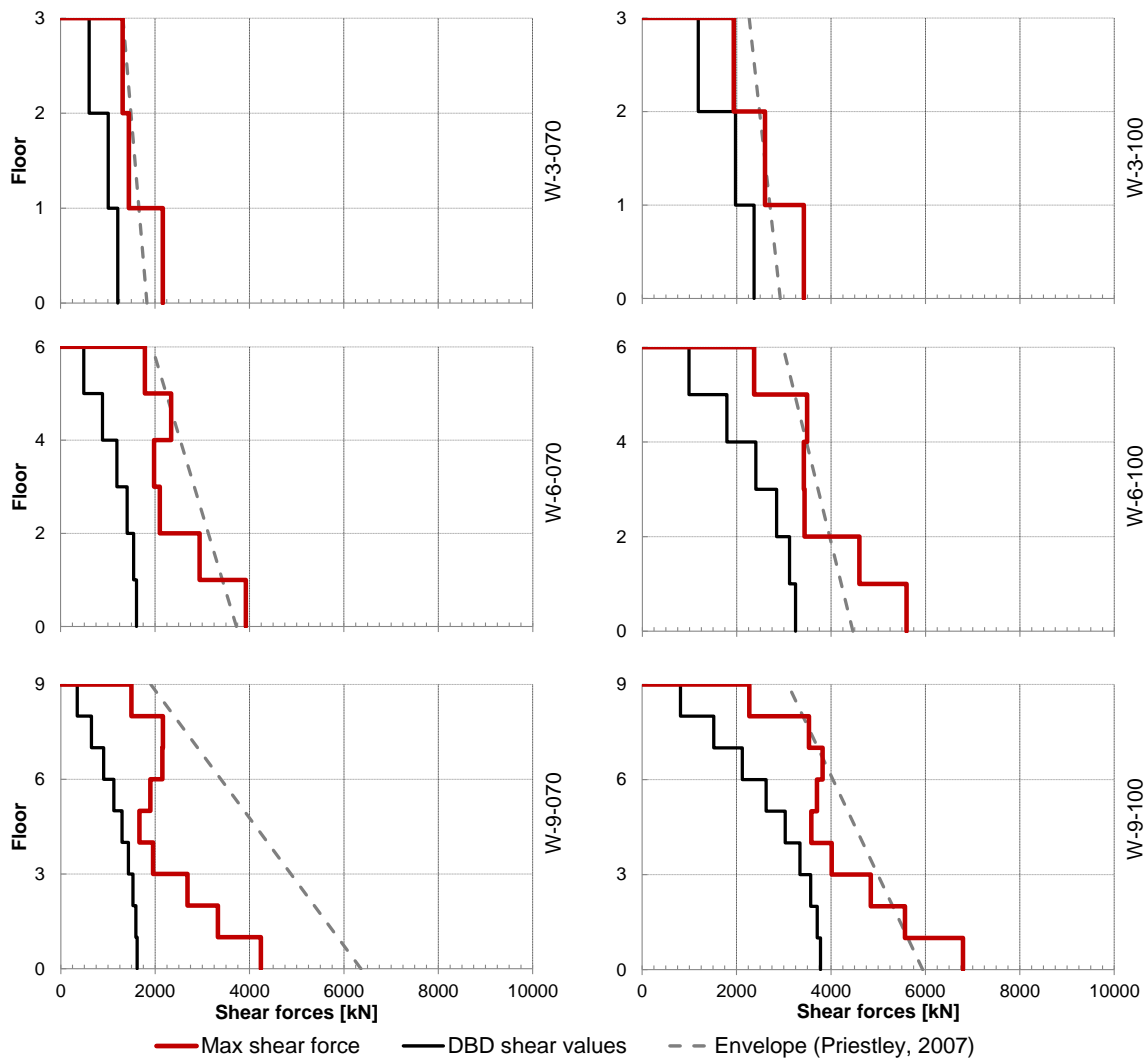


Figure 5.9 Maximum storey shear forces from the NLTH and suggested envelopes for wall structures

It can be clearly seen that higher modes significantly alter the base shear and storey shear force distribution. The suggested envelope predicts the peak values reasonably well with some conservatism for the 9 storey structures. For the non-dissipative structures the base shear is slightly underestimated for all cases.

Also for the non-dissipative wall structures, the ductility factor μ was set as 1 for the non-dissipative structures.

5.5.4.2 Prediction of moments in wall structures

Wall base moments are not amplified by higher modes since they are governed by the moment capacity at the wall-foundation interface. Interestingly a reduction for very tall structures can be seen caused by the presence of higher modes. At the same time it can be observed that the moments at mid-height are notably increased. This effects is almost absent for the wall structures with only 3 storeys, where higher modes have almost no influence.

Figure 5.10 shows the moment envelopes from Priestley et al. (2007) and Sarti (2015). Both methods slightly underpredict the moments for the short to medium structures. Better estimates were found for the taller structures.

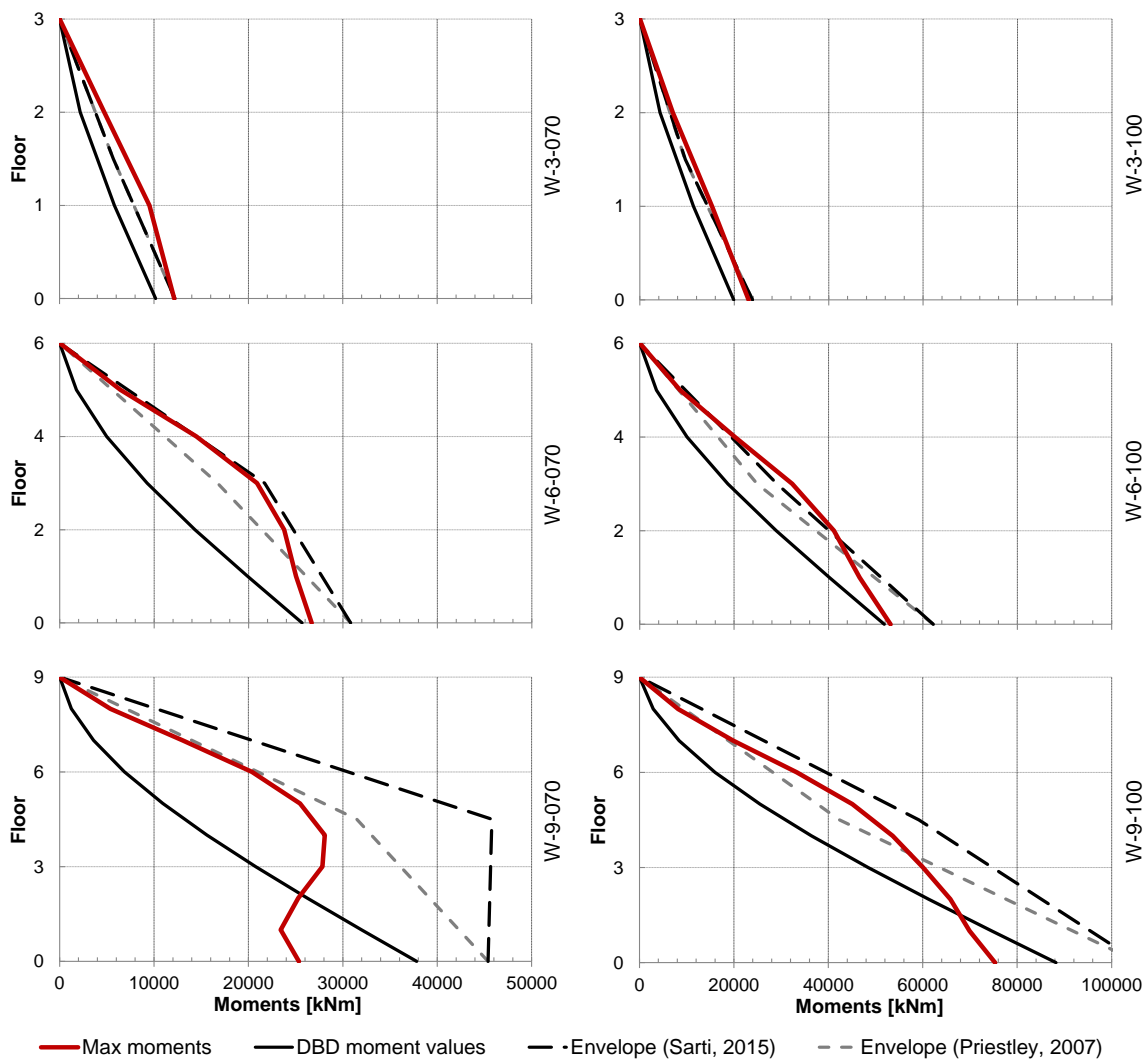


Figure 5.10 Maximum moments from the NLTH and suggested envelopes for wall structures

5.5.4.3 Prediction of floor forces in wall structures

Figure 5.11 shows the peak floor forces for the 6 different wall structures. In difference to the frame structures, the floor forces are in part significantly more influenced by the diaphragm stiffness. Semi-rigid diaphragms increased the force demand to up to 200% compared to the demand with rigid diaphragms for the lower levels of the 9 storey structures. Further are the floor forces at the lower half of all structures of the same size to the ones acting at the top storey, a result in clear contrast to the typical first mode force distribution suggested by an ESA.

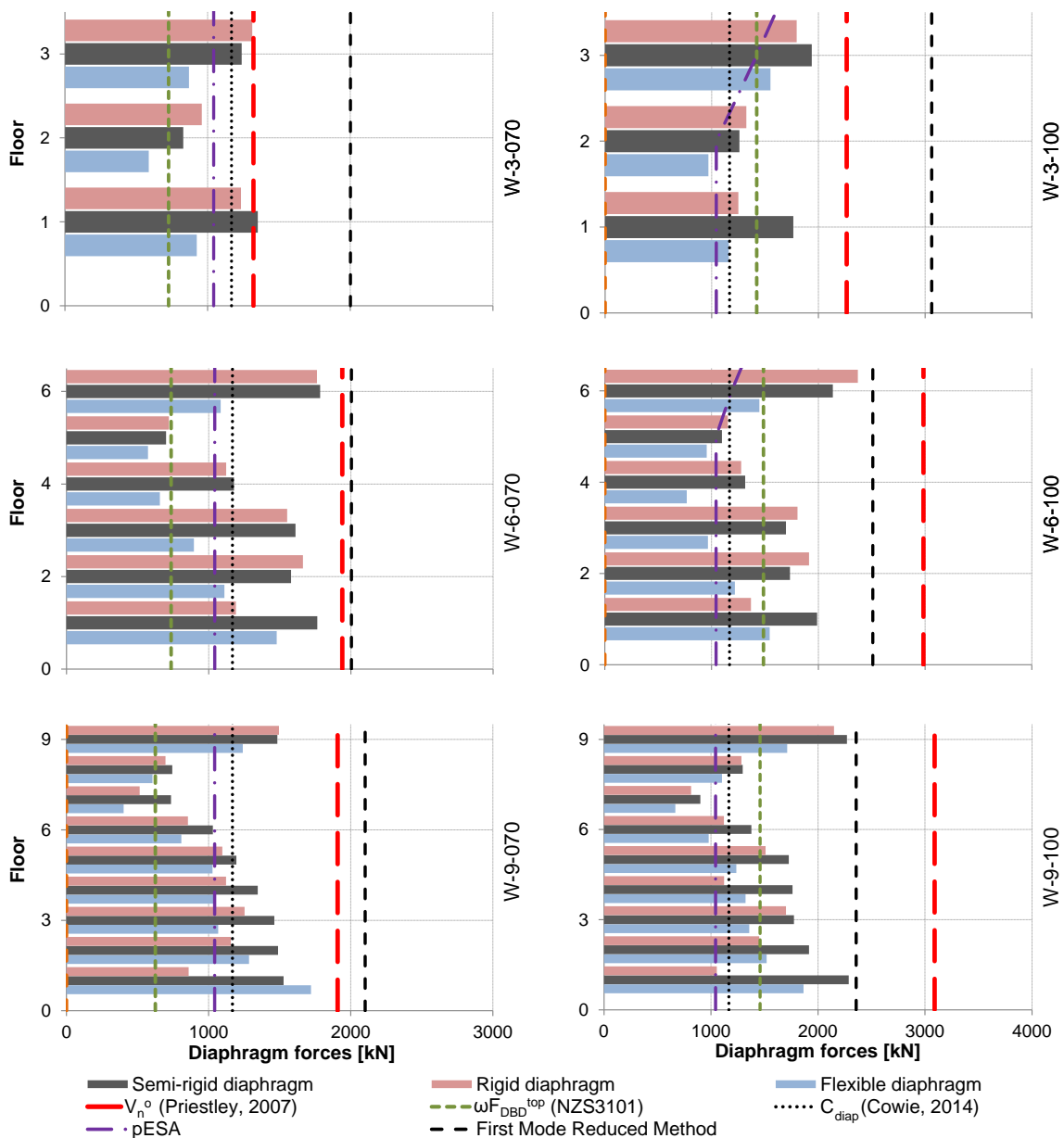


Figure 5.11 Diaphragm forces from the NLTH and suggested design values for wall structures

Figure 5.11 shows that the provisions from the New Zealand Concrete Code for the determination of amplified wall shears underpredict the top storey force for all cases analysed. Also the pseudo Equivalent Static Analysis (pESA) and the method proposed by Cowie underpredict the peak diaphragm forces. The First Mode Reduced Method estimates the peak forces relatively well with some conservatism for short structures. It has to be noted that the floor forces calculated with this method were obtained with a unitary S_p factor, in contrary to the original equation found in Rodriguez et al. (2002), where S_p would need to be considered.

The best results could be obtained by considering the amplified design shear force at the top of the building at overstrength V_n^o as proposed by Priestley et al. (2007) and already used in the preliminary diaphragm design carried out in Chapter 4.

Table 5.2 shows the measured and proposed diaphragm amplification factors ω_D for the analysed wall structures. The diaphragm demand for low structures ranges from about two times the top storey equivalent static force to 5 for the slender 9 storey structure.

Table 5.2 Diaphragm amplification factors for the wall structures with varying diaphragm flexibilities

ID	measured ω_D			Average	proposed ω_D
	Rigid	Semi-rigid	Flexible		
W-3-070	2.2	2.2	1.5	2.0	2.1
W-6-070	3.6	3.6	3.0	3.4	3.8
W-9-070	4.3	4.4	5.0	4.5	5.4
W-3-100	1.5	1.6	1.3	1.5	1.8
W-6-100	2.4	2.2	1.6	2.0	2.8
W-9-100	2.7	2.8	2.3	2.6	3.6

Like for frame structures it is recommended to design all diaphragms for the same maximum demand. Further analyses are required to verify this equation for wall structures designed with other ductility values.

5.6 DISCUSSION

This chapter summarized current code provisions for the determination of diaphragm forces. Only very little information was found to be provided, since most codes were limited in giving guidance for the determination of forces acting on the lateral load resisting system. Analysis methods like the equivalent static analysis, modal response spectrum analysis, and time history analyses are briefly explained and their suitability for the determination of diaphragm forces discussed. Further, research findings in regard to the diaphragm force determination are summarized. Since all information was based on concrete diaphragms in concrete

structures, no consensus on an appropriate method was given. Current desktop methods like the pseudo Equivalent Static Analysis (pESA) are not validated for multi-storey timber structures, where higher mode effects severely affect the dynamic behaviour.

The nature and importance of transfer forces in diaphragms were highlighted. Since simple desktop methods for timber structures are not available yet, more advanced analysis methods are recommended if transfer forces are expected. However, because of the more flexible behaviour of timber diaphragms, transfer forces are expected to be less pronounced. The method to determine transfer forces by Sabelli et al. (2011) should be further explored for the use with timber structures. For its application it would be required to investigate which force envelope along the structure's height is appropriate and what the magnitude of the single storey forces are.

It is recommended that design diaphragms work in the elastic range because of their importance in resisting lateral loads in structures and because of missing alternative load paths in the case of a diaphragm failure. To obtain this, both the overstrength of the lateral load resisting system and the dynamic amplification because of higher mode effects need to be taken into account. Existing desktop methods for concrete structures are based on capacity design principles only and don't account for the enhanced dynamic amplification found in timber structures.

Storey shear and moment envelopes of the structures with rigid, semi-rigid and flexible diaphragms were compared with suggested envelopes found in literature for both frame and wall structures. Relatively good agreement of the values proved the importance of considering higher modes in determining the shear and moment demand in frame columns and wall elements. Especially in wall structures these effects can be high and should never be neglected in design. The sole consideration of capacity design principles without the higher mode effects could result in non-conservative designs.

The peak diaphragm force distribution for both frame and wall structures significantly departed from the typical first mode distribution along the building height. Diaphragm forces at lower storeys were observed to be as high as the values at the top storey. It is therefore recommended that all diaphragms are designed for the same peak demand. These maxima can be approximately determined with a simple equation based on the amplified top storey column shear force for frame structures. For frame structures the existing formulation by

Priestley et al. (2007) to determine the top storey shear force can be used to determine the maximum diaphragm force demand.

As a general trend it was found that floor forces in frame structures undergo a dynamic amplification of 2 to almost 3 times compared to the top storey force from an equivalent static analysis. Further, it was observed that diaphragm flexibility has no significant effect on the force distribution. In wall structures, higher modes were responsible for an amplification of the diaphragm demand of up to 5 times the maximum value found from equivalent static analysis. Diaphragm flexibility did influence the force demand especially in the lower storeys and should therefore not be ignored. For the shear, moment and floor force envelopes for both frame and wall structures, the ductility factor μ should be taken as one if no additional hysteretic damping is applied to the structures.

Since only a limited number of structures have been analysed in this research, further analysis would be required to assure that suggested formulations are appropriate to estimate peak floor forces. Further, a desktop method for timber structures for the determination of transfer forces in timber structures needs to be developed. The measured peak forces occurred for very limited time intervals only. It would need to be determined if these peak values are caused by numerical errors from the time history analysis and if such large but short forces have the potential to damage the diaphragms.

The dynamic amplifications obtained from this analysis are relatively large and might lead to non-economical designs of the diaphragms or the connections between the diaphragms and the lateral load resisting system. To overcome this issue, the presence of ductile connections between the diaphragm panels could be taken into account to lower the diaphragm force demand. In this way, peak demands might cause some fasteners to experience plastic deformations, without compromising the performance of the remaining diaphragm. This approach would require some further analyses and possibly dynamic testing. Designers need to make sure that the chosen panel connections provide the required ductility, which is normally provided automatically if the fasteners are ductile nails or non-hardened screws. However the ductility of the panel fasteners should not be used to reduce the seismic demand of the whole building unless a specific special study is carried out.

5.7 CONCLUSIONS

The following conclusions can be drawn from this chapter

- Shear forces and moments determined with an equivalent static analysis do not include higher mode effects; procedures available in literature provided good estimates for the maximum forces and moments and can therefore be applied independently of the diaphragm flexibility;
- No international codes, except the ASCE 7-10 (ASCE 2010), provide special provisions for the determination of diaphragm forces;
- In addition to inertia forces, diaphragms need to resist transfer forces deriving from vertical irregularities along the building height (podium structures, discontinuous walls, set-backs etc.) or displacement incompatibilities of the lateral load resisting system (dual systems with frames and walls, walls with different stiffness etc.);
- To keep diaphragms in the elastic range, capacity design principles and dynamic amplification need to be included in the diaphragm demand calculations;
- The parametric analysis showed that the diaphragm force demand departed notably from the assumed first mode distribution; for frame structures forces are almost constant up the building height, but for wall structures larger forces are observed at the top and bottom storeys;
- Diaphragm flexibility does not influence the force demand in frame structures, but in wall structures diaphragm flexibility increases the force demand especially for lower storeys;
- For both frame and wall structures, all diaphragms up the height of the building should be designed for the same maximum force demand;
- Simple equations are provided to determine the peak diaphragm demand for frame structures and wall structures.

6 Diaphragm loads, massive timber diaphragms and deformation estimation

6.1 INTRODUCTION

This chapter investigates the influence of different load application types on the load path in light timber framing and massive timber diaphragms. Shear and longitudinal stress distribution, chord and reaction forces, as well as deflections are compared for different diaphragm types under distributed area, line, and concentrated forces. The increasing availability of engineered massive timber products change the way floor diaphragms are built. The behaviour of massive timber diaphragms is analysed and compared to the typical assumptions of traditional analysis methods. Since diaphragm flexibility influences the load distribution into the lateral load resisting system, it is essential to determine the deflection of diaphragms. Available methods and their applicability to massive timber diaphragms are discussed.

6.1.1 Load application

All codes discussed in Chapter 3, except the German National Appendix to Eurocode 5 (Eurocode 5 DIN NA 2010) and the New Zealand Earthquake Loading Code (Standards New Zealand 2004), assume load applications in form of a Uniformly Distributed Load (UDL) applied to the diaphragm compression edge. This is also the case for the majority of experimental diaphragm setups (Countryman 1952; Tissell 1966; Tissell and Elliott 2004). The question, however, arises if this idealized loading condition is representative for all possible diaphragm loads and if there are implications for the demand on the individual diaphragm components.

6.1.2 Massive timber diaphragms

The availability of Cross Laminated Timber (CLT), Laminated Veneer Lumber (LVL), and GLUed LAMinated timber (glulam) in form of large panels, gives the possibility to build massive timber flooring systems with larger spans and higher loads. The behaviour of these massive timber diaphragms under horizontal action is, however, relatively unknown. Even though the common assumption of rigid diaphragms is often appropriate (Ceccotti 2008; Dujic et al. 2010; Follesa et

al. 2013), it still requires the calculation of the load path and the subsequent element and connection design and verification.

6.1.3 Diaphragm deformation and stiffness

Chapters 3 and 4 showed that diaphragm stiffness influences both the global dynamic behaviour of the structure and the load distribution into the Lateral Load Resisting System (LLRS). Current code provisions on the diaphragm deflection are very limited and given formulations are based on regular geometries only. Since such cases are seldom of practical interest, alternative methods must be provided. No information on the deflection estimation for massive timber diaphragms is provided.

The implication of different load application types on regular and irregular diaphragms, built with LTF and massive timber panels, is analysed by a series of finite element models carried out with SAP2000 (CSI 2004). Results are discussed and methods to account for the differences are highlighted. The applicability of the girder analogy for massive timber diaphragms is also discussed based on finite element models. Implications of designs without chord beams are shown with special emphasis on the fastener demand. Deflection equations for regular LTF diaphragms are studied, showing the possibilities of their extension to real design applications.

6.2 TYPES OF LOAD APPLICATION AND THEIR INFLUENCE ON THE LOAD PATH

Types of loads to be resisted by diaphragms have been described in Chapters 2 and 5 and normally include seismic, wind and transfer forces, as well as concentrated forces from inclined columns or from the restraint of vertical elements in general. These actions can be further differentiated by the type of load application. The following sections discuss how loads can be applied to the diaphragm and how this type of application influences the load path, the demand on the different elements and the global diaphragm behaviour.

Types of loads generally acting on diaphragms are:

- area (surface) loads;
- line loads; and
- discrete loads.

These loads can generally be attributed to seismic action, wind action or concentrated loads from vertically offset walls respectively. Transfer forces can be treated like imposed displacements from the lateral load resisting system and have the same effects as concentrated forces.

In general, codes, guidelines and academic literature base the diaphragm design on a simply supported (or continuous) beam loaded with a uniformly distributed load. Normally no distinction is made if the loads are applied to either the compression or tension edge, applied to either the panels or framing elements or distributed over the sheathing panels. An exception can be found in the New Zealand Earthquake Loading Code NZS 1170.5, where its Commentary (Standards New Zealand 2004) requires that the inertia loads are to be distributed in accordance to the seismic masses. When finite element models are used, the real force application is modelled.

Table 6.1 summarizes how common loads on diaphragms can be modelled for analysis purposes.

Table 6.1 Sources of loads on diaphragms with corresponding idealized load type on diaphragm

Load type	Discrete loads [force]	Uniformly distributed line load ¹⁾ [force per length]	Uniformly distributed area load [force per area]
Seismic action			x
Transfer/Compatibility	x ²⁾		
Wind	x	x	
Soil/water pressure	x	x	
Buckling restrain	x ²⁾		
Sloping columns	x ²⁾		

¹⁾ Uniformly distributed line loads applied on the compression or tension edge of the diaphragm.

²⁾ If the force is introduced via a collector beam, then the force can be idealized as a uniformly distributed line load along the diaphragm depth.

To evaluate if such simplifications are appropriate for regular and irregular diaphragms LTF or massive timber diaphragms, a number of cases have been studied via a finite element analysis.

6.2.1 Load application types, example diaphragms and analysis method

To study the influence of the type of load application on LTF and massive timber diaphragms, four different sets of load applications as shown in Figure 6.1 were applied to two sample diaphragms. First a simply supported diaphragm with 6 panel elements was studied, and then the same load applications were applied to an irregular floor diaphragm as shown in Figure 6.2. Both diaphragms were modelled with a finite element model carried out in SAP2000 (CSI

2004) as discussed in Appendix B. Material properties of the LTF sheathing panels and of the massive timber panels are summarized in Table B.1. Framing elements had a cross section of $50 \times 100 \text{ mm}^2$ (this is considered to be the actual section size), all other beam elements had a cross section of $200 \times 400 \text{ mm}^2$. The modulus of elasticity of framing elements and beams was 11,000 MPa. For the simple diaphragm analysis (Figure 6.2a) the framing elements were not connected to each other (as assumed in the shear field analogy). For the irregular floor layout (Figure 6.2b) all beam and framing elements were connected with a linear spring with a stiffness of 9,000 N/mm in shear and tension based on a typical connection design. These connections were assumed as infinitely rigid when in compression, since the elements bear against each other. This assumption does not correspond necessarily to the reality, but the compression stiffness is much larger than the stiffness of the connection in tension and is therefore negligible. All panels were connected to the framing elements or to each other with linear springs placed at 150 mm having a stiffness of 1,000 N/mm.

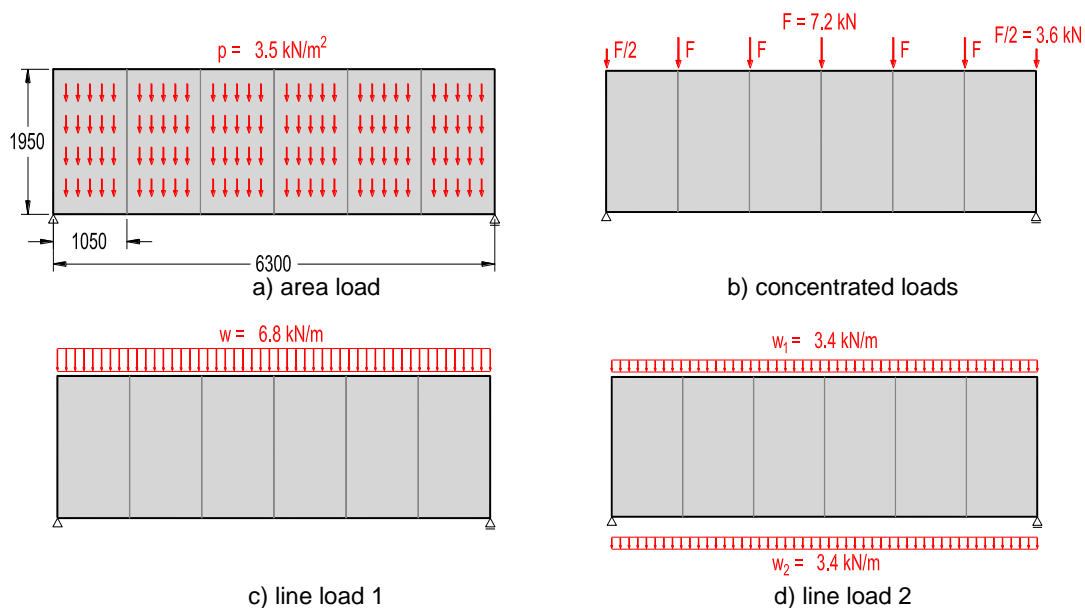


Figure 6.1 Load application types for diaphragm analysis

For load application a) a distributed load of 3.5 kN/m^2 was applied to all panel elements. For load application case b) with concentrated loads, the resultant force relative to each frame element was applied to the diaphragms. For load application case c) a uniformly distributed line load was applied to the compression edges. For load application case d) half the load was applied to the compression edges and the other half to the tension edges.

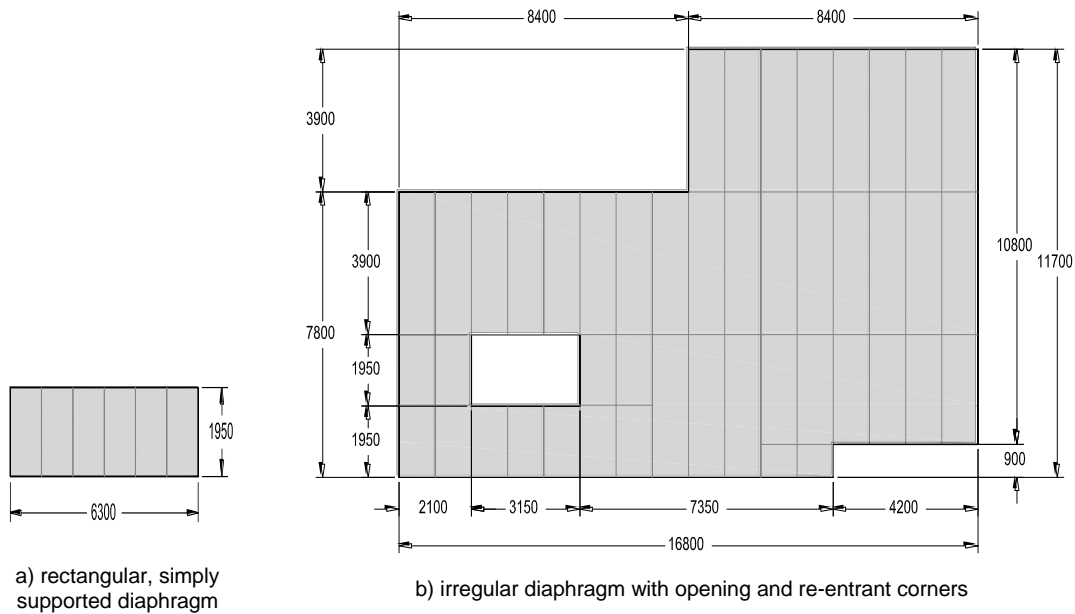


Figure 6.2 Sample diaphragms: a) rectangular, simply supported diaphragm; b) irregular diaphragm

6.2.2 Results and discussion for regular LTF diaphragms

To understand if the type of load application significantly influences the load path in diaphragms, the unit shear forces n_{xy} , and longitudinal unit forces n_x and n_y in the x and y directions respectively are plotted in Figure 6.3.

The comparisons of Figure 6.3 show that the distribution of unit shear forces is very similar throughout all four load cases for LTF diaphragms. For concentrated forces, which is the assumed load case for the shear field analogy discussed in Chapter 3, the shear forces n_{xy} are constant in each panel. For all other cases the shear forces vary linearly along the diaphragm span. Sheathing panels do slightly contribute with their longitudinal stiffness in the x direction for all four load applications, the resulting n_x stresses however are small and can be neglected. Stresses in the y direction are slightly more dominant and are mostly found close to the panel edges where bigger relative movements are observed. Of more importance, however, are the increased n_y forces for line loads c) and d). Since the loads are applied to the chord elements which are nailed to the panels, the panels are activated in their longitudinal direction. For c) n_y stresses are mostly in compression, for d) both compression and tension stresses are activated, since the forces are pushing and pulling respectively on the panels. Even if longitudinal stresses are normally not required for the panel verification, fasteners need to be designed for these forces perpendicular to the panel edge as discussed in section 6.2.6.

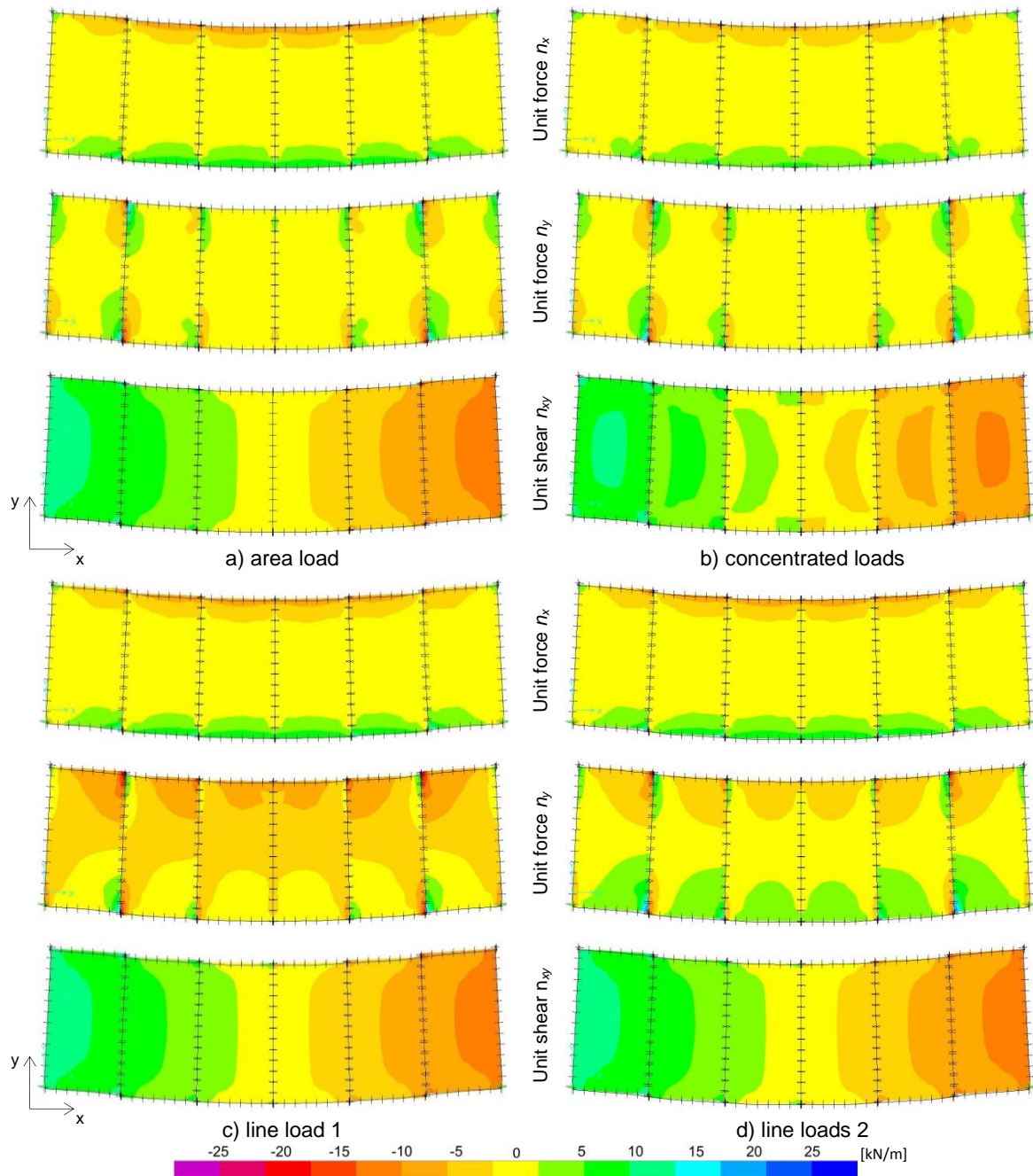


Figure 6.3 Resultant forces n_x , n_y and n_{xy} of a regular LTF diaphragm with different load types

6.2.3 Results and discussion for regular massive timber diaphragms

Figure 6.4 shows a similar trend regarding the shear forces in massive timber panels, only for the concentrated shear forces the distribution appears less uniform on the individual panels. A big difference to the LTF diaphragms can be seen in the large n_x stresses close to the diaphragm edges. Because the panels are relatively stiff in their longitudinal directions, they contribute to a bigger extent to the bending resistance of the diaphragm. For floor layouts with low chord beam stiffness, this tensile stresses need to be verified, because of the very low

tension capacity perpendicularly to the grain. Products like CLT or cross banded LVL panels normally can easily resist this tensile stresses because of perpendicularly oriented layers. Fasteners also need to be verified for this load component perpendicular to the panel edge. For load case b) local effects can be seen at the panel edge close to the force introduction. Because of the punctual load introduction and the local deformation, the panel locally works in tension. This undesired effect can be attributed to the mathematical formulation of the finite element analysis and does not have big relevance for practical purposes.

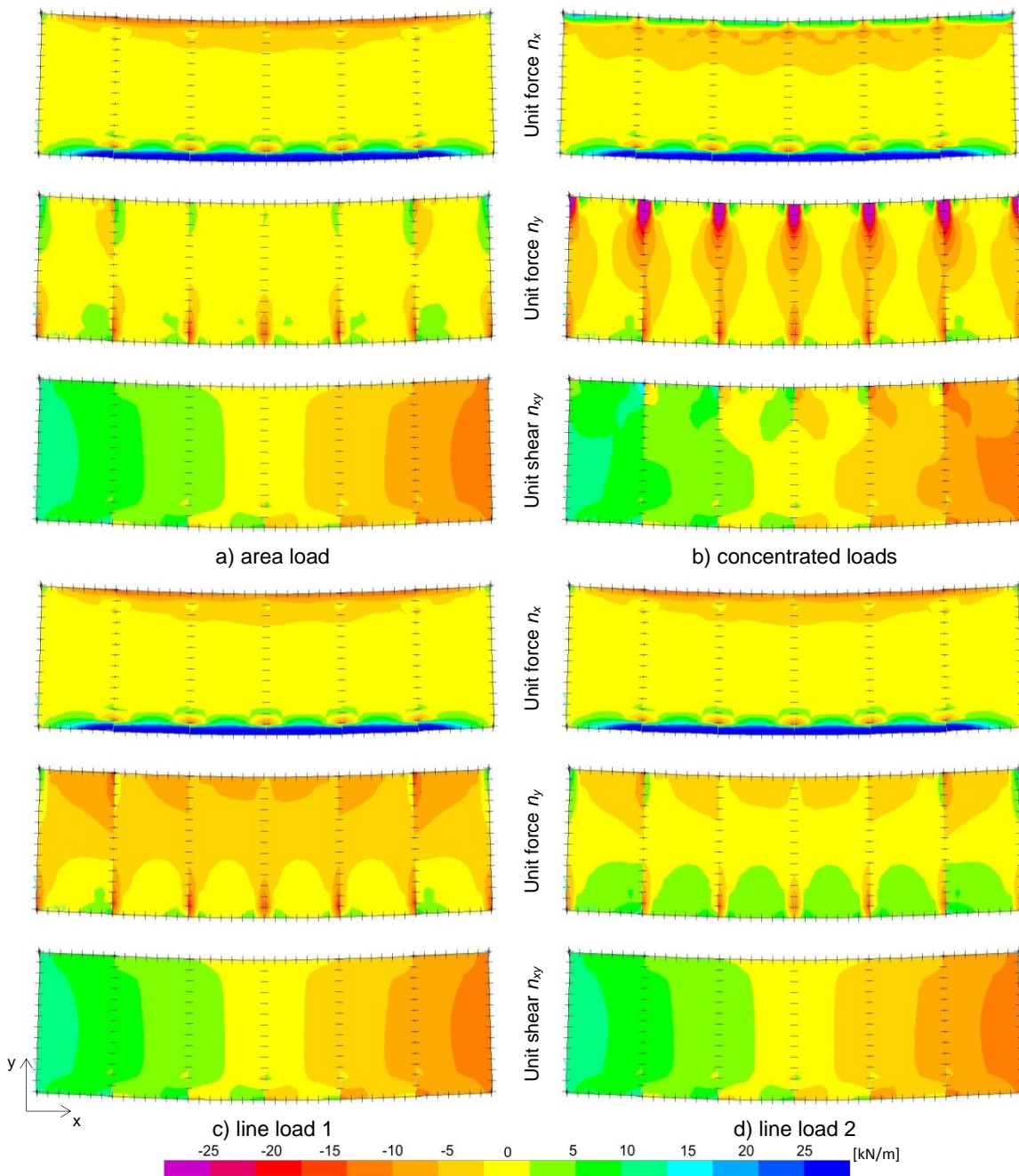


Figure 6.4 Resultant forces n_x , n_y and n_{xy} of a regular massive timber diaphragm with different load

Because of the missing framing elements, which normally introduce the loads into the diaphragm, higher n_y forces can be observed in massive timber panels. As long as the tension or compression capacity for concentrated loads is guaranteed, these stresses are not influencing the diaphragm behaviour.

6.2.4 Results and discussion for irregular LTF diaphragms

Figure 6.5 shows the stress distribution for an irregular LTF diaphragm on the 4 load application types. Shear stresses are well distributed over the diaphragm and they reflect the values expected from the girder analogy. For all four load conditions a higher shear stress demand adjacent to the re-entrant corner can be observed, but aside from that no significant change in the stress distribution for the four different load cases can be seen. This can be mainly explained by the force introduction by the framing elements.

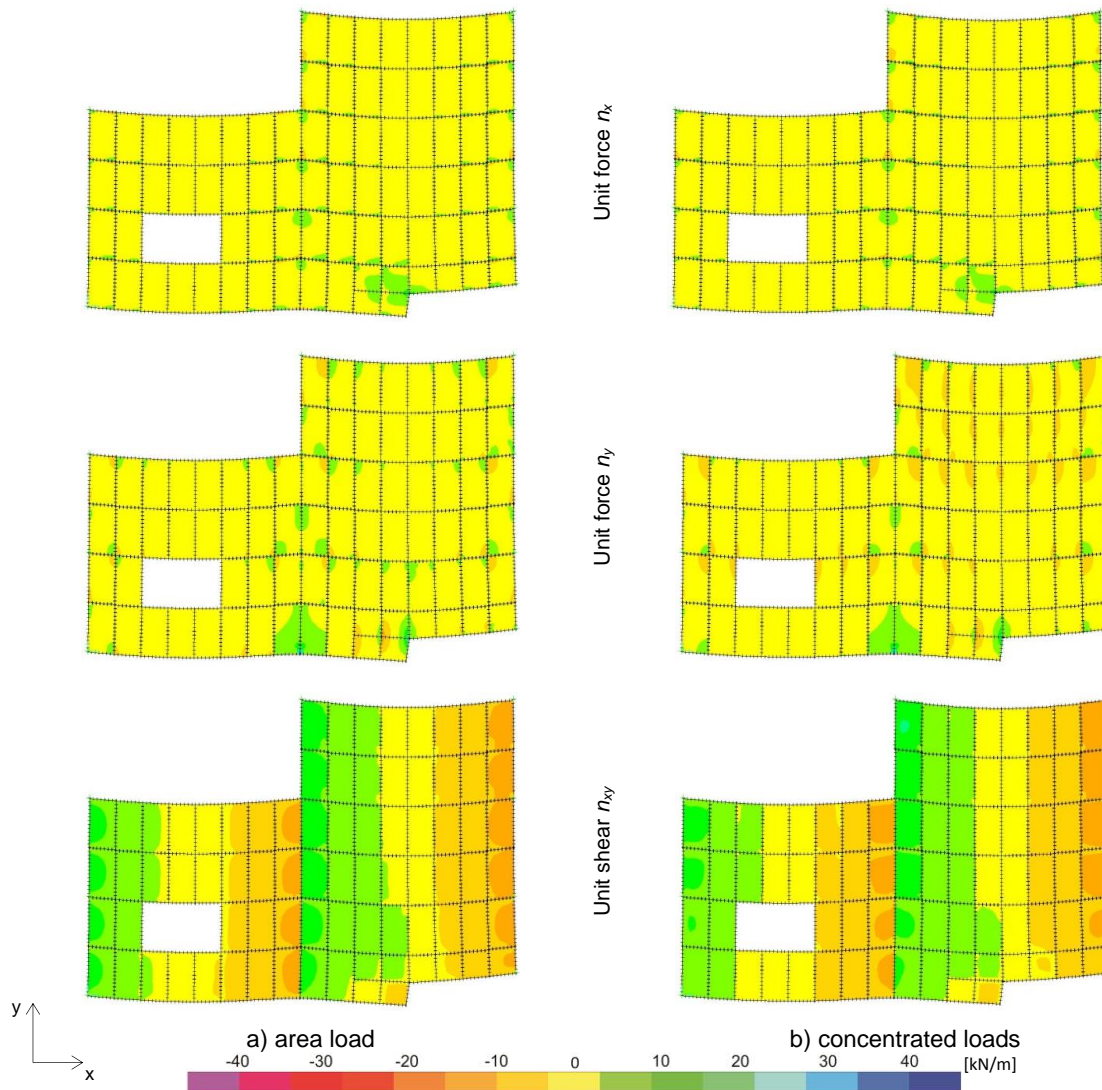


Figure 6.5 Resultant forces n_x , n_y and n_{xy} of an irregular LTF diaphragm with distributed and concentrated loads

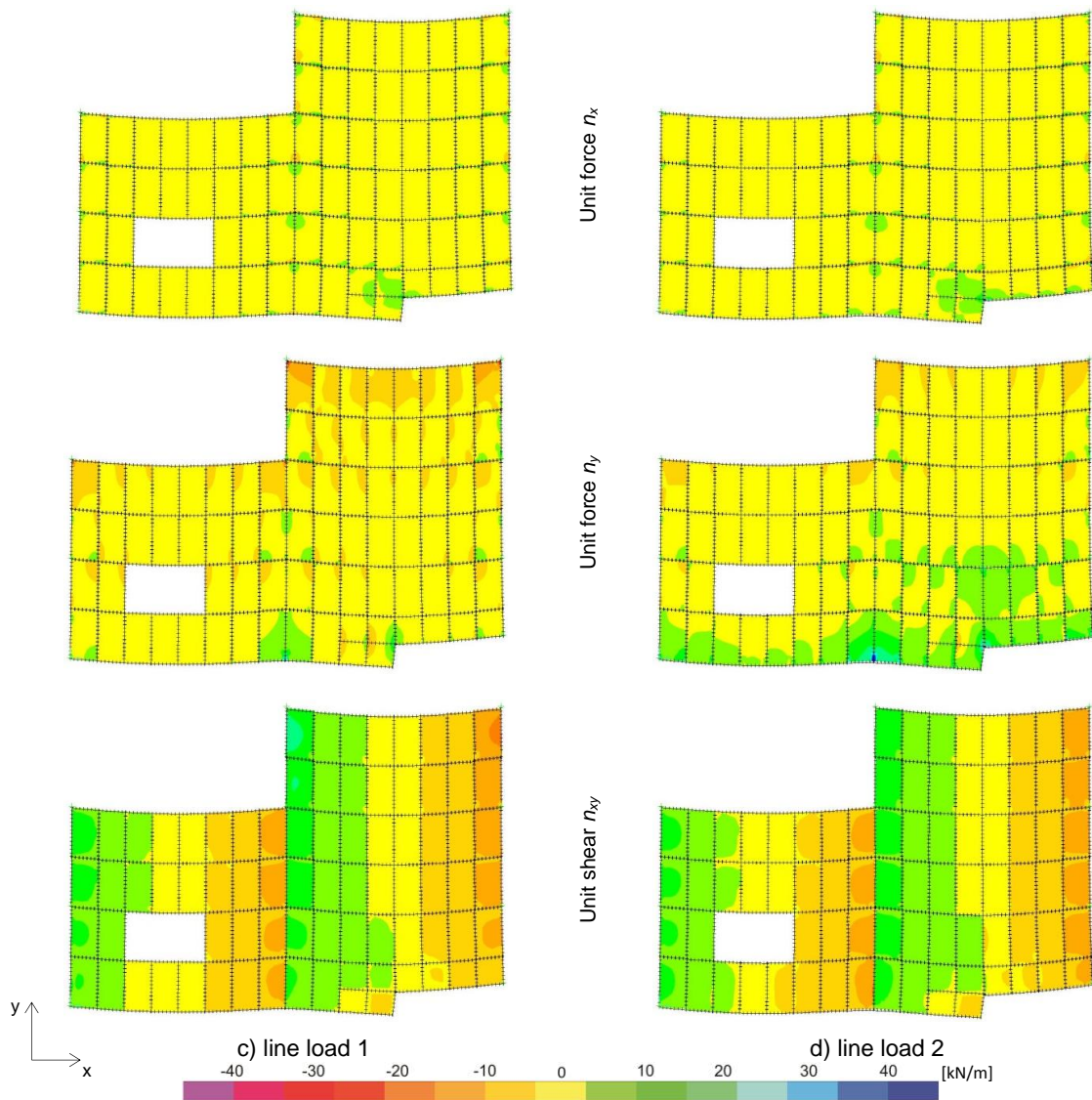


Figure 6.5 Resultant forces n_x , n_y and n_{xy} of an irregular LTF diaphragm with line loads 1 and 2

Figure 6.6 compares the forces transferred from the diaphragm into the lateral load resisting system. A comparison of these reaction forces shows some difference in their distribution into the individual supports. The values mainly reflect the position of the type of load application, i.e. higher reactions are obtained at supports closer to the load introduction point.

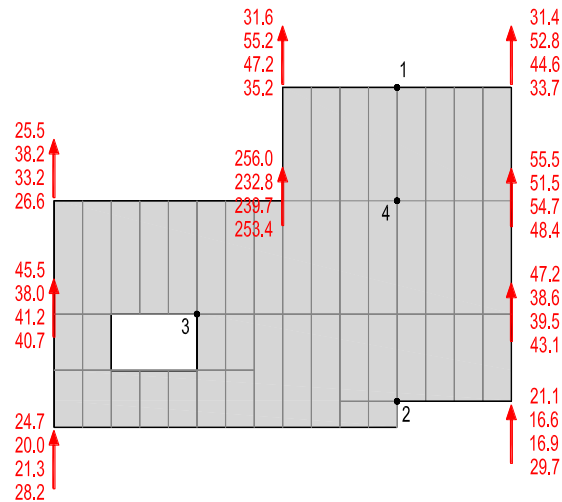


Figure 6.6 Reaction forces of an irregular LTF diaphragm with different load types (area load, concentrated loads, line load 1, line load 2)

A comparison of other key values like the diaphragm deflection or chord/strut beam forces summarized in Table 6.2 shows that the different load application types only have minor impact. This is explained by the fact that the framing elements can distribute the forces into the whole diaphragm and therefore activated it evenly. Therefore only difference of less than 20% can be seen in the key values shown.

Table 6.2 Deflections and chord forces of an irregular LTF diaphragm with different load types

Load type	Deflection (at p.t 1) [mm]	Axial force in chord (at p.t 1) [kN]	Axial force in chord (at p.t 2) [kN]	Axial force in strut beam (at p.t 3) [kN]	Load in fastener perp. to panel edge (at p.t 4) [kN]
Area load	4.5	24.8	8.5	4.5	0.0
Con. load	5.1	27.6	7.6	5.1	0.1
Line load 1	5.4	27.3	7.7	5.4	0.1
Line loads 2	4.7	24.5	9.2	4.7	0.1

6.2.5 Results and discussion for irregular massive timber diaphragms

Figure 6.7 shows the stress distribution for massive timber diaphragms, which compared to the stress distributions of LTF diaphragms, is less regular and shows high values of axial stresses. The unit shear forces are all relatively well distributed and reflect the expected distribution from a girder analogy. High stresses in the top panels can be seen for load applications at the compression edge as per load case b) and c). This is because the panel connections are not designed to transfer longitudinal stresses in x direction, and therefore panels further away from the force introduction are not activated. This is in difference to LTF

diaphragms, where framing elements are connected along their whole length and are able to distribute the longitudinal forces along the whole diaphragm depth.

The axial stress distribution in n_x direction suggests that the massive timber panels all contribute to the bending strength of the diaphragm. For load applications at one diaphragm edge only, high panel axial stresses are activated. For load case b) with concentrated forces, local deformation effects again create high axial forces which are not relevant for practical purposes.

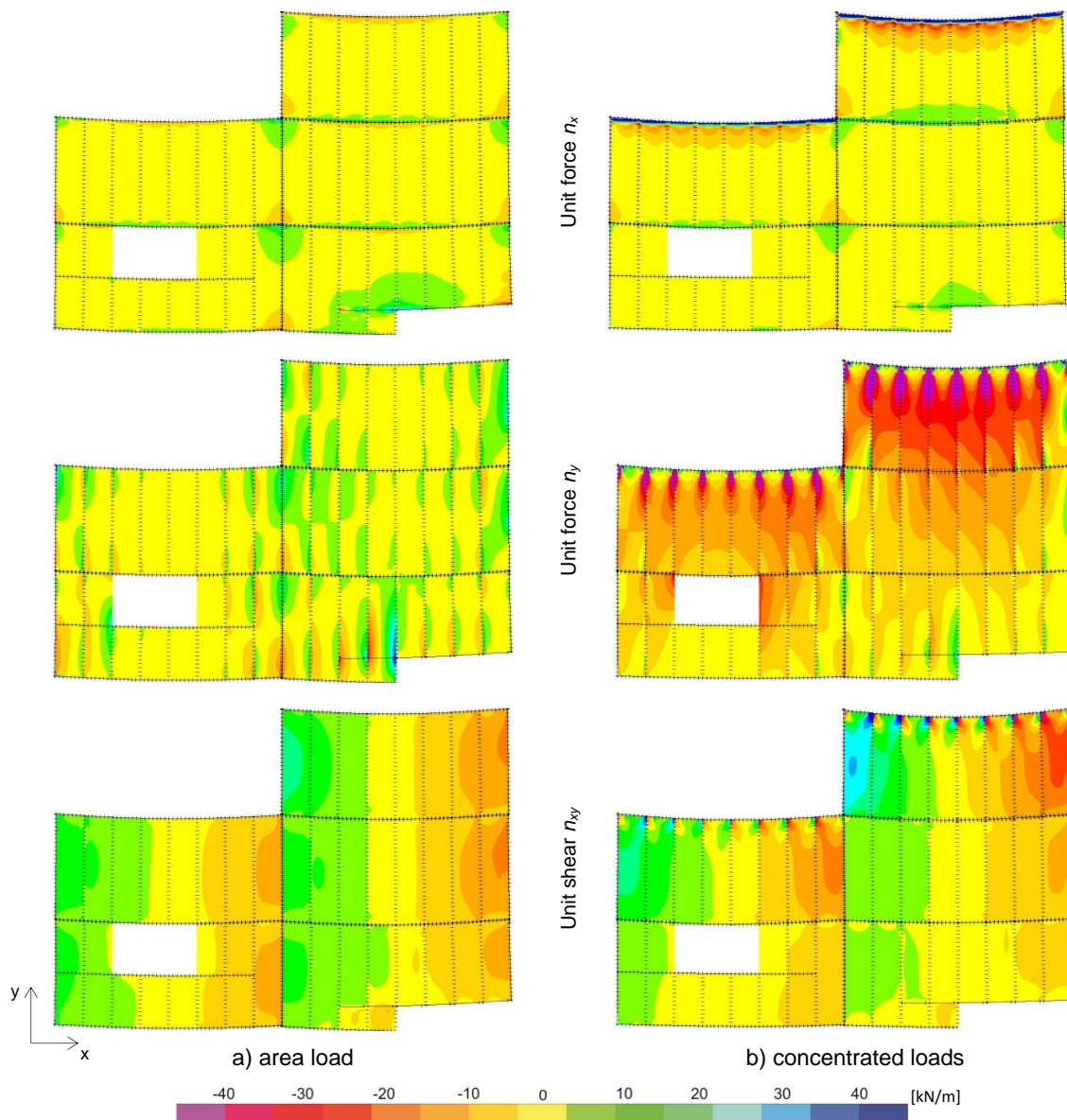


Figure 6.7 Resultant forces n_x , n_y and n_{xy} of an irregular massive timber diaphragm with area and concentrated loads

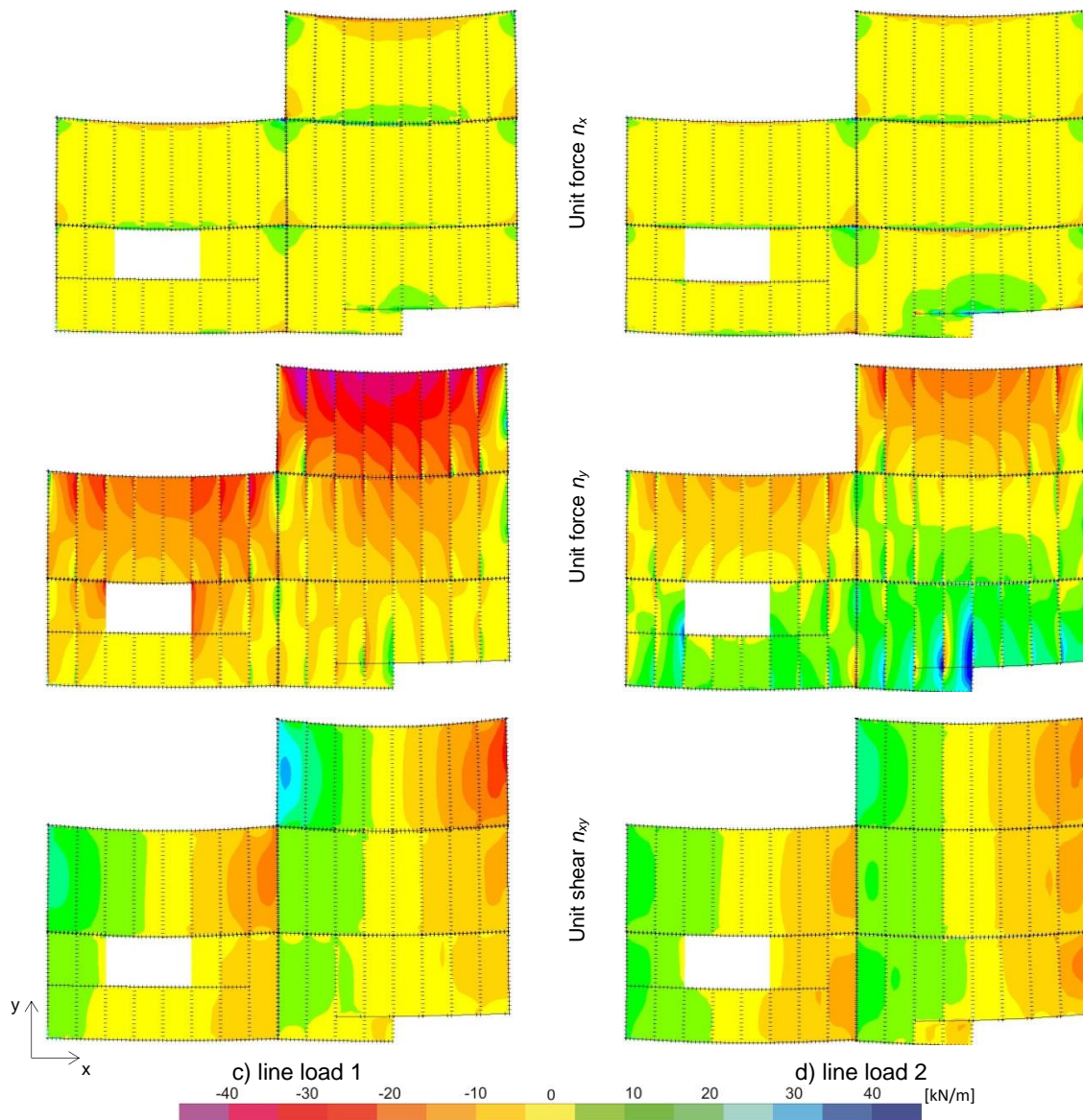


Figure 6.7 Resultant forces n_x , n_y and n_{xy} of an irregular massive diaphragm with line load 1 and 2

Axial stresses in y direction are becoming more noticeable for irregular diaphragms. Especially for concentrated loads and for line loads on one diaphragm edge only, forces need to be transferred from the load introduction point to the remaining diaphragm panels. The more the load is distributed over the diaphragm (either because of a well distributed load application or through axial force transfer through the panel connections), the more uniformly distributed are the diaphragm stresses. Especially for irregularities close to the load application point, n_y stresses should be checked and connections to adjacent panels designed for axial load transfer. Reaction forces as shown in Figure 6.8 have a similar trend as for LTF diaphragms.

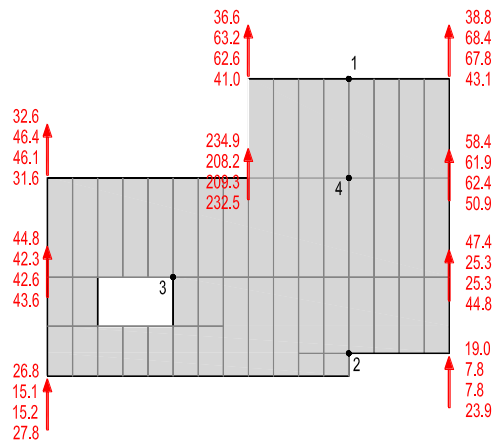


Figure 6.8 Reaction forces of an irregular massive timber diaphragm with different load types (distributed, concentrated, line load 1, line load 2)

In difference to the modelled LTF diaphragms, deflections and axial forces in beam elements are more affected by the type of load introduction. For the distributed load application types like the area load a) or the line loads applied to both diaphragm edges d), the diaphragm deflections, as summarized in Table 6.3, are smaller than for load types applied to one diaphragm edge only. Similarly are chord and strut forces higher if the force introduction is closer to their position.

This can be explained by the fact that panels are not designed and connected to transfer longitudinal forces (in load direction) to adjacent panels. Therefore only a part of the diaphragm is activated. On the other hand, if loads are applied over the whole diaphragm depth, then the whole diaphragm resists the loads. Because panel fasteners provide stiffness and strength both parallel and perpendicularly to the panel edge, part of the axial loads is still transferred. For a single fastener located at point 4 as shown in Figure 6.8, the force components perpendicular to the panel edge are shown in Table 6.3. Considering the maximum expected unit shear force in the diaphragm of 20 kN/m and a therefore resulting fastener load of 3 kN parallel to the panel edge, fasteners for load cases b) and c) must also resist to almost the same amount in their perpendicular direction. Fasteners therefore need to have a capacity equal to or bigger than the resultant of these forces and also need to respect the minimum spacing to loaded edges. For LTF diaphragms this problem is normally not encountered if all framing members are axially connected and therefore transfer the applied loads along the whole depth of the diaphragm. Fastener loads perpendicular to the panel edge can therefore normally be ignored as Table 6.2 suggests.

Table 6.3 Deflections and chord forces of an irregular massive timber diaphragm with different load types

Load type	Deflection	Axial force in chord	Axial force in chord	Axial force in strut beam	Load in fastener perp. to panel edge
	(at p.t 1) [mm]	(at p.t 1) [kN]	(at p.t 2) [kN]	(at p.t 3) [kN]	(at p.t 4) [kN]
Area load	2.7	29.2	10.3	9.4	0.2
Con. load	4.2	44.7	5.3	19.7	2.8
Line load 1	4.3	44.7	5.3	19.6	2.8
Line loads 2	2.9	30.8	11.4	7.3	0.6

6.2.6 Load introduction through the chord beam

As discussed above for both LTF and massive diaphragms, loads applied to a diaphragm edge are not activating the whole diaphragm if the applied forces are not distributed along the diaphragm depth. Framing beams along the loading direction can assume this role for LTF diaphragms. Similarly must loads applied directly to a chord beam, which is a common case for wind loads on a façade, also be transferred into the remaining diaphragm. This force transfer can be realised in two different ways:

- a) Force transfer via chord beam (LTF diaphragms only) (see Figure 6.9a):

The chord beam resists the forces in bending (in the diaphragm in-plane direction) and transfers the forces into the framing elements parallel to the load direction. Since this force can act in both tension and compression, an adequate tension connection between the chord beam and the framing members is necessary. The framing elements then continuously transfer the axial load into the sheathing panels.

- b) Force transfer via sheathing panels (LTF and massive timber diaphragms) (see Figure 6.9b):

The force is introduced from the chord beam directly into the sheathing panels, requiring the fasteners to resist forces perpendicular to the panel edges. This mechanism further creates longitudinal panel stresses. Since the fasteners already need to resist the unit shear force from the diaphragm action, it is necessary to check if they can also resist the additional load component from the direct load introduction. Further, also the minimum distance to the loaded panel edge needs to be guaranteed. For the diaphragms in Figure 6.3 the line loads of case c) and d) are transferred from the chord beams directly into the diaphragm panel. Fasteners at the outermost panel are activated for a force of ca 1.6 kN parallel to the panel edge. For a line load of 6.8 kN/m, fasteners spaced at 150 mm need to transfer 1 kN perpendicular to the panel

edge. This means fasteners have to carry a resultant force of 1.9 kN, which is about 20% higher than the demand from the pure unit shear force. When designing for such load applications, this additional fastener demand needs to be considered.

To account for the increased fastener load, the German National Appendix to Eurocode 5 (Eurocode 5 DIN NA 2010) requires the use of an effective diaphragm depth. This is defined as half or a quarter of the total diaphragm depth for cases with loads applied to both chords beams or to one chord beam respectively. The reduced depth results in an increased fastener demand, which covers the additional force component from the load introduction through the chord and panel connections.

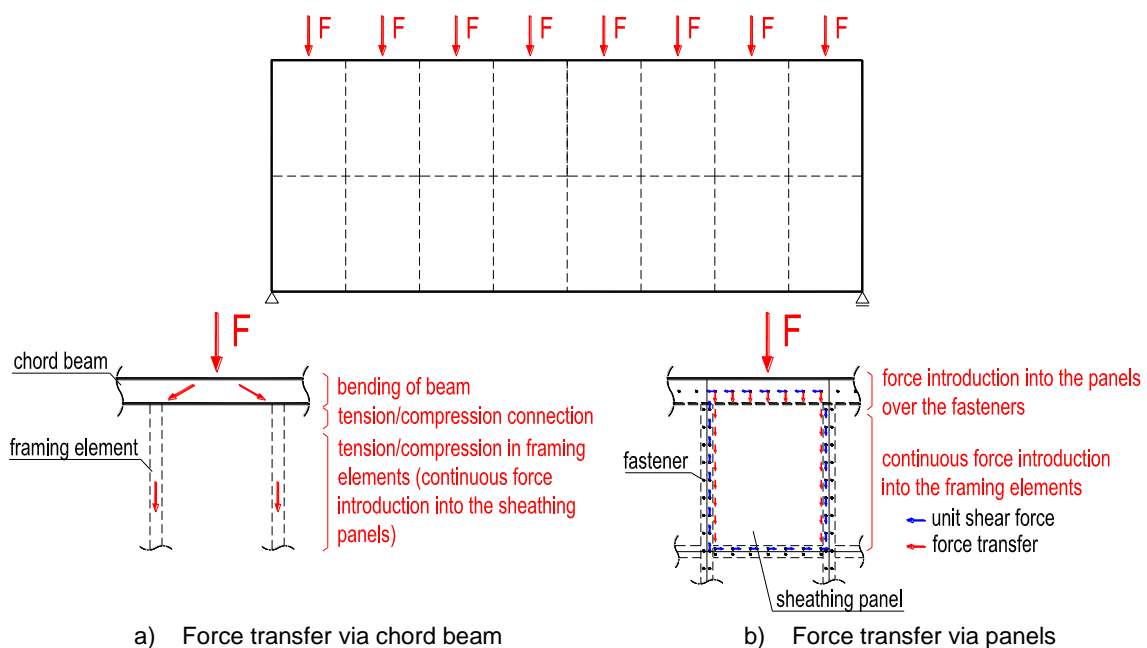


Figure 6.9 Concentrated force introduction offset from framing elements. Force transfer into diaphragm: a) via the bending of the chord beam, b) via fasteners into the sheathing panel

6.3 MASSIVE TIMBER DIAPHRAGMS

All available analysis methods for timber diaphragms, as discussed in the state-of-the-art summary in Chapter 3, were developed, tested and applied to LTF diaphragms only. Little is known about the behaviour of massive timber diaphragms.

Wallner-Novak et al. (2013) discussed the design of floor diaphragms made from CLT panels and referred also to the deep beam analogy as shown in Figures 6.10a and b. The panels and panel connections which resist the shear and tension/compression forces along the edges are resisted by chord beams or by appropriate panel connectors. For loading perpendicular to the

panel length (Figure 6.10c), the diaphragm can be assumed to work as a series of beams in parallel. A finite element analysis by Ashtari (2009) also confirmed the shear force distribution in Figure 6.10a, but the tension and compression forces in Figure 6.10b were not evaluated because the panels were connected with rigid links perpendicular to the panel edges. Both documents studied regular diaphragms with one row of panels.

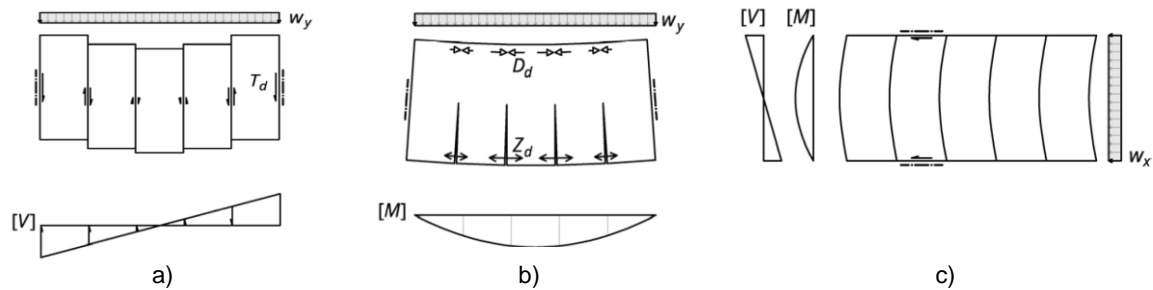


Figure 6.10 Mechanism of floor diaphragms: a) shear along panel connection, b) chord forces, c) diaphragms as series of beams (Wallner-Novak et al. 2013)

The finite element analyses carried out in the previous section confirm the deep beam behaviour of massive timber diaphragms in terms of the unit shear distribution. Results, however, also show that longitudinal stresses play a major role for certain load conditions. This behaviour becomes even more obvious in the case of diaphragms with multiple panel rows and for diaphragm with irregularities.

Because of the absence of framing elements in massive timber diaphragms, panel axial forces in load direction are activated. For forces applied to diaphragms edges, this is the only mechanism available to transfer the loads into the diaphragm. In addition, the panels also contribute to the bending stiffness of the diaphragm, which activates stresses perpendicular to the load direction. This can be clearly seen from the reduced chord forces and deflections when comparing Tables 6.2 and 6.3 for LTF and massive timber diaphragms respectively. Such effect should not be neglected, since panels without cross layers are activated in tension perpendicular to the grain and fasteners also need to resist force components perpendicularly to the panel edge. In the absence of special reinforcing elements (i.e. drag/strut beams, metal brackets etc.) massive timber panels are not only carrying unit shear forces, but also additional longitudinal forces deriving from the stress redistribution.

Wallner-Novak et al. (2013) suggested that tension and compression forces can also be resisted by the panel fasteners instead of the chord beams. Although this approach is technically feasible as long as panels and fasteners are designed for the forces, such diaphragms are not as efficient as the ones with chord beams. Figure 6.11 shows the SAP2000

analysis results of a diaphragm with a dimension of 1.2 x 4.8 m consisting of 8 CLT panels with and without chord beams under a load of 3.5 kN/m² (see Appendix B for material properties). Chord beams, if present, had a cross section of 189 x 400 mm². The panel fasteners were modelled with a stiffness of 3,000 N/mm, increasing to infinity after 1 mm of displacement when the panels were assumed to bear against each other.

For the diaphragm without chord beams, Figure 6.11 shows that the fasteners are not only heavily loaded perpendicularly to the panel edge (compared to the maximum fastener force from the unit shear force of 2.5 kN), but the diaphragm deflection is also increased by 250%. Shear stresses compare reasonably well, with a slightly less uniform distribution. The measured tension stress in the panels of 1.0 N/mm² reached the tension strength perpendicular to grain for some timber species.

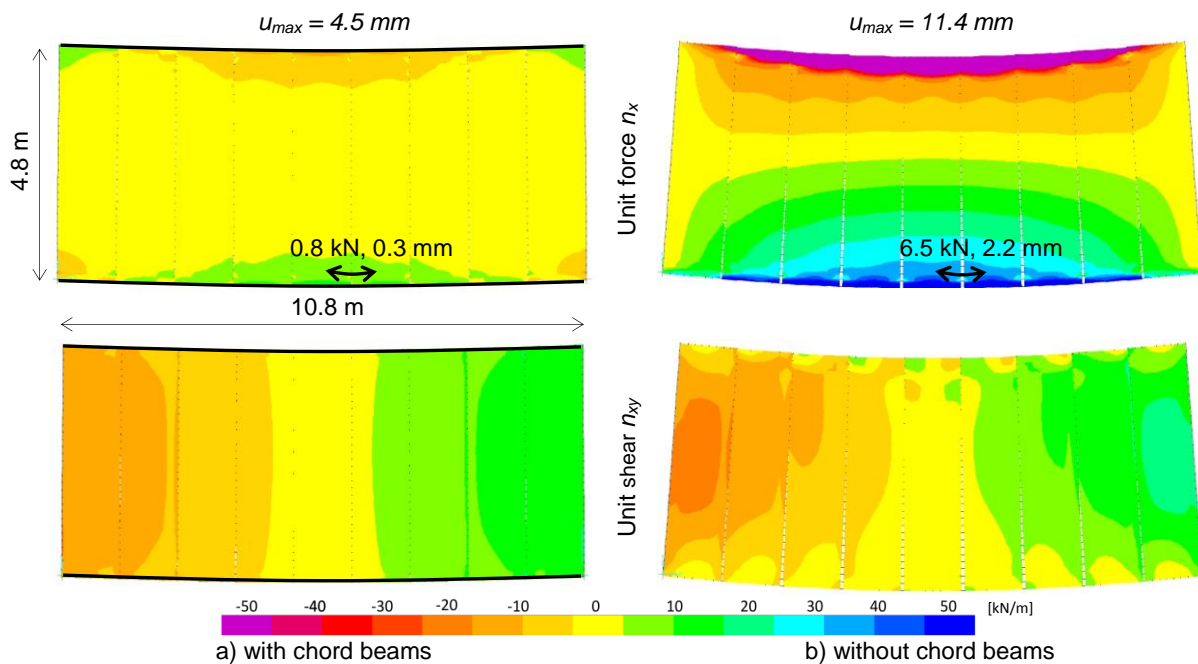


Figure 6.11 Simply supported diaphragms a) without and b) with chord beams

Although it is assumed that in the presence of chord beams no tension and compression forces are resisted by the diaphragm panels as shown in Figure 6.12a, connections will still have to carry nominal tension forces as per Figure 6.12b. From the analysis, a connection load component perpendicular to the panel edge of 0.8 kN can be observed, this values is about 30% of the unit shear force component. This effect can also be seen in the chord forces, which is 45 kN from the FEM analysis in respect to the 51 kN from the girder analogy.

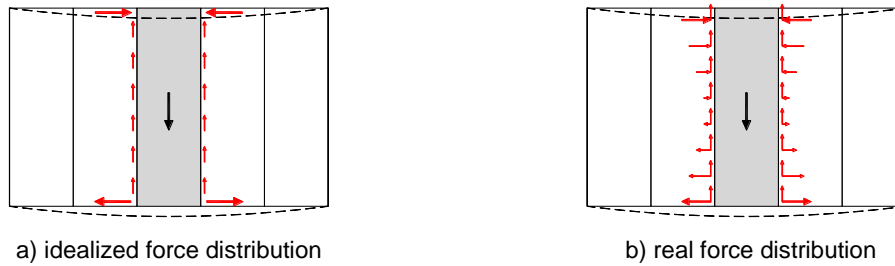


Figure 6.12 Force distribution in diaphragm panel connections with massive timber panels

In conclusion, massive timber diaphragm can be analysed with the girder or shear field analogy, as long as the loads are appropriately transferred into the diaphragm. This is always the case for area loads, but panel connections must be specifically designed for these longitudinal loads. Massive timber diaphragms without chord beams are relatively flexible and require a careful connection and panel design, since high axial forces arise from the required bending strength.

6.4 DEFORMATION OF TIMBER DIAPHRAGMS

The explicit calculation of diaphragm deformation is not required by most building codes as discussed in Chapter 3. Similarly, deflection limits for diaphragms are not provided, with one exception found in the German National Appendix of Eurocode 5 (Eurocode 5 DIN NA 2010), where a limit of $l/500$ is enforced to limit P-Delta effects on gravity supporting elements.

Because diaphragms link all structural and non-structural elements together, their deflection can have a major impact, not only on the structural behaviour of the building, but also on the expected structural and non-structural damage. Excessive movement of a diaphragm could compromise the lateral load resisting system and hinder the load path to the foundations. On the other hand, wall linings and glass facades can undergo substantial damage if their out-of-plane movements are not accounted for. Because large panelised wood diaphragms have more commonly been used for roofs in industrial warehouses, rather than for floor diaphragms in residential or commercial buildings, this issue was seldom addressed. By using timber diaphragms for irregular floor layouts with large spans like in real examples shown in Figure 6.13, the calculation of the horizontal deflection for both serviceability and ultimate limit state will be necessary in order to guarantee functionality and prevent dis-proportional damage in diaphragms and all other connected elements.

A far more important reason to calculate the deformation of diaphragms under design loads is the evaluation of the diaphragm stiffness. Depending on the relative stiffness of the diaphragm

and the lateral load resisting system, the force distribution from the floor into walls and frames is affected. Additionally, as was discussed in Chapter 4, the flexibility of diaphragms can have an influence on the dynamic behaviour of the whole building.

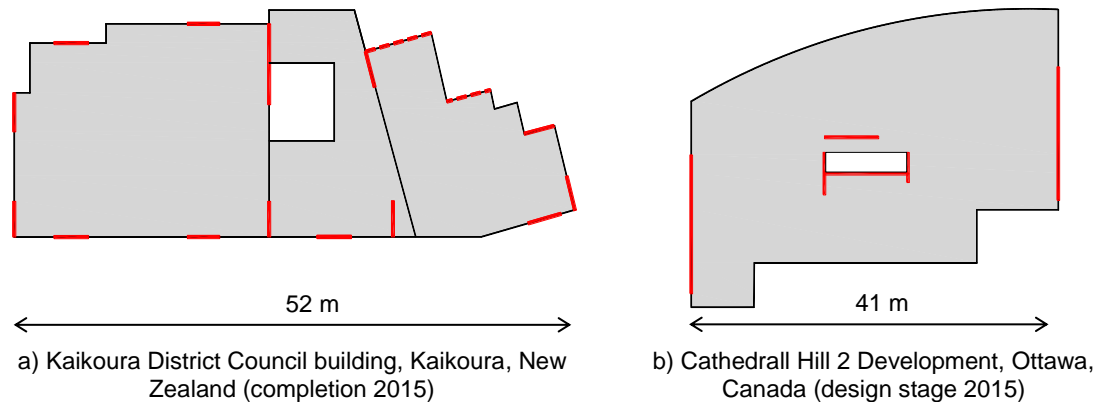


Figure 6.13 Floor layouts of recently built or planned buildings (LLRS in red)

6.4.1 Current knowledge in the calculation of diaphragm deflection

The first comprehensive publication concerning the design of timber diaphragms was the Guideline for the Design of Horizontal Wood Diaphragms (ATC 1981). It contains some considerations regarding diaphragm deflections and shows the derivation of a four term deflection equation. The fastener slip contribution derived by Countryman (1952), however, had an error, which was then later corrected (James 1984). The deflection equation, based on first principles as derived in Appendix A, is still in use in a number of timber design codes as shown below. The deflection of a diaphragm is attributed to the following four contributions:

- Bending deformation (of the chord beams);
- Shear deformation (of the sheathing panels);
- Fastener slip;
- Chord splice slip.

Similar to the strength evaluation of the diaphragm, it is assumed that all bending of the diaphragm is resisted by the chord beams and that the sheathing panels have a negligible axial stiffness. Likewise, the shear deformations are purely attributed to the sheathing elements. The fastener slip provides the biggest deflection contribution as shown in Figure 6.17. For its derivation it is assumed that fastener forces are all parallel to the panel edges, all panel edges are connected to each other (blocked diaphragm) and that the fastener spacing is constant over the whole diaphragm. Because of limited available beam lengths, chords need to be spliced. An additional term can account for the splice slip on the diaphragm deflection. Engineering judgement on the amount of splice slip to account in the equation is required (Skaggs and Martin 2004; Curtis 2009). To prevent large deformation contributions from the

chord splice, the former German Timber Standard DIN1052 (DIN 2008) required that chord splices are be designed as stiff as possible by increasing the chord demand by 1.5.

Following the deflection equation from three major timber codes are shown. All equations contain the single deflection contributions as mentioned above. For the detailed comparison of the code equations see Appendix A:

- New Zealand Timber Structures Code NZS 3603 (commentary clauses) (Standards New Zealand 1993):

$$u_{diaphragm} = \frac{5WL^3}{192EAH^2} + \frac{WL}{8GHt} + \frac{1}{2}e_n(1 + \alpha)m; \quad (6.1)$$

- Canadian Standard Engineering Design in Wood O86-14 (Standards Council of Canada 2014):

$$u_{diaphragm} = \frac{5}{96} \frac{tL^3}{EAH} + \frac{tL}{4B_v} + 0.000614 L e_n + \sum \frac{\Delta_c x}{2H}; \quad (6.2)$$

- Special Design Provisions for Wind and Seismic SDPWS2008 (AF&PA American Wood Council 2008):

$$u_{diaphragm} = \frac{5}{96} \frac{tL^3}{EAH} + \frac{tL}{4Gd} + 0.188 L e_n + \sum \frac{\Delta_c x}{2H}; \quad (6.3)$$

where: W lateral load applied to the diaphragm (resultant of the diaphragm load);
 L span of the diaphragm;
 E elastic modulus of the chord members;
 A cross sectional area of one chord;
 H distance between chord members (diaphragm height);
 d sheathing panel thickness;
 G shear modulus of the sheathing;
 m number of sheathing panels along the length of the chord member;
 α sheathing panel aspect ratio $\alpha = b/h$;
 e_n fastener slip of the panel-to-panel connection;
 t unit shear force $= \frac{W}{2H}$;
 Δ_c chord splice slip;
 x position of chord splice from the origin;
 B_v shear-through-thickness rigidity of the sheathing $= Gd$.

Note that equation (6.3) requires imperial units, whereas all other equations require SI units.

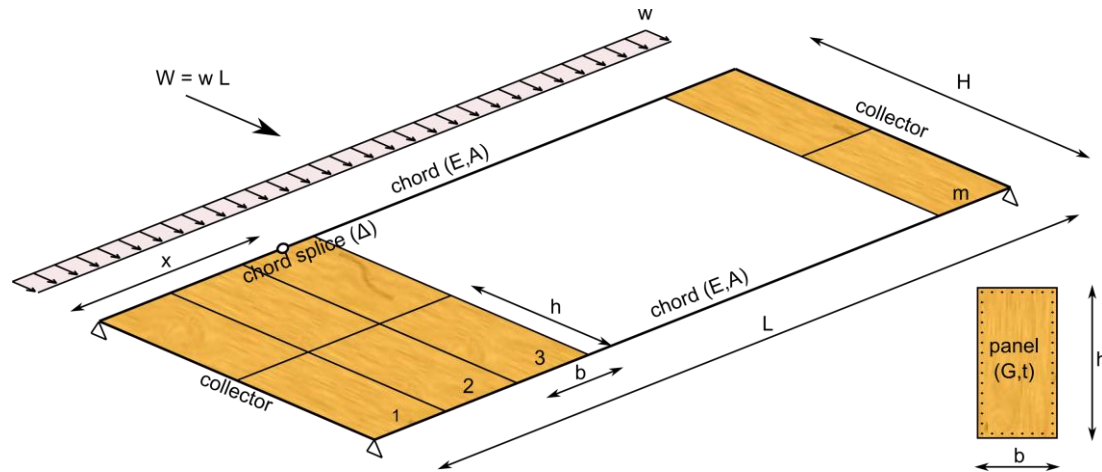


Figure 6.14 Diaphragm notation

Even though the New Zealand equation does not include the splice slip term, it provides the most general equation, as the panel dimension can be chosen arbitrarily. The fastener slip contribution is dependent on the slip of the single fastener e_n , but also on the panel aspect ratio $\alpha = b/h$ (b = panel length along the chord beam). This is to account for the fastener slip on the vertical and horizontal joints of the single panels.

Although the bending and shear deflection terms in the Canadian equation are equivalent to the New Zealand terms, the fastener slip term is determined for a standard plywood panel size of 4 x 8 feet (i.e. 1219 x 2438 mm, which is normally rounded to 1.2 x 1.4 m).

The American equation is equivalent to the Canadian equation, except of the imperial units used. Converted in SI units the fastener slip constant 0.188 from Equation (6.3) becomes $1/1,627$ which is exactly the value 0.000614 used in Equation (6.2). Although the fastener slip e_n is provided as a force-displacement relationship for nails in NZS3603, the North American codes provide empirical formulas for different fastener type and sizes and sheathing materials.

6.4.2 Deflection of unblocked diaphragms

According to Kessel and Schönhoff (2001) and Schulze and Schönhoff (1989), unblocked diaphragms have a displacement 4 times larger than an equivalent blocked diaphragm. The stiffness should therefore be taken as 25% of the stiffness of a blocked diaphragm. Research carried out by the American Plywood Association similarly suggests that the overall diaphragm deflection should be multiplied by 2.5 or 3, depending on the spacing of the framing elements (APA 2007). Because of the high loads, the connectors close to the unsupported edge might undergo extensive yielding and therefore lead to large deformations. Eventually the forces are

transferred by contact of the panels which are wedged together. This mechanism does not lead to immediate brittle failure, but leads to very large displacements.

6.4.3 Deflection of diaphragms with non-uniform fasteners

Especially for larger diaphragms, the fastener spacing is staggered to account for larger unit shear forces close to the supports and zero forces at mid-span. To account for this in the diaphragm deflection, the fastener slip term needs to be modified accordingly. This can be simply achieved by applying a factor which is the ratio of the average load on the fastener with uniform nailing v_n and the average load on the fastener with non-uniform nailing v_n' (ATC 1981). A sample can be found in Skaggs and Martin (2004) which is reproduced in Equation (6.4) and Figure 6.15.

$$factor = \frac{v_n'}{v_n} = \frac{Area_2 + Area_3}{Area_1} = \frac{0.5(100 + 75)20 + 0.5 \cdot 125 \cdot 50}{50 \cdot 100 \cdot 70} = 1.39 \quad (6.4)$$

In Figure 6.15 the derivation of the factor is shown on the hand of equivalent areas. Area 1 is proportional to the average fastener force v_n and the sum of Areas 2 and 3 is proportional to the average fastener force v_n' . The ratio is the factor which amplifies the fastener slip contribution.

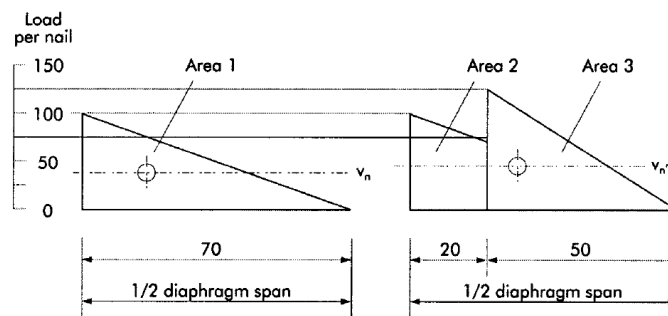


Figure 6.15 Floor layouts of recently built or planned buildings (Skaggs and Martin 2004)

6.4.4 Deflection of irregular diaphragms

For diaphragms with a limited number of irregularities, hand methods based on first principles are available to determine unit shear forces and axial forces in frame elements. For such cases the deflection equation can be integrated over parts of the diaphragm. Similarly can varying loading conditions or diaphragms with non-uniform depths and widths be analysed. A good source of examples with step-by-step calculations can be found in Malone and Rice (2012).

For very irregular diaphragms, the last resource for the determination of diaphragm deflections can be found in finite element analysis, requiring however high resources in terms

of software, and time. The truss analogy presented in Chapter 7 provides a simple and valid alternative for the determination of diaphragm deflections with irregularities with various types of loading types.

6.4.5 Floor stiffness in historic buildings and retrofit solutions

Several guidelines, like the FEMA 356 (American Society of Civil Engineers 2000) or the guidelines for the Assessment and Improvement of the Structural Performance of Buildings in Earthquakes (New Zealand Society for Earthquake Engineering 2006), provide reference values or simple equations to evaluate the stiffness of existing timber diaphragms, with and without blocking or chord beams. Brignola (2009) compared some of these values with experimental testing carried out at the University of Canterbury and test results by Peralta et al. (2004) and developed a new analytical formulation. Recently procedures for the seismic assessment and improvement of historical timber diaphragms in New Zealand have been published (Giongo et al. 2014).

The main emphasis of these and similar research projects are the determination of stiffness values for existing (historical) diaphragms and their retrofit. Several more publications about strengthening and retrofit of timber floors, mainly in masonry buildings can be found in literature (Piazza et al. 2008; Valluzzi et al. 2010; Wilson et al. 2011).

6.4.6 Parameters influencing the diaphragm deflection

An extensive experimental campaign regarding the stiffness evaluation of state-of-the-art timber diaphragms has been carried out by Dolan et al. (2003) in the CUREE-Caltech Wood Frame Project. The influence of several parameters like corner and centre openings, diaphragm blocking, adhesives and lateral walls were investigated. Although factors influencing the diaphragm stiffness have been identified, no additional guidance on the analytical estimation of diaphragm deflection is provided.



Figure 6.16: Fully sheathed 3 x 12,2m specimen (Dolan et al. 2003)

Another experimental campaign was carried out by Filiatrault et al. (2002) on diaphragms in a two storey wood frame building. Different variables were taken into account while studying the shear and flexural flexibility of the diaphragms. Nailing pattern only had minor influence on the shear flexibility, whereas blocking of the edges stiffened the diaphragm. Flexural flexibility on the other hand was only influenced by the presence of chord beams; these can be made up by the walls from the upper and lower storeys.

By considering the three fundamental deflection contributions of bending, shear and fastener slip in their most general form as written in Equation (6.5), the following inverse linear relationship can be seen (see Appendix A for notations and derivation of the equation):

- the bending stiffness is in proportion to the elastic modulus and the cross sectional area of the chord material;
- the shear stiffness is in proportion to the shear modulus and the thickness of the sheathing panel material; and
- the fastener slip is in proportion to the slip modulus and the spacing of the fasteners.

$$u_{diaphragm} = \frac{5}{192} \frac{W L^3}{EA H^2} + \frac{1}{8} \frac{W L}{Gt H} + \frac{1}{4} \frac{W s}{K_{ser}} \left(1 + \frac{b}{h}\right) \frac{1}{b} \frac{L}{H} \quad (6.5)$$

Aside from this linear dependency, the length-to-width ratio L/H is the term which is influencing the diaphragm deflection most. The ratio is in a linear dependency to the shear and fastener slip terms, but is non-linear proportional to the bending term.

A typical blocked LTF diaphragm with plywood sheathing panels of 1.2 x 2.4 m and nails has been considered to evaluate the deflection contributions. Figure 6.17 shows these values for a range of L/H values considering a diaphragm depth of 5 m.

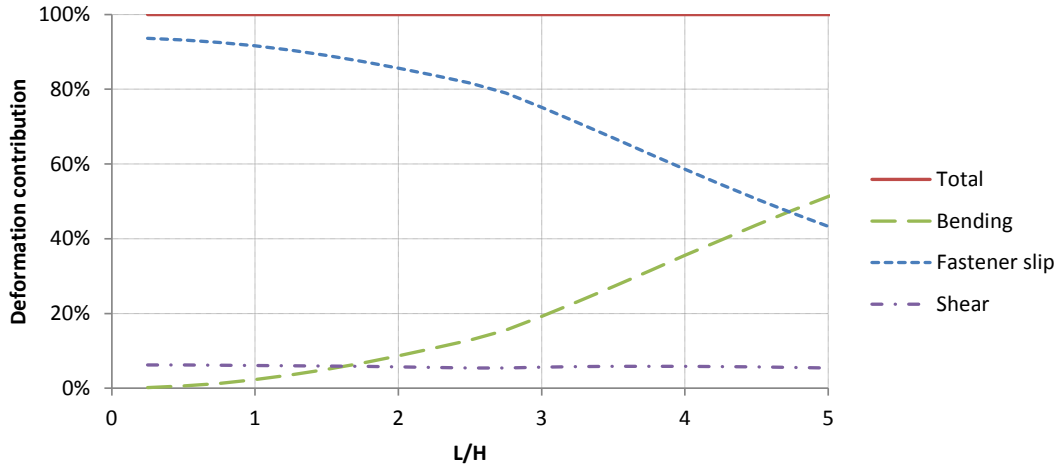


Figure 6.17 Diaphragm panel deflection due to panel shear deformation, vertical connector slip and horizontal connection slip

Although the shear deflection has a limited influence for all ratios, the bending term is becoming more dominant for longer diaphragm spans. This is expected, since the diaphragm behaviour is moving away from the typical deep beam behaviour. The figure also explains why diaphragm ratios are limited to an upper value of 5, where the diaphragm behaviour is not following the assumptions of the deep beam and excessive diaphragm flexibility would be achieved.

6.4.7 Flexibility of the connections between the diaphragm and the lateral load resisting system

In the majority of cases the evaluation of diaphragm flexibility is limited to the diaphragm panels, panel connections and chord beams only. The connection of the diaphragm to the lateral load resisting system introduces a further source of flexibility and needs to be considered as well. For diaphragms working as simply supported beams, this additional deformation can simply be accounted as

$$u_{connection LLRS} = \frac{1}{2} \frac{W}{K_{connection LLRS}} \quad (6.6)$$

Where W is the total load of the diaphragm and $K_{connection LLRS}$ is the slip in the connection between the diaphragm and the lateral load resisting system. In difference to the panel connections carried out by a series of small diameter fasteners, the connection to the lateral

load resisting system is often realized with discrete connectors of larger diameter. The detailing of such connectors often requires larger hole diameters, resulting in additional slip in the connection.

6.4.8 Deflection equation for diaphragms with solid timber panels

Assuming that the same design assumptions as for LTF diaphragms can be applied to massive timber diaphragms, the deflection for such kind of diaphragms can be assessed based on the same first principles. Aside from the thickness of the panels involved, the main difference of the two diaphragm types are the missing frame elements to connect the individual sheathing panels together. For massive timber diaphragms, the panel elements are most commonly directly connected to each other with screws. Therefore only the fastener slip term of Equation (6.1) needs to be amended.

The deflection equation for massive timber diaphragms therefore becomes:

$$u = \frac{5WL^3}{192EAH^2} + \frac{WL}{8GHd} + \frac{1}{4}e_n(c_1 + c_2\alpha)m; \quad (6.7)$$

where:	W	lateral load applied to the diaphragm;
	L	span of the diaphragm;
	E	elastic modulus of the chord members;
	A	cross sectional area of one chord;
	H	distance between chord members (diaphragm height);
	d	sheathing panel thickness;
	G	shear modulus of the sheathing;
	m	number of sheathing panels along the length of the chord member;
	α	sheathing panel aspect ratio $\alpha = b/h$ (b is the length in chord direction);
	e_n	fastener slip of the panel-to-panel connection;
	c_i	is the number of connections rows along sheathing panel edge;
	c_1	number of lines of fasteners between adjacent panels along the sheathing panel height h ;
	c_2	number of lines of fasteners between adjacent panels along the sheathing panel length b .

The fastener slip term has been modified to account for the fact that the unit shear force is normally transferred from one panel directly to the adjacent one. This means that only the connection slip along one panel edge in load direction needs to be considered, c_1 is therefore typically 1. Massive timber diaphragms are normally supported by gravity beams at their ends; the same beams are also used to transfer the shear force between adjacent panels, resulting in $c_2 = 2$. The connection slip along the panel heads is therefore accounted as for LTF diaphragms. If the massive timber panels are however connected by a strip of plywood, placed in a recess

and nailed to both panels, then same equation as for LTF diaphragms can be used ($c_1 = 2$). The fastener slip e_n is calculated for the maximum unit shear force at the support.

To evaluate the proposed equation, diaphragm deflections are compared with the outcomes of a finite element analysis. The regular diaphragms were assumed to be made of massive timber panels connected with screws placed in a lap joint. Material properties, section dimensions and detailed to the FEM analysis can be found in Appendix B. The diaphragm geometries are shown in Table 6.4.

Table 6.4 Diaphragm geometry description



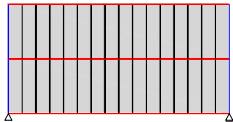
A	B	C
8 panels simply supported 1.95x1.05 m	8 panels simply supported 3.90x1.05 m	16 panels, 2 rows simply supported 3.90x1.05 m
		

Table 6.5 shows that for the 3 geometries the proposed equation provides quite accurate values when compared to a sophisticated finite element analysis. When the fastener stiffness perpendicular to the panel edges is ignored, as suggested by the shear field analogy, then a maximum error of 7% was found. If the fastener stiffness in both directions is accounted for, then a larger error of 18% was observed for a short diaphragm. This is because of the differential movement of the panels and the tendency of the chord beams to prevent this behaviour via their bending stiffness. For long diaphragm lengths this additional stiffness clearly decreases since the bending stiffness decreases. This effect is not specific to massive timber diaphragms, but is also found in LTF diaphragms.

Table 6.5 Deflection comparison between proposed equation and values from a finite element analysis

	equation	FEM 1	FEM 2
A	4.0	3.8 (107%)	3.4 (118%)
B	3.1	3.0 (103%)	2.8 (111%)
C	12.2	12.4 (99%)	12.2 (100%)

Note that FEM 1 considers zero fasteners stiffness perpendicular to the panel edges, FEM 2 considers the same stiffness parallel and perpendicular to the panel edges.

The comparison suggests that the proposed equation can be applied to obtain accurate deflection estimation of regular, simply supported timber diaphragms.

6.4.9 Limitations of the deflection equation

The provided equations provide a simple tool to estimate the deflection of LTF and massive timber diaphragms. Their application, however, is limited to blocked diaphragms which can be idealized as simply supported beams, with uniform nailing and no irregularities. Despite all simplifications and assumptions necessary to derive the equations, experimental results have shown that the theoretical values provide reasonable estimates (James 1984; Filiatrault et al. 2002; Skaggs and Martin 2004). Nevertheless such equations should only be considered as rough estimates and only applied using engineering judgement.

Major sources for the inaccuracy are the bending contribution of frame and chord beams, the axial and shear connections of framing elements, fastener stiffness activation perpendicular to the panel edge and the friction between panels and framing elements. The first three contributions could also be observed in the FEM analysis developed in this research.

Because of their complexity, real floor layouts normally do not allow for the use of the simplified equations. Even by integrating the equations over diaphragm, such methods soon reach their limit when applied with hand calculations only. A truss analogy as discussed in Chapter 7 provides an easy yet relatively sophisticated way to derive diaphragm deformations.

6.5 DISCUSSION

6.5.1 Load application

Diaphragms are often analysed with idealized models by applying a uniformly distributed load to the diaphragm compression edge. Although this is common in the case of wind loads applied to the façade of a building, the load transfer from the chord beam into the remaining diaphragm is normally not considered. Seismic loads and the introduction of concentrated force introduction are normally not specifically addressed.

6.5.2 Massive timber diaphragms

Finite element models of regular and irregular Light Timber Framing (LTF) and massive timber diaphragms under different load application types were carried out. Differences on the load distribution into the diaphragms for both LTF and massive timber diaphragms could be observed in the simple diaphragm models with only one row of panels. Additional effects on the force distributions and deflections were found in irregular diaphragms and especially in

case of massive timber panels. Under area loads LTF sheathing and massive timber panels were mainly working in shear with negligible longitudinal stresses. The same was observed for concentrated forces applied into the framing elements of LTF diaphragms. In massive timber diaphragms, concentrated loads and line loads created longitudinal stresses because of the absence of other axial load carrying members, like frame elements. Although axial loads normally can be resisted easily by massive panels, fasteners must be designed for these additional loads. Portions of the diaphragm close to the point of force introduction were activated to a higher degree than the more distant parts. The resulting additional fastener demand and partial diaphragm activation is recognized in the German National Appendix to Eurocode 5 (Eurocode 5 DIN NA 2010), and should be considered in general and specifically for massive timber diaphragms.

Finite element analysis under different load applications showed that massive timber diaphragms can be analysed with the girder analogy, as long as the external loads can be introduced into the diaphragm depth. Although this is always the case for area loads, panel connections must be designed for this additional force demand for loads applied to diaphragm edges. Because massive timber panels have high longitudinal stiffness, panels and fasteners also contribute to the bending strength of diaphragms. Panels therefore need to be checked for tensile stresses perpendicular to the grain and fasteners for force components perpendicular to the panel edges. This mechanism was found to be very pronounced for diaphragms without chord beams, also leading to very flexible diaphragm designs.

6.5.3 Diaphragm deformation and stiffness

Determining the diaphragm flexibility is essential because it has the potential to influence both the global dynamic behaviour of the building (Chapter 4) and the load distribution into the lateral load resisting system. Diaphragm deflections are also of importance for the serviceability of the building and the global stability of all other connected structural elements. Common diaphragm deflection equations are based on a number of assumptions and can be derived from first principles as shown in Appendix A. Despite its simplicity, these formulae provide still a reasonable estimate for the diaphragm deflection. Floor layouts however are normally far away from the model assumptions and, because of the lack of more sophisticated analysis tools, designers often skip the deflection check. To overcome some of these limitations, procedures to account for openings, staggered fastener pattern and diaphragms with unsupported edges are briefly shown. These methods are, however, mostly unknown to

designers and therefore never applied. It is therefore recommended that a truss analogy as shown in Chapter 7 is used, which also provides accurate deformation estimations of diaphragms.

In this chapter, a modified deflection equation for use on massive timber diaphragms is also introduced.

6.6 CONCLUSIONS

The following conclusions can be drawn from this chapter:

- In LTF diaphragms, the load application does not influence the load path, as long as forces are introduced and distributed via the framing elements;
- In massive timber diaphragms force introductions along the diaphragm edges generate longitudinal stresses in the diaphragm panels and create force components perpendicular to the panel edges to be resisted by the connections;
- In massive timber diaphragms longitudinal stresses need to be transferred along the panels in order to activate diaphragm portions away from the point of force introduction;
- Traditional analysis like the girder analogy can be used to analyse regular massive timber diaphragms as long as the force introduction into the diaphragm can be guaranteed by providing the transfer of longitudinal stresses along the individual panels across the diaphragm depth;
- Absence of chord beams result in very flexible diaphragms and generate high tensile forces in the fasteners, as well as transversal stresses which have the potential to created brittle failures;
- A number of procedures are available to extend the use of traditional diaphragm deflection formulations to irregular diaphragms. Their complexity, however, calls for an alternative approach to determine diaphragm deflections. A possible solution can be found in the Equivalent Truss Methods as discussed in Chapter 7;
- A simple deflection formulation is proposed for the calculation of the deflection of massive timber diaphragms.

7 Equivalent Truss Method for timber diaphragms

7.1 INTRODUCTION

This chapter describes the Equivalent Truss Method for the analysis of timber diaphragms, following on from Chapter 3 where the currently available analysis methods for diaphragms were summarized and briefly discussed, highlighting their limitations. Solving timber diaphragms with simple hand calculation methods like the girder analogy are the common approach in most design offices. While for rectangular and regular floor layouts this is a valid approach most floor diaphragms do not fall in this category. Complex floor plans with irregularities like openings, re-entrant corners, concentrated horizontal forces and the presence of multiple supports, which make the diaphragm statically indeterminate, make hand calculations soon reach their limit. Even if general purpose Finite Element Methods (FEM) analysis programs are becoming more accessible in design offices, their application to timber diaphragms is normally limited to special studies since it requires a great amount of modelling and post-processing time. To encourage the use and proper calculation of timber diaphragms in new construction, an intuitive and more cost efficient method for their analysis is therefore essential, which the Equivalent Truss Method can provide.

7.1.1 Strut-and-Tie Method

In New Zealand, the Strut-and-Tie Method is encouraged for the analysis of concrete diaphragms. It is codified in the New Zealand Concrete Standard NZS3101 (Standards New Zealand 2006) and will also be implemented in the upcoming amendment to the New Zealand Loading Standard for Earthquake Actions NZS1170.5 (Standards New Zealand 2004a). Although, the strut-and-tie method is generally applicable to any concrete element, it can be quite time consuming because of multiple possible strut-and-tie geometries especially with varying load conditions. Bull and Henry (2014) and Scarry (2015) therefore encourage the use of truss models as previously developed by Hrennikoff (1941). With this approach, the most probable load path is found automatically and multiple load conditions can be studied with the same model. Since the diaphragm flexibility can also be evaluated, it is suitable for determining the force distribution into the lateral load resisting system and to study torsional effects.

7.1.2 Equivalent Truss Method for timber diaphragms

Because of the simple yet powerful approach of truss models, such analogy is also desirable for LTF and massive timber diaphragms. In contrast to concrete diaphragms, which consist of continuous concrete slabs with orthogonal reinforcing, timber diaphragms consist of a number of sheathing panels connected to each other with flexible fasteners. The definition of the truss elements therefore needs to be based on different assumptions as, for example, used in the method defined by Kamiya (1990) which used equivalent bracing elements for the analysis of LTF diaphragms with openings. This method, however, has not found acceptance in the broader design community. Kessel and Schönhoff (2001) provided a more detailed characterisation of a truss analogy for LTF diaphragms, based on the shear field analogy. Although the approach is reasonably straight-forward in its application to real problems, its use has only found little application, probably because it is only documented in German.

7.1.3 Proposed enhancements to the Equivalent Truss Method for timber diaphragms

In this chapter, the principles behind the truss analogy for LTF timber diaphragms are derived and explained in detail, and subsequently verified against more accurate analysis methods. Because modern floor layouts tend to have an increasing number of irregularities, requiring reinforcement in form of steel brackets or strut beams, such elements also need to be considered in the analogy. The position of openings and re-entrant corners, as well as the availability of engineered panel dimensions with high aspect ratios require the refinement from one equivalent diagonal per panel to multiple diagonals per panel. The combination of multiple diagonals per panel and the derivation of the deflection formulae of massive timber panels provide the extension of the truss analogy to massive timber diaphragms. The enhanced truss analogy, referred to as Equivalent Truss Method, not only provides unit shear forces and diaphragm deflections, but also axial stresses in strut beams and other reinforcing elements. It further provides an estimate of the longitudinal forces in massive timber diaphragms, which are normally absent in LTF diaphragms.

The basic principles of the truss analogy for LTF diaphragms are explained on the shear field analogy. The method is applied to a cantilever diaphragm and results are compared to other available methods. Then, the analogy is extended to massive timber panels by deriving their deformation equation. The formulation for multiple diagonals is then described, also defining the properties of the remaining truss elements. Different diaphragm geometries are then

calculated and verified for two different truss geometries. Finally, the Equivalent Truss Method is applied to irregular LTF and massive timber diaphragms with different loading conditions and verified against finite element analysis. The chapter is concluded by the limitations of the analogy and a summary.

7.2 THE GENERAL PRINCIPLES OF THE TRUSS ANALOGY FOR TIMBER DIAPHRAGMS

The basic concepts and limitations of the truss analogy for the design of timber diaphragms have been discussed in Chapter 3. Following the analogy is described on the basis of first principles and then later applied to both LTF and massive timber diaphragms.

As known from solid mechanics, the shear force F causes the deformation of a rectangular element in a parallelogram with a shear angle γ as shown in Figure 7.1. The flexibility of the panel fasteners further increases the panel deflection. This deflection behaviour can be reproduced by a quadrilateral system with an equivalent diagonal as shown in Figure 7.1b. The stiffness of the equivalent diagonal is chosen in a way to have the same panel deformation under a load F as for the shear panel. Considering that the sheathing panel is surrounded by framing elements and connected with flexible fasteners, this analogy holds by assuming that the four bars are the framing elements pinned to each other and the diagonal provides the shear stiffness and fastener stiffness of the LTF floor panel.

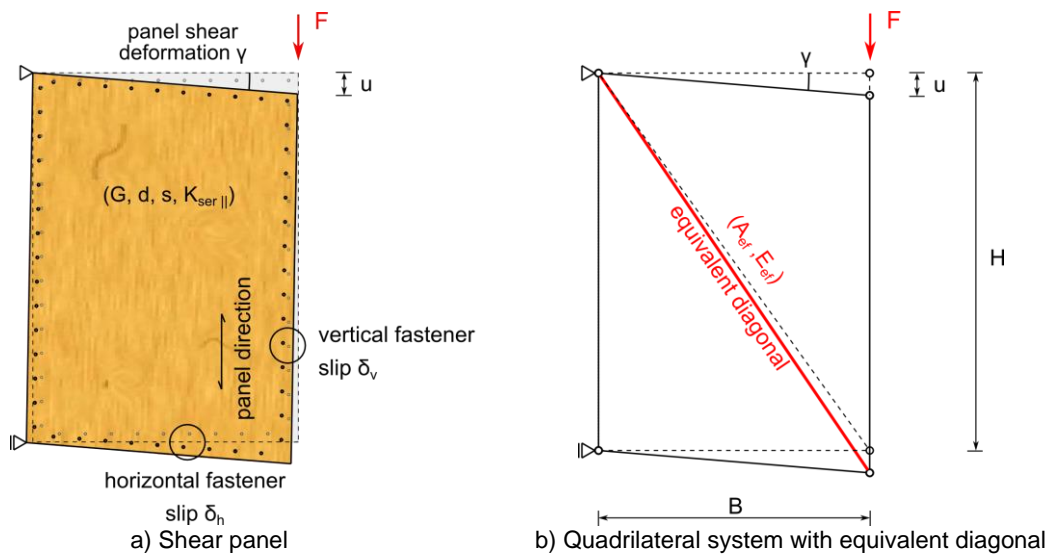


Figure 7.1 Shear panel with fastener stiffness and equivalent truss diagonal

If the assumptions of the shear field analogy as discussed in Chapter 3 are valid, the shear panel only resists shear forces and the framing elements only work in axial tension or compression. In the panelised system no force introduction occurs at the nodes, except for externally applied forces. Because the unit shear force is constant for each shear panel, the forces are transferred gradually along the framing elements to the sheathing panels. If it can be assumed that the fasteners are smeared along the panel edges, this force introduction is linear.

In the truss analogy, however, the resultant shear force in the panel is transferred via the diagonal to the nodes. It is therefore necessary to correct this concentrated force introduction by distributing the force along the panel edges to obtain the real forces in the framing elements. This procedure is shown for a generic truss in Figure 7.2, where the axial forces in the longitudinal and transversal elements are obtained by solving the truss. These forces are then corrected by adding the contribution from the unit shear force, which needs to be integrated along the element length, to the framing element at the node where a diagonal is connected. This can be done by simply adding (with the respective sign) the unit shear force of the panel times the length of the panel edge to which the framing member is attached to, to the axial force at the node of the framing element under consideration. The unit shear force in the panel can directly be obtained by the force acting in the equivalent diagonal. A design example in the following chapter will provide a numerical example of this procedure.

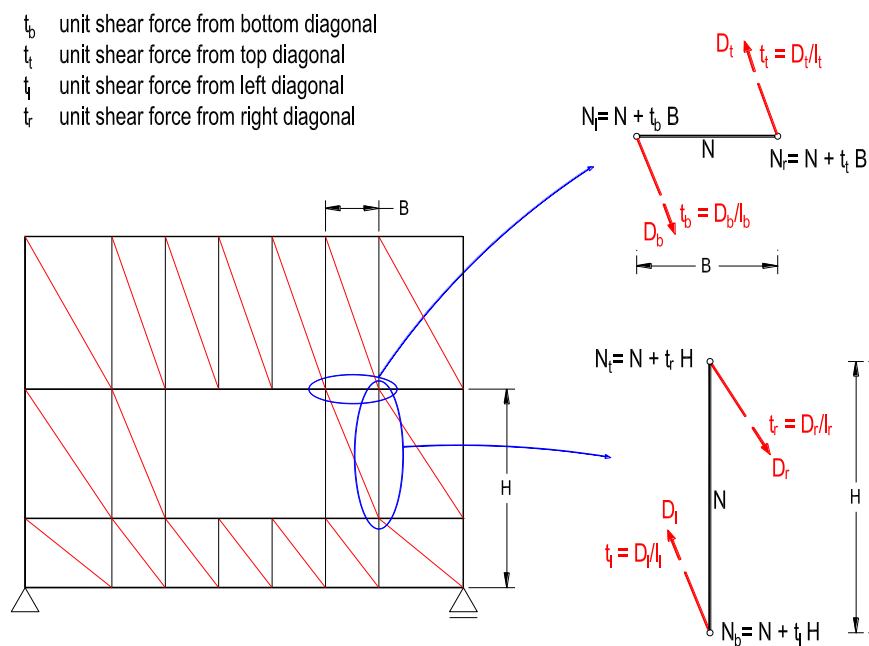


Figure 7.2 Post-calculation for the determination of the frame forces (modified from (Kessel and Schönhoff 2001))

To successfully analyse the unit shear force and the force in the framing elements, a consistent sign convention is paramount. The positive sign of the shear force, shear angle and unit shear force as shown in Figure 7.3 is used throughout this document. If the diagonals are placed from the top left corner to the bottom right corner of the quadrilateral systems, then a positive (tension) force in the diagonal equals an elongation of the idealised panel strip as shown in Figure 7.3b. This results in a positive unit shear force (shear flow) in the panel.

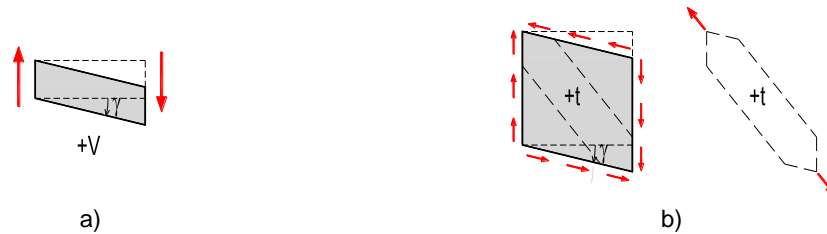


Figure 7.3 Sign convention for positive a) shear force and shear angle; b) unit shear force and shear angle

7.3 THE TRUSS ANALOGY FOR LTF DIAPHRAGMS

In order to define the equivalent stiffness of the sheathing panel connected to framing elements via flexible fasteners, the single deformation contributions as shown in Figure 7.1a derived in Appendix A can be written as follows.

$$u'_{panel\ shear} = \gamma B = \frac{\tau}{G} B = \frac{t}{Gd} B = \frac{1}{Gd} \frac{FB}{H}; \quad (7.1)$$

$$u'_{fastener\ v} = \frac{2s}{K_{ser}b} \frac{FB}{H}; \quad (7.2)$$

$$u'_{fastener\ h} = \frac{2s}{K_{ser}h} \frac{FB}{H}; \quad (7.3)$$

where

$u'_{panel\ shear}$	shear deflection of a cantilevered panel;
$u'_{fastener\ v}$	deflection due to slip in the vertical joints;
$u'_{fastener\ h}$	deflection due to slip in the horizontal joints;
γ	shear angular deformation;
τ	shear stress;
$t = \tau d$	unit shear force;
H	height of the shear panel;
B	length of the shear panel;
h	height of single sheathing panel;
b	length of single sheathing panel;
G	shear modulus;
d	sheathing panel thickness;
s	fastener spacing;
K_{ser}	fastener slip.

The reason why the height and length for the shear panel (uppercase H and B respectively) and the height and length for the sheathing panel (lowercase h and b respectively) are treated separately is that a number of sheathing panels might be required to make up one shear panel, and the additionally required panel connections provide additional flexibility to the shear panel. Designers can therefore decide to either setup a model with one diagonal replacing an entire shear panel as shown in Figure 7.4b (the diagonal stiffness includes the slip of the internal sheathing panel joints), or to model each individual sheathing panel with a diagonal including the respective framing elements as in Figure 7.4c. If the shear panel is made of one sheathing panel only, then $B = b$ and $H = h$.

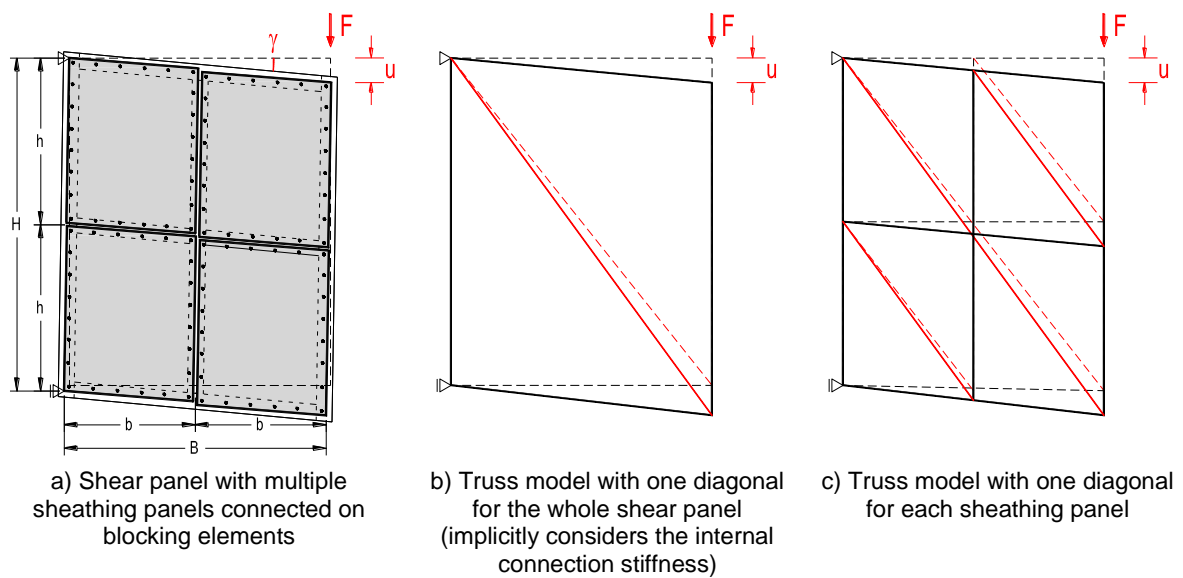


Figure 7.4 Truss models solutions for a shear panel with multiple sheathing panels

Summing Equations (7.1) to (7.3), the total deflection of the shear panel can be calculated in terms of an equivalent (or effective) shear-through-thickness rigidity $(Gd)_{ef}$.

$$\begin{aligned}
 u'_{shear\ panel} &= u'_{panel\ shear} + u'_{fastener\ v} + u'_{fastener\ h} \\
 &= \left[\frac{1}{Gd} + \frac{2s}{K_{ser}} \left(\frac{1}{b} + \frac{1}{h} \right) \right] \frac{FB}{H} \\
 &= \frac{1}{(Gd)_{ef}} \frac{FB}{H}.
 \end{aligned} \tag{7.4}$$

For LTF diaphragm this value can be written as

$$(Gd)_{ef\ LTF} = \frac{1}{\left[\frac{1}{Gd} + \frac{2s}{K_{ser}} \left(\frac{1}{b} + \frac{1}{h} \right) \right]} \tag{7.5}$$

The deformation of the quadrilateral system as shown in Figure 7.1a has been derived in Appendix A and equals

$$u'_{diagonal} = \frac{Fl^3}{E_{ef}A_{ef}H^2}; \quad (7.6)$$

where

$$l \quad \text{length of the diagonal} = \sqrt{H^2 + B^2}.$$

The force in the diagonal and the respective normal stress are

$$F_{Diagonal} = \frac{F}{\sin\alpha} = \frac{Fl}{H}; \quad (7.7)$$

$$\sigma = \frac{F_{Diagonal}}{A_{ef}} = \frac{Fl}{HA_{ef}}. \quad (7.8)$$

If for convenience the unit shear force in the panel $t = F/H$ is set equal to the axial stress σ as suggested by Kessel and Schönhoff (2001), then the diagonal area numerically equals the diagonal length

$$t = \frac{F}{H} = \sigma = \frac{Fl}{HA_{ef}}; \quad (7.9)$$

$$A_{ef} = l = \sqrt{H^2 + B^2}. \quad (7.10)$$

By equating $u'_{panel\ shear}$ and $u'_{diagonal}$ and by using Equation (7.10), the equivalent (or effective) modulus of elasticity can be obtained

$$E_{ef} = \frac{(Gd)_{ef} l^2}{HB}. \quad (7.11)$$

By formally equating the effective area to the diagonal length, the units of A_{ef} (length) and E_{ef} (force per length) don't have the expected mechanical meaning, but they allow the determination of the required unit shear force by obtaining the axial stress in the diagonal. Conceptually this can be avoided if the stress in the diagonal is equalled to the unit shear force divided by a unit length.

Contrary to the suggestion by Kamiya (1990), all remaining truss elements should be modelled with their real cross section and material properties, as they all contribute to the flexibility of the diaphragm.

As for every truss, the angle of the diagonals should not be overly obtuse or acute. Ideally this angle should be around 45 degrees.

7.4 EXAMPLE OF THE TRUSS ANALOGY ON A CANTILEVERED LTF DIAPHRAGM

To show the appropriateness of the truss analogy, a simple cantilevered diaphragm as shown in Figure 7.5 is solved using the truss analogy. The results are then compared with both the shear field analogy (as discussed in Chapter 3) and a FEM model (see Appendix B for details).

The sheathing panel was made of a 20 mm Oriented Strand Board (OSB) panel with a shear modulus of 1,080 MPa, framing elements had a cross section of 50 x 100 mm with a modulus of elasticity of 11,000 MPa. Fasteners with a slip modulus of 1,500 N/mm were placed every 150 mm.

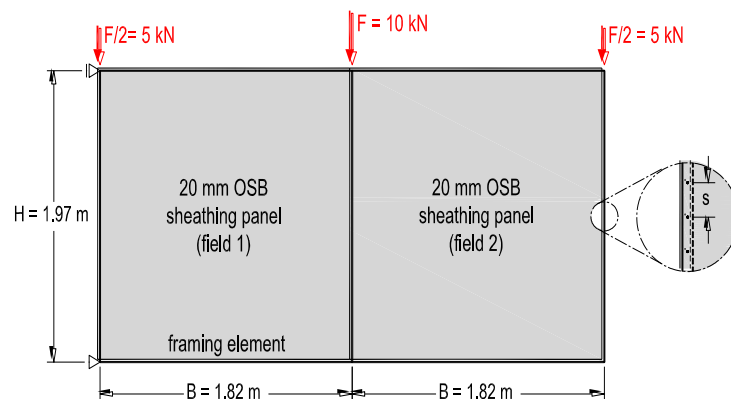


Figure 7.5 Cantilever diaphragm in LTF

For the given setup, the effective shear-through-thickness rigidity $(Gd)_{ef}$ was 3,880 kN/m from Equation (7.5), resulting in an effective modulus of elasticity E_{ef} equal to 7,785 kN/m and an effective area A_{ef} of 2.68 m from Equations (7.10) and (7.11) respectively.

By solving the truss, the axial forces as shown in Figure 7.6b were obtained. The unit shear forces derived from the diagonal forces were $t_1 = 7.6$ kN/m and $t_2 = 2.5$ kN/m respectively. These are the shear forces in the sheathing panels of field 1 and 2 respectively. The axial forces in the frame shown in Figure 7.6b were then corrected as shown in Figure 7.6c.

As an example the axial force in the framing element between the supports is shown next. The axial force from the truss has been calculated as being -20 kN. At the top of the framing element a diagonal is introducing a concentrated force of 20.42 kN. In reality this force is introduced linearly along its length and a correction to the axial force in the framing element is necessary. Since it is known that the force in the diagonal corresponds to a unit shear force of 7.6 kN/m, this value times the panel height of 1.97 m can be added to the axial force in the

framing element to obtain $-20 \text{ kN} + 7.6 \text{ kN/m} \cdot 1.97 \text{ m} = -5 \text{ kN}$. At the bottom of the framing member no diagonal is connected and therefore not unit shear force need to be added. This results in an axial force of -20 kN .

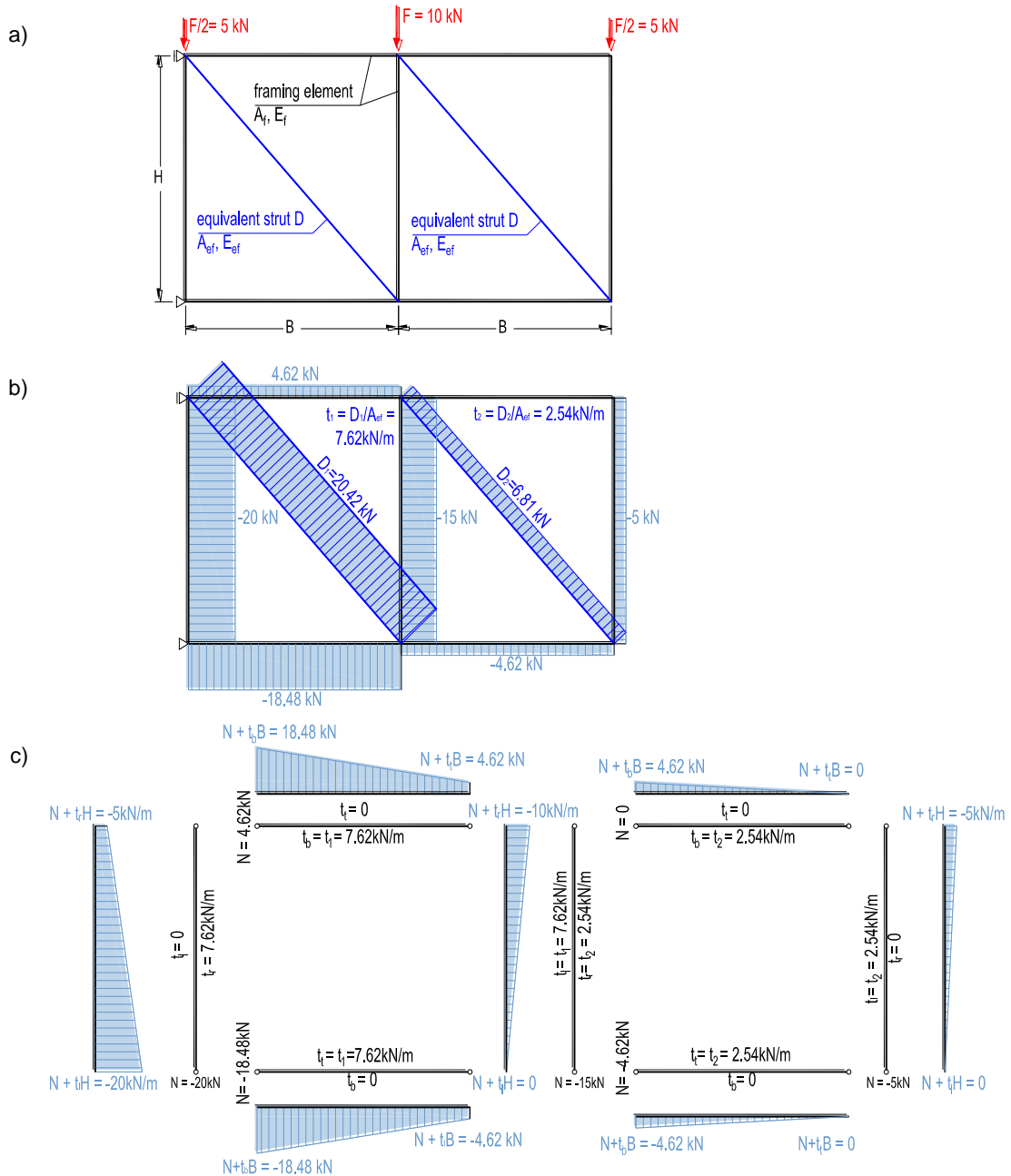


Figure 7.6 Panel shears and axial forces in the frame elements of a cantilevered diaphragm solved with an equivalent truss: a) cantilevered diaphragm representation with the truss beam analogy; b) axial forces in the truss beam; c) post-calculation to derive the axial forces in the framing members

The same system was solved with the shear field analogy as shown in Figure 7.7. Since the truss analogy is based on the shear field analogy, the unit shear force and the forces in the framing elements were the same.

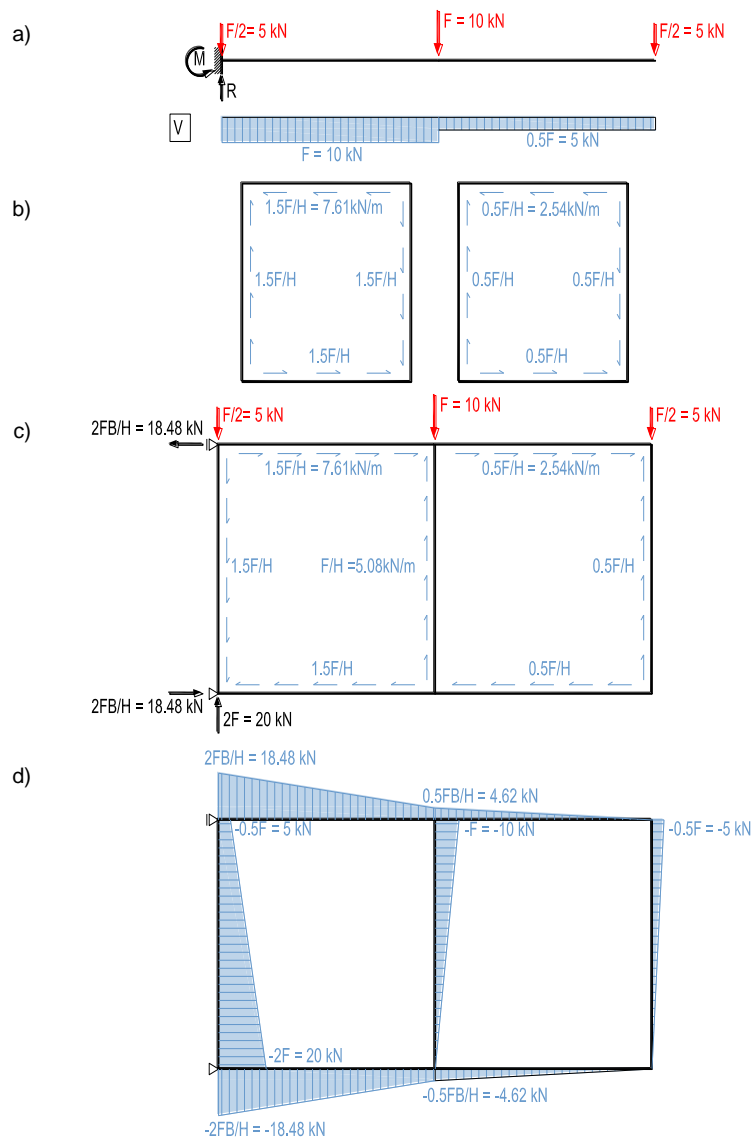


Figure 7.7 Panel shears and axial forces in frame elements of a cantilevered diaphragm according to the shear field analogy: a) equivalent static system and load assumption; b) unit shear in sheathing panel; c) unit shear on framing elements; d) axial force in framing elements

The definition of the longitudinal stresses n_{xx} and n_{yy} and shear stresses n_{xy} in plane elements is shown in Figure 7.8. It is noted that in this chapter $n_x = n_{xx}$, $n_y = n_{yy}$ and n_{xy} are shown as stresses multiplied by the panel thickness (forces per unit length).

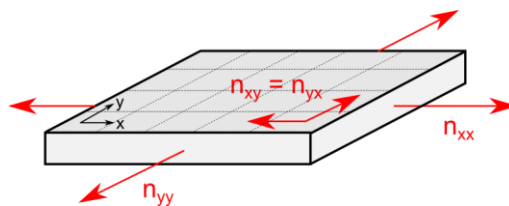


Figure 7.8 Definition of plane element stresses

Figure 7.9 shows the unit shear forces and the forces in the framing elements according to a FEM model. Except for some small variation in the shear force distribution over the panel elements, the values fit very closely with values obtained by the truss analogy.

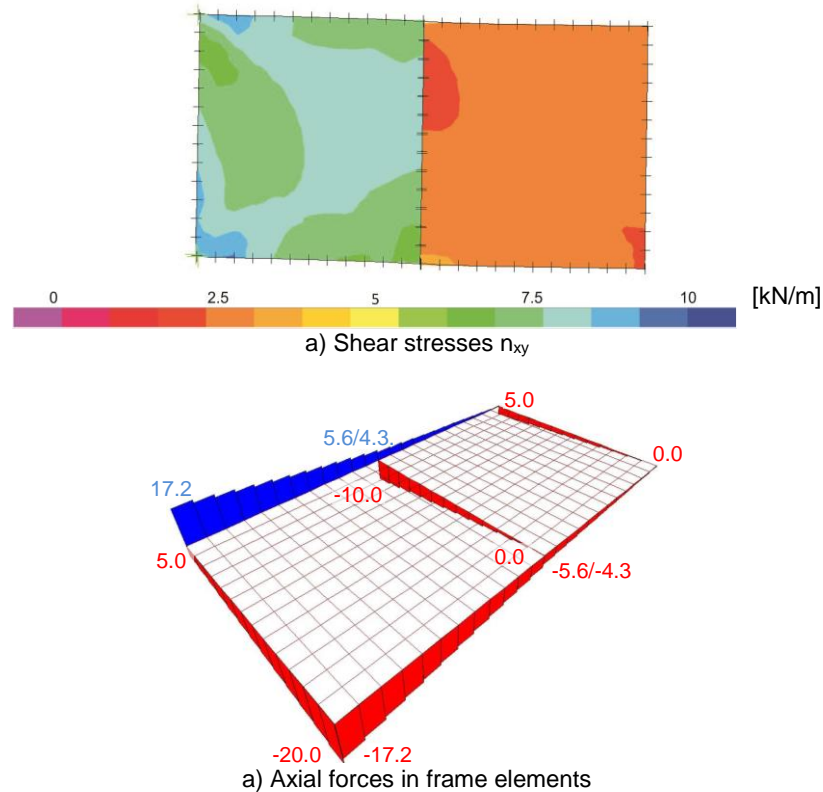


Figure 7.9 a) Shear stresses n_{xy} and b) forces in framing elements from the FEM analysis

Although the discussed example is statically determinate and therefore no stiffness considerations are required, the cantilever deflection from the truss analogy is compared to analytical equations and to the FEM analysis as well. Table 7.1 shows the cantilever deflection from the different approaches.

Table 7.1 Cantilever deflection of the system shown in Figure 7.5

	Truss analogy	Analytical formulation	FEM
Deflection [mm]	6.2	6.3	6.2

The deflection values from the truss analogy and the analytical formulation are very close. This is expected, since the shear and fastener slip contributions from the equation have been used to derive the diagonal stiffness. Differences in the deflection value are given by the bending contributions of the chord beams, which load demand is only an approximation to the assumed mechanism. For diaphragms with an increased number of panels, this difference will

become less noticeable. The deflection value from the FEM analysis is slightly smaller than from both the truss analogy and the analytical formulation, as additional effects like the bending resistance of the framing elements and stiffness of the fasteners perpendicular to the panel edge are activated.

From the comparison shown above, it can be concluded that the truss analogy provide a simple and accurate method to evaluate the force path and deformation for LTF diaphragms.

7.5 THE EQUIVALENT TRUSS METHOD FOR MASSIVE TIMBER DIAPHRAGMS

Similarly to the analysis of LTF diaphragms, the truss analogy can be used for massive timber diaphragms. Even though not all assumptions of the shear field analogy as discussed later are valid for this kind of diaphragms, the same procedure can be applied for the determination of the effective shear-through-thickness rigidity. Depending on the type of connection between the individual panels and between the panels and beams, $(Gd)_{ef}$ becomes

$$(Gd)_{ef} = \frac{1}{\frac{1}{Gd} + \frac{s}{K_{ser}} \left(\frac{c_1}{b} + \frac{c_2}{h} \right)}; \quad (7.12)$$

where

- c_i number of connections rows along the sheathing panel edge;
- c_1 number of lines of fasteners between adjacent panels along the sheathing panel height h ;
- c_2 number of lines of fasteners between adjacent panels along the sheathing panel length b ;

For massive timber panels no framing elements are necessary along the longitudinal panel edge, c_1 is therefore typically 1. The heads of the panels are sitting normally on a beam, requiring two lines of fasteners to transfer the forces and therefore $c_2 = 2$.

The effective area A_{ef} and modulus of elasticity E_{ef} of the equivalent diagonal can be derived with the same equations as for LTF diaphragms.

According to the shear field analogy for LTF, sheathing panels are to be connected to framing elements with flexible metallic fasteners. In the case of massive timber panels, framing elements are partly missing and the high axial stiffness and thickness of the panel elements activates longitudinal stresses. A simple comparison in Chapter 6 showed that the girder analogy still provides an adequate method to predict the demand in massive timber

diaphragms. To be able to use the truss analogy for massive timber diaphragms, the assumptions and the modifications to the analogy as shown in the next paragraph are applied.

Massive timber panels are normally spanning between two gravity carrying beams and are connected to them to guarantee diaphragm action. These beams are the truss elements running along the short length of the panels. An equivalent truss element needs to be placed along the panel-to-panel edge. The stiffness of this element is the same as the panel stiffness in this direction and the cross sectional area is the sum of half of the cross section areas of each of the two panels. In this way the longitudinal forces in the panel direction can be captured by the model.

7.6 MULTIPLE DIAGONALS PER SHEATHING PANEL

Because of very high aspect ratios of massive timber panels (available panel sizes in New Zealand can be up to 1.2 x 18.0 m or longer), the angle of the equivalent diagonals becomes very high, resulting in a poorly working truss. Additionally, the main assumption of the shear field analogy, stiffness of the framing elements much bigger than the longitudinal (axial) stiffness of the panel, is not valid for massive timber diaphragms. This implies that the panel fasteners also resist load components perpendicular to the panel edges and that the panel itself resists longitudinal stresses. This becomes even more accentuated for irregular diaphragms, because of increased diaphragm deformations and concentrated force introductions.

To account for these shortcomings and to be able to evaluate longitudinal stresses, a discretisation of the panel with multiple diagonals can be used. Diaphragm irregularities like openings and re-entrant corners can be modelled in this way with the inclusion of strut beams or other means of reinforcement.

Figure 7.10 shows the schematized equivalent truss for LTF and massive timber diaphragm panels for the case of multiple diagonals. The panel has been divided formally into 4 x 2 fields with additional longitudinal and transverse truss elements, all joined by diagonals. The spacing of the sub-division is a designer's choice and depends mostly on the panel geometry and the presence of irregularities. In order to reduce the number of diagonal properties to be calculated, the spacing should ideally be chosen in a way to cover the whole floor geometry with one diagonal type only as shown in Figure 7.13a. If this is not possible or desired, individual panels can also have irregular subdivisions as in the truss shown in Figure 7.12b. If

local refinement because of stress concentrations is required, then only a limited number of panels can be refined as shown in Figure 7.12c.

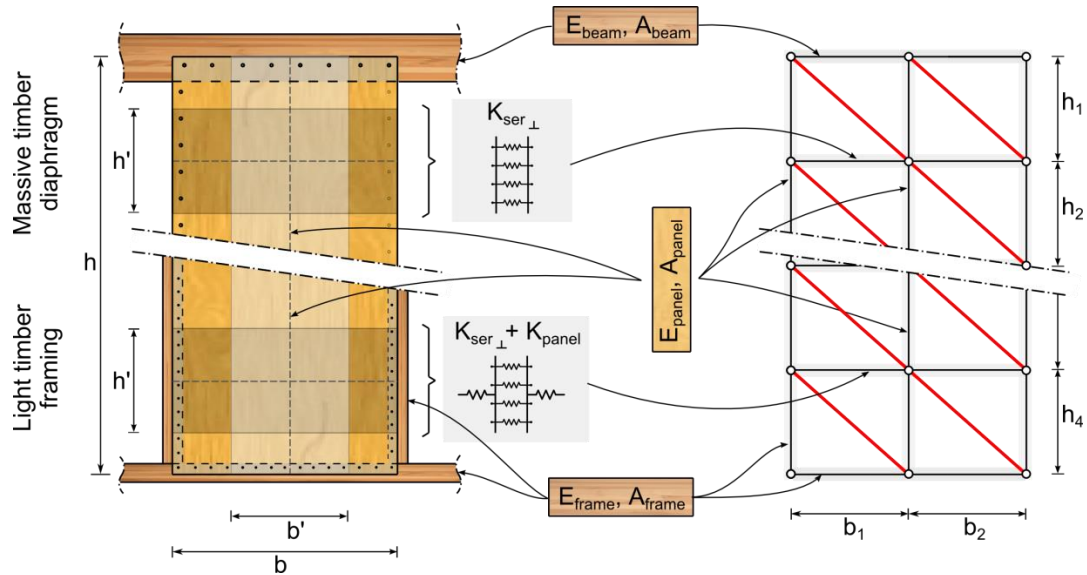


Figure 7.10 Timber panels and idealization in the equivalent truss model for the case of multiple diagonals for LTF diaphragms and massive timber diaphragms

For a diaphragm panel of dimensions $b \times h$ divided into $m \times n$ panels (m is the number of diagonals along the panel height and n is the number of diagonals along the panel length respectively) as in Figure 7.11a, the effective area A_{ef} and effective modulus of elasticity E_{ef} become

$$E_{ef,mxn} = mn \frac{(Gd)_{ef} l_{mxn}^2}{bh} ; \quad (7.13)$$

$$A_{ef,mxn} = l_{mxn} = \sqrt{\left(\frac{b}{n}\right)^2 + \left(\frac{h}{m}\right)^2} . \quad (7.14)$$

If the spacing of the panel sub-division is not regular as in Figure 7.11b, (i.e. the panels do not have equal lengths), then the values become

$$E_{ef,ij} = \frac{(Gd)_{ef} l_{ij}^2}{b_j h_i} ; \quad (7.15)$$

$$A_{ef,ij} = l_{ij} = \sqrt{b_i^2 + h_j^2} ; \quad (7.16)$$

where the index i is the number of sub-division along the panel height and j is the number of the sub-division along the panel width.

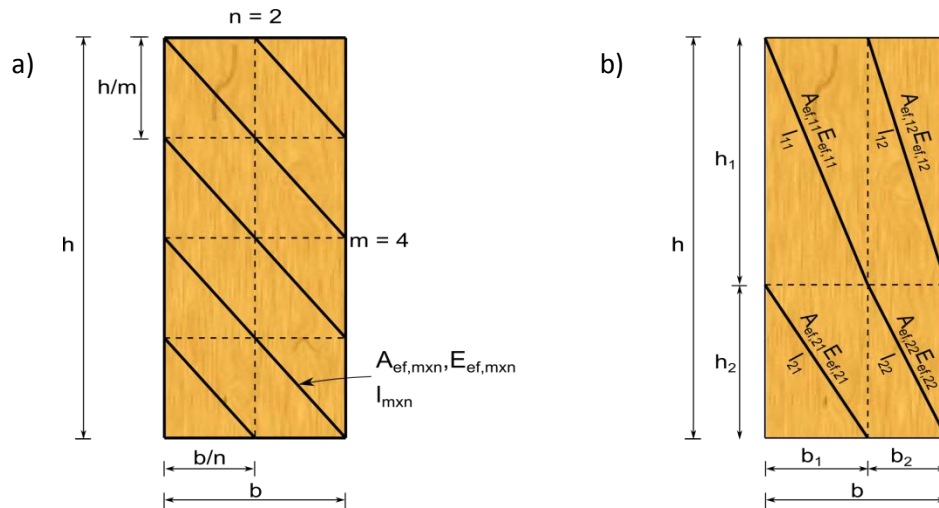


Figure 7.11 Multiple diagonals for a) regular $m \times n$ sub-divisions or for b) irregular sub-divisions

By using multiple diagonals, additional longitudinal and transverse truss elements are required. Their stiffness properties are chosen in a way to represent their contribution to the global diaphragm behaviour.

For the longitudinal truss elements, the properties and section of the framing element are assigned for LTF diaphragms as shown in Figure 7.10a. For massive panels the longitudinal elements are defined by a tributary panel strip with a cross section of $b' \times d$, being $b' = (b_i + b_{i+1})/2$ and d the panel thickness as shown in Figure 7.10b; the material properties are as for the panel element.

For the transverse truss element the stiffness of the tributary panel strip is summed (in series) to the fastener stiffness perpendicular to the panel edge ($K_{ser \perp}$). Considering a common sub-division of 2 diagonals along the panel width, the equivalent stiffness for a LTF diaphragm can be calculated as

$$K_{ef,transverse\ truss,LTF} = \frac{1}{\frac{1}{\frac{E_{90}A'}{b'}} + \frac{1}{n' K_{ser \perp}}}; \quad (7.17)$$

where

E_{90}	panel stiffness perpendicular to the panel direction;
A'	tributary cross section of transverse truss = $h' d$;
d	panel thickness;
b'	tributary width of longitudinal truss element = $(b_i + b_{i+1})/2$;
h'	tributary width of transverse truss element = $(h_i + h_{i+1})/2$;
n'	number of fasteners along h' ;
$K_{ser \perp}$	slip modulus of fasteners perpendicular to panel edge.

In the case of a massive timber diaphragm the axial stiffness of the transverse truss element is much bigger than the stiffness of the fasteners and can normally be ignored. Considering a common sub-division of 2 diagonals along the panel width, the number of fasteners is multiplied by (3-c) to account of the number of lines of fasteners necessary to transfer the forces. In case of a single line of fasteners (c = 1), the fastener stiffness is doubled, since it is shared between two adjacent panels. For a spline connection with two lines of fasteners (c = 2), each transverse truss considers the stiffness of one line of fasteners.

$$K_{ef,transverse\ truss,masive} = \frac{1}{\frac{1}{\frac{E_{90}A'}{b'}} + \frac{1}{(3-c)n'K_{ser\perp}}} \cong (3-c)n'K_{ser\perp}. \quad (7.18)$$

For the examples shown in the next sections, with a panel division of 4 x 2, the stiffness of the transverse truss elements becomes (for panel dimension and material properties see next sections)

$$K_{ef,transverse\ truss,LTf} = \frac{1}{\frac{1}{\frac{3,000(20 \cdot 975)}{525}} + \frac{1}{19.5 \cdot 1,000}} = \frac{1}{\frac{1}{111,428} + \frac{1}{19,500}} = 16,596\ N/mm \quad (7.19)$$

$$K_{ef,transverse\ truss,masive} = \frac{1}{\frac{1}{\frac{4,000(150 \cdot 975)}{525}} + \frac{1}{2 \cdot 6.5 \cdot 3,000}} = \frac{1}{\frac{1}{1,114,286} + \frac{1}{39,000}} \frac{37,681N}{mm} \cong 39,000\ N/mm \quad (7.20)$$

If a truss analysis with multiple diagonals is used, the unit shear force demand in the panel should be taken as the average over all diagonals.

7.7 COMPARISON OF DIFFERENT TRUSS MODEL GEOMETRIES

In order to evaluate the appropriateness of the Equivalent Truss Method, some sample massive timber diaphragms are analysed with the method with two different truss geometries and then compared with a finite element analysis (see Appendix B for FEM details).

For the analyses a number of different floor geometries as shown in Table 7.2 were considered. These cases were all multiples of the basic diaphragm geometry shown in Figure 7.13a. For model D an additional intermediate support has been added. For model F with dimension as per Figure 7.13b, irregularities in the form of a re-entrant corner and an opening have been added (this is the sample diaphragm as used in Chapter 6). Panel and beam dimensions as well as material properties and fastener details are summarized in Table 7.3. Supports are considered as rigid, the structure has been loaded with a distributed area load of

3.5 kN/m², corresponding to the seismic load of a typical commercial multi-storey timber building situated in Wellington, New Zealand. These loads were lumped to the vertical truss members as uniformly distributed line loads. Alternatively the loads can be applied as concentrated forces to the nodes, obtaining approximately the same results.

Table 7.2 Model and diaphragm geometry description

Description	Model		
	Finite Element Modelling (FEM)	Equivalent <i>truss 1</i> (1 diagonal per panel ¹)	Equivalent <i>truss 2</i> (4x2 diagonals per panel ²)
A 8 panels simply supported 1.95x1.05			
B 8 panels simply supported 3.90x1.05			
C 16 panels 2 rows simply supported 3.90x1.05			
D 2x8 panels 2 rows continuous diaphragm 3.90x1.05			
E 16 panels 3 rows continuous diaphragm 3.90x1.05			
F 16 panels 5 rows continuous diaphragm irregular 3.90x1.05			
		(see Figure 7.12)	(see Figure 7.12)

Note: ¹ For *model F*, 2 diagonals per panel were used in the correspondence of truss beams;
² For *model A*, the panel was subdivided into 2x2 diagonals.

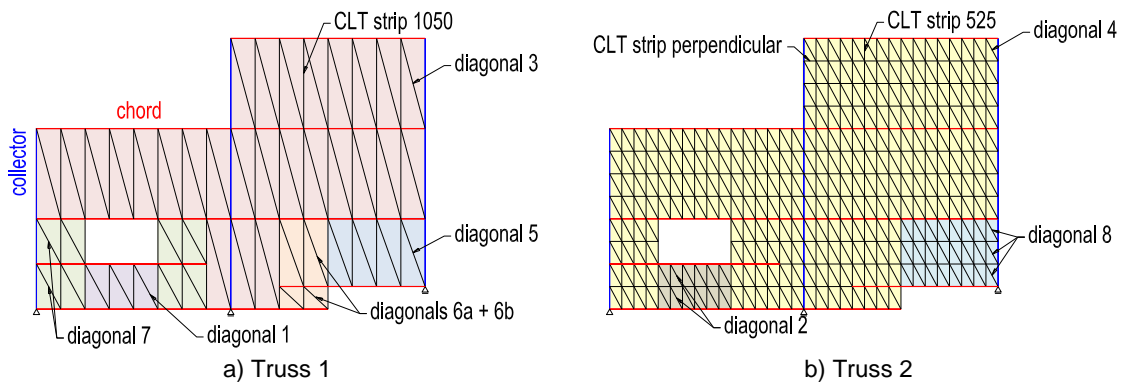


Figure 7.12 Diagonal layout for model F: a) truss 1; b) truss 2

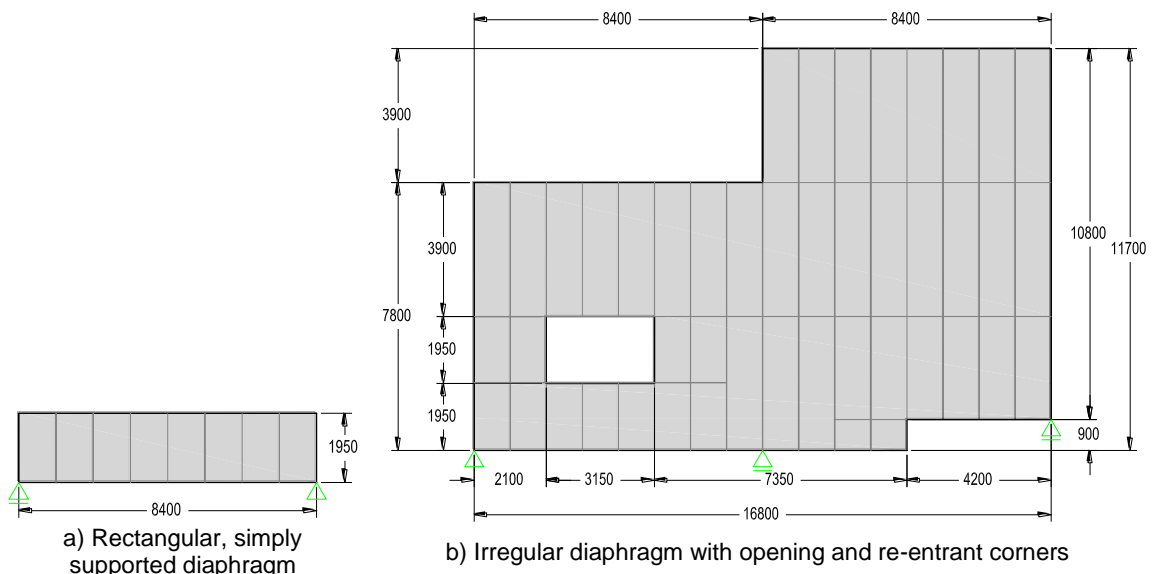


Figure 7.13 Sample diaphragms: a) rectangular, simply supported diaphragms (model A); b) irregular diaphragm (model F)

The truss method was carried out with two different grid geometries. In *truss 1* a single diagonal was used to represent the whole diaphragm panel. In *truss 2* the panels were divided into 4 x 2 diagonals. Only for model F a number of additional diagonals needed to be defined in order to allow for the connection of the drag beams to the panels. The denomination of these additional diagonals is shown in Figure 7.12.

It has to be noted that if the properties of diagonal 4 were used in *truss 2*, only a marginal error was obtained. This simplifies the use of the truss method with multiple diagonals per panel for irregular floor layouts.

Table 7.3 Properties of the structural elements of the massive timber diaphragms

Element	Properties	Element	Properties
Diagonal 1 (Case A, Truss 1, panel 1.95x1.05)	$A = 2,214,732 \text{ mm}^2$ $E = 21.8 \text{ N/mm}$ (1x1 diagonal)	Chords, collectors, struts	$A = 200 \times 400 \text{ mm}^2$ $E = 11,000 \text{ MPa}$
Diagonal 2 (Case A, Truss 2, panel 1.95x1.05)	$A = 1,107,362 \text{ mm}^2$ $E = 21.8 \text{ N/mm}$ (2x2 diagonals)	Fasteners	$s = 150 \text{ mm}$ $K_{ser} = 3,000 \text{ N/mm}$
Diagonal 3 (Case B-F, Truss 1, panel 3.9x1.05)	$A = 4,038,874 \text{ mm}^2$ $E = 47.2 \text{ N/mm}$ (1x1 diagonal)	CLT strip 525	$A = 525 \times 150 \text{ mm}^2$ $E = 8,000 \text{ MPa}$
Diagonal 4 (Case B-F, Truss 2, panel 3.9x1.05)	$A = 1,107,362 \text{ mm}^2$ $E = 28.4 \text{ N/mm}$ (4x2 diagonals)	CLT strip 1050	$A = 525 \times 150 \text{ mm}^2$ $E = 8,000 \text{ MPa}$
Diagonal 5 (Case F, Truss 1, panel 2.925x1.05)	$A = 3,107,752 \text{ mm}^2$ $E = 33.8 \text{ N/mm}$ (1x1 diagonal)	CLT strip perpendicular	$A = 526 \text{ mm}^2$ $E = 39,000 \text{ MPa}$ (see equation (7.20))
Diagonal 6 (Case F, Truss 1, panel 3.9x1.05)	$A_a = 3,107,752 \text{ mm}^2$ $E_a = 37.3 \text{ N/mm}$ $A_b = 1,432,873 \text{ mm}^2$ $E_b = 23.8 \text{ N/mm}$ (2x1 irregular diagonals)	Shell element for FEM analysis (CLT)	$E_1 = 8,000 \text{ MPa}$ $E_2 = 4,000 \text{ MPa}$ $E_3 = 500 \text{ MPa}$ $G_{12} = 600 \text{ MPa}$ $G_{13} = 500 \text{ MPa}$ $G_{23} = 100 \text{ MPa}$ $v_{12} = 0.07$ $v_{13} = 0.35$ $v_{23} = 0.35$ $t = 150 \text{ mm}$
Diagonal 7 (Case F, Truss 1, panel 3.9x1.05)	$A = 2,214,700 \text{ mm}^2$ $E = 28.4 \text{ N/mm}$ (1x2 diagonals)		
Diagonal 8 (Case F, Truss 1, panel 2.925x1.05)	$A = 1,107,362 \text{ mm}^2$ $E = 25.8 \text{ N/mm}$ (3x2 diagonals)		

Table 7.4 summarizes the outcomes of the different diaphragm models for all three analysis cases (FEM, *truss 1* with one diagonal per panel and *truss 2* with 4x2 diagonals per panel). Key values like the diaphragm deflection, the maximum and the average shear stress in the panels, chord forces and the reaction forces are provided. All values are compared to the outcomes from the FEM analysis, providing the most reliable data available at this stage.

The comparison of the analysis results suggest that the Equivalent Truss Method provides reliable estimates. The key parameters differ by a maximum of 15% which is an acceptable margin, considering all uncertainties and fabrication tolerances involved. There is no general correlation between the degree of irregularity and the error in the analysis output.

For the given panel and floor geometry, both truss models provide approximately the same accuracy. It is therefore more of a designer's choice of how a diaphragm is discretized for the Equivalent Truss Method. For more complicated geometries and slender panels, a more refined panel discretization is suggested.

Table 7.4 Comparison of some key values for models A-F with massive timber panels from the FEM analysis and the simple and refined truss analysis

	Model	A	B	C	D	E	F
Deflection [mm]	FEM	3.4	2.8	12.2	3.2	3.5	4.2
	truss 1	3.8 (+12%)	3.1 (+11%)	13.5 (+11%)	3.4 (+6%)	3.8 (+9%)	4.1 (-2%)
	truss 2	3.9 (+15%)	3.1 (+11%)	13 (+7%)	3.4 (+6%)	3.7 (+6%)	3.8 (-10%)
Max shear stress ¹⁾ [kN/m]	FEM	14.7	14.7	29.4	15.0	14.7	14.8
	truss 1	12.9 (-12%)	12.9 (-12%)	27.6 (-6%)	12.9 (-14%)	12.7 (-14%)	12.9 (-13%)
	truss 2	12.9 (-12%)	12.9 (-12%)	27.6 (-6%)	12.9 (-14%)	12.7 (-13%)	12.7 (-14%)
Average shear stress ²⁾ [kN/m]	FEM	14.7	14.7	29.4	15.0	14.7	14.8
	truss 1	12.9 (-12%)	12.9 (-12%)	27.6 (-6%)	12.9 (-14%)	12.7 (-14%)	12.9 (-13%)
	truss 2	12.9 (-12%)	12.9 (-12%)	27.6 (-6%)	12.9 (-14%)	12.7 (-13%)	12.7 (-14%)
Chord force [kN]	FEM	27.8	27.6	119.3	28.8	30.8	26.2
	truss 1	30.9 (+11%)	30.9 (+12%)	125.4 (+5%)	32.5 (+13%)	34.5 (+12%)	30.1 (+15%)
	truss 2	30.9 (+11%)	31.0 (+12%)	123.5 (+4%)	31.9 (+11%)	34.6 (+12%)	28.9 (+10%)
Reactions ³⁾ [kN]	FEM	28.6	57.4	229.5	287.3	287.3	282.8
	truss 1	28.6 (0%)	57.4 (0%)	229.5 (0%)	289.4 (+1%)	282.8 (-2%)	282.0 (0%)
	truss 2	28.6 (0%)	57.4 (0%)	229.5 (0%)	286.4 (0%)	283.1 (-1%)	278.6 (-1%)

Note: ¹⁾ Maximum shear stress in highest loaded shear panel;

²⁾ Average shear stress in shear panels along the collector beam with highest axial force (average over several panels);

³⁾ Reaction force at the external support for *models A-C* and for the internal support for *models D-F*.

7.8 VERIFICATION OF THE TRUSS MODEL

In this section the Equivalent Truss Method is verified against a finite element model for the irregular floor geometry shown in Figure 7.13b. For both LTF and massive timber diaphragms shear stresses, deflection and chord forces as well as reaction forces are compared to a FEM analysis.

For the LFT diaphragm, OSB panels fixed on framing elements were assumed; element sections and material properties are summarized in Table 7.5. The diaphragm geometry is shown in Figure 7.13b, the support conditions however have been changed in order to reflect the lateral

load resisting system as shown in Figure 7.14a. The sheathing panels were discretized by 2 x 2 diagonals as shown in Figures 7.14b and d.

Table 7.5 Properties of the structural elements of the LTF diaphragm

Element	Properties	Element	Properties
Diagonal (panel 1.95x1.05)	$A = 1,107,400 \text{ mm}^2$ $E = 12.4 \text{ N/mm}$ (2x2 diagonal)	OSB strip perpendicular	$A = 526 \text{ mm}^2$ $E = 16,596 \text{ MPa}$ (see equation (7.19))
Frame elements	$A = 50 \times 100 \text{ mm}^2$ $E = 11,000 \text{ MPa}$	OSB strip 525	$A = 525 \times 20 \text{ mm}^2$ $E = 8,000 \text{ MPa}$
Chords, collectors, struts	$A = 200 \times 300 \text{ mm}^2$ $E = 11,000 \text{ MPa}$	Shell element for FEM analysis (OSB)	$E_1 = 3,800 \text{ MPa}$ $E_2 = 3,000 \text{ MPa}$ $E_3 = 3,500 \text{ MPa}$ $G_{12} = 1,080 \text{ MPa}$ $G_{13} = 1,080 \text{ MPa}$ $G_{23} = 1,080 \text{ MPa}$ $\nu_{12} = 0.22$ $\nu_{13} = 0.16$ $\nu_{23} = 0.16$ $t = 20 \text{ mm}$
Fasteners	$s = 150 \text{ mm}$ $K_{ser} = 3,000 \text{ N/mm}$		

The material properties and the element sections for massive timber diaphragms are the same as in the previous section (see Table 7.3), only the support conditions have been changed as shown in Figure 7.15a. The truss method is carried out by dividing the massive timber panels into 4 x 2 diagonals, using the effective area and stiffness values as for Diagonal 4 in Table 7.3.

The unit shear forces, chord forces, reactions and deflections are compared for each example. For the massive timber diaphragms the forces in the longitudinal and transversal truss elements (as discussed in section 7.6) are also compared to the FEM analysis. Since the accuracy of the truss method has already been proven for LTF diaphragms by Kamiya (1990), only one example loaded in $-y$ is shown. For massive timber diaphragms the same structure has been loaded in $-y$ and $+y$ direction, as well as for the case with a full load in x and 30% of the load in $-y$ direction, as required by some loading codes (Eurocode 8 2004; Standards New Zealand 2004). The seismic loads were applied as distributed area loads over the panel elements in the FEM analysis, and as uniformly distributed line loads to the truss elements. For these analysis cases the supports were assumed to be rigid. To model the interaction with the lateral load resisting system, the rigid supports can be replaced with springs and by assigning the respective lateral load resisting system element stiffnesses.

7.8.1 LTF diaphragm loaded in -y direction

Shear stresses n_{xy} shown in Figure 7.14 suggest that the truss method can accurately predict the unit shear forces in the sheathing panels when compared to the outcomes from the FEM analysis. The equivalent shear from the diagonals provides some higher peak values; this can be avoided by considering the average over all diagonals of one panel. Chord forces are generally overestimated, providing a conservative demand. The forces in the frame beams around the opening and the re-entrant corner can also be predicted accurately, therefore guaranteeing an appropriate reinforcement design around these areas. The deformation and therefore diaphragm stiffness is also estimated with sufficient accuracy, the same can be said for the reaction forces.

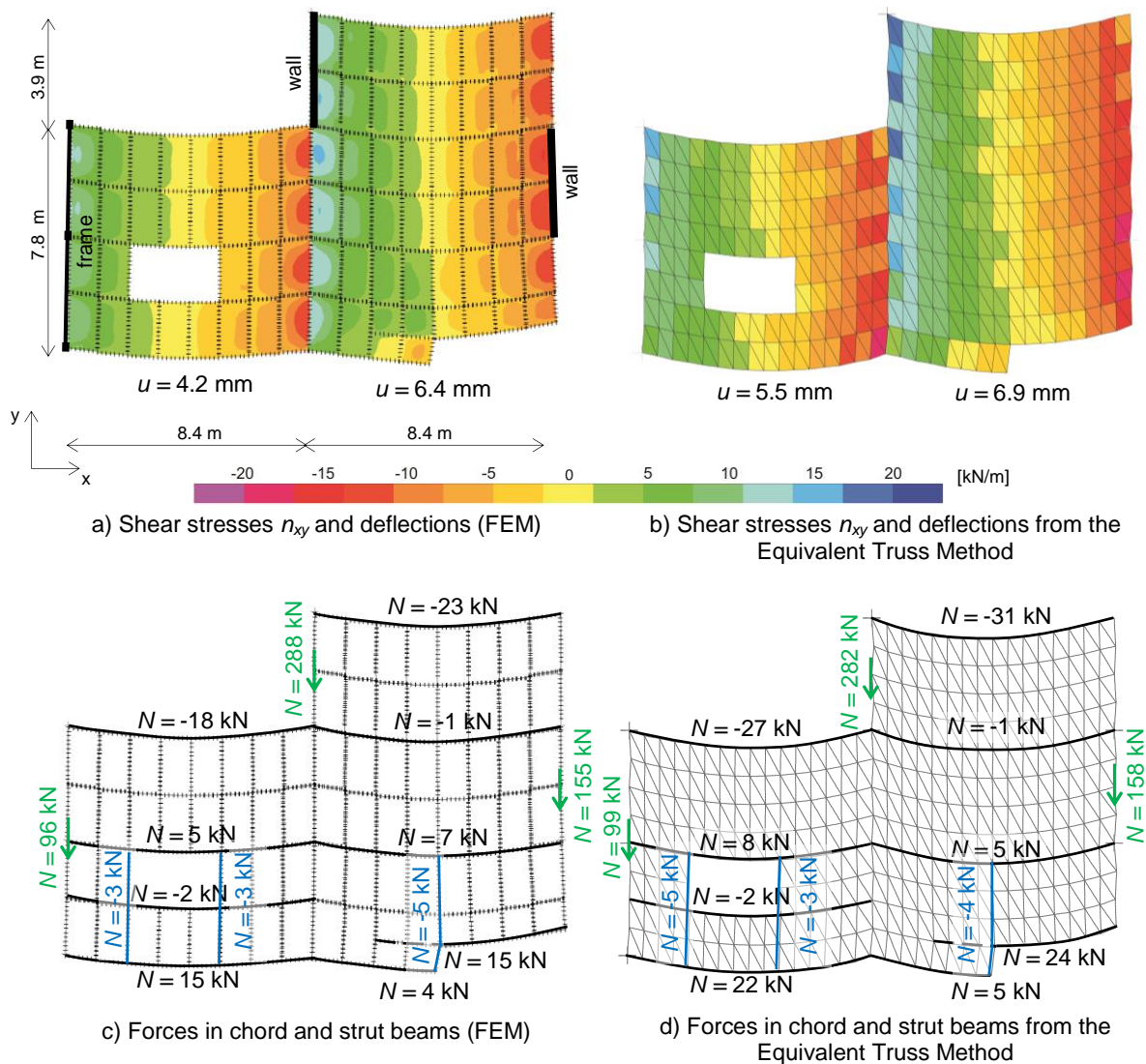


Figure 7.14 Shear stress distribution, chord forces and deflections for an irregular LTF timber diaphragm from FEM and Equivalent Truss Method (load case $-E_y$ with a seismic load of 3.5 kN/m^2)

7.8.2 Massive timber diaphragm loaded in -y direction

The comparison of Figures 7.15a and b show that the distribution and magnitude of the shear stresses can be derived very accurately with the truss method also for massive timber diaphragms. In proximity of chord beams and especially of the supports, the shear stresses from the individual diagonal can be slightly over-estimated. This is due to the higher stiffness from the beams or supports, which attracts more force. The shear stress should therefore be averaged over the individual shear panel for design purposes. Diaphragm deflections can be predicted in a satisfying manner.

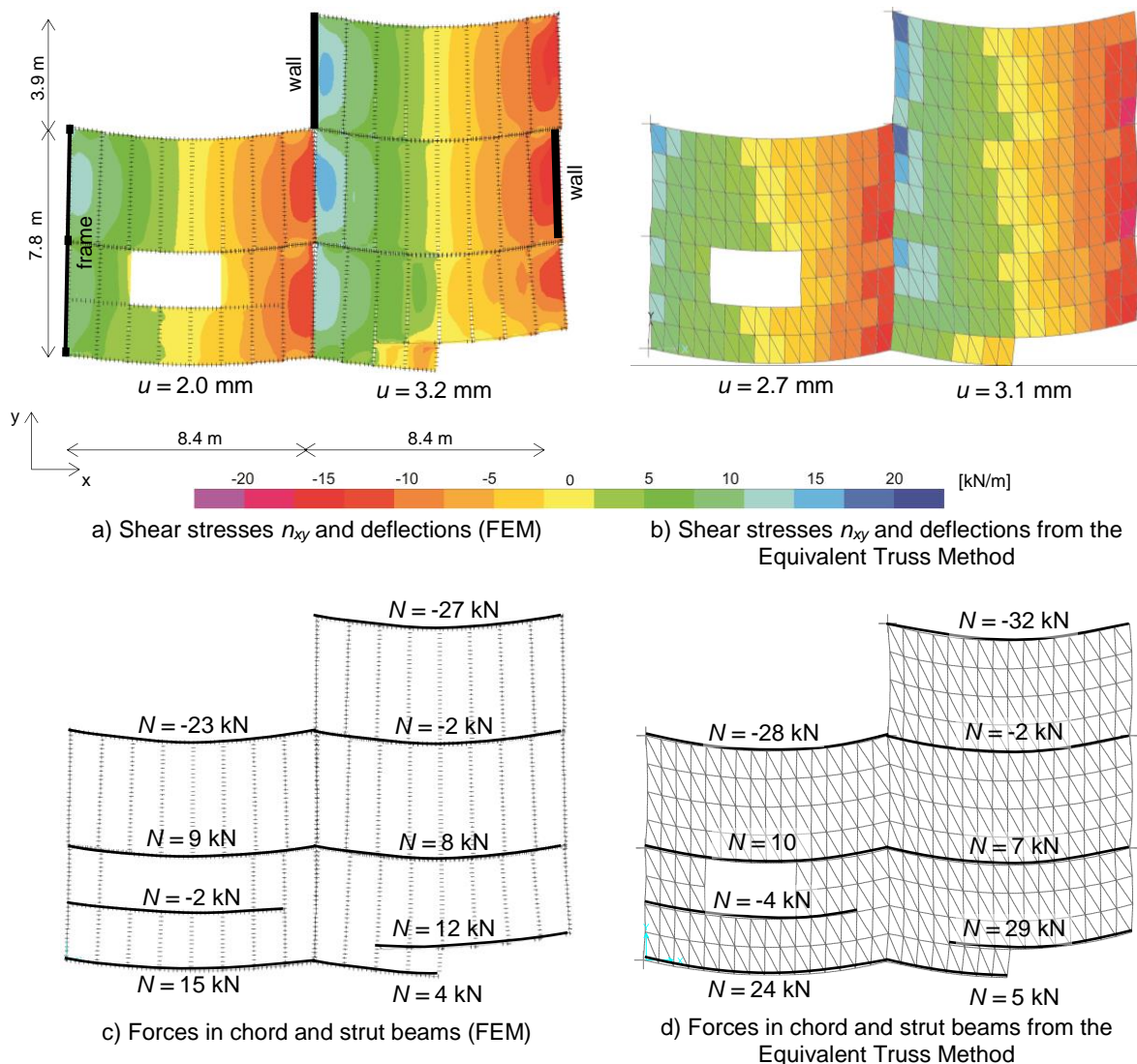


Figure 7.15 Shear stress distribution, chord forces and deflections for an irregular massive timber diaphragm from FEM and Equivalent Truss Method (load case $-E_y$ with a seismic load of 3.5 kN/m^2)

A comparison of the chord forces shown in Figures 7.15c and d indicates that the truss method most of the times overestimates these values. A look at Figure 7.16a explains the lower chord

forces from the FEM analysis. Since the massive timber panels do not satisfy all assumptions of the shear field analogy, both fastener forces perpendicular to the panel edge and longitudinal stresses in the panels are activated. By summing the resultants of the n_{xx} stresses from Figure 7.16a to the chord forces in Figure 7.15d, the forces from the truss method can be matched more appropriately. The forces in the transversal trusses obtained from the sub-divisions of the panel in multiple diagonals approximately provide the amount of load transferred by the fastener perpendicular to the panel edge, as can be seen from the comparison of Figures 7.16a and b.

Reaction forces also compare very well, which is expected after considering the accurate estimation of the diaphragm deformation.

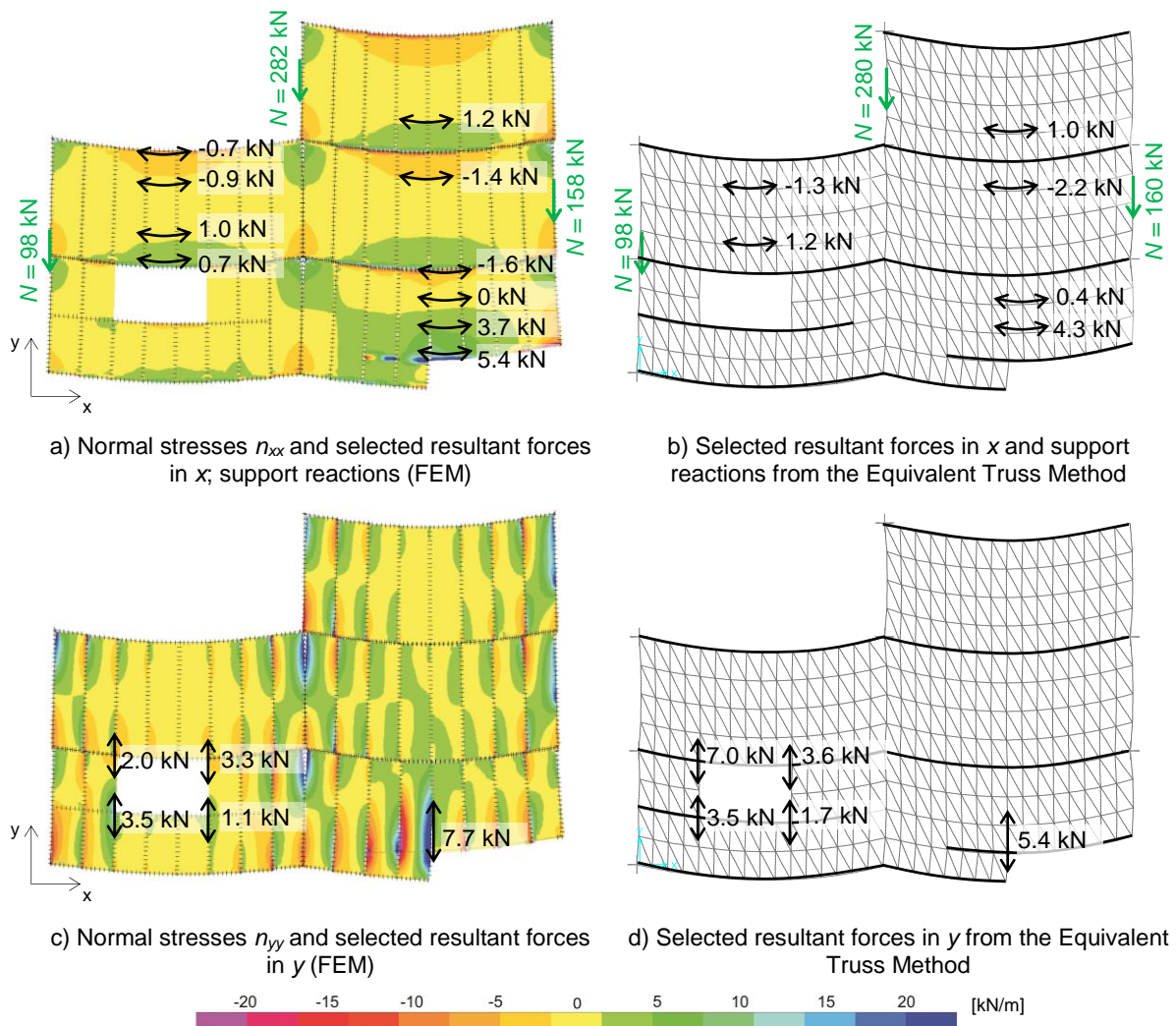


Figure 7.16 Shear stress distribution, chord forces and deflections for an irregular massive timber diaphragm from FEM and Equivalent Truss Method (load case $-E_y$ with a seismic load of 3.5 kN/m^2)

Figure 7.16c shows the normal stress in y direction as well as a number of selected resultant forces at diaphragm irregularities. The derivation of these forces is essential for the design of irregular diaphragms. The comparison between these resultant forces and the forces from the vertical truss elements from Figure 7.16d show that the truss method provides accurate values.

7.8.3 Massive timber diaphragm loaded in x and y direction

It is common practice in seismic engineering to only consider earthquake attacks in the principal directions of the building layout. Structural members which provide enough strength under seismic loads in x and y direction can normally withstand earthquakes in any arbitrary direction. Seismic codes like Eurocode 8 (Eurocode 5 2008) or the New Zealand seismic loading code NZS 1170.5 (Standards New Zealand 2004a), however, require the analysis of the structure for a combined earthquake attack of 100% in one direction and 30% in the perpendicular direction ($E_x \pm 0.3E_y$ and $E_y \pm 0.3E_x$).

In Figures 7.17 and 7.18 the diaphragm is loaded for a combined seismic loading condition of $E_x - 0.3E_y$. An additional frame and a wall have been added to resist the horizontal loads in the x direction. Even though the unit shear forces are almost doubled for this load case, the fastener configuration has not been changed to maintain the same stiffnesses as used for the previous examples. Because the load attack occurs from both the x and y direction, the beam elements are working as chords and as collectors at the same time. Because of the presence of the supports the beam forces cannot easily be presented in the following graphs and are therefore omitted.

The comparison of the shear stresses, deflections and chord/collector forces shown in Figure 7.17 suggest that the truss method provides again very accurate values, even for seismic loads applied in both the x and y directions. To match some of the chord/collector forces, the resultant n_{xx} forces from Figure 7.18 need to be considered.

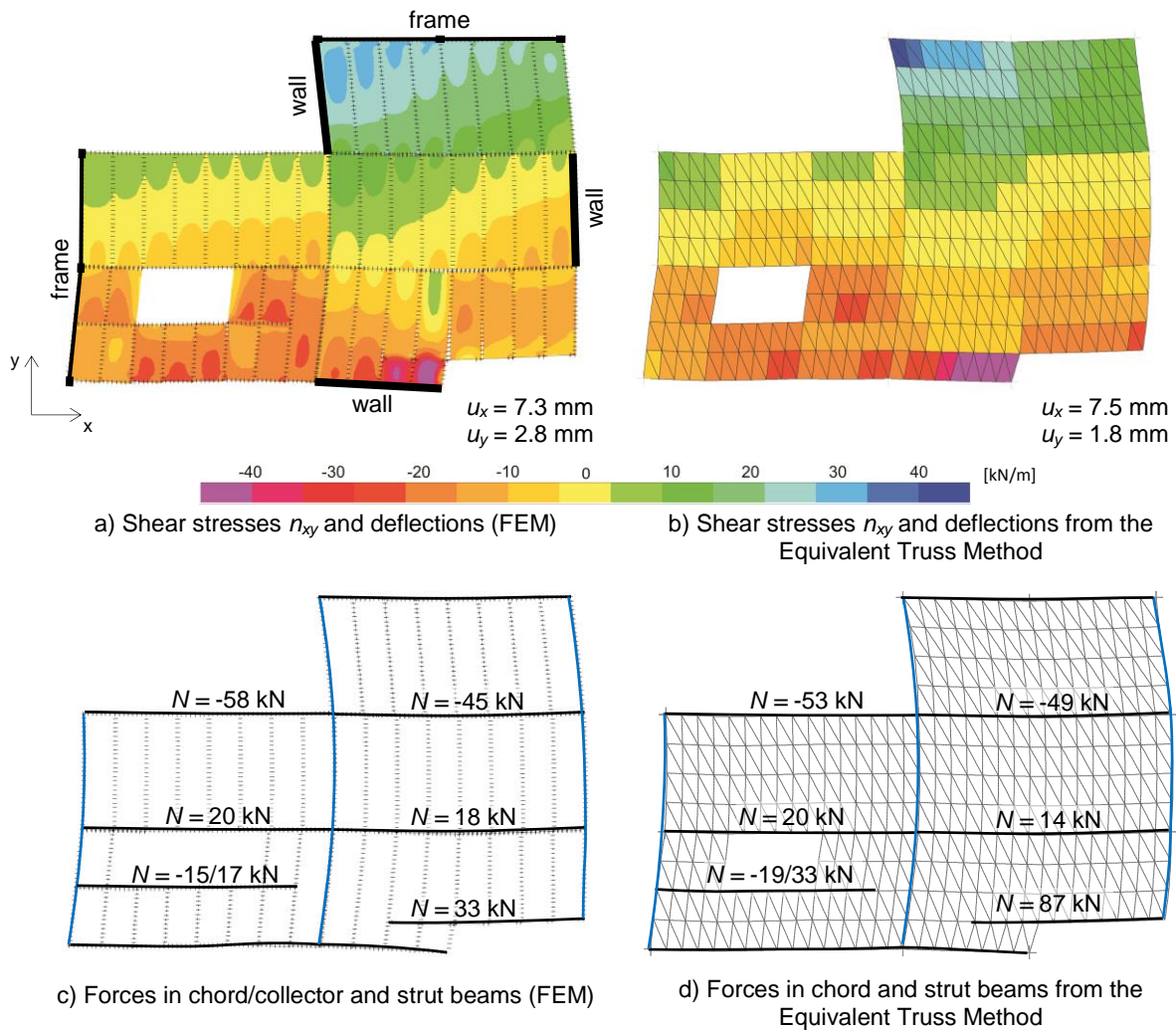


Figure 7.17 Shear stress distribution, chord/collector forces and deflections for an irregular massive timber diaphragm from FEM and Equivalent Truss Method with supports in x and y direction (load case $E_x + 0.3 E_y$ with a seismic load of 3.5 kN/m^2)

Figure 7.18 shows that the reaction forces as well as the forces around the re-entrant corner and the opening can be accurately predicted. It is worth noting that forces in y direction in the panels adjacent to the diaphragm irregularities are much higher than for the previous load cases in y direction only. The massive timber panels however will easily provide enough capacity to resist these forces.

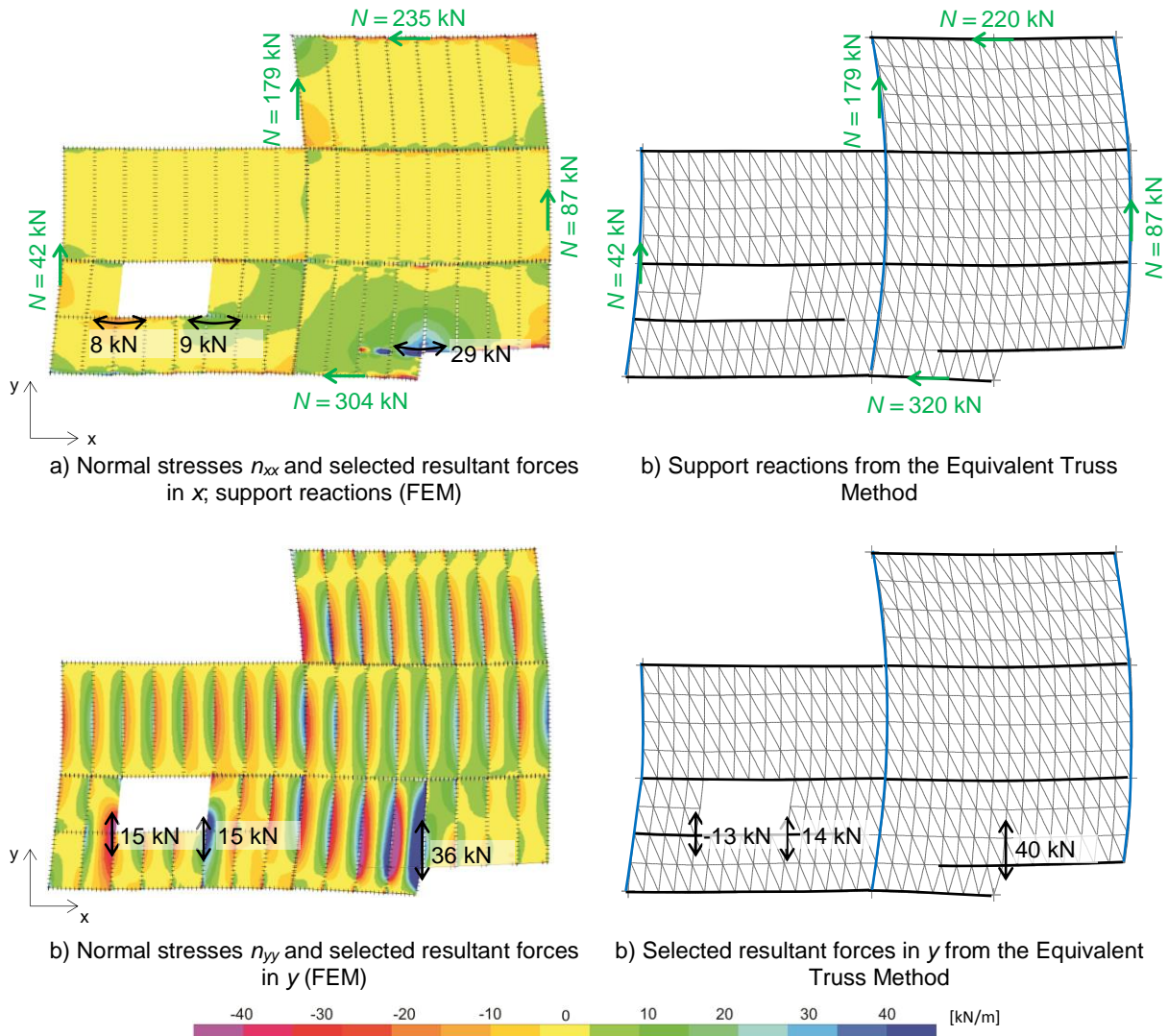


Figure 7.18 Shear stress distribution, chord forces and deflections for an irregular massive timber diaphragm from FEM and Equivalent Truss Method (load case $E_x + 0.3 E_y$ with a seismic load of 3.5 kN/m^2)

7.9 NON-LINEAR DIAPHRAGM BEHAVIOUR

The truss method discussed so far has only been applied to linear elastic cases. Even though diaphragms are supposed to remain essentially elastic, certain design situations might require non-linear analysis. Since all timber material elements have an almost perfectly linear behaviour until a brittle failure, the only source of non-linearity is found in the fasteners used to connect the individual panels.

The truss method can easily be extended to reflect the non-linear force-displacement behaviour of panel connections. This implies that the force-displacement curve of the specific fasteners needs to be known. Such information can be found in code provisions (Standards New Zealand 1993) or needs to be obtained from experimental evidence. The effective shear-

through-thickness rigidity $(Gd)_{ef}$ and the effective modulus of elasticity of the diagonal E_{ef} need to be derived for the varying force level in the connector and are therefore a function of the varying slip modulus K_{ser} .

The analysis of a simply supported LTF diaphragm with 6 panels is shown under consideration of the force-displacement curve for nails from the New Zealand Timber Standard (Standards New Zealand 1993) as shown in Figure 7.19a.

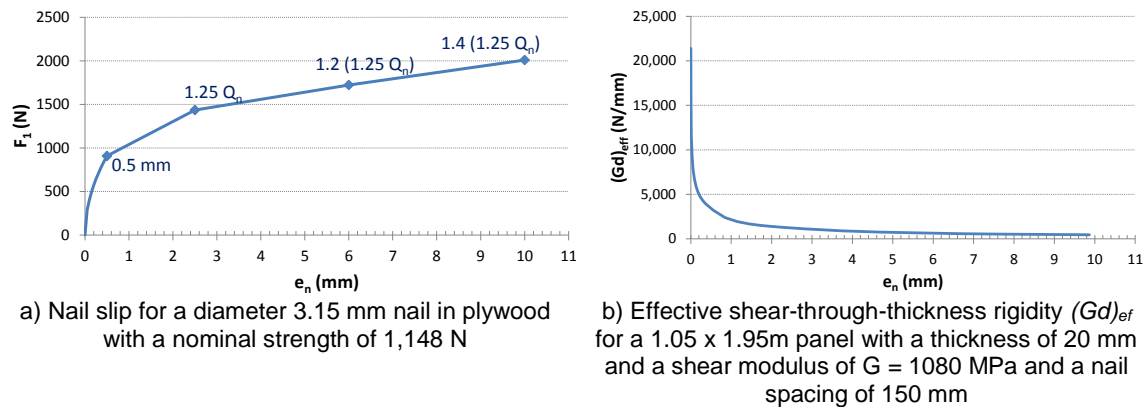


Figure 7.19 a) Nail slip according to NZS 3603 (Standards New Zealand 1993); b) effective shear-through-thickness rigidity $(Gd)_{ef}$

The effective shear-through-thickness rigidity $(Gd)_{ef}$ was calculated as a function of the fastener displacement e_n by using Equation (7.5), plotted in Figure 7.19b. Once the values for E_{ef} were calculated according to Equation (7.11), the non-linear properties of the diagonal were implemented in the analysis software. Depending on the software used, the properties are normally entered in form of a stress-strain relationship for a beam element with an area A_{ef} or as a link element with a force-displacement curve $F'-u'$ (force in the diagonal versus elongation of the diagonal) derived with equations provided in Appendix A.

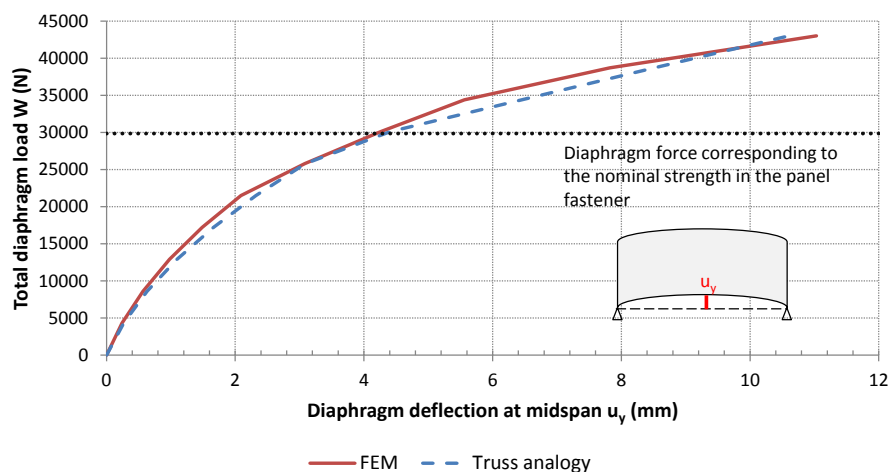


Figure 7.20 Comparison between the diaphragm deflection from a non-linear FEM and from the truss method

Figure 7.20 shows that the non-linear behaviour of panel fasteners can be predicted very accurately when compared to a non-linear finite element analysis.

7.10 LIMITATIONS OF THE EQUIVALENT TRUSS METHOD

The Equivalent Truss Method is based on the shear field analogy which assumes that sheathing panels are only carrying shear forces and that fasteners are only transferring loads parallel to the panel edge. These assumptions are not necessarily always fulfilled in LTF diaphragms, since framing elements contribute with their bending resistance and the panels often also carry longitudinal stresses. These actions create loads in the fasteners perpendicular to the panel edge. Similarly, massive timber panels possess substantial axial stiffness which is activated under diaphragm action, creating also force components perpendicular to the panel edge. These effects are only partially considered in the truss method. Connection stiffnesses between chord, collector and strut beams are normally considered as perfectly pinned connection, which is also not corresponded to reality, but has little effect on the analysis outcomes. Nevertheless of all shortcomings, this theory provides very reasonable demands of the diaphragm components based on a simple approach.

Although the model setup of a truss requires less time than a FEM model, quite a number of elements (frame elements, chord and collector beams, equivalent diagonals, additional longitudinal and transverse truss elements etc.) need to be defined and implemented in the model. Depending on the floor geometry, panels are discretized by one or a number of equivalent diagonals, all requiring a stiffness definition. Similar to FEM analyses, the discretisation of the panel elements is to be chosen carefully. If the panel or fastener layout (stiffness and/or spacing) needs to be changed, all diagonal stiffnesses need to be recalculated and the model updated. Once the model is solved, shear stresses and deflections can be immediately obtained. To evaluate the forces in the beam elements, additional calculations are required, which imply the consequent use of the sign convention.

7.11 DISCUSSION

Floor geometries in modern buildings are often far away from being perfectly rectangular and commonly include irregularities like openings and re-entrant corners. The use of the classic girder analogy, therefore, becomes inappropriate, leaving design engineers with the question of how to determine the diaphragm demand for timber floors. Like for concrete diaphragms, an intuitive approach like the strut-and-tie method, to be used with standard structural beam

analysis software, is required for the analysis and design of LTF and massive timber diaphragms.

In this chapter, a truss method was applied to both LTF and massive timber diaphragms and compared to a more sophisticated finite element analysis. To derive the stiffness of the equivalent diagonal used in the truss method, the deflections of a quadrilateral system braced with a diagonal and a cantilevered LTF shear panel were equated. Once the equivalent stiffness was derived from both the panel and the fasteners stiffnesses, a truss with equivalent diagonals was used to obtain the diaphragm deformation and the unit shear forces in the individual panels. Only the axial forces in framing and beam elements required minimal post-processing, since the concentrated forces applied at the truss nodes needed to be transformed into distributed loads along the panel edges.

The analogy was then extended to use with massive timber panels. Because the basic assumption of the shear field analogy, sheathing panel connected with flexible fasteners to axially stiff framing elements, is violated and massive timber panels can have very high aspect ratios, the panels were formally divided into a number of diagonals. The additionally introduced transversal and longitudinal truss elements were used to simulate the longitudinal stiffness and the fastener force components perpendicular to the panel edges.

The suitability of the truss method was verified on a number of LTF and massive timber diaphragm examples, including cantilever, simply supported and continuous diaphragms, with and without irregularities. Results showed that all relevant values like unit shear forces, axial forces in frame and beam elements, deflection and reaction forces could be predicted in an accurate manner. Stress concentrations around openings and forces in the reinforcement elements like strut beams were also derived accurately. Considering all uncertainties involved in the design and construction of timber diaphragms, the results from the truss method provided enough accuracy to determine the demand in the single diaphragm elements and the force distribution into the lateral load resisting system.

It can therefore be concluded that the Equivalent Truss Method provides a suitable yet simple method to study the deflection and load path of both LTF and massive timber diaphragms, independent of irregularities or staggered connection patterns. This method only requires a little analytical input and can be implemented in a generic structural analysis program, not requiring the use of more complex shell elements and flexible link elements.

Unfortunately, only little experimental evidence is available on the behaviour of large scale LTF diaphragms, especially in the presence of irregularities. To fully verify the truss method, as well as the finite element analysis adopted, these results would need to be compared to test data.

Since diaphragms are required to remain elastic, most of the verification examples are carried out in the elastic range only. If non-linear behaviour is expected or required, the diagonal properties in the truss method can be calculated accordingly and used in the calculation software. The non-linear force-displacement behaviour of fasteners, however, is not always readily available, especially with load components parallel and perpendicular to the panel edges. More analysis cases including plastic behaviour of the fasteners and, therefore, diagonals, would be required.

All analysis cases shown in this chapter involve distributed loads only, further cases with concentrated loads or line loads could be carried out to validate the truss method for more loading conditions.

7.12 CONCLUSIONS

The following conclusions can be drawn from this chapter:

- An Equivalent Truss Method based on the panel shear and fastener stiffnesses can predict the load path in light timber framing diaphragms;
- By the use of multiple equivalent truss diagonals per panel and by adding further longitudinal and transverse truss members, the behaviour of massive timber panels can be accurately predicted;
- The Equivalent Truss Method allows for the determination of the unit shear forces (shear flow), fastener forces, axial forces in frame elements, chord beams, collector beams and strut beams as well as reaction forces;
- Since all stiffness contributions are considered in the Equivalent Truss Method, diaphragm deflections can be estimated accurately;
- If the stiffness of the lateral load resisting system is included in the model, the actual force distribution in the structure including torsional effects can be determined;
- The Equivalent Truss Method can easily be extended to include non-linear fastener behaviour.

8 Displacement incompatibilities between diaphragms and frame structures

8.1 INTRODUCTION

This chapter describes the sources and effects of displacement incompatibilities on diaphragms in frame structures. The experimental behaviour of two different timber diaphragm designs in moment resisting timber frame structures is studied and conceptual design recommendations are given.

8.1.1 Background

Most moment-resisting frame structures are subjected to the effects of beam elongation during cyclic lateral loading. This is independent of the construction material and happens in traditional systems (such as reinforced concrete structures), in jointed-ductile systems (like in PREcast Seismic Structural Systems PRESSS (Priestley 1996) or in Prestressed Laminated Pres-Lam structures (Palermo et al. 2005; Newcombe 2011; Smith 2014)) and in other ductile timber moment resisting frame structures like frames with glued in rods (Buchanan and Fairweather 1993) or frames with tube type connectors (Wrzesniak 2014). The recent earthquake series in Canterbury has caused a number of near diaphragm failures because of large cracks along the diaphragm perimeter. Investigations have shown (Kam et al. 2011; Canterbury Earthquake Royal Commission 2012; Elwood 2013; Bull and Henry 2014) that the damage was caused by frame elongation and the unavailability of concrete diaphragms to accommodate the imposed displacement demand. This inability in current diaphragm design practice also needs to be addressed for diaphragms in multi-storey timber frame structures.

The two experimental setups have been carried out on post-tensioned Pres-Lam timber frame structures. The first of these was the test of a two bay post-tensioned frame with a stressed-skin-panel floor under quasi-static loading. Loads were applied to the panel elements which had to accommodate the displacement demand from the beam-column-joint gap opening. Two different connection details were tested on their ability to transfer diaphragm shears while accommodating the floor gap opening. The second experimental setup was a three-storey post-tensioned timber frame building with a solid timber floor under dynamic loading. Measurements of individual diaphragm elements investigated the fasteners capability to allow for the displacement incompatibility.

Based on the results of the experiments the mechanisms of how timber diaphragms can accommodate the required displacement demands are discussed and conceptual design recommendations for traditional and massive timber diaphragms are given.

8.2 DISPLACEMENT INCOMPATIBILITIES IN FRAME STRUCTURES

Most moment-resisting frame structures are subjected to the effects of beam elongation during cyclic lateral loading. This is independent from the construction material and happens in traditional systems (such as reinforced concrete structures) and also in jointed-ductile systems. In timber frames, the displacement incompatibility is to be expected because of geometric gap opening (Pres-Lam frames) or because of material dependent gap opening (frames with glued in rods or with tube connectors).

The displacement incompatibilities between the floor and the frame, in particular at the beam-column joint level as shown in Figure 8.1 can cause damage to the floor diaphragm. These incompatibilities have the potential to compromise the load paths within the structure and hinder seismic resistance.

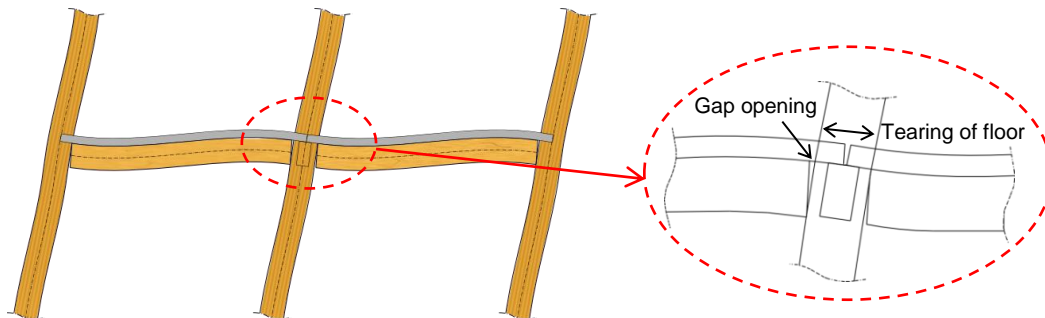


Figure 8.1 Tearing of the floor due to frame elongation

The mechanisms of reinforced concrete frame elongation because of the formation of plastic hinges has been reported since the 1970s (Fenwick and Fong 1979) and further studied in the 1990s (CAE 1999), but implications of these displacement incompatibilities on the design and behaviour of diaphragms have only recently been addressed by researchers (Bull 2004). Experiments by Matthews et al. (2003) simulated the collapse of precast flooring systems because of beam elongation and the resulting pushing out of columns and beams as shown in Figure 8.2. Subsequent research by Lindsay et al. (2004) and MacPherson et al. (2005) led to detailing improvements to guarantee the diaphragm behaviour in the case of a seismic event; these solutions however still allow substantial damage.

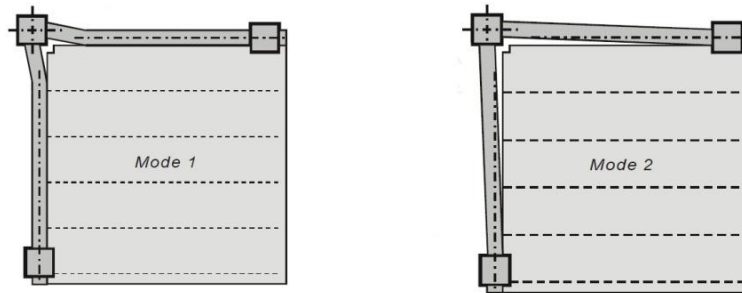


Figure 8.2 Particular deformation modes because of beam elongation (Matthews et al. 2003)

8.3 REVIEW OF CURRENT DESIGN APPROACHES TO AVOID DIAPHRAGM DAMAGE IN FRAME STRUCTURES

8.3.1 Connections in multi-storey concrete frame buildings

The effect of beam elongation in precast concrete structures has been a concern in New Zealand over the last decades and a number of researchers worked on solutions to overcome the problem. In a laboratory testing carried out by Matthews et al. (2003) a hollowcore unit adjacent to the frame beam collapsed in a similar way as observed for precast buildings in the 1994 Northridge Earthquake. The failure was attributed to beam elongation, which caused the central column to become detached from the diaphragm. Additionally, the out of plane deflections of the diaphragm (simple curvature) and the frame beam (double curvature) were not compatible. The formation of cracks in the floor and the missing load path in the diaphragm led to a brittle collapse. Further research by MacPherson et al. (2005) and Lindsay et al. (2004) led to some improvements like seating details, additional ties to connect the columns to the floor and a link slab made of a timber infill with a thin concrete topping to allow for the differential movements of the floor in respect to the frame. Taylor (2004) studied the optimum location of discrete floor-frame connectors in precast-concrete systems by developing shape functions. Based on this procedure, McKenzie (2004) analyzed structures with special connectors between the floor slabs and frame beams in the positions where the deformation incompatibility was minimal. This solution was previously implemented in the 5 storey PRESS building (Priestley et al. 1999) in the form of X-welded connectors. The stress distribution in concrete diaphragms connected in discrete locations was shown by Jensen (2004) to be higher than for continuously connected diaphragms. It is also shown that the high shear forces in connectors govern the design, considering the limited capacity of commercially available connectors. Vides and Pampanin (2015) further studied the ideal position of the connectors and showed that by using dissipative jointed ductile connectors, seismic forces in

the diaphragm could be reduced. All these solutions intend to allow for out-of-plane displacement incompatibilities, but do not address frame elongation.

Amaris et al. (2008) addressed both the frame elongation and out-of-plane displacement incompatibilities and tested a slotted beam connection in conjunction with a non-tearing floor solution. Results showed satisfactory performance but because of the complexity of the construction of the beams with the special hinge element, as well as the sliding connections for the floor as shown in Figure 8.3, this solution was never used in real buildings.

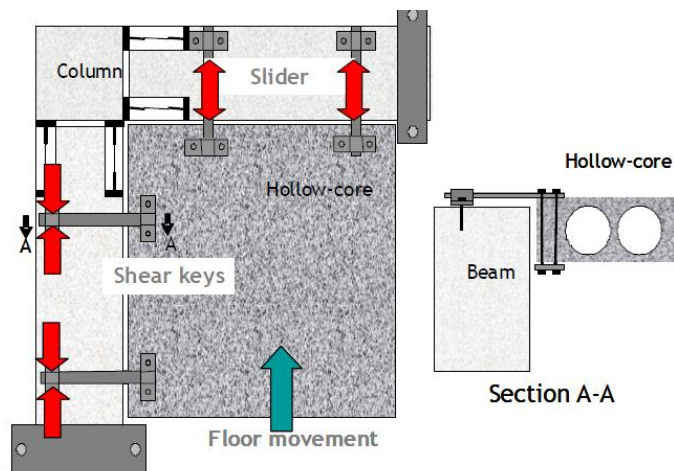


Figure 8.3: Articulated floor connection (Amaris et al. 2008)

The idea of minimizing beam elongation in concrete beams is not new and has been proposed earlier in Japan by Ohkubo et al. (1999) and at a similar time in the US during the PRESSS research program (Priestley 1996). In continuation of Amaris's results, Leslie et al. (2010) developed and tested a number of different slotted beam connection details for precast and semi-precast beams. Beam elongation could be successfully minimized, but bar buckling, confinement and shear pinching compromised the performance at higher drifts. Au (2010) studied and tested slotted beam details for conventional monolithic concrete beams shown in Figure 8.4. A number of tested beam column joints led to new design recommendations. The experimental results however showed issues regarding the bond of longitudinal bars and the joint shear mechanism, which were addressed and solved by Byrne and Bull (2012). Because all cited research was based on small subassemblies, Muir et al. (2012) evaluated the performance of the slotted beam connection on a full scale three-dimensional structure. Results showed the very satisfactory performance of the connection detailing with reduced beam elongation, with limited damage to the floor slab. The correct detailing of the diagonal

hangers however was shown to be crucial, since they need to resist bending, torsion and shear.

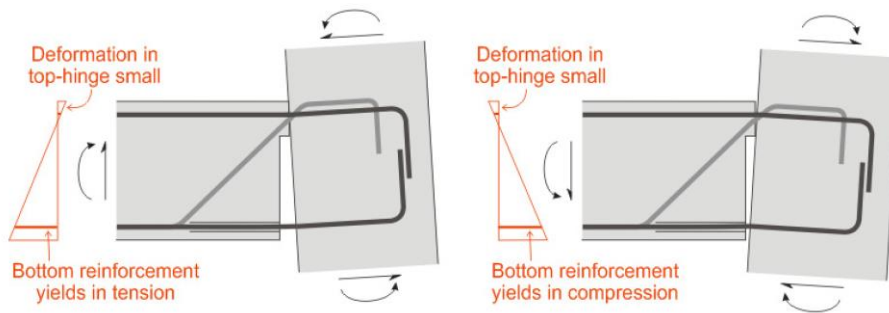


Figure 8.4: Slotted reinforced concrete beam showing how the beam rotation is accommodated via opening and closing of slot (Au 2010)

8.3.2 Connections in multi-storey steel frame buildings

As for concrete structures, the displacement incompatibility between frame beams and floor diaphragms has become of increasing interest with the introduction of rocking steel structures. Since traditional concrete diaphragms in post-tensioned steel frame systems restrain beam-column-joint gap opening, Garlock and Li (2008) suggested the use of flexible collector beams, perpendicular to the post-tensioned frame as shown in Figure 8.5. These beams need to allow for bending to accommodate the gap opening, while still providing enough stiffness to transfer the diaphragm forces. Aside from this design challenge, only a limited part of the diaphragm is able to carry the shear forces to the central bays of the frame. This theoretically possible, but practically challenging solution only works for perimeter post-tensioning frames

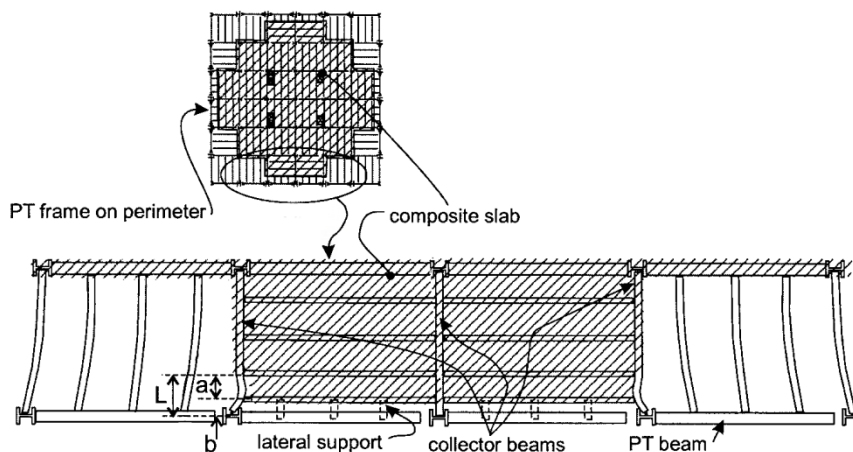


Figure 8.5 Special collector beams for steel self-centering moment frames (modified from Garlock and Li (2008))

Similarly, King (2007) suggested the use of one single collector bay instead of activating all frame beams. To accommodate the displacement demand, the diaphragm is considered to slide along all other frame beams. It was suggested that the high diaphragm forces are

transferred by a horizontal steel shear plate to the collector bay. Care needs to be taken to allow for the sliding of the diaphragm.

Another sliding floor solution is suggested by Kim and Christopoulos (2009), where single slab portions are fixed to beams along two edges and are able to slide on Teflon pads placed on the beams on the remaining edges. The slabs can therefore accommodate the required displacement demand by sliding respectively to each other. Elastic filler material is placed into the sliding edges and steel plates prevent concrete crushing. It is however unclear how shear transfer can be guaranteed between the different slab portions.

Chou et al. (2008) carried out full scale cyclic tests on post-tensioned steel beam-column connections assembled with a composite slab. Experimental results showed that the addition of the slab increased the strength and the stiffness of specimen when compared to the bare beam-column sub-assembly. To allow for the gap opening, cracks formed in the slab along the beam-column interfaces as shown in Figure 8.6 until the wired mesh ruptured. Like suggested later in the chapter, unbonded longitudinal rebars were placed over the cracked area, but no information on their capacity in transferring shear forces was provided.

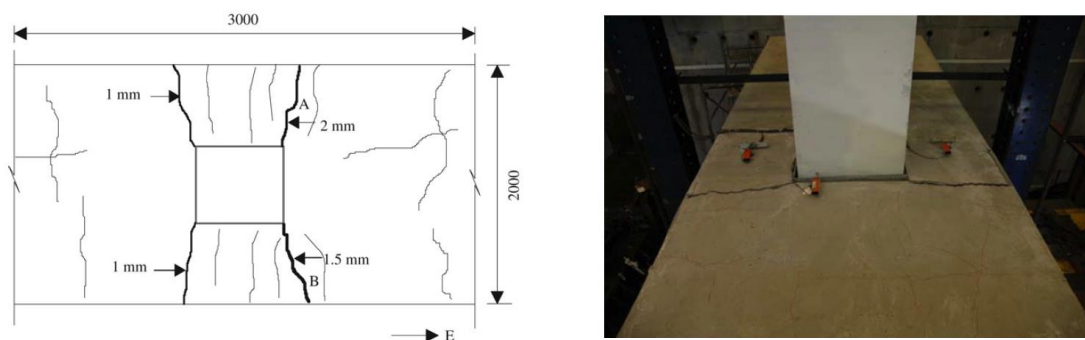


Figure 8.6 Cracking pattern at beam-column-joint (Chou et al. 2008)

The influence of the concrete slab in steel structures has also been investigated at the University of Canterbury (MacRae and Clifton 2013; MacRae et al. 2013; Hobbs 2014). The authors showed that composite slabs increased the strength of beams, but in case of traditional detailing this effect should not be accounted for in the beam design, since it becomes missing under larger drifts. Beam elongation was shown to be small for composite steel beams, because the beams could yield both in compression and tension. Chaudhari et al. (2014) are currently carrying out further experimental tests including a new confinement concept at the beam-column-joint and a new low damage connection based on non-prying sliding hinge joints.

8.3.3 Connections in multi-storey timber frame buildings

Only little information is available on the interaction between diaphragms and the lateral load resisting system in post-tensioned multi-storey timber buildings. Smith (2008) tested an external beam-column joint sub-assembly with a concrete floor slab added on top as shown in Figure 8.7. The presence of the floor created an asymmetric response of the joint since it partially prevented the top gap opening of the beam. The gap opening and the rocking of the gravity beam on the timber corbel caused some floor tearing; crack widths however were small and would close at the end of each cycle. It was suggested that in the case of an internal joint, the displacement incompatibility would have added noticeable strength and stiffness to the system and caused bigger cracks in the slab. This interaction is recommended to be taken into account for the design of such structures.

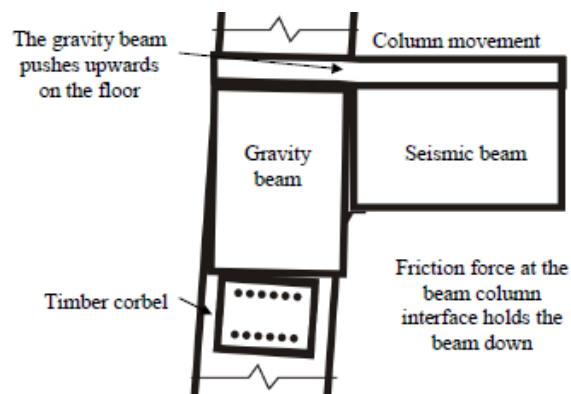


Figure 8.7: Movement of gravity beam during positive drift (Smith 2008)

Frame elongation due to gap opening has also been observed by Pino (2011) while studying the dynamic behaviour of post-tensioned timber frame buildings. At the lower floor of the scaled 5 storey building tested on the shake table, a gap opening of 10 mm (real scale) was measured. Since the frame was tested without realistically attached floor diaphragms, no information on the interaction between frame beams and the slabs are provided.

Newcombe (2011) tested a 2/3 scaled building with timber-concrete-composite floors shown in Figure 8.8. Frame elongation has been measured to be less than 4 mm under unidirectional loading and up to 8 mm for bidirectional loading. The relatively small values were explained by the elastic compression deformation in the beam-column joint, later described by van Beerschoten (2013) and Smith (2014). Still, an increase in strength due to interaction was measured to be around 20%, when compared to the structure without diaphragms. Crack widths in the slab were relatively small and were deemed to be easily repairable.



Figure 8.8: Two-thirds scale test building at the University of Canterbury (Newcombe 2011)

For a gravity rocking system with continuous timber beams and continuous steel columns, Jamil et al. (2012) and later Jamil et al. (2014) showed an alternative connection system to minimize floor damage. The beams were supported by cantilevers fixed to the columns, and under rocking provided eccentric gravity loads guaranteeing self-centering of the structure. With this mechanism, all beams and therefore also the diaphragms underwent the same vertical movement, avoiding any displacement incompatibilities. The beam to column connection needs to be designed carefully, since diaphragm shear forces must be transferred while allowing for the columns rotation. Vertical displacement incompatibilities will arise if the diaphragm is connected to any other gravity resisting system.

Similarly to the systems suggested by King (2007), the Massey University's College of Creative Arts building in Wellington, New Zealand, designed by Dunning Thornton Consultants, has the floor diaphragm connected to one bay of the moment resisting frame. The remaining diaphragm portion can slide on top of the remaining beams (Davies 2012). For the Trimble Navigation Building in Christchurch, New Zealand, the timber-concrete-composite floors are pre-cracked along the beam-column-joint lines to allow for the gap opening to happen. Unbonded rebars are placed over the crack, which elongate elastically in case of gap opening and transfer shear forces via dowel action for earthquake attack perpendicular to the frame direction (Brown et al. 2012). As discussed later, this design solution needs some further research, since dowel action will imply large displacements and kinking of the bars in the case of large crack openings.

8.4 FINDINGS FROM A POST-TENSIONED TWO BAY FRAME

To study the implications of a timber floor diaphragm connected to a frame system subjected to beam elongation, a low damage Press-Lam frame system as shown in Figure 8.9 has been erected and tested under quasi-static lateral load in the structural engineering laboratories at the University of Canterbury. An exhaustive description of the experimental setup, the loading protocol and the results are described in Appendix C. Following an overview of the setup and the main findings, together with design recommendations, are given.



Figure 8.9 Experimental setup of a two bay post-tensioned timber frame with floor panels

8.4.1 Experimental setup

The full scale two bay frame with a total length of 12 meters was tested under quasi-static lateral loads. Stressed-skin flooring panels made of LVL joist and cross-banded LVL panels of 2 meters length were fixed to the frame beams via blocking members. The horizontal load from the hydraulic ram was applied to the floor panels as shown in Figure 8.10. The frame was loaded to drift levels of up to 3.5%, a deformation limit normally accepted for a Maximum Credible Earthquake (MCE) event. For normal design situations, drifts of 2.5% for Design Basis Earthquake (DBE) events were targeted.

To obtain benchmark values, the frame was first tested without the flooring elements by applying loads to the beams directly (test setup 1). Successively flooring panels were mounted on the frame beams and the load was applied through these to the frame. All floor elements were connected via inclined screws in order to transfer shear forces, except of the panels at the central column where the displacement incompatibilities occurred. The floor portions on the left and right hand sides of the central columns were left unconnected in order to measure the displacement demand on the diaphragm panels (test setup 2).

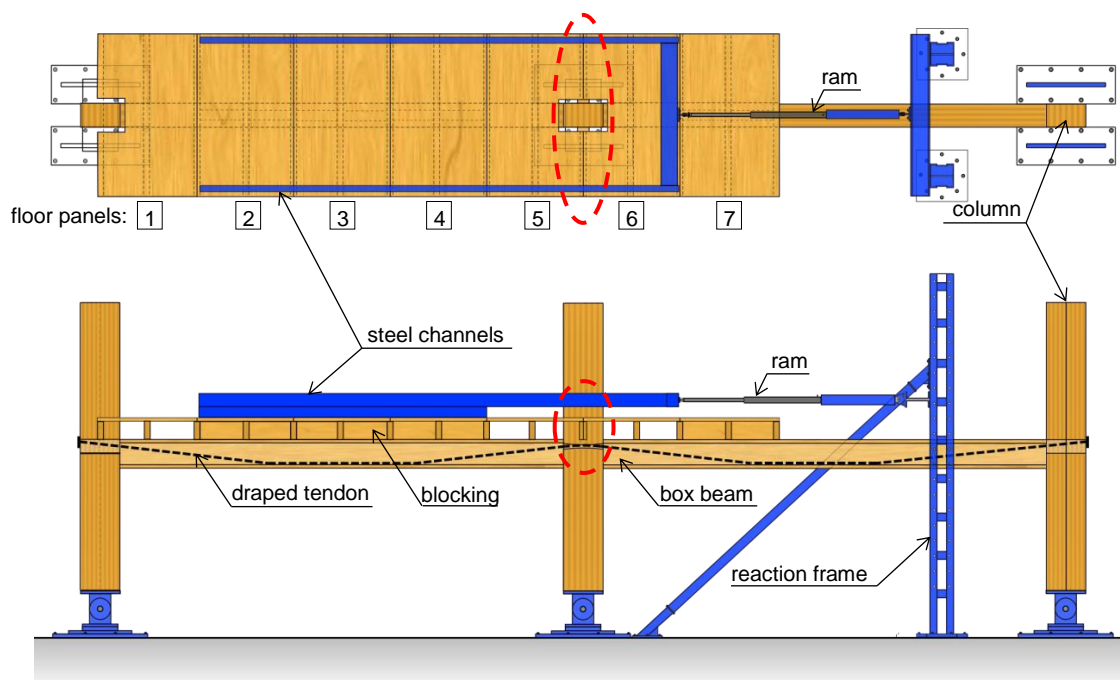


Figure 8.10 Schematic test setup of the post-tensioned two bay frame

Table 8.1 Summary of the test setups

Test Setup	Description	Displacement incompatibility accommodated by	Load application
1	Bare frame	-	Frame beam
2	Sliding floors	Sliding of floor panels	Floor panels
3	Concentrated gap	One concentrated panel gap	Floor panels
4	Spread gap	Multiple panel gaps and panel elongation	Floor panels

To guarantee diaphragm action also the panels at the central column were connected by fully threaded screws placed at the bottom of the joist. This setup represents the '*concentrated gap opening*' solution (test setup 3) shown in Figure 8.12a, which accommodates the displacement demand by bending of the joists. By connecting all panels with screws just under the floor skin, as shown in Figure 8.12b, all panel connections had the same stiffness, leading to the '*spread gap opening*' solution (test setup 4) with a number of smaller gap openings.

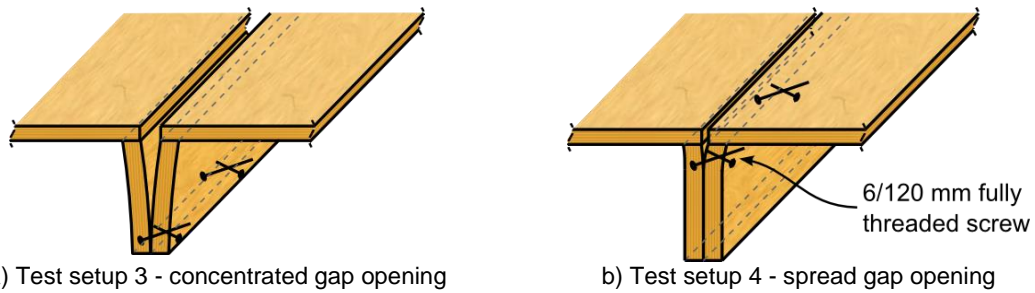


Figure 8.11 Panel connection at the central column, where displacement incompatibilities occur (connection between panels 5 and 6)

8.4.2 Test results

Figure 8.12 shows the beam-column-joint gap opening behaviour at the central column for the concentrated gap solution (test setup 3) during the cyclic testing. Also shown is the gap opening between the panels at the central column (panels 5 and 6); all other floor panel gap openings were close to zero and therefore not shown. The elongation of floor panel 5 is plotted as well, with similar values for panel 6 (not shown).

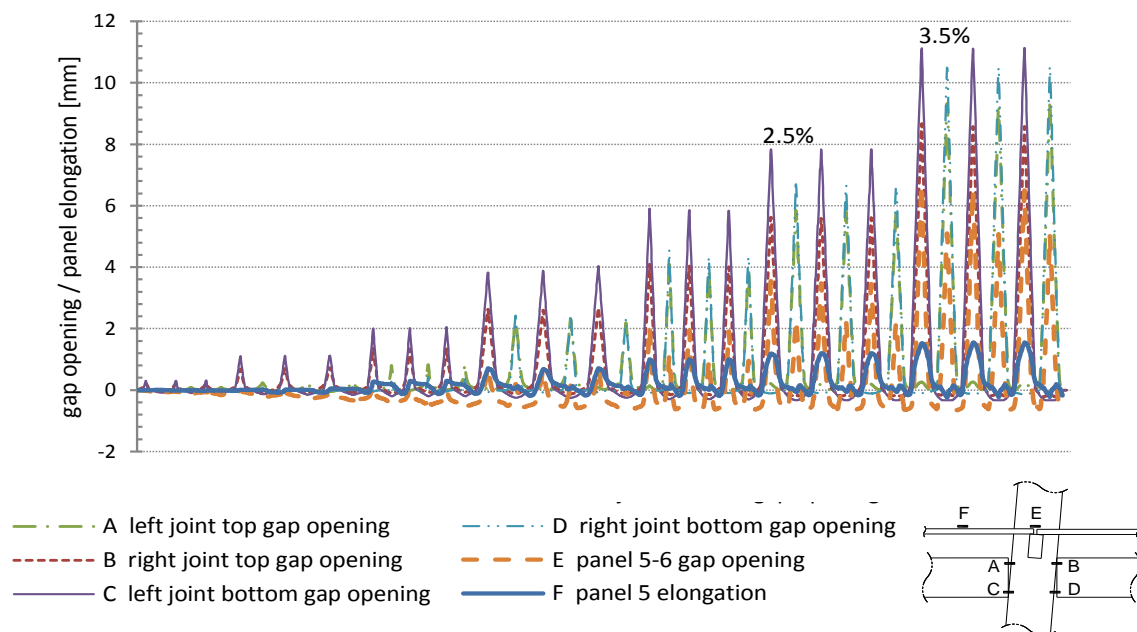


Figure 8.12 Central beam-column-joint gap openings overlaid with the gap opening between floor panels 5 and 6 and the elongation of floor panel 5 for drift levels up to 3.5% (Test setup 3 - concentrated floor gap opening)

Even though the floor panels at the central column were connected, the beam-column-joint opening is the same as for the test with sliding floor panels as show in Table 8.2. The panel gap opening between panels 5 and 6 is reduced to half the value, with the remaining displacement demand provided by panel elongation and smaller gap openings in adjacent panels.

Results for the spread gap opening (test setup 4) are plotted in Figure 8.13. The beam-column-joint gap openings are not shown as they are identical with previous setups (compare Table

8.2). All floor gap openings, together with the elongation of panel 5, are shown. It can be seen that the gap openings close to the beam-column-joints are bigger and tend to zero for panels further away from the disturbed area. Since the gap between panels 5 and 6 is smaller than for the concentrated gap opening solution, the panel elongation becomes more dominant.

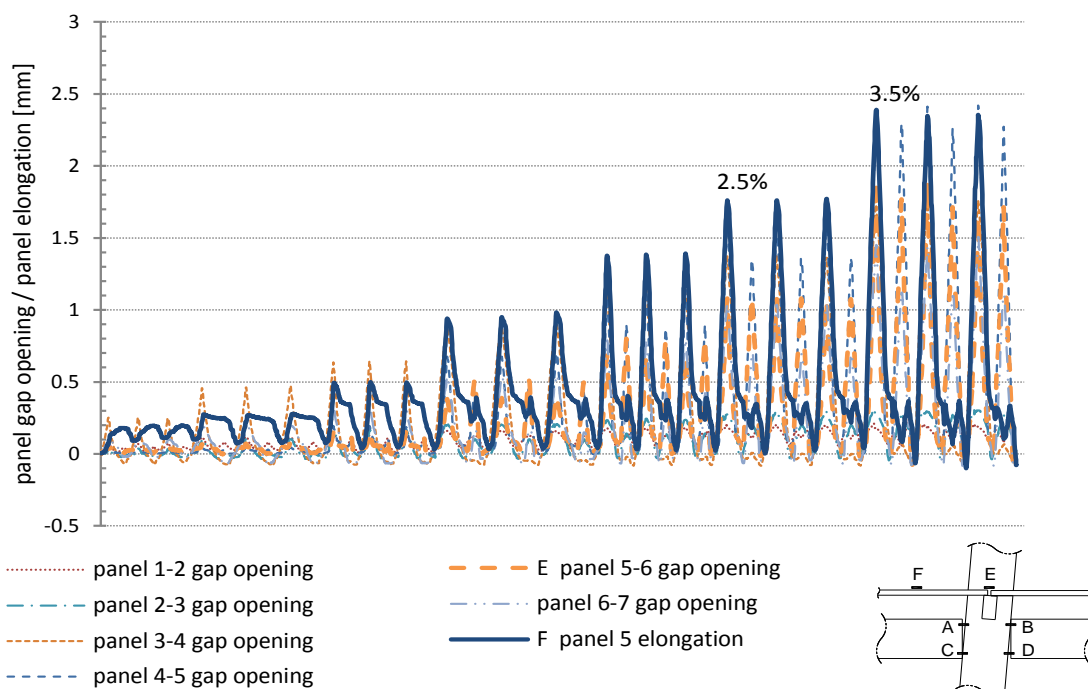


Figure 8.13 Gap opening of the different floor panels and the elongation of floor panel 5 (Test setup 4 – spread floor gap opening and panel elongation)

Table 8.2 further shows that the beam-column-joint opening is about 6 mm at the top and about 7 mm at the bottom for all setups. The difference between top and bottom values is caused by the draped profile of the tendon and the resulting pre-camber of the beam.

Table 8.2 Key values in mm for all four setups for 2.5% drift (values in parenthesis are at 3.5% drift)

Test Setup	Beam-column-joint gaps				Panel	
	top left	top right	bottom left	bottom right	gap 5-6	elongation
	A	B	C	D	E	F
1 - Bare frame	4.9	6.1	8.3	7.0	n.a.	n.a.
2 - Sliding floor	5.7	6.1	7.9	6.1	6.6	0.3
3 - Concentrated gap	5.9 (9.3)	5.6 (8.7)	7.8 (11.1)	6.7 (10.5)	3.6 (6.7)	1.2 (1.6)
4 - Spread gap	5.8 (9.3)	5.3 (8.2)	7.7 (11.2)	6.9 (10.8)	1.1 (1.9)	1.8 (2.4)

8.4.2.1 Influence of the diaphragm on the frame behaviour

The results from the four different setups shown in Figure 8.14 indicate that the frame has the same behaviour independently if loaded directly via the beam or through the floor diaphragm.

The negligible difference in stiffness and strength is given by the higher loading point (the diaphragm level is above the top of the beam) and by the tolerances in the initial post-tensioning force applied.

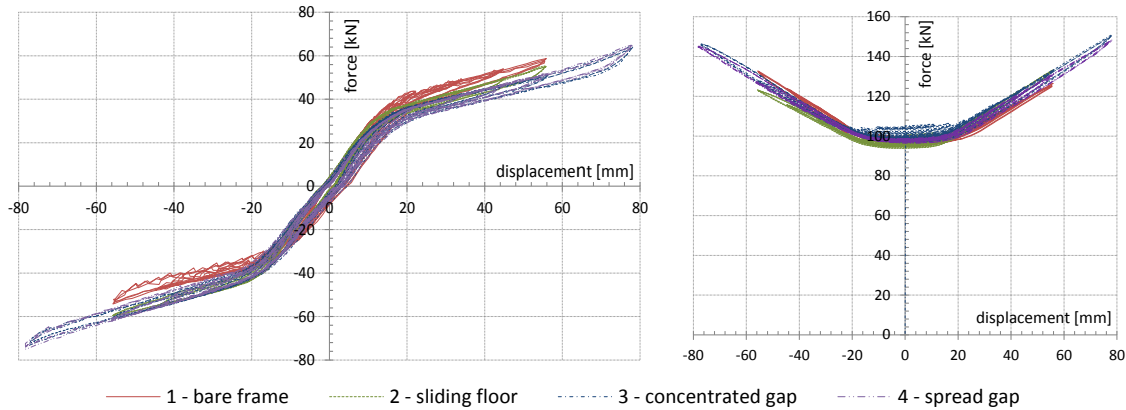


Figure 8.14 Force-displacement curve (left) and post-tensioning force (right)

More importantly, also for the setups with the concentrated and the spread gap solution, there was no significant difference in the global behaviour of the frame. This means that even though tearing forces tended to move the floor elements apart, no stiffening of the overall structural system occurred and the performance of the frame remained unaffected.

8.4.2.2 Performance of different connection detailing

For the concentrated gap solution (test setup 3) the floor elements 5 and 6 moved apart because of transverse bending of the LVL joists over their height. This behaviour can be clearly seen in Figure 8.15. By comparing the values in Table 8.2 it can be seen that the beam-column-joint gap openings remained essentially the same, another indication that the presence of the floor did not interfere with the overall performance of the frame. Because of the flexible connection, the floor gap opening tended to be smaller than in the case of the totally unconnected test setup 2 (3.6 mm and 6.6 mm respectively for a drift ratio of 2.5%). The remaining displacement was provided by the internal elongation of panels 5 and 6 (about 1.2 mm for a drift ratio of 2.5%) and some additional smaller floor gap openings in adjacent panels.

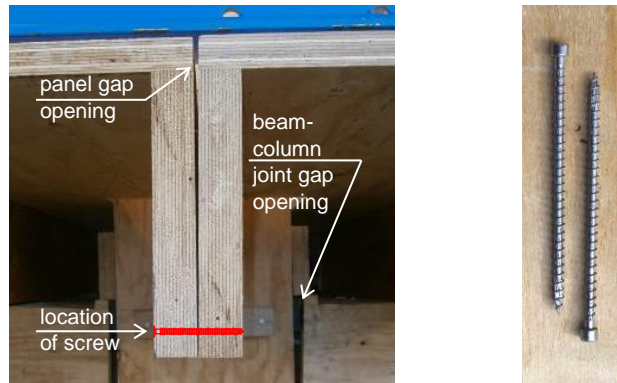


Figure 8.15 Beam-column joint and floor gap opening with undamaged fasteners of the two-bay frame system (Test setup 3 - concentrated gap solution)

By connecting the floor elements by a much stiffer top flange connection (test setup 4, spread gap opening), the imposed displacement could not be taken solely by a single concentrated gap, but was spread out over several floor elements. This can be clearly seen in Figure 8.13, where the magnitude of floor gap openings is smaller, but occurs in more positions, with higher values close to the central column. Additionally, the panel elongation was higher than in test setup 3 (2.4 mm instead of 1.6 mm for 3.5% drift); this behaviour was expected also in panel 6 and in a lesser extent in adjacent panels. By summing up the single floor gaps and the panel elongations, the displacement required from the beam-column-gap opening can be obtained.

After unloading the frame, no residual deformation or damage in the timber elements or connections was observed. This can be explained by the flexibility of the timber elements and their connections.

8.4.3 Design recommendations

Depending on the flexibility of floor finishing and linings of adjacent internal and external walls to move with the floor, the designer can choose from 2 solutions to accommodate the displacement in the floor diaphragm:

- **Concentrated floor gap:** The required deformation should occur mainly in a single gap between floor panels, which will need special detailing. If the floor joists are flexible enough in transverse bending, a bottom flange connection with screws is sufficient. The connection still needs to guarantee the full shear transfer between the panels. If required, special steel elements, which allow the panels to move apart, can be used. Seismic gaps in the floor finishing and the wall linings may have to be provided.

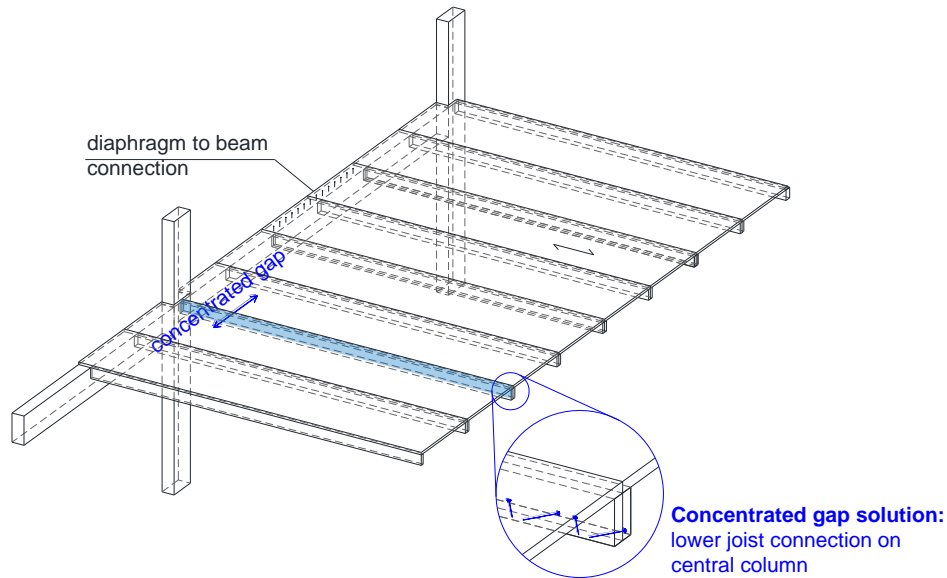


Figure 8.16 Concentrated floor gap solution

- Spread floor gaps and panel elongation:** All floor panels can be connected to each other by metallic connectors like nails or small diameter screws, which give some local flexibility. The connections need to guarantee the full shear transfer between panels. Gluing to connect floor panels should not be used, as it results in a very stiff and brittle connection, which cannot accommodate the required deformations. The panels close to the disturbed area should not be directly connected to the beam, as this would prevent the development of gap openings and panel elongations further away from the beam-column joint. The diaphragm to beam connection should not be a brittle type of connection. The floor finishing should be chosen to be elastic enough to allow for the formation of spread gaps or might require some cosmetic repair after a major seismic event.

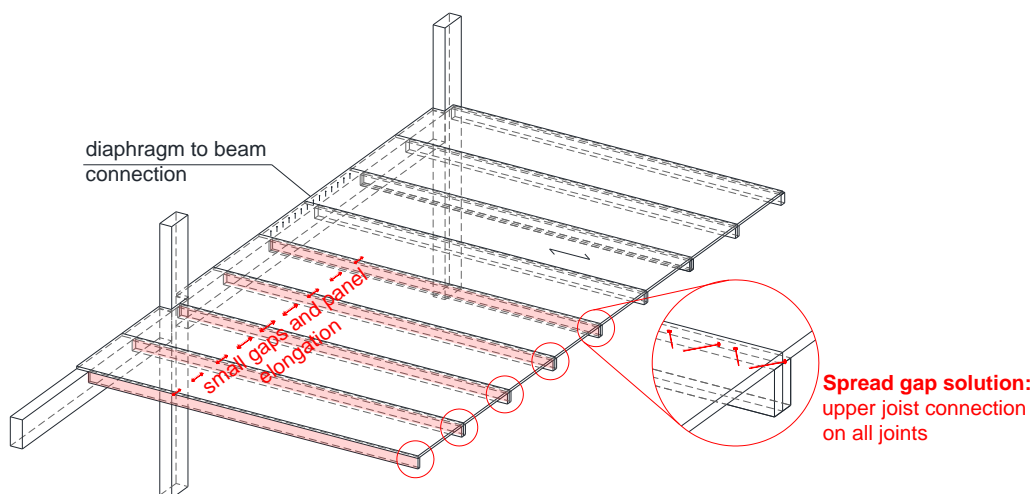


Figure 8.17 Spread floor gaps and panel elongation solution

A design example for both a timber only and a timber-concrete composite floor in a frame structure can be found in Appendix E.

8.4.4 Concrete diaphragms

Timber-Concrete-Composite (TCC) floor diaphragms or other diaphragms where the concrete topping is providing diaphragm action should be designed using the concentrated floor gap option. The concrete topping should be pre-cracked along the required gap line. Instead of providing continuous steel reinforcement over the crack, the shear transfer can be obtained by dowel action of unbonded rebars. It is important to note that contrary to the timber-only solution, the deformation of the steel rebars might give some additional strength and stiffness to the frame. Further research is required to investigate the capability of the rebar to transfer the diaphragm shear forces under dowel or kinking action in case of wider cracks (CAE 1999; Fenwick et al. 2010).

As an alternative, the concrete slab can be pre-cracked along two parallel timber joists, each connected to the slab at either side of the crack. The necessary shear connection between the joist and the slab is normally guaranteed by the connection mechanism used for the composite action. The shear forces can then be transferred between the two joists like for the timber concentrated gap solution with screws at the bottom of the joist.

For concrete topped diaphragms where the topping is non-structural, cracking is to be expected along the gap line. This causes only cosmetic damage and does not influence the behaviour of the structure. Even though it is assumed that this kind of diaphragm does not provide any composite action, the friction between the timber and the concrete might increase the stiffness of the frames. It is recommended to pre-crack the concrete topping along the expected gap line.

8.5 FINDINGS FROM A THREE STOREY POST-TENSIONED FRAME STRUCTURE UNDER DYNAMIC LOADS

Displacement incompatibilities of floor diaphragms in frame buildings have also been investigated on a three-storey Pres-Lam building tested on a shaking table. The test structure shown in Figure 8.18 was designed, erected and tested for a research project carried out at the University of Basilicata in Italy in collaboration with the University of Canterbury. More information on the research project can be found in Smith (2014). A detailed description of the test setup, the loading protocol and the results can be found in Appendix C.



Figure 8.18 Experimental setup of the 3 storey post-tensioned glulam frame building

8.5.1 Experimental setup

The 2/3 scale test building as shown in Figure 8.19 with an interstorey height of 2 m and a footprint of 4 m by 3 m was entirely built of glulam beams and columns and connected by high-strength post-tensioning rods in both directions. The building was designed by assuming a live load for offices of 3 kN/m^2 with the final storey being a rooftop garden.

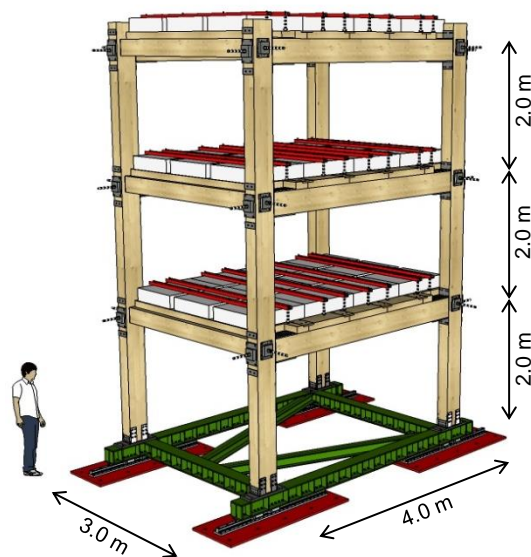


Figure 8.19 Schematic test setup of the 3 storey post-tensioned glulam frame building (modified from Smith (2014))

The timber diaphragms consisted of 100 mm thick glulam panels connected with plywood splines and screws working in shear. The whole diaphragm panel was connected to the perimeter beams in the loading direction by inclined fully threaded screws as shown in Figure

8.20. In the transverse direction the panels were fixed to the beams by in beam direction inclined screws.

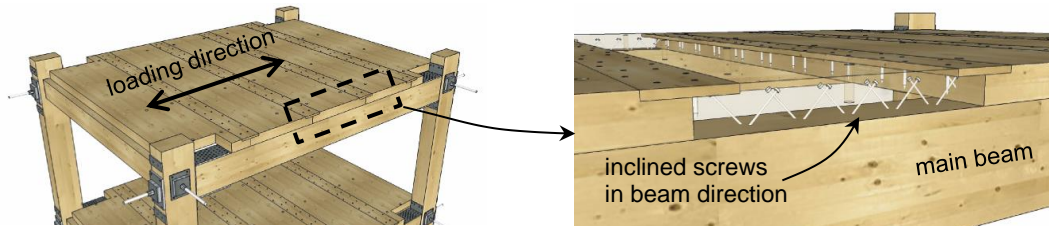


Figure 8.20 Experimental setup of the 3 storey post-tensioned glulam frame building; timber flooring, attachment and additional mass arrangement (modified from Smith (2014))

In the case of beam-column-joint gap opening, the main beam moves away from the column and the attached secondary beam. The diaphragm, which is attached to both the main and the secondary beam, restrains this movement causing displacement incompatibilities. Because of the high stiffness of screws working in their axial direction (connection to the main beam) and their lower stiffness when working in shear (connection to the secondary beams) as shown in Figure 8.21, latter was thought to provide enough elastic displacement to accommodate the imposed demand.

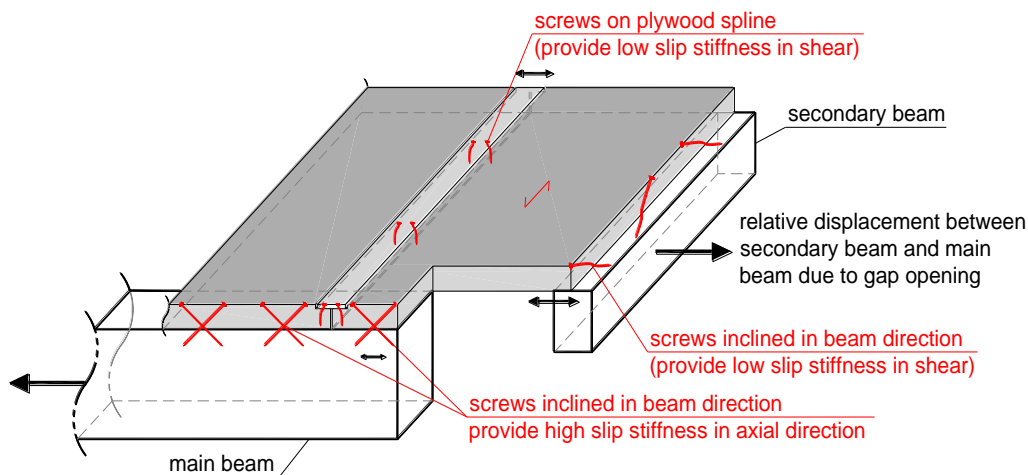


Figure 8.21 Fastener deformation to accommodate displacement incompatibilities

Additional mass was added to the floors to simulate the factored live load and to account for the scaled prototype structure. The mass was made up of a combination of concrete blocks and steel hold downs.

The loading input was a set of 7 spectra compatible earthquakes selected from the European strong-motion database (Izmit 1999, Turkey; Montenegro 1979, Serbia; Erzican 1992, Turkey; Tabas 1978, Iran; Campano Lucano 1980, Italy and South Iceland 2000 with two different peak ground accelerations). The code spectrum was defined in accordance with the current

European seismic design code Eurocode (Eurocode 8 2004) having a PGA of $a_g = 0.35$ g and a soil class B giving a Peak Ground Acceleration (PGA) for the design spectrum of 0.44 g. The shake table tests were performed with and without additional dissipative element with increasing PGA levels.

For the initial test series carried out in 2013, no dedicated instrumentation to measure diaphragm displacements was installed. In a subsequent test series a number of linear potentiometers were used to measure the displacements of the diaphragm.

8.5.2 Test results

Records obtained from initial testing (testing phase 1) showed that top gap openings of about 5 mm occurred at the beam-column-joint interface as shown in Figure 8.22 (Moroder et al. 2014). No stiffness or strength degradation was observed even after building drifts of 3.5% were measured. No visible damage to the diaphragm panels or other structural elements could be observed. Several diaphragm fasteners were extracted from the specimen and no damage to the fasteners was observed as shown at the bottom of Figure 8.22.



Figure 8.22 Beam-column-joint gap opening (top) and undamaged fastener of the diaphragm connection to the secondary beam (bottom)

In successive dynamic tests (testing phase 2), potentiometers measured diaphragm displacements at the locations where fastener slip or panel gap openings were expected. As outlined in Figure 8.21, most of the displacement demand was accommodated by the deformation of the connections to the secondary beam. Gap opening between the first and the second diaphragm panels together with some slip of the panel connection to the main beam could also be measured, adding some smaller displacements.

Figure 8.23 shows the measured diaphragm displacements for the Erzican, Turkey 1992 earthquake, where beam-column-joint gap openings of 2.2 mm were measured. The sum of the measured diaphragm displacements accommodated almost 0.9 mm, providing about 40% of the displacement demand. Visual inspection during subsequent tests suggests that the remaining displacements were accommodated by the rotation of the secondary beam. Depending on the connection of the secondary beams to the columns, this movement might not be possible in real building designs, requiring higher deformations at the panel-beam connection instead. Considering the relatively small diaphragm gap openings, this demand is normally guaranteed by the elastic deformation of the fasteners.

Even in the case of structures with multiple bays, rotation of the secondary beams still might occur, since the floor of the adjacent bay is connected with the same flexible connections. A concentrated gap in the floor panels at the secondary beam will open to accommodate the displacement demand.

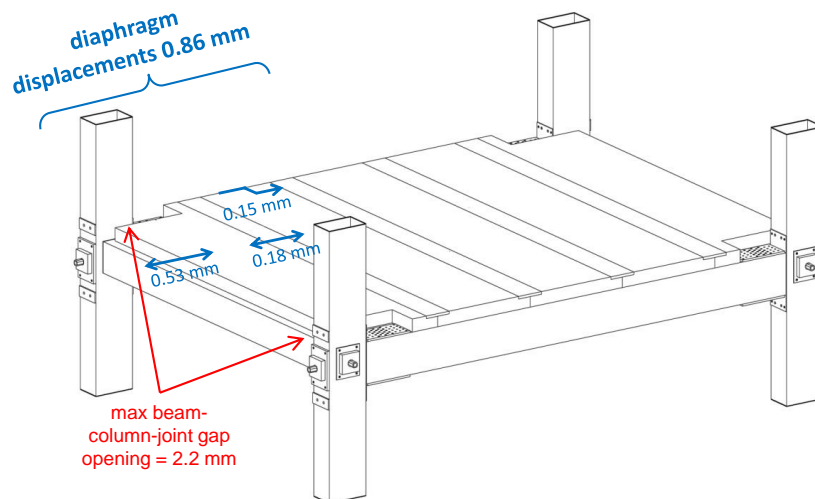


Figure 8.23 Beam-column-joint gap opening and diaphragm displacements for the Erzican, Turkey 1992 earthquake with a maximum building drift of 3.45%

Table 8.3 summarizes the maximum lateral interstorey drift at level 1 and the measured beam-column-joint-gap opening and total diaphragm displacements for the seven earthquake records. For all earthquakes except for the Tabas 1978 record, the measured diaphragm displacements accommodated between 30% and 60% of the displacement demand. For the Tabas earthquake, the relatively high displacement demand was accommodated elsewhere. The reason for this different behaviour is unclear, but the high intensity of the earthquake might have created panel slips at another location.

Table 8.3. Diaphragm displacement values for the seven earthquake records

ID	Maximum interstorey drift at level 1 [%]	Beam-column-joint gap opening at level 1 [mm]	Diaphragm displacements [mm]	Diaphragm uplift at secondary beam [mm]
Izmit, Turkey 1999	1.15	1.07	0.49	0.73
Montenegro, Serbia 1979	1.99	2.74	0.79	1.35
Erzican, Turkey 1992	3.78	2.20	0.86	2.02
Tabas, Iran 1978	3.69	6.09	0.58	2.24
Campano Lucano, Italy 1980	2.29	2.72	1.11	1.42
South Iceland, Iceland 2000	2.46	0.69	0.39	1.47
South Iceland, Iceland 2000	1.46	1.10	0.55	0.95

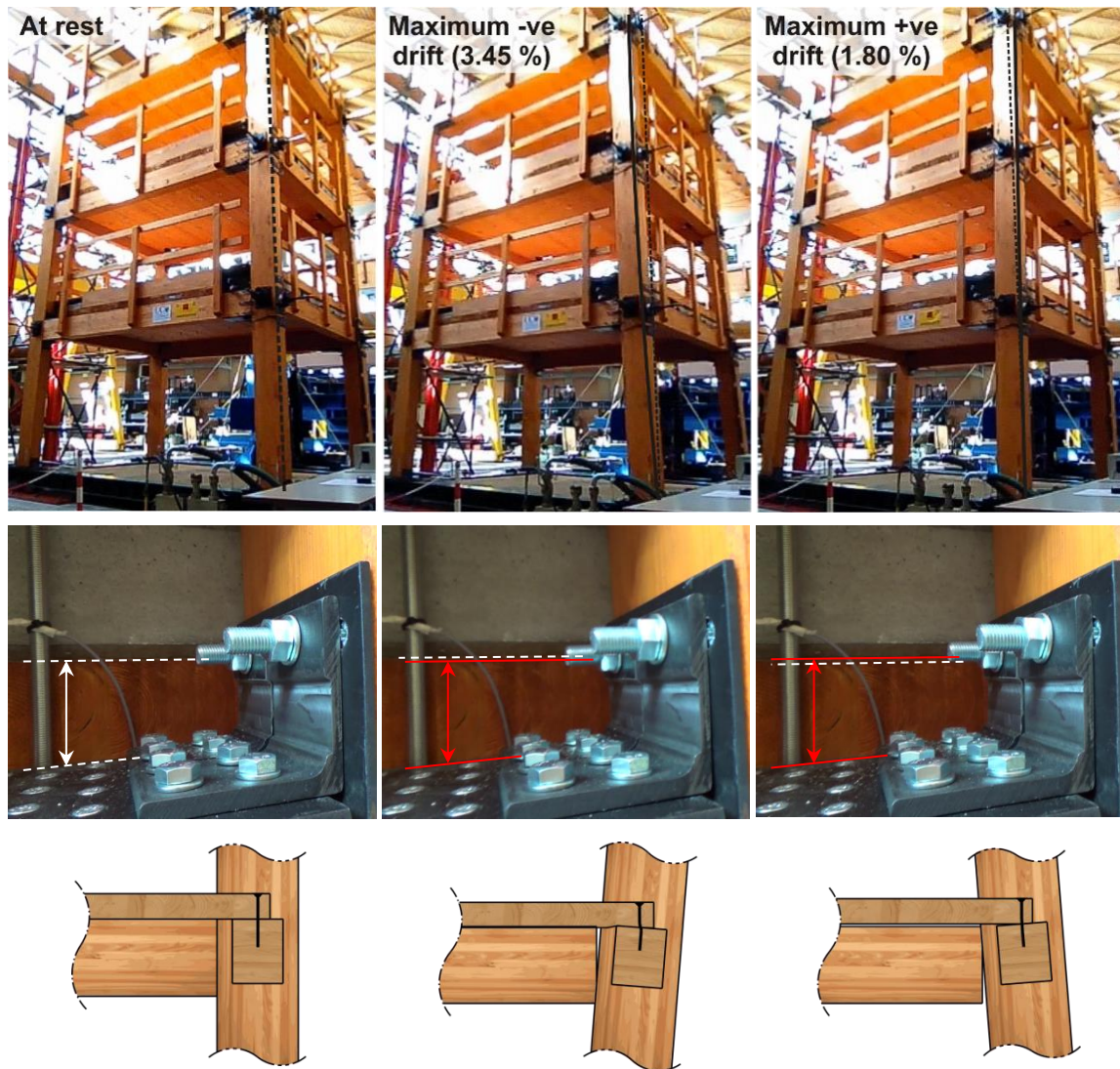


Figure 8.24 Photos and sketches showing maximum positive and negative drift response of the structure and respective vertical movement of the floor diaphragms

The rocking of the frames also caused some vertical displacement incompatibility of the diaphragms. As shown in Figure 8.24, the secondary beams rotated with the columns and as the diaphragm panel was fixed to them, it was forced to follow these movements. As a result, the diaphragm panel was pushed up and down relatively to the frame beams. Because of the notch at the outermost diaphragm panel, necessary to place the steel dissipators, this relative movement was easily accommodated by the flexibility of the timber elements and the connection between the panels. As discussed above, the secondary beam was not rigidly fixed to the columns, allowing for some rotation of the beam around their longitudinal axis. Figure 8.24 shows that in the case of beam-column-gap opening the floor panel and/or secondary beam undergo some compression deformation. Visual inspection suggested that most of this deformation was reversible or only caused very limited damage. Table 8.3 shows the relative vertical movement between the diaphragm panel and the secondary beam.

8.5.3 Design recommendations

Similarly to the two bay frame with stressed-skin-panels, the displacement incompatibilities were accommodated by the flexibility of the connections and, to a limited extent, by the flexibility of the timber elements. Therefore it is important to design a connection which allows for the required movement throughout a seismic event without compromising its capacity also for future events.

For a floor setup with massive timber panels running perpendicular to the frame direction, the displacement demand should be provided mainly by the connection of the panels to the secondary beam. This can be achieved by the use of a connection with in beam direction inclined screws as shown in Figure 8.25 or with screws or nails working in shear as in Figure 8.26. In the case of beam-column-joint gap opening the screws will deform elastically in dowel action but will keep transferring shear when the seismic load acts perpendicularly to the frame direction. This force transfer is important for seismic attacks in the perpendicular direction, where diaphragm forces need to be transferred to guaranteed diaphragm action.

Only little panel elongation can be expected for floors made with massive timber panels; however the connections between the single panels can provide additional elastic deformation. To enhance this behaviour, the first panel(s) adjacent to the disturbed areas should not be connected to the main beam. In this way the panel can slide and panel gap opening can be accommodated. The diaphragm shear needs to be transferred from the remaining panels into the lateral load resisting system.

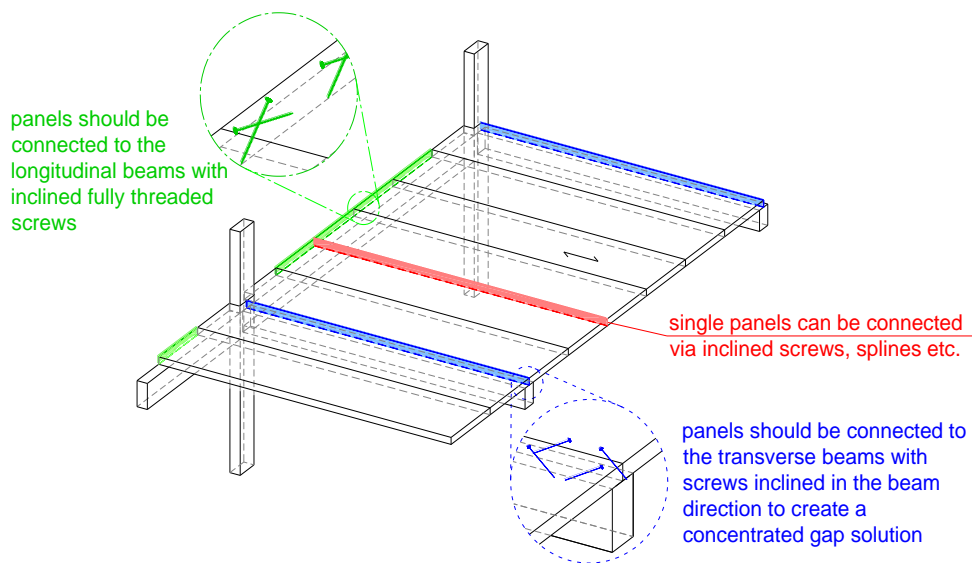


Figure 8.25 Design for solid panels

This solution is therefore conceptually the same as the concentrated floor gap solution mentioned above, where the panel joint should be conveniently located at the transverse beam in case of multiple frame bays as shown in Figures 8.25 and 8.26.

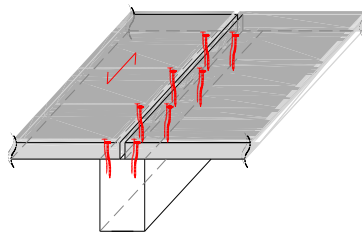


Figure 8.26 Close up of the floor panel gap opening at the secondary beam, connections working in shear allow for the displacement by elastic slip

8.6 DISCUSSION

This chapter studied the displacement incompatibilities between diaphragms and moment resisting frame structures. The outcomes of two different experimental setups showed insight on the interaction of the diaphragm and frame structures and strategies to accommodate displacement demand from gap openings are suggested.

Experimental evidence and damage after recent earthquakes have shown that the behaviour of concrete diaphragms and the respective lateral load resisting system can be strongly compromised because of displacement incompatibilities. Frame elongation can cause diaphragm cracking, unwanted stiffening of the frames or the pushing out of columns. In order to study such effects on diaphragms in timber frame structures, two experimental tests were conducted. For convenience, the experiments were carried out on post-tensioned Pres-Lam

frame structures, but the results and design recommendations given are valid for most ductile timber moment resisting frame structures.

The two bay post-tensioned frame was equipped with floor diaphragm elements and loaded horizontally. The floor elements were connected in two different ways to accommodate the displacement incompatibilities at the central beam-column-joint. The results showed that the presence of the floor did not alter the frame stiffness and that proper panel connections allowed for the displacement demand without compromising the diaphragm behaviour. Further, a three dimensional, three storey post-tensioned frame building with massive timber panels was tested under dynamic loads. Visual inspection and subsequent instrumentation showed that the required displacement demand due to frame elongation was accommodated by the metallic fasteners without noticeable damage or stiffness deterioration.

The first experimental setup presented here was not capable of investigating the diaphragm behaviour of a whole building, as it would have required the setup of a full scale diaphragm between a second frame, which was not possible during the research program. Diaphragms with concrete slabs have not been tested in this research program. The design of a pre-cracked slab with unbonded rebars is theoretically possible, but dowel action over larger cracks still needs to be investigated.

8.7 CONCLUSIONS

Based on the experimental testing on the two frame structures, which showed no damage under numerous loading cycles, it can be concluded that:

- the displacements created by the beam-column gap openings were accommodated within the diaphragm due to the flexibility in the connections and, to a lesser extent, by the elongation of the timber components of the diaphragm;
- the beam-column joint gap openings were not restrained by the presence of the floor diaphragm.

Two alternative connection details are proposed:

- A *concentrated floor gap* at the position of the beam-column joint. This is the preferred connection when using stressed-skin panels with a rigid floor finish, solid timber panels and timber-concrete-composite floors (not tested in this programme);
- *Distributed floor gaps and elongation* of the floor diaphragm over several floor panels. This is the preferred connection detail in the case of a flexible timber floor.

9 Displacement incompatibilities between diaphragms and wall structures

9.1 INTRODUCTION

In the previous chapter, the effect of displacement incompatibilities in frame structures was shown, and in this chapter the interaction between floor diaphragms and shear walls will be discussed. In two experimental setups, one with a single rocking wall connected to floor beams and one with a stairwell core structure connected to orthogonal floor beams, the behaviour of a number of different connections between collector beams and rocking timber shear walls is investigated.

9.1.1 Background

Because of the formation of plastic hinges in cast-in-situ reinforced concrete walls or the geometric gap opening in controlled rocking walls, floor slabs are forced to undergo vertical movements and also allow for imposed rotations. The required displacements are either allowed by out-of-plane deformation of the floor, or are restrained by the floor by increasing the stiffness of the wall. The latter mechanism can further cause additional axial forces in the wall or adjacent gravity columns. This behaviour, if not accounted for, can cause damage in the floors, hinder the force transfer from the diaphragm into the wall or lead to brittle wall failures.

In timber structures, the uplift and rotation demand on the floor diaphragm can be found in traditional Light Timber Framing (LTF) walls, where the tension chord and hold downs elongate, in Cross Laminated Timber (CLT) walls, where hold downs or wall-to-wall connections yield and allow for rocking, in purposely designed rocking timber walls like in the Prestressed Laminated (Pres-Lam) wall structures (Palermo et al. 2005; Newcombe 2011; Sarti 2015) or in gravity rocking walls with friction dissipaters (Loo et al. 2014).

To investigate the magnitude of displacement incompatibilities in timber wall structures and to study possible connections able to transfer diaphragm forces by allowing for the displacement demand, two different post-tensioned rocking walls were tested. First, a single rocking, two storey, scaled wall with and without end columns was tested. The loads were applied via two pairs of collector beams connected with ten different connection configurations to the wall. A

cost analysis compares the effectiveness of the different tested connection designs. A second setup studied the interaction of a CLT stairwell core and the collector beams. Two different beam-to-wall connections were studied, as well as the connection between the collector beams.

Depending on the out-of-plane stiffness of the floor, different connection configurations for design purposes are recommended.

9.2 DISPLACEMENT INCOMPATIBILITIES IN WALL STRUCTURES

Past research on post-tensioned and gravity rocking walls has highlighted the need to consider and resolve displacement incompatibilities between floor diaphragms and the lateral load resisting system (Priestley et al. 1999; fib 2003). As shown for a post-tensioned timber wall in Figure 9.1, the floor diaphragms are subjected to out-of-plane bending when the wall undergoes rocking, because of the rotation and uplift from the foundation. This behaviour can be found in traditional wall structures, like cantilever cast-in-situ concrete walls where the rotation and uplift are spread along the plastic hinge (fib 2003), as well as in controlled rocking concrete (*PREcast Seismic Structural Systems - PRESSS*), timber (Prestressed Laminated Timber Structures - Pres-Lam) and steel walls, where geometric gaps opening are encouraged. Similarly, also traditional Light Timber Framing (LTF) and Cross Laminated Timber (CLT) walls with yielding hold-downs or spread yielding along the panel connections undergo uplift and rotation, creating incompatibilities with the floor diaphragms.

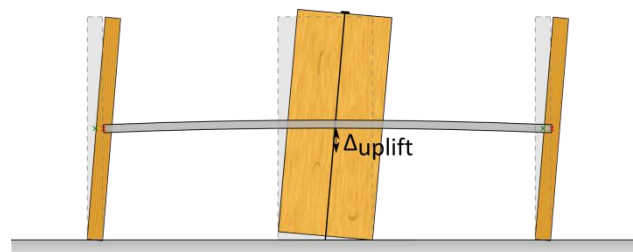


Figure 9.1 Floor out-of-plane bending due to wall rotation and uplift

The Canterbury earthquakes series in 2010-2011 has caused damage to reinforced concrete walls because of excessive compression loads, leading to shear and bar buckling failures. One of the reasons for the increased axial load were the relatively stiff floor slabs which prevented the uplift and/or the rotation of the walls (Canterbury Earthquake Royal Commission 2011; Structural Engineering Society of New Zealand 2011). Henry (2011) shows that the compression force in a reinforced concrete shear wall can be increased by 25% or more because of the presence of rigid floors.

9.3 REVIEW OF CURRENT DESIGN APPROACHES TO AVOID DAMAGE IN DIAPHRAGMS IN WALL STRUCTURES

9.3.1 Connections in multi-storey concrete wall buildings

Almost from its original conception, the research on post-tensioned and gravity rocking walls have highlighted the need to consider and resolve displacement incompatibilities of floor diaphragms with the lateral load resisting system. Solutions with slotted holes have been tested successfully in large scale pseudo-dynamic tests or on shaking table tests (Priestley et al. 1999; fib 2003). Figure 9.2 shows a further refined version of such a slotted connection used by Schoettler et al. (2009).

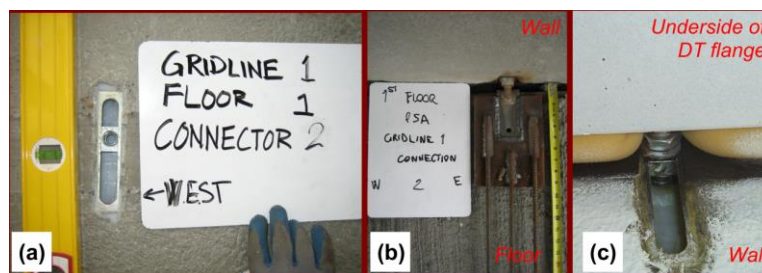


Figure 9.2 Wall-to-floor connection a) vertical slot in wall, b) insert tab welded to floor embed plate, and c) underside view of slotted connection (Schoettler et al. 2009)

Numerical analysis by Henry (2011) showed that rigidly connected concrete slabs can increase the shear wall flexural strength up to 45-50%. If this is not accounted for, capacity design principles might be compromised, leading to either brittle shear failures or buckling failures in the walls or nearby gravity columns due to the increased axial forces. Further, the stiffened wall can decrease the buildings' period and therefore increase the seismic demand. To prevent the interaction and possible floor diaphragm damage, it was suggested to connect the floor to the wall through special devices with slotted holes.

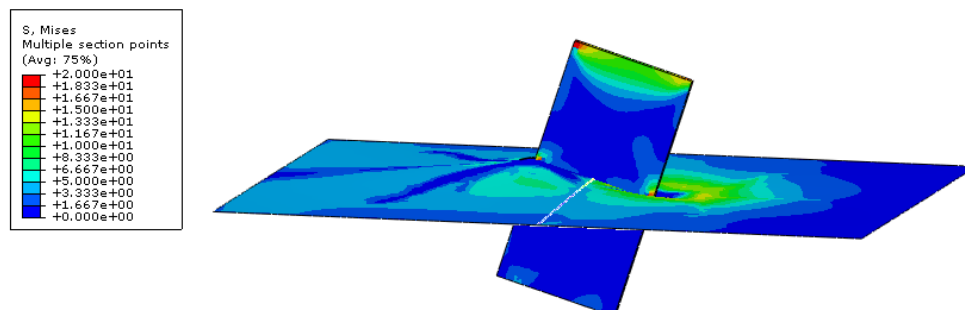


Figure 9.3 Calculated displaced shape of the floor section FEM at 3% wall drift (displacements magnified 10 times) (Henry 2011)

As an alternative, the Precast Wall with End Columns System (PreWEC) was suggested as shown in Figure 9.4. The system solves the displacement incompatibilities by having the floor slab connected to two external columns. Since the columns are fixed to the foundation, no uplift force is imposed to the floor slab. The horizontal forces are transferred by friction and pinned struts into the wall, as proposed by Sritharan et al. (2008).

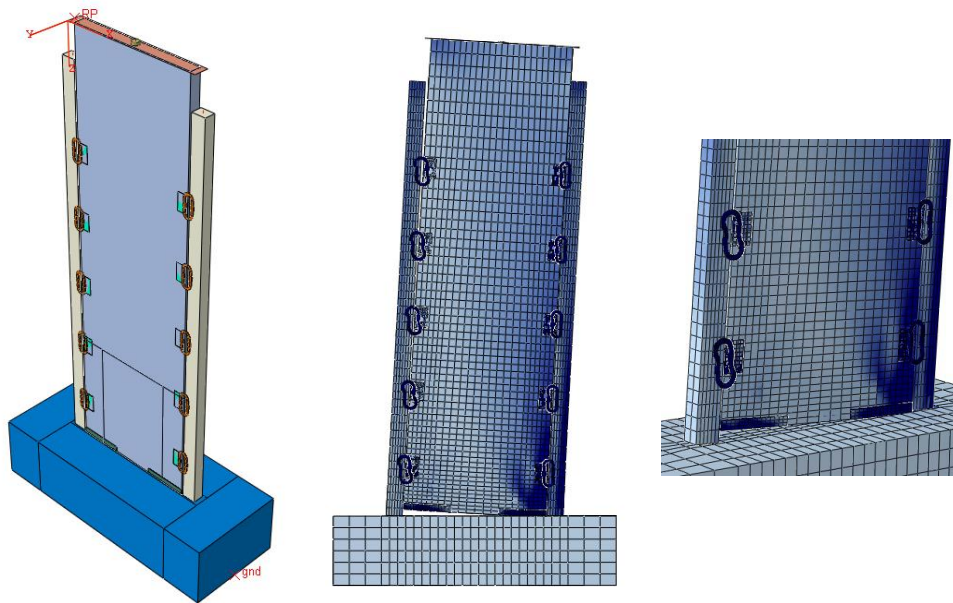


Figure 9.4 Schematic layout of the PreWEC system and FEM analysis results (Henry 2011)

The blind prediction competition of the seven storey NEES building tested on a shake table at the University of California at San Diego shows that the wall-to-floor interaction is a commonly ignored issue (Waugh and Sritharan 2010). The large moment couple created by the gravity columns and out-of-plane rigid floor increased the lateral resistance by 24%.

9.3.2 Connections in multi-storey steel wall buildings

Eatherton (2010) proposed a number of different connection designs between the floor slabs and the steel rocking frame in order to prevent localized damage from the uplifting column. The configuration shown in Figure 9.5a requires two collector beams running parallel to the steel frame. The beams are connected to the frame by thin shear plates which can transfer the horizontal forces but allow for the rocking motion by out-of-plane bending. For the solution shown in Figure 9.5b the forces are transferred via contact through rollers. Chancellor et al. (2011) proposed a similar solution, whereas instead of rollers, bearings with brass plates are used to transfer the horizontal force to the gravity columns. This solution has the advantage of providing additional energy dissipation via friction.

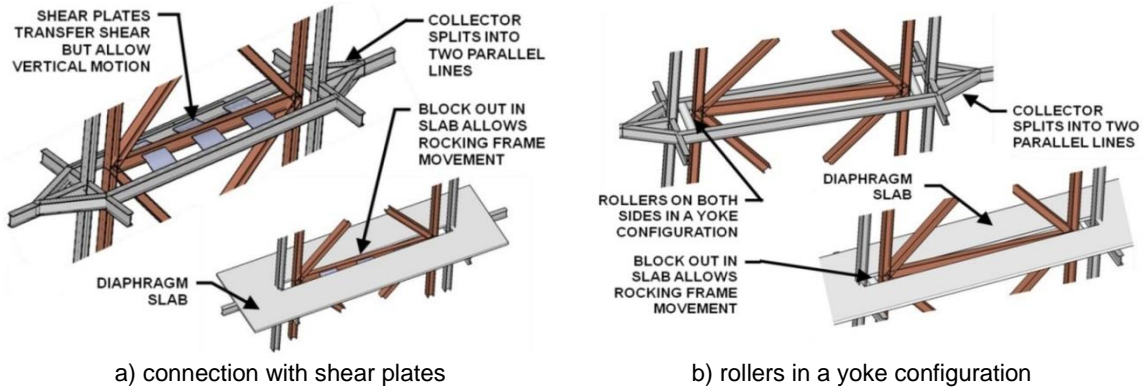


Figure 9.5 Proposed diaphragm connections for steel wall structures (Eatherton 2010)

In their feasibility study, Latham et al. (2013) showed other diaphragm connections for post-tensioned steel rocking walls. In order to allow for the rotation and uplift of the wall, a round pin in a slotted hole provides the required degrees of freedom. Because of the localized contact area, which could cause high localised stresses, the pin is inserted in a rectangular steel casting which can move in a slotted hole as shown in Figure 9.6a. Because of friction, this solution has been further modified to a protruding tongue plate, which allows for small rotations and uplifts. The bearing area can be designed specifically to minimize friction and, in case of higher than expected seismic load demands, the plate has a ductile behaviour. Also a link system with two pins was presented as shown in Figure 9.6c. Although required displacement demands are allowed for, out-of-plane movements cannot be restrained. As an outcome of this report, the Kilmore Medical Centre in Christchurch has been designed using the protruding tongue connection.

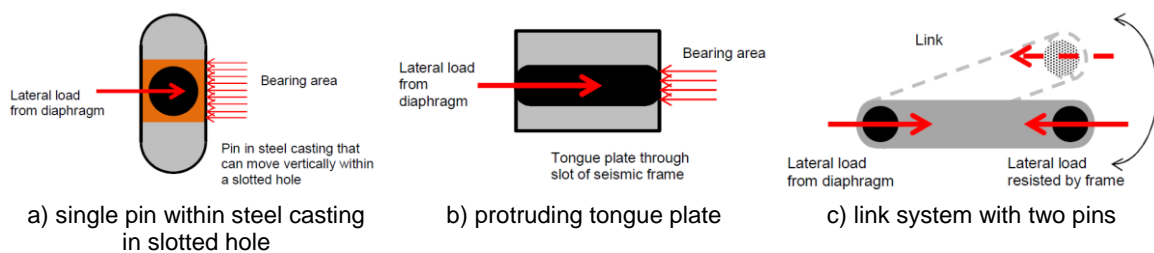
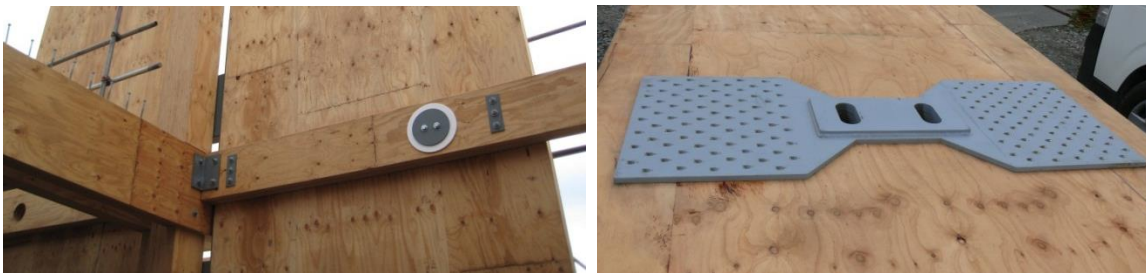


Figure 9.6 Floor diaphragm to seismic frame connection (Latham et al. 2013)

9.3.3 Connections in multi-storey timber wall buildings

Newcombe (2011) studied the response of a Pres-Lam building erected and tested under lateral loading at the University of Canterbury. When the building was loaded in the wall direction, a noticeable increase in the system strength was observed after a timber-concrete-composite floor was added to the structure. The increase of 20% however was attributed to the fact that the stiff collector beams have been connected to the external edges of the

coupled walls. While one edge of a wall was uplifting, the edge of the other wall was immobile because of the compression force, bending the collector beam over a very short span. This connection setup caused a high increase in stiffness and decreased the expected wall-to-foundation gap opening and the relative movements between the two walls required to activate the dissipation devices. Eccentric connections shall in general be avoided as the stiffness of the wall-beam system changes notably and damage to the connection or the floor diaphragm is likely to occur.



a) NMIT Building in Nelson with a large diameter pin (photo courtesy by Andy Buchanan) b) Trimble Building in Christchurch with a steel-to-steel connection

Figure 9.7 Connection of collector beams to walls

The diaphragm-to-wall connection detail chosen in the design of the NMIT Arts and Media Building in Nelson designed by Aurecon (Devereux et al. 2011), shown in Figure 9.7a, comprised 200 mm diameter steel pins between the collector and each of the coupled walls. In this case the pins were slightly offset from the centre of the wall to avoid the central post-tensioning cables. The non-continuity of the collector beam and the distance between the pins create little restraint in case of wall uplift. Furthermore, the pin acts as a hinge, decoupling the rotation between the walls and the beams.

Another connection detail designed to eliminate any displacement incompatibilities has been used in the Trimble Navigation Building in Christchurch designed by Opus International Consultants (Brown et al. 2012) as shown in Figure 9.7b. Both the wall and the collector beams were assembled with steel plates, one with a slotted and one with a round hole respectively. A simple steel pin sitting in slotted steel plates, which are connected to the walls and beams, transfers the horizontal forces by allowing for uplift and rotation.

In the currently under construction Kaikoura District Council Building designed by Nelson Timber Solutions Ltd, the diaphragm-to-wall connections were designed as a group of bolts arranged in a circular pattern. Because of the confined connection geometry, rotation is expected to be allowed for; uplift of the beam however needed to be accounted for by checking the bending strength and stiffness of the collector beams.



Figure 9.8 Pin connection between collector beams and walls in the Richmond Warehouse, New Zealand

Similarly as for the NMIT Arts and Media Building, the Richmond Warehouse designed by Craig Thelin Engineering has large diameter pins to connect the collector beams to the rocking walls. Figure 9.8a shows the connection at the first storey, where the collector can pivot on top of the pin while transferring both vertical and horizontal loads. For the second storey Figure 9.8b shows the pin which directly connects the collector to the wall.

9.4 CONCEPTUAL DESIGN SOLUTION

For wall structures the imposed uplift and rotation to the floor can be accommodated by a combination of the flexibility of the connection and the bending flexibility of the beam itself or by decoupling the vertical uplift and/or the rotation. While rotational decoupling can be realized by connections with a single pin, vertical uplift can ideally be allowed for by vertically slotted holes. The rotational flexibility of connections with a group of dowels derives from the low slip modulus and the small spacing between the fasteners. All wall-to-beam connection types used in the experimental program presented in this chapter can be grouped into the following three categories as shown in Figure 9.9:

- Connections with translational and rotational interaction (no decoupling);
- Connections with translational interaction (rotation decoupling); and
- Connections without interaction (decoupling of rotation and vertical uplift).

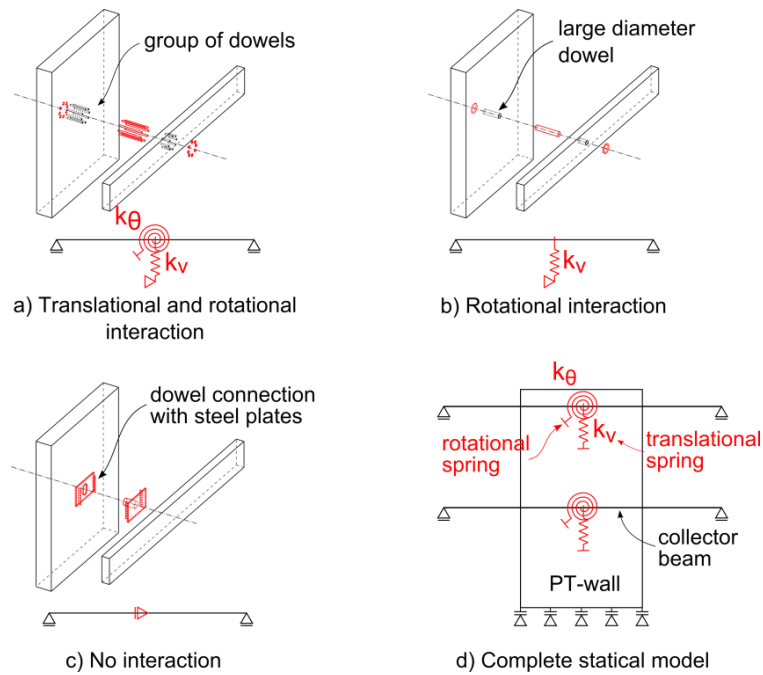


Figure 9.9: Summary of three proposed wall-to-beam connections: a) translational and rotational interaction, b) translational interaction and c) no interaction with the collector beam. d) shows the complete statical model

If the interaction between the wall and the collector beams needs to be evaluated, the translational and rotational stiffnesses of the connection and the beam can be added to the statical system of the wall. In this way the stiffness contributions can be incorporated to determine the force-displacement curves of post-tensioned walls. More information on the topic can be found in Chapter 10.

A different approach to reach a high degree in the mitigation of the interaction between walls and floor diaphragms is the use of end wall as suggested for concrete structures by Henry (2011) and later proposed for timber walls by Sarti (2015). With this option, the floor forces are transferred to end columns which are fixed or pinned to the foundation and can therefore not uplift. The columns bear against the wall and transfer the horizontal forces by contact. Since the columns cannot uplift, only rotation incompatibility needs to be accounted for.

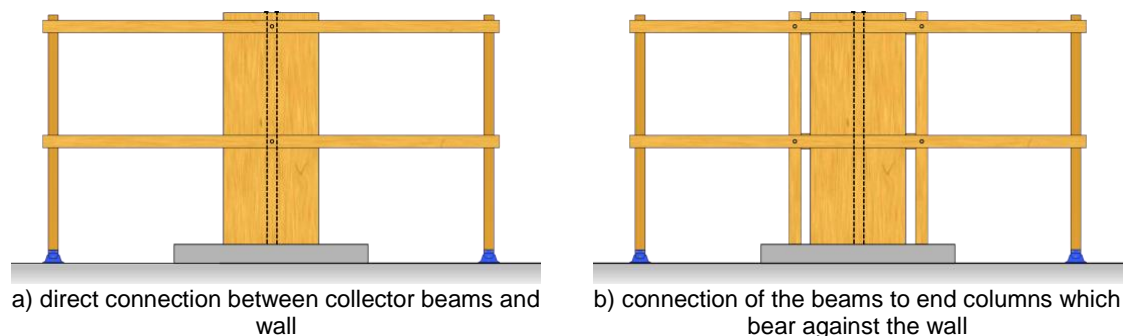


Figure 9.10 Different diaphragm force introduction into the wall by a) direct connection to the wall or b) by the use of end columns

9.5 FINDINGS FROM A POST-TENSIONED WALL

The interaction between rocking timber walls and floor diaphragms has been tested by the use of a low-damage Pres-Lam post tensioned wall erected and tested in the structural engineering laboratories at the University of Canterbury as shown in Figure 9.11. The full description of the experimental setup, the loading protocol and the results of the experiment are described in Appendix C. Following an overview of the setup and the main findings, together with design recommendations and a cost analysis, are given.

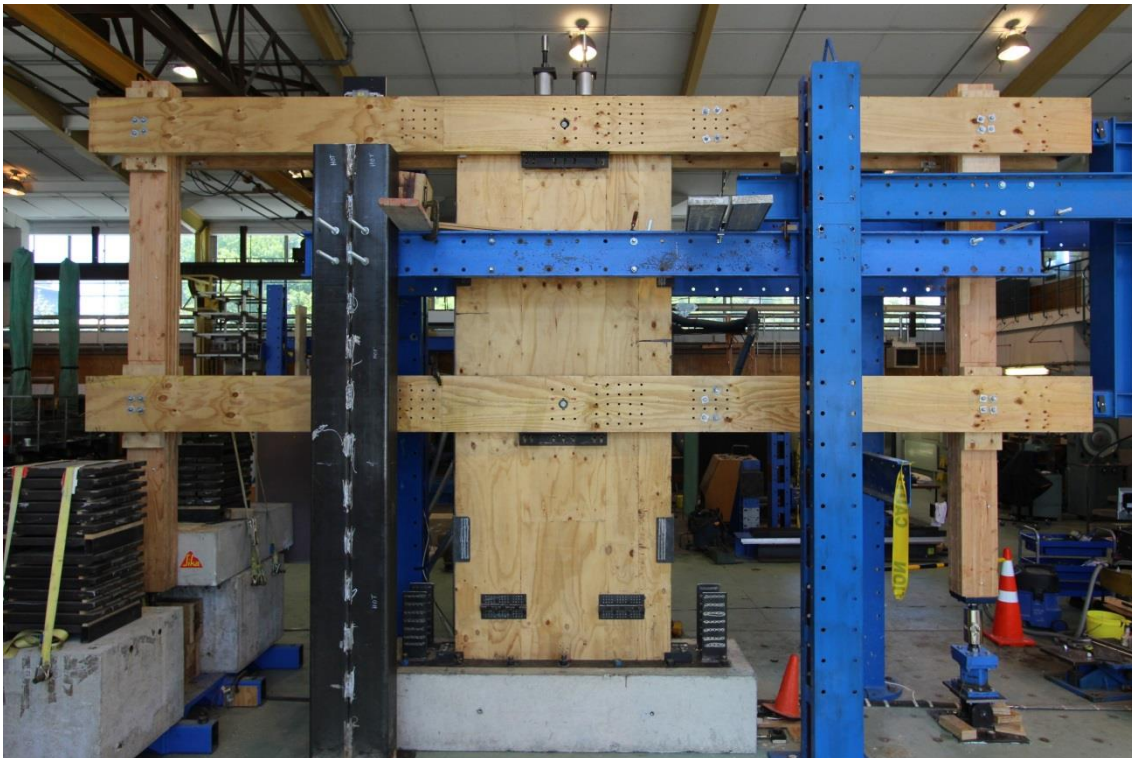


Figure 9.11 Experimental setup of a post-tensioned rocking wall with collector beams

9.5.1 Experimental setup

The 2/3 scale wall in Figure 9.14 was fitted with two sets of beams to resemble the collector beams which accumulate and transfer the diaphragm forces to the wall. Gravity columns at each end of beams were holding them into position by only allowing for the horizontal movements of the system under lateral loads. The collector beams were designed assuming a concrete-composite floor in order to represent a scenario with very high floor out-of-plane stiffness. A number of different connection details were applied at both levels to study the behaviour of the system. Loads were applied by a hydraulic ram and a spreader beam simulating a triangular load distribution. The quasi-static cyclic loads led to drift levels of 2.0%, considered as an acceptable drift limit for Maximum Credible Earthquake (MCE, 2500 years

return period) events. Drifts of 1.0 % are normally targeted for Design Basis Earthquake (DBE, 475 years return period) events.

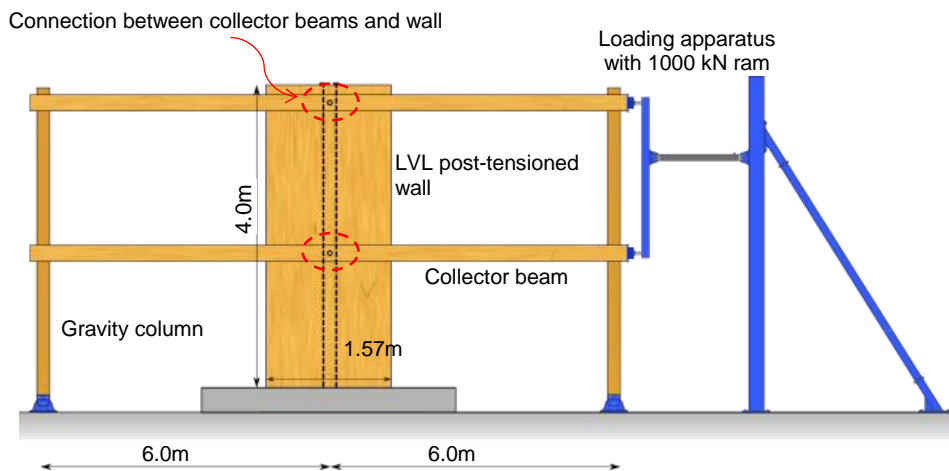


Figure 9.12 Test setup of the post-tensioned wall loaded through collector beams which were connected to the wall by several connection details (setup with end columns not shown)

Eight different connections were used to transfer the horizontal load from the collector beams to the wall (Figure 9.13 connections 1-8 and Figure 9.14a):

- 1) Group of 12 x M16 mm bolts at the centre of the wall;
- 2) Group of 25 x M16 mm bolts, 400 mm offset from the centre of the wall;
- 3) External timber blocks pushing against the edge of the wall, bolted to the beams with 16 mm bolts;
- 4) A 65 mm diameter round steel pin through a circular hole at the centre of the wall;
- 5) A 65 mm diameter round-square-round steel pin through a vertical slot at the centre of the wall;
- 6) A steel angle with 7 x M16 mm bolts in slotted holes;
- 7) A steel-to-steel connection with a 40 mm diameter round-square-round steel pin in a slotted hole;
- 8) 10 fully threaded $\varnothing 10/350$ mm screws inclined at 30° .

Subsequently, two end columns were added on each side of the wall as shown in Figures 9.10a and 9.14b. The columns were bearing against the wall in order to transfer the horizontal forces from the beams. The following two connections were used to transfer the load from the beams to the columns (Figure 9.13 connections 9-10 and Figure 9.14b):

- 9) Group of 12 x M16 mm bolts;
- 10) A 65 mm diameter round steel pin through a circular hole.

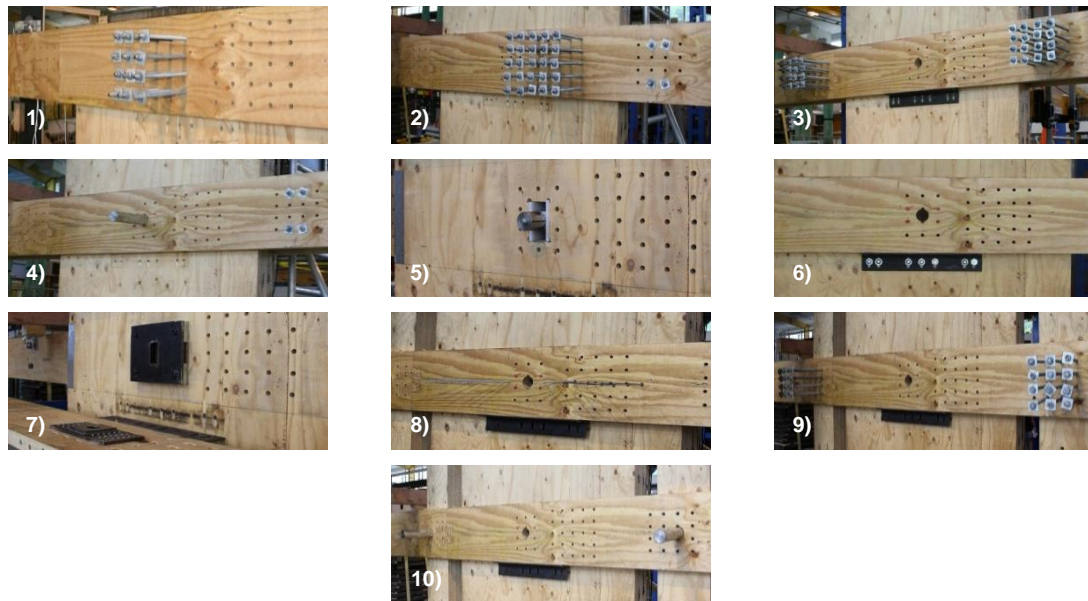


Figure 9.13 The ten tested connection details between the collector beams and the wall (1-8) and columns (9-10) respectively

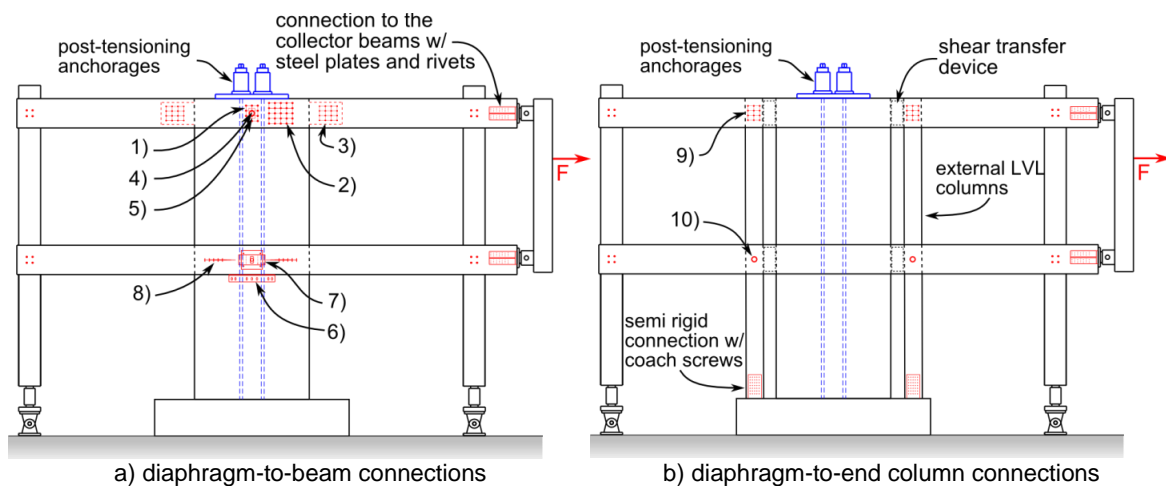


Figure 9.14 Alternative connections for the a) diaphragm-to-wall connections and the b) diaphragm-to-end beam connections

It is worth mentioning that when the collector beams also have to provide support for gravity loads (i.e. the floor is spanning perpendicularly to the beam), the designer needs to decide if the wall should also act as a vertical support. If no gravity should be taken by the wall (the collector beam hence spans freely between gravity columns), the wall-to-beam connection has to allow for the deflection of the beam under serviceably load. In case the wall is acting as a vertical support for the beam, the connection also has to carry additional vertical loads. The supplementary vertical force component in the wall increases the moment capacity and adds to the recentering of the wall.

9.5.2 Test results

The results of main interest are the degree of release (decoupling) of the rotations and the uplifts between the wall and the collector beams. Table 9.1 summarizes these values for both setup cases (wall with and without end columns) for all ten connections. Values are provided for both DBE (1.0% drift) and MCE (2.0% drift) design cases. Values are also compared to the outcomes of the bare wall tested. All values are averages of the maxima during the three cycles at 1.0% (DBE) and 2.0% (MCE) drift respectively.

Table 9.1. Average values for the peak drifts at 1.0% (DBE in black) and 2.0% (MCE in red and italic) for some key values

Connection type	Horizontal force on wall		Upper beam				Axial force in external columns [kN]
	[kN]	[%] ^{1) 2)}	rotation [mrad]	[%]	uplift [mm]	[%] ³⁾	
1) Group of 12 bolts	170	(123%)	1.7	(17%)	3.6	(123%)	14
	<i>248</i>	<i>(114%)</i>	<i>2.6</i>	<i>(14%)</i>	<i>7.3</i>	<i>(100%)</i>	<i>26</i>
2) Eccentric group of 25 bolts	173	(127%)	1.2	(12%)	6.6	(224%)	29
	<i>272</i>	<i>(127%)</i>	<i>2.6</i>	<i>(15%)</i>	<i>13.3</i>	<i>(182%)</i>	<i>55</i>
3) External blocks with dowels	162	(119%)	1.5	(15%)	6.5	(221%)	21
	<i>248</i>	<i>(116%)</i>	<i>2.3</i>	<i>(13%)</i>	<i>9.5</i>	<i>(130%)</i>	<i>32</i>
4) Large diameter pin	156	(113%)	0.5	(5%)	3.8	(129%)	7
	<i>232</i>	<i>(106%)</i>	<i>0.9</i>	<i>(5%)</i>	<i>7.4</i>	<i>(101%)</i>	<i>14</i>
5) Large diameter pin and slot in wall	154	(111%)	0.4	(4%)	4.4	(148%)	9
	<i>231</i>	<i>(108%)</i>	<i>1.0</i>	<i>(5%)</i>	<i>7.9</i>	<i>(108%)</i>	<i>17</i>
6) Steel angle with slots	161	(118%)	2.9	(29%)	3.9	(131%)	14
	<i>251</i>	<i>(117%)</i>	<i>4.4</i>	<i>(24%)</i>	<i>7.4</i>	<i>(100%)</i>	<i>27</i>
7) Steel-to-steel connection with slots	150	(109%)	0.6	(6%)	3.1	(103%)	5
	<i>231</i>	<i>(106%)</i>	<i>0.8</i>	<i>(5%)</i>	<i>6.7</i>	<i>(92%)</i>	<i>12</i>
8) Fully threaded screws	142	(103%)	0.7	(7%)	2.7	(92%)	5
	<i>221</i>	<i>(102%)</i>	<i>1.4</i>	<i>(8%)</i>	<i>4.4</i>	<i>(62%)</i>	<i>8</i>
9) End columns with group of bolts	140	(110%)	0.8	(8%)	0.5	(16%)	8
	<i>237</i>	<i>(99%)</i>	<i>1.4</i>	<i>(8%)</i>	<i>0.8</i>	<i>(11%)</i>	<i>13</i>
10) End columns with large diameter pin	135	(101%)	0.3	(3%)	0.9	(30%)	5
	<i>225</i>	<i>(93%)</i>	<i>0.7</i>	<i>(4%)</i>	<i>1.1</i>	<i>(15%)</i>	<i>7</i>

¹⁾ Ratios are relative to the max force value of 137 kN (DBE) and 215 kN (MCE) respectively of the wall tested without beams (bare wall) for connections 1-8 without end columns.

²⁾ Ratios are relative to the max force value of 130 kN (DBE) and 247 kN (MCE) respectively of the wall tested without beams (bare wall) for connections 9-10 with end columns.

³⁾ Ratios are relative to the average wall rotation of 10 mrad (DBE) and 20 mrad (MCE) respectively and wall uplift of 3.0 mm (DBE) and 7.5 mm (MCE) respectively.

As expected, the beam rotations for all connections were much lower than the imposed wall rotations. Although all connections allowed for some differential rotation, for the solution with the large diameter pins the beams essentially remained straight. Connections with bolts, on the other hand, forced the beam to rotate slightly. Vertical uplift of the beam could only be

slightly reduced with a steel-to-steel connection with a pin in slotted holes and with the connection with fully threaded screws. For the remaining connections, vertical movement was either not released (dowel connections), or friction prevented sliding. For the wall setup with end columns the vertical uplift was absent. The measured axial forces in the two external gravity columns also provided information of how much interaction the beam-wall system underwent. If imposed displacements are completely decoupled, then the beam will remain straight without activating any forces in the columns.

In the following section the behaviour of the single connections is briefly discussed:

Connection type 1 - centred group of 12 bolts: the collector beams followed closely the wall uplift and also underwent some rotation as the connection had a small rotational stiffness. The strength of the system increased slightly when compared to the wall tested without beams.

Connection type 2 - eccentric group of 25 bolts: the eccentric connection imposed higher uplift in the beams and also increased the system strength, since the beams had to bend closer to the support.

Connection type 3 - external blocks with dowels: the rotation of the beams was similar to that with bolted connections; however, the friction at the bearing plates made the beam uplift equal to the wall edges uplift, which is higher than the wall centre uplift. The interaction between the beams and the wall was relatively high.

Connection type 4 - large diameter pin: as expected, no rotations were transferred to the beam and the uplift of the beam closely followed the wall uplift. There was only little interaction between the beams and the wall in terms of strength.

Connection type 5 - large diameter pin with slotted hole: the rotational behaviour was similar to connection type 4; unexpectedly the uplift of the beam increased slightly. This behaviour was attributed to the fact that the pin does not slide in the slotted hole due to friction and to an unintended alteration in the test setup due to the change of connection.

Connection type 6 - steel angle with slotted holes: Because of the high friction between the external bolts and the steel angle, no sliding occurred along the slotted holes. Due to the length of the steel angle, higher rotations were imposed to the beam. A higher degree of interaction could be observed between the beams and the wall.

Connection type 7 - steel-to-steel connection with slotted holes: Rotation incompatibility was almost absent for this connection. Vertical decoupling of the beam did not occur to the expected degree, this was again attributed to high friction.

Connection type 8 – fully threaded screws: Because of the low stiffness of the screws when working in dowel action, this connection minimized both rotational and uplift incompatibilities. This was also reflected in the unaltered system strength when compared to the bare wall strength.

Connection type 9 – end columns with group of bolts: Uplift of the beams could be avoided in this connection, whereas still a small amount of rotation was introduced. System strength remained almost unchanged.

Connection type 10 – end columns with large diameter pin: Both rotation and uplift could be successfully avoided in the collector beams.

Connections which were able to decouple the imposed rotations showed only a small increase in system strength, additionally the axial forces in the gravity columns were smaller than with other connections. Avoiding rotation incompatibilities has therefore a bigger impact on the system behaviour than vertical displacement incompatibilities. This conclusion can also be drawn from the analytical analysis discussed in Chapter 10.

Because of the relatively small stiffness of the beams under a point load at mid-span ($k_v = 48 EI/l^3 = 1.64 \text{ kN/m}$), the vertical displacement incompatibility was often accommodated by beam bending rather than by sliding of the connection. Only a force as little as 12.3 kN is required to yield a mid-span deflection of 7.5mm (which corresponds to the MCE uplift). Thus, considering a horizontal force of $2/3 \cdot 231 \text{ kN} = 154 \text{ kN}$ (connection 7) in the upper collector beam, a friction coefficient smaller than 0.08 would be required to allow for the sliding. Considering that the imposed uplift for an MCE event leads to a beam deflection smaller than $l/800$ (the span between the mid-length of the wall and the gravity column was 6 m), which is considerably smaller than deflections under the serviceability limits state, the imposed uplift is normally not of big concern.

Except for connection 8 with fully threaded screws no damage could be observed in either the structural elements or the connections for drifts up to 2.0%. The screws were slightly bent due to the formation of two plastic hinges as shown in Figure 9.15; they however could still transfer horizontal loads.



Figure 9.15 $\varnothing 10/350$ mm long fully threaded screws from connection 8 after several MCE cycles

9.5.3 Cost analysis

Table 9.2 shows a cost and time estimation of the ten connection configurations. More detail on the costing can be found in Appendix C. The costs include material costs for the connection itself and any other component necessary to achieve the force transfer into the wall, as well as the labour involved to prepare and assemble the connection. The time to assemble the end columns and the shear transfer devices for connections 9 and 10 have not been taken into account. All costs and times are compared in relative terms to connection 1 with the centric bolts.

It can be seen that classical timber connections with bolts and screws are relatively cheap in cost and required only limited labour. Steel-to-steel connections increase the material cost notably and are also more labour intensive. Assemblies with end columns required the biggest cost and labour of all tested connections.

Table 9.2 Cost and time estimation and comparison of the ten connection configurations

Connection type	Cost	Time
1) Group of 12 bolts	400\$ (100%)	1h40' (100%)
2) Eccentric group of 25 bolts	625\$ (156%)	2h30' (150%)
3) External blocks with dowels	1260\$ (315%)	4h30' (270%)
4) Large diameter pin	60\$ (15%)	40' (40%)
5) Large diameter pin and slot in wall	90\$ (23%)	1h (60%)
6) Steel angle with slots	700\$ (175%)	2h20' (140%)
7) Steel-to-steel connection with slots	1420\$ (355%)	5h (300%)
8) Fully threaded screws	180\$ (45%)	2h20' (140%)
9) End columns with group of bolts	2000\$ (500%)	3h20' (200%)
10) End columns with large diameter pin	1300\$ (325%)	1h20' (80%)

When comparing the obtained performance of the different connectors with the respective costs, it can be seen that relatively cheap timber-to-timber connections with dowels, pins or fully threaded screws are an economic yet reliable solution. Steel-to-steel connections only have a marginal better behaviour in reducing the interaction between the beams and the wall,

requiring a much higher cost. Similarly can assemblies with end columns minimize interaction, these solutions however implies elevated costs.

9.5.4 Design recommendations

For ordinary design situations with out-of-plane flexible floors, an economic and reliable connection is recommended consisting of a group of bolts placed at or near the centre of the wall, of a large diameter pin or of (in beam direction) inclined fully threaded screws. Non-central connections, if needed because of geometrical constraints or the presence of post-tensioning bars, will induce slightly higher rotations and vertical displacements in the beams. Large diameter pins need to be designed carefully, since embedment strengths for large diameters fasteners are not available. Reinforcement to prevent splitting is therefore highly recommended. For stiffer floor beams (i.e. short spans and thick concrete slab), steel-to-steel connections with slotted holes can further mitigate displacement incompatibilities. The steel-to-steel solution minimizes the interaction between the wall and the beams, but will result in higher construction costs as shown above. For solutions with slotted holes, special precautions to minimize friction are paramount to achieve the required behaviour. Only for very special situations where vertical uplift and rotations of the beam need to be kept as small as possible (for example for wall connections very close to gravity columns and in the presence of very stiff beams), end columns should be used to transfer the diaphragm forces indirectly to the wall.

Table 9.3 Summary of connections including the degree of participation of beam rotation and uplift when compared to the respective wall values

Connection types	Benefit	Degree of participation of beam	
		rotation	uplift
Group of bolts, large steel pin, inclined screws	reduction in rotation interaction	8-14 %	60-100%
Steel-to-steel connection	reduction in rotation and uplift interaction	9%	90%
End-columns	minimization of interaction	6%	13%

9.6 FINDINGS FROM A POST-TENSIONED CLT CORE-WALL STRUCTURE

To study the behaviour of timber core-wall structures loaded in the presence of floor diaphragms, two two-storey CLT stairwell cores have been built and tested under quasi-static lateral load in the structural engineering laboratories at the University of Canterbury (Dunbar 2014). The bi-directional loads have been applied to the structure by collector beams which simulated the floor diaphragm. A detailed description of the experimental setups including geometry and material properties, the loading protocol, the instrumentation and the full set of results can be found in Appendix C.

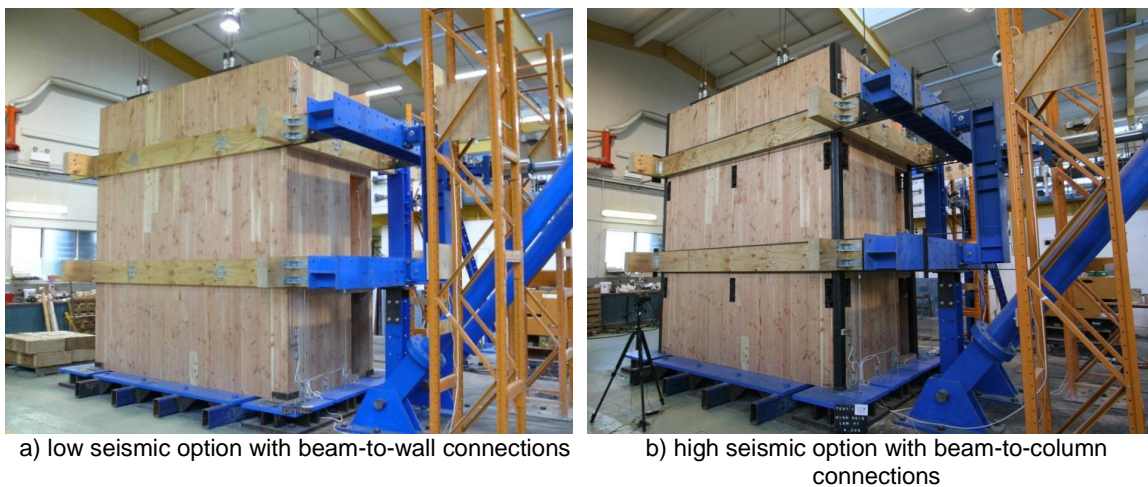


Figure 9.16 Experimental setup of the two storey post-tensioned CLT core structure

The two prototype specimens were built as a timber only structure for areas with low seismic loads (Figure 9.16a) and as a structure with timber walls and steel corner columns with dissipation devices for areas with high seismic loads (Figure 9.16b).

9.6.1 Experimental setup

The half scale two storey stairwell core shown in Figure 9.17 was made of 100 mm thick Cross Laminated Timber (CLT) panels made of Douglas Fir SG8 boards. The footprint of the specimen was 1.9 x 3.4 meters with two storeys with an interstorey height of 1.5 meters. The whole core had a height of 3.75 meters. Doorway openings provided access to the inside of the core, where a wooden half-flight stair case with landings was installed. In the longitudinal direction two coupled walls resisted the lateral loads; in the transverse direction single walls provided the lateral load resisting system. All walls were fixed to the foundation by post-tensioning strands. The forces in the tendons were varied in order to simulate gravity loads on the walls or to act as recentering rocking Pres-Lam walls.

The structure was tested under quasi-static bi-directional loading. The loads were applied as a triangular load pattern to the sets of beams on the two storeys. The beams were representing gravity and collector beams of the floors and diaphragms. To study the interaction between the core and the diaphragm, the structure was loaded to drift levels of up to 1.5% to represent typical DBE design levels. The structure subsequently underwent also drift levels of more than 3% without any damage to the collector beams and connections.

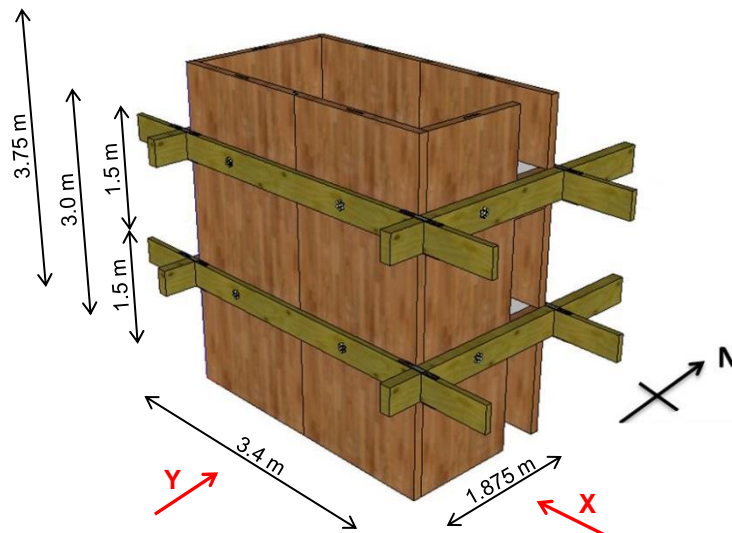


Figure 9.17 Test setup of the CLT core – low seismic option (modified from Dunbar (2014))

The core has been designed and tested in two following options, the

- *low seismic option*; and the
- *high seismic option*.

The former was designed for areas with small seismic actions and the latter was designed to resist high seismic actions with very limited damage. Both specimens were built out of the same CLT panels and had the same loading apparatus, including the collector beams.

For the low seismic option the individual panels were connected by screws working in shear. Together with the post-tensioning strands, the screws provided a semi-rigid connection coupling the parallel and perpendicular walls together and therefore increased the lateral load resistance of the core structure. Under bigger displacements the screws yielded and provided some energy dissipation.

For a rocking core structure the displacement incompatibilities between the diaphragm and the core-walls cannot only be found in the uplift and rotation of the wall, which the collector beams needed to follow as shown in Figure 9.18a, but also in the differential displacement between the orthogonally running beams. To allow for the rotations of the wall, the collector

beams were connected by a ring of bolts to each individual wall panel as shown in Figure 9.18b. To allow for the displacements between the collector beams, the discontinuous beam was spliced with two top and bottom riveted steel plates. The connection was designed to allow for the axial force transfer, but also to allow for the differential movement by elastic out-of-plane bending of the plates as will be discussed later and shown in Figure 9.24.

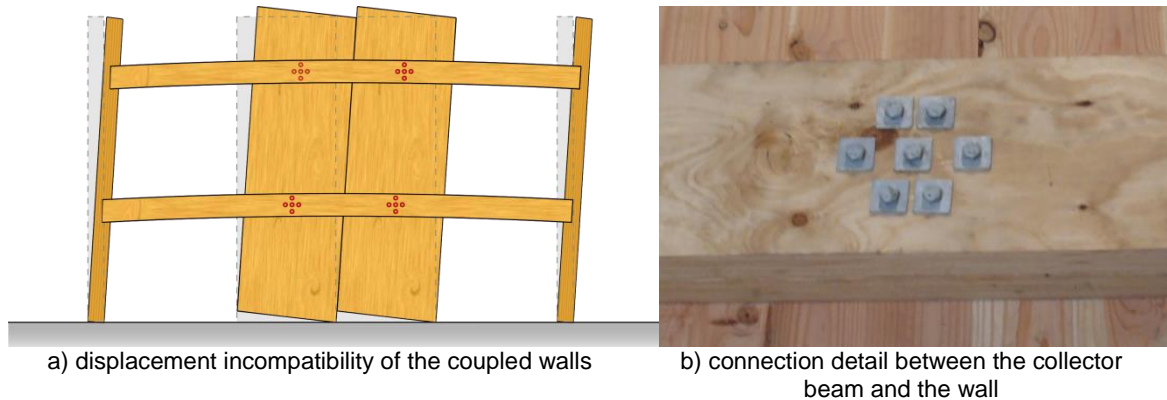


Figure 9.18 Diaphragm-to-wall connection for the low seismic option

For the high seismic option the parallel wall panels were connected with U-shaped Flexural Plates (UFPs) (Kelly et al. 1972) to each other. Hollow steel columns were fixed in the four corners and also connected to the walls via UFPs. These special steel devices do not only couple the wall elements together, but also provide stable hysteresis loops. These elements can undergo a number of loading cycles without damage, but can be replaced if necessary after a very large seismic event.

To avoid displacement incompatibilities with the collector beams, the beams were connected to the corner steel columns via a single bolt as shown in Figure 9.19b. Since the columns were fixed to the foundation and can therefore not uplift and the bolt provides a hinged connection, neither uplift nor rotation was imposed to the beams as in Figure 9.19a.

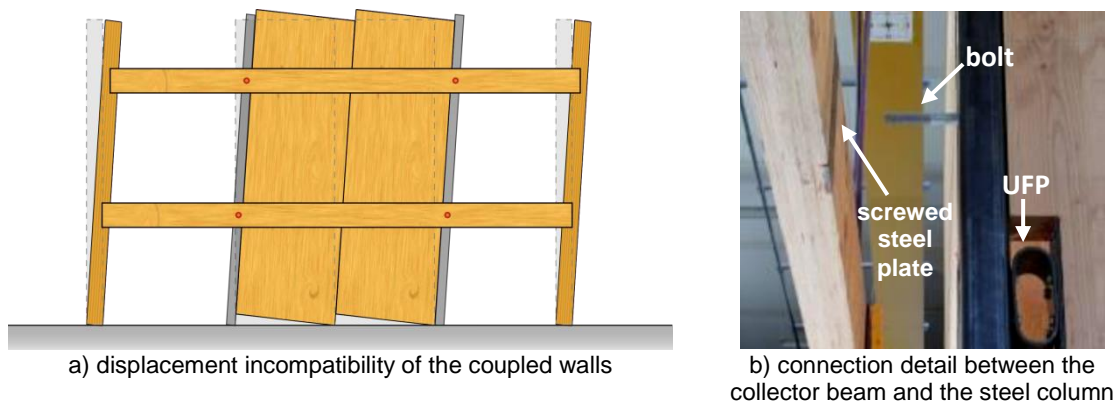


Figure 9.19 Diaphragm-to-wall connection for the high seismic option

9.6.2 Test results

For both the low and the high seismic options the rotation between the beams and the walls as well as the beam uplift are of interest and will be shown in the following sections. Other relevant results and additional graphs can be found in Appendix C.

The beam and wall rotations as well as uplifts are measured in the positions as shown in Figure 9.20.

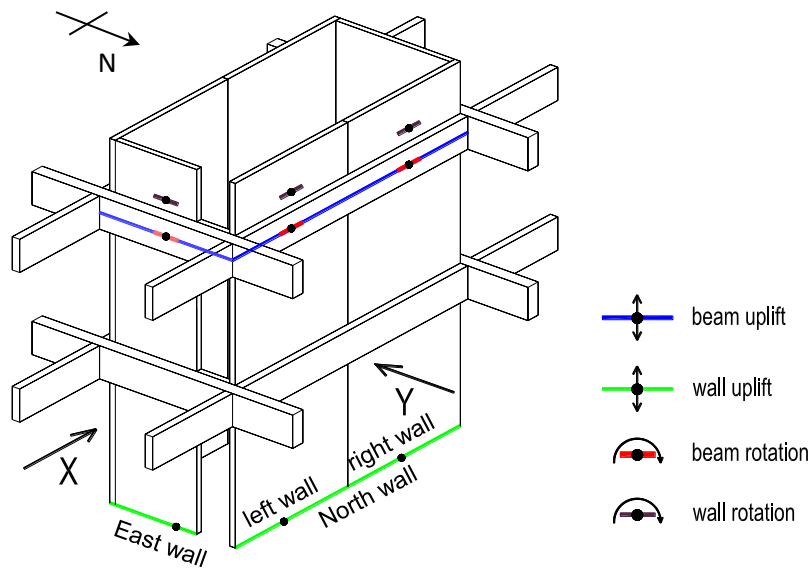


Figure 9.20 Position of beam deflection and rotation measurement points

9.6.2.1 Low seismic option

The test specimen was tested under bi-directional loads in the X and Y directions up to drift levels of 1.5%. Figure 9.21a shows the required ram forces to achieve the required core drifts. As expected, higher loads were required in the longitudinal direction, where the coupled walls resisted the load, when compared to the required forces in the transverse direction.

Figures 9.21b and c show the left and right wall uplifts of the North wall at mid-length and the respective beam uplifts. It can be seen that for the left wall the uplift was amplified for loads in the X direction. This is because the loading apparatus was slightly inclined upwards when pushing against the beams; more information on this unwanted effect can be found in Appendix C. For the right wall the beams followed closely the wall uplift for loads in the X direction. For load applications in the Y direction, the North walls uplifts were relatively small and only showed minimal torsional and other unwanted effects due to the loading apparatus. The beam deflections were relatively high and were caused by the interaction between the perpendicularly running collector beams.

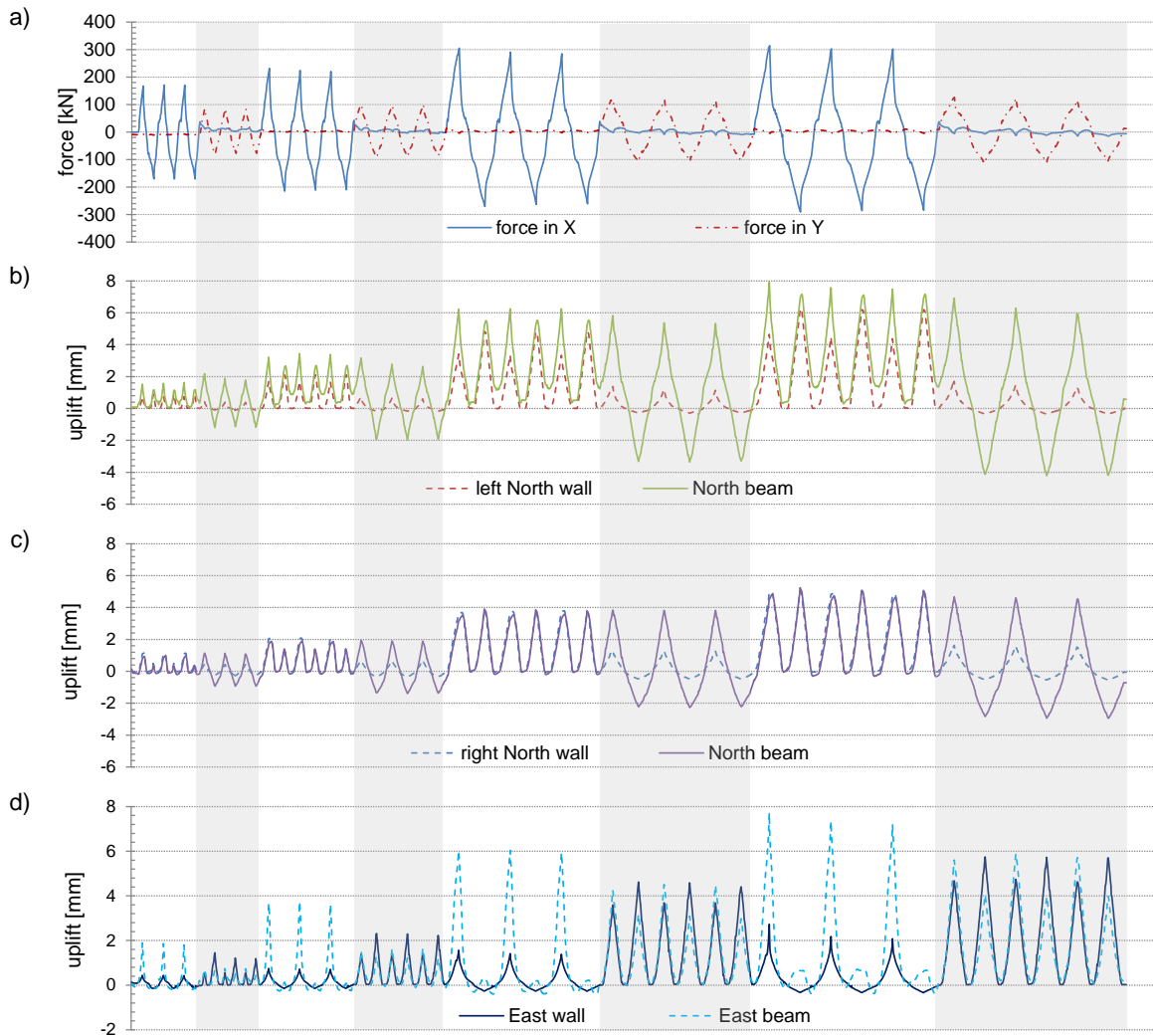


Figure 9.21 Low seismic option under bi-directional loading: a) Ram forces, b-d) walls and beams uplift at wall mid-length (non-shaded areas correspond to loading in the X direction, shaded areas correspond to loading in the Y direction)

A very similar behaviour can be seen for the East wall and relative collector beams as shown in Figure 9.21d. For loads in the Y direction the beams underwent amplified uplift when the ram was pushing against the beams and slightly smaller uplift when the beams were pulled. Under forces in the X direction the wall uplifts were small with relatively high beam uplifts. Although the wall uplifts are again created by secondary effects, the beam uplifts were created by the interaction with the beams running in the opposite direction.

Figure 9.23 shows the wall and beam rotations for both the North and the East walls for loads in both directions. The collector beams along the North walls underwent only small rotations, since they were fixed at the mid-length of both walls and were flexibly restrained by the connection to the perpendicularly running beams as shown in Figure 9.22b. Since the beams were undergoing double bending, the measured deformations were relatively small.

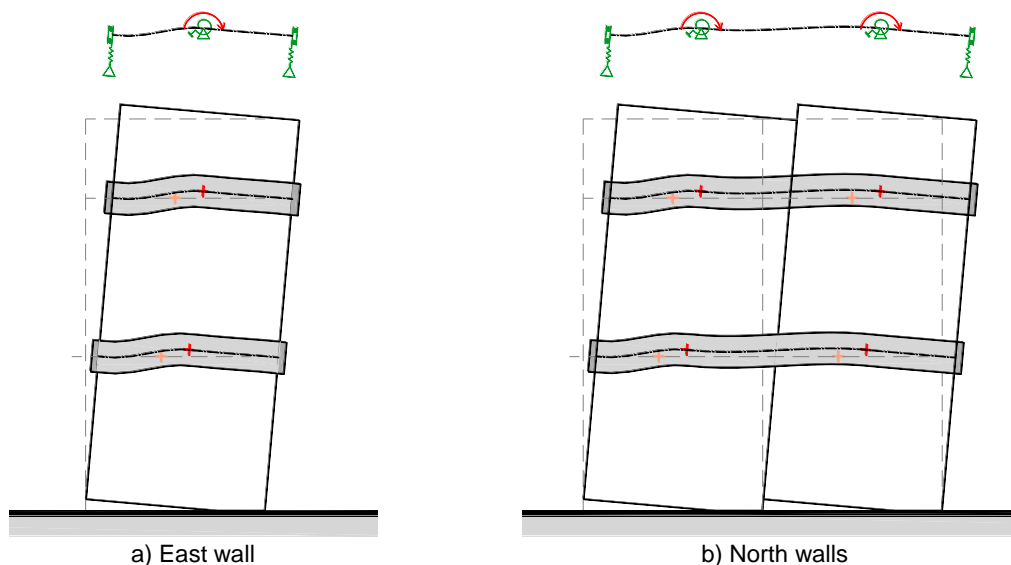


Figure 9.22 Deformed shape and statical system of the collector beams for the low seismic option

The beams along the East wall followed the wall rotations much closer. This was due to the fact that the beams were solely connected to the single wall and were restrained by the flexible connection to the orthogonally running collector beams as shown in Figure 9.22a.

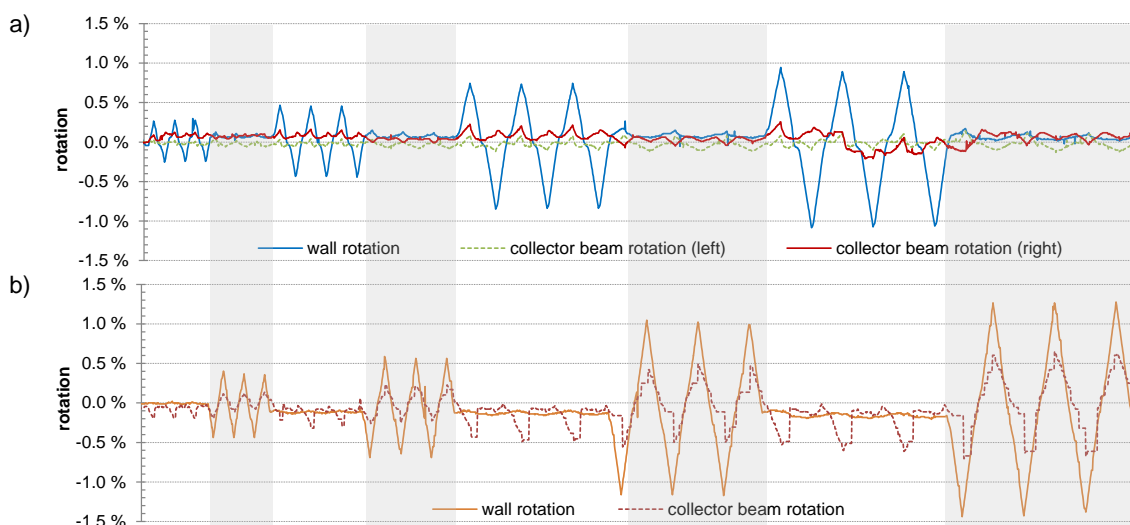


Figure 9.23 Comparison between the wall and the collector beam rotation for the low seismic option: a) the North wall and b) East wall (non-shaded areas correspond to loading in the X direction, shaded areas correspond to loading in the Y direction)

The relative rotations and uplifts of the collector beams were allowed by the out-of-plane flexible splice of the longitudinal beams as shown in Figure 9.24. For the low seismic option the connection plate accommodated relative beam movements of up to 6 mm for a drift level of 1.5%. Axial forces in the collectors could still be transferred and neither the plate nor the rivets showed any sign of damage.



Figure 9.24 Elastically deformed top and bottom splice plate of the collector beams under 1.5% drift

9.6.2.2 High seismic option

Figure 9.25a shows the force required to achieve drift levels of 1.5% of the core structure in the two principal directions. The forces are notably higher when compared to the low seismic option.

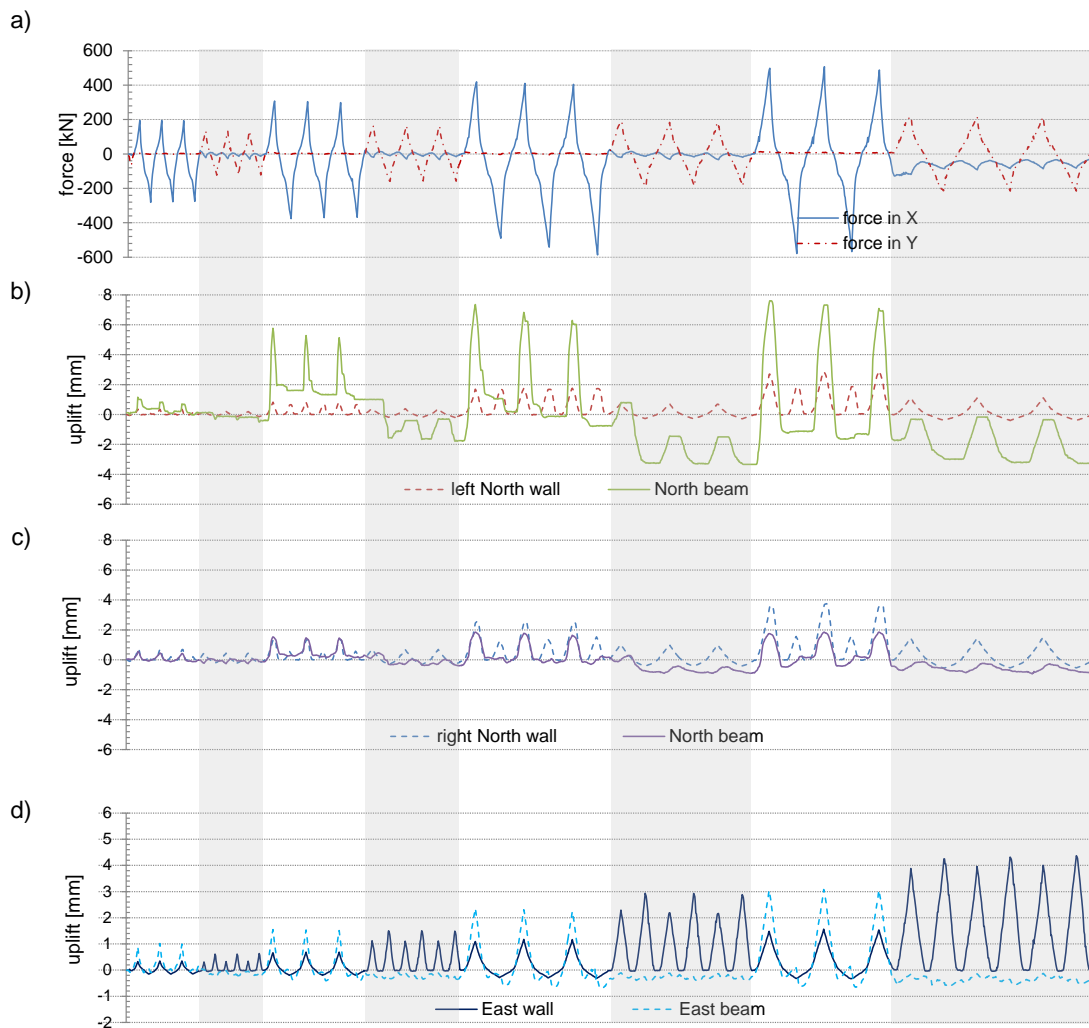


Figure 9.25 High seismic option: a) Ram forces for the bi-directional loading, b-d) walls and beams uplift at wall mid-length (non-shaded areas correspond to loading in the X direction, shaded areas correspond to loading in the Y direction)

Figures 9.25b and c show the uplift of the left and right North wall respectively as well as the beam movements. Even though the collector beams were not connected to the walls, they still underwent some vertical movement. The spikes in the beams on the left wall (Figure 9.25b) were due to the upwards pushing of the ram and should be disregarded. The vertical displacements shown in Figure 9.25c are closer to a real building behaviour and show that beam movements could be reduced.

For loading in the Y direction, the wall and beam uplifts along the East wall shown in Figure 9.25d suggest that the vertical uplift could be successfully decoupled. Beam uplift was however still imposed for loads in the X direction.

Figure 9.26 shows that the beam rotations could be successfully reduced for the collector beams in both directions. Since the beams were connected with bolts to the columns, the small measured beam rotations have been imposed by the out-of-plane rotation of the walls perpendicular to the load direction.

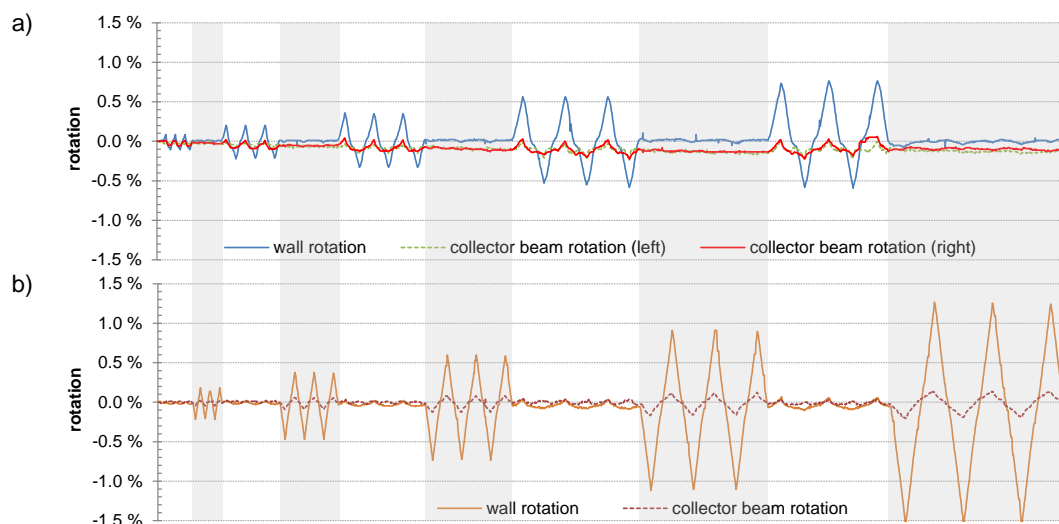


Figure 9.26 Comparison between the wall and the collector beam rotation for the high seismic option: a) the North wall and b) East wall (non-shaded areas correspond to loading in the X direction, shaded areas correspond to loading in the Y direction)

The above results relating to the collector beam deformations under bi-directional loads show the complexity of the system involved. Beams are imposed to uplift and rotations from both the rocking and the out-of-plane wall rotations in both directions. Even the high seismic option, where beam deformations were generally lower, showed interaction of all elements. Unfortunately the behaviour of the specimens was largely influenced by the loading apparatus, which imposed additional uplift forces when pushing against the beam. Such action is not expected in real buildings.

The low seismic option presented was not detailed as a *low damage design*, therefore damage to the walls, beams and relative connectors was allowed as long as forces could still be transferred. For the high seismic option, effort was put in eliminating or at least reducing displacement incompatibilities. Test results showed that both systems could successfully transfer the forces from the collector beams into the core walls and no damage was observed. Displacement incompatibilities were allowed for by the beam bending, the partial or total rotational release of the beam-to-wall connections and the flexible connections between the collector beams. Both beam rotation and uplift could be reduced in the high seismic option.

9.6.3 Design recommendations

For the design of diaphragms in core structures it is paramount that the load path is well detailed for both principal directions until the forces are transferred into the walls. Displacement incompatibilities from the rocking and the out-of-plane rotation of the walls need to be considered.

Aside from the beam-to-wall connections which should be positioned and detailed in order to minimize imposed uplift and rotations as discussed in section 9.5, the connections between the perpendicular collector beams need to allow for differential vertical displacements. A steel splice plate, connected to the beams with metallic fasteners with appropriate thickness and length can be used. These dimensions need to guarantee a low out-of-plane stiffness and should accommodate the differential vertical movements by elastic bending.

The unit shear forces from the diaphragm shall be introduced to the collector beams at a certain distance from the intersection point of the collector beams. In these disturbed areas the relative vertical movement of the beams might result in pull-out of the panel fasteners. Shear transfer in this area should not be relied on and ideally panel connections should be avoided in this area as shown in Figure 9.27.

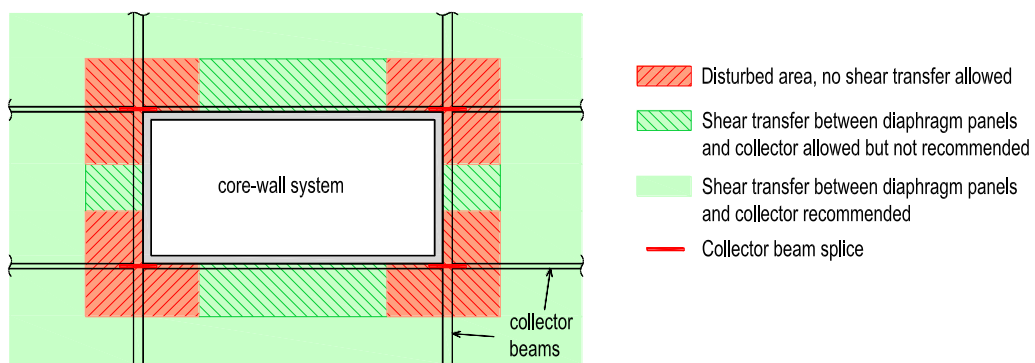


Figure 9.27 Recommended and prohibited areas for the force transfer between the core and the floor diaphragms

In the case of rigid out-of-plane diaphragms, either because of a floor slab or of stiff collector beams, a design solution like for the high seismic option should be used. Imposed vertical uplift and rotation from the rocking walls is limited or reduced and only the out-of-plane rotation of the walls needs to be allowed for by the collector beams.

9.7 DISCUSSION

Both uplift and rotation of walls cause diaphragm damage because of out-of-plane deformations and unwanted stiffening of the walls, causing increased axial loads in walls or other gravity carrying elements and potential buckling failures. In order to study such effects in timber buildings two experimental tests were carried out. The setup of a post-tensioned rocking wall studied 8 different connections between the walls and the collector beams and two additional connections to end columns on either side of the wall. All tested connections showed very satisfying results; the effectiveness and cost of different timber-to-timber, timber-to-steel, steel-to-steel and solutions with end columns were evaluated in detail. Rotational incompatibilities proved to have bigger impact on the global behaviour of the wall-diaphragm assembly than uplift incompatibilities. Further, a setup of a CLT stairwell core loaded under bi-directional loads was tested with two different design solutions with special focus on the connection between the orthogonal collectors and the connection to the walls. Both design options allowed for the required displacements proving the detailing was adequate.

Results from both setups showed that closely spaced bolts, inclined fully threaded screws or large diameter bolts provide very satisfactory results for floors with a relatively low out-of-plane stiffness. For stiffer floors a steel-to-steel solution with a pin in a slotted hole is recommended to avoid displacement incompatibilities. Special measures to avoid friction in these connections need to be undertaken to allow for the vertical decoupling. To further reduce interaction, collector beams can be connected to timber or steel columns at the ends of the wall. A cost analysis shows that the more interaction is limited with a specific connection, the higher the construction cost will be. For core wall structures the same connection detailing between the collectors and the walls should be used as for single walls. Collector beams should be spliced with out-of-diaphragm-plane flexible connections. Shear transfer from the diaphragm panel into the collectors should occur outside the corner regions of the core.

The experimental setups presented here were not capable of investigating the diaphragm behaviour of a whole building, as it would have required the setup of a full scale diaphragm, which was not possible during the research program. The interaction of some diaphragm-to-wall connection increased the wall stiffness and strength; Chapter 10 presents a procedure to account for this behaviour.

9.8 CONCLUSIONS

For single, coupled or core walls the following connection details are recommended:

- closely spaced bolts, inclined fully threaded screws or large diameter bolts for floors with a relatively low out-of-plane stiffness;
- steel-to-steel connections with a pin in a slotted hole for stiffer floors;
- collector beams can be connected to timber or steel columns (boundary columns) at the ends of the wall for very stiff floors.

To allow for vertical sliding special measures to avoid friction might be necessary. Rotational incompatibilities showed to have bigger impact on the global behaviour of the wall-diaphragm assembly than uplift incompatibilities. The strength of the wall-beam system increased by up to 25% for some connections, this increase need to be taken into account for design as shown in Chapter 10.

Around core-wall systems orthogonal collector beams should be spliced with out-of-diaphragm-plane flexible connections. Shear transfer from the diaphragm panels into the collectors should occur outside the corner regions of the core.

10 Analytical modelling of a post-tensioned wall with collector beams

10.1 INTRODUCTION

This chapter compares the force-displacement curves of the experimentally tested wall-beam assembly presented in Chapter 9 with values determined by an iterative analytical procedure. A brief parametric study investigates some key parameters on their influence on the wall-beam interaction.

10.1.1 Background

Chapter 9 showed the effects of displacement incompatibilities on walls connected to collector beams based on laboratory testing. It was observed that the beams and connections could accommodate the imposed displacement demand by beam bending, elastic deformation of the metallic fasteners or by decoupling the rotation and/or uplift demand by a specific connection detail. Depending on the connection type, and therefore on the translational and rotational stiffnesses, the system strength and stiffness might increase. These additional strengths and stiffnesses need to be determined, since they influence the dynamic behaviour of the system. An increase in wall stiffness changes the fundamental period, reduces the gap opening necessary to activate the dissipator, and influences the wall-beam connection design.

To account for the beam interaction on the wall behaviour, an advanced computer model with special multi-spring contact elements which simulates wall uplift and rotation could be used as shown by Sarti (2015). In this chapter a procedure to determine the pushover curve of the wall-beam assembly based on an existing iterative moment-curvature procedure is developed. The modified approach accounts for the compatibility forces deriving from the imposed deformations in the beams. This is based on the formulation of the beam-connection system stiffness, which is derived in full detail in Appendix D. The obtained moment-curvature curves can be used to determine the force-displacement curve for the wall-beam assembly.

10.2 ANALYTICAL PROCEDURES

Figure 10.1 shows two different statical models of a rocking wall connected to collector beams. Model a), which is used in this chapter, is based on the Modified Monolithic Beam Analogy (MMBA) (Palermo 2004). The MMBA overcomes the violation of the Euler-Bernoulli theory of plane sections in rocking elements by the introduction of an equivalent monolithic element. This approach allows for the determination of the moment-curvature curve at the wall-foundation interface. This moment-curvature information can be used to analytically determine the pushover curve of the wall.

Model b) is a more sophisticated approach, where the wall sits on a number of springs (multi-spring element) which simulate the rocking interface of the wall with the foundation. This model can directly be used for cyclic push-pull analysis or for time history analysis of a full tri-dimensional building model. Furthermore, stiffness degradation of materials can be implemented. The disadvantage of this method is that the calibration of the springs requires the moment-curvature behaviour from experimental results or from the analytical procedure as above (Sarti 2015).

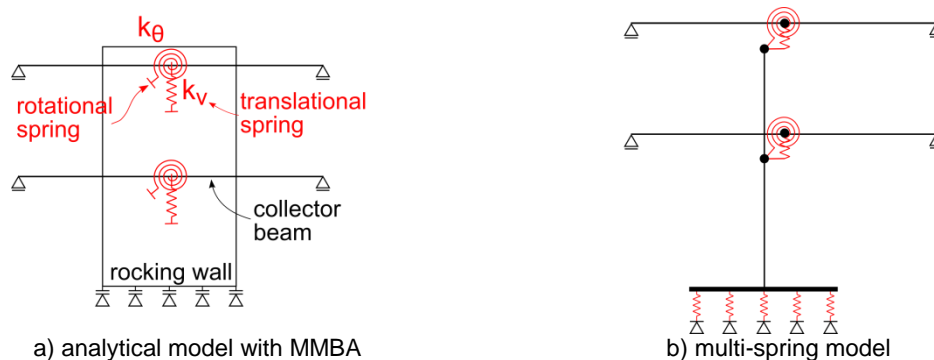


Figure 10.1 Statical model of a rocking wall connected to collector beams

Both models are able to provide the uplift of the wall at an arbitrary position along the wall-foundation interface as well as the rotation of the wall along its height. This information is important if the interaction with the collector beams and relative connections needs to be studied. Sarti (2015) uses the multi-spring model to replicate the wall-beam system behaviour for some of the test configurations presented in Chapter 9. In this chapter the pushover curve for the wall-beam system is studied based on the analytical moment-curvature analysis which is extended in order to include the behaviour of the wall-beam connection and the beam stiffness.

10.2.1 Iterative moment-curvature procedure

The iterative determination of the moment-curvature behaviour of post-tensioned rocking elements has been described by Pampanin et al. (2001) and is referred to as Monolithic Beam Analogy (MBA). This procedure was later modified by Palermo (2004) to account for the elastic behaviour before yielding. This Modified Monolithic Beam Analogy (MMBA) can also be used on post-tensioned rocking Pres-Lam elements (Newcombe et al. 2008). Because the Euler-Bernoulli theory of plane sections is violated at the rocking interface, the MMBA considers global strain compatibility by assuming that the displacement of the rocking element is equal to that of a monolithic element.

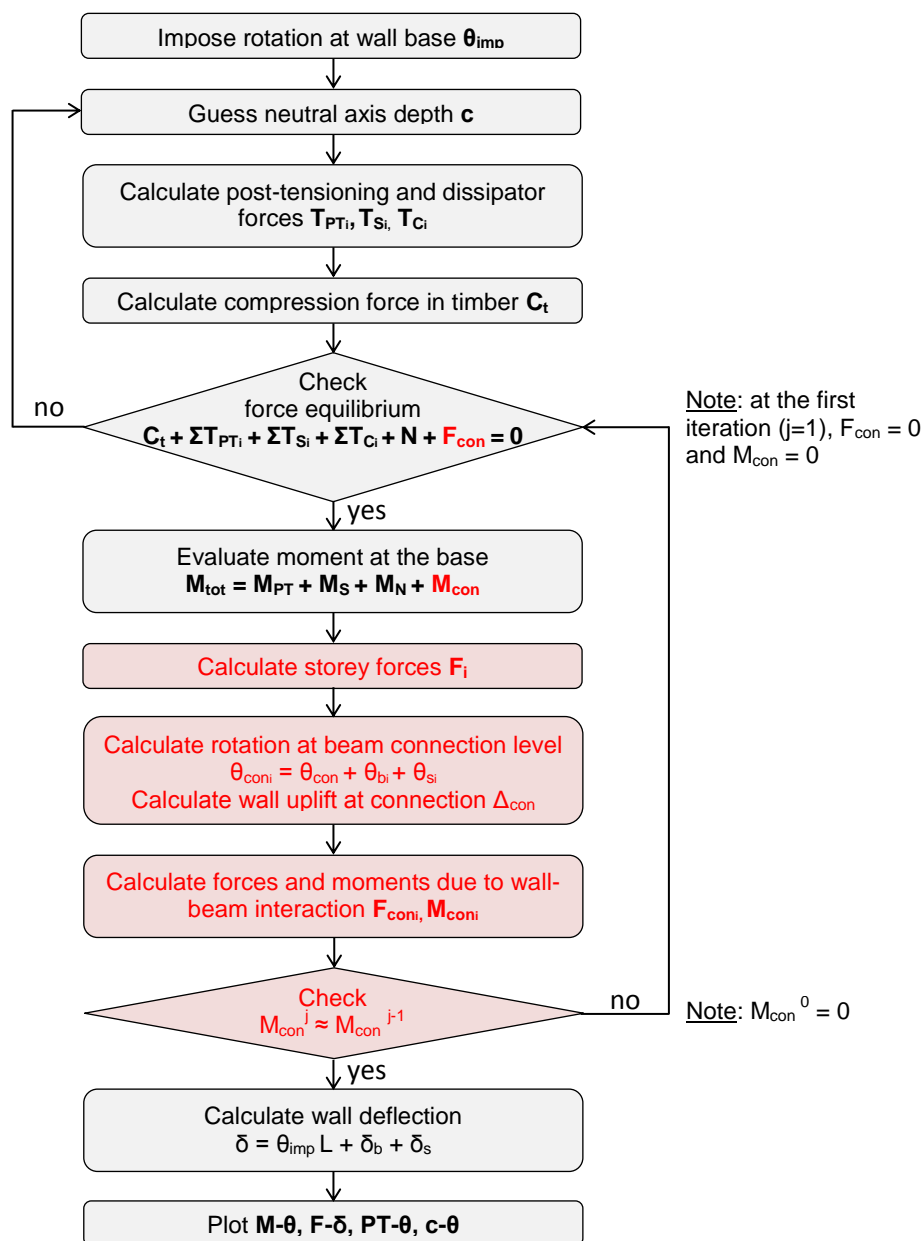


Figure 10.2 Procedure to calculate the moment-curvature and force-displacement curves of the wall-beam system

The procedure is summarized on a step by step basis in the next sections and then extended in order to consider the additional incompatibilities forces and moments from the wall-beam interaction. A schematic representation of the procedure is shown in Figure 10.2, the additional steps to account for the wall-beam interaction are in red.

Figure 10.3 shows deformed wall and all involved forces with relative distances from the compressed wall edge.

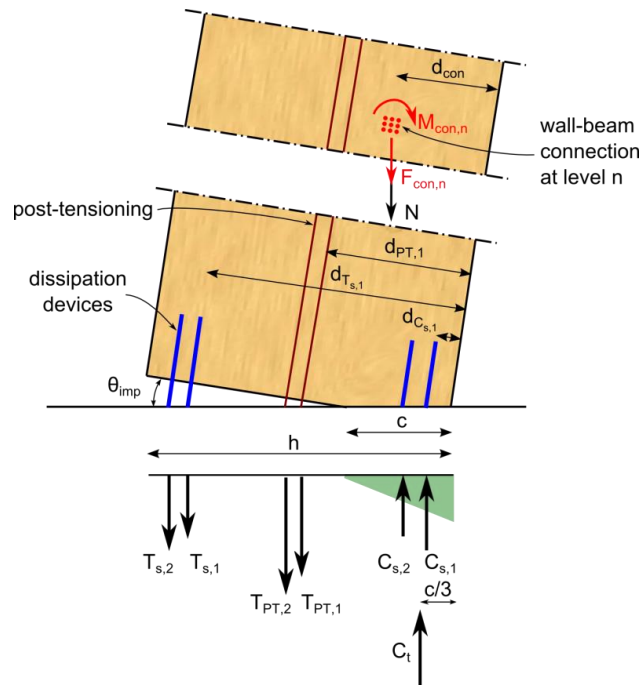


Figure 10.3 Forces and moments acting on the rocking wall

10.2.1.1 Decompression moment

Until the moment at the base of the wall M_{tot} is smaller than the decompression moment, no gap opening occurs. The decompression point is reached when the external moment is bigger than the stabilizing moment from the post-tensioning and axial forces.

$$M_{dec} = \frac{Z}{A} (T_{PT,0} + N); \quad (10.1)$$

where

- M_{dec} decompression moment;
- Z elastic section modulus;
- A cross sectional area of the wall;
- $T_{PT,0}$ initial post-tensioning force;
- N axial forces (i.e. from gravity loads).

10.2.1.2 Impose rotation and guess neutral axis

The imposed rotation θ_{imp} at the bottom of the wall is an arbitrary chosen input parameter. This rotation will differ from the wall drift because of the elastic contributions (bending and shear deformations). An initial neutral axis depth c needs to be guessed; this will then later be subject to iteration in order to achieve force equilibrium.

10.2.1.3 Calculate post-tensioning and dissipator forces

Based on the neutral axis depth c and the imposed rotation θ_{imp} , the vertical uplift of the wall at each reinforcement layer (post-tensioning and dissipators) needs to be calculated.

$$\Delta_{PT,i} = \theta_{imp}(d_{PT,i} - c); \quad (10.2)$$

$$\Delta_{s,i} = \theta_{imp}(d_{s,i} - c); \quad (10.3)$$

where

- $\Delta_{PT,i}$ elongation of the i^{th} post-tensioning layer;
- $\Delta_{s,i}$ elongation of the i^{th} dissipator layer;
- $d_{PT,i}$ distance from the compressed edge to the position of the i^{th} post-tensioning layer;
- $d_{s,i}$ distance from the compressed edge to the position of the i^{th} dissipator layer.

Next the increase in strain and post-tensioning force for each layer is calculated:

$$\Delta\varepsilon_{PT,i} = \frac{\Delta_{PT,i}}{l_{ub}}; \quad (10.4)$$

$$\Delta T_{PT,i} = \Delta\varepsilon_{PT,i} E_{PT} A_{PT,i}; \quad (10.5)$$

where

- $\Delta\varepsilon_{PT,i}$ strain increase of the i^{th} post-tensioning layer;
- l_{ub} unbonded length of the post-tensioning elements;
- $\Delta T_{PT,i}$ force increase in the i^{th} post-tensioning layer;
- E_{PT} modulus of elasticity of the post-tensioning steel;
- $A_{PT,i}$ cross sectional area of the i^{th} post-tensioning layer.

Finally the post tensioning force can be calculated as

$$T_{PT,i} = T_{PT,0,i} + \Delta T_{PT,i}; \quad (10.6)$$

where

- $\Delta T_{PT,i}$ force in the i^{th} post-tensioning layer;
- $T_{PT,0,i}$ initial force in the i^{th} post-tensioning layer.

There are a number of different dissipation devices which can be used in rocking timber walls. Generally internal or external mild steel dissipators are used which dissipate energy by tension or compression yielding of fused steel bars. Depending on the type of dissipator and relative

connection detailing, the unbonded length l'_{ub} needs to be calculated. More information on this can be found in Sarti (2015).

The increase in strain in the dissipators is calculated as

$$\varepsilon_{s,i} = \frac{\Delta_{s,i}}{l'_{ub}}; \quad (10.7)$$

where

$\varepsilon_{s,i}$ strain in the i^{th} dissipator layer;
 l'_{ub} unbonded length of the dissipator.

The stress in the mild steel dissipator can be estimated by using a bi-linear stress-strain relationship

$$f_{s,i} = f_{s,y} \left[1 + r \left(\frac{\varepsilon_{s,i}}{\varepsilon_{s,y}} - 1 \right) \right]; \quad (10.8)$$

where

$f_{s,i}$ stress in the i^{th} dissipator layer;
 $f_{s,y}$ steel yield strength;
 $\varepsilon_{s,y}$ steel yield strain;
 r post-yielding stiffness ratio (assumed as 0.008).

The force in the dissipators then becomes

$$F_{s,i} = f_{s,i} A_{s,i}; \quad (10.9)$$

where

$A_{s,i}$ cross sectional area of the the i^{th} dissipator layer.

10.2.1.4 Calculate compression force in timber

The compression strain in the timber is calculated based on the MMBA

$$\varepsilon_t = c \left(\frac{3\theta_{imp}}{L_{cant}} + \phi_{dec} \right); \quad (10.10)$$

where

ε_t maximum strain in the timber;
 L_{cant} cantilever length (distance from the base to the centroid of the applied post-tensioning forces);
 ϕ_{dec} curvature at decompression;
 $\phi_{dec} = \frac{M_{dec}}{k_{gap} E_t I}$
 k_{gap} = 0.7, reduction factor for timber walls (STIC 2013);
 E_t modulus of elasticity of the timber;
 I moment of inertia of the wall.

Since the wall is supposed to work in the elastic range, the total compression force can be calculated based on a triangular stress distribution and becomes

$$C_t = \frac{1}{2} k_{gap} E_t \varepsilon_t b c; \quad (10.11)$$

where

b , width of the wall.

10.2.1.5 Check force equilibrium and calculated base moment

Until this stage all calculation steps were closely followed as for the classic procedure (STIC 2013) bare rocking walls. Because of the displacement incompatibilities, additional vertical forces and moments will act on the wall at the position of the beam-wall connection. These need to be added to guarantee the force equilibrium in the system. The additional actions are dependent on the imposed uplift and rotation at the connection for each collector beam. To obtain these compatibility forces and moments it is therefore necessary to know the wall deformation along its height, which is a function of the storey forces, given by the base shear.

Since these forces are not known at the first iteration, the force equilibrium and total moment at the base is first calculated as for the bare wall. Based on these values the storey forces and resulting wall rotations at each beam connection can be calculated. By including the beam and connection stiffnesses, the compatibility forces and moments acting on the wall can be calculated. Finally the force equilibrium is verified by iterating the neutral axis depth until it is satisfied.

The force equilibrium equations are shown next, with the derivation of the compatibility force F_{con} shown later.

$$-C_t + \sum_i T_{PT,i} + \sum_i F_{s,i} + N + F_{con} = 0; \quad (10.12)$$

where

h , length of the wall;
 N axial force from gravity loads (normally introduced via the wall-beam connection);
 F_{con} compatibility force due to displacement incompatibilities as calculated later. $F_{con} = 0$ for the first iteration.

The neutral axis depth c needs to be iterated until the force equilibrium is achieved. Finally the base moment M_t of the wall can be calculated as

$$M_{tot} = \sum_i T_{PT,i} \left(d_{PT,i} - \frac{c}{3} \right) + \sum_i F_{s,i} \left(d_{s,i} - \frac{c}{3} \right) + N \left(d_{con} - \frac{c}{3} \right) + F_{con} \left(d_{con} - \frac{c}{3} \right) + M_{con} = 0; \quad (10.13)$$

where

- d_{con} distance from the compressed edge to the position of the wall-beam connection.
- M_{con} compatibility moment due to displacement incompatibilities as calculated later. $M_{con} = F_{con} = 0$ for the first iteration.

10.2.2 Compatibility forces and moments

The rocking mechanism of a wall requires rotation and uplift at the base of the wall. Every element connected to the wall needs to undergo the same movements, less the elastic losses along the wall height. Depending on the type of connection between the wall and the collector beams, the beams also might need to follow these movements as shown in Figure 10.4. If the vertical movement is therefore not decoupled, as discussed in the previous chapter, then the beam needs to bend out-of plane. Similarly, if the rotation is not decoupled by the connection, the beam needs to deform in double curvature.

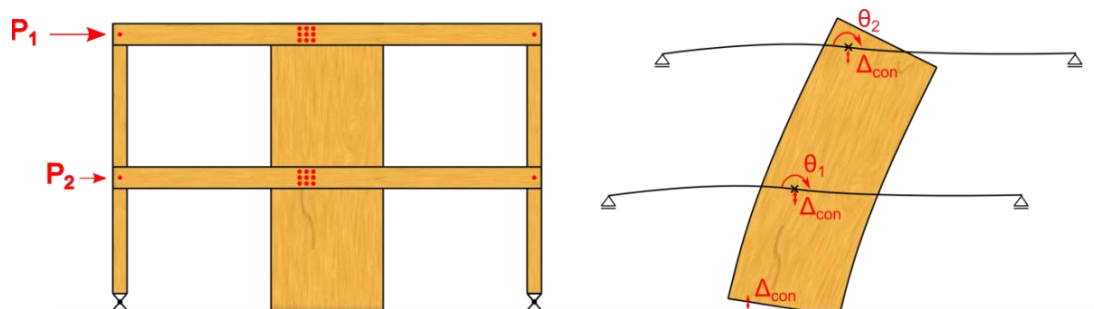


Figure 10.4 Imposed displacements to the collector beams

Even though the beams and the connections have an inherent flexibility due to bending stiffness and fastener slip respectively, they will restrain the wall rocking mechanism. The compatibility forces and moments acting on the wall can be calculated based on the stiffness of the beam-connection system.

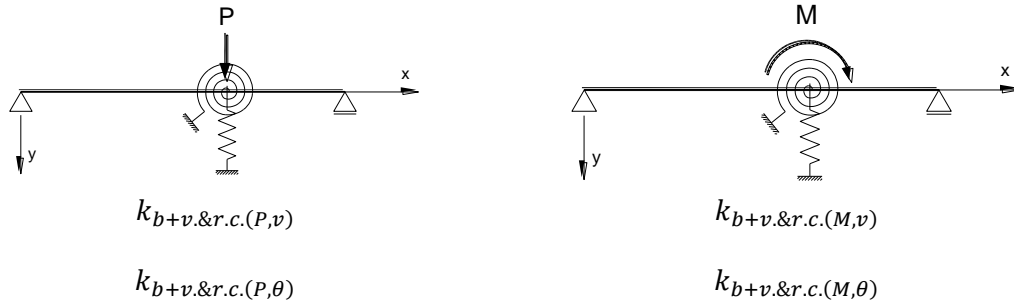


Figure 10.5 Statical system of the beam-connection stiffness for imposed deflection and rotations at the connection location

The stiffness formulations for the beam-connection system shown in Figures 10.1a and 10.5 are derived in their most general form in Appendix D for an eccentric connection. In the following procedure the stiffnesses as shown in Figure 10.5 are used. The subscript ‘b,v.c.&r.c.’ denominates the combination of the *beam bending stiffness*, the *connection vertical translational stiffness* and the *connection rotational stiffness*. Further the term in parenthesis denominates the action caused (P for vertical force and M for moment) by the imposed deformation (ϑ for rotation and v for vertical uplift).

The system stiffness for (P,ϑ) and (M,v) is zero for connections at mid-span of the beam. If the connection is not at mid-span, an imposed rotation or uplift will cause both vertical force and moment in the connection.

10.2.2.1 Compatibility forces for imposed uplift

Firstly the wall uplift at the position of the connection needs to be calculated

$$\Delta_{con} = \theta_{imp}(d_{con} - c) \quad (10.14)$$

where

d_{con} distance from the compressed edge to the position of the wall-beam connection.

Considering the wall as axially rigid, the same uplift will be imposed to all connections. The vertical force in the connection due to imposed uplift can be calculated as

$$F_{con(\Delta)} = \Delta_{con} k_{b,v.c.&r.c.(P,v)}; \quad (10.15)$$

the corresponding restraining moment in the wall due to the imposed uplift is

$$M_{con(\Delta)} = F_{con(\Delta)} \left(d_{con} - \frac{c}{3} \right). \quad (10.16)$$

In the case of connections placed away from the beam mid-span, the additional moment because of the deformation compatibility becomes

$$M_{con(F_{con(\Delta)})} = F_{con(\Delta)} \frac{k_{b,r.c.(M,\theta)}}{k_{b(p,\theta)}} = \Delta_{con} k_{b,v.c.\&r.c.(M,v)}. \quad (10.17)$$

10.2.2.2 Determination of the wall rotation at the connections

To determine the compatibility forces and moments due to the imposed rotations, the wall rotation at each connection needs to be determined. Since these values are a function of the total base moment, an additional iteration as shown in Figure 10.2 is required to determine the moment-curvature behaviour of the wall.

The rotation at an arbitrary position of the wall is the sum of the rotation at the base, the elastic rotations due to bending and shear deformations. Latter two can be determined in the general case as

$$\theta_b = \int \frac{M(z)}{E_t I_t} dz; \quad (10.18)$$

$$\theta_s = \int \frac{V(z)}{G_t A_s} dz; \quad (10.19)$$

where

θ_b	elastic rotation due to bending;
$M(z)$	moment distribution along the wall height;
E_t	modulus of elasticity of the wall;
I_t	moment of inertia of the wall;
θ_s	elastic rotation due to shear;
$V(z)$	shear distribution along the wall height;
G_t	shear modulus of the wall;
A_s	shear area of the wall (2/3 of the cross section for a rectangular section).

For the two storey wall, as studied in Chapter 9, the elastic rotation contributions can be calculated as a function of the storey forces as shown in Figure 10.6. The symbol θ_{ij} indicates the rotation at position i because of a force applied in position j .

$$\theta_{22} = \frac{P_2 L^2}{2 E_t I_t}; \quad (10.20)$$

$$\theta_{12} = \frac{3 P_2 L^2}{8 E_t I_t}; \quad (10.21)$$

$$\theta_{11} = \frac{P_1 L^2}{8 E_t I_t} = \theta_{21}. \quad (10.22)$$

where:

P_i	force applied in position i ;
L	length of the wall;
E_t	modulus of elasticity of the wall;
I_t	moment of inertia of the wall.

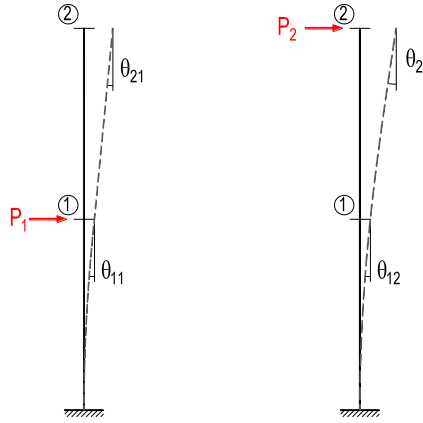


Figure 10.6 Elastic rotation contributions at the two levels because of floor forces in the case of a two storey wall

The rotations at the two different levels can therefore be calculated as

$$\theta_{con,1} = \theta_{11} + \theta_{12} + \theta_{imposed}; \quad (10.23)$$

$$\theta_{con,2} = \theta_{22} + \theta_{21} + \theta_{imposed}. \quad (10.24)$$

The base shear in the wall due to the total moment for the case of N storeys with a constant storey height of N can be written as

$$V_b = \frac{M_b}{L} \frac{3N}{2N+1}; \quad (10.25)$$

and the force at the i^{th} storey assuming a triangular distribution becomes

$$P_i = \frac{M_b i}{H \sum i^2}. \quad (10.26)$$

In the case of $N = 2$ the base shear and the storey forces become

$$V_b = \frac{6}{5} \frac{M_b}{L}; \quad (10.27)$$

$$P_1 = \frac{1}{5} \frac{M_b}{H} \text{ and } P_2 = \frac{2}{5} \frac{M_b}{H}. \quad (10.28)$$

10.2.2.3 Compatibility forces for imposed rotation

Once the rotations at the respective connections are calculated, the compatibility moments at each connection can be calculated as

$$M_{con(\theta),i} = \theta_{con,i} k_{b,v.c.\&r.c.(M,\theta)}. \quad (10.29)$$

In the case of connections placed away from the beam mid-span, also the translational springs get activated, causing an additional vertical force in the connection

$$F_{con(M_{con(\theta),i})} = -M_{con(\theta),i} \frac{k_{b,v.c.(P,v)}}{k_{b(M,v)}} = -\theta_{con,i} k_{b+v.\&r.c.(P,\theta)}. \quad (10.30)$$

This force in turn creates an additional moment

$$M_{con(F_{con(M_{con(\theta),i})})} = F_{con(M_{con(\theta),i})} d_{con}. \quad (10.31)$$

10.2.2.4 Sum of the compatibility forces

The sum of all compatibility forces needs to be added to the equilibrium Equation (10.12)

$$F_{con} = N F_{con(\Delta)} + \sum_{i=1}^N F_{con(M_{con(\theta),i})} \quad (10.32)$$

where:

N number of storeys.

To the total moment at the base obtained with Equation (10.13), all compatibility moments as calculated above need to be added

$$M_{con,tot} = \left[M_{con(\Delta)} + M_{con(F_{con(\Delta)})} \right] N + \sum_{i=1}^N \left[M_{con(\theta),i} + M_{con(F_{con(M_{con(\theta),i})})} \right]. \quad (10.33)$$

As will be shown in section 0, the compatibility forces and movements due to connections away from the beam mid-span, shown in blue in Equations (10.32) and (10.33), are normally small and can be ignored.

10.2.3 Force-displacement curve

Once the moment-curvature relationship of the rocking wall is defined, the force-displacement curve can be plotted. As already shown in Equation (10.25), the total force on the wall can be written as a function of the base moment. The top wall displacement is the sum of the elastic deformations due to wall bending deformation, shear deformation and the displacement due to gap opening as shown in Figure 10.7.

For the most general load combination on the wall, the elastic displacements due to bending δ_b and shear δ_s can be calculated as

$$\delta_b = \int \int \frac{M(z)}{E_t I} dz; \quad (10.34)$$

$$\delta_s = \int \int \frac{V(z)}{G_t A_s} dz. \quad (10.35)$$

These equations can be simplified considering a triangular force distribution and a constant interstorey height H . This allows writing the elastic wall displacement contributions as a function of the base moment

$$\delta_b = \frac{M_{tot}H^2}{6E_tI_t} \frac{6}{(N+1)(2N+1)} \sum i^3 \left(3 - \frac{1}{N}\right); \quad (10.36)$$

$$\delta_v = \frac{M_{tot}}{G_tA_s}. \quad (10.37)$$

The top wall displacement can be equated as

$$\delta_{tot} = \theta_{imp}L + \delta_b + \delta_v; \quad (10.38)$$

where:

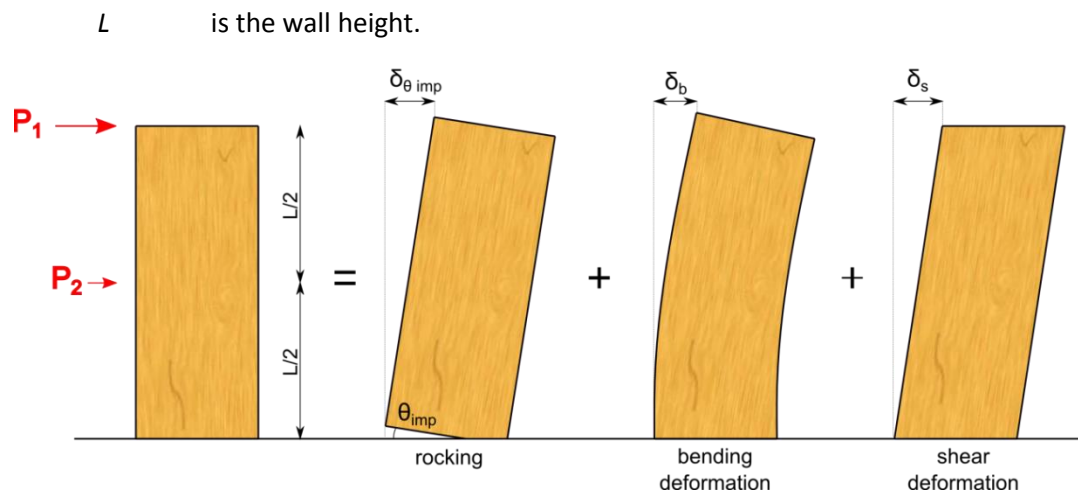


Figure 10.7 Displacement contributions of the wall

10.3 COMPARISON WITH EXPERIMENTAL VALUES

The analytical pushover curve, which can be obtained from the procedure outlined above, is compared to the experimental data of the post-tensioned wall with collector beams as described in Chapter 9. Before the force-displacement and moment-rotation curves of the wall-beam system are compared, the appropriateness of the analytical formulation for the base wall needs to be verified. This is carried out by determining the moment-rotation behaviour as shown in Figure 10.2, without the terms in red related to the compatibility forces.

10.3.1 Validation on the bare wall

The post-tensioned timber rocking wall has been tested up to Maximum Credible Earthquake (MCE) drift levels of 2% for a number of times in previous experiments carried out by Sarti (2015), before the collector beams were assembled and further tests were carried out. These severe tests caused some crushing of the timber especially towards the edges, resulting in a slight convex surface as can be seen in Figure 10.8.

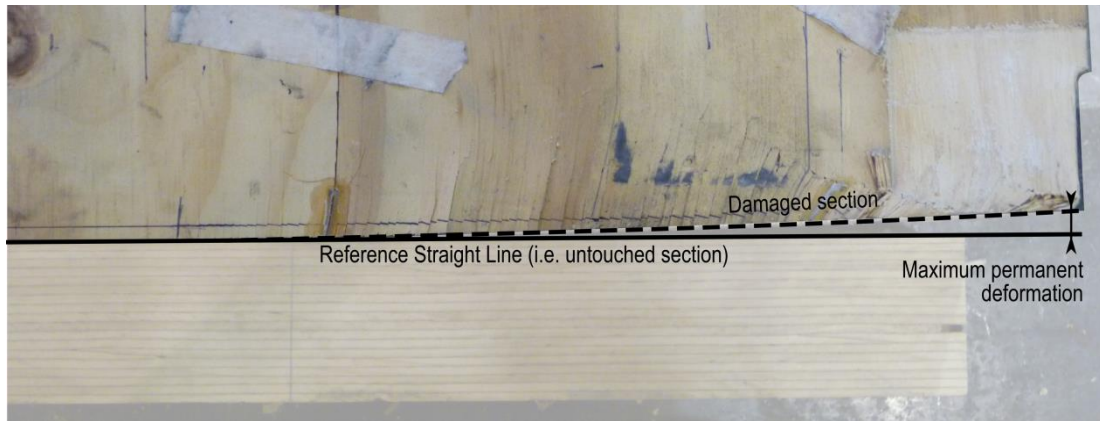


Figure 10.8 Wall damage from MCE testing (modified from Sarti (2015))

As a result, the initial stiffness of the wall before gap opening was reduced. This can be seen in Figure 10.9, where the experimental force-displacement and moment-rotation curves of the wall at the beginning and at the end of all test are compared. Once the decompression point was reached, the original wall stiffness is restored and for higher drifts also the full strength is reached.

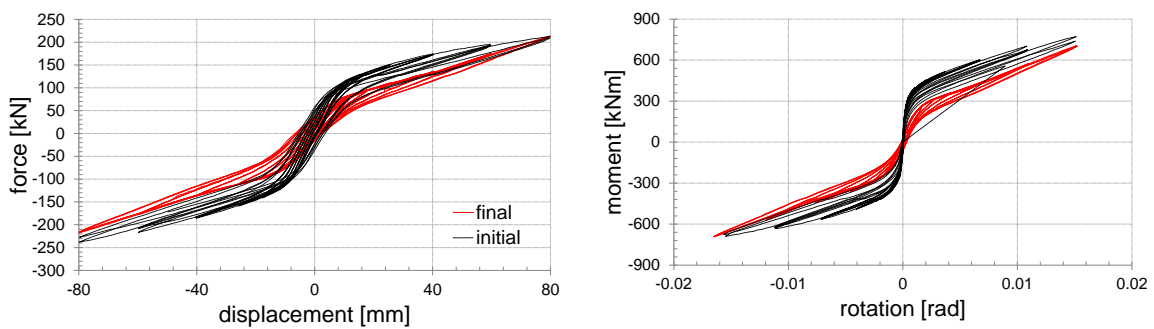


Figure 10.9 Experimental force-displacement (left) and moment-curvature (right) curves for the bare wall at the beginning and the end of the test campaign

Figure 10.10 shows the experimental and analytical force-displacement and moment-rotation curves of the bare wall at the beginning of the experimental campaign. It can be seen that the results from the analytical procedure match the experimental results very well. For positive drifts the experimental values were slightly higher, because of some restraining action of the test frame, which prevented out-of-plane movements of the wall.

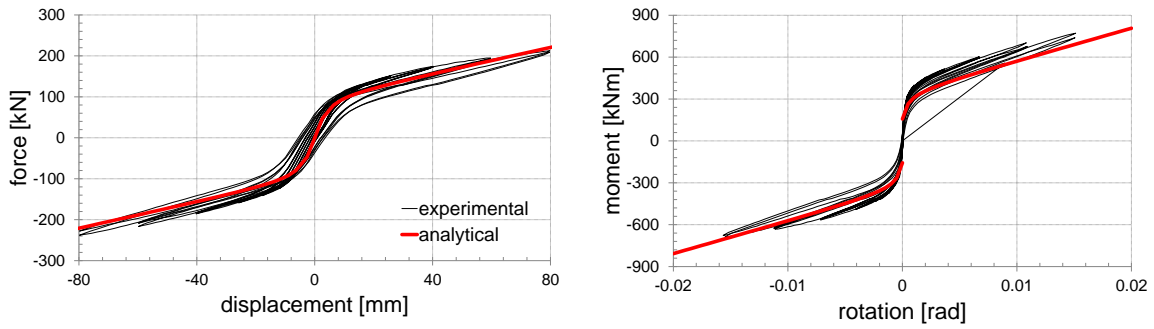


Figure 10.10 Force-displacement (left) and moment-curvature (right) curves for the bare wall at the first test

Figure 10.11 shows the same plots for the bare wall at the end of the test campaign. To resemble the slightly more flexible wall at lower drifts until almost full restoration at higher drifts, the section depth h of the wall was reduced to 85% of the section depth at 0% drift, which linearly increased until the full depth at 2% drift. The reduction to 85% of the section depth is based on the measured plastic deformation of the wall and from the fitting of the analytical data. With increasing wall rotation at the base, the gap from the convex shape is reduced and the wall original section depth is linearly reached.

The figure additionally also shows the post-tensioning forces and the neutral axis depth. The slight discrepancies of the values for negative drifts are thought to be caused by a slight inclination of the post-tensioning tendons over their height.

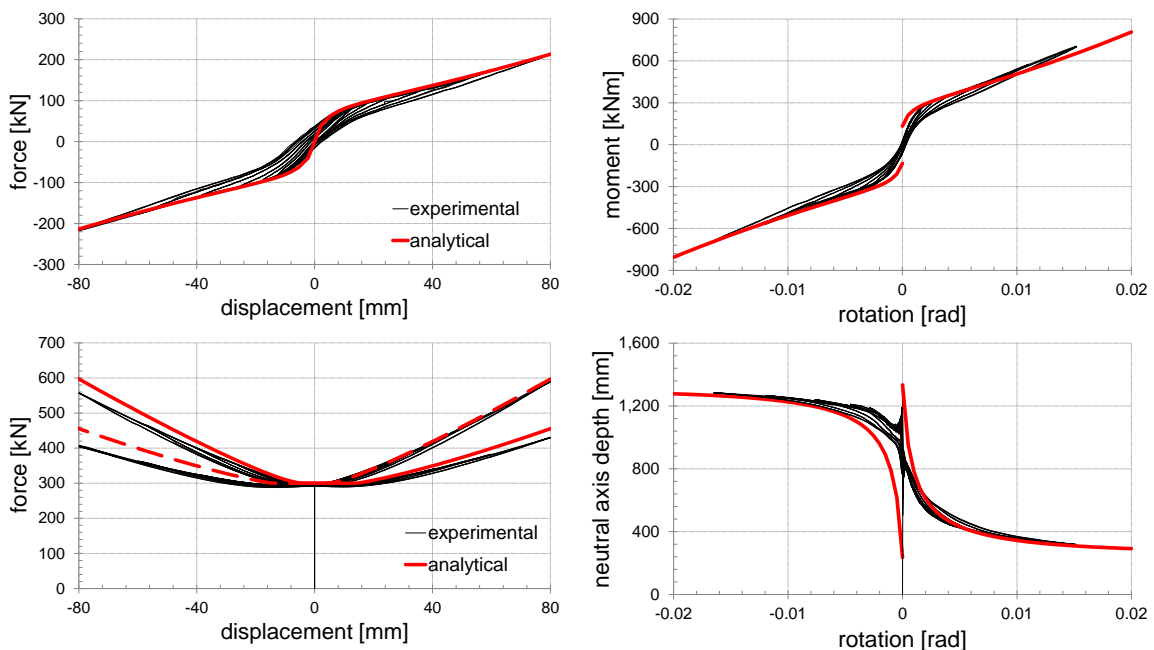


Figure 10.11 Force-displacement curve (top left), moment-curvature curve (top right), post-tensioning forces for both the left and the right post-tensioning bar (bottom left) and neutral axis (bottom right) for the bare wall at the end of all tests

10.3.2 Comparison for the wall-beam system

To simulate the behavior of the wall with the collector beams with connection type 1, with a centered group of 12 bolts, the translational and rotation connection stiffnesses were calculated with the equations presented in Appendix D. The fastener stiffness was calculated in accordance with Eurocode 5, considering a medium LVL density of 597 kg/m^3 (Franke and Quenneville 2011). Since the connection was designed to work in the elastic range, the slip modulus for the serviceability limit state was considered.

Figure 10.12 shows the comparisons of the force-displacement curve, moment-curvature curve, post-tensioning force and neutral axis depth of the system. The close match of the results suggests that the proposed model captures not only the rocking mechanism of the wall but also the restraining action from the collector beams.

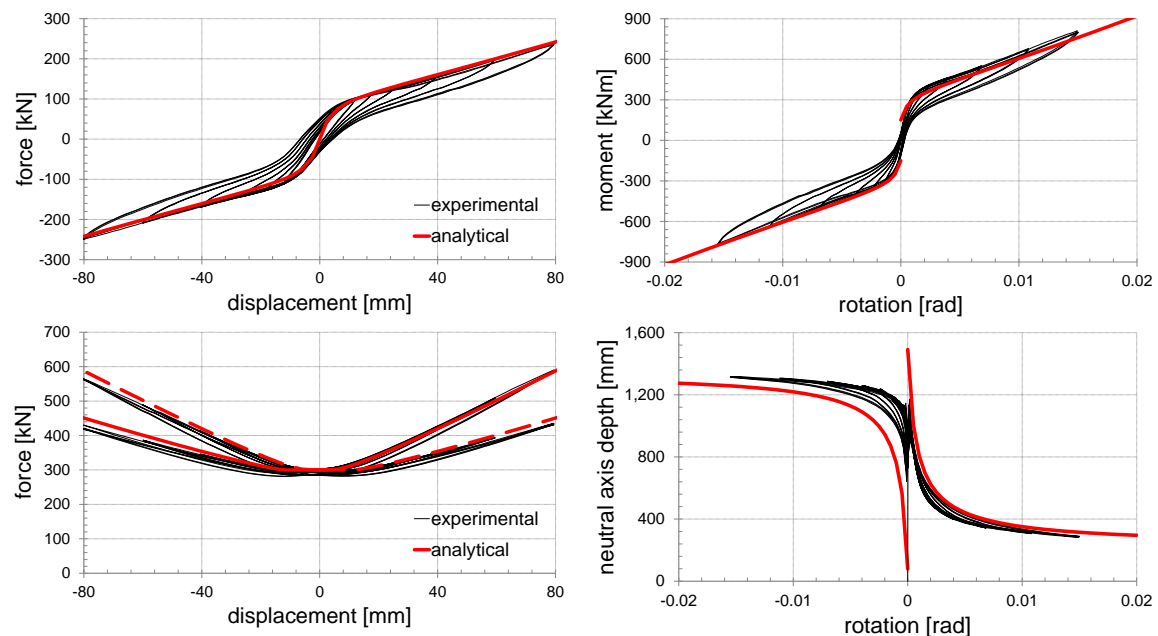


Figure 10.12 Force-displacement curve (top left), moment-curvature curve (top right), post-tensioning forces (bottom left) and neutral axis (bottom right) for the wall connected to the collectors with connection type 1 with a centred group of 12 bolts

The magnitude of the restraining action from the collector beams due to the imposed vertical displacement and rotation is shown in Figure 10.13. Whereas small rotations due to elastic bending and shear deformation in the wall already activate the compatibility forces, the increased strength and stiffness of the system can be clearly seen after the decompression point is reached. This is because at decompression the gap opening occurs, activating the vertical displacement incompatibility and increasing the wall rotation. The figure also shows

that the moment contribution due to the compatibility forces is a linear function of the imposed drift.

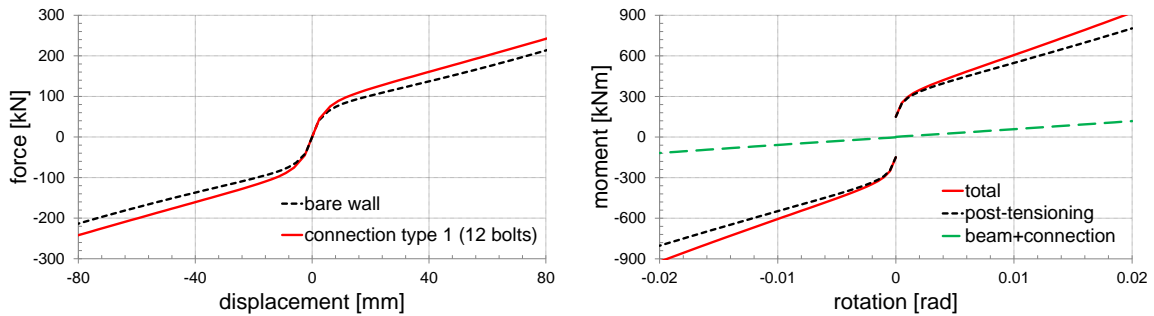


Figure 10.13 Change in the force-displacement behaviour (left) and moment-rotation behaviour (right) due to the connection between the wall and the collector beams for connection type 1 with a centred group of 12 bolts

For connection type 2, with a group of 25 bolts placed eccentrically in respect to the wall, the compatibility forces also need to consider the position of the connection away from the mid-length of the beam. For the specific case studied, the additional restraint however only accounts for 1% additional base moment and could be ignored. Figure 10.14 shows the comparison between the experimental and the analytical values. The slight asymmetry in the force-displacement curve and the difference in the maximum and negative peak forces of 14 kN from the experiment and 16 kN from the analytical procedure suggest that the eccentric placement of the connection does not cause great differences in the system behaviour. This also reinforces the conclusion of Chapter 9, that uplift incompatibility has less impact than the rotational incompatibility (Bigger displacements were imposed to the beam when the wall was rocking in one direction because of the eccentric connection in respect to the wall. The imposed rotation however was always the same).

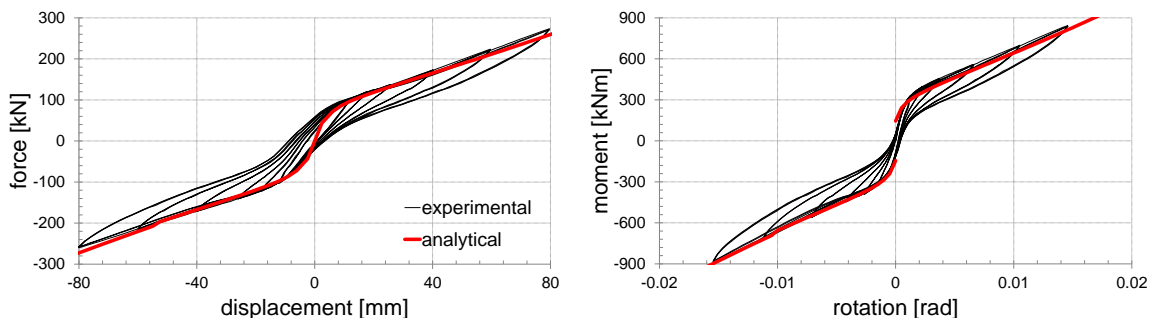


Figure 10.14 Force-displacement (left) and moment-rotation (right) curves for the wall connected to the collectors with connection type 2 with an eccentric group of 25 bolts

For connection type 4, with a large diameter pin, no rotations were imposed to the beam. Only the vertical movement of the wall created compatibility forces. Figure 10.15 shows the

comparison of the experimental and analytical values, confirming the accuracy of the proposed procedure.

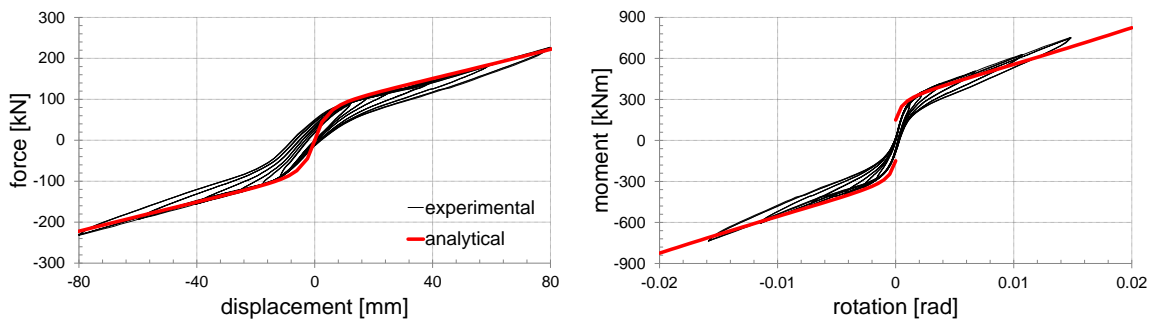


Figure 10.15 Force-displacement (left) and moment-curvature (right) curves for the wall connected to the collectors with connection type 4 with a large diameter pin

For connection type 6, with a steel comb with slotted holes, it was observed during testing that the bolts did not slide in the slots. The connection stiffness was therefore equated as for a connection with 7 bolts in a row placed in normal boltholes. Figure 10.16 shows the results for this configuration, confirming the finding that sliding did not occur in the connection.

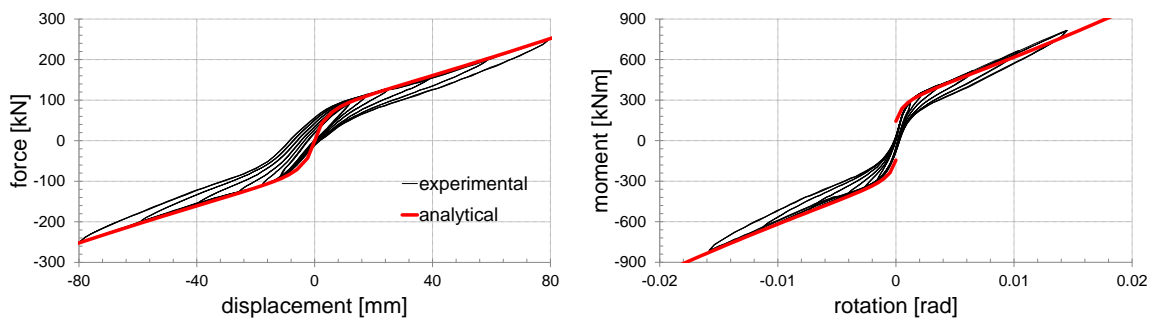


Figure 10.16 Force-displacement (left) and moment-curvature (right) curves for the wall connected to the collectors with connection type 6 with a steel comb with slotted holes

10.4 PARAMETRIC ANALYSIS

The analytical procedure permits studying the influence of the collector beam geometry and connection stiffness on the wall-beam system behaviour by varying some key parameters like beam length, beam height, position along the beam and connection stiffness. In this section a parametric analysis is carried out in order to understand the influence of these parameters on the global behaviour of the wall. Most of the presented force-displacement graphs are based on the configuration used for the experimental test with connection type 1 where one parameter has been varied. All figures also show the force-displacement curve of the bare wall (black dashed line) as a reference value.

10.4.1 Influence of the beam length and the number of fasteners

Figure 10.17a shows the results for the wall-beam system with varying collector beam lengths. The shorter the span, the higher the compatibility forces and the bigger the increase in wall stiffness and strength. With longer spans the interaction between wall and beams becomes smaller but the difference is quickly decreasing. Figure 10.17b is showing the force-displacement curves for increasing numbers of fasteners in the connection, which equals to an increase in connection stiffness. For a pinned connection the behaviour is close to the bare wall, since only vertical uplift is imposed to the wall. With increasing number of fasteners especially the rotational stiffness rapidly increases, causing more interaction between the wall and the beams. The influence however eventually attenuates, since the rotational beam stiffness tends to govern as can be seen later in Figure 10.21.

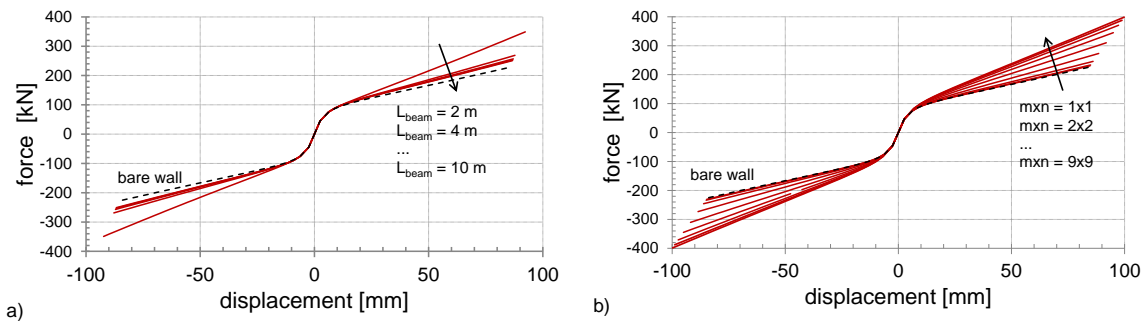


Figure 10.17 Parametric study of the wall-beam system with a) varying beam length and b) varying number of fasteners

10.4.2 Influence of the connection position on the collector beam

Figure 10.18 shows the influence of the position of the connection along the collector beam for two different connection configurations with 12 and 36 fasteners respectively. For both cases a connection very close to the support increases the wall-beam interaction. For the stiffer connection this interaction is much more pronounced.

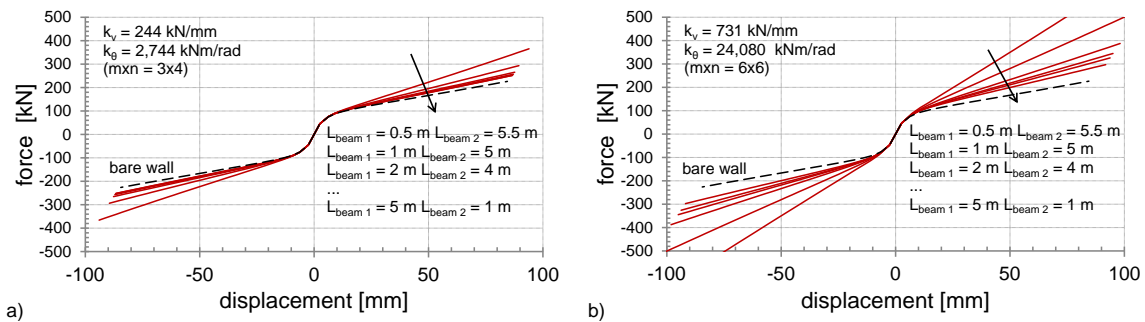


Figure 10.18 Parametric study of the wall-beam system with varying position of the connection along the beam for two different fastener configurations

10.4.3 Influence of the beam height

Figure 10.19 shows the influence of the beam height on the system behaviour for two different fastener configurations with 12 and 36 fasteners respectively. Whereas it is obvious that the beam height directly influences the beam stiffness and therefore the compatibility forces, the change in stiffness is different for the two different connection configurations as seen in Figures 10.19a and d. This indicates that the interaction is governed by the relative stiffnesses of the beam and the connection.

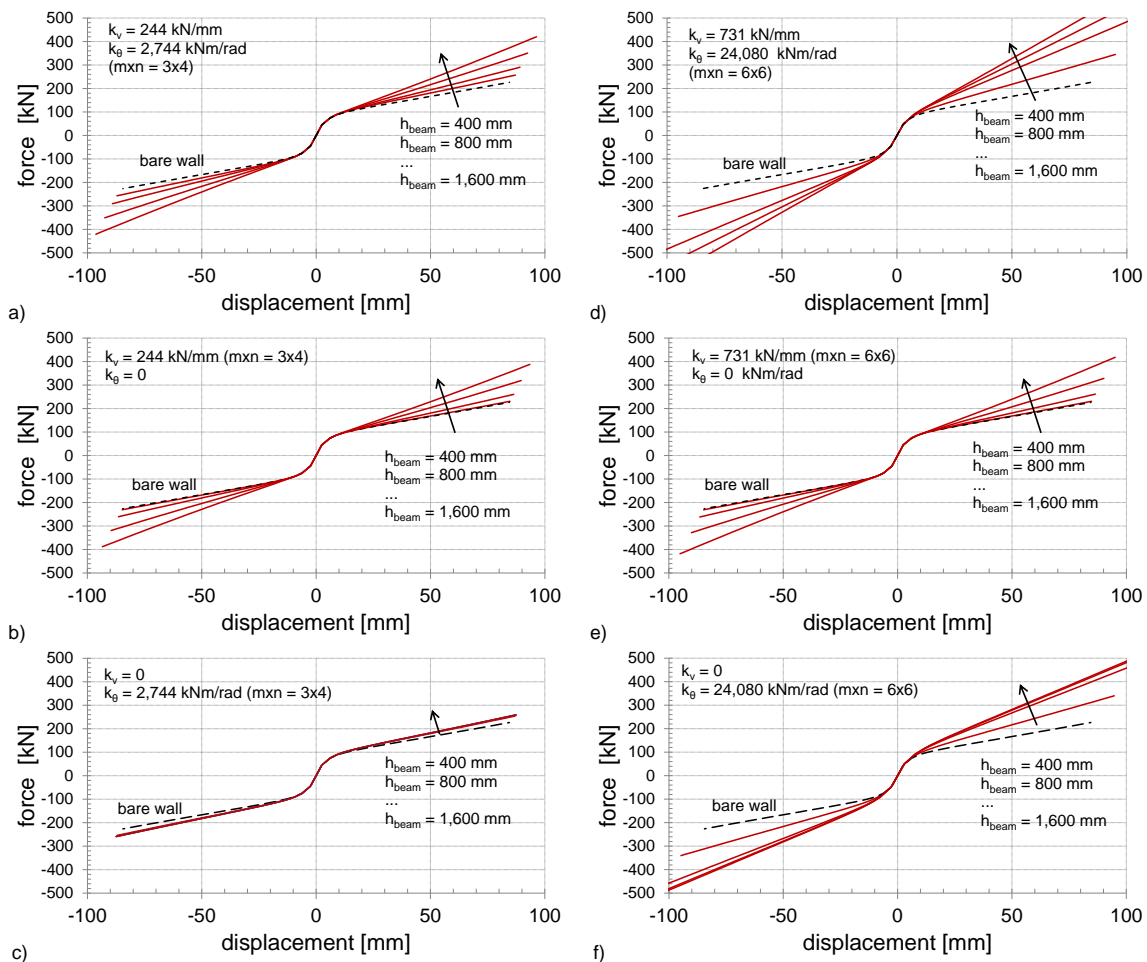


Figure 10.19 Parametric study of the wall-beam system with varying beam height considering the influence of the translational (k_v) and rotational (k_θ) springs for two different fastener configurations

When studying the influence of the beam height, by ignoring the connection rotational stiffness (i.e. the connection is considered a perfect hinge), it can be seen from Figures 10.19b and e that the behaviour is very similar for both connections. This is because the connection translational stiffness is bigger than the beam stiffness, and therefore only the latter influences the behaviour. It can also be seen that for the beam height of 400 mm, as used for the experiments, the vertical displacement incompatibility did not change the system behaviour

notably as already discussed in Chapter 9. For larger beam heights the wall uplift does cause bigger interaction.

Figure 10.19c shows that when studying the system behaviour by ignoring the connection translational stiffness (i.e. the connection can slide), the influence from the beam height is almost negligible. This is because the connection rotational stiffness with 3x4 fasteners is very low and acts almost as a hinge. For the connection with 6x6 fasteners the connection rotational stiffness becomes comparable with the beam rotational stiffness and the interaction between the beam and the wall becomes more pronounced as shown in Figure 10.19d.

10.4.4 Connections placed at a distance from the mid-span of the collector beam

Figures 10.20 and 10.21 can be used to explain the limited influence from the connection placed at a distance from the mid-span of the beam, as encountered in connection type 2 with 25 eccentric bolts. The curves were plotted resembling the tested configuration considering a varying number of fasteners.

For the connection with 25 bolts, because of the relatively small beam deflection stiffness $k_{beam(P,v)}$, the increase in the system stiffness of the rotational spring is from 1.7 kN/mm to 1.75 kN/mm and is therefore barely noticeable. Therefore, also the increase of the combined rotational stiffness from the beam and the connection vertical stiffnesses $k_{beam+rotational(M,\theta)}$ to the total stiffness $k_{beam+vertical+rotational(M,\theta)}$ is very small. For the specific geometry considered, the eccentric connection with 25 bolts therefore does not influence the wall-beam system a lot.

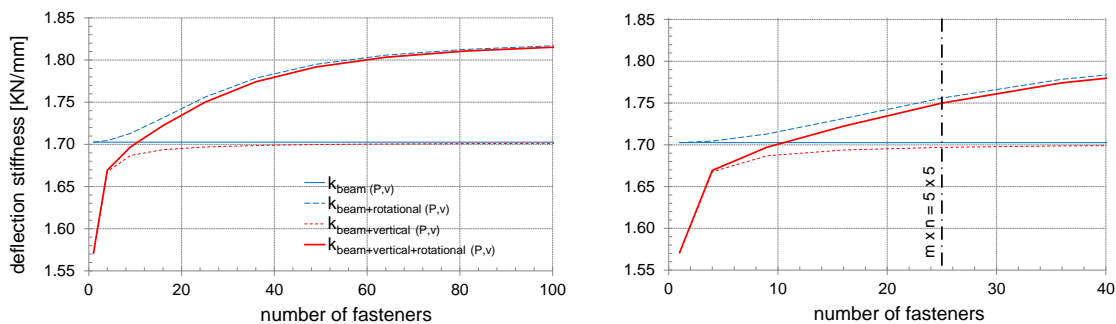


Figure 10.20 System deflection stiffness for the geometry with connection type 2 as described in Chapter 9 for varying number of fasteners

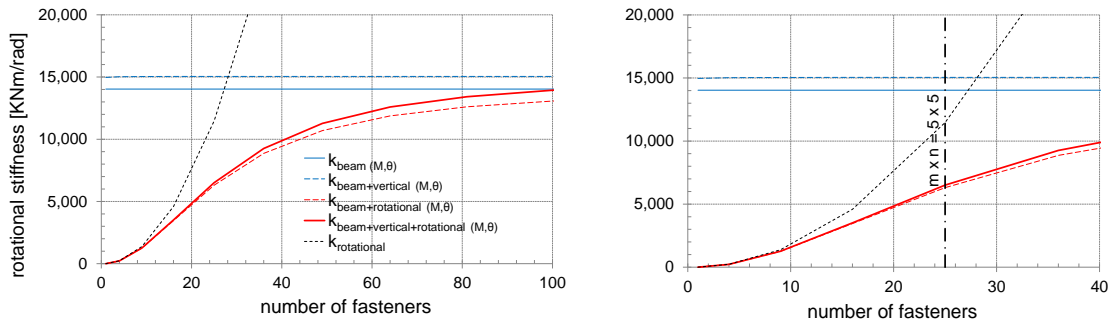


Figure 10.21 System rotational stiffness for the geometry with connection type 2 as described in Chapter 9 for varying number of fasteners

If the same connection with 25 bolts is moved further to about 1 meter from the right support, the influence of the eccentricity becomes much more pronounced as shown in Figure 10.22. With an increasing number of fasteners, and therefore stiffer connection, this interaction would become even bigger, creating a pronounced asymmetric force-displacement behaviour of the system.

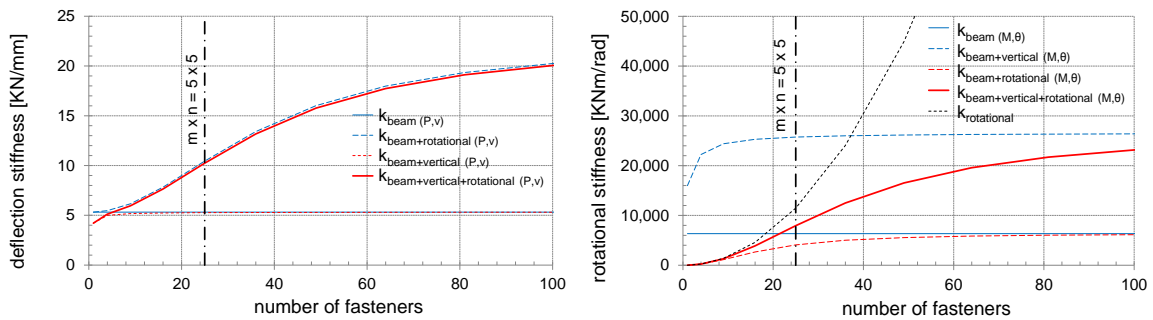


Figure 10.22 System rotational and translation stiffnesses for the geometry with connection type 2 as described in Chapter 9 at 1 meter from the right support for varying number of fasteners

10.5 DISCUSSION

To study the behaviour of post-tensioned rocking timber walls loaded through collector beams, the iterative moment-curvature procedure described in Newcombe et al. (2008) was extended by the inclusion of the compatibility forces and moments caused by the imposed displacement to the collector beams. Since these actions are a function of the floor forces, which depend on the system stiffness, a second iteration needed to be introduced in the procedure. The system stiffness of the beams and the relative connections to the wall were derived in their most general form in Appendix D, and were implemented in the procedure. Based on the moment-curvature curve, the force-displacement of the wall-beam system was finally derived.

The moment-curvature procedure was compared to the experimental results of the bare wall described in Chapter 9. Because of crushing at the edges of the wall, caused by repeated severe simulated earthquake loading over design loading, the wall stiffness was slightly reduced until the decompression point was reached. This was accounted for in the analytical procedure by an 85% reduced section depth at 0% drift, which linearly increased until the full depth at 2% drift. With this modification, which is only necessary for walls which already underwent a certain number of high drift cycles, the experimental pushover curves matched perfectly.

Further, the behaviour of the wall-beam assembly connected with a centric group of 12 bolts, an eccentric group of 25 bolts, with a large diameter pin and a slotted steel comb was obtained with the analytical procedure and compared to the experimental values. For all these cases the iterative procedure predicted the values in a very precise fashion. It can, therefore, be concluded that the analytical procedure allows practitioners to quickly determine the strength and stiffness of the wall and also the forces in the wall-to-beam connection as well as the deformation of the beams.

A parametric analysis showed the influence of the beam length, position of the connection along the beam, number of fasteners and beam height on the system behaviour. Although any increase of rotational or translational stiffness in the beam or connection increased the wall-beam stiffness, no general rule of which parameter influenced the wall-beam stiffness most could be observed. This is because the system stiffness is accounted for by several springs in series, and any trend would need to be based on relative rather than absolute stiffnesses. The influence on the position of the connection along the beam was also investigated. For connections only slightly offset from the beam mid-span only a small increase in the system stiffness and strength were observed, connections further away caused higher interaction.

Generally, it can be concluded that the connection vertical stiffness has negligible influence on the system behaviour, since it is normally greater than the beam bending stiffness. The rotational stiffness of a compact connection was able to decouple the imposed rotations from the beam. For connections with many dowels or with increased fastener distances, the connection rotational stiffness soon became very large and increased compatibility forces because of beam bending were created.

The force-displacement curves derived analytically for the wall-beam system could also be extended for the column-wall-column system as reported in Chapter 9. For this, the analytical

procedure developed by Sarti (2015) would need to be extended by accounting for the rotation incompatibility between the column and the beam if the connection is not acting as a hinge.

10.6 CONCLUSIONS

The proposed iterative procedure based on the force equilibrium method, modified to include the wall-beam compatibility forces and moments, predicted the actual strength and stiffness values of the tested wall-beam assemblies precisely. The compatibility forces and moments can be determined as a function of the beam and connection stiffnesses and their position to the wall. The actual beam deformation and increased connection forces can also be determined.

A parametric study confirms that although for the tested design configuration vertical displacement incompatibilities only cause small compatibility forces and moments, and compact connections can successfully limit the rotational interaction, no general trend can be given as to which parameter, like beam height, or number and position of fasteners, most influences the interaction. This is because the compatibility forces and moments are a function of the beam bending and rotational stiffnesses as well as the rotational stiffness of the connection.

11 Recommendations for the design of diaphragms in multi-storey timber buildings

This chapter provides recommendations for the design of diaphragms in multi-storey timber buildings. Key findings of this thesis are presented for direct use in practical design. The recommended method to determine the diaphragm force demand has been evaluated on - tensioned Pres-Lam buildings only. However, since timber structures are normally deflection governed, the same findings can be applied to engineered timber structures in general. Further research is currently carried out on the determination of floor forces with additional guidance soon available. Guidance on the load paths in diaphragms and displacement incompatibilities between the lateral load resisting system and the floor slabs is independent from the structural system and is therefore valid for any timber structure.

11.1 DETERMINATION OF THE DIAPHRAGM FORCE DEMAND

All information provided in this section can be found in more detail in Chapter 5.

11.1.1 Fundamental period of vibration

Flexible diaphragms increase the structure's fundamental period. This effect is more pronounced for stiff buildings, like short wall structures, and tends to be negligible for flexible buildings, like tall frame structures. Although a longer period normally decreases the seismic demand, higher modes attributed to diaphragm flexibility counteract this effect by increasing the base shear and the forces acting on the lower stories. It is therefore recommended to use the fundamental period calculated for the structure with rigid diaphragms.

If the fundamental period of the structure with non-rigid diaphragms needs to be determined, the following equations can be used (Nakaki 2000). This equation is valid independently from the structural type, as long as all diaphragms have the same stiffness

$$T' = T_{rigid} \sqrt{\frac{1 + \alpha^2}{\alpha^2}}; \quad (11.1)$$

$$\alpha = \frac{T_{rigid}}{T_{diap}}; \quad (11.2)$$

$$T_{diap} = 2\pi \sqrt{\frac{M}{K_{eq}}}; \quad (11.3)$$

$$K_{eq} = K_{eq,d+c} = \left(\frac{1}{K_{diap}} + \frac{1}{K_{con}} \right)^{-1}; \quad (11.4)$$

where

T'	is the structure's fundamental period including diaphragm flexibility [s];
T_{rigid}	is the structure's fundamental period with rigid diaphragms [s];
T_{diap}	is the diaphragm's period [s];
M	is the mass applied on the diaphragm [kg];
K_{eq}	is the combined diaphragm and connection stiffness [N/m];
K_{diap}	is the diaphragm stiffness [kN/m];
K_{con}	is the diaphragm connection stiffness [kN/m].

11.1.2 Diaphragm stiffness in frame structures

Because of the typically small grid spacing of moment resisting frame structures, timber diaphragms in frame structures can normally be categorized as rigid or semi-rigid. Concrete diaphragms typically behave as rigid. Although for rigid diaphragms the force distribution into the lateral load resisting system is a function of the stiffness of the latter, for semi-rigid diaphragms both the diaphragm stiffness and the stiffness of the lateral load resisting elements need to be considered. For the analysis of semi-rigid diaphragms the Equivalent Truss Method as discussed later in section 11.2.3 is recommended. The frame stiffness can be accounted for by specific sub-model in a 3D model, or by a spring element with an equivalent stiffness determined by a pushover analysis of the frame.

11.1.3 Force demand in frame structures

The seismic demand of frame structures in terms of storey shear, moment and drifts is not significantly influenced by diaphragm flexibility. To account for higher mode effects and overstrength in the lateral load resisting system, the column shear and moment amplification factor as proposed by Priestley et al. (2007) can be applied.

All diaphragms up the height of the structure should be designed based for the maximum diaphragm demand determined by the following equation

$$E_{diap}^* = \phi^o V_{E,top} + 0.2\mu V_{E,base}; \quad (11.5)$$

where

E_{diap}^*	is the diaphragm force demand;
ϕ^o	is the overstrength factor of the lateral load resisting system;
μ	is the ductility of the structure (taken as 1 in case of structures with no additional hysteretic damping);
$V_{E,top}$	is the shear value at the top storey found from the equivalent static analysis;
$V_{E,base}$	is the base shear value.

Until overstrength factors for timber structures are available, conservative assumptions based on engineering judgement or preliminary experimental testing should be used.

11.1.4 Diaphragm stiffness in wall structures

Diaphragms in wall structures can range from flexible to rigid depending on the span and the type of flooring setup. Both the diaphragm and wall flexibilities should be considered when determining the load distribution. For wall structures, it is recommended that diaphragms be considered as semi-rigid and be modelled with the Equivalent Truss Method as discussed later in section 11.2.3. The wall stiffness can be accounted for by a wall element in a 3D model, or by a spring element with an equivalent stiffness determined by a pushover analysis of the wall.

11.1.5 Force demand in wall structures

Diaphragm flexibility has a minor effect on the shear and moment distribution up the height of the wall. Higher mode effects and overstrength of the lateral load resisting system can be accounted for by using the envelopes determined by Priestley et al. (2007) and Sarti (2015).

Diaphragm flexibility does influence the diaphragm demand especially in the lower stories and should be included in an analysis. The amplified design shear force at the top of the building at overstrength according to Priestley et al. (2007) provides good estimates of the peak diaphragm force demand for commonly encountered diaphragm stiffnesses

$$E_{diap}^* = V_n^o; \quad (11.6)$$

where

E_{diap}^*	is the diaphragm force demand;
V_n^o	is the amplified design shear force at the top of the building at overstrength which can be calculated with the use of the following equations

$$V_B^o = \phi^o \omega_V V_{E,base}; \quad (11.7)$$

$$V_n^o = C_{3,T} V_B^o; \quad (11.8)$$

$$\omega_V = 1 + \frac{\mu}{\phi^o} C_{2,T}. \quad (11.9)$$

$$C_{2,T} = 0.067 + 0.4(T_i - 0.5) \leq 1.1; \quad (11.10)$$

$$C_{3,T} = 0.9 - 0.3T_i \geq 0.3. \quad (11.11)$$

where

- ϕ^o is the overstrength factor of the lateral load resisting system;
- μ is the ductility of the structure (taken as 1 in case of structures with no additional hysteretic damping);
- T_i is the elastic fundamental period of the building.

Until overstrength factors for timber structures are available, conservative assumptions based on engineering judgement or preliminary experimental testing should be used.

To protect gravity carrying elements, facades and other non-structural elements attached to the diaphragms, the interstorey drift values should also include the diaphragm deflection. If no special study is carried out, the following expression provides estimates for the total interstorey drift. It has to be noted that for flexible diaphragms this procedure can result in very conservative values.

$$\theta_{total,max} = \theta_{LLRS,base} + \theta_{diap}; \quad (11.12)$$

$$\theta_{diap} = \frac{E_{diap}^*}{H K_{diap}}; \quad (11.13)$$

where

- $\theta_{total,max}$ is the maximum estimated interstorey drift at the mid-span of the diaphragm;
- $\theta_{LLRS,base}$ is the interstorey drift at the first level according to the equivalent static analysis (inelastic deformation);
- θ_{diap} is the maximum estimated diaphragm interstorey drift;
- H is the interstorey height;
- E_{diap}^* is the maximum diaphragm demand;
- K_{diap} is the diaphragm stiffness.

The diaphragm stiffness should be determined by the deflection Equation (11.26) or through the Equivalent Truss Method as per section 11.2.3.

11.1.6 Transfer forces

Transfer forces are generated in diaphragms because of deformation incompatibilities of the lateral load resisting system (often also denominated compatibility forces) or because of sudden changes in the stiffness or location of lateral load resisting elements up the building height (i.e. decreasing wall lengths or discontinuous walls).

Compatibility forces and transfer forces in diaphragms are likely to occur in diaphragms if one or more of the following situations occur:

- Lateral load resisting elements with different stiffnesses working in parallel (horizontal stiffness irregularity);
- Dual structures with wall and frames;
- Lateral load resisting elements with changing stiffness up the building height (vertical stiffness irregularity);
- Discontinuous or missing walls up the building height;
- Non continuous lateral load resisting elements up the building height;
- Podium structures or structures with set-backs.

Transfer forces are intimately linked to the inertia forces; in case they are created by displacement incompatibilities they however do not necessarily occur at the same instant in time. The above suggested diaphragm forces do not occur simultaneously and should not be applied to the structure to determine compatibility forces in the diaphragms, as it would provide very conservative values. If transfer or compatibility forces are expected in the diaphragms, special studies should be relied on.

11.2 DIAPHRAGM ANALYSIS AND LOAD PATHS

11.2.1 Girder analogy

For regular and rectangular diaphragms, the load path and the internal actions in the diaphragm components can be determined by the girder or deep beam analogy as shown in Figure 11.1. The shear forces are resisted by the diaphragm panels and can be assumed as constant along the diaphragm depth. The bending moment is resisted by the chord beams, acting in tension and compression respectively.

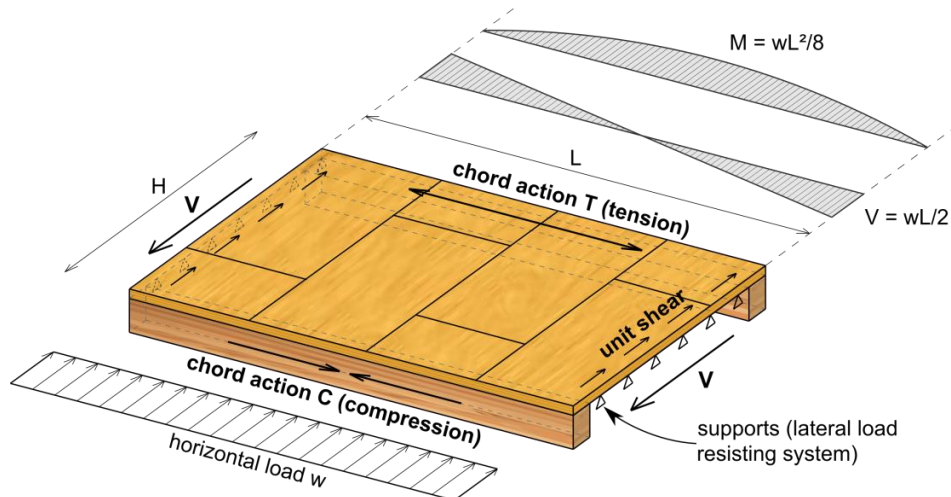


Figure 11.1 Girder analogy for regular diaphragms

The tension and compression forces in the chord beams can be determined as

$$T = C = \frac{M}{H} = \frac{wL^2}{8H}; \quad (11.14)$$

where

- T is the tension force in chord beam;
- C is the compression force in chord beam;
- w is the uniformly distributed load;
- L is the diaphragm span;
- H is the diaphragm depth;
- M is the moment from the uniformly distributed load.

The unit shear force, defined as the shear force per unit length, can be calculated as

$$v = \frac{V}{H} = \frac{wL}{2H}; \quad (11.15)$$

where

- v is the unit shear force;
- V is the reaction force at the diaphragm supports.

In the case of individual diaphragm panels (precast concrete or wooden panels), the panel shear demand and the fasteners demand (discrete or smeared) can be determined based on the unit shear forces obtained as shown in Figure 11.2. For larger diaphragms, fastener spacing can be reduced towards the centre of the diaphragm. Chord beams and any eventual splices have to be designed to resist the axial force demand.

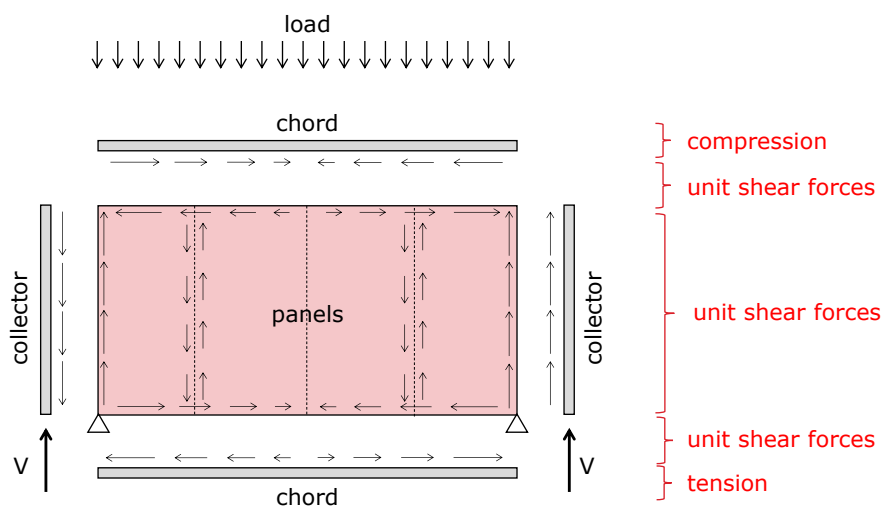


Figure 11.2 Free body diagram of a simply supported diaphragm without irregularities

More information on the girder analogy can be found in Chapters 3 and 6.

11.2.2 Strut-and-Tie Method – concrete diaphragms

For regular and irregular concrete diaphragms a strut-and-tie analysis (Schlaich et al. 1987) is recommended. In the case of very complex and statically indeterminate diaphragms it is recommended that the stress distribution (in form of stress trajectories for example) is determined beforehand with the use of an elastic finite element analysis. This allows determining the likely force path, and therefore the most appropriate strut-and-tie geometry. It is worth mentioning that different loading conditions might require different strut-and-tie geometries.

Once the forces from the strut-and-tie analysis are determined, the concrete struts, tension ties and node areas need to be verified. This verification needs to be carried out in accordance to the relevant design code (Eurocode 8 2004; Standards New Zealand 2006; Standards Australia 2009; ACI 2014).

A more enhanced method of the strut-and-tie method can be found by modelling the diaphragm with an equivalent truss (grillage) according to the framework method developed by Hrennikoff (1941). Guidance on this method can be found in Bull and Henry (2014).

11.2.3 Equivalent Truss Method – timber diaphragms

The derivation and full explanation of the Equivalent Truss Method for timber diaphragms can be found in Chapter 7. The following sections provide the relevant information for its practical application.

For blocked Light Timber Framing (LTF) and massive timber diaphragms the Equivalent Truss Method is recommended. A diaphragm can be defined as blocked, when all panel edges are connected to each other and can transfer the unit shear force. The truss analogy allows the analysis of statically indeterminate diaphragms in presence of irregularities and concentrated forces. If the deflected shape of the lateral load resisting systems is imposed to the diaphragm, transfer forces can be evaluated as well.

With the Equivalent Truss Method the horizontal diaphragm is modelled by a grillage of elements representing framing members and beams as well as the axial stiffness of each panel which includes the fastener stiffness perpendicular to the panel edges. For each panel the shear stiffness and fastener flexibility is modelled by equivalent diagonals, characterized by the following properties:

$$(Gd)_{ef} = \frac{1}{\left[\frac{1}{Gd} + \frac{s}{K_{ser||}} \left(\frac{c_1}{b} + \frac{c_2}{h} \right) \right]}; \quad (11.16)$$

$$E_{ef} = \frac{(Gd)_{ef} l^2}{hb}; \quad (11.17)$$

$$A_{ef} = l = \sqrt{h^2 + b^2}. \quad (11.18)$$

where

- $(Gd)_{ef}$ is the equivalent shear-through-thickness rigidity of the panel;
- G is the shear modulus of the sheathing;
- d is the sheathing panel thickness;
- E_{ef} is the equivalent modulus of elasticity of the diagonal;
- A_{ef} is the equivalent cross sectional area of the diagonal;
- $K_{ser||}$ is slip modulus of the fastener parallel to the panel edge;
- s is the fastener spacing;
- b is the panel width;
- h is the panel height;
- l is the diagonal length;
- c_i number of connections rows along sheathing panel edge;
- c_1 number of lines of fasteners between adjacent panels along the sheathing panel height h ;
- c_2 number of lines of fasteners between adjacent panels along the sheathing panel length b ;

For LTF diaphragms, the panels are connected via framing elements, requiring two lines of connections, therefore $c_1 = c_2 = 2$. For massive timber panels no framing elements are necessary along the longitudinal panel edge, c_1 is therefore typically 1 (if a connection with a splice plate is used, $c_1 = 2$). The heads of the panels are sitting normally on a beam, requiring two lines of fasteners to transfer the forces and therefore $c_2 = 2$.

- LTF diaphragms with nails
 $c = 2$
- Massive timber diaphragm with lap joint and screws
 $c = 1$
- Massive timber diaphragm with single spline joint and screws/nails
 $c = 2$

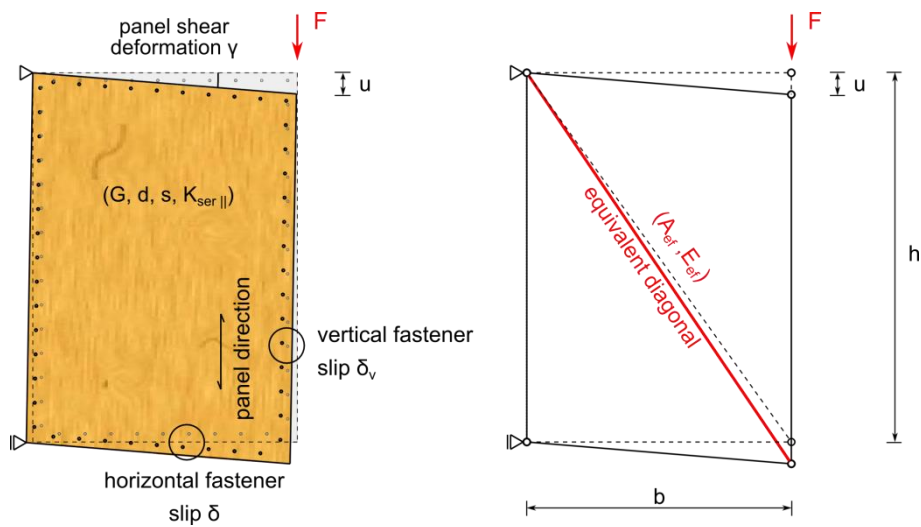
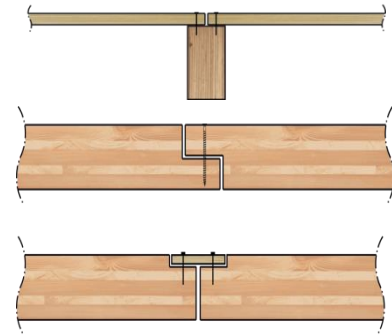


Figure 11.3 Shear panel with fastener stiffness and equivalent truss diagonal

By setting the equivalent diagonal cross sectional area A_{ef} equal to the diagonal length l (this does not have any physical meaning, but provides some simplification in the method), the unit shear force t in the panel (that is the shear force per length) can be obtained as the normal stress in the diagonal

$$t = \sigma = \frac{F_{diagonal}}{A_{ef}} = \frac{F_{diagonal}}{l}; \quad (11.19)$$

where:

- t is the unit shear force in the panel;
- σ is the axial stress in the diagonal;
- $F_{diagonal}$ is the force in diagonal;
- A_{ef} is the diagonal area, which equals to the diagonal length l .

To obtain the tension/compression forces in the chord and collector beams, the integration of the unit shear forces along the element length needs to be added to the axial forces from the truss elements. This is because the diagonal introduces the equivalent panel force in the nodes, whereas in reality it is introduced gradually through the fasteners along the panel edge.

The diaphragm loads are best applied as concentrated loads to the respective nodes.

11.2.3.1 Multiple diagonals per sheathing panel

Because massive timber panels possess relatively high axial stiffness compared to LTF panels, normal stresses along the two main directions need to be accounted for. Additionally, fasteners will not only transfer forces parallel to the panel edges, but also perpendicularly to them. By dividing the panels into multiple diagonals as shown in Figure 11.4, the transverse truss elements (along the panel width b) can account for these effects by including the fastener stiffness perpendicular to the panel edges.

Because of stiffness considerations, in the case of panel subdivision into multiple diagonals, higher forces are attracted close to stiffer elements like beams or supports. In such cases the average of all diagonals belonging to one panel element should be considered.

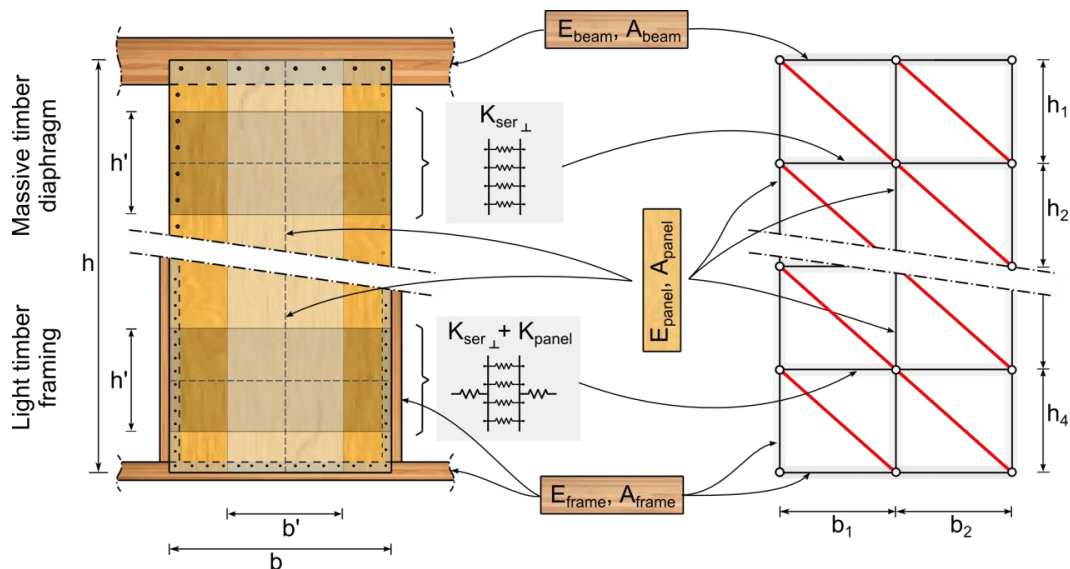


Figure 11.4 Timber panels and idealization in the equivalent truss model for the case of multiple diagonals for LTF diaphragms and massive timber diaphragms

The individual diaphragm panel can be sub-divided in a regular pattern obtaining $m \times n$ equivalent diagonals or by diagonals with varying lengths according to Table 11.1 and Figure 11.5.

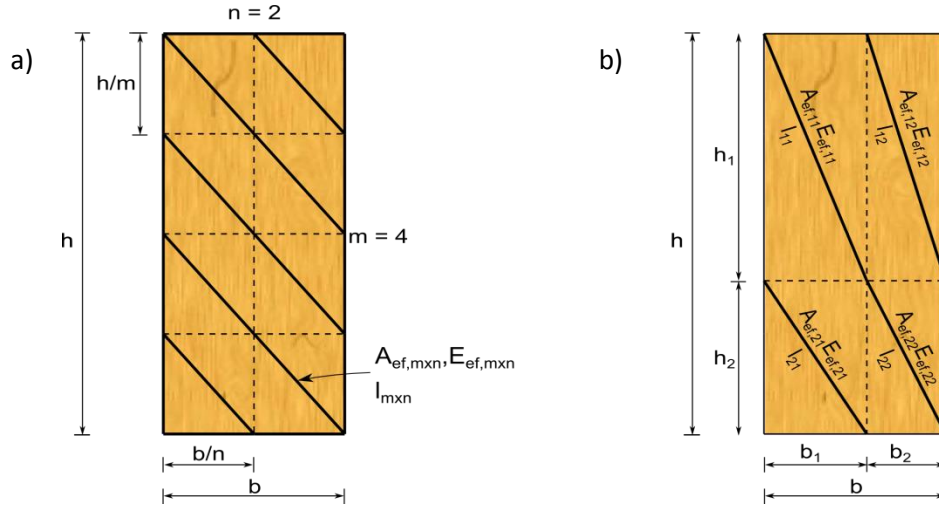

 Figure 11.5 Multiple diagonals for a) regular $m \times n$ sub-divisions or for b) irregular sub-divisions

Table 11.1 Diagonal properties in case of regular and irregular panel sub-divisions

$m \times n$ regular diagonals	irregular diagonals
$E_{ef,mxn} = mn \frac{(Gd)_{ef} l_{mxn}^2}{bh} \quad (11.20)$	$E_{ef,ij} = \frac{(Gd)_{ef} l_{ij}^2}{b_j h_i} \quad (11.21)$
$A_{ef,mxn} = l_{mxn} = \sqrt{\left(\frac{b}{n}\right)^2 + \left(\frac{h}{m}\right)^2} \quad (11.22)$	$A_{ef,ij} = l_{ij} = \sqrt{b_i^2 + h_j^2} \quad (11.23)$

All beams (collector, chord, strut beams) and framing elements as well as other reinforcing elements are modelled with their real axial stiffness. The remaining longitudinal truss elements (along the panel height h) are to be modelled with the axial panel stiffness corresponding to the tributary width b' of the truss element as shown in Figure 11.4.

For the transverse truss element (along the panel width b) not corresponding to beams or framing elements, the stiffness of the tributary panel strip is summed (in series) with the fasteners stiffness perpendicular to the panel edge ($K_{ser \perp}$). Considering a common sub-division of two diagonals along the panel width, the equivalent stiffness (in force per length) of the transverse member for a LTF diaphragm can be calculated as

$$K_{ef,transverse\ truss,LTF} = \frac{1}{\frac{1}{\frac{E_{90} A'}{b'}} + \frac{1}{n' K_{ser \perp}}}; \quad (11.24)$$

where

- E_{90} is the panel stiffness perpendicular to the panel direction;
- A' is the tributary cross section of the transverse truss element = $h' d$;
- d is the panel thickness;
- b' is the tributary width of the longitudinal truss element = $(b_i + b_{i+1})/2$;

- h' is the tributary width of the transverse truss element = $(h_i + h_{i+1})/2$;
 n' is the number of fasteners along h' ;
 $K_{ser \perp}$ is the slip modulus of the fasteners perpendicular to the panel edge.

In the case of a massive timber diaphragm, the axial stiffness of the transverse truss element is much bigger than the stiffness of the fasteners and can normally be ignored. For a common sub-division of two diagonals along the panel width, the equivalent stiffness of the transverse member in a massive timber panel can be calculated as

$$K_{ef,transverse\ truss,massive} = \frac{1}{\frac{1}{\frac{E_{90}A'}{b'}} + \frac{1}{(3-c)n'K_{ser \perp}}} \cong (3-c)n'K_{ser \perp}. \quad (11.25)$$

where

- c number of fastener lines to transfer the unit shear force from one panel to the other.

11.2.3.2 Diaphragm flexibility

Loading and material codes often define diaphragms as either flexible or rigid (Eurocode 8 2004; Standards New Zealand 2004; ASCE 2010). In case of a flexible diaphragm the force distribution into the lateral load resisting elements can be determined according to tributary area approach. For rigid diaphragms, on the other hand, the horizontal forces are distributed in function of the stiffness of the lateral load resisting elements.

In reality there is however no distinct change in the force distribution behaviour of diaphragms, and normally an intermediate behaviour of the two extreme cases occurs. Especially timber diaphragms often work in this intermediate range, commonly defined as semi-rigid, where the force distribution is in function of both the diaphragm and the lateral load resisting system stiffnesses. The analysis of semi-rigid diaphragms is seldom carried out, since simple analysis methods are missing. Designers often avoid the issues by applying an envelope method, where the highest forces from both extreme cases are considered.

The Equivalent Truss Method is based on stiffness considerations and can effectively simulate the diaphragm stiffness and the correct force distribution into the lateral load resisting elements. The stiffness of the lateral load resisting system can be added to the truss model in the form of non-linear springs determined by a pushover analysis. Alternatively the lateral load resisting stiffness can be modelled directly with vertical equivalent trusses for walls. Because the Equivalent Truss Method can model the diaphragm stiffness, a correct force distribution because of torsional effects (geometric or accidental torsion) can also be achieved.

It has to be noted that this procedure might require iteration for the design of both the diaphragm and the lateral load resisting system. This is because section sizes or fastener stiffness first have to be defined in a preliminary design before the load path in both the diaphragm and the lateral load resisting system can be determined. Higher than expected loads might require the re-design of some elements and therefore cause a change in the elements stiffness, influencing the load path in the structure.

11.2.3.3 Choice of truss grid spacing

The choice of the truss grid spacing depends on the diaphragm layout and the panel dimensions. Slender panels can result in very inclined diagonals, which like for any truss system lead to unfavourable behaviour and should therefore be sub-divided into smaller, square elements. To account for irregularities in the floor geometry and to obtain the forces in the relative strut/collector beams or other types of reinforcement, subdivisions might be necessary as shown in Figure 11.17a and b. By choosing a smaller grid spacing as shown in Figure 11.17c, only a reduced number of different diagonal types need to be considered (ideally only one). It is reminded that any sub-division of the panels requires the definition of additional longitudinal and transverse truss members.

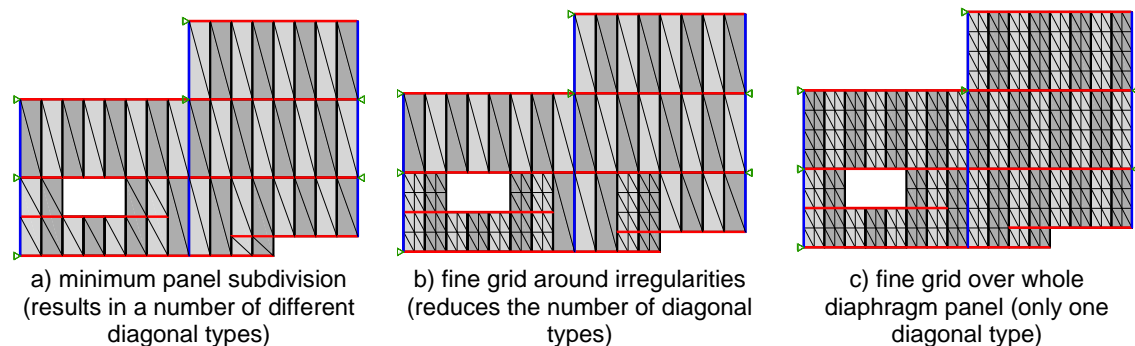


Figure 11.6 Examples of different truss grid spacing

Stress concentrations are normally avoided by transferring or redistributing them over a certain length via nailed steel strips or drag beams into neighbouring undisturbed portions of the diaphragm. Numerical issues with stress concentrations as known from other materials are therefore less common and the use of a more refined mesh in such position is not necessary. If discrete forces are to be transferred locally (via metallic fasteners or special steel elements), the connection needs to be verified considering appropriate increased edges distances and by preventing any possible brittle connection failure (i.e. tension perpendicular to grain).

11.2.4 Diaphragm deflection

The deflection of timber diaphragms can be determined directly with the Equivalent Truss Method outlined above.

In the case of regular diaphragms spanning between two supports, the mid-span deflection Δ can also be determined as

$$\Delta = \Delta_{bending} + \Delta_{shear} + \Delta_{fastener\ slip} + \Delta_{splice}; \quad (11.26)$$

where

- $\Delta_{bending}$ is the flexural deflection of the diaphragm considering the chords acting as a moment resisting couple;
- Δ_{shear} is the deflection of the diaphragm resulting from the shear deformation of the sheathing panel;
- $\Delta_{fastener\ slip}$ is the deflection of the diaphragm due to fastener slip;
- Δ_{splice} is the deflection of the diaphragm due to chord connection slip.

$$\Delta_{bending} = \frac{5WL^3}{192EAH^2}; \quad (11.27)$$

$$\Delta_{shear} = \frac{WL}{8GHd}; \quad (11.28)$$

$$\Delta_{fastener\ slip} = \frac{1}{4}\delta(c_1 + c_2\alpha)m; \quad (11.29)$$

$$\Delta_{splice} = \frac{\sum \delta_s x}{2H}; \quad (11.30)$$

where

- W is the lateral uniformly distributed load applied to the diaphragm;
- L is the span of the diaphragm;
- E is the elastic modulus of elasticity of the chord members;
- A is the cross sectional area of one chord;
- H is the distance between chord members (diaphragm height);
- d is the sheathing panel thickness;
- G is the shear modulus of the sheathing;
- m is the number of sheathing panels along the length of the chord member;
- α is the sheathing panel aspect ratio $\alpha = b/h$ (b is the length in chord direction);
- δ is the fastener slip of the panel-to-panel connection at the diaphragm support from code provisions or experimental data;
- x is the distance of the splice from the origin;
- δ_s is the splice slip in the chord;
- c_i is the number of connections rows along sheathing panel edge;
 - c_1 number of lines of fasteners between adjacent panels along the sheathing panel height h ;
 - c_2 number of lines of fasteners between adjacent panels along the sheathing panel length b ;

For LTF diaphragms, the panels are connected via a framing element, requiring two lines of connections, therefore $c_1 = c_2 = 2$. For massive timber panels no framing element is necessary along the longitudinal panel edge, c_1 is therefore typically 1 (if connection a connection with a splice plate is used, $c_1 = 2$). The heads of the panels are sitting normally on a beam, requiring two lines of fasteners to transfer the forces and therefore $c_2 = 2$.

11.3 DIAPHRAGM CONNECTIONS AND DISPLACEMENT INCOMPATIBILITIES

The diaphragm panel connections and the diaphragm connection to the lateral load resisting system depend on the flooring type and diaphragm forces involved, as well as on the connection's cost, manufacturer capabilities and builders' preference. Therefore a number of different connection options are available and no unique best performing solution can be given.

From a structural performance point of view, the connection capacity, the connection stiffness, the type of connection failure mode and possible displacement incompatibilities will influence the type of connection.

11.3.1 Connections between single timber floor elements

To connect two single wooden panels together, the connection systems shown in Figure 11.7 are suggested:

- a) nailing of adjacent panels with half-lapped joint;
- b) wooden spline in recess between panels with screws or nails;
- c) inclined fully threaded screws, or regular screws at 90° between floor joists;
- d) nailing of panel to the next joist/framing member;
- e) double inclined screws in shear between solid panels;
- f) tongue and groove with double inclined fully threaded screws.

These connections are of general validity and are to be designed in accordance with code provisions or manufacturer information in order to guarantee adequate shear transfer.

Gluing of diaphragm panels is generally not recommended, as it would result in very brittle failure modes. If panels are glued to the framing elements/joists, then at least the connection between the joints should be designed with metallic fasteners (see Figure 11.7c). In general it is recommended to consider connections with yielding failure mechanisms to prevent brittle

diaphragm failure in the case of higher than predicted seismic loading prevent brittle diaphragm failure.

Because of the possible displacement incompatibilities as discussed later, special detailing for floor panel connections close to the beam-column-joints may be necessary.

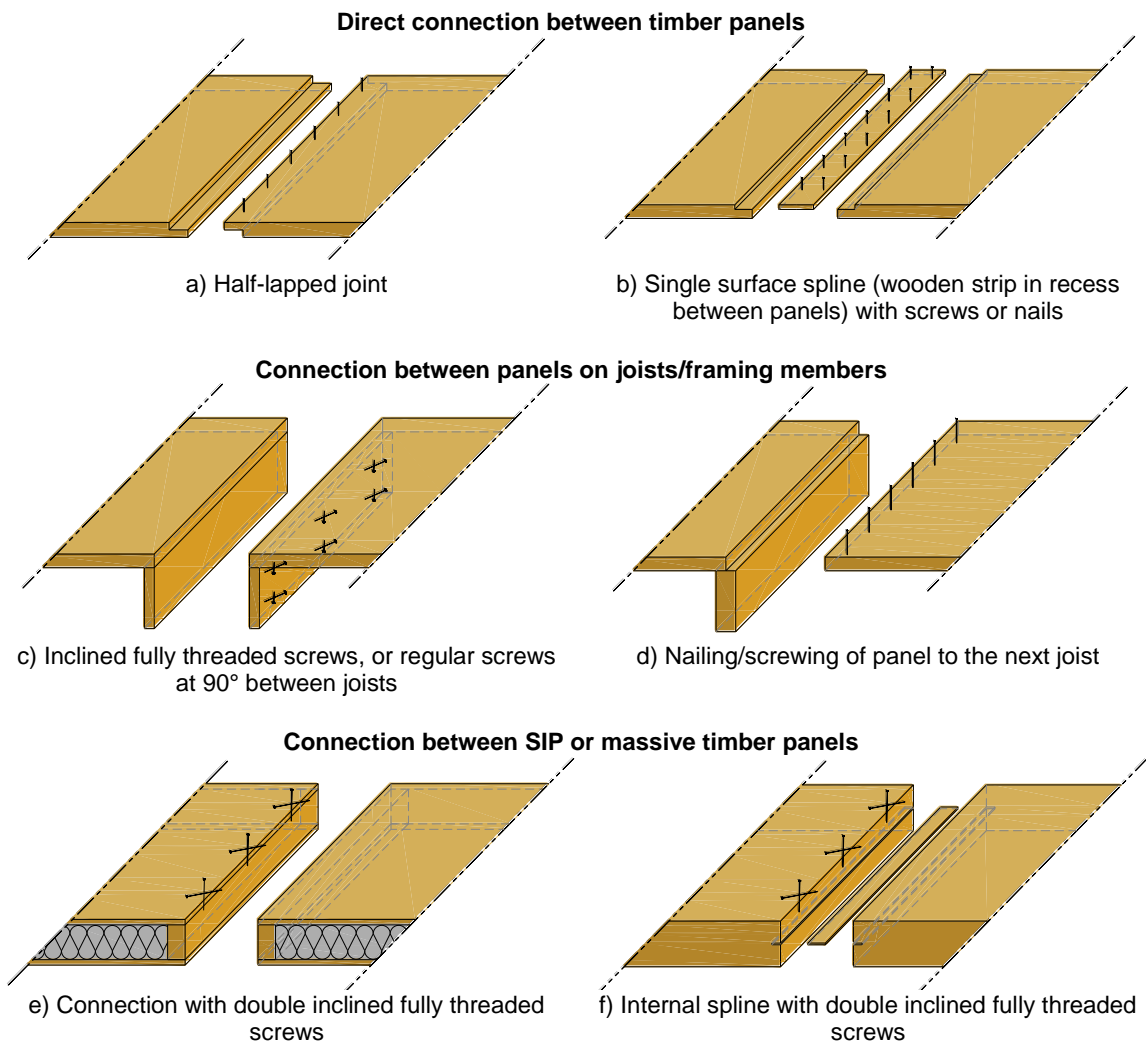


Figure 11.7. Connection details between floor elements

11.3.2 Chord beams

Chord beams are required to resist the diaphragm bending in the form of tension and compression forces. It is paramount that any splices in the chord beams are designed correctly for both tension and compression forces due to load reversals. Chord splices also influence the diaphragm stiffness and should be designed as stiff as possible.

In the case of re-entrant corners or diaphragm set-backs, the forces in the chords need to be transferred via the panel elements to the next chord or strut beam as shown in Figure 11.8 in

order to provide force continuity. Stress concentrations in the panels and the forces in the beams can be determined with the Equivalent Truss Methods.

Alternatively, the discontinuous chord can also be ignored and the next continuous internal beam can be considered as the chord beams. The internal chord beam needs to carry higher forces because of the smaller lever arm. Higher displacements and therefore potential damage at the discontinuities need to be taken into account with this approach.

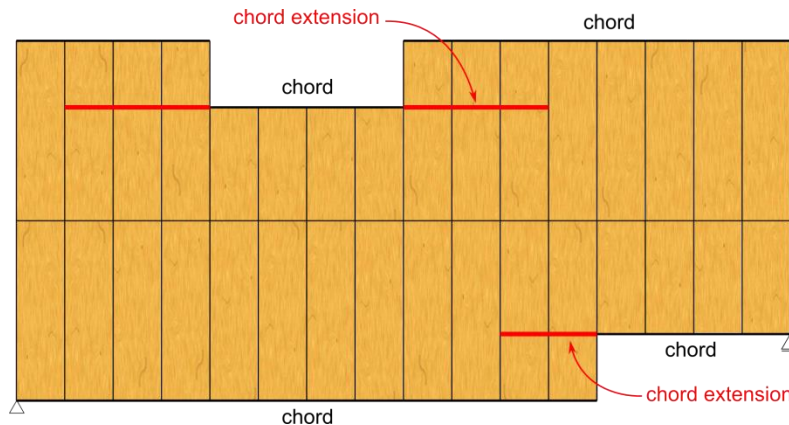


Figure 11.8 Chord discontinuities

11.3.3 Collector and strut beams

Collector beams collect the unit shear forces along the diaphragm depth and transfer them to the next lateral load resisting element. The same element therefore needs to work in tension and compression. Because of openings and other floor irregularities, additional strut/drag beams have to be placed to transfer the forces from the disturbed areas to the remaining diaphragm. The forces in these members need to be determined with rational analysis, like the Equivalent Truss Method.

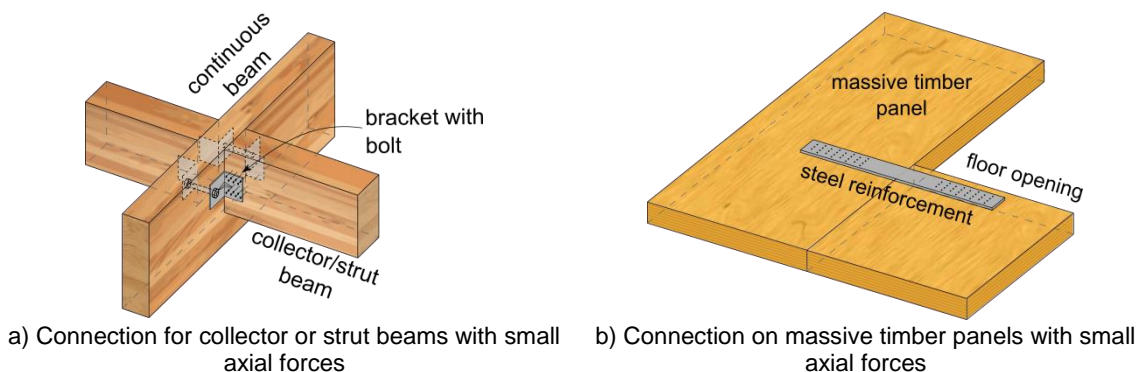


Figure 11.9 Force transfer in timber diaphragms due to irregularities

The biggest challenge in the design of these beams is the potential intersection with other members. Since it is of paramount importance to transfer the axial forces correctly,

connections need to be designed accordingly. Figure 11.9a shows a connection for smaller axial forces for two orthogonally running beams. Tension forces are transferred by the bolt and the steel angles, compression forces are transferred by compression. In the case of massive timber panels, dedicated strut beams can sometimes be avoided by transferring tension forces through a nailed steel strip to the adjacent panel(s) as in Figure 11.9b. For such cases possible tension forces perpendicular to grain need to be considered.

Figure 11.10a shows a Quick-Connect connection (Quenneville et al. 2011) suitable for larger load transfer like for chord beams. A steel version of this connection is shown in Figure 11.10b used in the Kaikoura District Council Building.

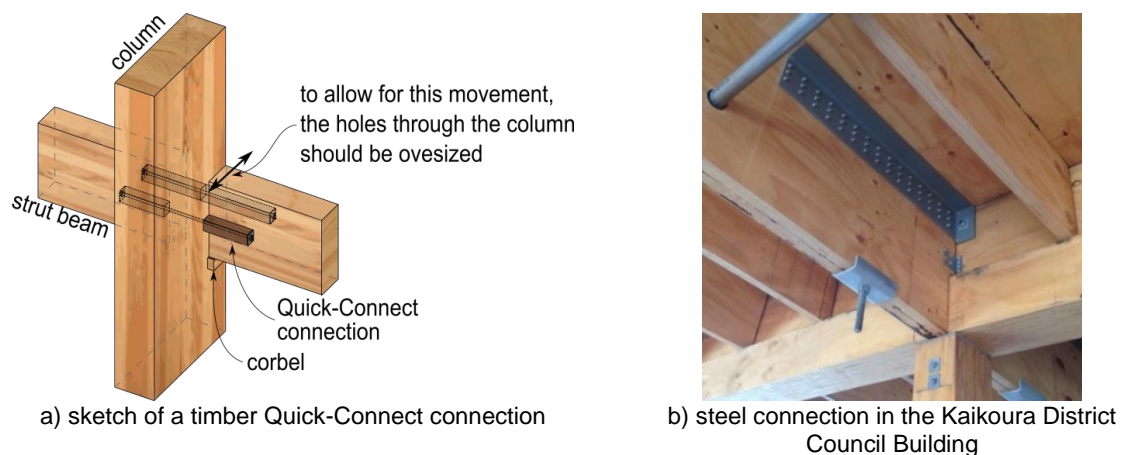


Figure 11.10 Possible details for a chord/strut beam splice

Most of these collector and strut beams also carry gravity loads, so their section size and connection design needs to be carried out based on the respective load combinations.

Depending on the direction of the earthquake attack, chord and collector beams swap their functions. It is therefore necessary to determine the force demand in the elements from all possible load scenarios (line of attack and direction) and to determine appropriate section sizes and design splices accordingly.

11.3.4 Connections between diaphragms and frames

11.3.4.1 Diaphragm panel to frame connections and frames

In this section, timber-only floors running perpendicular to the seismic and gravity frames are considered. The floors are considered to transfer vertical gravity forces and horizontal shear forces to the frame beam, which acts as a collector or strut. For floors sitting in between the beams, gravity loads can be transferred by a timber corbel, a pocket in the main beam or steel

hanger brackets as shown in Figure 11.11. The horizontal shear forces in the diaphragm can be transferred directly by nailing or screwing the sheathing panels to the top of the beam.

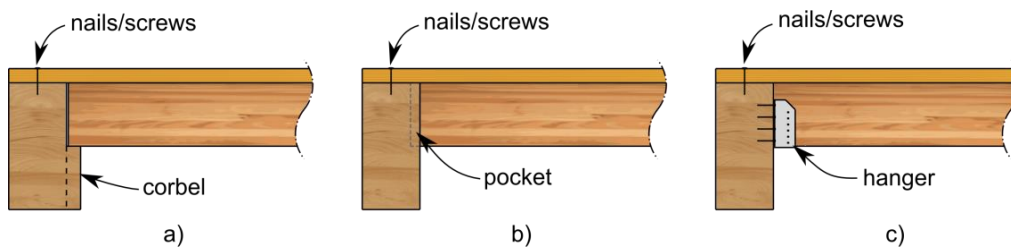


Figure 11.11 Suggested floor to frame connections (floor joists flush with beam): a) floor joist on corbel, b) floor joist in pocket, c) steel bracket/hanger

Where the floors sit on top of the beams, gravity forces are transferred by direct contact. Shear forces can be transferred by using inclined fully threaded screws or by connecting the sheathing panels to blocking elements which are again joined to the beam by screws or steel plate elements (see Figure 11.12).

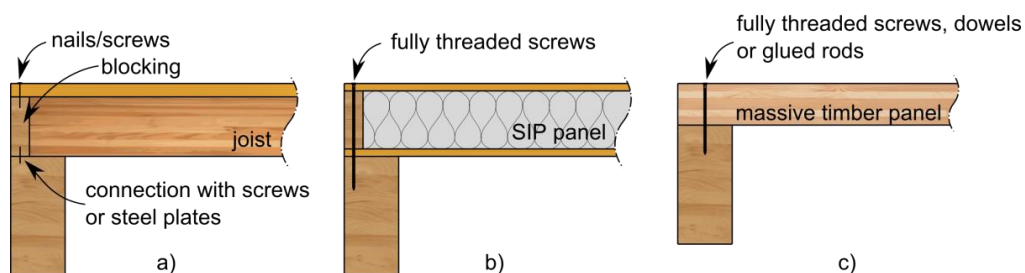


Figure 11.12 Suggested diaphragm to frame connections (floor joists on top of beam): a) floor joist sitting on beam – additional blocking required, b) Structural Insulated Panel (SIP) on beam, c) solid timber floor on beam

Independently from the seating detail chosen, enough bearing surface must be guaranteed also in case of gap opening at a beam-column interface due to geometric beam elongation.

11.3.4.2 Panel connections to accommodate frame elongation

Information on the experimental testing and derivation of the design recommendation for the diaphragm design in frame structures can be found in Chapter 8.

Ductile timber frames will experience beam elongation under design earthquakes due to geometric gap opening (in post-tensioned Pres-Lam frames) or yielding of the steel elements (yielding of the glued rod, external steel plate etc.) at the beam-column-interface. Although this effect is desired in order to achieve ductility and/or damping in the system, this displacement demand has the potential to lead to tearing in the floor as shown in Figure 11.13.

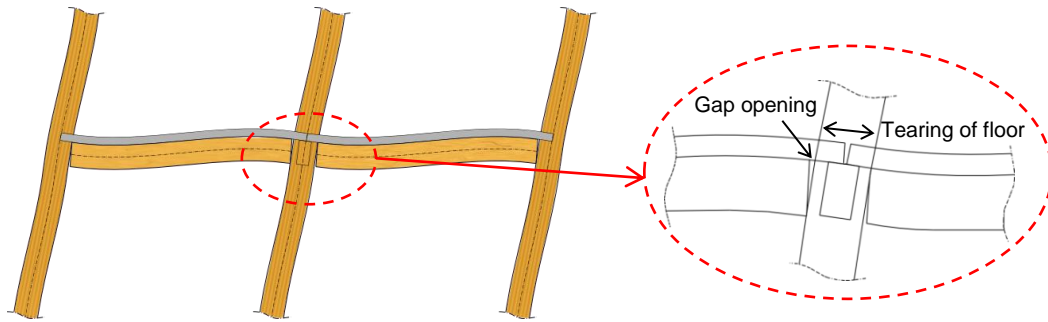


Figure 11.13 Tearing of the floor due to frame elongation

This elongation of the floor has to be allowed for without a brittle tearing of the plate element, as it would cause permanent damage and compromise the shear transfer. The flexibility of the timber elements and the low stiffness of the steel connections allow for two simple design solutions for engineered timber floor panels:

Solution 1 - Concentrated gap (see Figure 11.14):

As the required deformation in the floor level occurs only at the beam-column-joint, a joint between two adjacent floor panels should be positioned accordingly. This joint needs special detailing, whereas other panel joints can be designed normally.

- For floors with sheathing panels and slender joists, only the lower part of the joist should be connected, so that the joist can bend up its height, but still guarantee shear transfer (see Figure 11.15a). The sheathing panel to joist connection should be designed with sufficient capacity and appropriate minimum distances to allow for the joist bending (i.e. the corresponding forces are perpendicular to the joist edge as opposed to the shear forces which are acting parallel to the panel edges).
- For floors with stiff joists, special steel elements can be used. These should allow the panels to move apart from each other, but still transfer shear forces (an example is shown in Figure 11.15b). Seismic gaps in the floor finishing and the wall linings have to be provided in order to allow these deformations to occur.
- For a floor with massive timber panels running perpendicular to the frame direction, the displacement demand should be provided mainly by the connection of the panels to the transverse beam. This can be achieved by the use of a connection with inclined screws as shown in Figure 11.14. In the case of gap opening, the screws will deform elastically in dowel action but will keep transferring shear when the seismic action runs perpendicular to the frame direction. The seismic shear forces should be transferred to the longitudinal beams with inclined fully threaded screws.

To achieve some panel gap spreading on panels further away from the beam-column-joint location, the panels close to the disturbed area should not be connected to the main beams. The remaining panels however will need to transfer bigger diaphragm shear forces to the main beam.

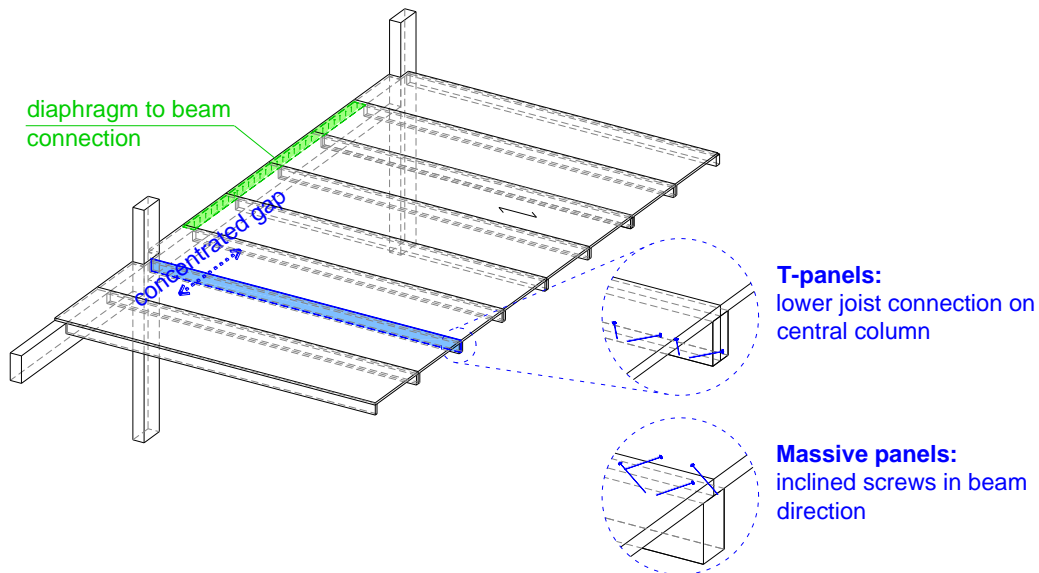


Figure 11.14 Sample design for a concentrated floor gap

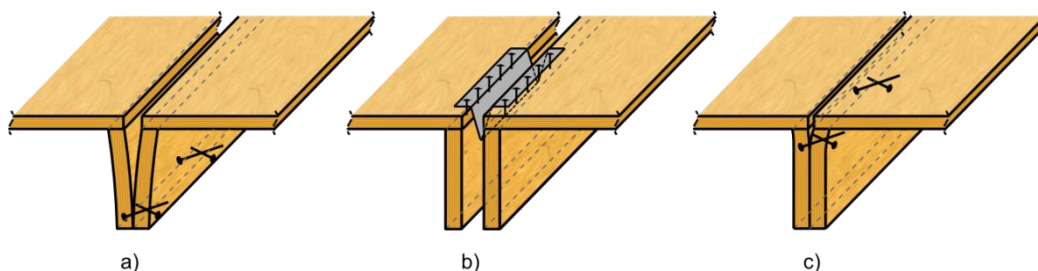


Figure 11.15 Details for a concentrated floor gap a) lower joist connection, b) connection with thin steel plate, c) upper joist connection

Solution 2: Spread floor gaps and panel elongation (see Figure 11.16):

As an alternative to a concentrated gap at each column location, detailing for uniformly spread gaps can be used. The required deformation will be accommodated by a number of small panel gap openings and the elongation of the sheeting panel itself.

Two to three floor elements each side of the interested beam-column-joint should be connected to each other by means of metallic connectors like nails or screws (like an upper joist connection shown in Figure 11.15c or a connection with a nailed spline as in Figure 11.7b). The connection needs to guarantee full shear transfer between the elements, but should be flexible enough to allow for a small displacement. Small gaps will hence open in several panel joints and the sheeting panels will elongate. The panels close to the beam-column-joint(s)

should not be connected to the beam to transfer diaphragm forces, as this would prevent the development of floor gap openings and panel elongations further away from the area of interest.

The floor finishing should be chosen to be elastic enough to follow the formation of the spread gaps or it might require some cosmetic repair after a bigger seismic event.

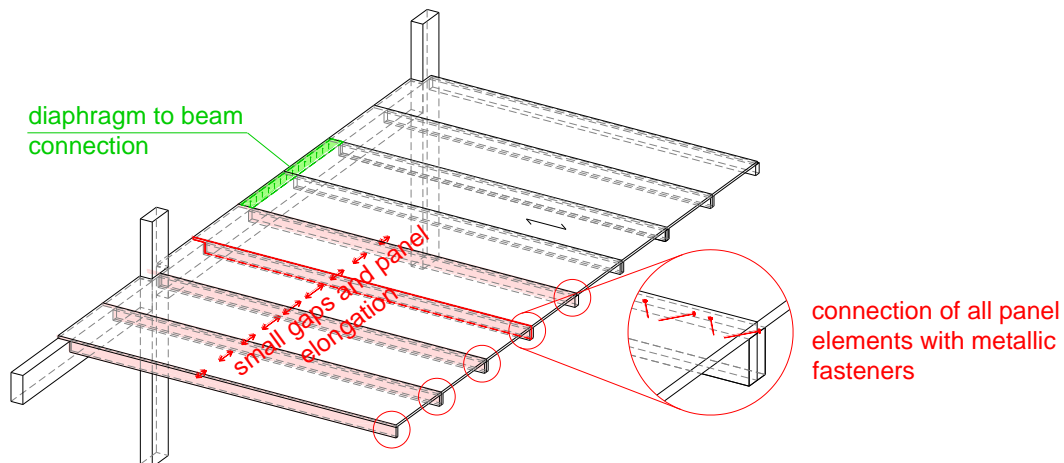


Figure 11.16 Sample design for a spread floor gap

Independently from the type of panel connection chosen, a gap in the panels around all frame columns should be provided to further prevent interaction and potential damage to the columns and/or floor elements. The size of the gap can be estimated from the calculated gap opening at the beam column joint.

Transverse beams should be well connected to the frame columns, so to prevent a possible pushing out of the columns due to the beam elongation. This tie action in the beams is also necessary to provide buckling restraint to the frame columns under gravity loads. The New Zealand Concrete Code NZS 3101 (Standards New Zealand 2006) provides methods to estimate the force demand in the ties; such values should also be used in timber structures.

In Pres-Lam frames, the frame beams are normally tied together by post-tensioning strands through the columns. When these beams are acting as chords, tension forces are introduced. These additional force needs to be taken into account when designing the post-tensioning and anchorages.

A different solution to avoid the frame elongation problem on a multi-bay frame consists of connecting the diaphragm only to one bay and letting the diaphragm slide over the remaining beams. This solution however might result in high shear forces at the connection between the

diaphragm and the beam and would require proper detailing to allow for the sliding of the diaphragm in respect to all other elements.

11.3.4.3 Displacement incompatibilities of the external columns

At the external columns the frame elongation can be accommodated by a flexible connection similarly as for the massive timber panels, or by the sliding of the transverse beams on the corbel as shown in Figure 11.17. A gap in the flooring elements around the column prevents direct contact between the column and the diaphragm. The collector beam transfers the forces to a shear wall or other lateral load resisting system.

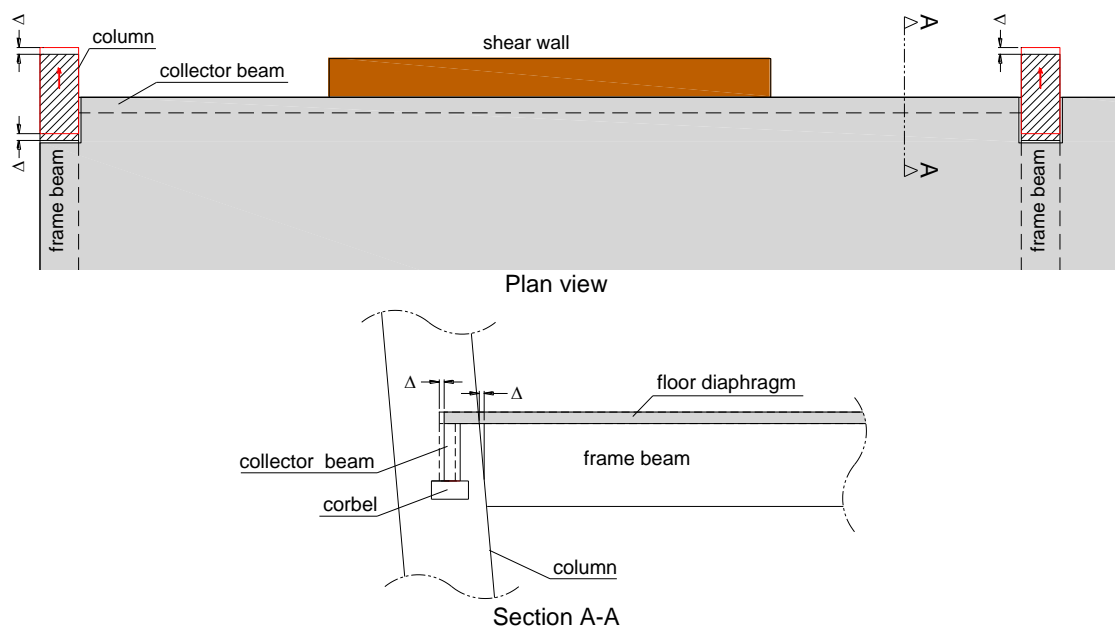


Figure 11.17 Frame elongation effect on external column – the floor diaphragm is sliding on the corbel

11.3.4.4 Connections to accommodate frame elongation for concrete floor topping

The introduction of a concrete topping in a ductile timber frame structure requires more attention in the diaphragm design because displacement incompatibilities cannot be accommodated in the same way as they can in engineered timber. As a result of the low tensile strength of concrete, tearing forces due to frame elongation and bending forces due to uplift and rotation of the walls tend to crack the diaphragm topping. If these cracks become larger, the force transfer is interrupted and the diaphragm action is compromised (Bull 2004).

For frame structures with Timber-Concrete-Composite floors (TCC), the displacement incompatibility required from the beam-column-gap opening can be accommodated similarly as to the concentrated floor gap solution already described for timber diaphragms. As

suggested in Figure 11.18, the concrete should be pre-cracked along the line of the beam-column-joint.

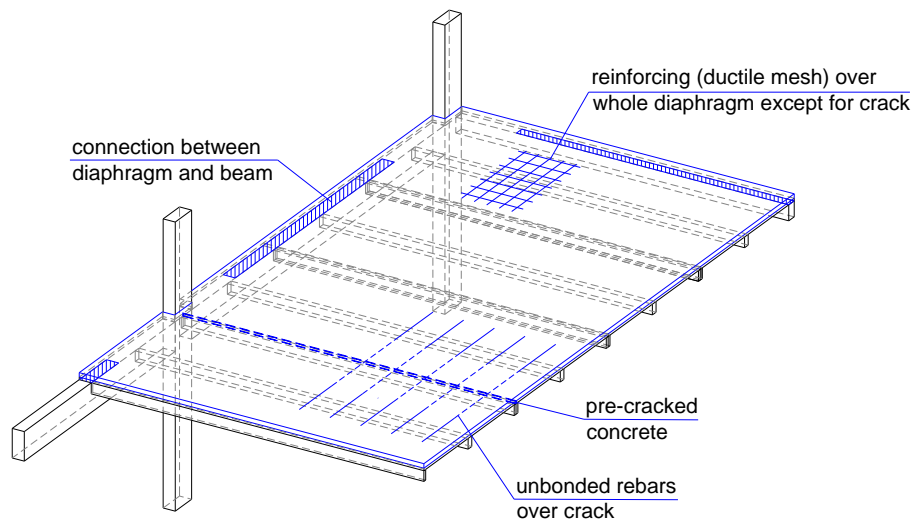


Figure 11.18 Suggested detailing for a TCC floor in a frame system

For the internal columns the frame elongation effect is given by the gap opening Δ_1 minus the elastic losses Δ_2 of the beam pushing into the column (see Figure 11.19). This causes tearing forces around the column and therefore the formation of cracks in the concrete topping.

To guarantee the shear transfer between the sub-diaphragms, which is needed for the diaphragm action in the transverse direction and to link the single sub-diaphragms together, unbonded rebars can be placed over the potential crack line. The unbonded length is chosen in order to have only elastic deformation if the crack would open along the entire line. After a crack has occurred and therefore the shear-friction mechanism cannot be activated anymore, the bars can still transfer shear in dowel action.

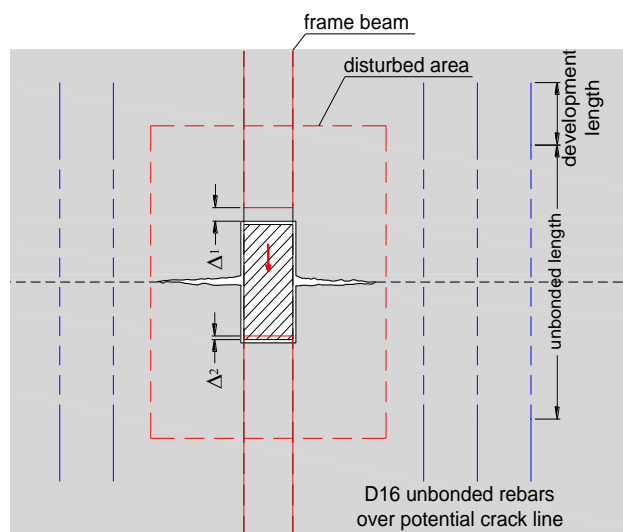


Figure 11.19 Cracking due to frame (beam) elongation on an internal column

It has to be noted that this solution for TCC floor is only based on theoretical considerations. Even though already implemented in real constructions like the Trimble Navigation Building (Brown et al. 2012), further investigation and some experimental testing is recommended. Dowel action might be delayed in case of large gap openings until a kinking effect allows for the shear transfer. Latter however implies plasticization of the unbonded rebars and potentially large deformations.

The diaphragm has to be tied appropriately to the collector beams. One way of doing this is shown in Figure 11.20, where staggered starter bars are cast into the concrete slab. The force transfer from the diaphragm to the beam should be guaranteed in the central portion of the beams, leaving it unconnected close to the beam-column-joints (in the disturbed areas shown in Figure 11.21). In this way frame elongation will not compromise the force transfer which starts away from the disturbed areas where the displacement incompatibility is attenuated.

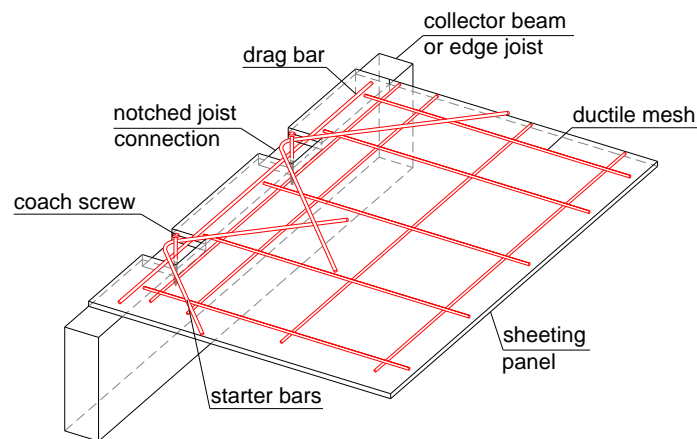


Figure 11.20 Suggested connection between the concrete topping and the timber beam

If the floor gap opening occurs along a collector beam or tie back, care has to be taken as the cracking of the concrete can compromise the force transfer. Ideally the pre-crack should be placed away from any connection to the beams.

Figure 11.20 shows a suggested connection between the concrete topping and the collector or frame beam. The diaphragm shear is introduced to the beam via notched connections used for the TCC design (see Gerber et al. (2012)). If the concrete topping is connected to the beam directly, the beam has to be designed as a composite section. As an alternative, an edge joist from the TCC floor can be connected to the frame beam via a timber-timber connection. Starter bars are normally required by design codes, to tie the collector/strut beams to the diaphragm.

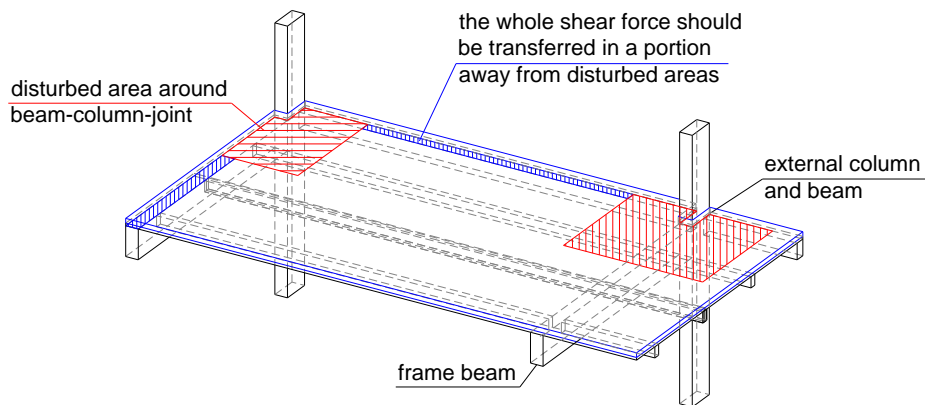


Figure 11.21 Shear transfer between the concrete topping and beams

For the design of concrete diaphragms the design recommendations given in Bull and Henry (2014) should be considered.

11.3.4.5 Out-of-plane rocking of frames

In the case where the earthquake force acts perpendicular to the frame, the whole building will undergo a certain drift (depending on the lateral load resisting system in this direction) and hence the frame may have to rotate out of plane. As indicated in Figure 11.22 it is suggested to leave a construction gap between the floor elements and the beams (also useful for construction tolerance and variances in ambient conditions). This will allow the beam to rotate, without damaging the timber floor or the connection to it. The connection between the beam and the floor also needs to transfer the dragging force to rotate the frame out of plane.

It needs to be guaranteed that enough seating area is provided, also for larger than expected deformation, caused by a large seismic event (MCE event).

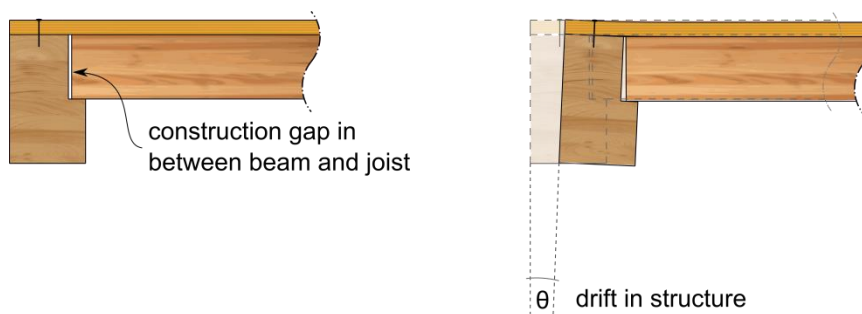


Figure 11.22 Construction gap between a timber floor and supporting beam to allow for rotation undeformed state (left) and deformed state (right)

The frame beams might however also undergo rotational deformation in respect to their columns. The combination of a seating detail with corbels and the presence of the post-tensioning strand can allow for the rotation without any damage. As an alternative, shear keys

inserted in the hollow core of the box section can also allow for the rotation. High deformation in the timber elements may occur because of high local stress concentration; such effects however are reversible once the seismic load drops and the structure returns to its initial position.

11.3.5 Connections between diaphragms and walls

Information on the experimental testing and derivation of the design recommendation for the diaphragm design in wall structures can be found in Chapter 9.

Cantilevered shear walls, in the form of post-tensioned rocking walls, LTF walls, massive timber walls with ductile hold downs or connected with ductile fasteners along their vertical joints, will rotate and uplift under design earthquakes. Such behaviour is desired to achieve wall-foundation gap opening, and therefore to yield the hold downs or other reinforcement devices or to yield the smeared fasteners along the vertical joints. Because of the presence of diaphragm-to-wall connections, necessary to transfer the horizontal forces, the floor diaphragms are subjected to out-of-plane bending, because of the rotation and uplift from the foundation as shown in Figure 11.23.

This imposed deformation demand has the potential to damage the floor slab as well as to increase the wall strength and stiffness and to increase axial forces in the wall and other connected gravity resisting elements. The displacement incompatibility can be accommodated by the out-of-plane flexibility of the floor and the flexibility of the connection. Ideally the incompatibilities can be removed by releasing the rotational or vertical movement degrees of freedom.

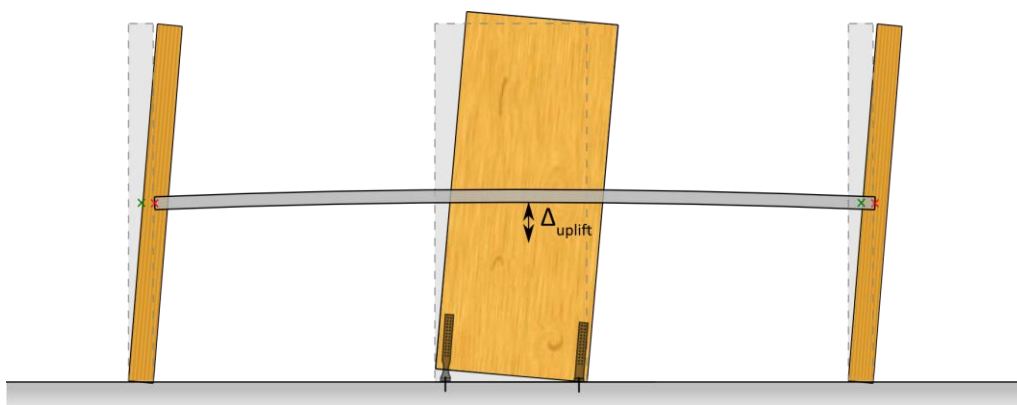


Figure 11.23 Floor out-of-plane bending due to wall rotation and uplift

For wall structures, the diaphragm and possible gravity forces may be transferred via the collector beam to the lateral load resisting system as shown in Figure 11.24. The diaphragm

panel element is directly connected to the collector beam with nails or screws with configurations similar to those in Figures 11.11 and 11.12. The most appropriate connection detail to link the collector beam to the walls depends on the span direction and out-of-plane stiffness of the floor. For floor elements running parallel to the wall only horizontal forces have to be transferred, otherwise gravity forces have to be resisted as well.

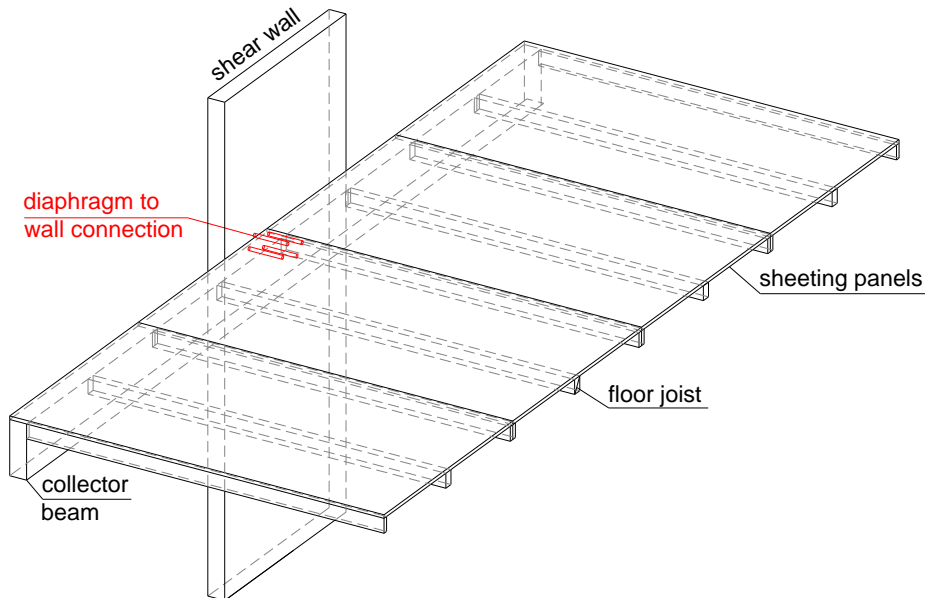


Figure 11.24 Scheme of a typical diaphragm to wall connection

To minimize the effects of displacement incompatibilities, the collector beam should be connected to the wall by a single connection placed near the centre of the wall. An eccentric connection will induce bigger rotations and uplifts in one direction of rocking. Because the vertical displacement incompatibility is normally much smaller than the deflection limit under serviceability loads, it generally does not create any damage to structural or non-structural elements.

For flexible floors with a relatively low out-of-plane stiffness, economical connections with closely spaced bolts, inclined fully threaded screws or large diameter bolts can be used. For stiffer floors a steel-to-steel solution with a pin in a slotted hole is recommended to avoid displacement incompatibilities. To minimize friction, brass shims or Teflon pads should be used at areas of contact. Boundary columns can be provided at each end of the wall to reduce interaction of the floor diaphragm with the wall, in which case the collector beams should be pin-connected to these boundary columns via closely spaced bolts or a large diameter dowel.

These solutions apply to all floor systems including timber only and concrete floors. Recommended solutions are listed in Table 11.2 in order of increasing cost and reduced interaction between the wall and floor.

Table 11.2. Possible wall to collector beam connections

Connection type	Force transfer	Displacement incompatibilities		Comments
Large diameter dowel	Horizontal shear and gravity	Rotation is allowed	Uplift is not allowed	The embedment strength needs to be determined carefully and splitting of timber avoided
Closely spaced bolts	Horizontal shear and gravity	Rotation is partially allowed ¹⁾	Uplift is not allowed	Simple and cost effective solution, the flexibility of the connection allows for some rotation
Inclined fully threaded screws	Horizontal force only	Rotation is allowed	Uplift is allowed	Inelastic behaviour of the screws might occur, damaged screws can be replaced or additional screws added. Very economical solution.
Slotted steel plate	Horizontal force only	Rotation is allowed	Uplift is allowed ²⁾	Relatively expensive and laborious connection, the interaction is significantly reduced.
Wall end-columns and pinned connection	Horizontal shear and gravity	Rotation is allowed	Uplift is allowed	Essentially eliminates the interaction, increases the construction cost significantly.

¹⁾ given the possibility of using oversized holes in timber and by accounting for the relatively flexible dowel connection, the rotation of the wall normally can be accommodated for limited drift ratios.

²⁾ special measures to reduced friction at the contact interface are required.

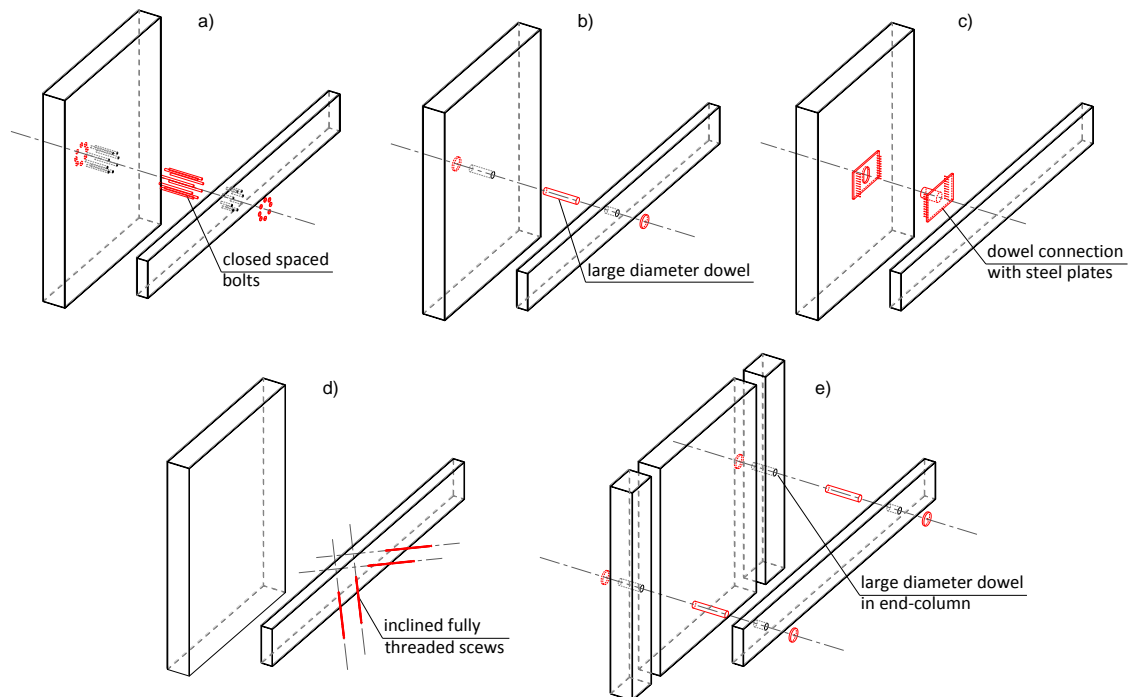


Figure 11.25 Recommended beam-to-wall connections: a) closely spaced bolts, b) large diameter dowel, c) steel plates with slotted hole and pin, d) inclined fully threaded screws, e) large diameter dowel in end-columns

11.3.5.1 Modelling of the floor-wall interaction

If the displacement incompatibilities between the wall and the floor beams are not avoided by a special connection, the interaction between the two needs to be taken into account, since both the strength and the stiffness of the lateral load system increases. This is because the imposed rotation and uplift is counteracted by the beam, providing additional re-centering forces and moments to the wall as shown in Figures 11.26b and c.

A number of software packages allow for pushover analysis to be carried out on a system like those shown in Figure 11.27. To obtain realistic wall rotations and uplifts, the modelling of the wall-foundation interface with multi-springs or other elements is necessary.

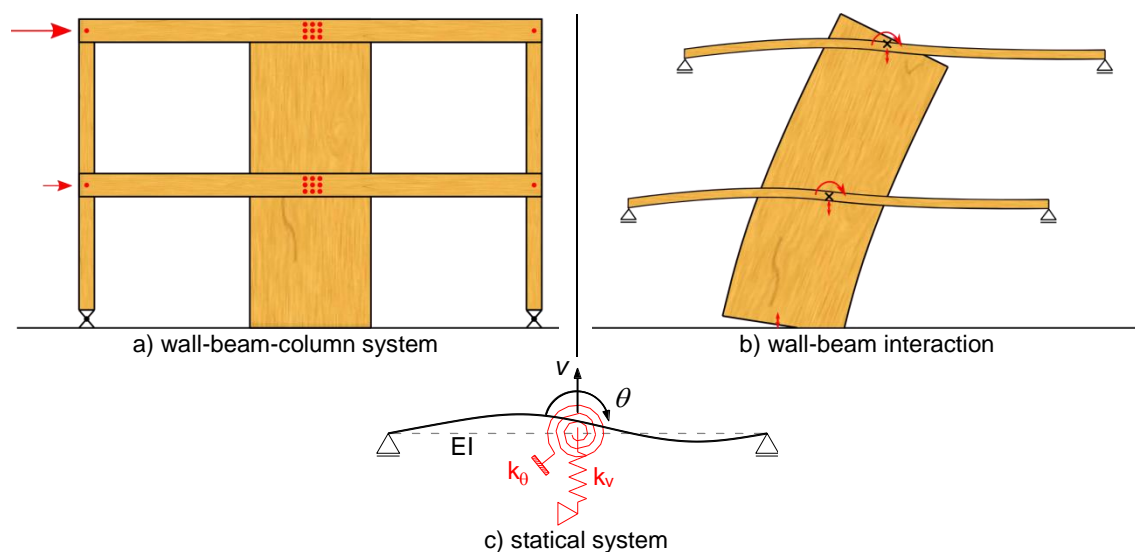


Figure 11.26 Wall-to-beam system with statical system

The pushover analysis of the wall-to-beam system can also be obtained by an analytical procedure. For each imposed rotation in the wall, the force and moment equilibrium at the wall-foundation interface can be obtained by iteration. For the given deformed shape, the vertical force and moment at the wall-to-beam connection due to the displacement incompatibility needs to be determined. These re-centering actions, which are a function of the beam bending stiffness EI , the connection rotational and translational stiffness k_θ and k_v respectively, need to be considered in the equilibrium conditions.

Such a procedure for a post-tensioned Pres-Lam wall is presented in Chapter 10. Depending on the connection type chosen, different connection stiffnesses as outlined in Figure 11.27 need to be considered. The general formulation for the beam-connection stiffness is derived in Appendix D.

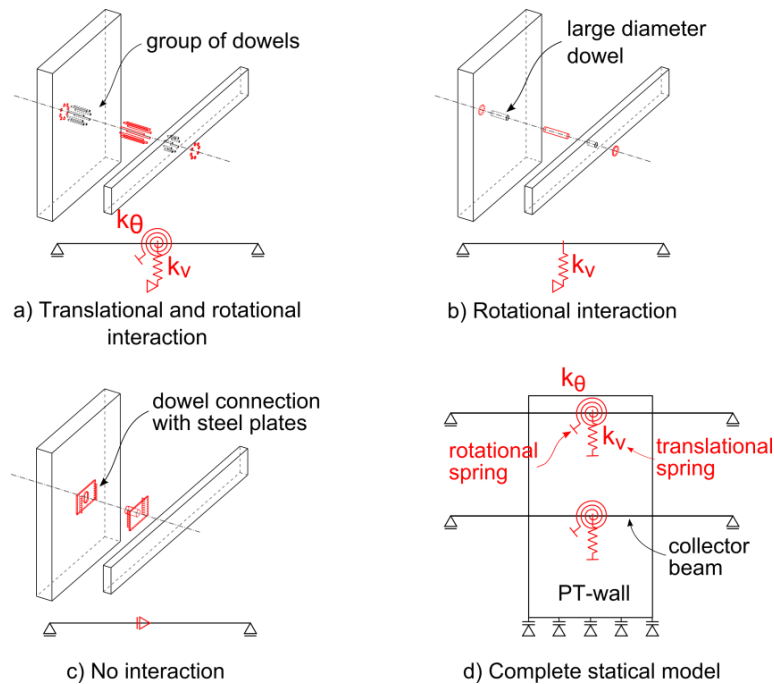


Figure 11.27 Summary of three proposed wall-to-beam connections: a) translational and rotational interaction, b) translational interaction and c) no interaction with the collector beam. d) shows the complete statical model

11.3.5.2 Connection to core-wall systems

In core-wall systems the same design recommendations regarding the diaphragm-to-wall connections as for single walls should be followed. More attention however must be given to the displacement incompatibilities arising from the out-of-plane rotations of the walls.

Because core-wall systems normally resist horizontal loads in both principal directions, collector beams in both directions need to be connected to the walls. The beams must be connected to the walls with connection details allowing for the displacement incompatibilities. Because of height constraints, collector beams are normally placed at the same height and need to be spliced at their intersection at the core-wall. To allow for both the axial force transfer in the beams and to allow for the vertical displacement imposed from the orthogonal walls, thin out-of-plane flexible steel plates as shown in Figure 11.28 are suggested. Steel plates fixed at the top and bottom of the beams can be connected by nails, rivets or fasteners at a sufficiently long distance from the intersection to allow for elastic bending of the plates. The flexibility of the beam-to-wall connection, the bending of the beams and the flexible splice plate must allow for the expected displacements.

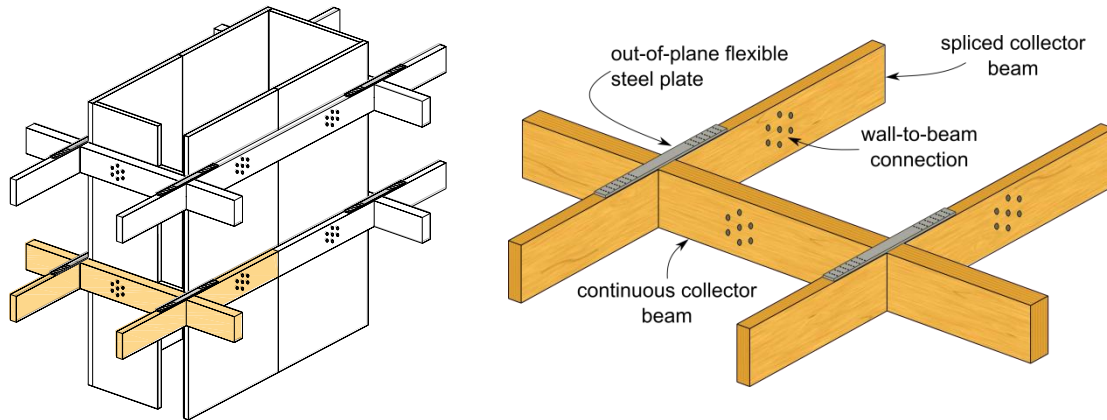


Figure 11.28 Collector beam connection with out-of-plane flexible steel plates

The unit shear forces from the diaphragm should be introduced to the collector beams at a distance from the intersection point of the collector beams, because in these disturbed areas the relative vertical movement of the beams might result in pull-out of the panel fasteners. Shear transfer in this area should not be relied on and ideally panel connections should be avoided in this area as shown in Figure 11.29, by transferring forces to the collectors at remote locations.

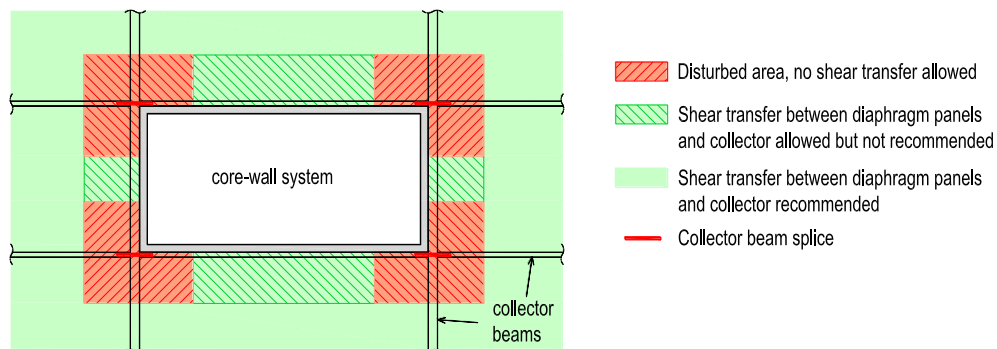


Figure 11.29 Recommended and prohibited areas for the shear force transfer between the core and the floor diaphragms

In the case of rigid out-of-plane diaphragms, a design solution with boundary columns at the corner of the core-wall system should be used. Imposed vertical uplift and rotation from the rocking walls is reduced and only the out-of-plane rotation of the walls needs to be allowed for by the collector beam splices.

11.3.5.3 Connection of concrete floor diaphragms to timber walls

It is generally recommended not to connect a concrete slab directly to the timber walls, but to transfer horizontal forces first along a timber collector beam. In this way the force transfer occurs between the wall and the collector beam and the connection can be designed following the recommendations as discussed above.

The connection between a concrete slab and a collector beam can be carried out as per Figure 11.20, resulting in a solution as outlined in Figure 11.30, where a bolted connection has been assumed.

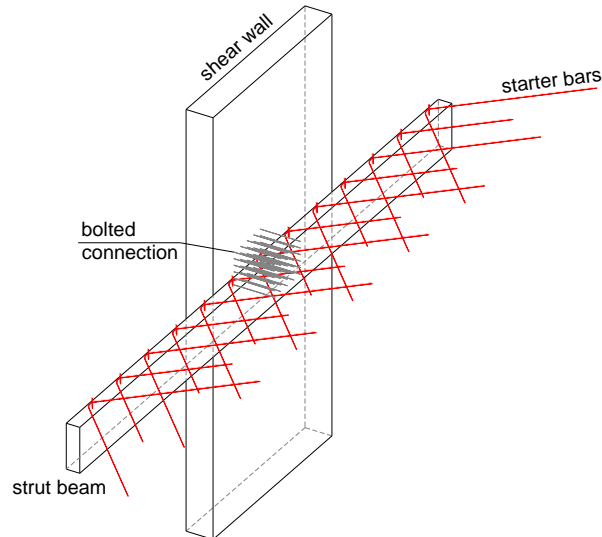


Figure 11.30 Conceptual connection of the diaphragm to the timber strut beam and its connection to the wall

11.3.5.4 Out-of-plane rocking of walls

As for frame structures, the connections between the floor diaphragm, the collector beam and the wall itself have to transfer not only the unit shear forces from the diaphragm action, but also the drag force from the out of plane deformation of the wall. These forces as represented in Figure 11.31 can be wind suction at leeward walls, inertia forces on the façade, or dragging forces from the constraint of vertical elements to move with the rest of the structure under a certain drift.

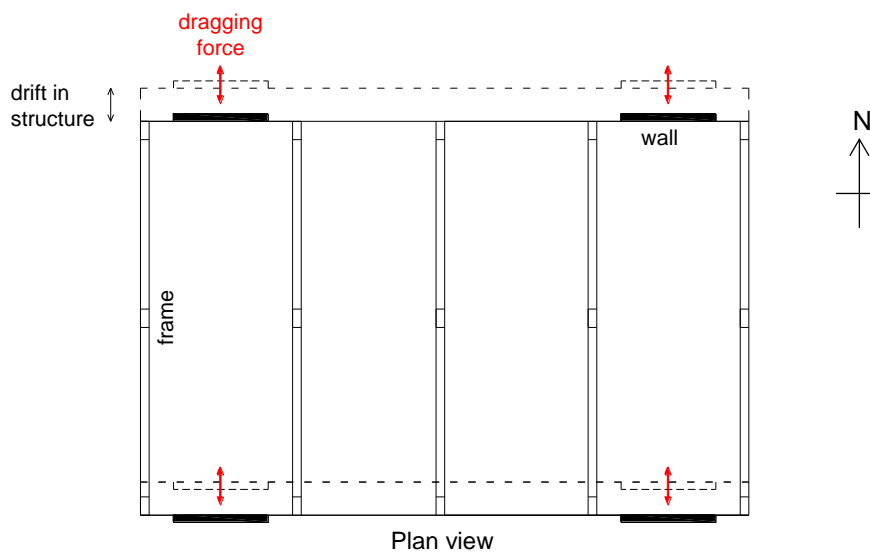


Figure 11.31 Out-of-plane dragging forces on walls from drift in structure

Construction gaps between the floor and the walls as shown in Figure 11.32 must accommodate the displacement incompatibilities.

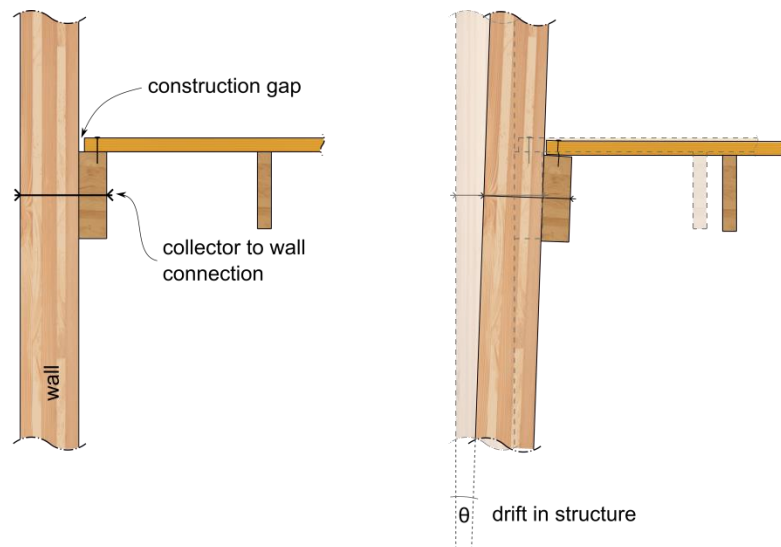


Figure 11.32 Construction gap between a timber floor and supporting beam to allow for rotation undeformed state (left) and deformed stat (right)

12 Conclusions and recommendations for future research

12.1 CONCLUSIONS

This thesis provides tools for estimating the seismic demand and for analysing and designing timber diaphragms in modern timber buildings.

The principal objectives of this work, as presented in Chapter 1, were to provide the design community with tools able to:

- establish the diaphragm force demand under seismic loading;
- analyse the load path and determine the deflections of timber diaphragms;
- provide diaphragm connections to the lateral load resisting system able to accommodate displacement incompatibilities.

These objectives have led to a series of questions which have been addressed with design tools through parametric numerical analyses of multi-storey timber wall and frame structures, a simple Equivalent Truss Model verified through a finite element representation of timber diaphragms and four different experimental setups under quasi-static and dynamic horizontal loading.

For each of the three objectives, the main conclusions are summarized next.

Diaphragm force demand under seismic loading:

- To keep diaphragms in the elastic range, capacity design principles and dynamic amplification need to be included in the diaphragm demand calculations;
- Diaphragm force demand departed notably from the assumed first mode distribution: for frame structures forces were almost constant up the whole building height, for wall structures large forces were observed at the top and bottom stories;
- Diaphragm flexibility did not influence the force demand in frame structures, in wall structures diaphragm flexibility increased the force demand in the lower stories when compared to the results with rigid diaphragms;
- For both frame and wall structures all diaphragms up the height of the building should be designed for the same force demand;
- Simple equations are provided to determine the peak diaphragm demand for frame and wall structures independently of the diaphragm stiffness;

- For non-rigid diaphragms the diaphragm interstorey drift values were notably higher than the target wall drifts and need to be checked in design to protect structural and non-structural elements connected to the diaphragms;
- Storey shear and moment distributions for both frame and wall structures were not significantly influenced by diaphragm flexibility; higher mode effects however need to be taken into account;
- Even though flexible diaphragms increased the structure's period, which normally decreases the seismic demand, the period relative to the structure with rigid diaphragms should be taken to compensate for higher mode effects;
- In addition to inertia forces, diaphragms need to resist transfer forces deriving from vertical irregularities up the building height (podium structures, discontinuous walls, set-backs etc.) or displacement incompatibilities forces of the lateral load resisting system (dual systems with frames and walls, walls with different stiffness etc.);
- Peak floor diaphragm forces occur at different times during an earthquake and should not be applied simultaneously to determine displacements of the structure and therefore transfer forces, as this could lead to conservative values.

Analysis of the load path and determination of the deflections of timber diaphragms:

- An Equivalent Truss Method based on the panel shear stiffness and fastener stiffness can accurately predict the load path in light timber framing and massive timber floor diaphragms, even if the diaphragms are statically indeterminate or have other irregularities;
- The Equivalent Truss Method allows for the determination of the unit shear forces (shear flow), fastener forces (parallel and perpendicular to the panel direction), axial forces in frame elements, chord beams, collector beams and strut beams as well as reaction forces. Since it is based on a stiffness analogy, it can estimate the diaphragm deflections, distribute the forces to the lateral load resisting elements in function of their relative stiffnesses and account for torsional effects;
- The Equivalent Truss Method can easily be extended to include non-linear fastener behaviour;
- In LTF diaphragms the load application type does not influence the load path, as long as forces are introduced and distributed via the framing elements;

- In massive timber diaphragms force introductions along the diaphragm compression and tension edges generate longitudinal stresses in the diaphragm panels and create force components perpendicular to the panel edges which the connections must resist;
- In massive timber diaphragms longitudinal stresses need to be transferred along the panels in order to also activate diaphragm portions away from the point of force introduction, this creates fastener force components perpendicular to the panel edges which need to be taken into account in design;
- Traditional analysis like the girder analogy can be used to analyse regular massive timber diaphragms as long as the force introduction into the diaphragm can be guaranteed;
- Absence of chord beams in massive timber diaphragms result in very flexible diaphragms and generate high tensile forces in the fasteners as well as transverse stresses which have the potential to create brittle failures;
- A simple three term equation is provided to determine the deflection of simply supported regular massive timber diaphragms.

Diaphragm connections to the lateral load resisting system and mitigation of displacement incompatibilities:

Frame structures

- Experimental evidence showed that displacements created by the beam-column gap openings were accommodated within the diaphragm due to the flexibility in the connections and, to a lesser extent, by the elongation of the timber panel members;
- The beam-column joint gap openings were not restrained by the presence of the floor diaphragms;
- *The following two connection options for the floor panels are recommended:*
 1. *A concentrated floor gap* at the position of the beam-column joint. This is the preferred connection for stressed-skin panels with a rigid floor finish, solid timber panels and timber-concrete-composite floors (not tested in this programme);
 2. *Distributed floor gaps and elongation* of the floor diaphragm over several floor panels. This is the preferred detail in the case of a flexible timber floor.

Wall structures

- Experimental evidence showed that the strength of the wall-beam system increased by up to 25% for some connections when compared to the bare wall;
- An iterative analytical procedure including incompatibility forces from the collector beams allows for the accurate determination of the moment-curvature and force-displacement curves of the wall-beam assembly;
- The compatibility forces can be calculated with provided stiffness formulations which are a function of the beam stiffness and fastener stiffness as well as their position relative to the wall;
- The procedure also allows for the determination of the forces and moments acting on the connection and the deformation of the collector beams;
- Based on the experimental evidence, the following connection details between the collector beams and the walls are recommended:
 - *closely spaced bolts, inclined fully threaded screws or large diameter pin* for floors with a relatively low out-of-plane stiffness;
 - *steel-to-steel connections* with a pin in a slotted hole for stiffer floors;
 - *boundary columns* bearing against the walls and connected to the collector beams for very stiff floors.
- To allow for vertical sliding in the steel-to-steel connections, special measures to avoid friction are necessary;
- Rotational incompatibilities proved to have bigger impact on the global behaviour of the wall-diaphragm assembly than uplift incompatibilities.
- Around core-wall systems, orthogonal collector beams should be spliced with out-of-diaphragm-plane flexible connections. Shear transfer from the diaphragm panels into the collectors should occur outside the corner regions of the core.

12.2 ANSWERS TO THE RESEARCH QUESTIONS

The answers to the research questions, as presented in Chapter 1, are listed below:

Determination of the seismic demand in multi-storey timber buildings

1. *Can current seismic analysis methods predict the seismic demand in multi-storey timber buildings?*

Non-linear time history analyses of a series of post-tensioned Pres-Lam timber frame and wall structures with varying heights showed that higher mode effects significantly alter the storey shear force and moment demands as well as displacements. Such effects were found to be more pronounced for timber structures because of the inherent flexibility of the material. Although simplified methods like the equivalent static analysis are normally adequate to design the ductile elements of the lateral load resisting system, all other elements need to be designed for an increased demand including overstrength and dynamic amplification.

Wall structures showed increased storey shear forces at the top stories as well as increased moments in the middle levels for tall structures. Design target drift values were respected, except for very slender walls. Column shears and moments in frame structures were less affected by higher modes, whose effects also contributed to a reduction of interstorey drift.

To account for higher mode effects and overstrength, the methods proposed by Priestley et al. (2007) and later modifications have been applied to the analysed structures leading to very satisfactory estimates of storey shears and moments.

Even though the analysis was only carried out on Pres-Lam post-tensioned frame and wall buildings, the same trend can be expected in other modern buildings made of engineered timber materials, since such structures are normally deflection governed and designed for the same drift limits and therefore have a similar stiffness.

2. *What is the effect of diaphragm flexibility on the seismic behaviour of timber structures*

Results from the numerical analyses showed that diaphragm flexibility increases the fundamental period of the structures. This effect was more pronounced in stiff buildings like in short and medium wall structures. Frame structures, because of their inherent flexibility, showed very little increases in period. The higher mode vibration periods of the structures converged to the diaphragm period, leading to closely spaced modes.

The analysis further showed that diaphragm flexibility had only a small effect on the storey shear and moment distribution and can normally be ignored. The displacements of the lateral

load resisting system were independent from the diaphragm stiffness for frame structures and decreased with increasing diaphragm flexibility for wall structures. Diaphragm displacements (relative to the lateral load resisting system), however, were notably increased for wall structures, resulting in much higher diaphragm interstorey drifts when compared to the drifts measured at the lateral load resisting system. Gravity supporting elements, façade elements and any other non-structural elements attached to the diaphragm could be affected by these increased displacements. It is, therefore, recommended that diaphragm flexibility is included in the verification of maximum displacements or interstorey drifts especially in wall structures.

Diaphragm force demand did not seem to be affected by the diaphragm flexibility in frame structures. On the other hand, for wall structures the diaphragm demand increased in presence of flexible diaphragms, especially at lower stories. In certain cases the peak force at lower stories was of the same magnitude as the top story demand.

3. Is the definition of flexible diaphragms according to current codes adequate to evaluate the dynamic behaviour of a timber structure?

Current code definitions for flexible diaphragms are based on, and intended for, the force distribution from the diaphragms into the lateral load resisting system. The chosen ‘semi-rigid’ diaphragms for the analysed wall structures, even though classifiable as rigid according to New Zealand code provisions, showed increased interstorey drifts and floor forces at lower stories, which need to be considered in design. The current definition should, therefore, not be used to exclude the influence of diaphragm stiffness in the dynamic behaviour of timber buildings.

4. Are current capacity design principles adequate to protect timber diaphragms under seismic loading?

In agreement with a number of international design codes, it is recommended that timber diaphragms be designed as elastic if no specific study is carried out. To achieve this, capacity design principles need to be applied to determine the diaphragm demand. Current loading codes require the application of overstrength factors when designing diaphragms or other capacity protected (brittle) elements. Timber material codes, however, fail to provide overstrength factors for timber structures. Definitions of these factors found in literature were not in agreement in between each other and the choice of these values is normally left to the designer’s interpretation and judgement.

It is recommended that conservative overstrength factors are used for the design of timber diaphragms and, if possible, experimental data relied upon to determine the overstrength of

the ductile elements or connections. Dynamic amplification factors in determining the diaphragm design also need to be considered as discussed in the next question.

In case bigger than expected seismic demands occur (like in the case of a Maximum Credible Earthquake, MCE), brittle failures of diaphragms need to be excluded. To guarantee the resilience of timber structures, it is therefore recommended that panel-to-panel or diaphragm-to-lateral load resisting system connections, which fail in a ductile way, are used.

5. How can the diaphragm force demand in timber structures be evaluated?

The two major contributors to the diaphragm demand are inertial and transfer forces. The former occurs because of the acceleration of masses, and is therefore always present under dynamic excitation. The latter only occurs in structures with lateral load resisting systems which are not regular in stiffness (i.e. dual systems with walls and frames, walls with different stiffnesses, podium structures, structures with set-backs etc.) and are a result of the inertial forces. Transfer forces are often overlooked in design, mostly because of limited design tools or negligence. To date, no information on transfer forces in timber structures is available, especially because no timber structures where such forces can be expected have been built. Design procedures for dual frame-wall structures in timber do not exist and, therefore, no desktop method for transfer forces can be provided. Transfer forces created in wall structures due to change of stiffness are normally small because of the higher diaphragm flexibility and can be ignored (Cobeen et al. 2014). If transfer forces in diaphragms are expected, more sophisticated analysis methods, like a time history analysis, are required.

Non-transfer diaphragms need to resist the peak floor inertial forces. Maximum forces from non-linear time history analysis proved to be several times larger than the static forces from an equivalent static analysis. For both frame and wall structures, maximum forces found in top stories were also found in lower stories, not reflecting the typical triangular distribution from an equivalent static analysis. Diaphragm forces were up to 2.5 times higher than the top equivalent static force for frame structures and 5 times higher for tall wall structures.

For frame structures a simple equation based on a modified formulation of the amplified top shear storey force as defined by Priestley et al. (2007) provided good estimates for the diaphragm demand. In wall structures the peak diaphragm demand was influenced by the diaphragms stiffness and should be considered in the analysis. The current method to determine the top storey shear force by Priestley et al. (2007) was able to conservatively

predict the peak diaphragm demand in wall structures. It is further recommended that all diaphragms be designed for the same maximum demand obtained with these methods.

The pseudo Equivalent Static Analysis (Bull 2004; Gardiner et al. 2008) provides unconservative predictions and should not be applied to timber frame and wall structures. Dynamic amplification factors provided in the New Zealand Concrete Standard (Standards New Zealand 2006) also proved to be inadequate to determine the force demand in timber structures.

Load path and deflections in diaphragms

6. Are current analysis methods adequate to design timber diaphragms and to determine the component demand?

Current diaphragm analysis methods consist of either a simplistic deep beam/girder analogy or sophisticated finite element analyses. The former is not suitable for floors with irregularities and does not account for diaphragm stiffness, while the latter is rarely applied in design offices because of limited knowledge, time and analysis software.

The girder analogy recently has been further extended by the 'shear field analogy' and the use of sub-diaphragms. These procedures, however, have not found widespread use in design offices because of the soon reached complexity.

Because of the lack of more general analysis tools and limited understanding of the diaphragm behaviour, floor openings often are ignored, chord beams made discontinuous and displacement incompatibilities between the diaphragm and the lateral load resisting system overlooked. Defining diaphragms as rigid is often erroneously interpreted as being strong enough for any force demand. It is, therefore, of great importance to provide the engineering community with a simple desktop method for the analysis of irregular timber diaphragms.

7. Can the principles of such methods be applied to massive timber diaphragms?

Finite element modelling showed that regular massive timber diaphragms can be analysed with the same commonly available tools as used with light timber framing diaphragms, as long as chord beams are used.

In the absence of chord beams, panels and the panel connections need to withstand substantial tension forces, also leading to very flexible diaphragms. Such effects cannot be evaluated with the girder analogy.

If loads are applied to the diaphragm edges only, the massive timber panels need to transfer these loads into the remaining part of the diaphragm further away from the point of load

application, activating longitudinal stresses and causing force components in the fasteners perpendicular to the panel edges. This effect is not found in LTF diaphragms, where framing elements transfer these forces. In case of seismic loads, such forces are normally negligible.

8. Can a strut-and-tie or truss analysis be used to analyse timber diaphragms?

Strut-and-tie analysis (Schlaich et al. 1987) provides a simple and reliable tool to analyse concrete diaphragms and concrete elements in general. This method is based on the distinct compression and tension capacities of the concrete and the steel reinforcement respectively, which allows for the direct development of truss models. Such behaviours with compression struts and tension ties do not occur in timber diaphragms, where panels are connected by metallic fasteners. As such, the force transfer and deformation mechanisms cannot directly be considered with a truss model.

According to the shear field analogy, the individual panels in light timber frame diaphragms work exclusively in shear, and the fasteners along the edges transfer these forces to adjacent panels via framing elements. Based on the panel shear and fastener slip stiffnesses, an equivalent diagonal can be defined. Together with the framing elements and boundary beams an Equivalent Truss Model can be obtained for the analysis of statically indeterminate and irregular diaphragms. Panel unit shear forces can be directly obtained from the stresses in the diagonals.

Comparison with a finite element analysis showed very good agreement in terms of panel, fastener and chord forces, as well as reactions and diaphragm deflections. Because the stiffness of the panels is directly considered, the Equivalent Truss Model can automatically distribute the forces into the lateral load resisting system. Geometric torsional effects are also considered in this analysis method.

This Equivalent Truss Model was further modified to be used for massive timber diaphragms. By dividing the normally slender panels into multiple diagonals and by using additional transverse and longitudinal elements, these panels and their fasteners can also be modelled with an equivalent truss model. Comparison with finite element analysis showed very good agreement.

The Equivalent Truss Model can easily be extended for the analysis with non-linear fasteners, as long as their force-slip behaviour is available.

9. How can diaphragm stiffness be assessed?

Code provisions provide equations to estimate the deflection of regular light timber frame diaphragms which can be idealized as simply supported beams. These equations have been modified in order to predict the deflection of massive timber diaphragms.

For irregular diaphragms the Equivalent Truss Method is suggested, which also provides the deflection for statically indetermined diaphragms.

10. How can the force distribution into the lateral load resisting system be determined?

Code provisions acknowledge the fact that both the diaphragm stiffness and the stiffness of the lateral load resisting system influence the force distribution into the lateral load resisting system. Recent research and examples carried out in this research have shown that a rigid diaphragm assumption is not always appropriate for timber diaphragms. Diaphragms are therefore often best described as 'semi-rigid'. Thus it is suggested to model diaphragms with the use of a truss method in a 3D structural model or by simply considering the behaviour of the lateral load resisting system with spring elements in a bi-dimensional model. This approach provides further the possibility to account for torsional effects.

Since the force distribution is dependent on the relative stiffnesses of the lateral load resisting system and the diaphragms, iterations on this distribution might be necessary during design, as section sizes and connections of both the lateral load resisting system and the diaphragms can change from the preliminary assumed values.

Connection of the floor diaphragms to the lateral load resisting systems and displacement incompatibilities:

11. What displacement incompatibilities can occur in timber buildings?

To achieve ductility and damping in seismic resistant structures, mechanisms like concrete plastic hinge formation, steel yielding or gap opening due to rocking are activated. All these mechanisms require local displacements which are imposed to all other attached structural and non-structural elements.

In timber frame structures such displacement incompatibilities occur at the beam-column-joint interface in case of gap opening because of controlled rocking or yielding of the moment-resisting connectors. Floor diaphragms connected to the frame beams need to accommodate this local displacement demand, otherwise creating tearing forces leading to diaphragm damage.

Timber wall structures rotate and tend to uplift connected floor beams. This behaviour is evident for Pres-Lam walls with a distinct rocking mechanism, but also occurs in massive timber walls connected with yielding metallic fasteners and hold-downs and to a lesser extent in light timber framing walls. A rigidly attached floor beam is forced to follow this movement, creating diaphragm uplift and out-of-plane bending. Simultaneously the floor elements can increase the stiffness and strength of the wall, leading to large axial forces in the wall and other gravity carrying elements.

Collector beams around core-wall structures undergo the same displacement incompatibilities as wall structures, but in addition also need to allow for the movement from orthogonally running beams.

12. How can displacement incompatibilities be allowed for in frame structures?

Based on the experimental testing on two frame structures, which showed no damage under numerous loading cycles, it could be concluded that:

- the displacements created by the beam-column gap openings were accommodated by the diaphragm due to the flexibility in the connections and, to a lesser extent, by the elongation of the timber members;
- the beam-column joint gap openings were not restrained by the presence of the floor diaphragms.

Two alternative connection details are proposed:

- *A concentrated floor gap* at the position of the beam-column joint. This is the preferred connection in the case of stressed-skin panels with a rigid floor finish, solid timber panels and timber-concrete-composite floors (not tested in this programme);
- *Distributed floor gaps and elongation* of the floor diaphragm over several floor panels. This is the preferred detail in the case of a flexible timber floor.

13. How can displacement incompatibilities be allowed for in wall structures?

Test results on a wall and a stairwell structure showed that collector beams connected with closely spaced bolts, inclined fully threaded screws or one large diameter pin give very satisfactory results for floors with a low-to-medium out-of-plane stiffness. For stiffer floors a steel-to-steel solution with a pin in a slotted hole is recommended to avoid displacement incompatibilities. To further reduce interaction, collector beams can be connected to timber or steel columns at the ends of the wall.

For core wall structures the same connection detailing between the collectors and the walls proved very satisfying behaviour. Orthogonally running collector beams should be connected to each other with out-of-diaphragm-plane flexible connections. Shear transfer from the diaphragm panel into the collectors should occur outside the corner regions of the core.

A cost analysis showed that the more interaction is eliminated with a specific connection, the higher the construction cost will be. Timber-to-timber connections with bolts or screws are less expensive both in terms of material cost and labour. Sliding steel-to-steel connections have an increased cost from the steel elements, fasteners and labour. In case displacement incompatibilities are minimized by the use of wall boundary columns, the cost of the columns, the shear transfer devices as well as the fasteners need to be accounted for, leading to a very costly solution.

14. How can the wall-to-diaphragm interaction be quantified for design purposes?

Pushover analyses are a simple yet powerful tool in determining the moment-rotation or force-displacement behaviour for structures under horizontal loading. Such capacity curves are used to determine the performance point of Pres-Lam walls under seismic action. An existing iterative moment-curvature procedure was extended by the inclusion of the compatibility forces and moments caused by the imposed displacement to the beams. Such formulation depends on the uplift and rotation of the wall, the bending stiffness of the beam and the translational and rotational stiffnesses of the connection. Comparison with experimental values showed very good agreement with the analytical procedure, giving engineers a simple tool to evaluate the increase of strength and stiffness of the wall-beam system.

A parametric analysis showed that the connection vertical stiffness has little influence on the system behaviour, since it is normally greater than the beam bending stiffness. The rotational stiffness of a compact connection with a limited number of fasteners was able to decouple the imposed rotations from the beam. For larger connections, the connection rotational stiffness soon became dominant and large compatibility forces because of beam out-of plane bending were created.

12.3 RECOMMENDATIONS FOR FURTHER RESEARCH

While carrying out this research, many shortcomings and knowledge gaps in the design of diaphragms in multi-storey timber buildings have been identified. Although many questions were answered in this work, a number of issues still need to be addressed. The following recommendations for future research can be made:

- The dynamic behaviour of Pres-Lam frame and wall structures under spectrum compatible ground motions was studied in Chapter 4. The conclusions drawn were based on structures designed with one target ductility only, so more structures with additional ductility values need to be analysed. Further it was assumed that other types of modern timber frame and wall structures show a similar trend. Such assumptions need to be verified with additional numerical analysis on different structural systems.
- Provided formulae allow for the determination of peak diaphragm forces, which can be up to 5 times the peak floor forces determined with an equivalent static analysis. It needs to be determined if such high peak values are affected by numerical effects/errors from the time history analysis and if the values are meaningful, since they only occur for a very short instance in time.
- Simplified methods to determine peak floor inertial forces in post-tensioned wall and frame buildings were validated. Such forces occur at different moments in time and cannot be used to determine the structure's displacements and diaphragm compatibility forces. Current methods like the pseudo Equivalent Static Analysis underpredicted the peak inertial forces for both timber frame and wall structures. A simple but robust method to determine diaphragm compatibility forces in timber buildings still need to be developed. The method by Sabelli et al. (2011) should be further explored for the use with timber structures. It is however assumed that the higher flexibility of timber diaphragms leads to much smaller transfer forces than in concrete diaphragms.
- Diaphragm compatibility forces are a typical phenomenon found in dual frame and wall structures. Such timber structures with a dual lateral load resisting system are still very uncommon and design procedures non-existing. New procedures would be required to promote the use of dual structures.
- Diaphragm designs based on force demands including overstrength and dynamic amplification can result in non-economical designs. Allowance of yielding in diaphragm panel connections has shown promising results in pre-cast concrete diaphragms

(Fleischman 2014). Such procedures could be applied to timber diaphragms with discrete or smeared ductile connections. A research programme including numerical analysis and dynamic tests would be required to evaluate if this method would successfully reduce the amplification of diaphragm forces.

- The Equivalent Truss Method has been developed based on deflection equations as provided by current timber design codes and verified against finite element models. Such finite element models need to be verified against experimental evidence. Only very little experimental evidence is available on the behaviour of large scale diaphragms, especially in the presence of irregularities. The models further need to be verified for massive timber diaphragms, which allow for large diaphragm spans and large force demands.
- Since most diaphragms are designed to remain elastic, most of the verification examples are carried out with elastic material properties. It was shown that if non-linear behaviour is expected or required, the diagonal properties in the Equivalent Truss Method can easily be adapted. The non-linear force-displacement behaviour of fasteners is however not always readily available, especially for load components both parallel and perpendicular to the panel edge. Such values would need to be codified, if non-linear diaphragm behaviour is to be achieved. More analysis cases including hysteretic behaviour of the fasteners and therefore diagonals would also be required.
- The experimental setup of the two bay frame presented in this thesis was not capable of investigating the diaphragm behaviour of a whole building, as it would have required the setup of a full scale diaphragm between a second frame, which was not possible during the research program. The second frame specimen was tested dynamically in one principal direction only; its diaphragm behaviour under a seismic attack in an arbitrary direction would need to be tested.
- Diaphragms in timber buildings with concrete slabs have not been tested in this research program. Although the design of a pre-cracked slab with unbonded rebars is theoretically possible, dowel action over larger cracks still needs to be investigated both experimentally and analytically.

References

- ACI (2014). ACI 318-14 Building Code Requirements for Structural Concrete and Commentary. American Concrete Institute.
- ACI Committee 374 (2005). Acceptance Criteria for Moment Frames Based on Structural Testing and Commentary. American Concrete Institute.
- ACI Innovation Task Group 5 (2008). ITG-5.1-07 Acceptance criteria for special unbonded post-tensioned precast structural walls based on validation testing and commentary: an ACI standard. American Concrete Institute, Farmington Hills, Michigan.
- AF&PA American Wood Council (2008). ASD&LRFD. Wind & Seismic. Special Design Provisions for Wind and Seismic, Washington DC, USA.
- Amaris, A., Pampanin, S., Bull, D. and Carr, A. (2008). Experimental Investigation on a Hybrid Jointed Precast Frame with Non-tearing Floor Connections. New Zealand Society for Earthquake Engineering Conference 2008, Wairakei, New Zealand.
- American Forest & Paper Association - American Wood Council (2005). ANSI/AF&PA SDPWS-2005. Special Design Provisions for Wind and Seismic with Commentary. A. W. Council. American Wood Council, Washington, DC, USA.
- American Society of Civil Engineers (2000). Prestandard and Commentary for the Seismic Rehabilitation of Buildings. Federal Emergency Management Agency. Federal Emergency Management Agency,, Washington, D.C.
- APA (2007). Diaphragms and Shear Walls. Design/Construction Guide. The Engineered Wood Association. Tacoma, WA.
- Ardalany, M., Deam, B., Fragiacomio, M. and Crews, K.I. (2010). Tension Perpendicular to Grain Strength of Wood, Laminated Veneer Lumber (LVL), and Cross-Branded LVL (LVL-C). 21st Australasian Conference on the Mechanics of Structures and Materials, Melbourne, Australia.
- Armstrong, T., Smith, T., Buchanan, A. and Pampanin, S. (2014). Seismic Detailing of Post-Tensioned Timber Frames. World Conference on Timber Engineering, Quebec City, Canada.
- ASCE (2010). ASCE 7-10. Minimum design loads for buildings and other structures. American Society of Civil Engineers, Reston, Va.
- Ashtari, S. (2009). In-plane Stiffness of Cross-laminated Timber Floors. Masters Thesis, The University of British Columbia. Vancouver, Canada.
- ATC (1979). Proceedings of a workshop on design of horizontal wood diaphragms. Applied Technology Council, Berkeley, California.
- ATC (1981). Guidelines for the design of horizontal wood diaphragms. Applied Technology Council, Berkeley, California.
- Au, E.V. (2010). The Mechanics and Design of a Non-tearing Floor Connection using Slotted Reinforced Concrete Beams. Masters Thesis, University of Canterbury. Christchurch.
- Blaauwendraad, J. and Hoogenboom, P.C.J. (1996). Stringer Panel Model for Structural Concrete Design. Structural Journal 93(3).
- Blaß, H.J., Ehlbeck, J., Kreuzinger, G. and Steck, G. (2004). Erläuterungen zur DIN 1052:2004-08. Entwurf, Berechnung und Bemessung von Holzbauwerken ("Commentary to the DIN 1052:2004-08. Design of Timber Structures"). DGFH Innovations- und Service GmbH, Munich, Germany.

- BRANZ (1999). Evaluation and Test Method EM1: Structural Joints - Strength and Stiffness Evaluation. Building Research Association of New Zealand. Porirua City, New Zealand.
- Brignola, A. (2009). Evaluation of the In-plane Stiffness of Timber Floors for the Performance based Retrofit of URM Buildings. PhD Thesis, University of Genoa.
- Brignola, A., Podesta, S. and Pampanin, S. (2008). In-plane stiffness of wooden floor. New Zealand Society for Earthquake Engineering Conference 2008, Wairakei, New Zealand.
- Brown, A., Lester, J., Pampanin, S. and Pietra, D. (2012). Pres-Lam in Practice: A Damage-Limiting Rebuild Project. SESOC Conference 2012, Auckland, New Zealand.
- Brühl, F., Schänzlin, J. and Kuhlmann, U. (2014). Ductility in Timber Structures: Investigations on Over-Strength Factors. Materials and Joints in Timber Structures. Editors S. Aicher, H. W. Reinhardt and H. Garrecht. Springer Netherlands. 9: 181-190.
- Brunner, R., Jung, P., Seiger, R., Wenk, T. and Wirz, N. (2010). Erdbebengerechtes Entwerfen und Konstruieren von mehrgeschossigen Holzbauten ("Seismic design of multistorey timber buildings"). Lignum. Zürich, Switzerland.
- Buchanan, A., Carradine, D. and Jordan, J. (2011b). Performance of Engineered Timber Structures in the Christchurch Earthquakes. Bulletin of the New Zealand Society for Earthquake Engineering 44(4).
- Buchanan, A., Carradine, D., Beattie, G. and Morris, H. (2011a). Performance of Houses during the Christchurch Earthquake of 22 February 2011. Bulletin of the New Zealand Society for Earthquake Engineering 44(4).
- Buchanan, A.H. and Fairweather, R.H. (1993). Seismic Design of Glulam Structures. Bulletin of the New Zealand Society for Earthquake Engineering 26(4): 415-436.
- Buchanan, A.H. and Smith, T. (2015). The Displacement Paradox for Seismic Design of Tall Timber Buildings. New Zealand Conference of Earthquake Engineering, Rotorua, New Zealand.
- Buchanan, A.H., Palermo, A., Carradine, D. and Pampanin, S. (2011). Post-tensioned Timber Frame Buildings. The Structural Engineer 89(17): 24-30.
- Bull, D. (2004). Understanding the complexities of designing diaphragms in buildings for earthquakes. Bulletin of the New Zealand Society for Earthquake Engineering 37(2): 70-88.
- Bull, D. and Henry, R. (2014). Strut and Tie. Seminar Notes. Technical Report No.R57. The New Zealand Concrete Society.
- Byrne, J.D.R. and Bull, D.K. (2012). Design and testing of reinforced concrete frames incorporating the slotted beam detail. New Zealand Society of Earthquake Engineering Conference, Christchurch, New Zealand.
- C.F. Møller (2013). Wooden Skyscraper. <http://www.cfmoller.com/r/Wooden-Skyscraper-i13265.html>, 30th May, 2014.
- CAE (1999). Guidelines for the use of structural precast concrete in buildings. Centre for Advanced Engineering, University of Canterbury.
- Canadian Commission of Building and Fire Codes (2010a). National Building Code of Canada. National Research Council of Canada, Ottawa, Canada.
- Canadian Commission of Building and Fire Codes (2010b). User's guide - NBC 2010 - Structural Commentaries (Part 4 of Division B). National Research Council of Canada, Ottawa, Canada.
- Canadian Wood Council and Natural Resources Canada (2013). Tall Wood Structure Demonstration Projects. <http://www.cwcdemoproject.ca/en/index.php>.
- Canterbury Earthquake Royal Commission (2011). Interim Report. Christchurch, New Zealand.

- Canterbury Earthquake Royal Commission (2012). Final Report - Volume 3 - Low-Damage Building Technologies. Christchurch, New Zealand.
- Carney, J.M. (1975). Bibliography on wood and plywood diaphragms. *Journal of the Structural Division* 101(ST11): 2423-2436.
- Carr, A. (2006). Ruamoko 2D and Ruamoko 3D: Inelastic Dynamic Analysis Software.
- Ceccotti, A. (2008). New technologies for construction of medium-rise buildings in seismic regions: The XLAM case. *Structural Engineering International: Journal of the International Association for Bridge and Structural Engineering (IABSE)* 18(2): 156-165.
- Ceccotti, A., Follesa, M., Lauriola, M. and Sandhaas, C. (2006). SOFIE Project – Test Results on the Lateral Resistance of Cross-Laminated Wooden Panels. 1st ECEES 2006, Geneva, Switzerland.
- CEIArchitecture (2011). 40-Storey Wood Office Tower.
<http://www.ceiarchitecture.com/project/naiop-design-competition-2012>, 30th May, 2014.
- CEN (1999). EN 1194:1999. Timber Structures - Glued Laminated Timber - Strength Classes and Determination of Characteristic Values. European Committee for Standardization.
- Chancellor, N., Akbas, G., Sause, R., Ricles, J., Tahmasebi, E. and Joó, A. (2011). Evaluation of performance-based design methodology for steel self-centering braced frame. *Behaviour of Steel Structures in Seismic Areas*. CRC Press: 737-743.
- Chaudhari, T., MacRae, G., Bull, D., Chase, G., Hobbs, M., Clifton, C. and Hicks, S. (2014). Composite slab effects on beam-column subassemblies: further development. *New Zealand Society of Earthquake Engineering*.
- Chiou, B., Darragh, R., Gregor, N. and Silva, W. (2008). NGA project strong-motion database. *Earthquake Spectra* 24(1): 23-44.
- Chopra, A.K. and Goel, R.K. (1999). Capacity-demand-diagram methods based on inelastic design spectrum. *Earthquake Spectra* 15(4): 637-655.
- Chou, C.-C., Wang, Y.-C. and Chen, J.-H. (2008). Seismic design and behavior of post-tensioned steel connections including effects of a composite slab. *Engineering Structures* 30(11): 3014-3023.
- Christovasilis, I.P., Filiatrault, A. and Wanitkorkul, A. (2007). Seismic Testing of a Full-Scale Two-Story Light-Frame Wood Building: NEESWood Benchmark Test. *Development of a Performance-Based Seismic Design Philosophy for Mid-Rise Woodframe Construction*. Buffalo, NY.
- Cleland, N.M., Fleischman, R.B. and Ghosh, S.K. (2012). Seismic Design Methodology for Precast Concrete Floor Diaphragms NEES/EERI Research to Practice Webinar. PCI/NSF/CPF.
- Cobeen, K.E., Dolan, J.D., Thompson, D. and van de Lindt, J. (2014). *Seismic Design of Wood Light-Frame Structural Diaphragm Systems: a Guide for Practicing Engineers*. NEHRP Seismic Design Technical Brief No. 10. NIST. Gaithersburg, MD.
- Colling, F. (2011). *Gebäudeaussteifung bei Gebäuden in Holztafelbauart. Grundlagen, Beanspruchungen, Nachweise nach DIN und EUROCODE*. Ingenieurbüro Holzbau, Karlsruhe
- Consiglio Superiore dei Lavori Pubblici (2008). *Norme tecniche per le costruzioni ("Design code for structures")*, Rome, Italy.
- Consiglio Superiore dei Lavori Pubblici (2013). *Bozza delle Norme tecniche per le costruzioni ("Draft of the Design Code for Structures")*, Rome, Italy.
- Countryman, D. (1952). Lateral tests on plywood sheathed diaphragms. Laboratory Report No. 63. Douglas Fir Plywood Association. Tacoma, WA.
- Cowie, K.A., Fussell, A.J., Clifton, G.C., MacRae, G.A. and Hicks, S.J. (2014). Seismic design of composite metal deck and concrete-filled diaphragms – A discussion paper. *New Zealand Society of Earthquake Engineering Conference*, Auckland, New Zealand.

- CSI (2004). SAP2000: Static and Dynamic Finite Analysis of Structures. CSI Computers and Structures Inc.
- CUREE (2000). CUREE-Caltech Woodframe Project.
<http://www.curee.org/projects/woodframe/index.html>, 22nd May.
- Curtis, E. (2009). Deflection of Light Frame Wood Diaphragms. Washington State University.
- Dassault Systèmes HQ (2011). Abaqus FEA. ABAQUS Inc.: Finite element analysis software.
- Davies, M. (2012). Personal communication regarding the diaphragm design of the Massey University's College of Creative Arts building.
- Deam, B.L. (1996). The seismic design and behaviour of multi-storey plywood sheathed timber framed shearwalls. PhD Thesis, University of Canterbury.
- Dean, J.A. (1982). Sheated Construction. Timber Engineering Seminar.
- Dean, J.A., Moss, P.J. and Stewart, W. (1984). A design procedure for rectangular openings in shearwalls and diaphragms. Pacific Timber Engineering Conference, Auckland, New Zealand.
- Dekker, D. and Chung, S. (2012). Carterton Events Centre Auditorium Pres-Lam Wall Design and Construction New Zealand Conference of Earthquake Engineering, Christchurch, New Zealand.
- Devereux, C.P., Holden, T.J., Buchanan, A.H. and Pampanin, S. (2011). NMIT Arts & Media Building - Damage Mitigation Using Post-tensioned Timber Walls. PCEE, Auckland, New Zealand.
- Diekmann, E.F. (1982). Design of Wood Diaphragms. *Journal of Materials Education* 8(1-2).
- Diekmann, E.F. (1995). Diaphragms and Shear Walls. *Wood Engineering and Construction Handbook*. Editors K. F. Faherty and T. G. Williamson. McGraw-Hill: 8.1-8.68, New York.
- Diekmann, E.F., Faherty, K.F. and Williamson, T.G. (1997). Diaphragms and shearwalls. *Wood Engineering and Construction Handbook*. Editors McGraw-Hill, New York.
- DIN (1988). DIN 1052-1:1988-04 Structural use of timber; design and construction. Deutsches Institut für Normung e.V., Berlin, Germany.
- DIN (2008). DIN1052:2008-10 Design of timber structures - General rules and rules for buildings. Deutsches Institut für Normung e.V., Berlin, Germany.
- Dolan, J.D., Carradine, D.M., Bott, J.W. and Easterling, W.S. (2003). Design Methodology for Diaphragms. CUREE-Caltech Wood Frame Project Task 1.4.2 – Diaphragm Studies.
- Dujic, B., Strus, K., Zarnic, R. and Ceccotti, A. (2010). Prediction of dynamic response of a 7-storey massive XLam wooden building tested on a shaking table. World Conference on Timber Engineering, Riva del Garda, Italy.
- Dunbar, A. (2014). Seismic Design of Core-Wall Systems for Multi-Storey Timber Buildings. Masters Thesis, University of Canterbury. Christchurch, New Zealand.
- Eatherton, M.R. (2010). Large-scale cyclic and hybrid simulation testing and development of a controlled-rocking steel building system with replaceable fuses. PhD Thesis, University of Illinois at Urbana-Champaign. Urbana, Illinois.
- Elliott, J.R. (1979). Wood diaphragm testing - past, present, planned. Proceedings on a Workshop on Design of Horizontal wood diaphragms, Applied Technology Council, Berkeley, California.
- Elwood, K.J. (2013). Performance of concrete buildings in the 22 February 2011 Christchurch earthquake and implications for Canadian codes. *Canadian Journal of Civil Engineering* 40(8): 759-776.
- Eurocode 2 (2005). EN 1992:2004. Design of concrete structures - Part 1-1: General rules and rules for buildings. European Committee for Standardization.
- Eurocode 5 (2008). EN 1995-1-1:2004/A1:2008 Design of timber structures. Part 1-1: General - Common rules and rules for buildings. European Committee for Standardization.

- Eurocode 5 DIN NA (2010). DIN EN 1995-1-1:NA:2010. National Annex - Nationally determined parameters - Eurocode 5: Design of timber structures. Part 1-1: General - Common rules and rules for buildings. Deutsches Institut für Normung.
- Eurocode 8 (2004). EN 1998-1:2004/AC:2009. Design of structures for earthquake resistance. Part 1: General rules, seismic actions and rules for buildings. European Committee for Standardization.
- Falk, R.H. and Itani, R.Y. (1989). Finite-element modeling of wood diaphragms. *Journal of Structural Engineering-ASCE* 115(3): 543-559.
- Fenwick, R., Bull, D.K. and Gardiner, D. (2010). Assessment of hollow-core floors for seismic performance. Research Report. Civil and Natural Resources Engineering. University of Canterbury.
- Fenwick, R.C. and Fong, A. (1979). The Behaviour of Reinforced Concrete Beams under Cyclic Loading. *Bulletin of the New Zealand Society for Earthquake Engineering*. Vol 12(1): 158-167.
- fib (2003). Seismic design of precast concrete building structures: state-of-art report. *Fédération internationale du béton*, Bulletin n. 27 (Chairman R. Park, F. Watanabe), Lausanne, Switzerland.
- fib (2011). Design examples for strut-and-tie models: technical report. International Federation for Structural Concrete, Lausanne.
- Filiatrault, A., Fischer, D., Folz, B. and Uang, C.-M. (2002). Experimental parametric study on the in-plane stiffness of wood diaphragms. *Canadian Journal of Civil Engineering* 29(4): 554-566.
- Fleischman, R. (2014). Seismic Design Methodology Document for Precast Concrete Diaphragms. Charles Pankow Foundation.
- Fleischman, R., Naito, C. and Restrepo, J. (2008). Development of a seismic design methodology for precast concrete floor diaphragms. *Tailor Made Concrete Structures*. CRC Press: 55-55.
- Fleischman, R., Restrepo, J., Naito, C., Sause, R., Zhang, D. and Schoettler, M. (2013). Integrated Analytical and Experimental Research to Develop a New Seismic Design Methodology for Precast Concrete Diaphragms. *Journal of Structural Engineering* 139(7): 1192-1204.
- Fleischman, R.B. and Farrow, K.T. (2001). Dynamic behavior of perimeter lateral-system structures with flexible diaphragms. *Earthquake Engineering & Structural Dynamics* 30(5): 745-763.
- Fleischman, R.B., Farrow, K.T. and Eastman, K. (2002). Seismic Performance of Perimeter Lateral-System Structures with Highly Flexible Diaphragms. *Earthquake Spectra* 18(2): 251-286.
- Fleischman, R.B., Restrepo, J., Ghosh, S.K., Naito, C.J. and Sause, R. (2005). Seismic design methodology for precast concrete diaphragms - Part 1: Design framework. *PCI Journal* 50(5): 68-68.
- Follesa, M., Christovasilis, I.P., Vassallo, D., Fragiacomano, M. and Ceccotti, A. (2013). Seismic design of multi-storey cross laminated timber buildings according to Eurocode 8. *Ingegneria Sismica* 4.
- Folz, B. and Filiatrault, A. (2000a). CASHEW: A Computer Program for Cyclic Analysis of Wood Shear Walls. The CUREE-Caltech Woodframe Project, CUREE Publication No. W-8.
- Folz, B. and Filiatrault, A. (2000b). SAWS: A Computer Program for Seismic Analysis of Woodframe Structures. The CUREE-Caltech Woodframe Project, CUREE Publication No. W-21.
- Foschi, R.O. (1977). Analysis of wood diaphragms and trusses. Part I: Diaphragms. *Canadian Journal of Civil Engineering* 4(3): 345-352.
- Foschi, R.O. (1999). DAP3D shear wall/diaphragm analysis program.
- Foschi, R.O. (2000). Modeling the Hysteretic Response of Mechanical Connections for Wood Structures. World Conference on Timber Engineering, Whistler, Canada.
- FPIInnovations (2013). Technical Guide for the Design and Construction of Tall Wood Buildings in Canada. 90% DRAFT. E. Karacabeyli. Vancouver.

- Fragiacomo, M., Amadio, C., Sancin, L. and Rinaldin, G. (2012). Seismic analysis of a light - frame timber building with and without friction pendulum base isolation. World Conference on Timber Engineering, Auckland, New Zealand.
- Fragiacomo, M., Batchelar, M., Wallington, C. and Buchanan, A. (2010). Moment Joints in Timber Frames using Glued-in Steel Rods- Experimental Investigation of Long-Term Performance. World Conference on Timber Engineering, Riva del Garda, Trentino, Italy.
- Franke, S. and Quenneville, P. (2011). Bolted and dowelled connections in Radiata pine and laminated veneer lumber using the European Yield Model. Australian Journal of Structural Engineering Vol. 12 (No. 1): 13-28.
- Gagnon, S., Pirvu, C. and FPInnovations (2011). CLT Handbook: Cross-Laminated Timber, Québec, Canada.
- Gardiner, D. (2011). Design recommendations and methods for reinforced concrete floor diaphragms subjected to seismic forces. PhD Thesis, University of Canterbury. Christchurch, New Zealand.
- Gardiner, D.R., Bull, D. and Carr, A. (2008). Internal forces of concrete floor diaphragms in multi-storey buildings. New Zealand Society of Earthquake Engineering Conference, Wairakei, New Zealand.
- Garlock, M.E.M. and Li, J. (2008). Steel self-centering moment frames with collector beam floor diaphragms. Journal of Constructional Steel Research 64(5): 526-538.
- Gerber, C., Crews, K. and Shrestha, S. (2012). Design Guide Australia and New Zealand. Timber Concrete Composite Floor Systems. Structural Timber Innovation Company, Christchurch, New Zealand.
- Giongo, I., Wilson, A., Dizhur, D., Derakhshan, H., Tomasi, R., Griffith, M., Quenneville, P. and Ingham, J. (2014). Detailed seismic assessment and improvement procedure for vintage flexible timber diaphragms. Bulletin of the New Zealand Society for Earthquake Engineering 47(2): 97-118.
- Graf, W. (2008). The ShakeOut Scenario - Supplemental Study: Woodframe Buildings. United States Geological Survey, California Geological Survey.
- Gray, G.W. (1979). Field Performance of wood diaphragms in structures subjected to seismic forces. Proceedings on a Workshop on Design of Horizontal wood diaphragms, Applied Technology Council, Berkeley, California.
- He, M., Lam, F. and Foschi, R.O. (2001). Modeling three-dimensional timber light-frame buildings. Journal of Structural Engineering-ASCE 127(8): 901-913.
- Henry, R.S. (2011). Self-centering Precast Concrete Walls for Buildings in Regions with Low to High Seismicity. PhD Thesis, The University of Auckland. Auckland.
- Hobbs, M. (2014). Effects of Slab-Column Interaction in Steel Moment Resisting Frames with Steel-Concrete Composite Floor Slabs. Masters Thesis. University of Canterbury.
- Hollings, J. (1968). Reinforced concrete seismic design. Bulletin of the New Zealand Nation Society for Earthquake Engineering 2(3): 217-250.
- Holzbau Austria (2015). 24-storey Wooden Tower in Vienna. [http://www.holzbauaustria.at/index.php?id=111&tx_ttnews\[tt_news\]=5825&cHash=bf2db5a74efee99acdce447217048c90](http://www.holzbauaustria.at/index.php?id=111&tx_ttnews[tt_news]=5825&cHash=bf2db5a74efee99acdce447217048c90).
- Hrennikoff, A.P. (1940). Plane stress and bending of plates by method of articulated framework. Thesis, Massachusetts Institute of Technology. Cambridge, Massachusetts.
- Hrennikoff, A.P. (1941). Solution of Problems of Elasticity by the Framework Method. Journal of Applied Mechanics 8: A169-175.
- Humar, J. and Popovski, M. (2013). Seismic response of single-storey buildings with flexible diaphragms. Canadian Journal of Civil Engineering 40(9): 875-886.

- Ilgadi, O.B. (2013). Advanced three-dimensional analysis of concrete structures using nonlinear truss models. Thesis, Colorado School of Mines. Golden, Colorado.
- International Code Council (2011). 2012 International Building Code. International Code Council.
- Iqbal, A. (2011). Seismic Response and Design of Subassemblies for Multi-Storey Prestressed Timber Buildings. PhD Thesis, University of Canterbury. Christchurch, New Zealand.
- Jain, S.K. and Jennings, P.C. (1985). Analytical models for low-rise buildings with flexible floor diaphragms. *Earthquake Engineering & Structural Dynamics* 13(2): 225-241.
- James, G.W. (1984). Plywood diaphragms and shearwalls. Research Report. University of Auckland.
- Jamil, M., Quenneville, P. and Clifton, C. (2012). Low-damage moment resisting timber multi-storey buildings. World Conference on Timber Engineering, Auckland.
- Jamil, M., Quenneville, P. and Clifton, C. (2014). Low-Damage Design Using a Gravity Rocking Moment Connection. *Materials and Joints in Timber Structures*. Editors S. Aicher, H. W. Reinhardt and H. Garrecht. Springer Netherlands. 9: 307-321.
- Jamil, M., Quenneville, P. and Clifton, C. (2015). Scaled shake table tests of a novel gravity rocking moment frame system. New Zealand Society of Earthquake Engineering Conference 2015, Rotorua, New Zealand.
- Jensen, J. (2004). Diaphragm Action Issues in a Jointed Precast Concrete System. 3rd Professional Year Project, University of Canterbury. Christchurch.
- Jephcott, D.K. and Dewdney, H.S. (1979). Analysis methods for horizontal wood diaphragms. Proceedings on a Workshop on Design of Horizontal wood diaphragms, Applied Technology Council, Berkeley, California.
- Johnston, H., Watson, C., Pampanin, S. and Palermo, A. (2014). Shake table testing of an integrated low damage building system. European Conference on Earthquake Engineering and Seismology, Istanbul, Turkey.
- Jorissen, A. and Fragiacomio, M. (2011). General notes on ductility in timber structures. *Engineering Structures* 33(11): 2987-2997.
- Ju, S.H. and Lin, M.C. (1999). Comparison of Building Analyses Assuming Rigid or Flexible Floors. *Journal of Structural Engineering* 125(1): 25-31.
- Judd, J. and Fonseca, F. (2005). Analytical Model for Sheathing-to-Framing Connections in Wood Shear Walls and Diaphragms. *Journal of Structural Engineering* 131(2): 345-352.
- Jung, P. (2009). Bemessung von Scheiben ("Design of diaphragms"). *Holzbautag Biel*, Biel, Switzerland.
- Kærn, J.C. (1979). The Stringer Method Applied to Discs with Holes. Final Report. IABSE Colloquium Plasticity in Reinforced Concrete, Copenhagen.
- Källsner, B. and Girhammar, U.A. (2009). Plastic models for analysis of fully anchored light-frame timber shear walls. *Engineering Structures* 31(9): 2171-2181.
- Kam, W.Y., Pampanin, S. and Elwood, K. (2011). Seismic performance of reinforced concrete buildings in the 22 February Christchurch (Lyttelton) earthquake. *Bulletin of the New Zealand Society for Earthquake Engineering* 44(4): 239-278.
- Kamiya, F. (1990). Horizontal plywood sheathed diaphragms with openings: static loading tests and analysis. Proceedings of the International Timber Engineering Conference, Tokyo, Japan.
- Kamiya, F. and Itani, R.Y. (1998). Design of Wood Diaphragms with Openings. *Journal of Structural Engineering* 124(7): 839-848.
- Kelly, J.M., Skinner, R.I. and Heine, A.J. (1972). Mechanisms of Energy Absorption in Special Devices for use in Earthquake Resistant Structures. *Bulletin of the New Zealand Society for Earthquake Engineering* 5(3): 63-88.

- Kessel, M.H. (2001). Tafeln ("Diaphragms"). *Karlsruher Tage*, Karlsruhe, Germany.
- Kessel, M.H. and Schönhoff, T. (2001). Entwicklung eines Nachweisverfahrens für Scheiben auf der Grundlage von Eurocode 5 und DIN 1052 neu ("Development of a design methodology for diaphragms based on Eurocode 5 and DIN1052:2008"). *Fraunhofer IRB Verlag*, Braunschweig, Germany.
- Kim, H.-J. and Christopoulos, C. (2009). Seismic design procedure and seismic response of post-tensioned self-centering steel frames. *Earthquake Engineering & Structural Dynamics* 38(3): 355-376.
- King, A.J. (2007). Design of collector elements for steel self-centering moment resisting frames. Masters Thesis, Purdue University.
- Kunnath, S.K., Panahshahi, N. and Reinhorn, A.M. (1991). Seismic Response of RC Buildings with Inelastic Floor Diaphragms. *Journal of Structural Engineering* 117(4): 1218-1237.
- Latham, D.A., Reay, A.M. and Pampanin, S. (2013). Kilmore Street Medical Centre: Application of a post-tensioned steel rocking system. *Steel Innovations Conference*, Christchurch, New Zealand.
- Lee, H.J., Aschheim, M.A. and Kuchma, D. (2007). Interstory drift estimates for low-rise flexible diaphragm structures. *Engineering Structures* 29(7): 1375-1397.
- Leslie, B.J., Bull, D. and Pampanin, S. (2010). The Seismic Performance of a Non-Tearing Floor Precast Concrete Structural System. *New Zealand Society of Earthquake Engineering Conference*, Wellington.
- Li, M., Foschi, R.O. and Lam, F. (2012). Modeling Hysteretic Behavior of Wood Shear Walls with a Protocol-Independent Nail Connection Algorithm. *Journal of Structural Engineering* 138(1): 99-108.
- Li, M.H. and Foschi, R.O. (2004). *FLOOR2D User's Manual*.
- Lindsay, R.A., Mander, J.B. and Bull, D.K. (2004). Preliminary results from experiments on hollow-core floor systems in precast concrete buildings. *New Zealand Society of Earthquake Engineering Conference*, Rotorua.
- Loo, W.Y., Kun, C., Quenneville, P. and Chouw, N. (2014). Experimental testing of a rocking timber shear wall with slip-friction connectors. *Earthquake Engineering & Structural Dynamics* 43(11).
- MacPherson, C.J., Mander, J.B. and Bull, D.K. (2005). Reinforced concrete seating details of hollow-core floor systems. *New Zealand Society of Earthquake Engineering Conference 2005*, Wairakei, New Zealand.
- MacRae, G.A. and Clifton, C. (2013). Low damage design of steel structures. *Steel Innovations 2013 Workshop*, Christchurch, New Zealand.
- MacRae, G.A., Hobbs, M., Bull, D., Chaudhari, T., Leon, R., Clifton, G.C. and Chase, J.G. (2013). Slab Effects on Beam-Column Subassemblies - Beam Strength and Elongation Issues. *Composite Construction VII Conference*, Palm Cove, Queensland, Australia.
- Malone, R.T. and Rice, R.W. (2012). *The Analysis of Irregular Shaped Structures - Diaphragms and Shear Walls*. McGraw Hill.
- Marriott, D. (2009). The Development of High-Performance Post-Tensioned Rocking Systems for the Seismic Design of Structures. PhD Thesis, University of Canterbury. Christchurch, New Zealand.
- Matthews, J.G., Bull, D.K. and Mander, J.B. (2003). Preliminary results from the testing of a precast hollowcore floor slab building. *Pacific Conference on Earthquake Engineering*, Christchurch, New Zealand.
- McKenna, F., Fenves, G.L., Scott, M.H. and Jeremic, B. (2000). *Open System for Earthquake Engineering Simulation (OpenSees)*. Pacific Earthquake Engineering Research Center. University of California.

- McKenzie, R. (2004). Feasibility Study and Optimum Location of Discrete Floor-Frame Connectors in a Precast Concrete System. 3rd Professional Year Project, University of Canterbury. Christchurch.
- McSaveney (1997). Precast concrete flooring systems design and detailing for seismic purposes. New Zealand Concrete Society Conference, New Zealand Concrete Society, Auckland.
- Menegotto, M. and Pinto, P.E. (1973). Method of analysis for cyclically loaded R.C. plane frames including changes in geometry and non-elastic behaviour of elements under combined normal force and bending. Resistance and Ultimate Deformability of Structures Acted on by Well Defined Repeated Loads: Symposium, International Association for Bridge and Structural Engineering, Lisbon, Portugal.
- Meyer, M. (2006). Deckentafeln mit freien Plattenrändern ("Diaphragms with unsupported edges"). Forschungskolloquium, Holzbau Forschung und Praxis, Institut für Konstruktion und Entwurf, Universität Stuttgart, Stuttgart, Germany.
- mgb (2012). THE CASE FOR Tall Wood BUILDINGS - How Mass Timber Offers a Safe, Economical, and Environmentally Friendly Alternative for Tall Building Structures. mgb ARCHITECTURE + DESIGN, Equilibrium Consulting, LMDG Ltd and BTY Group.
- Mitchell, D., Tremblay, R., Karacabeyli, E., Paultre, P., Saatcioglu, M. and Anderson, D.L. (2003). Seismic force modification factors for the proposed 2005 edition of the National Building Code of Canada. Canadian Journal of Civil Engineering 30(2): 308-308.
- Moehle, J.P., Hooper, J.D., Kelly, D.J. and Meyer, T.R. (2010). Seismic Design of Cast-in-Place Concrete Diaphragms, Chords, and Collectors: a Guide for Practicing Engineers. NEHRP Seismic Design Technical Brief No. 3. NIST. Gaithersburg, MD.
- Moon, S.-K. and Lee, D.-G. (1994). Effects of inplane floor slab flexibility on the seismic behaviour of building structures. Engineering Structures 16(2): 129-144.
- Moroder, D., Smith, T., Simonetti, M., Ponzo, F.C., Cesare, A.D., Nigro, D., Pampanin, S. and Buchanan, A.H. (2014). Experimental behaviour of diaphragms in post-tensioned timber frame buildings. European Conference on Earthquake Engineering and Seismology, Istanbul, Turkey.
- Morris, H.W., Wang, M. and Zhu, X. (2011). The long term instrumentation of the NMIT Arts Building - EXPAN shear walls. New Zealand Timber Design Journal 20(1): 13-24.
- Mörsch, E. (1912). Der Eisenbetonbau, seine Theorie und Anwendung ("Reinforced concrete, theory and application"). Verlag Konrad Wittwer, Stuttgart, Germany.
- MPI (2014). A summary of the MPI-commissioned survey on engineered timber use. Ministry for Primary Industries. Wellington, New Zealand.
- Muir, C.A., Pampanin, S. and Bull, D.K. (2012). Preliminary observations from biaxial testing of a two-storey, two-by-one bay, reinforced concrete slotted beam superassembly. Bulletin of the New Zealand Society for Earthquake Engineering Vol. 45(3): 97-104.
- Muir, C.A., Pampanin, S. and Bull, D.K. (2012). Preliminary observations from biaxial testing of a two-storey, two-by-one bay, reinforced concrete slotted beam superassembly. New Zealand Society of Earthquake Engineering Conference, Christchurch.
- Nakaki, S.D. (2000). Design guidelines for precast and cast-in-place concrete diaphragms. NEHRP Professional Fellowship Report. Earthquake Engineering Research Institute. Oakland, California.
- New Zealand Society for Earthquake Engineering (2006). Assessment and Improvement of the Structural Performance of Buildings in Earthquakes. Wellington, New Zealand.
- Newcombe, M.P. (2011). Lateral Force Design of Post-Tensioned Timber Frame and Wall Buildings. PhD Thesis, University of Canterbury. Christchurch.

- Newcombe, M.P., Pampanin, S. and Buchanan, A.H. (2010). Numerical Modelling and Analysis of a Two-Storey Post-Tensioned Timber Frame with Floor Diaphragms. 14th European Conference on Earthquake Engineering, Ohrid, Republic of Macedonia.
- Newcombe, M.P., Pampanin, S., Buchanan, A. and Palermo, A. (2008). Section Analysis and Cyclic Behavior of Post-Tensioned Jointed Ductile Connections for Multi-Story Timber Buildings. *Journal of Earthquake Engineering* 12(1): 83–110.
- Ni, C., Chui, Y.H. and Karacabeyli, E. (2010). Mechanics-based approach for determining the shear resistances of shearwalls and diaphragms. World Conference on Timber Engineering, Riva del Garda, Italy.
- Ohkubo, M., Zhu, W. and Hamamoto, T. (1999). Seismic Characteristics and Cracking Behavior of R/C Slotted Beams. *Proc. of Japan Concrete Institute* 24(2): 301-306.
- Palermo, A. (2004). The Use of Controlled Rocking in the Seismic Design of Bridges. PhD Thesis, Politecnico di Milano. Milan.
- Palermo, A., Pampanin, S. and Carr, A. (2005). Efficiency of Simplified Alternative Modelling Approaches to Predict the Seismic Response of Precast Concrete Hybrid Systems. fib symposium "Keep Concrete Attractive, Budapest, Hungary.
- Palermo, A., Pampanin, S., Buchanan, A. and Newcombe, M. (2005). Seismic Design of Multi-Storey Buildings using Laminated Veneer Lumber (LVL). New Zealand Society for Earthquake Engineering Conference 2005, Wairakei, New Zealand.
- Pampanin, S., Priestley, N. and Sriharan, S. (2001). Analytical Modelling of the Seismic Behaviour of Precast Concrete Frames Designed with Ductile Connections. *Journal of Earthquake Engineering* 5(3): 329-367.
- Pang, W. and Hassanzadeh, M. (2010). Next generation numerical model for non-linear in-plane analysis of wood-frame shear walls. World Conference on Timber Engineering, Riva del Garda.
- Pang, W. and Rosowsky, D. (2007). Direct Displacement Procedure for Performance-Based Seismic Design of Multistory Woodframe Structures. Development of a Performance-Based Seismic Design Philosophy for Mid-Rise Woodframe Construction. Texas A&M University. College Station, Texas.
- Park, R., Bull, D.K. and Paulay, T. (1997). Seismic design of reinforced concrete structures. Technical Report No.20. New Zealand Concrete Society.
- Pathak, R. (2008). The effects of diaphragm flexibility on the seismic performance of light frame wood structures. PhD Thesis, Virginia Polytechnic Institute and State University.
- Paulay, T. (1996). Seismic design of concrete structures: the present needs of societies (Paper No 2001). World Conference on Earthquake Engineering, Acapulco, Mexico.
- Paulay, T. and Park, R. (1975). Reinforced concrete structures. Wiley & Sons, New York.
- Paulay, T. and Priestley, M.J.N. (1992). Seismic Design of Reinforced Concrete and Masonry Buildings. John Wiley & Sons, Inc.
- Peralta, D.F., Bracci, J.M. and Hueste, M.B.D. (2004). Seismic behavior of wood diaphragms in pre-1950s unreinforced masonry buildings. *Journal of Structural Engineering* 130(12).
- Peterson, J. (1983). Bibliography on Lumber and Wood Panel Diaphragms. *Journal of Structural Engineering* 109(12): 2838-2852.
- Piazza, M., Baldessari, C. and Tomasi, R. (2008). The Role of In-plane Floor Stiffness in the Seismic Behaviour of Traditional Buildings. World Conference on Earthquake Engineering, Beijing, China.
- Pino, D. (2011). Dynamic response of post-tensioned timber frame buildings. Masters Thesis, University of Canterbury. Christchurch, New Zealand.

- Popovski, M. and Karacabeyli, E. (2005). Framework for lateral load design provisions for engineered wood structures in Canada. CIB Working Commission W18 - Timber Structures, Karlsruhe, Germany.
- Priestley, M.J.N. (1991). Overview of PRESSS Research Program. *PCI Journal* 36(4): 50-57.
- Priestley, M.J.N. (1996). The PRESSS program – Current status and proposed plans for phase III. *PCI Journal* 42(2): 22-40.
- Priestley, M.J.N. (2003). *Myths and fallacies in earthquake engineering, revisited*. IUSS Press, Pavia, Italy.
- Priestley, M.J.N., Calvi, G.M. and Kowalsky, M.J. (2007). *Displacement-Based Seismic Design of Structures*. IUSS Press.
- Priestley, N., Sritharan, S., Conley, J. and Pampanin, S. (1999). Preliminary Results and Conclusions from the PRESSS Five-Story Precast Concrete Test Building. *PCI Journal* 44(6): 42-67.
- Prion, H.G.L. (2003). *Shear Walls and Diaphragms*. Timber engineering. Editors S. Thelandersson and H. J. Larsen. Wiley+Sons: 383-408, New York.
- Quenneville, P., Franke, S. and Swager, T. (2011). *Design Guide New Zealand*. Timber Portal Frames, Christchurch, New Zealand.
- Rainer, J.H. and Karacabeyli, E. (2000). Ensuring good seismic performance with platform-frame wood housing. *Construction Technology Update*. Institute for Research in Construction.
- Rawlinsons (2015). *Rawlinsons New Zealand Construction Handbook*. Rawlinsons Publishing.
- Ritter, W. (1899). Die Bauweise Hennebique ("The Hennebique System"). *Schweizerische Bauzeitung* XXXIII(7).
- Rodriguez, M.E., Restrepo, J.I. and Carr, A.J. (2002). Earthquake-induced floor horizontal accelerations in buildings. *Earthquake Engineering & Structural Dynamics* 31(3): 693-718.
- Sabelli, R., Pottebaum, W. and Dean, B. (2009). *Diaphragms for seismic loading. A philosophy for analysis and design*. Structural Engineer.
- Sabelli, R., Sabol, T.A. and Easterling, W.S. (2011). *Seismic Design of Composite Steel Deck and Concrete-filled Diaphragms: a Guide for Practicing Engineers*. NEHRP Seismic Design Technical Brief No. 5. NIST. Gaithersburg, MD.
- Sadashiva, V.K., MacRae, G.A., Deam, B.L. and Spooner, M.S. (2012). Quantifying the seismic response of structures with flexible diaphragms. *Earthquake Engineering & Structural Dynamics*.
- Saffarini, H.S. and Qudaimat, M.M. (1992). In-Plane Floor Deformations in RC Structures. *Journal of Structural Engineering* 118(11): 3089-3102.
- Sarti, F. (2015). *Seismic Design of Low-Damage Post-Tensioned Timber Wall Systems*. PhD Thesis, University of Canterbury.
- Sarti, F., Palermo, A. and Pampanin, S. (2015). Quasi-Static Cyclic Testing of Two-Thirds Scale Unbonded Posttensioned Rocking Dissipative Timber Walls. *Journal of Structural Engineering*.
- Sarti, F., Palermo, A., Pampanin, S. and Berman, J. (2014). Evaluation of the seismic performance factors of post-tensioned timber wall systems. *European Conference on Earthquake Engineering and Seismology*, Istanbul, Turkey.
- Scarry, J.M. (2014). Floor diaphragms – Seismic bulwark or Achilles' heel. *New Zealand Society for Earthquake Engineering Conference 2014*, Wellington, New Zealand.
- Scarry, J.M. (2015). Floor Diaphragms and a Truss Method for their Analysis. *Bulletin of the New Zealand Society for Earthquake Engineering* 48(1): 41-62.
- Schick, M., Vogt, T. and Seim, W. (2013). *Connections and anchoring for wall and slab elements in seismic design*. CIB Working Commission W18 - Timber Structures, Vancouver, Canada.

- Schlaich, J., Schafer, K. and Jennewein, M. (1987). Toward a consistent design of structural concrete
Journal Prestressed Concrete Institute 33(6): 177-179.
- Schoettler, M.J., Belleri, A., Zhang, D., Restrepo, J.I. and Fleischman, R.B. (2009). Preliminary results of the shake-table testing for the development of a diaphragm seismic design methodology. PCI Journal 54(1): 100-124.
- Schulze, H. and Schönhoff, T. (1989). Bemessungsvorschläge für Deckenscheiben in Holzbauart mit dreiseitiger Lagerung ("Design recommendations for timber diaphragms with three-sided support"). Technical University Braunschweig. Stuttgart, Germany.
- SIA (2003a). SIA 261:2003 Actions on Structures. Swiss Society of Engineers and Architects, Zurich, Switzerland.
- SIA (2003b). SIA 265:2003 Timber Structures. Swiss Society of Engineers and Architects, Zurich, Switzerland.
- Skaggs, T.D. and Martin, Z.A. (2004). Estimating Wood Structural Panel Diaphragm and Shear Wall Deflection. Practice Periodical on Structural Design and Construction 9(3): 136-141.
- Smith, P.C., Dowrick, D.J. and Dean, J.A. (1986). Horizontal timber diaphragms for wind and earthquake resistance. Bulletin of the New Zealand Society for Earthquake Engineering 19(2): 135-142.
- Smith, T. (2008). Feasibility of Multi Storey Post-tensioned Timber Buildings. Masters Thesis, University of Canterbury. Christchurch, New Zealand.
- Smith, T. (2014). Post-tensioned Timber Frames with Supplemental Damping Devices. PhD Thesis, University of Canterbury.
- Smith, T., Watson, C., Moroder, D., Pampanin, S. and Buchanan, A. (submitted 2015). Lateral performance of a gravity designed Pres-Lam system. Engineering Structures.
- SOM (2013). Timber Tower Research Project. Skidmore, Owings and Merrill. Chicago, IL.
- Spangler, B.D. (1979). Field Performance of wood diaphragms in structures subjected to wind forces. Proceedings on a Workshop on Design of Horizontal wood diaphragms, Applied Technology Council, Berkeley, California.
- SPAX International GmbH & Co. KG (2012). European Technical Approval. ETA-Danmark A/S, Charlottenlund, Denmark.
- Spieth, H.A., Carr, A.J., Murahidy, A.G., Arnolds, D., Davies, M. and Mander, J.B. (2004). Modelling of Precast Prestressed Concrete Frame Structures with Rocking Beam-Column Connections. New Zealand Society of Earthquake Engineering Conference, Rototua.
- Spooner, M.S. (2008). Quantifying the Dynamic Response of Flexible Floor Diaphragms. 3rd Professional Year Project, University of Canterbury. Christchurch.
- Sritharan, S., Aaleti, S., Henry, R.S., Liu, K.Y. and Tsai, K.C. (2008). Introduction to PreWEC and Key Results of a Proof of Concept Test. Proceedings of the M. J. Nigel Priestley Symposium, King's Beach, CA.
- Standards Australia (2009). AS 3600. Concrete Structures. Standards Australia, Sydney, Australia.
- Standards Australia (2012). AS 1720.1. Timber Structures - Part 1: Design Methods, Sydney, Australia.
- Standards Council of Canada (2014). O86-14. Engineering design in wood, Ottawa, Canada.
- Standards New Zealand (1992). NZS 4203 General Structural Design and Design Loadings for Buildings. Standards New Zealand, Wellington, New Zealand.
- Standards New Zealand (1993). NZS 3603 Timber Structures Standard, Wellington, New Zealand.
- Standards New Zealand (1995). NZS 3101 Concrete Structures Standard. The Design of Concrete Structures, Wellington, New Zealand.

- Standards New Zealand (2004a). NZS 1170.5 Structural Design Actions Part 5: Earthquake Actions - New Zealand.
- Standards New Zealand (2004b). NZS 1170.5 Supp Structural Design Actions Part 5: Earthquake Actions - New Zealand - Commentary.
- Standards New Zealand (2006). NZS 3101 Concrete Structures Standard. The Design of Concrete Structures, Wellington, New Zealand.
- Standards New Zealand (2015). DZ 1170.5 Commentary A1 - Public Comment Draft NZS 1170.5 Supp1: Structural Design Actions – Part 5: Earthquake actions – New Zealand – Commentary.
- STIC (2013). Design Guide Australia and New Zealand - Post-Tensioned Timber Buildings. Structural Timber Innovation Company, Christchurch, New Zealand.
- Structural Engineering Society of New Zealand (2011). Preliminary observations from Christchurch earthquakes. Report prepared for the Canterbury Earthquakes Royal Commission.
- Sustersic, I. and Dujic, B. (2011). Influence of connection properties on the ductility and seismic resistance of multi-storey cross-lam buildings. CIB Working Commission W18 - Timber Structures, Alghero, Italy.
- SWG Schraubenwerk Gaisbach GmbH (2012). European Technical Approval ETA-11/0470. Three-dimensional nailing plate (Connector for timber to-steel connections), ETA-Danmark A/S, Charlottenlund, Denmark.
- Taylor, L. (2004). Vertical Displacement Incompatibility between Floor Slabs and Seismic Resisting Systems. 3rd Professional Year Project, University of Canterbury. Christchurch.
- TDA (2015). Final Report for Commercial Building Costing Cases Studies – Traditional Design versus Timber Project. Project Number PNA 308-1213. Timber Development Association NSW Ltd. Melbourne, Australia.
- Tena-Colunga, A. and Abrams, D.P. (1996). Seismic Behavior of Structures with Flexible Diaphragms. *Journal of Structural Engineering* 122(4): 439-445.
- The Norwegian Barents Secretariat (2009). Barents House. <http://www.barents.no/barents-house.4607296-139566.html>, 30th May, 2014.
- Thelandersson, S. and Larsen, H.J. (2003). Timber engineering. J. Wiley, New York.
- Tissell, J.R. (1966). Horizontal Plywood Diaphragm Tests. Laboratory Report No. 106. American Plywood Association. Tacoma, WA.
- Tissell, J.R. and Elliott, J.R. (2004). Plywood Diaphragms - Report 138. APA - The Engineered Wood Association. Tacoma, WA.
- Tremblay, R. and Stiemer, S.F. (1996). Seismic behavior of single-storey steel structures with a flexible roof diaphragm. *Canadian Journal of Civil Engineering* 23(1): 49-62.
- Uma, S., Zhao, J. and King, A. (2009). Floor Response Spectra for Frame Buildings under Ultimate and Serviceability Limit States. Structures Congress 2009.
- Valluzzi, M.R., Garbin, E., Dalla Benetta, M. and Modena, C.C. (2010). In-plane strengthening of timber floors for the seismic improvement of masonry buildings. World Conference on Timber Engineering, Riva del Garda.
- van Beerschoten, W. and Newcombe, M. (2010). The Effects of Diaphragm Flexibility on the Response of Post-Tensioned Timber Buildings. Masters Thesis, University of Canterbury. Christchurch, New Zealand.
- van Beerschoten, W.A. (2013). Structural Performance of Post-tensioned Timber Frames under Gravity Loading. PhD Thesis, University of Canterbury.

- van Beerschoten, W.A., Carradine, D.M. and Palermo, A. (2013). Compressive strength and stiffness of Radiata Pine laminated veneer lumber. *European Journal of Wood and Wood Products* 71(6): 795-804.
- Van De Kuilen, J.W.G., Ceccotti, A., Xia, Z. and He, M. (2011). Very tall wooden buildings with Cross Laminated Timber. *Procedia Engineering* 14: 1621-1628.
- van de Lindt, J. and Pei, S. (2010). SAPWood. <https://nees.org/resources/sapwood>.
- van de Lindt, J., Pei, S., Pryor, S.E., Shimizu, H. and Isoda, H. (2010). Experimental Seismic Response of a Full-Scale Six-Story Light-Frame Wood Building. *Journal of Structural Engineering* 136(10).
- Vides, R. and Pampanin, S. (2015). Towards a performance-based design of precast concrete diaphragms using jointed dissipative connectors: concept and feasibility study. *New Zealand Conference of Earthquake Engineering*, Rotorua, New Zealand.
- Wagner, H. (1929). Ebene Blechwandträger mit dünnem Stegblech ("Flat sheet metal girders with very thin metal webs". NASA Technical Reports Server, Reports NACA-TM 604, 605 and 606, 1931). *Zeitschrift für Flugtechnik und Motorluftschiffahrt* 20(8-12).
- Wallner-Novak, M., Koppelhuber, J. and Pock, K. (2013). Brettsperrholz Bemessung - Grundlagen für Statik und Konstruktion nach Eurocode ("Cross Laminated Timber Design - Construction and Design according to Eurocode"), Vienna, Austria.
- Waugh, A., Wells, M. and Linegar, M. (2010). Tall Timber Buildings: Application of Solid Timber Constructions in Multi-Storey Buildings. *International Convention of Society of Wood Science and Technology and United Nations Economic Commission for Europe - Timber Committee*, Geneva, Switzerland.
- Waugh, J.D. and Sritharan, S. (2010). Lessons Learned from Seismic Analysis of a Seven-Story Concrete Test Building. *Journal of Earthquake Engineering* 14(3): 448-469.
- Wilson, A., Quenneville, P. and Ingham, J. (2011). Experimental testing of full-scale timber floor diaphragms in unreinforced masonry buildings. *Pacific Conference on Earthquake Engineering*, Auckland, New Zealand.
- Winkel, M.H. (2006). Behaviour of light-frame walls subject to combined in-plane and out of plane loads. *Masters Thesis, The University of New Brunswick*. Fredericton, New Brunswick.
- Wrzesniak, D. (2014). Connection systems in multi storey timber buildings under seismic action. PhD Thesis, Università degli studi di Trieste.
- Wrzesniak, D., Amadio, C., Rinaldin, G. and Fragiacommo, M. (2013). Non-linear cyclic modelling of moment-resisting timber frames. *ANIDIS Conference*, Padua, Italy.

A Appendix – Derivation of the diaphragm deformation equations

A.1 DEFORMATION EQUATIONS FOR LIGHT TIMBER FRAMING DIAPHRAGMS

A.1.1 Bending deformation

It is assumed that the sheathing panels are not contributing to resist the bending of the diaphragm, as their axial stiffness is negligible compared to the axial stiffness of the framing elements. The presence of panel joints also interrupts the flow of longitudinal stresses.

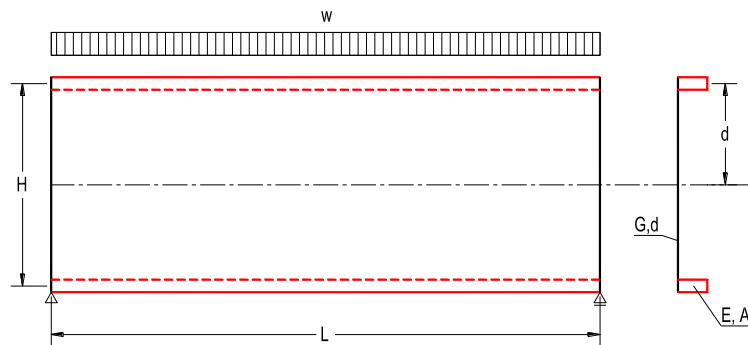


Figure A.1 Bending deformation of a diaphragm

A simply supported equivalent beam with a uniform distributed load as shown in Figure A.1 is considered. The deflection equation for this common case is

$$u_{bending} = \frac{5}{384} \frac{wL^4}{EI} \quad (A.1)$$

where

- $u_{bending}$ diaphragm deflection contribution due to bending;
- w uniform distributed load along the equivalent beam;
- L the length of the diaphragm;
- E modulus of elasticity of the chord beams;
- I the second moment of inertia of the chord beams.

The second moment of inertia of the chord beams to the centroidal axis of the diaphragm is

$$I = 2(I_o + Ad^2) \cong 2Ad^2 = 2A \left(\frac{H}{2}\right)^2 = A \frac{H^2}{2} \quad (A.2)$$

where

- I_o second moment of inertia of the chord relative to its centroid;
- A chord area;
- d distance between the centroid of the chord and the centroid of the diaphragm;

H height of the diaphragms (distance between the chord beams).

The approximation in Equation (A.2) can be justified, as the second moment of inertia of the chord around its centroid is much smaller than the Huygens–Steiner term. By inserting equation (A.2) in (A.1) we obtain

$$u_{bending} = \frac{5}{192} \frac{wL^4}{EAH^2}. \quad (\text{A.3})$$

Often the load applied to the diaphragms is written in terms of the resultant concentrated force W instead of a distributed load w

$$u_{bending} = \frac{5}{192} \frac{WL^3}{EAH^2}. \quad (\text{A.4})$$

A.1.2 Shear deformation

Similarly to the bending deformation term, a simply supported beam with a uniformly distributed load w is considered. It is assumed that only the sheathing panels resist the shear in the diaphragm. This is justified, since the cross section of the chord beams is much smaller than the one of the sheathing panels. Unlike classic beam theory, it is assumed that the shear is uniformly distributed along the diaphragm height. This assumption has been proven correct by the outcomes of several shear tests on plywood diaphragms in the US (ATC 1979).

The general equation for the shear deflection of a simply supported beam can be written as

$$u_{shear} = \frac{1}{8} \frac{\kappa wL^2}{AG} \quad (\text{A.5})$$

where

u_{shear}	diaphragm deflection contribution due to shear;
G	shear modulus;
κ	shear coefficient (taken as $\kappa = 1.0$ as explained above);
A	shear area.

This equation can be rewritten for the diaphragms case as

$$u_{shear} = \frac{1}{8} \frac{wL^2}{GdH} \quad (\text{A.6})$$

where

H	height of diaphragm;
d	sheathing panel thickness;

and if written for the total load on the diaphragm

$$u_{shear} = \frac{1}{8} \frac{WL}{GdH}. \quad (\text{A.7})$$

A.1.3 Fastener slip

For the derivation of the fastener slip contribution, a single cantilevered shear panel is assumed as shown in Figure A.2. A concentrated force F is applied at the panel end. The shear panel of size $B \times H$ is assumed to consist of individual sheathing panels of dimensions $b \times h$, connected by nails to the framing elements on all edges.

For completeness, also the cantilever shear deformation of the shear panel is evaluated. A concentrated force applied to the shear panel will cause the following deformation:

$$u'_{panel\ shear} = \gamma B = \frac{\tau}{G} B = \frac{t}{Gd} B = \frac{1}{Gd} \frac{FB}{H} = \frac{FB}{GA} \quad (A.8)$$

where

$u'_{panel\ shear}$	shear deflection of a cantilevered panel;
γ	shear angular deformation;
τ	shear stress;
t	unit shear force;
H	height of the shear panel;
B	length of the shear panel;
G	shear modulus;
d	sheathing panel thickness.

To determine the deformation of the shear panel given by the fastener slip, first the slip of the single fastener needs to be calculated

$$\delta = \frac{F_1}{K_{ser}} \quad (A.9)$$

where

δ	fastener slip;
F_1	force on one fastener;
K_{ser}	slip modulus (connection stiffness).

Having assumed that the unit shear force is constant along the panel edge, and knowing that the unit shear forces is the same on all panel edges because of the compatibility requirement, the force and therefore the fastener slip can be calculated as

$$F_1 = t \cdot s = \frac{F}{H} s \quad (A.10)$$

$$\delta = \frac{Fs}{HK_{ser}} \quad (A.11)$$

where

s	fastener spacing.
-----	-------------------

To calculate the deflection of the shear panel due to the fastener slip, the force is assumed to be applied to the individual framing members, which introduce the force into the sheathing

panel along their length. Additional framing elements are placed on the shear panel edges and any other sheathing panel edge (blocked diaphragm assumption).

The deflection due to slip in the vertical joints $u'_{fastener v}$ can be calculated as

$$u'_{fastener v} = \delta \cdot n_v \quad (A.12)$$

where n_v is the number of vertical panel connections in the shear panel. Each panel has two vertical connected edges and considering that B/b sheathing panels make up the shear panel length, we get

$$u'_{fastener v} = \frac{Fs}{HK_{ser}} \cdot 2 \frac{B}{b} = \frac{2s}{K_{ser}b} \frac{FB}{H} \quad (A.13)$$

Similarly the deflection due to slip in the horizontal joints $u'_{fastener h}$ can be calculated as

$$u'_{fastener h} = \delta \cdot n_h \cdot \frac{B}{H} \quad (A.14)$$

The last term of the equation is necessary to transform the horizontal panel deformation into a vertical deformation. The number of horizontal connections n_h is calculated similarly as above, considering that H/h are the number of sheathing panels along the shear panel height.

$$u'_{fastener h} = \frac{Fs}{HK_{ser}} \cdot 2 \frac{H}{h} \cdot \frac{B}{H} = \frac{2s}{K_{ser}h} \frac{FB}{H} \quad (A.15)$$

Summing equations (A.8), (A.13) and (A.15), the total deflection of the cantilever shear panel can be obtained. This equation does not consider the bending contribution of the chord beams. This equation is essential for the determination of the equivalent diagonal stiffness for the truss analogy discussed in Chapter 7.

$$\begin{aligned} u'_{shear panel} &= u'_{panel shear} + u'_{fastener v} + u'_{fastener h} \\ &= \frac{1}{Gd} \frac{FB}{H} + \frac{2s}{K_{ser}b} \frac{FB}{H} + \frac{2s}{K_{ser}h} \frac{FB}{H} \\ &= \left[\frac{1}{Gd} + \frac{2s}{K_{ser}} \left(\frac{1}{b} + \frac{1}{h} \right) \right] \frac{FB}{H} \end{aligned} \quad (A.16)$$

where

$u'_{shear panel}$ is the deflection of a cantilevered shear panel connected to surrounding frame elements as shown in Figure A.2.

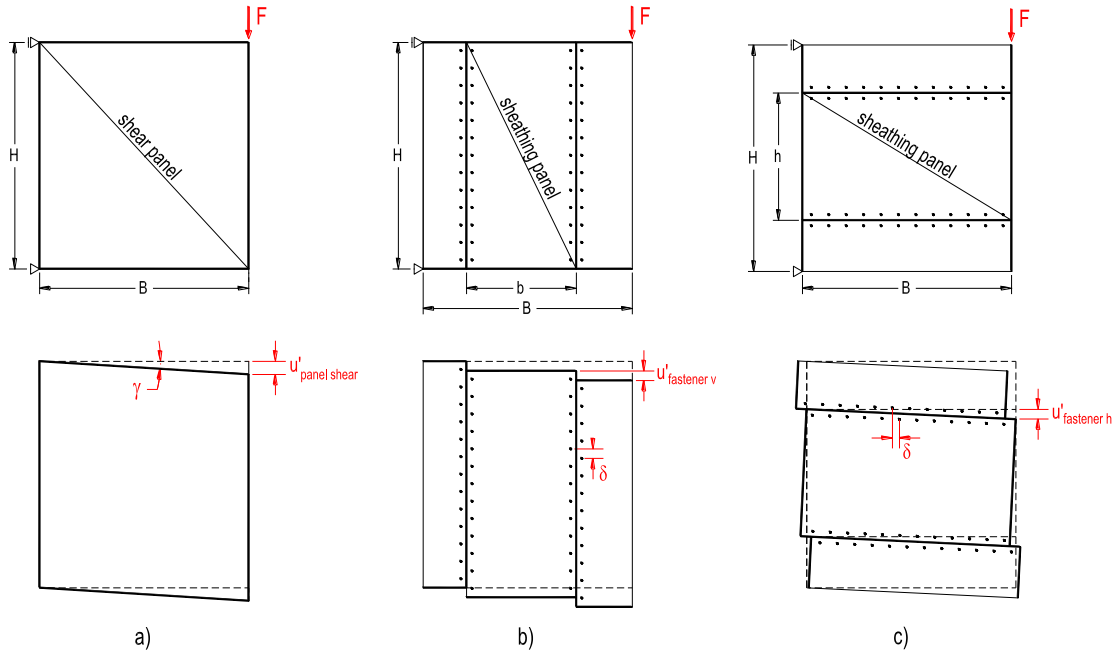


Figure A.2 Diaphragm panel deflection due to a) panel shear deformation, b) vertical connection slip and c) horizontal connection slip

Writing only the two connection slip components of equation (A.16)

$$u'_{connection} = \frac{2s}{K_{ser}} \left(\frac{1}{b} + \frac{1}{h} \right) \frac{FB}{H} \quad (A.17)$$

and by using equation (A.11), the following equation can be derived

$$u'_{connection} = 2\delta \left(1 + \frac{b}{h} \right) \frac{B}{b} = 2\delta(1 + \alpha)m \quad (A.18)$$

where

- $u'_{connection}$ deflection of a cantilevered panel due to fastener slip;
- $\alpha = b/h$ sheathing panel aspect ratio, where b is the length of the sheathing panel edge parallel to the chord beams;
- m number of panels along the chord beam.

Equation (A.18) is valid for a cantilever shear panel with a concentrated load. Considering that the nail slip δ is a linear function of the applied force on the panel, the equation can be easily extended to a simply supported diaphragm. The diaphragm deflection at mid-span is required and therefore involves the deformation of $m/2$ panels. Furthermore the shear distribution and therefore also fastener slip varies from a maximum at the support to 0 at mid-span. The fastener slip contribution can therefore be written as

$$u_{fastener slip} = 2\delta(1 + \alpha) \frac{m}{2} \cdot \frac{1}{2} = \frac{1}{2} \delta(1 + \alpha)m. \quad (A.19)$$

where

- $u_{fastener slip}$ diaphragm deflection contribution due fastener slip

A.1.4 Chord beam splice slip

An eventual slip in the chord beam splice causes a further diaphragm deflection in the direction of load. The change of length in the chord causes rigid body rotation of the two diaphragm parts on either side of the splice as shown in Figure A.3

For small angles the following equations can be found from geometry:

$$\tan \alpha = \frac{u_{splice\ x}}{x} = \frac{\Delta_1}{H}; \quad (A.20)$$

$$\tan \beta = \frac{u_{splice\ x}}{L - x} = \frac{\Delta_2}{H}. \quad (A.21)$$

where Δ_1 and Δ_2 are the deflections as defined in Figure A.3 and x is the distance of the splice from the origin.

Solving both equations for u_{splice} and equating them provides

$$(\Delta_1 + \Delta_2)x = \Delta_2 L. \quad (A.22)$$

Considering that $\Delta = \Delta_1 + \Delta_2$, we obtain

$$\Delta_2 = \frac{\Delta x}{L}. \quad (A.23)$$

Using this result in Equation (A.21) we obtain the diaphragm deflection at the position of the splice

$$u_{splice\ x} = \frac{\Delta x}{LH} (L - x). \quad (A.24)$$

The deflection at midspan of the diaphragm can found to be

$$u_{splice} = \frac{u_{splice\ x} L}{L - x} \frac{L}{2} = \frac{\Delta x (L - x) L}{LH (L - x) 2} = \frac{\Delta x}{2H}. \quad (A.25)$$

where

u_{splice} diaphragm deflection contribution due to chord splice slip.

Since the diaphragm deflection from each chord splice slip is independent from each other, the general equation can be found to be

$$u_{splice} = \frac{\sum \Delta x}{2H}. \quad (A.26)$$

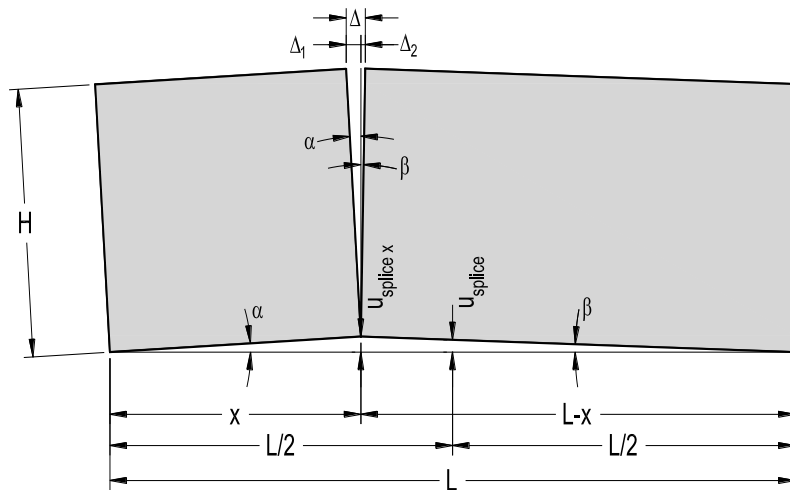


Figure A.3 Deflection of a diaphragm due to chord splice slip at a location x from the origin

A.1.5 Diaphragm deflection for LTF diaphragms

Summing the bending contribution from equation (A.4), the shear contribution from equation (A.7), the fastener slip from equation (A.19) and the chord beam splice slip from equation (A.26), the general equation for LTF diaphragms can be obtained

$$u_{diaphragm} = \frac{5}{192} \frac{WL^3}{EAH^2} + \frac{1}{8} \frac{WL}{GdH} + \frac{1}{2} \delta(1 + \alpha)m + \frac{\sum \Delta x}{2H}. \quad (A.27)$$

A.1.6 Code implementation of the deflection equation

In this chapter some code provisions for the calculation of the LTF diaphragm deflection are shown and briefly discussed. The equations are reproduced as found in the relative codes, only the notations were changed to be congruent with the ones used in this document.

A.1.6.1 New Zealand Timber Structures Code NZS 3603:1993

A commentary clause in New Zealand Timber Structures Code (Standards New Zealand 1993) provides the following diaphragm deflection equation

$$u_{diaphragm} = \Delta_1 + \Delta_2 + \Delta_3 = \frac{5WL^3}{192EAH^2} + \frac{WL}{8GHd} + \frac{1}{2} e_n(1 + \alpha)m \quad (A.28)$$

The single terms in this equation are equivalent to equations (A.4), (A.7) and (A.19) derived before. The fastener slip e_n is provided in the form of a non-linear force-displacement relationship for nails.

A.1.6.2 Canadian Standard Engineering Design in Wood O86-14

The Canadian Engineering Design in Wood Standard O86-14 (Standards Council of Canada 2014) provides the following four term equation

$$u_{diaphragm} = \frac{5}{96} \frac{tL^3}{EAH} + \frac{tL}{4B_v} + 0.000614 L e_n + \sum \frac{\Delta_c x}{2B}. \quad (A.29)$$

Both the bending and the shear deflection term are related to equations (A.4) and (A.7), but are written in terms of the maximum unit shear force t , instead of the total diaphragm load W . The maximum unit shear force is

$$t = \frac{V}{H} = \frac{wL}{2H} = \frac{W}{2H} \quad (A.30)$$

where

- t unit shear force [force/length];
- V shear at the support.

By using equation (A.30) in equation (A.4) we obtain

$$u_{bending} = \frac{5}{96} \frac{tL^3}{EAH}. \quad (A.31)$$

For the shear contribution, the Canadian standard introduces the shear-through-thickness rigidity of the sheathing B_v , which is the product of the shear modulus G and the thickness of the sheathing panels t . Combining equations (A.7) and (A.30) and introducing B_v , we obtain

$$u_{shear} = \frac{1}{4} \frac{tL}{Gd}. \quad (A.32)$$

The fastener slip term is a special case to equation (A.19) where the standard dimension of the North American plywood sheathing panel of 4x8 feet is used. Equation (A.19) is rewritten for commodity

$$u_{connection} = \frac{1}{2} e_n \left(1 + \frac{b}{h}\right) \frac{L}{b} = L e_n \left(\frac{1 + \frac{b}{h}}{2b}\right). \quad (A.33)$$

The term in parenthesis yields to 0.000615 for a standard plywood panel of 4x8 feet, with the longer edge parallel to the chord beams and with all dimensions in SI units (i.e. 1219x2438 mm). The fastener slip e_n can be evaluated with a provided equation.

A.1.6.3 Special Design Provisions for Wind and Seismic with Commentary SDPWS2008

The commentary to the Special Design Provisions for Wind and Seismic (American Forest & Paper Association - American Wood Council 2005) provides the following four term equation:

$$u_{diaphragm} = \frac{5}{96} \frac{tL^3}{EAH} + \frac{tL}{4Gt} + 0.188 L e_n + \sum \frac{\Delta_c x}{2B}. \quad (A.34)$$

This equation is identical to the Canadian provision, except for the constant in the fastener slip term. This is due to the imperial units considered, and leads to the same results. The fastener

slip e_n can be evaluated with empirical equations provided in the code for different fastener sizes and for different sheathing materials.

A.2 DEFORMATION EQUATION OF A QUADRILATERAL SYSTEM WITH A DIAGONAL

In this section the deformation equation of a quadrilateral system with a diagonal is derived.

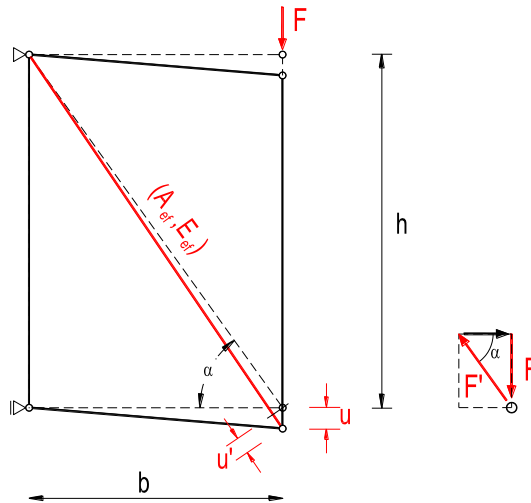


Figure A.4 Quadrilateral system with diagonal

For the system in Figure A.4, loaded by a force F , the force in the diagonal can be calculated as

$$F' = \frac{F}{\sin\alpha} \quad (\text{A.35})$$

with the angle α being

$$\sin\alpha = \frac{h}{\sqrt{h^2 + b^2}} = \frac{h}{l} \quad (\text{A.36})$$

According to Hook's law the force in the diagonal can also be calculated in function of its deformation

$$F' = k u' = \frac{E_{ef} A_{ef}}{l} u' \quad (\text{A.37})$$

Considering the relation between the vertical deformation of the system and the extension of the diagonal

$$u = \frac{u'}{\sin\alpha} \quad (\text{A.38})$$

and by inserting u' as derived in Equation (A.37), the deformation can be written as

$$\mathbf{u} = \frac{F'l}{E_{ef}A_{ef}} \frac{1}{\sin\alpha} = \frac{Fl}{E_{ef}A_{ef}} \frac{1}{(\sin\alpha)^2} = \frac{Fl^3}{E_{ef}A_{ef}h^2} \quad (\text{A.39})$$

A.3 DEFORMATION EQUATIONS FOR MASSIVE TIMBER DIAPHRAGMS

A diaphragm made of solid timber panels has similar deflection behaviour as the one made of LTF. Major differences can be found in the connection between the single panel elements.

Figure A.5 schematically shows the possible connection layout of a solid timber panel diaphragm. To adopt the deflection equation for this type of diaphragms, only the fastener slip term needs to be changed. It is assumed that all panel edges are connected to the chord beams with the same fastener type and spacing. All panel to panel connections are assumed to the same.

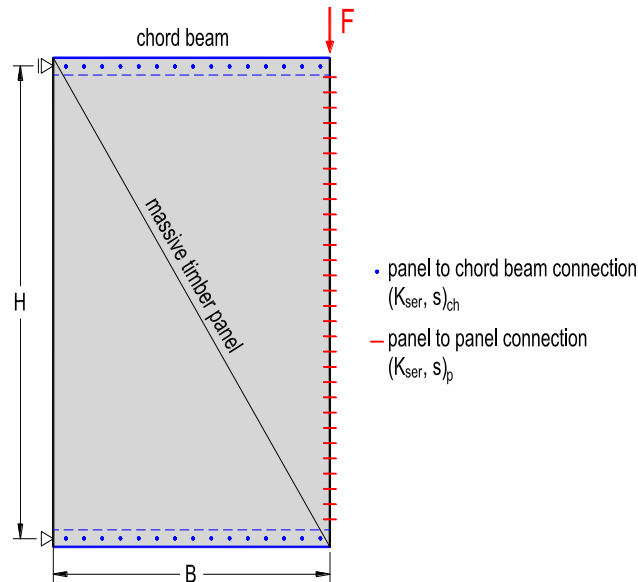


Figure A.5 Shear panel with connection layout

Considering the shear panel in Figure A.5, a single panel has two horizontal connections to the boundary beams (perpendicular to load direction). If it is assumed that the panels are directly connected to each other, then one vertical panel edge is fixed and the other one is connected with flexible fasteners. Repeating the same steps used to obtain Equations (A.13) and (A.15) for LTF diaphragms, the deformation of the shear panel due to fastener slip becomes

$$\begin{aligned} u''_{fastener\ slip} &= u''_{fastener\ v} + u''_{fastener\ h} \\ &= \frac{s_p}{K_{ser\ p} b} \frac{FB}{H} + \frac{2s_{ch}}{K_{ser\ ch} h} \frac{FB}{H} \end{aligned} \quad (\text{A.40})$$

$$\begin{aligned}
 &= \frac{s_p}{K_{ser\ p}} \frac{FB}{b\ H} + \frac{2s_{ch}}{K_{ser\ ch}} \frac{FB}{h\ H} \\
 &= (\delta_p + 2\delta_{ch}\ \alpha)m.
 \end{aligned}$$

where

$u''_{fastener\ slip}$	deflection of a cantilevered massive timber panel due to fastener slip;
δ_p	fastener slip of the panel-to-panel connection;
δ_{ch}	fastener slip of the panel-to-chord connection;
$\alpha = b/h$	sheathing panel aspect ratio;
m	number of panels along the chord beam.

Similarly as for equation (A.16), the panel shear and the fastener slip along the panel edges can be summarized in one single equation. The total deflection of the cantilever shear panel, ignoring the bending contribution of the chord beams, becomes

$$\begin{aligned}
 u'_{shear\ panel} &= u'_{panel\ shear} + u''_{fastener\ v} + u''_{fastener\ h} \\
 &= \frac{1}{Gd} \frac{FB}{H} + \frac{s_p}{K_{ser\ p}} \frac{FB}{b\ H} + \frac{2s_{ch}}{K_{ser\ ch}} \frac{FB}{h\ H} \\
 &= \left[\frac{1}{Gd} + \left(\frac{s_p}{K_{ser\ p}} \frac{1}{b} + \frac{s_{ch}}{K_{ser\ ch}} \frac{2}{h} \right) \right] \frac{FB}{H}.
 \end{aligned} \tag{A.41}$$

This equation is essential for the determination of the equivalent diagonal in the truss analogy discussed in Chapter 7.

Repeating the same procedure as for LTF panels, the fastener slip term for the whole diaphragm can be written as:

$$u_{fastener\ slip} = (\delta_p + 2\delta_{ch}\ \alpha) \frac{m}{4}. \tag{A.42}$$

Finally the total deformation for massive timber diaphragms can be written as

$$u_{diaphragm} = \frac{5WL^3}{192EAH^2} + \frac{WL}{8GHt} + (\delta_p + 2\delta_{ch}\ \alpha) \frac{m}{4}. \tag{A.43}$$

In the case where the connections between the panels and the chord beams have the same connection layout (i.e. the same fastener stiffness and spacing), equation (A.43) can be simplified into

$$u_{diaphragm} = \frac{5WL^3}{192EAH^2} + \frac{WL}{8GHt} + \delta(1 + 2\ \alpha) \frac{m}{4}. \tag{A.44}$$

B Appendix – Finite element modelling of timber diaphragms

In order to verify the appropriateness of the girder analogy and the deflection equation for massive timber diaphragms (see Chapter 3 and 6 respectively), in order to study the implication of different load types on the diaphragms (see Chapter 6) and in order to evaluate the effectiveness of the Equivalent Truss Method for timber diaphragms (see Chapter 7), different finite elements models have been setup with the analysis software SAP2000 (CSI 2004).

Because this research is aimed to be as practical as possible, a computer software which is readily available in design offices has been chosen. A number of in-house software packages like Floor 2D (Li and Foschi 2004) or SapWood (van de Lindt and Pei 2010) would probably yield more accurate results and allow for a more detailed analysis, but these packages are not readily available and their usage is often limited to research purposes.

The finite element models carried out in this work are not aimed to provide the best fit for real diaphragm assemblies, but should provide reference values which follow first principles and which can be easily reproduced in design offices for everyday use. For this reason, the force-displacement curves of the fasteners are not calibrated towards experimental values; stiffness values are instead calculated from design standards like Eurocode 5 (Eurocode 5 2008).

B.1.1 Definition of the finite element diaphragm models

All FEM models are two dimensional and are solved with a linear static or non-linear static solver (Newton-Raphson) as required.

Chord, collector and strut beams, as well as framing elements, have been modelled as beam elements with a modulus of elasticity of $E = 11.000$ MPa. Section sizes are as described below or as defined in the individual models.

The sheathing panels for LTF diaphragms are modelled as orthotropic shell elements with membrane properties only (i.e. only in-plane loads and deflections can be analysed). Properties are taken as for a standard oriented strand board (OSB) panel as shown in Table B.1 with an assigned thickness of 20 mm.

Table B.1 Material properties of panel elements

OSB panel	CLT panel
Orthotropic membrane element	Anisotropic membrane element
$E_1 = 3,800 \text{ MPa}$	$E_1 = 8,000 \text{ MPa}$
$E_2 = 3,000 \text{ MPa}$	$E_2 = 4,000 \text{ MPa}$
$G = 1,080 \text{ MPa}$	$E_3 = 500 \text{ MPa}$
$\nu_{12} = 0.22$	$G_{12} = 600 \text{ MPa}$
	$G_{13} = 500 \text{ MPa}$
	$G_{23} = 100 \text{ MPa}$
	$\nu_{12} = 0.07$
	$\nu_{13} = 0.35$
	$\nu_{23} = 0.35$

The massive timber panels are modelled as membrane elements with anisotropic material properties to simulate a 150 mm thick cross laminated timber (CLT) panel. The properties are taken from Ashtari (2009) and are summarized in Table B.1.

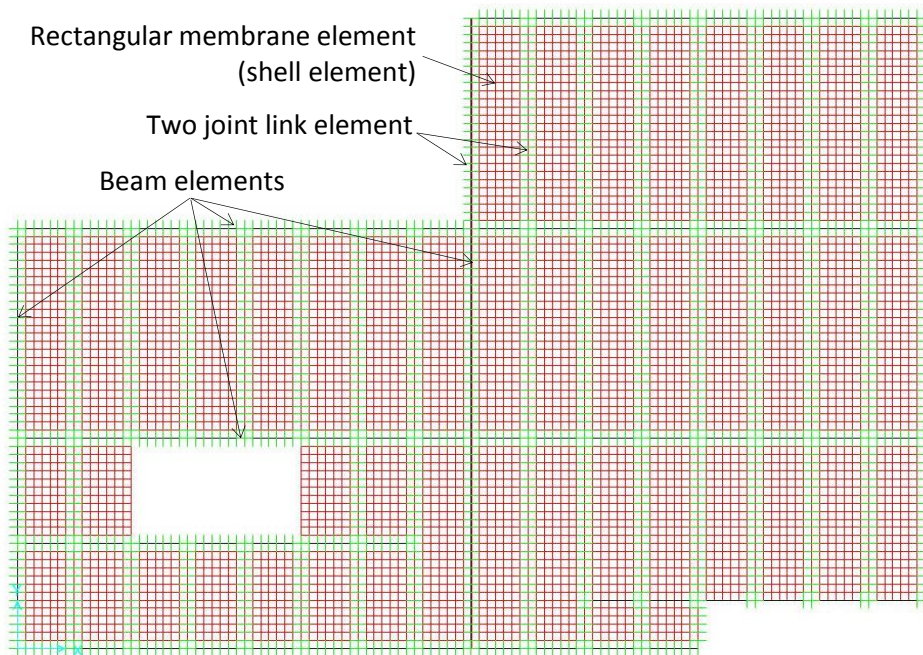


Figure B.1 SAP2000 finite element model

For LTF diaphragms, the framing elements are modelled as beams with a cross section of 50 x 100 mm². Each panel edge is connected to the framing elements with two-joint link elements every 150 mm. In the case of massive timber diaphragms, panels are connected directly by two-joint link elements every 150 mm.

Except when explicitly stated, stiffness values for the link elements are assigned for both the direction parallel and perpendicular to the panel edge. The distance between the panel edge and the centreline of the framing elements or in between adjacent panel edges is kept to a minimum of 1 to 2 mm to avoid secondary effects from the eccentricity. Because the model

are in 2D only, eccentricities between the panel plane and the centreline of the beam elements are not considered. This effect might need to be checked for the diaphragm design, but is considered not to affect the load path and deformations of diaphragms.

Chord, collector and strut beams have been assumed to be 200 x 400 mm².

The connection of framing elements to chord and collector beams as well as framing elements are also modelled with two-joint link elements with an axial stiffness of 9,000 N/mm in tension and an almost infinite stiffness in compression. The shear stiffness was assigned as 9,000 N/mm. The connection between chord and collectors beams is similarly modelled with two-joint link elements with an axial stiffness of 35,000 N/mm in tension and a very high stiffness in compression, since the elements bear against each other. The shear stiffness was assigned as 9,000 N/mm. These stiffness values were assumed without in depth calculations, as the connection design would often be governed by gravity loads and are outside the scope of this research.

B.1.2 Definition of the stiffness values for the link elements

For an assumed unit shear force of approximately 20 kN/m, a nailing spacing of 50 mm with diameter 3.1 nails has been considered. The stiffness of the single nail according to Eurocode 5 (Eurocode 5 2008) can be calculated as for non-predrilled nails

$$K_{ser} = \frac{\rho_m^{1.5} d^{0.8}}{30} = \frac{502^{1.5} 3.1^{0.8}}{30} = 927 \text{ N/mm}; \quad (\text{B.1})$$

$$\rho_m = \sqrt{\rho_{m \text{ OSB}} \cdot \rho_{m \text{ framing}}} = \sqrt{600 \cdot 420} = 502 \text{ kg/m}^3; \quad (\text{B.2})$$

which for the lumped link element at 150 mm spacing becomes roughly 3,000 N/mm.

Similarly, the massive timber panels are assumed to be connected with a lap joint with diameter 8 mm timber screws on 150 mm centres working in shear only. The stiffness can be calculated as for screws

$$K_{ser} = \frac{\rho_m^{1.5} d}{23} = \frac{420^{1.5} 8}{23} = 2,993 \text{ N/mm}; \quad (\text{B.3})$$

assuming a medium density of both the beam elements and CLT panels of 420 kg/m³. The stiffness of the link element at 150 mm is approximated as 3,000 N/mm.

Because both nails and screws have the same stiffness parallel and perpendicularly to the fibres when working in shear, the same stiffness values has been assigned to both the axial and

shear direction of the two-joint link element. The fact that the stiffness values are un-coupled in SAP2000 and thus yield to higher stiffnesses than measured in reality (Judd and Fonseca 2005), is well known to the author. For the sake of simplicity of the model, and the non-availability of coupled link elements in SAP2000 and similar software, this effect has been neglected. It is however thought that this increase in diaphragm stiffness can compensate for the friction effects between the panel elements not considered in the model but certainly occurring in real diaphragm assemblies.

C Appendix – Experimental setups

C.1 EXPERIMENTAL SETUP OF A POST-TENSIONED TWO BAY FRAME UNDER QUASI STATIC LOADS

The Pres-Lam two bay frame setup with draped tendons was initially designed and tested to study its behaviour under gravity loading (van Beerschoten 2013). In order to study the effect of frame elongation due to gap opening on the diaphragm, floor panels were added and the loading apparatus modified as described below. After this testing series, further experiments on the same specimen with external dog-bone dissipaters has been carried out (Smith et al. submitted 2015).

C.1.1 Test setup

The full scale, two-bay frame shown in Figure C.1 was assembled with engineered timber-only floor elements, sitting on top of the main beams. In order to simulate diaphragm forces, the frame was loaded by applying horizontal forces to the floor elements via a hydraulic ram.

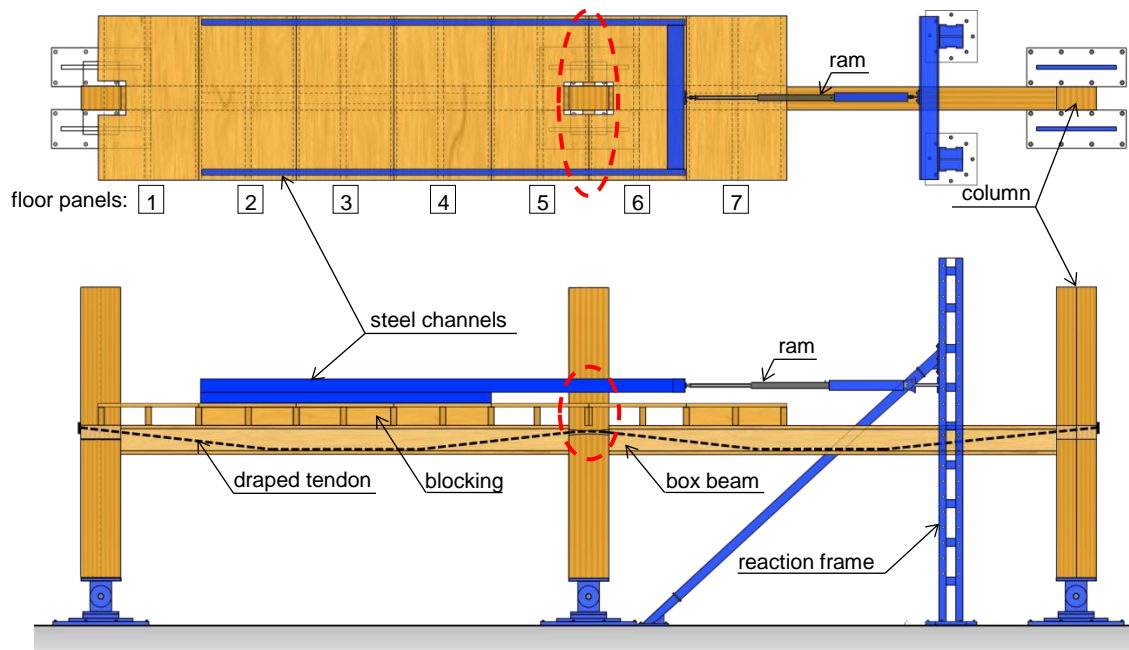


Figure C.1 Test setup of the 2 bay frame with floor panels

The frame with bay lengths of 6 m consisted of 3 solid columns (288 x 500 mm) and two hollow beams (288 x 360 mm), where the webs and flanges were made of 45 mm elements. All

elements were made of LVL11. The beams were sitting on steel corbels and connected to the columns by four 7-wire pre-stressing strands (diameter 12.7 mm). Due to the gravity dominated nature of the frame, the internal tendons were draped to balance a portion of the vertical loading. Material properties are listed in Table C.1.

Table C.1. Material properties of Pres-Lam frame

LVL11		Post-tensioning tendons	
Compression strength parallel to grain	$f_{c,0} = 45$ MPa	Yield stress	$f_y = 1530$ MPa
Compression strength perp to grain	$f_{c,90} = 12$ MPa	Ultimate stress	$f_u = 1760$ MPa
Shear strength	$f_s = 6$ MPa	Elastic modulus	$E_{pt} = 200$ GPa
Characteristic elastic modulus perp to grain	$E_{90} = 0.55$ GPa	Diameter	$D_{pt} = 12.7$ mm
Average elastic modulus parallel to grain	$E_{0,mean} = 11$ GPa	Area	$A_{pt} = 404$ mm ²
Shear modulus	$G = 0.55$ GPa		

20 mm thick and 90 mm deep steel plates were placed at the interface between the beam and the columns in correspondence of the flanges of the timber box beam. The area behind the plates on the column side has been reinforced with 14 fully threaded screws ($\varnothing 10 \times 200$ mm) creating a ‘heal-and-toe’ type connection.

To simulate the timber-only floor diaphragm, seven 2 m long floor panels, as shown in their unassembled state in Figure C.4, were mounted on top of the frame beams. These were designed as stressed-skin-panels for a span of 7.4 m resisting dead and live loads of 2 kN/m² and 3 kN/m² respectively. The top skin was a 36 mm cross-banded LVL panel, the internal and external joists were 90 x 290 mm and 45 x 290 mm respectively. Around the columns a 25 mm gap in the floor panels was created to allow for the rocking movement without any interference with the floor panels.

The joists and, where present, the blocking elements, were connected to the top skin by nail-gluing, using 3.3 x 90 mm gun-nails at 50 mm centres. The blocking was necessary to transfer the horizontal shear forces from the diaphragm skin to the beams through panels 2, 3 and 4 as shown in Figure C.1. Panel 7 was connected to the beam of the second bay so that also the floor portion on the right hand side of the central column is connected to the frame. The 45 x 290 mm blocking elements were connected to the web of the beams by steel plates with six $\varnothing 8/80$ mm wood screws and four M10 bolts respectively. By assuming a unit shear force of 20 kN/m in the diaphragm, the single floor elements except of panels 5 and 6 were connected to each other via 45° inclined $\varnothing 6/120$ mm fully threaded screws placed in the floor joists at 150 mm centres immediately under the floor skin. With this setup only limited diaphragm action can be achieved in the floor panels as the load application is relatively close to the beam.

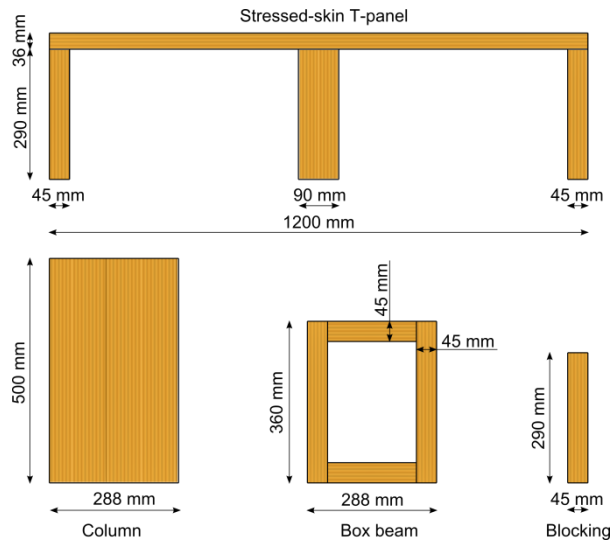


Figure C.2 Section sizes used in test frame

Since the behaviour of the floor at the position of the central column (circled in Figure C.1) was of main interest, the specimen was tested by considering the following four different setups, summarized in Figure C.3:

Setup 1 Pure frame

Benchmark test, frame is loaded directly;

Setup 2 Frame with sliding floor elements

Panels 5 and 6 at the central column are not connected, i.e. left and right portion of floor elements on either side of the central column can slide respectively to each other;

Setup 3 Frame with floor elements with bottom joist connection

Panels 5 and 6 are connected at the bottom of the external joists by fully threaded screws;

Setup 4 Frame with floor elements with full connection

All panels are connected at the top of the joist by fully threaded screws.

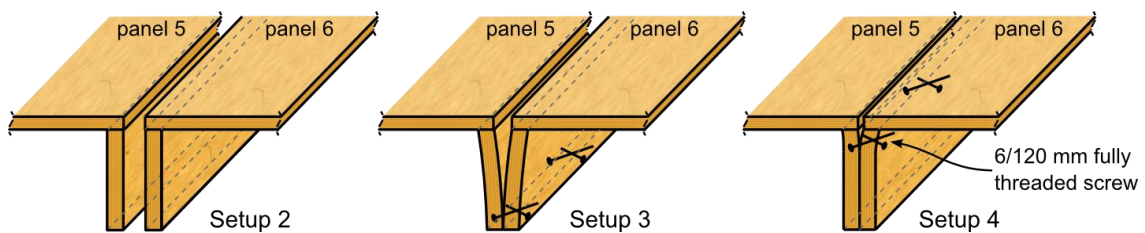


Figure C.3: Connection of floor elements at the central beam-column joint: Setup 2) no connection; Setup 3) bottom flange connection; Setup 4) top flange connection

The first test, Setup 1, is a benchmark test to study the behaviour of the bare frame under lateral loads. Setup 2 was necessary to measure the amount of floor gap opening to expect and does not involve diaphragm action. The two successive connection details Setup 3 and Setup 4 provided the ‘concentrated’ and the ‘spread gap solutions’ respectively.

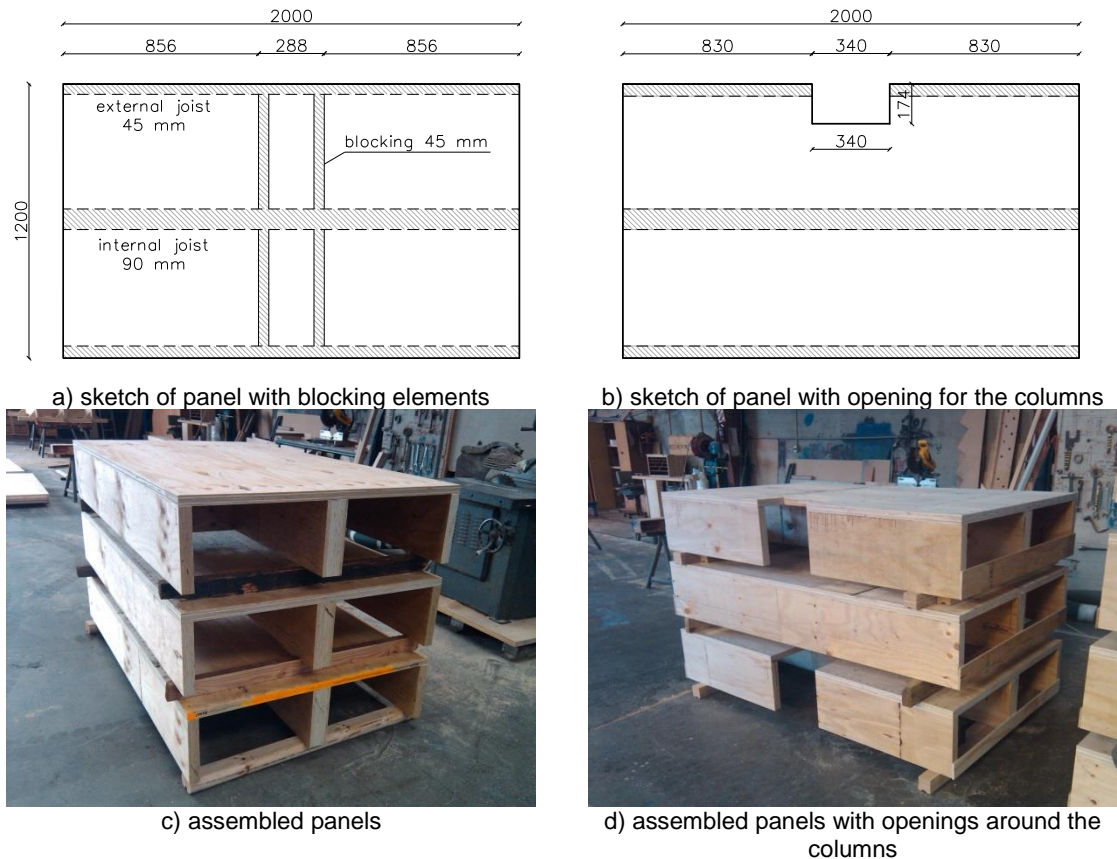


Figure C.4 Stressed skin floor diaphragm panels (Hunter Laminates Ltd)

C.1.2 Loading protocol and instrumentation

The frame was loaded horizontally through the floor panels 2, 3 and 4. Figure C.5 shows the quasi-static cyclic loading protocol with the frame’s interstorey drift values, based on ACI 374.1-05 (ACI Committee 374 2005), omitting the small cycles in between the 3 repetitive cycles.

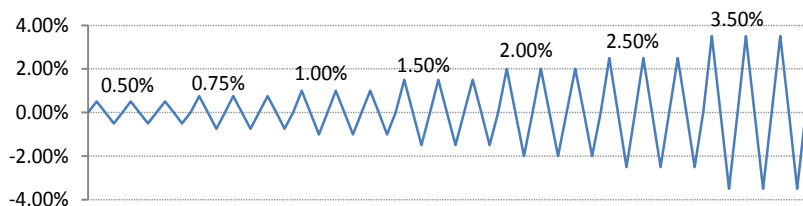


Figure C.5: Quasi-static cyclic loading protocol with building drift values

For a Design Basis Earthquake (DBE), design level drifts of up to 2.5 % needed to be allowed for; this equals to a frame displacement of approximately 56 mm. For a Maximum Credible Earthquake (MCE) drift levels of about 3.5% needed to be considered, demanding a 78 mm displacement of the frame.

Linear displacement potentiometers were used to measure the gap opening at the beam-column-joints (Figure C.6 b) and between the floor panels, as well as any elongation of the panels (Figure C.6 a).

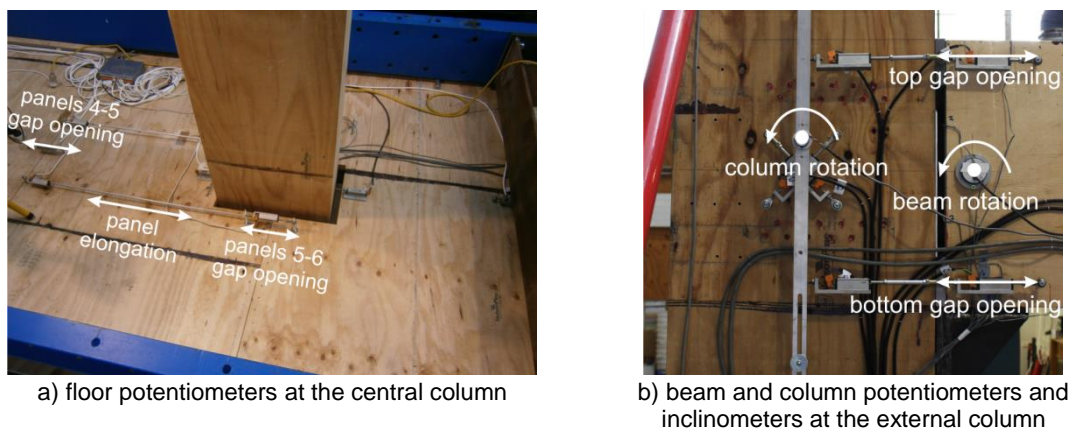


Figure C.6 Floor, beam and column instrumentation

C.1.3 Results

Figure C.7 shows the force-displacement curves for test setup 1 with initial post-tensioning values of 50, 100, 150 and 200 kN. For drift levels of 3.5 % (the figure only shows drifts until 2.5 %, but further test were carried out) a distinctive non-linear elastic behaviour of the frame was observed. Differences in the force values in both the force-displacement curves and the post-tensioning for the positive and negatives drifts are due to the force introduction to one of the two frame beams only.

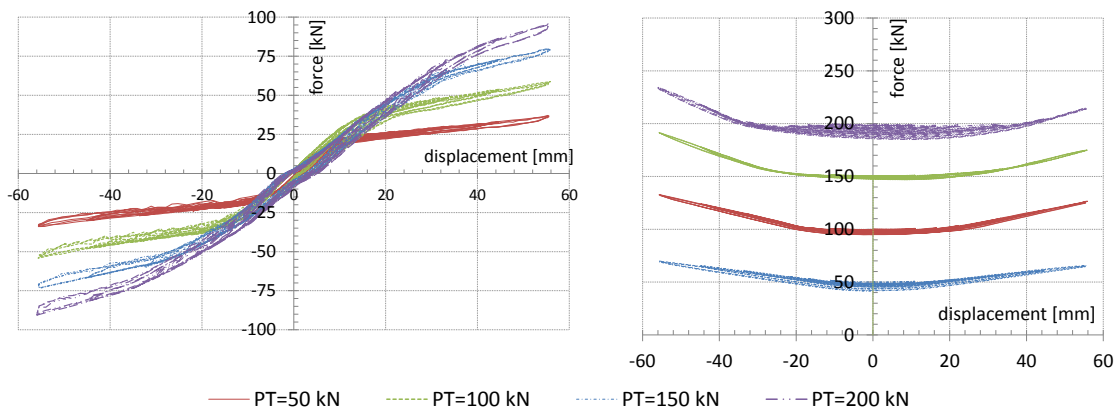


Figure C.7 Force-displacement curve (left) and post-tensioning force (right) of the bare frame (setup 1) for different post-tensioning levels

Figure C.8 shows the frame force-displacement and post-tensioning forces for the frame with an initial post-tensioning value of 100 kN. For test setup 2 values are shown for drifts up to 2.5 %, for setups 3 and 4 drift levels of 3.5 % were reached. The comparison between the graphs for setup 2 with sliding floors (no stiffening of the frame because of floor displacement restrains at the internal column) and setups 3 and 4 with connected floor panels suggest, that the presence of the floor diaphragm does not interfere with the frame behaviour.

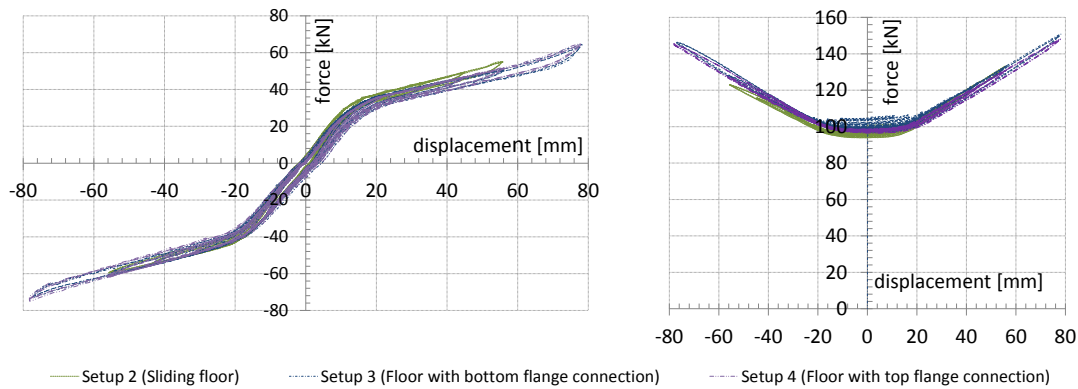


Figure C.8 Force-displacement curve (left) and post-tensioning force (right) for test setups 2, 3 and 4

Figure C.9 shows the beam-column-gap openings at the central column for drift levels of 2.5 %. Since the floor panels on the left and right side of the central column were unconnected, they could slide respectively to each other. The panels were mounted with an initial gap of 10 mm; potentiometer measurements were zeroed for this position. Because of the draped configuration of the post-tensioning strands and the therefore resulting counter flexure of the frame beams, the top gap openings are smaller than the bottom gap openings. Since the floor panels are sitting on top of the framing beams, the gap opening between panels 5 and 6 is geometrically amplified. For beam-column gap openings of about 6 mm, the panels move apart 6.6 mm, clearly showing the presence of displacement incompatibilities.

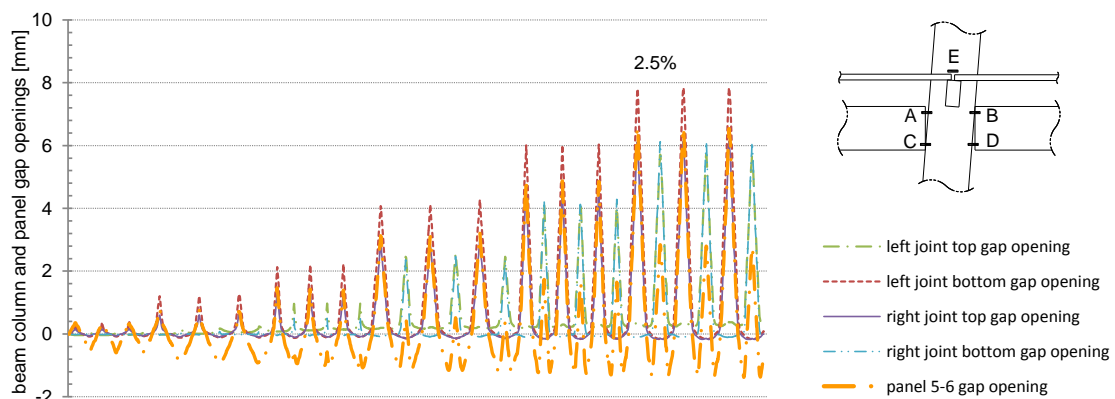


Figure C.9 Beam-column gap openings and floor panel 5-6 gap opening at the central column for test setup 2 with sliding floor panels

For test setup 3 the bottom of the joist at the interface of panels 5 and 6 were connected to each other by the use of fully threaded screws. By placing the connectors at the bottom of the joist, shear forces deriving from diaphragm action could still be guaranteed, while the joist could bend along the height to accommodate the displacement incompatibilities as shown in Figure C.3 b. The connection slip between the floor panels and the frame beams via blocking elements has been monitored, proving a very stiff connection with slips in the order of 0.1 mm.

Figure C.10 shows all floor panel gaps for drift levels up to 3.5 %. Since the connection between panels 5 and 6 was more flexible because of the bottom joist connection, larger openings as expected have been measured at this location. Panel gap openings further away from the central column could be observed as well, with decreasing magnitudes further away from the central column where the displacement incompatibility occurs. The gap opening at panel 5 and 6 decreased to half when compared to setup 2. The remaining displacement required to allow for the beam-column-gap opening was given by the accumulated gap opening from the remaining channels and some panel elongation.

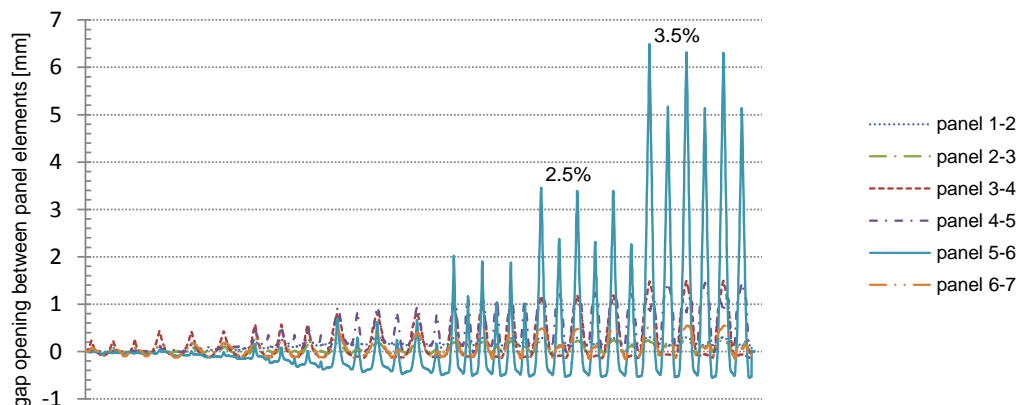


Figure C.10 Gap opening between floor panels for test setup 3

By connecting all floor panels via screws in the joist just under the floor skin, the larger gap opening at panels 5-6 observed in setup 3 were reduced. The displacement demand from the beam-column-gap opening is accommodated by a number of smaller gap openings, mostly between panels 3 and 7. Panel elongation has also been activated to allow for the required displacement.

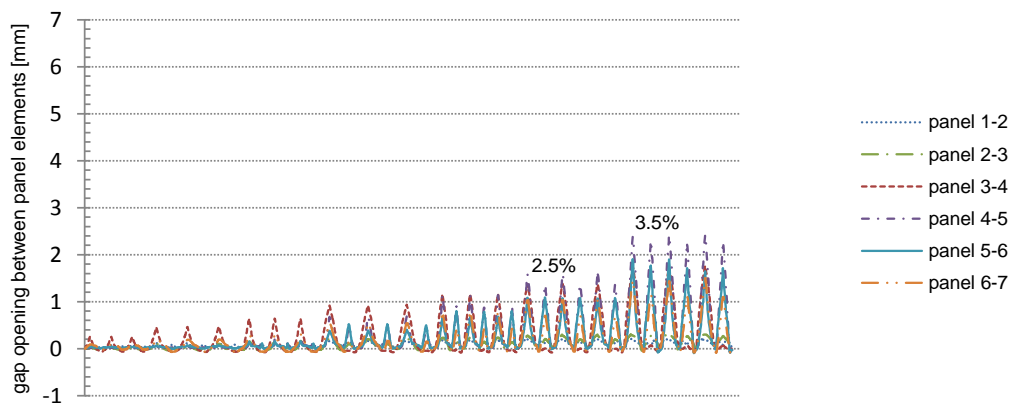


Figure C.11 Gap opening between floor panels for test setup 4

C.1.3.1 Stress check in joist for setup 3

For setup 3 the displacement demand in the floor panels is accommodated by the bending of the floor joists along their height. Independently from the material of the joist (solid timber, LVL or glulam), the stresses created due to this bending action need to be verified. This is because tension stresses perpendicular to grain are activated, which exceedance can lead to brittle failures.

Figure C.12 shows the joist geometry and a simplified model for the calculation of the bending moment in the joists. To account for all sources of flexibilities, both the screw axial stiffness and the stiffness perpendicular to grain of the timber joist have been considered by elastic spring elements. The screw stiffness has been calculated according to ETA-12/0114 (SPAX International GmbH & Co. KG 2012) for a diameter 6 mm screw with an effective length of 42 mm at an insertion angle of 45°. The elastic modulus of the joist has been selected as 371 MPa as suggested in van Beerschoten et al. (2013).

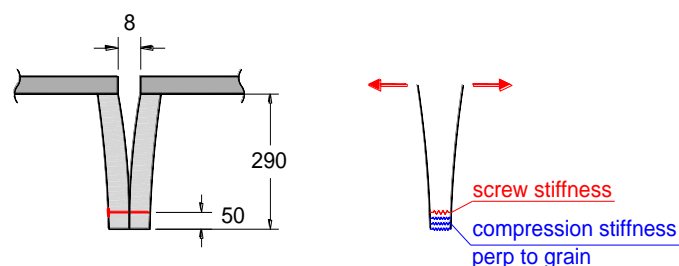


Figure C.12 Joist bending due to displacement incompatibilities

By assuming a gap opening of 8 mm, a bending moment of 0.34 kNm per meter of joist can be obtained. This equals to a stress value of 1 MPa, which compared to observed values from experiments from Ardalany et al. (2010) of 1.43 MPa provide enough safety margin. Care

should be taken for larger gap openings or in the case of other joist geometries. The forces in the screws are 8.7 kN per meter length, a demand easily resisted by the screws.

Similarly to the stress verification in the joists, also the flooring panels need to be verified. The gap opening activates tension stresses perpendicular to grain in the panel skin if the grain direction is parallel to the joist. Large panel thicknesses or cross layers (cross-banded LVL or CLT) can normally easily accommodate the implied stresses.

C.2 EXPERIMENTAL SETUP OF A THREE STOREY POST-TENSIONED FRAME STRUCTURE TESTED UNDER DYNAMIC LOADS

The three storey post-tensioned frame structure made of glued laminated timber (glulam) has been built and tested on a shaking table in the material and structures laboratory “*Laboratorio Prove Materiali e Strutture – SisLab*” at the University of Basilicata in Italy. The structure was part of a separate research program, carried out in collaboration with the University of Canterbury, investigating the dynamic behavior of Pres-Lam frames with and without additional damping devices. For a detailed description of the test setup and the results of the structure refer to Smith (2014).

C.2.1 Test setup

The prototype three-storey Pres-Lam frame structure had a food print of 6 m x 4.5 m and an interstorey height of 3 m. The structure with single bays in both directions was designed for a live load of 3 kN/m^2 with the final storey being a rooftop garden. The design and detailing of the structure was carried out according to the Italian design codes NTC 2008 (Consiglio Superiore dei Lavori Pubblici 2008).

To fit the shaking table dimensions at the University of Basilicata, the test structure as shown in Figure C.13 had to be scaled by 2/3. This resulted in a scaled interstorey height of was 2 m and a footprint of 4 m by 3 m.

The sections of the columns and beams are shown in Figure C.14; all elements were made of glulam grade 32h according to EN 1194:1999-05 (CEN 1999). The structure had post-tensioned frames in both directions, but was loaded in the long (4 m) direction only. The frame connections were realized with the aid of 26.5 mm diameter high strength steel bars, all post-tensioned up to an initial value of 150 kN.

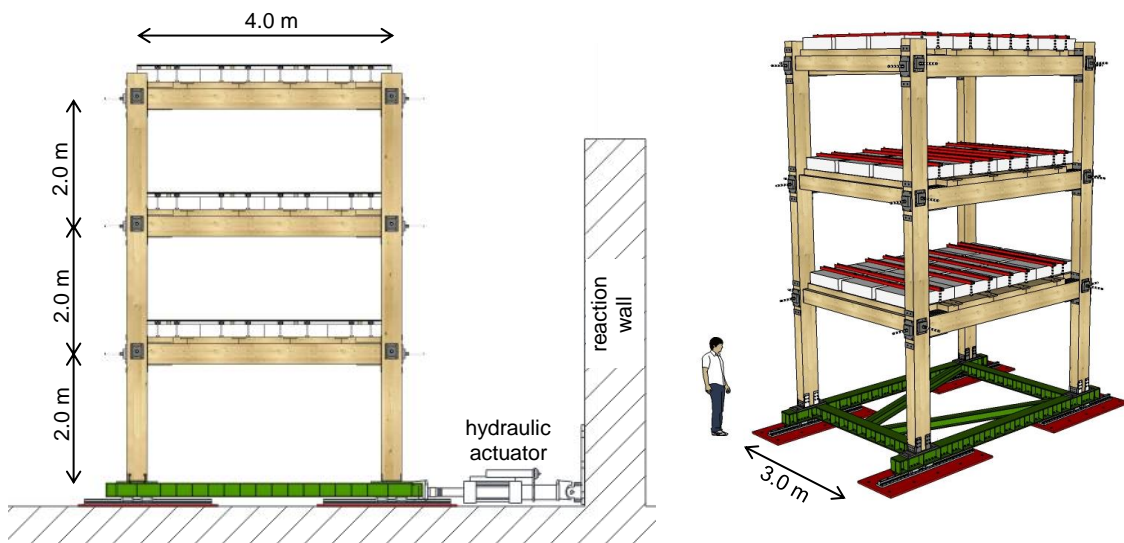


Figure C.13 Experimental setup of the 2/3 scale three storey post-tensioned glulam frame building on the shaking table (image courtesy of Dr. Tobias Smith)

The timber structure was fixed to the shaking foundation testing rig, which consisted of a steel frame sitting on four frictionless sliders. A dynamic actuator with a capacity of ± 500 kN and a stroke of ± 250 mm, placed between a 6 meter thick reaction wall and the test rig, provided the mono-directional movement of the testing rig. Because of the scaled nature of the test structure, mass similitude had to be maintained. Therefore the seismic masses of the floor, resulting from the self-weight of the floor, the weight of the façade and the factored lived load of the original structure, had to be scaled by $(2/3)^2$. The additional mass which had to be placed on the building was obtained by detracting the mass of the test building from the scaled mass. Concrete blocks fixed with steel hold downs on the 3 floor levels provided the required mass.

Table C.2. Material properties of the Pres-Lam multi-storey frame building

Glulam GL32h		Post-tensioning bar	
Bending strength	$f_b = 32$ MPa	Yield stress	$f_y = 1050$ MPa
Compression strength parallel to grain	$f_{c,0} = 29$ MPa	Elastic modulus	$E_{pt} = 170$ GPa
Compression strength perp to grain	$f_{c,90} = 3.3$ MPa	Bar diameter	$D_{pt} = 26.5$ mm
Shear strength	$f_s = 3.8$ MPa	Area per bar	$A_{pt} = 552$ mm ²
Characteristic elastic modulus perp to grain	$E_{90} = 0.46$ GPa		
Average elastic modulus parallel to grain	$E_{0,mean} = 11.1$ GPa		
Shear modulus	$G = 0.85$ GPa		

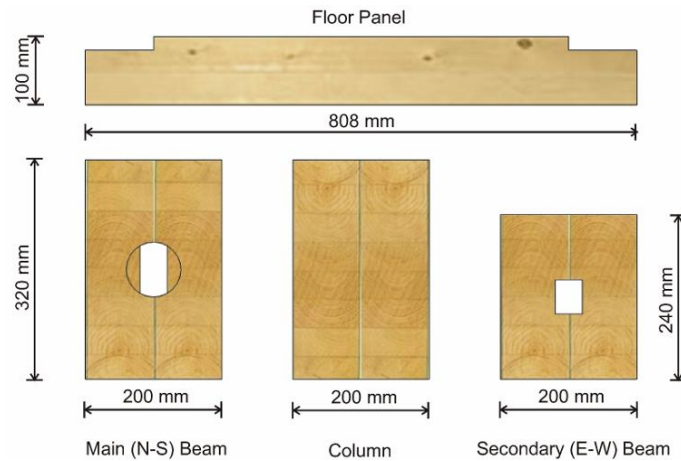


Figure C.14 Section sizes used in glulam test frame (Smith 2014)

The timber diaphragms were designed for a unit shear force of 15 kN/m and consisted of 100 mm thick and 808 mm wide glulam panels. These were connected to each other with a 20 mm thick plywood spline placed in a recess and connected with $\text{Ø}6/80 \text{ mm}$ partially threaded screws in shear every 150 mm as shown in Figure C.15. The diaphragm was connected to the main beams in the loading direction by pairs of $\text{Ø}7/220 \text{ mm}$ fully threaded screws at 45° every 200 mm. Perpendicular to the direction of loading the panels were fixed to the secondary beams by $\text{Ø}6/240 \text{ mm}$ partially threaded screws inclined 45° in beam direction every 186 mm.

Under earthquake loads the structure elastically deforms until the decompression point of the beam-column joint is reached. After this point gap opening at the beam-column joint occurs and the dissipation devices, if present, are activated. The gap opening at the interface however tends to tear the floor panels apart, since they are connected to both the main and secondary beams. To accommodate this displacement incompatibility, the floor panels are connected to the secondary beams by in beam direction inclined screws. Since the screws are relatively flexible in shear, in case of gap opening the panel can slightly move away from the secondary beam. On the other hand the stiffness of the connection in load direction was required to be higher in order to avoid relative slips between the diaphragm panels and the main beams. This could be obtained by the high axial stiffness of fully threaded screws.

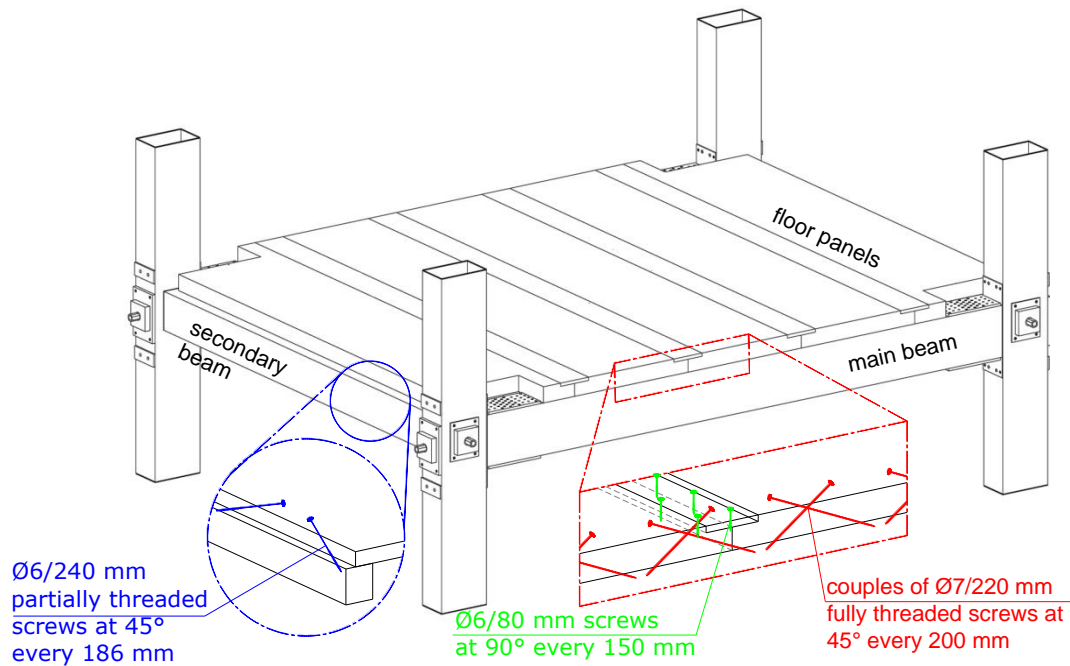


Figure C.15 Connection of the panel elements to each other and the diaphragm to the main and secondary beams

C.2.2 Loading protocol and instrumentation

The loading consisted of a set of seven spectra compatible earthquakes selected from the European strong-motion database as summarized in Table C.3. The code spectrum was defined in accordance with the current European Seismic Design Code (Eurocode 8 2004) with a ground acceleration of $a_g = 0.35$ g, a soil class B and a return period of 1 in 475 years, leading to a PGA of 0.44 g. Because of the 2/3 scale of the structure, the time of the earthquake input was scaled by $(2/3)^{0.5}$. Four of the earthquakes were additionally scaled in acceleration to guarantee a closer fit to the code spectrum (compare Figure C.16). The shake table tests were performed with and without additional dissipation devices with increasing PGA levels.

Table C.3. Information on the seven input earthquakes

ID	Location	Year	M_w	PGA	Epicentral distance	Scale factor
				[g]		
001228x	Izmit, Turkey	1999	7.6	0.36	47	1.5
000196x	Montenegro, Serbia	1979	6.9	0.54	25	1.0
000535y	Erzican, Turkey	1992	6.6	0.77	13	1.5
000187x	Tabas, Iran	1978	7.3	0.93	57	1.0
000291y	Campano Lucano, Italy	1980	6.9	0.26	16	1.5
004673y	South Iceland	2000	6.5	0.72	15	1.5
004677y	South Iceland	2000	6.5	0.23	21	1.0

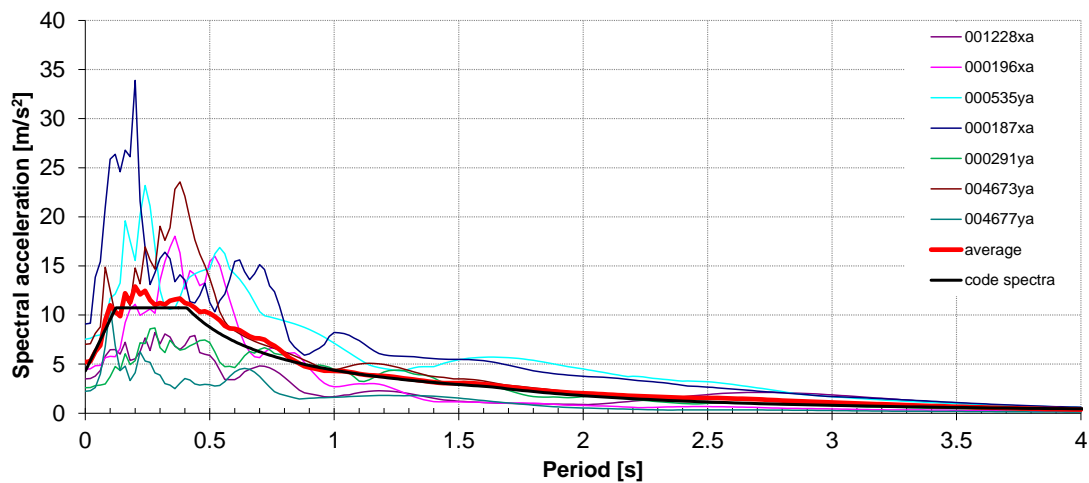


Figure C.16 Code spectra and selected earthquake input for testing

For the initial testing series carried out in 2013, no specific instrumentation to measure diaphragm displacements was available. Before the successive testing series in 2014, additional instrumentation to capture diaphragm displacements and accelerations were installed. Figure C.17 shows the four potentiometers used to measure the relative movement between the first diaphragm panel and the secondary beam, the gap opening between the first two diaphragm panels, the slip between the second diaphragm panel and the main beam, as well as the vertical movement of the first diaphragm panel and the secondary beam. The potentiometer measuring the top beam-column-gap opening which was installed since the beginning of the testing program is also shown. All instrumentation was mounted on the floor at level 1, since the beam-column-gap openings are maximum at this level.

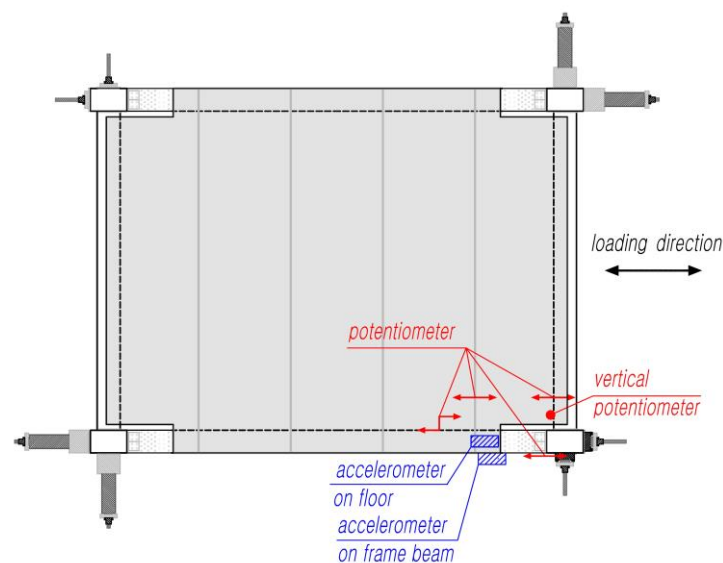


Figure C.17 Instrumentation layout on floor level 1

C.2.3 Results

For the initial test series carried out in 2013 no specific instrumentation to measure diaphragm displacements was installed. Results shown in Smith (2014) show that gap opening at the beam-column joints occurred as expected. No substantial degradation of the building strength and stiffness could be observed after a number of tests. Visual inspection of the diaphragm connections did not show any sign of inelastic deformation of the fasteners after building drifts of up to 3.45%.

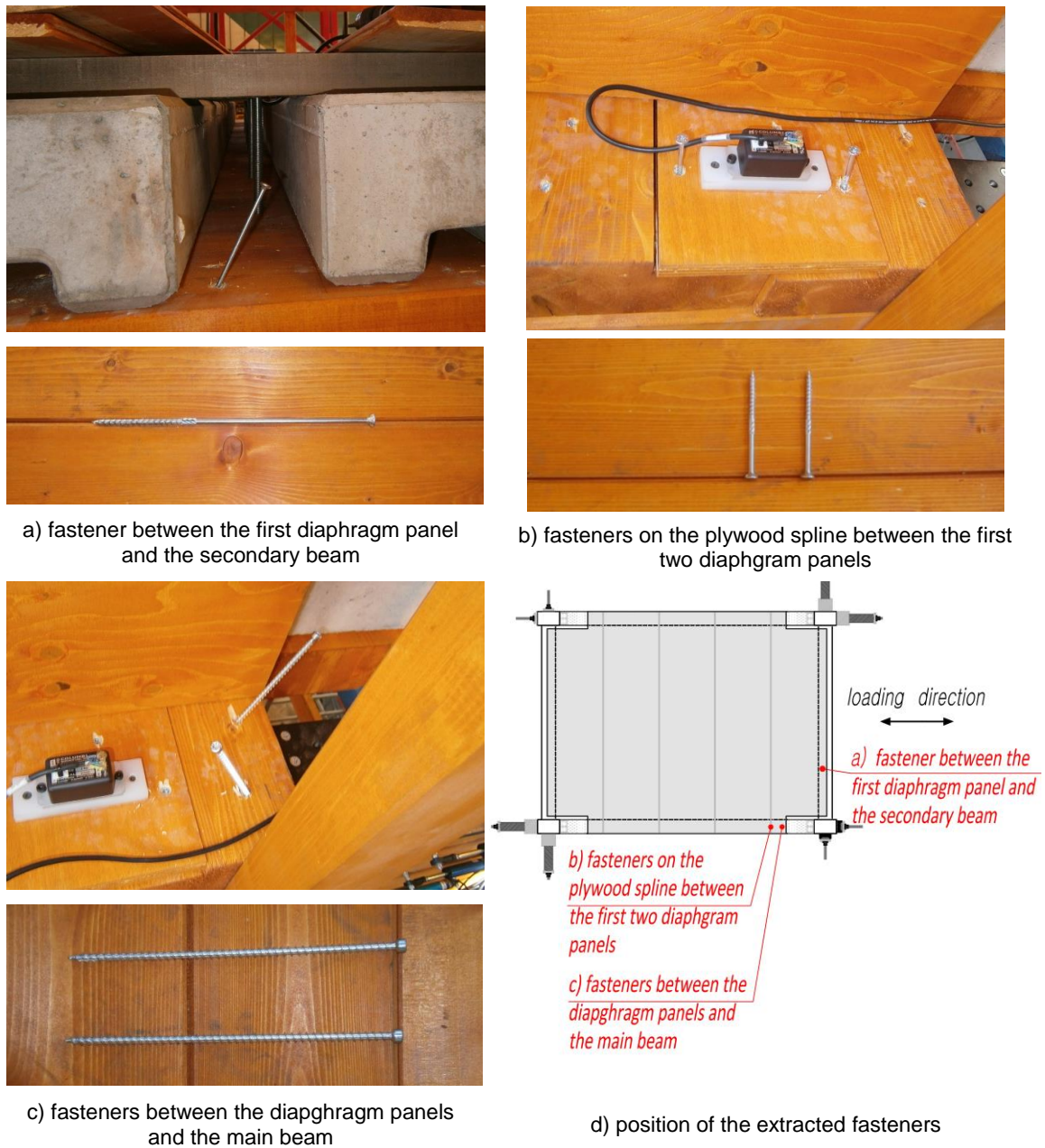


Figure C.18 Pictures from the inspection of diaphragm connections

Figure C.18 shows examples of diaphragm fasteners extracted at the three main connections: a) diaphragm-to-secondary beam connection, b) diaphragm-panels connections, and c) diaphragm-to-main beam connection. The fasteners in the diaphragm-to-secondary beam connection were expected to provide the biggest amount of elastic movement to accommodate the displacement incompatibilities. Because the first floor panel (at the secondary beam) had only a limited connection to the main beam with two screws shown in Figure C.18 b, the screws on the plywood splice were also thought to allow for some elastic panel gap opening. None of the fasteners showed any plastic deformation and the holes in the timber members did not show the typical oval shape due to excessive embedment stresses.

In the successive test series with external dissipation devices carried out in 2014, additional instrumentation as shown in Figure C.17 was used to measure the contributions of the diaphragm displacements. Figure C.19 shows the plot of the three main displacement components allowing for the top beam-column-joint gap opening for the Erzican, Turkey 1992 earthquake. The biggest contribution is provided by the displacement between the diaphragm panel and the secondary beam, followed by the panel-to-panel connection and finally the slip between the diaphragm panel and the main beam. Also shown is the total displacement as the sum of these single contributions.

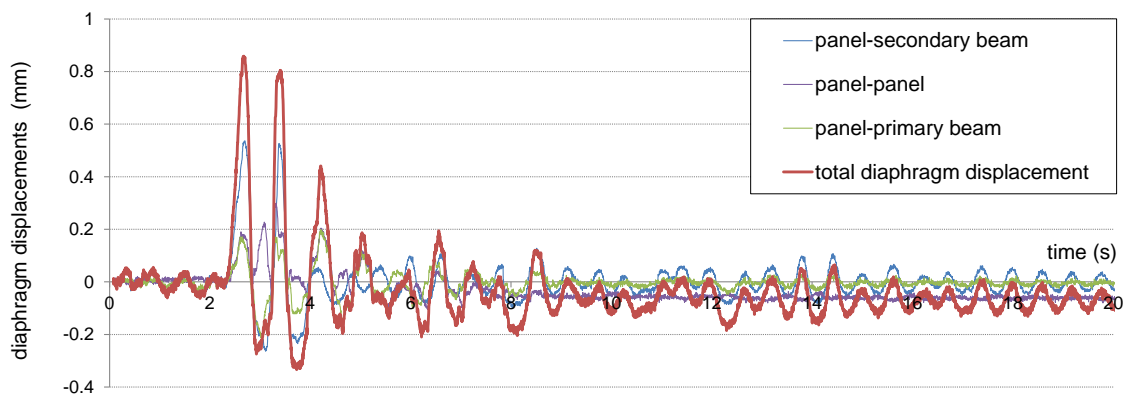


Figure C.19 Diaphragm displacement contributions for the Erzican, Turkey 1992 earthquake

In Figure C.20 the total diaphragm displacements are plotted against the top beam-column-joint gap opening for the same earthquake. Positive values show the values for the case of gap opening, negative values represent the displacements when the top flange of the beam pushes against the column causing local compression. In latter case the diaphragm displacements are reduced since the displacement incompatibility is limited to the compression deformation of the column.

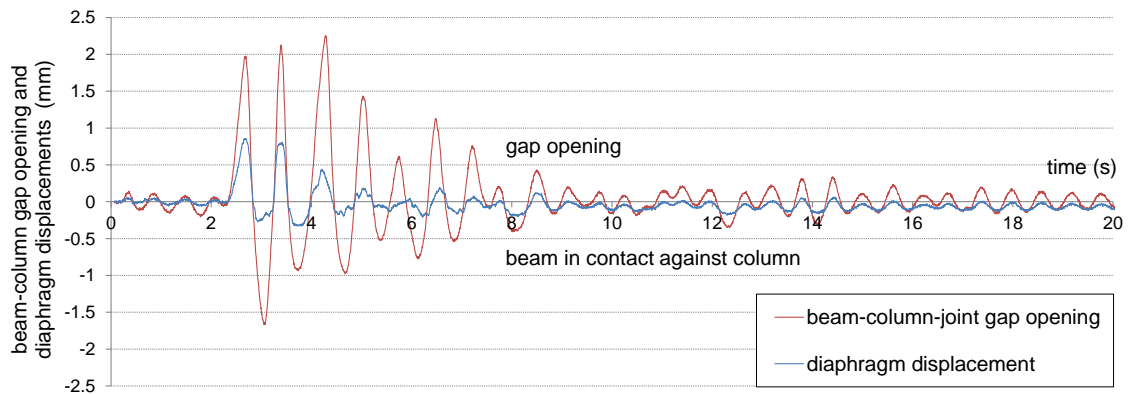


Figure C.20 Beam-column-gap opening and diaphragm displacements for the Erzican, Turkey 1992 earthquake

In the case of beam-column-joint gap opening, the diaphragm deformation allows for a portion of the imposed displacement. From visual inspection during the test it was observed that the remaining displacement demand was provided by the rotation of the secondary beam around its own axis.

Figure C.21 shows the same plot for the remaining earthquakes which the structure could withhold without any damage. Except for the Tabas, Iran (1978) earthquake, the diaphragm could always accommodate displacements of about 1/3 to 1/2 of the gap opening. It is not clear why the diaphragm could not accommodate the joint gap opening for the Tabas earthquake. The displacement incompatibilities have been accommodated elsewhere for this very intense earthquake record. Further testing will address this issue.

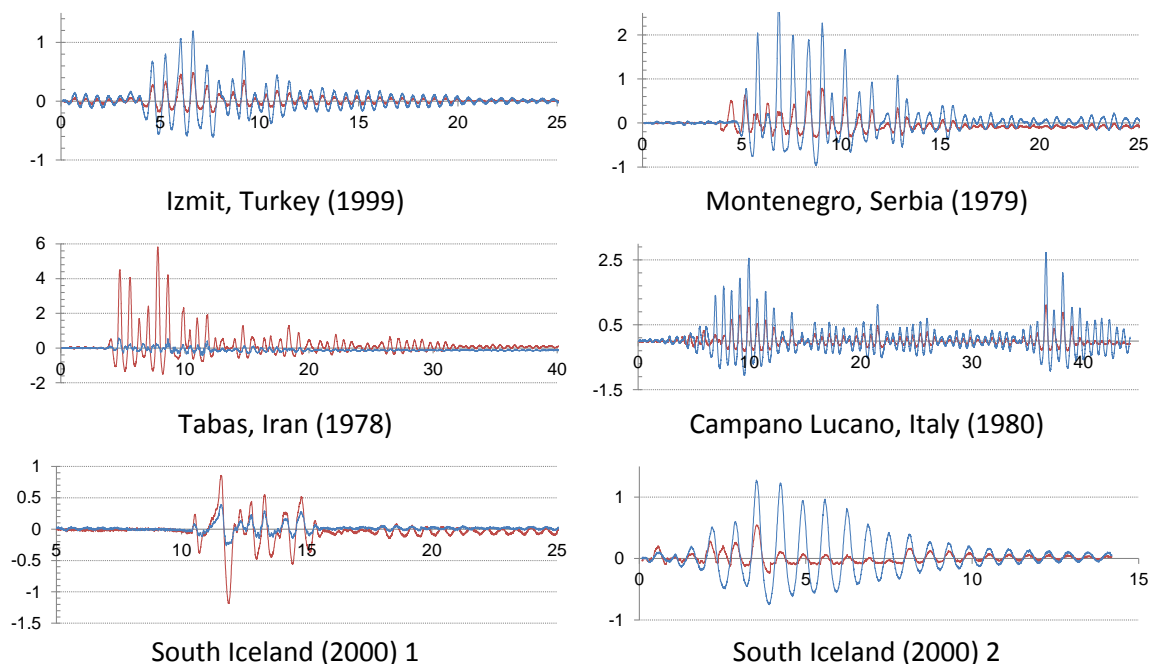


Figure C.21 Beam-column-gap opening and diaphragm displacements for the remaining six earthquakes (vertical axis: beam-column gap opening and diaphragm displacements in mm; horizontal axis: time in seconds)

Figure C.22 shows the vertical movement of the diaphragm relative to the secondary beam. This measurement was thought to provide information on vertical displacement incompatibilities between the diaphragm and the secondary beams as observed in concrete rocking frame buildings (Johnston et al. 2014). In the case of beam-column-joint gap openings the floor panel would move upwards and move downwards if the gap is closed. Because of the flexibility of the diaphragm panels, the flexibility of the connection and the low stiffness in compression perpendicular to the grain, no damage or interference due to this vertical displacement incompatibility could be observed.

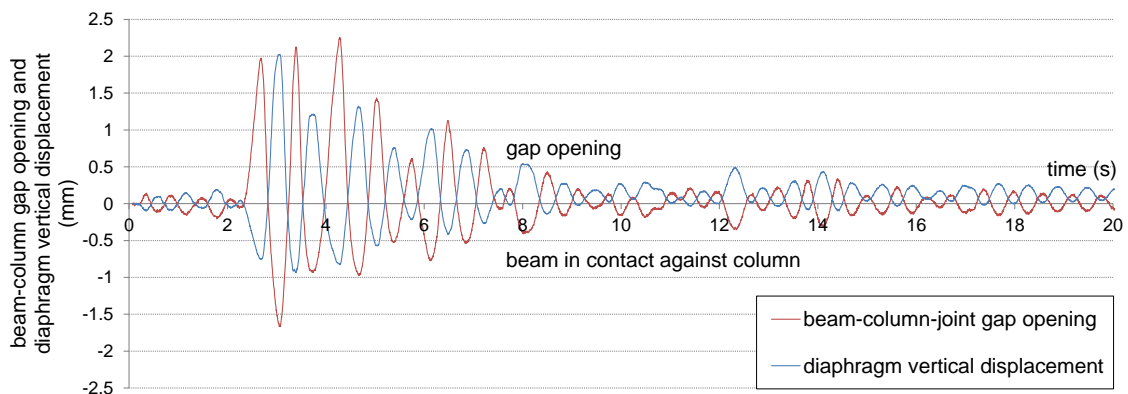


Figure C.22 Beam-column-gap opening and vertical diaphragm displacements for the Erzican, Turkey 1992 earthquake

C.3 EXPERIMENTAL SETUP OF A POST-TENSIONED WALL UNDER QUASI STATIC LOADS

The post-tensioned rocking wall shown in Figure C.23 was initially designed and tested without the floor beams and columns; further details and results on this previous test setup can be found in Sarti et al. (2015). In order to investigate the influence of wall displacement incompatibilities on floor diaphragms, the test specimen was subsequently modified by adding collector beams and external gravity columns. The wall was loaded horizontally through the beams which were connected to each other via a number of different connections as described later and shown in Figures C.25 and C.26. In a further testing stage end columns were added on each side of the wall. The collector beams were connected to those columns through two additional connection configurations as shown in Figures C.27 and C.28. The horizontal forces were transferred via special contact elements to the wall.

C.3.1 Test setup

The 2/3 scale post-tensioned rocking wall was loaded under cyclic lateral loads through two pairs of floor beams. A number of different connection setups were tested in order to investigate the vertical uplift and rotational interaction between the wall and the beams.

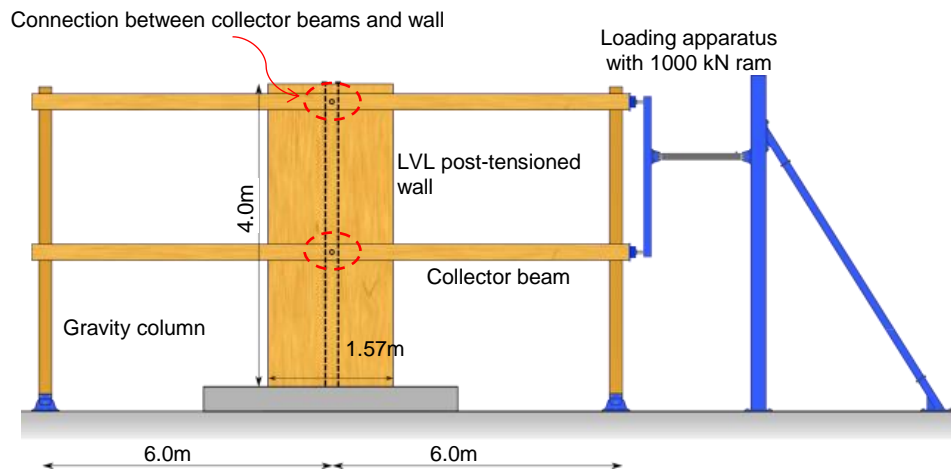


Figure C.23 Test setup of the post-tensioned wall loaded through collector beams which were connected to the wall by several connection details (setup with end columns not shown)

The LVL wall was 1570 mm wide, 189 mm deep and 4.0 m high, and was post-tensioned to the concrete foundation using two 32 mm MacAlloy bars with an initial post-tensioning force of 300 kN each. The interaction with the floor diaphragm was simulated by a pair of 6 m long collector beams for each of the two floor levels. These 63 x 400 mm LVL beams have been designed to have the same stiffness as a Timber-Concrete-Composite (TCC) floor with a 90 mm concrete slab connected to two 90 x 350 mm LVL beams with trapezoidal notches (Gerber et al. 2012). This represents the worst case scenario in terms of floor out-of-plane stiffness, considering a traditional plywood floor, a glued stressed-skin timber floor and a TCC floor.

Table C.4. Material properties of Pres-Lam wall

LVL11		Post-tensioning bar	
Compression strength parallel to grain	$f_{c,0} = 45$ MPa	Yield stress	$f_y = 835$ MPa
Compression strength perp to grain	$f_{c,90} = 12$ MPa	Ultimate stress	$f_u = 1030$ MPa
Shear strength	$f_s = 6$ MPa	Elastic modulus	$E_{pt} = 170$ GPa
Characteristic elastic modulus perp to grain	$E_{90} = 0.55$ GPa	Bar diameter	$D_{pt} = 32$ mm
Average elastic modulus parallel to grain	$E_{0,mean} = 11$ GPa	Area per bar	$A_{pt} = 804$ mm ²
Shear modulus	$G = 0.55$ GPa		

The collector beams were connected to the 300 x 189 mm gravity columns with four 16 mm bolts, which were assumed to work as a hinge to hold the beams down when they were pushed upwards by the rocking wall. Hinged steel connections linked the columns to the floor and load cells measured the axial forces in the columns. Because of limitations in the

laboratory, one foundation was fixed to the strong floor via bolts; the second foundation was created by concrete blocks weighting about 3 tons. This second foundation was therefore not perfectly fixed, but uplift measurements guaranteed minimal influence on the testing results. The horizontal load was applied to the collector beams via a spreader beam and a 1,000 kN hydraulic ram, simulating a triangular load.

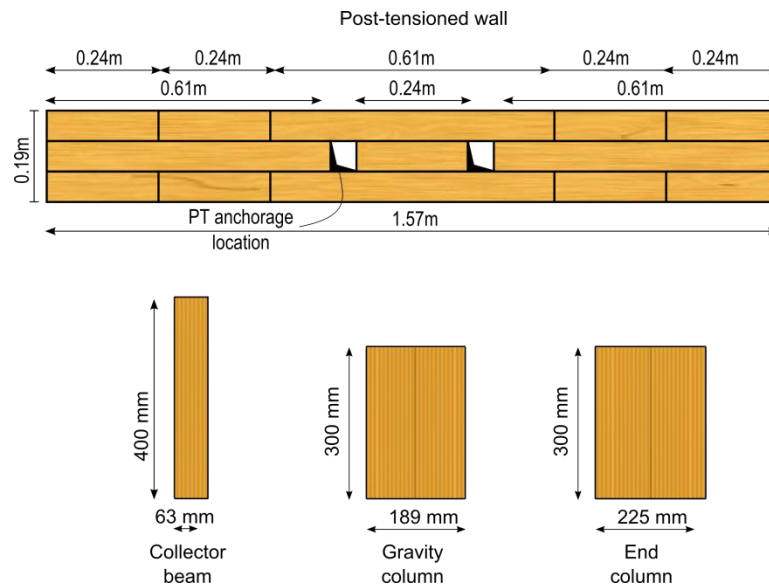


Figure C.24 Section sizes used in test setup

Eight different connections were used to transfer the horizontal load from the collector beams to the wall (see Figures C.25 and C.26):

- 1) Group of 12 x M16 mm bolts at the centre of the wall;
- 2) Group of 25 x M16 mm bolts, 400 mm offset from the centre of the wall;
- 3) External timber blocks pushing against the edge of the wall, bolted to the beams with 16 mm bolts;
- 4) A 65 mm diameter round steel pin through a circular hole at the centre of the wall;
- 5) A 65 mm diameter round-square-round steel pin through a vertical slot at the centre of the wall;
- 6) A steel angle with 7 x M16 mm bolts in slotted holes;
- 7) A steel-to-steel connection with a 40 mm diameter round-square-round steel pin in a slotted hole;
- 8) 10 fully threaded $\varnothing 10/350$ mm screws inclined at 30° .

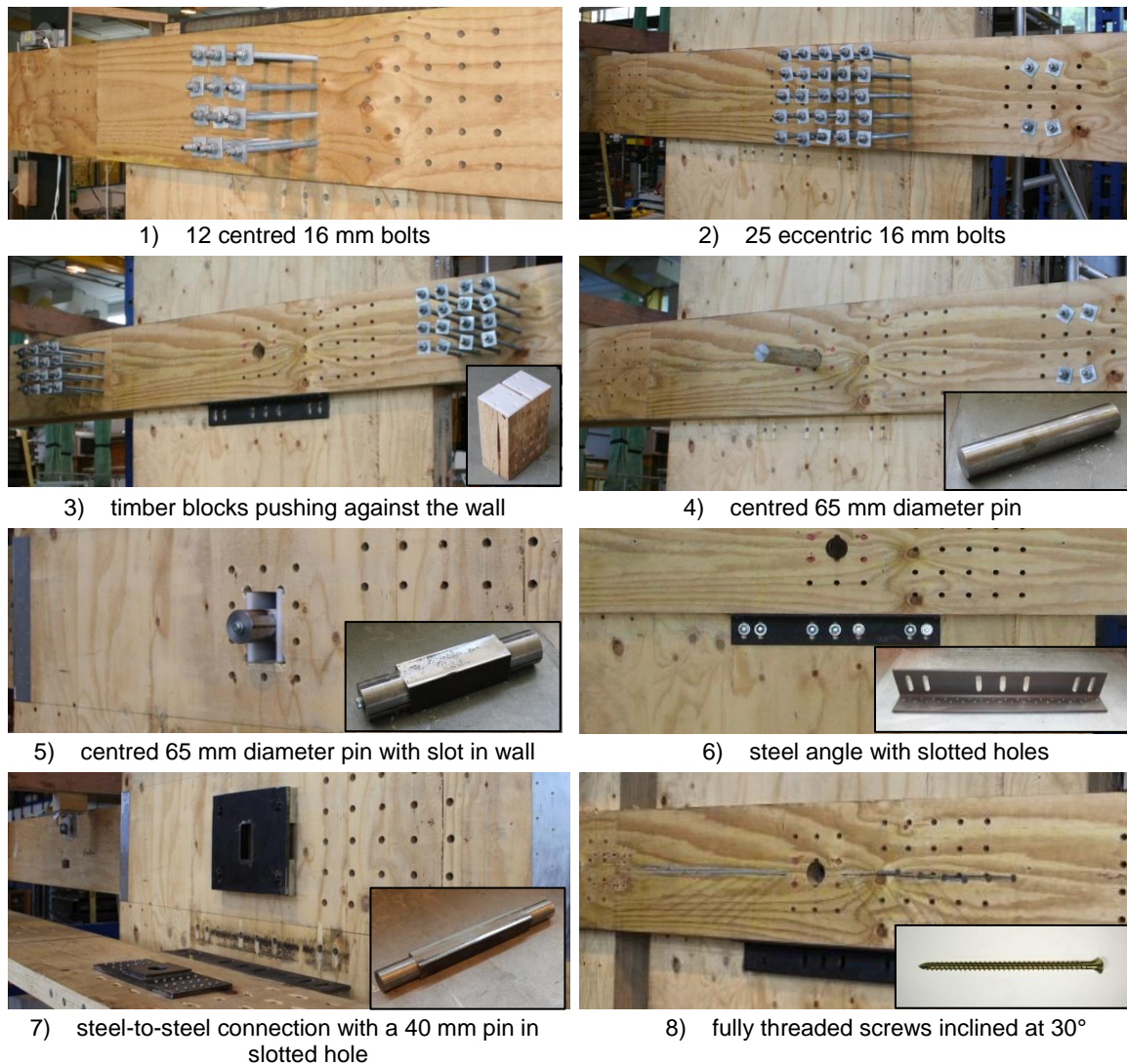


Figure C.25 The eight tested connection details between the collector beams and the wall

Because of the length of the bolts, M16 Grade 8.8 threaded bars were used for connections type 1 to 3. To avoid splitting, the beams were reinforced with fully threaded screws in accordance to Blaß et al. (2004). Connection type 1 was designed to transfer the horizontal forces and the imposed vertical force and moment due to the displacement incompatibilities. Assuming that the floor would span perpendicularly to the collector beams, connection type 2 was designed to also transfer gravity forces resulting in a higher force demand in the connection. The increased numbers of fasteners required to move the connection 400 mm offset from the wall centre to avoid the central location of the post-tensioning bars. For connection type 3, two timber blocks were bolted to the beam, each with a tight fit against the edges of the wall, so that horizontal forces in the beam could be transferred into the wall by contact. The timber blocks were assembled with a High Density Polyethylene (HDPE) plate, while the wall was covered with a stainless steel plate to reduce friction.

Embedment strengths are not available for large diameter steel pins in timber (diameter larger than 32 mm are not codified), so values need to be chosen conservatively. Fully threaded screws were added in the beams on either side of the hole to prevent splitting. For connection type 5, the sliding pin was bearing against two HDPE plates to avoid local crushing of the timber perpendicular to the grain and to minimize friction. Although for connection type 4 round pins were used, connection types 5 and 7 had special machined pins with an inner square section where they passed through the wall to avoid stress concentrations on the bearing areas and round sections where they were bearing against the beams. The steel ‘angle’ consisted of an L-shaped steel profile connected with 65 mm long rivets to the beams and seven M16 bolts in slotted holes against the wall. For connection type 7 one steel plate was connected to the beam by 65 mm long rivets and the other was fixed to the wall by ZD plates (SWG Schraubenwerk Gaisbach GmbH 2012) with $\varnothing 10 \times 280$ mm fully threaded screws inclined at 30° . Connection type 8 consisted of 10 fully threaded $\varnothing 10/350$ mm screws inclined at 30° . The screws were positioned along one line and had 5 screws working in tension and 5 in compression. In between the collector beams and the wall was a gap of 18 mm.

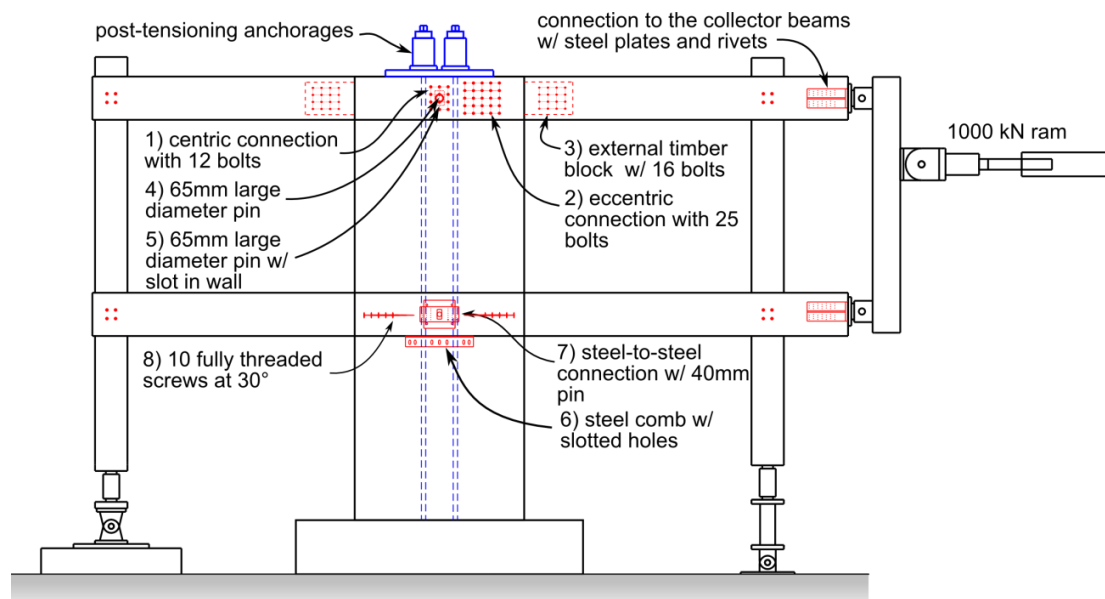


Figure C.26 Diaphragm-to-wall connections: 1) central connection with bolts; 2) eccentric connection with bolts; 3) external timber block with bolts; 4) 65 mm pin; 5) 65 mm pin with slot in wall; 6) steel angle with slotted holes; 7) steel-to-steel connection with 40 mm pin; 8) fully threaded screws at 30°

Connections type 1 and type 2 are not perfect hinges, but they do allow for some rotation because of the confined geometry and the flexibility of each single fastener. The remaining connections were designed not to transfer any rotation to the beam. Connections 3, 5, 6 and 7 were designed to allow the wall to move upwards without lifting the beams. In connection 8

horizontal forces were transferred by axial action of the screws while uplift and rotation was allowed by the low shear stiffness of the screws, especially in presence of the 18 mm gap.

In a subsequent test phase two additional 300 x 225 mm LVL end columns were added on each side of the wall as shown in Figure C.28. Special shear transfer devices consisting of HDPE plates on the columns and stainless steel plates were used to transfer the horizontal forces to the wall while minimizing friction (more information on this setup and detailing of the connection can be found in Sarti et al. (2015)). The collector beams were connected to the end columns by connections type 9 and 10 as shown in Figures C.27 and C.28:

9) Group of 12 x M16 mm bolts;

10) A 65 mm diameter round steel pin through a circular hole.



Figure C.27 The two tested connection details between the collector beams and the end columns

Since no vertical displacement (uplift) of the end columns was expected, the connections only needed to accommodate rotation. Similar to connections 1 and 4, the collector beams were connected first by a group of 12 M16 Grade 8.8 threaded rods to achieve a hinge-like connection. Successively a 65 mm round pin was used to transfer the horizontal loads.

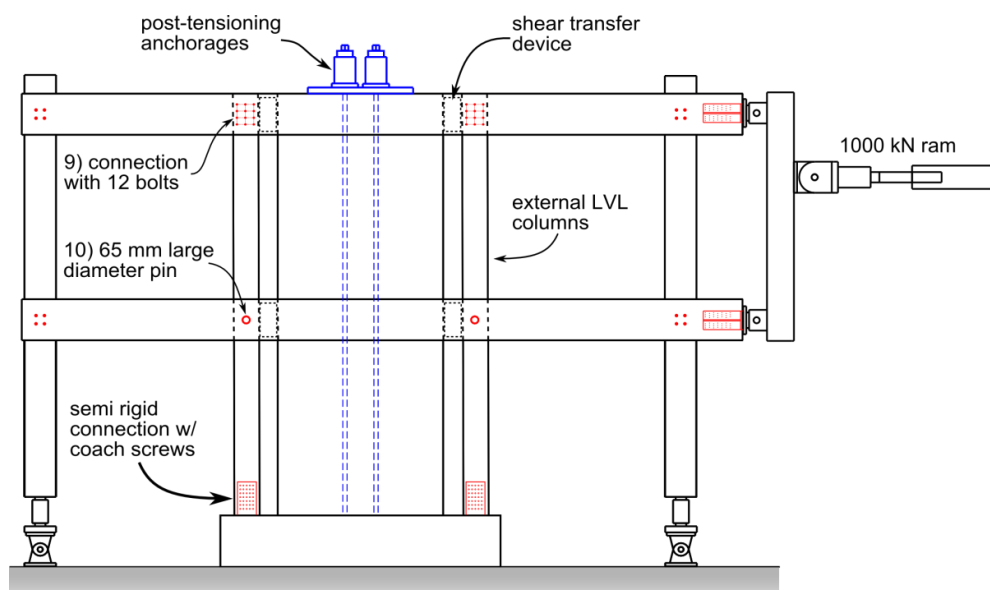


Figure C.28 Diaphragm-to-end-column connections: 9) connection with bolts; 10) 65 mm large diameter pin

C.3.2 Loading protocol and instrumentation

The wall was loaded following a quasi-static cyclic loading protocol according to ACI ITG-5.1-07 (ACI Innovation Task Group 5 2008) plotted in Figure C.29. The imposed displacements were applied with increasing amplitudes of three cycles each with corresponding drift values of 0.3%, 0.45%, 0.6%, 1.0%, 1.5% and 2.0%. For a Design Basis Earthquake (DBE), design level drifts of up to 1.0 % were targeted; this equals to a wall lateral displacement of approximately 40 mm. For a Maximum Credible Earthquake (MCE) drift levels of 2.0% were chosen, demanding an 80 mm displacement of the wall.

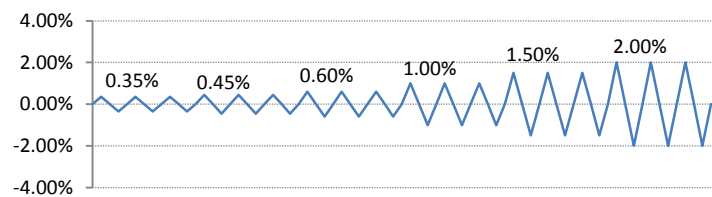


Figure C.29 Quasi-static cyclic loading protocol with building drift values

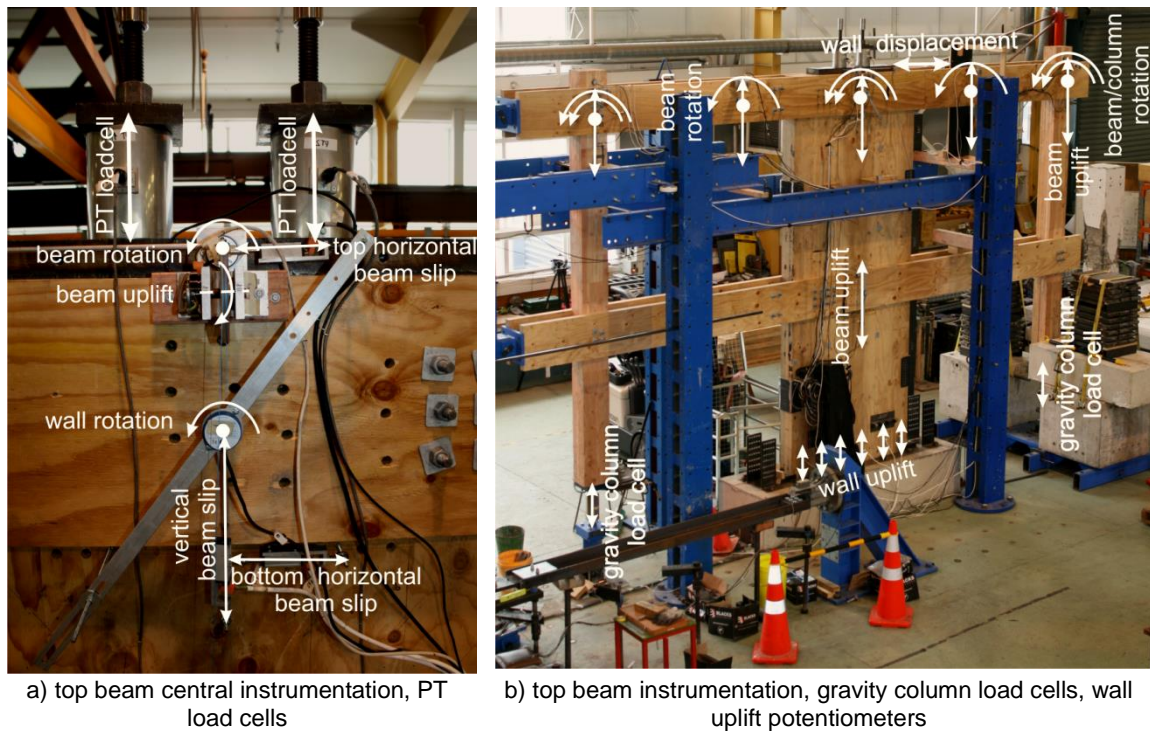


Figure C.30 Wall, beam and column instrumentation

The displacements were measured directly on the wall, thus taking into account any slip in the connections or the loading apparatus. The vertical and horizontal slips of the top collector beam in respect to the wall have been measured with potentiometers as shown in Figure C.30a. Inclinometers were installed to measure beam, column and wall rotations as shown in Figures C.30a and b. Five string pots on the top beam and one string pot at the bottom beam

were used to measure the absolute uplift of the collector beams. Two load cells on top of the wall measured the force in the PT bars; two additional load cells measured the axial force in the gravity columns to evaluate the uplifting forces in the beams. Six potentiometers were measuring the uplift of the wall from the foundation.

C.3.3 Results

The results of main interest are the rotation and uplift of the beam relative to the initial position. Horizontal movement is common to the whole building under any horizontal loading and therefore irrelevant. Another indicator for the wall-beam interaction is the axial forces in the gravity columns.

To characterize the wall-beam system, the wall was tested with three different post-tensioning levels of 300, 400 and 600 kN for connection 1 with centric bolts. Figure C.31 shows the force-displacement curves and the post-tensioning forces. It can be seen that the system does not behave perfectly symmetric. It is assumed that this is due to construction tolerances, the not perfectly fixed foundation on one gravity column and the restraint from the rollers which prevent out-of-plane movements of the wall.

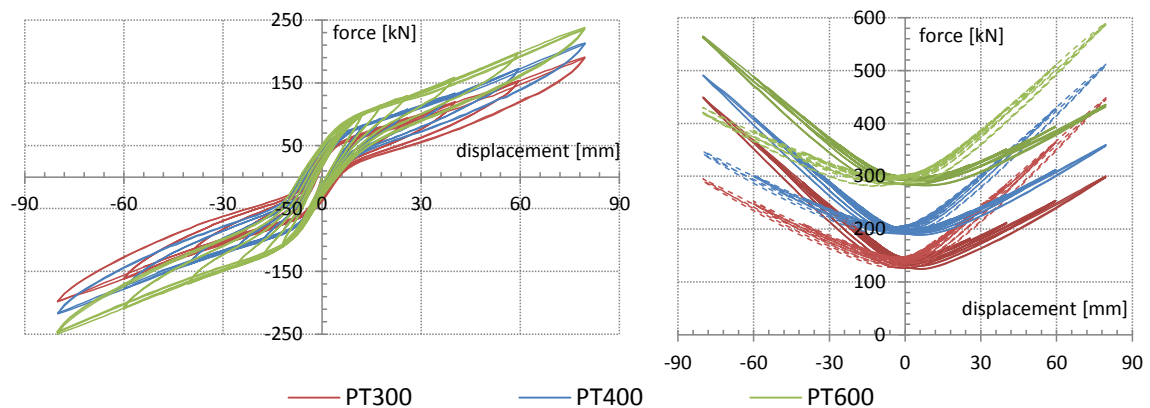


Figure C.31 Force-displacement and post-tensioning forces of the wall connected to the collector beams by connection 1) with 12 centric bolts for 3 different initial post-tensioning forces

Figure C.32 plots the top of the wall rotation against the upper beam rotation at mid-span (at the connection location except of type 2 which was eccentric) for some selected connection configurations. The beam rotations were much smaller than the wall rotations, because all the connections allowed some differential rotation. For the timber-to-timber connections the centric bolts reduced the rotational interaction, with the large diameter pin almost completely decoupling the two elements. The steel angle caused the beam to follow the wall rotation to a relatively high degree, with the steel-to-steel connection on the other hand reducing beam

rotations. Both connections through the end columns minimized beam connections, it has however to be noticed that for these setup the mid-span of the beam also represents the point of contraflexure.

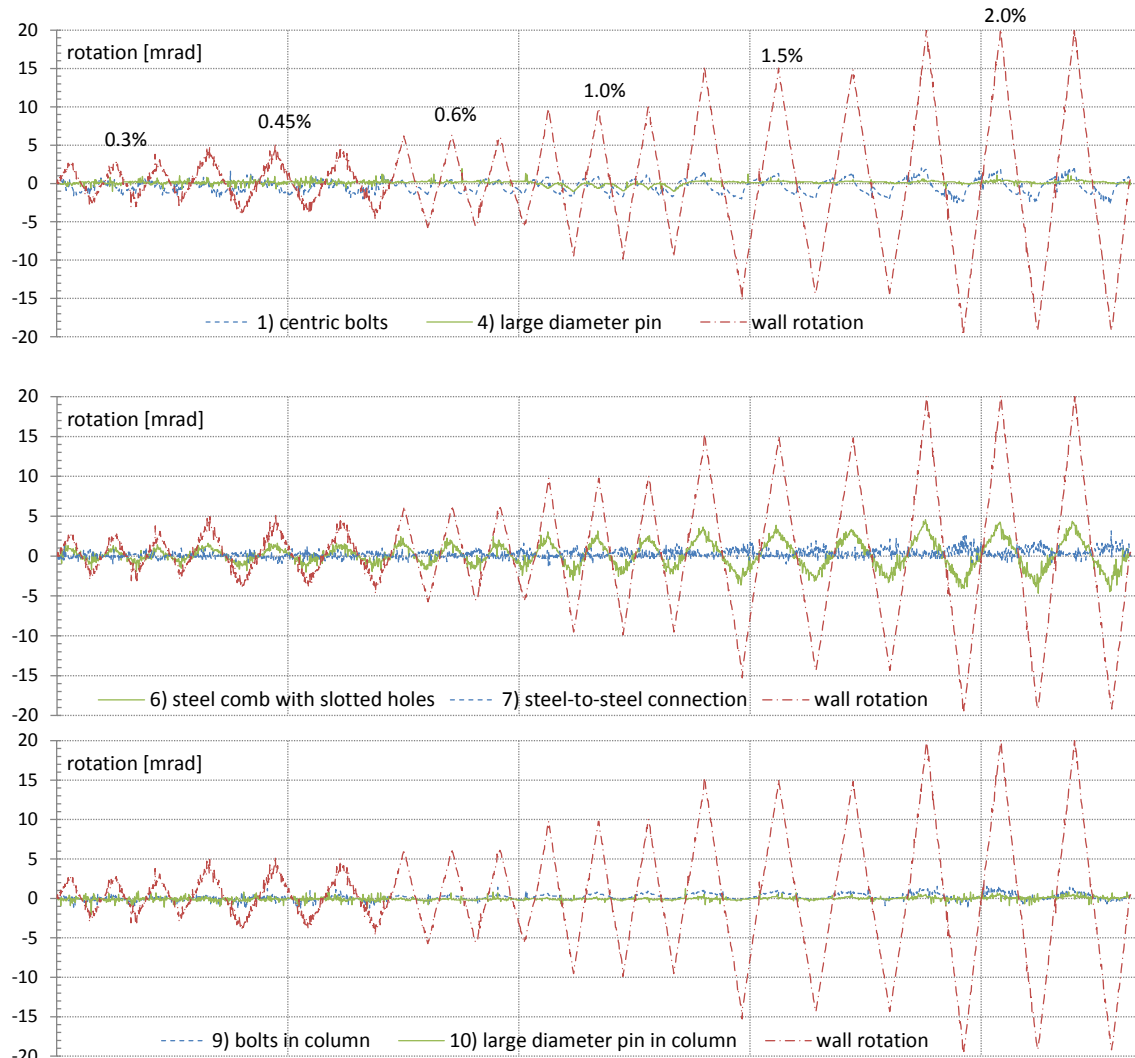


Figure C.32 Wall rotation and upper beam rotation for some selected connections

The absolute vertical displacement of the upper beam at mid-span measured from the ground is plotted in Figure C.33 for the 2.0% drift cycles. As the vertical slip in connection type 1 can be ignored, the uplift of the beam was equal to the uplift of the wall. The slightly asymmetric behaviour is attributed to the loading apparatus and the different behaviour of the wall, when being pushed or pulled. In the case of the eccentric bolted connection (type 2) the uplift at the centre was higher when pulled and almost nil when pushed. The connection with external blocks (type 3) showed a very different behaviour with much higher uplifts than the wall itself. The beam was first being pushed down and then uplifted quite rapidly. When unloaded, the beam lowered back to the initial position with some delay due to friction. Both steel

connections were not able to fully decouple the vertical displacements of the wall and the beam. Connection 8 with fully threaded screws shows a reduction in the vertical interaction, the measured displacements are however not symmetric. This behaviour is likely because of construction tolerances. For the setup with the external columns, the vertical beam uplift is successfully decoupled from the wall movement.

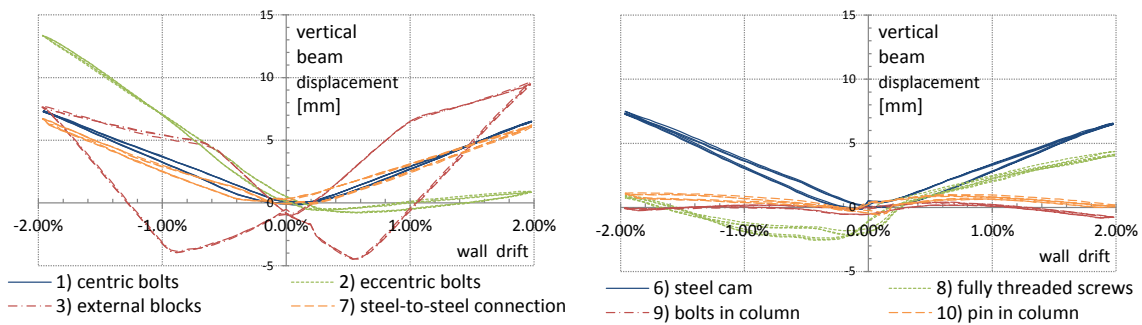


Figure C.33 Absolute vertical beam displacement at mid-span at the 2.0% drift cycles for selected connection setups

A good indicator of how much interaction between the beams and the walls is occurring, are the axial forces in the gravity columns. If rotational or uplift incompatibilities are successfully decoupled, the floor beam remains straight and only follows the horizontal movements. In this case the gravity columns are unloaded. Figure C.34 shows the axial force of both gravity columns plotted against the wall drift for four different connections setup.

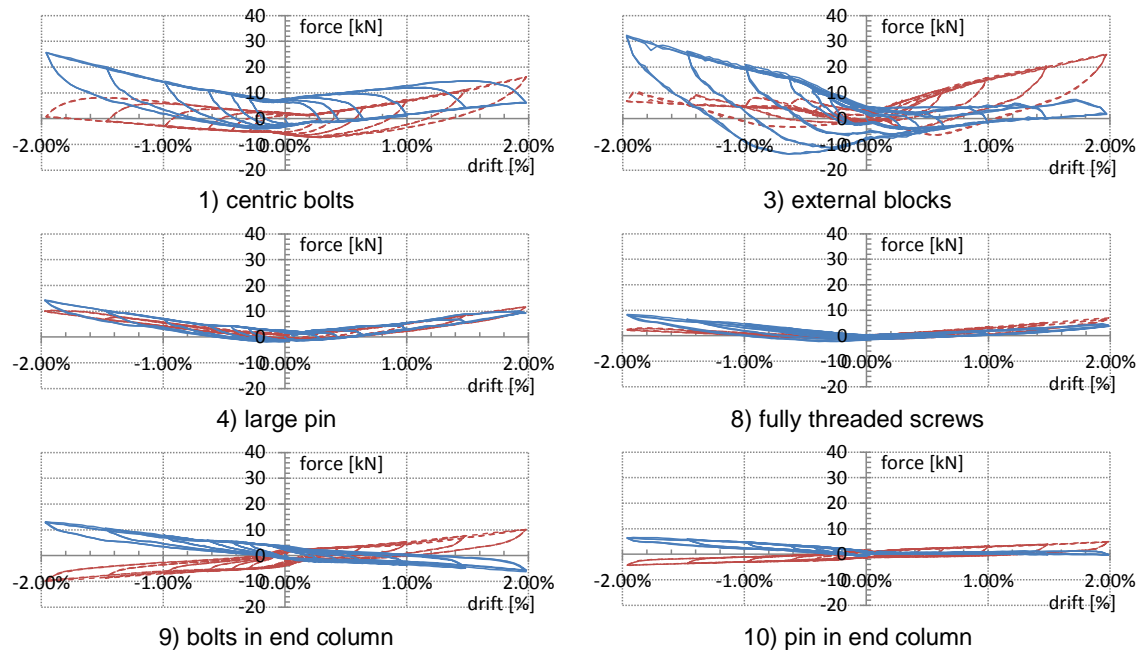


Figure C.34 Axial force in gravity columns

A comparison between the results from connection 1 and 4 with centric bolts and a large pin respectively suggests that with equal uplift demand in the beams, the imposed rotation causes higher interaction. The incomplete rotational decoupling also causes some residual forces in the columns. This behaviour is even more accentuated for the connection with external blocks, where frictional forces at the interface are present. The connection with fully threaded screws is able to minimize interaction while decoupling both uplift and rotation. For connections through the end columns interaction is relatively small, but imposed rotations with connection 9 cause some axial forces.

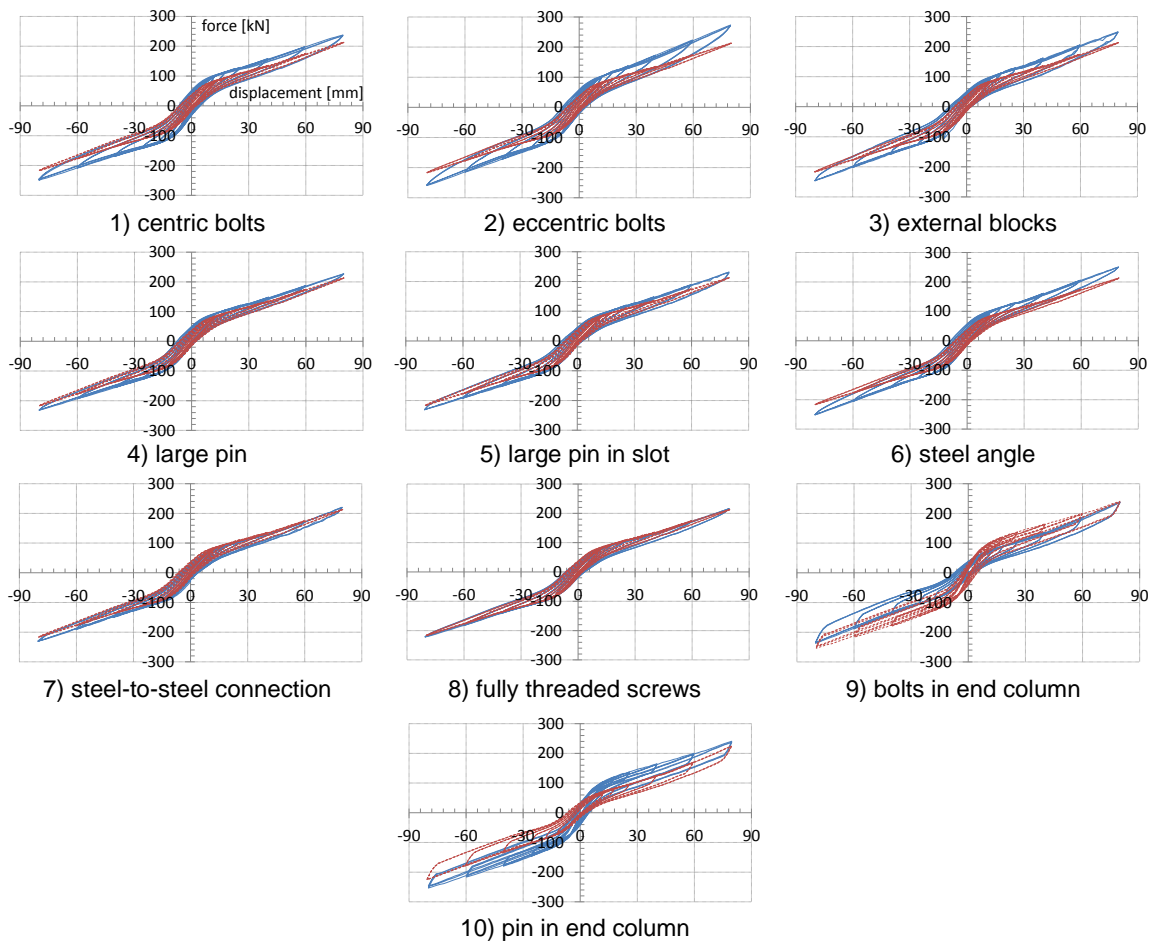


Figure C.35 Force-displacement curves of wall with connection assembly (blue solid line) compared against naked wall (1-8) and naked wall with end columns (9-10)

Figure C.35 provides a comparison of the strength and stiffness values of the wall-beam assembly compared to the bare wall for the whole loading protocol. Records of the bare wall without end columns were taken after the whole testing series (from previous testing from Dr. Francesco Sarti and this testing program), where strength and stiffness are slightly lower when compared to the records from initial testing as Figure C.36 shows. This is because of the high number of testing cycles under high stress levels for drifts corresponding to MCE design

assumptions, whose events caused some crashing of the wall at the foundation interface. The force-displacement curve of the bare wall with end columns has been recorded at an earlier stage, where damage was less accentuated. This explains the slightly lower values in strength and stiffness of the assemblies of the beams on the wall with end columns when compared to the bare wall with end columns.

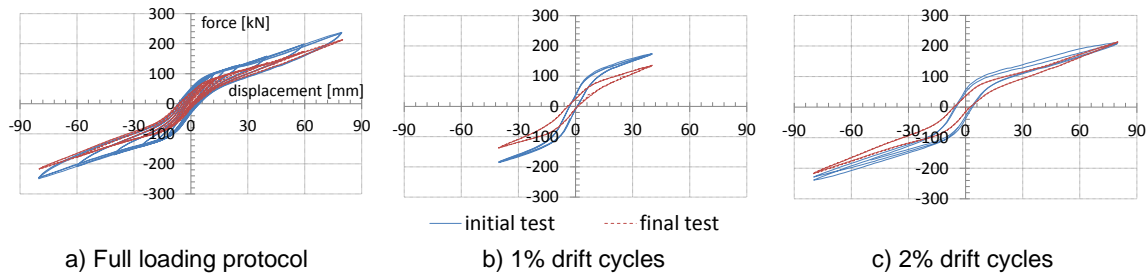


Figure C.36 Force-displacement curves of the bare wall at the first test and at the end of all tests carried out

Depending on the degree of decoupling from imposed displacements between the collector beams and the wall, stiffness and strength are normally increased when loads are applied through floor beams. As suggested already above connections 2 with eccentric bolts, 3 with external blocks and 6 with the steel angle show a higher interaction when compared to other setups. This is mainly because wall rotations were imposed to the beams to a higher degree. Connections with round pins (connections 4, 5 and 7), even when not preventing imposed uplift, show only a slight increase in strength and stiffness, reinforcing the conclusion that rotational incompatibility has a larger impact on the whole system than uplift incompatibility. The connection with fully threaded screws provided the best results in minimizing the interaction between the beams and the wall.

A comparison of the force-displacement curves of the setups with end columns suggest that the interaction between the floor beams and the wall can be successfully minimized and that connections with negligible rotational stiffness lead to an even higher degree of decoupling from imposed deformations.

C.3.4 Cost analysis

To evaluate the viability of the tested connections in real buildings, a cost analysis has been carried out in collaboration with Dr. Tobias Smith from the University of Canterbury. The costs summarized in Table C.5 are based on recorded construction times from the laboratory setup and on assumed times spend by a professional builder. Material and labour costs are

based on the Rawlinsons New Zealand Construction Handbook (Rawlinsons 2015). Both the indicated times and costs are relative to the connection of one pair of beams to the wall.

Table C.5. Cost and time estimation of the ten connection configurations including material list

Connection type	Cost	Time
1) Group of 12 bolts <i>16 bolts – M16, l = 400mm Grade 8.8 (including washers and nuts)</i>	400\$	1h40'
2) Eccentric group of 25 bolts <i>25 bolts – M16, l = 400mm Grade 8.8 (including washers and nuts)</i>	625\$	2h30'
3) External blocks with dowels <i>2x16 bolts – M16, l = 400mm Grade 8.8 (including washers and nuts)</i> <i>2x timber blocks 450x300x189 mm</i> <i>2x stainless steel plates 290x400x1mm</i> <i>2x High-Density Polyethylene sheet (HDPE) 300x190x20 mm</i> <i>Fasteners for plates</i>	1260\$	4h30'
4) Large diameter pin <i>Steel pin 65x325 mm</i> <i>4x fully threaded Ø10x400 for timber reinforcement</i>	60\$	40'
5) Large diameter pin and slot in wall <i>Machined steel pin 65x325 mm</i> <i>2x HDPE plates 110x190x20 mm</i> <i>4x fully threaded Ø10x400 for timber reinforcement</i>	90\$	1h
6) Steel angle with slots <i>2x Steel angle 75x100x10</i> <i>2x7 bolts – M16 l = 240 mm Grade 8.8 (including washers and nuts)</i> <i>2x32 rivets 6x65mm</i>	700\$	2h20'
7) Steel-to-steel connection with slots <i>Machined steel 40x325 mm</i> <i>2x36 rivets 6x65</i> <i>2x4 ZD plates (SWG Schraubenwerk Gaisbach GmbH 2012)</i> <i>2x16 fully threaded screws Ø10x280 to fix ZD plates</i> <i>2xsteel plate on wall side</i> <i>2xsteel plate on beam side</i> <i>2x4 bolts – M16 l = 35mm Grade 10.9</i>	1420\$	5h
8) Fully threaded screws <i>2x10 fully threaded screws Ø10x320</i>	180\$	2h20'
9) End columns with group of bolts*) <i>2x16 bolts – M16, l = 500mm Grade 8.8 (including washers and nuts)</i>	2000\$	3h20'
10) End columns with large diameter pin*) <i>2xSteel pin 65x325 mm</i> <i>8x fully threaded screws Ø10x400 for timber reinforcement</i>	1300\$	1h20'

*) For connections 9 and 10 the material cost of the end columns and the shear transfer devices including the HDPE plates and galvanized steel plates are included. The connection of the end columns to the foundations however has not been included in the cost analysis.

C.4 EXPERIMENTAL SETUP OF A 1/2 SCALE POST-TENSIONED CLT STAIRCASE CORE UNDER QUASI STATIC LOADS

To investigate the performance of floor diaphragms in combination with core-wall lateral load resisting systems, two post-tensioned Cross Laminated Timber (CLT) stairwell core structures were loaded through two sets of orthogonally running collector beams. One test specimen was designed for loads in a low seismic region and one in high seismic region. More information on the design of the specimens and the performance under lateral loads can be found in Dunbar (2014).

C.4.1 Test setup

The 1/2 scale stairwell core shown in Figure C.37 was made of CLT panels produced by XLam Ltd in Nelson, New Zealand and was assembled and tested in the structures laboratory of the University of Canterbury. The panels with material properties summarized in Table C.7 are made up of 20 mm thick standard Douglas Fir SG8 planks, three in the longitudinal direction and two in the transverse direction.

The core was loaded in both directions by quasi-static loads applied through the collector beams. For the *low seismic option* the individual panels were connected by wood screws working in shear and the collector beams transferred the forces directly into the wall panels. For the *high seismic option* the panels were coupled with U-shaped Flexural Plates (UFPs)(Kelly et al. 1972). The horizontal forces were introduced to the steel columns at the corners which were bearing against the wall.

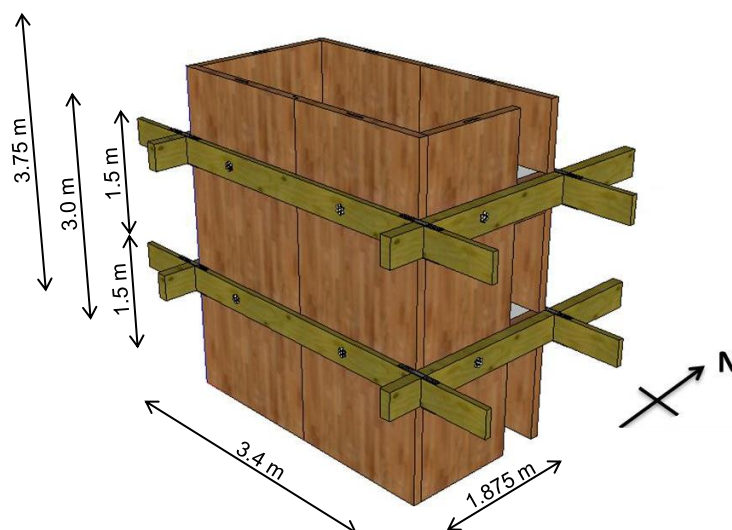


Figure C.37 Test setup of the CLT core – low seismic option (modified from Dunbar (2014))

12.7 mm post-tensioning strands for the coupled walls and 15.2 mm strands for the single walls were guaranteeing the rocking mechanism of the walls under horizontal loading. The post-tensioning force varied for the different test configurations to either simulate gravity loads only (low PT force) or to have a specifically designed post-tensioned rocking wall (high PT force). Force values are summarized in Table C.6.

Table C.6. Summary of the forces in the post-tensioning strands for both the low and high seismic option

PT level	12.7 mm strands	15.2 mm strands
low	40 kN	80 kN
high	100 kN	150 kN

The prototype stairwell core was designed as part of a three storey office building. The ½ scaled footprint of the structure as in Figure C.37 was 3.4 m in the longitudinal direction and 1.875 m in the transversal direction. The interstorey height was 1.5 m and the total core height was 3.75 m. Access to the stairs was given by a 1.1 m high and 0.45 m wide doorway.

The longitudinal wall was made of two coupled 100 mm thick CLT panels; the transversal walls were made of single 100 mm thick CLT panels as can be seen in Figure C.38. The opening for the doorway was cut out directly from the panels. Inside the specimen a half-flight stair case with landings all made of CLT panels was installed.

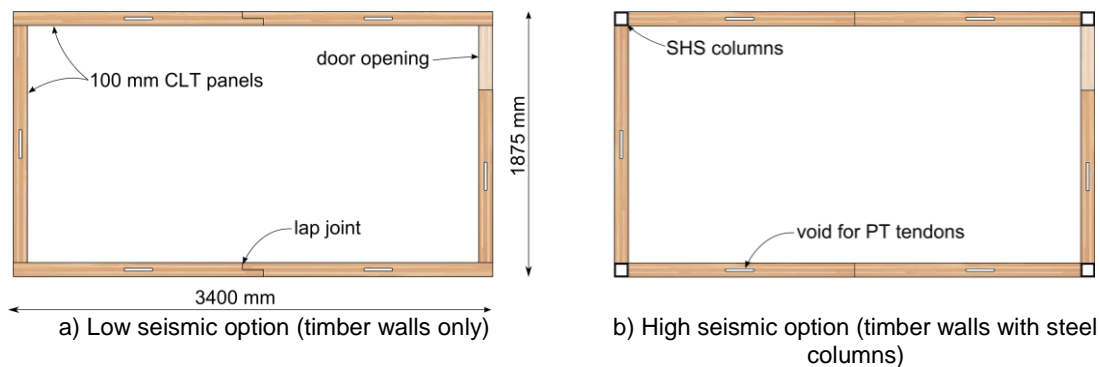


Figure C.38 Plan views of the two experimental setups

Collector beams were running both along the long direction and short direction of the core. These beams were simulating the floor slabs and the diaphragms. The beams running in the longitudinal direction with a cross section of 63 x 300 mm made of LVL 11 were designed to only act as collector (drag) beams for the diaphragm action. The beams were spliced by a top and bottom steel plate of 6 x 60 mm and 21 timber rivets with a length of 65 mm for each connection as shown in Figure C.39. The thin steel plate was designed to carry tension loads, but also to allow for the floor out-of-plane movements because of deflections and rotations of the core under horizontal loads. The beams in the short direction with a cross section of 126 x

300 mm made of LVL 11 were continuous and were designed to act as both gravity and collector beams. The loading apparatus with spreader beams and hydraulic rams as shown in Figure C.43 was connected to the ends of the collector beams by glued rods or steel brackets.

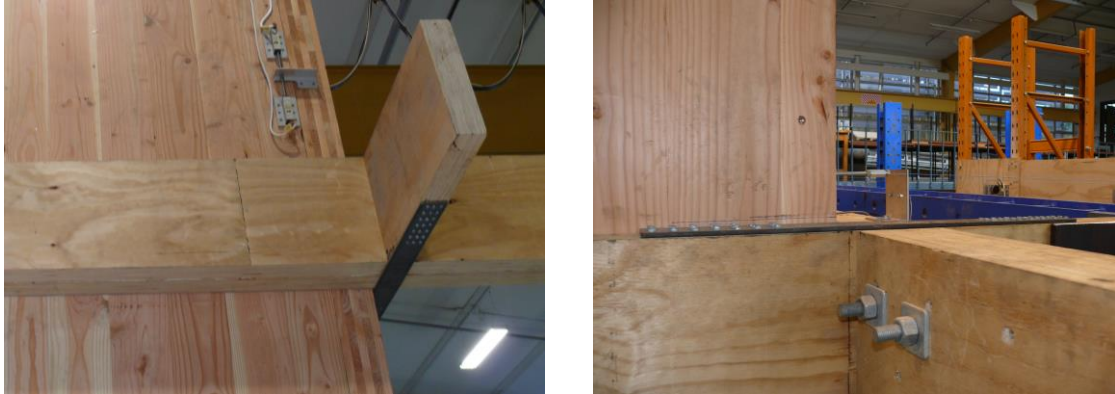


Figure C.39 Collector beam splice

Table C.7. Material properties of core structure

CLT			Post-tensioning tendons		
Compression strength parallel to grain	$f_{c,0} =$	14 MPa	Yield stress	$f_y =$	1530 MPa
Compression strength perp to grain	$f_{c,90} =$	12 MPa	Ultimate stress	$f_u =$	1760 MPa
Tensile strength	$f_t =$	6 MPa	Elastic modulus	$E_{pt} =$	200 GPa
Shear strength	$f_s =$	3.8 MPa	Area (12.7 mm strand)	$A_{pt} =$	99 mm ²
Average elastic modulus parallel to grain	$E_{0,mean} =$	8 GPa	Area (15.2 mm strand)	$A_{pt} =$	143 mm ²
Shear modulus	$G =$	0.5 GPa			

LVL11			UFPs		
Compression strength parallel to grain	$f_{c,0} =$	45 MPa	Yield stress	$f_{sy} =$	375 MPa
Compression strength perp to grain	$f_{c,90} =$	12 MPa	Elastic modulus	$E =$	200 GPa
Shear strength	$f_s =$	6 MPa			
Characteristic elastic modulus perp to grain	$E_{90} =$	0.55 GPa	Steel columns		
Average elastic modulus parallel to grain	$E_{0,mean} =$	11 GPa	Yield stress	$f_{sy} =$	300 MPa
Shear modulus	$G =$	0.55 GPa	Elastic modulus	$E =$	200 GPa

C.4.1.1 Low seismic option

For the low seismic option the core structure is a combination of post-tensioned rocking walls and traditionally jointed CLT panels. Were the post-tensioning provides lateral resistance and self-centering, the semi-rigid connection between the panels made of wooden screws acting in shear provided some additional resistance and energy dissipation.

In the longitudinal direction the panels were connected by 6 x 100 mm wood screws along an 80 mm long lap joint. The spacing of the screws varied for the different test setups (i.e. 3 and 20 screws per joint). For the corner connections, 6 x 200 mm wood screws were driven from the flat side of one wall into the small side of the perpendicular wall.

The collector beams were connected with seven M16 bolts to the centre of each wall panel. Even though the confined geometry of the ring of bolts acts almost as a pin, the connection restrains any vertical movement between the walls and the beams. Therefore the floor diaphragm was expected to undergo some out-of-plane displacements as shown in Figure C.42a. Relative movement between the orthogonal running collector beams was accommodated by the elastic out-of-plane bending of the splice steel plates.

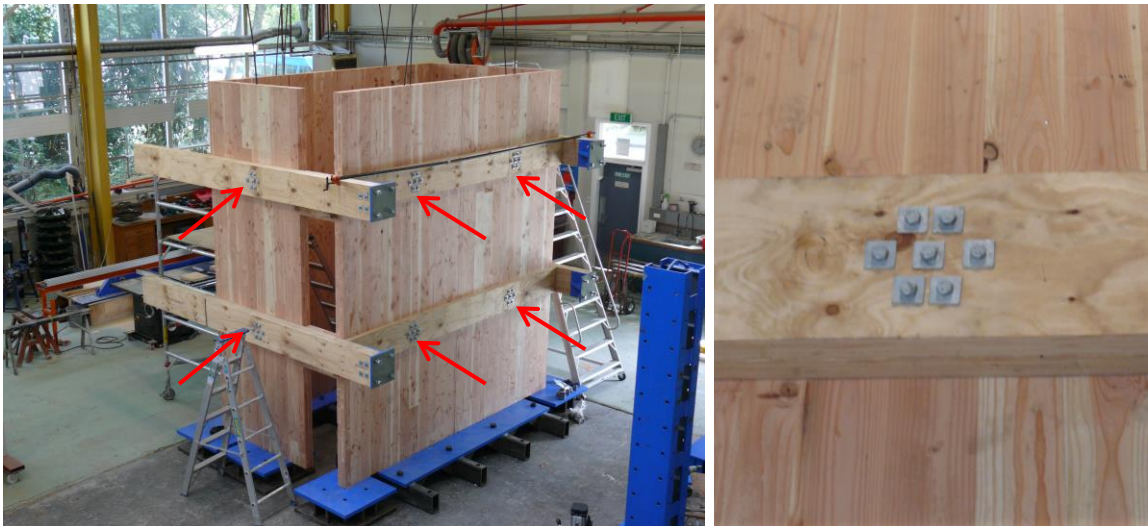


Figure C.40: Test specimen with wall-to-collector beam connections for the low seismic option

C.4.1.2 High seismic option

In order to resist high seismic actions and to achieve high dissipation for the high seismic option, the wall panels were connected to each other via UFP plates (Kelly et al. 1972). These plates are activated for small relative vertical displacements and provide very stable hysteresis loops under cyclic loading. Displacement incompatibilities between the walls and the floor diaphragm were avoided by connecting the collector beams to end columns.

Wall and beam geometries were the same as for the low seismic option. In the corners 100x100x10 square hollow steel sections were bolted to the foundation by a single M24 Grade 10.9 bolt. Steel UFPs with a width of 100 mm, a thickness of 8 mm and a radius of 40 mm were bolted to the steel section and the walls. To avoid rotation and uplift incompatibility between the rocking walls and the collector beams as in Figure C.42 b), the transversal beams were connected to the columns with a single M24 bolt as in Figure C.41. Because of the limited embedment strength of timber, the collector beams were reinforced with a steel plate and 26 8 x 80 mm wood screws. Additional epoxy resin was put to close the gap between the steel plate and the rebate in the timber, this however would not be necessary in real building

applications. For the erection, the bolt was inserted in the column before the walls were installed. The collector beams were then lifted in and fixed with the bolt as shown in Figure C.42c. The collector beams in the longitudinal direction were not directly connected to the walls or columns. Horizontal forces from the longitudinal beams are transferred over the steel splice to the transversal beams which bear against the columns.

Figure C.42c also shows the connection of the UFP plates to the CLT walls with an 8 mm thick steel plate connected with 28 timber rivets with a length of 65 mm into the rebate on the wall. The UFPs, which can be replaced after a major seismic event, are fixed with the use of four M14 bolts.

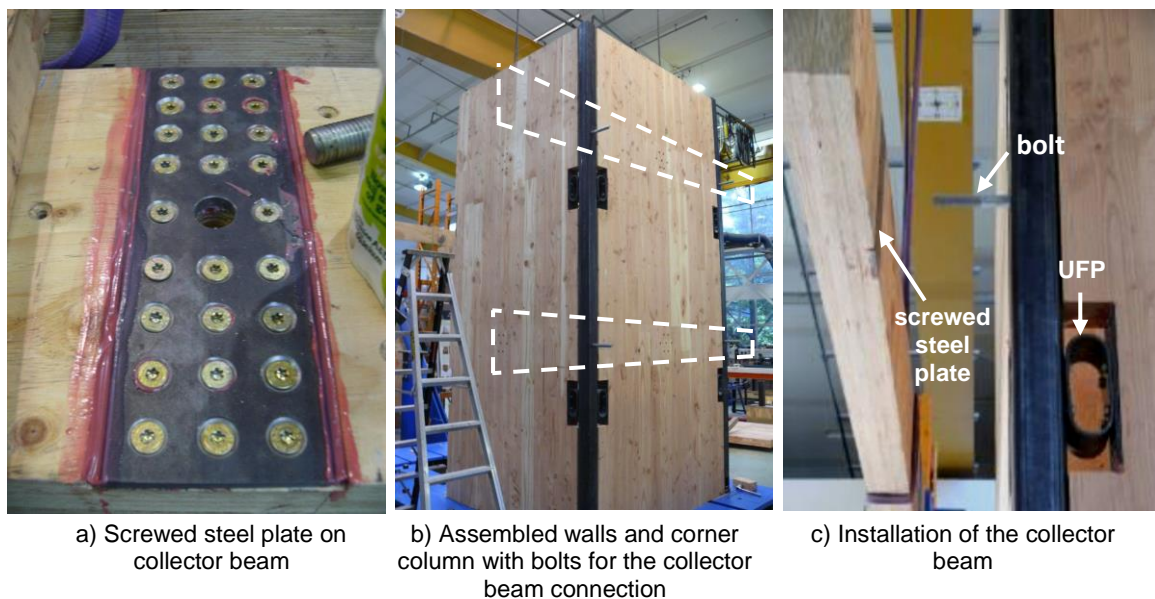


Figure C.41: Test specimen with column-to-collector beam connections for the high seismic option

Because of the pinned connections at the column base and between the columns and the beams, the floor beams remained level. The horizontal forces were transferred through contact from the steel columns to the walls.

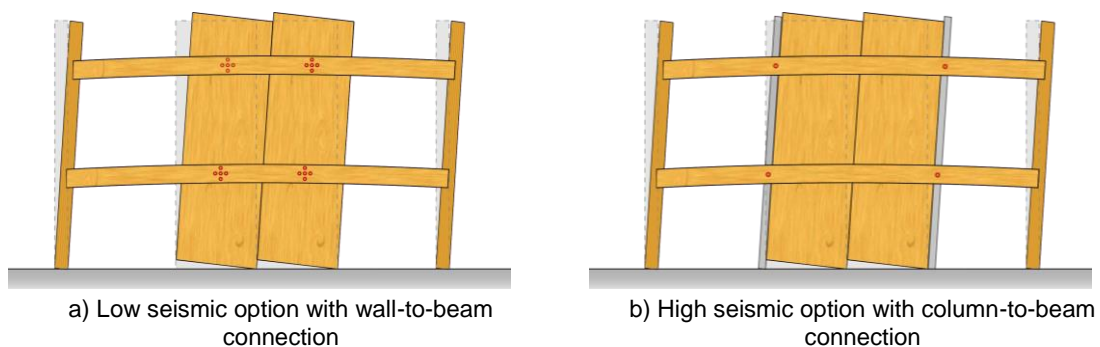


Figure C.42 Diaphragm to wall connection and displacement incompatibilities for the two design options

C.4.2 Loading protocol and instrumentation

The core structure was tested under quasi-static cyclic loads in the two main directions. Table C.8 summarizes the maximum drift level achieved for both the low and high seismic load options for different test configurations. The loads were applied in subsequent increasing cycles in the X and Y directions, first independently in the single directions and later in both directions contemporary by using a ‘cloverleaf’ protocol.

To investigate the behaviour of the floor beams, only test 1 for both the low and high seismic options is studied in detail. Measurements and visual inspection of the floor beams and connection for all other test configurations provided similar results as for test 1.

Table C.8. Summary of the test schedules for both low and height seismic options

Low seismic					High seismic				
Test	PT level	Screws x joint	Loading	Maximum drift (%)	Test	PT level	UFPs x joint	Loading	Maximum drift (%)
1	low	3	X+Y	1.5	1	low	2	X+Y	1.5
2	low	20	X+Y	0.5	2	low	2	clover	1.05
3	high	3	X+Y	1.5	3	high	2	X+Y	1.0
4	high	3	clover	1.25	5	high	1	X	1.25
5	high	20	X+Y	1.25	6	high	2	Y	1.75
6	high	20	clover	1.05	7	high	0	Y	3.5
					8	high	0	X	3

Typically a 1.5% drift limit for the ULS for a wall structure is targeted. For test 1 the stairwell core was tested alternatively in the X and Y directions as shown in Figure C.43 by applying the quasi static loading protocol shown in Figure C.44. The displacement controlled loading followed the guidelines of the American Concrete Institute for un-bonded post-tensioned precast structural walls (ACI Innovation Task Group 5 2008).



Figure C.43 Loading apparatus and loading direction

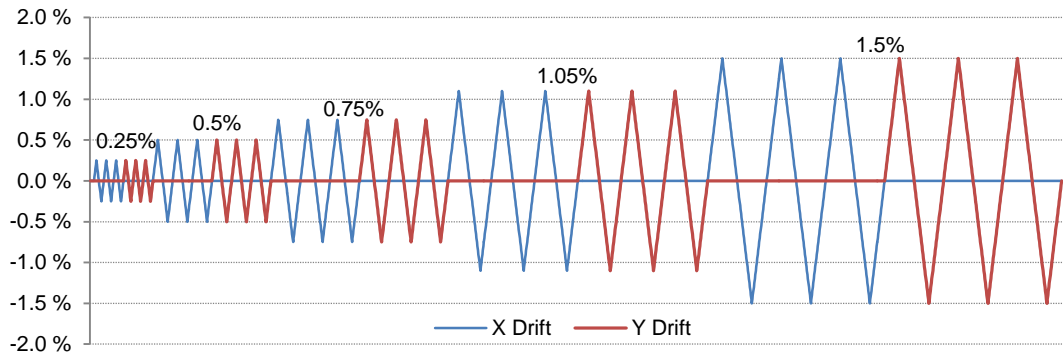


Figure C.44 Quasi-static cyclic loading protocol with building drift values for loading in X and Y directions

Figure C.43 also shows the spreader beams and hydraulic rams used to load the structure. In the East-West (X) direction, a single 1000 kN ram was used to apply loads to the collector beams. In the North-South (Y) direction two individual 300 kN rams were used to apply loads to the beams. A series of spreader beams were used to apply a triangular load pattern along the structure's height. The specimen was assembled on and fixed to a steel foundation.

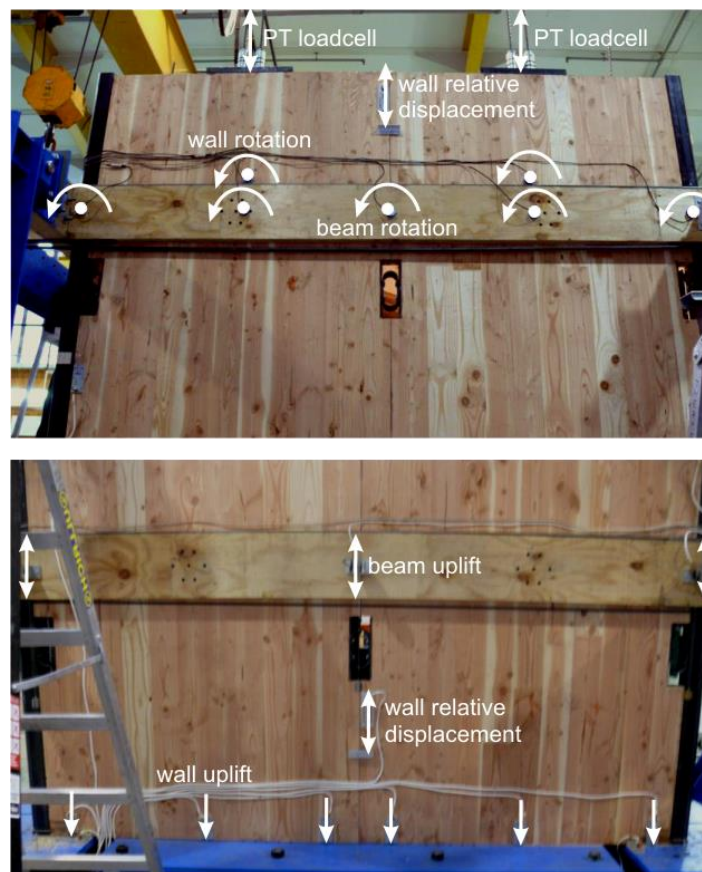


Figure C.45 Upper and lower beam and wall and instrumentation (North walls)

Aside from the loadcells, used to measure the forces in the post-tensioning strands, and the potentiometers, used to measure the structure's drift, panel uplifts and relative

displacements, the top North and East collector beams and the top of the walls were fitted with inclinometers to measure their rotations as shown in the top of Figure C.45. The lower collector beams were equipped with rotary string potentiometers (North beams) and linear potentiometers (East beam) to measure their absolute uplift.

C.4.3 Results

In the following chapter only the results of test 1 for both the low and high seismic options are shown. Similar results could be observed for all other test regimes.

Figure C.46 shows the force-displacement curves of the specimen in both directions. For the Y direction with the single walls, the typical bi-linear behaviour of post-tensioned rocking walls can be observed. The initial stiffness is given by the flexural and shear deformations of the walls until the decompression point. After this point the wall uplifts and the neutral axis decreases. In the X direction this behaviour is not clearly visible, since high friction forces contributed notably to the structure's strength. The force transfer at the lap joint for the low seismic option and the contact between the steel columns and wall elements for the high seismic options were responsible for the high friction component. A comparison between the low and high seismic options not only shows the increased higher strength and stiffness of the core, but also higher energy dissipation because of the presence of UFP devices.

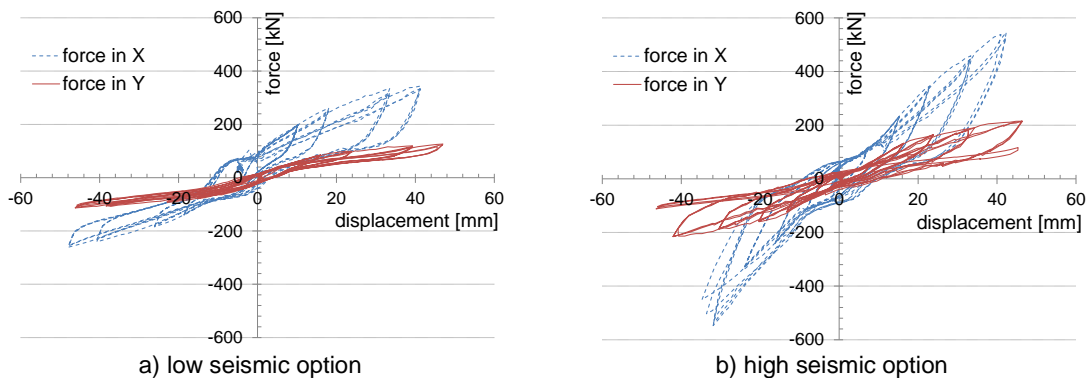


Figure C.46 Force-displacement curves for test 1 for drift levels of up to 1.5% for the low and high seismic option respectively

The core drift has been monitored by direct measurement of the wall rotation with inclinometers. The displacement controlled hydraulic jacks were relying on the measured displacements of the walls (imposed drift). Figure C.47 plots the imposed drift values and the real wall rotations along the loading protocol. It can be seen that especially in the East-West direction (coupled walls) the measured wall drifts were smaller than the imposed drifts. This can be attributed to unwanted displacements in the loading apparatus and slips between the

steel foundation plate and the laboratory's strong floor as well as slips between the walls and the foundation plate. This discrepancy is less pronounced in the North-South direction, probably because of the smaller forces required to push the single walls.

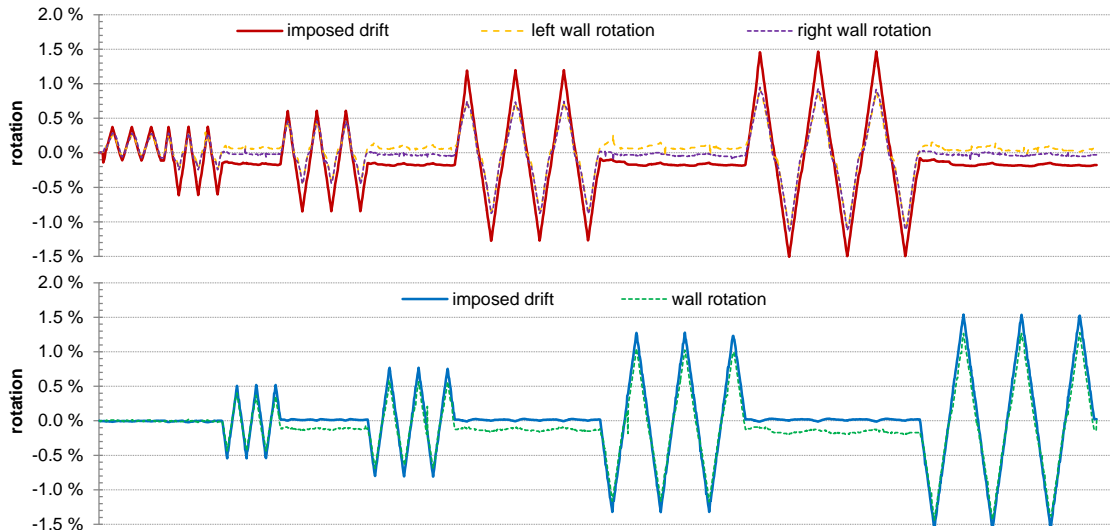


Figure C.47 Imposed drift and measured drift values on the walls for the low seismic option, test 1, for the coupled walls East-West (top) and the single wall North-South (bottom)

C.4.3.1 Collector beam behaviour for loading in X, low seismic option, test 1

To study the behaviour of the collector beams during the rocking of the core-wall system, the wall rotations and the beam rotations are plotted along the entire loading protocol in Figure C.48. Both the left and right East-West walls undergo the same rotations, the beam rotations are measured at the connection to the wall. It can be seen that the connection, consisting of a ring of bolts, can successfully decouple imposed rotations from the wall into the beams.

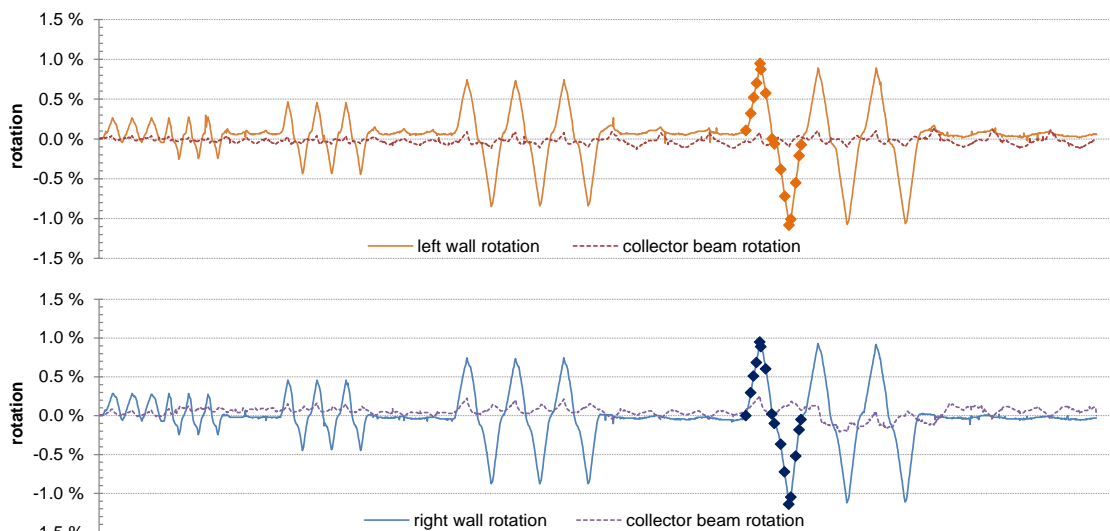


Figure C.48 Wall and collector beam rotations for the low seismic option in the East-West direction; 16 loading points for the 1.5% drift cycle are marked

It is interesting to note that during the loading in the North-South direction (the intermediate flatter sections in the graph), the East-West walls and beams undergo some rotation.

For both the North and the East collector beams, rotations are measured at the upper beams and deflections are measured for the lower beams. Since the top and the lower beams are connected in the same way to the wall, their deformation was deemed to be identical. Figure C.49 shows schematically the position of the measurement points. The beams are coloured in blue with a number of rotation indicators in red.

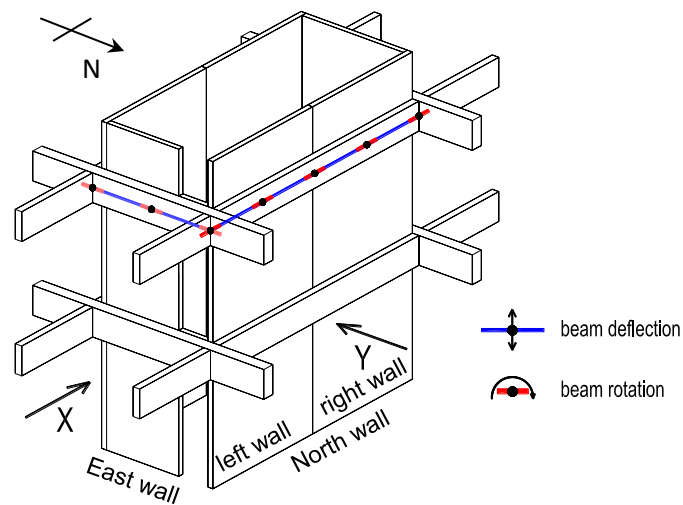


Figure C.49 Position of beam deflection and rotation measurement points

Figure C.50 shows the ram forces and wall rotations for the first 1.5% drift cycle. 15 distinct loading points are marked, which are also shown in Figure C.48. Both walls undergo identical deformation and follow the force pattern.

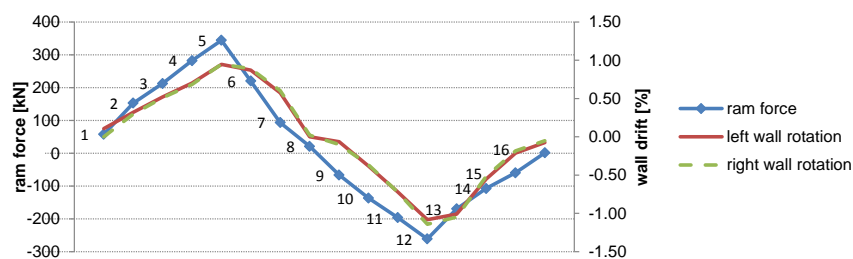


Figure C.50 Ram forces and respective wall rotations for the low seismic option in the East-West direction for the 16 loading points

In Figure C.51 the East and North collector beam deflections (in blue) and rotations (in red) are shown for the 16 loading points. The different plots represent the deformed shape increasing positive drift levels up to 1.5% and then down to zero. Then the same cycle is repeated for negative drifts up to -1.5%. It can be seen that the measured beam rotations follow the deformed shape of the beams.

As expected, the collector beam in the loading direction (right plots in Figure C.51) lifts up because of the walls uplift and rotation. The beams deformed quite differently on their left and right ends respectively. This is caused by the way the load is applied to the collector beams, rather than the rotations of the walls. Because the force is applied at the left side of the beam, when the beams are pushed (positive cycles), the ram is pushing slightly upwards. This caused bigger displacements at the left end of the beam, compared to the right side.

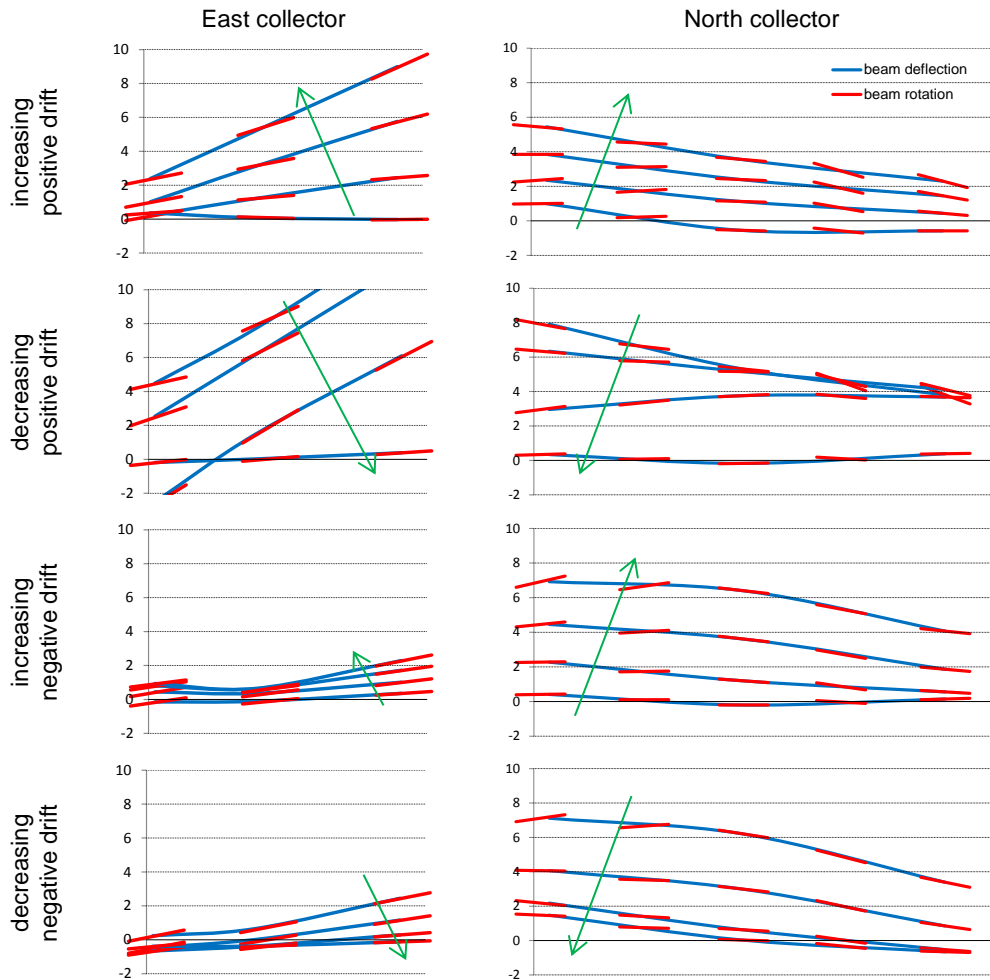


Figure C.51 Collector beam deflections and rotations along the single (left) and the coupled (right) walls for the low seismic option in the East-West direction for the 16 loading points

The unloaded collector beams on the East wall (left plots in Figure C.51) were connected eccentrically in respect to the mid-length of the wall because of the doorway opening. Therefore, when the loaded North collector beams were trying to uplift, the East collector beams rotated, resulting in bigger uplifts on the right side. This is thought to have caused the bigger deflections in the East collector beam, together with the additional displacements from the out-of-plane rotation of the East wall. For negative drift cycles, where the beams were pulled, the East collector beams only had limited uplift.

The differential displacement between the orthogonally collector beams was allowed for by elastic out-of-plane bending of the splice steel plate of the collector beams in longitudinal direction. The capacity of the splice was not influenced by this behaviour and the steel plate did not show residual deformations after testing.

C.4.3.2 Collector beam behaviour for loading in Y, low seismic option, test 1

Figure C.52 shows the East wall and beam rotations when the core is loaded in the transverse (Y) direction. Even though the beam rotations were reduced when compared to the wall, the collector beam along the single wall underwent bigger rotations than the beams along the coupled wall in the previous load case (loaded in X). This is because the collectors along the coupled wall are restrained by two wall connections, limiting the vertical movement of the beams.

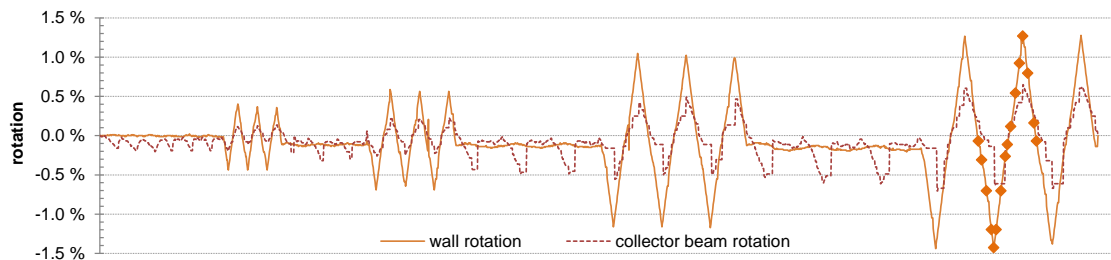


Figure C.52 Wall and collector beam rotations for the low seismic option in the North-South direction; 16 loading points for the 1.5% drift cycle are marked

Figure C.52 also shows the 16 loading points for the second 1.5% drift cycles in the North-South direction. Figure C.53 shows ram force and wall rotation for the same loading points.

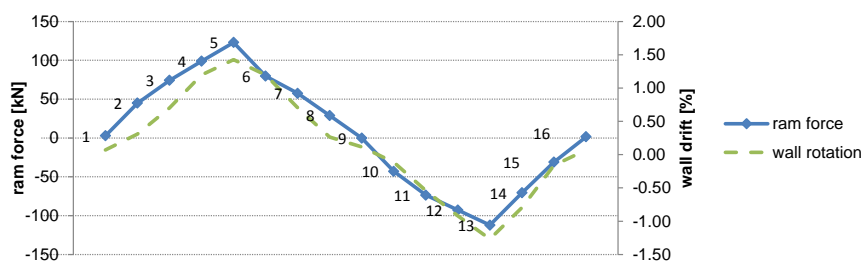


Figure C.53 Ram forces and respective wall rotations for the low seismic option in the North-South direction for the 16 loading points

The plots in Figure C.54 suggest that for loads applied in the North-South direction, the longitudinal collector beams remain almost straight while rigidly moving up and down. Only for the positive drift levels the beams are slightly bending upwards at their ends, as the East and West collector beams lift up.

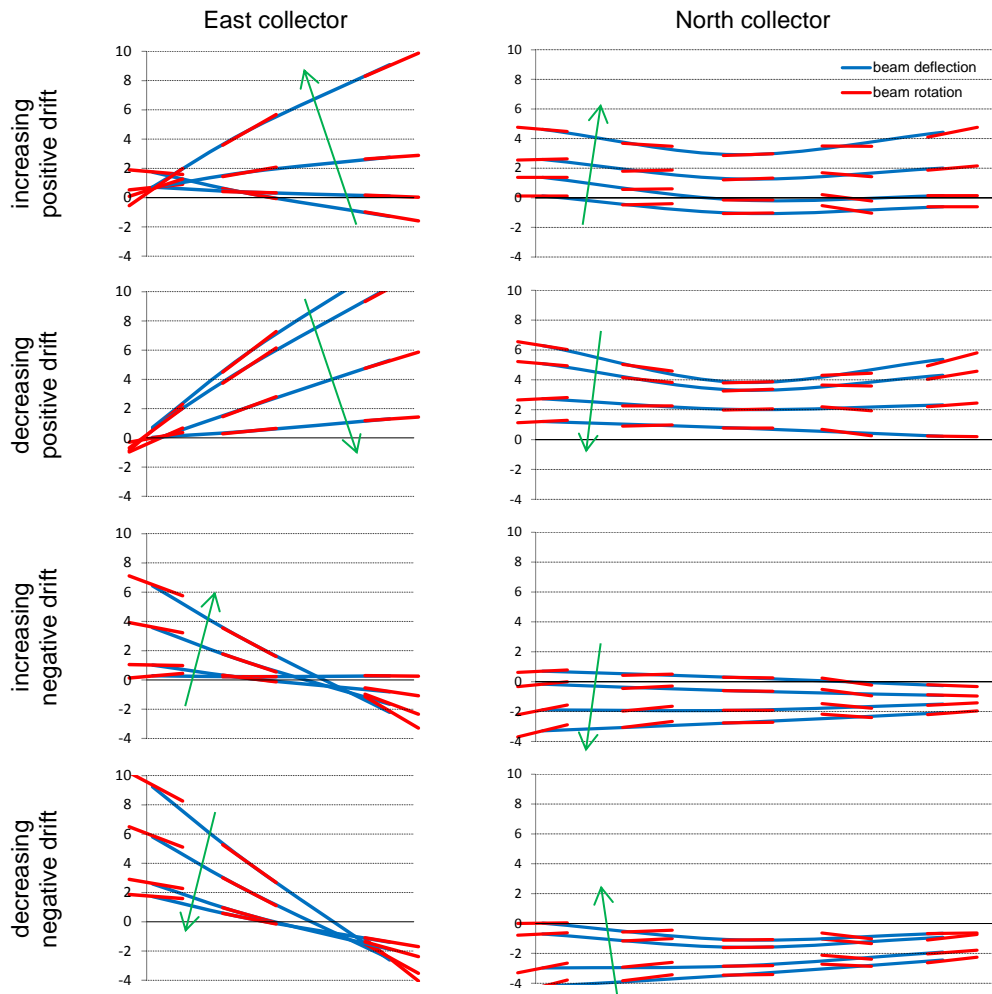


Figure C.54 Collector beam deflections and rotations along the single (left) and the coupled (right) walls for the low seismic option in the North-South direction for the 16 loading points

For positive drift levels the loaded East collector beam is pushed up on the right side. This is because in addition of the imposed uplift of the wall, also the horizontal force is applied there. When the beams are pushed, the ram is pushing slightly upwards. For negative drift levels the beam is pushed upwards by the wall uplift, but because the beam-to-wall connection is eccentric to the left respect to the mid-length of the wall, the beam rotates and provides high uplifts on the left side only.

The differential displacements between the orthogonally running beams are again taken by the splice plates, which were still able to carry the axial loads.

C.4.3.3 Collector beam behaviour for loading in X, high seismic option, test 1

Figure C.55 shows that the pinned beam to the steel column connection is able to almost decouple the wall rotations from the beams. The remaining beam rotations are imposed by the out-of-plane rotation of the single walls and respective collector beams.

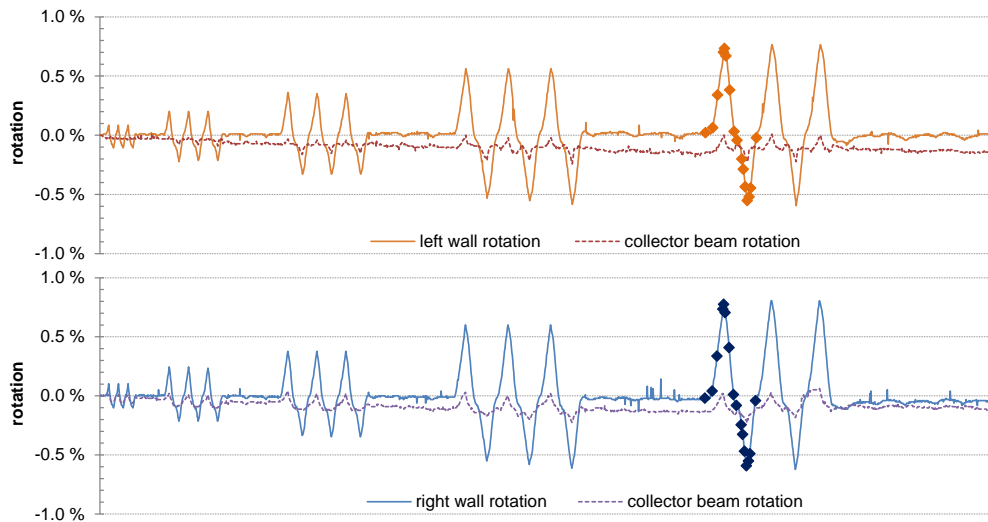


Figure C.55 Wall and collector beam rotations for the high seismic option in the East-West direction; 16 loading points for the 1.5% drift cycle are marked

Figure C.56 shows the ram forces and respective wall drifts for the selected loading points. In difference to Figure C.50, for the high seismic option the rotations of the coupled walls are slightly different. This is because the walls are not loaded equally through the collector beams, but by contact from the steel column to the first wall and then to the second wall.

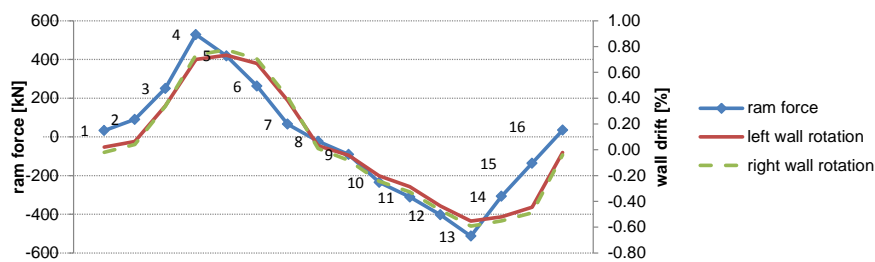


Figure C.56 Ram forces and respective wall rotations for the high seismic option in the East-West direction for the 16 loading points

Figure C.57 shows that when then core is pushed to positive drift levels, the loaded collector beams uplift on the left hand side. This is again because the ram is slightly rotated upwards when pushing against the beams. The orthogonal collector beams on the East wall slightly follow this movement.

For negative drifts, when the ram is pulling on the beams, both collector beams remain essentially straight. This can be considered as a more realistic behaviour of the sub-structure in a real building under horizontal loads.

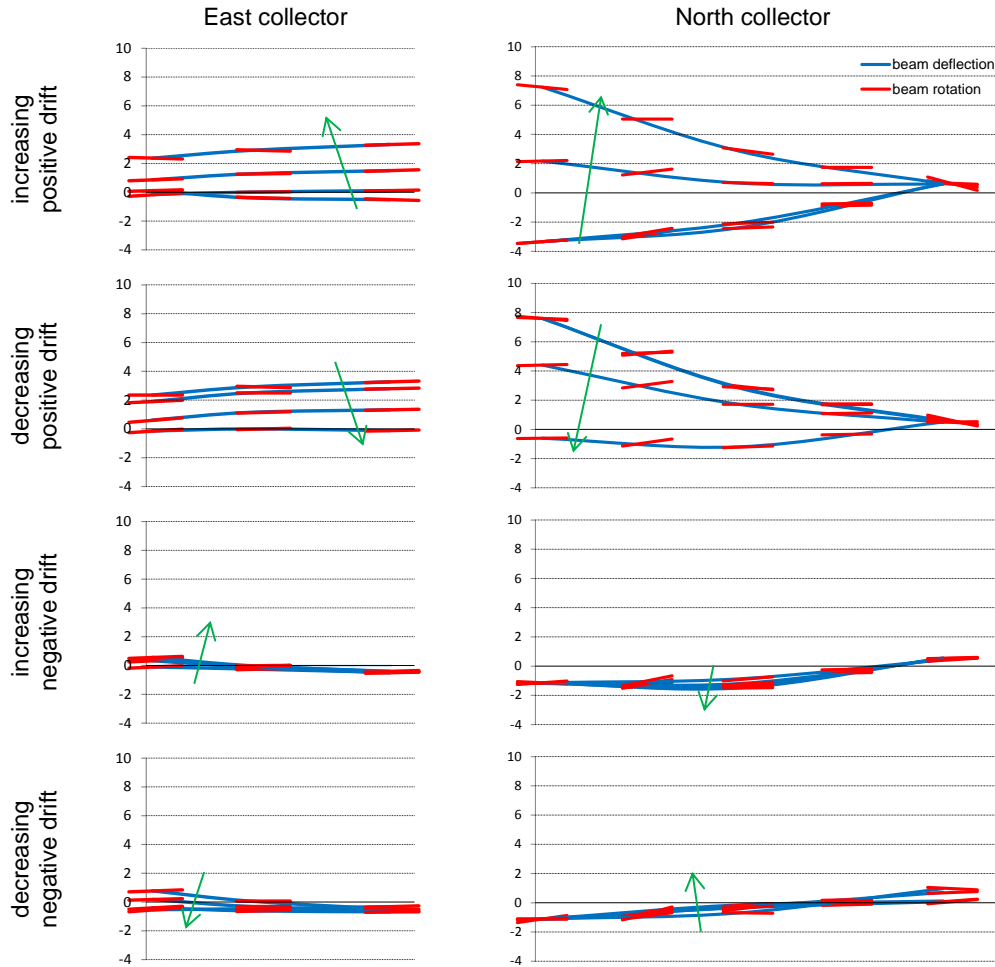


Figure C.57 Collector beam deflections and rotations along the single (left) and the coupled (right) walls for the high seismic option in the East-West direction for the 16 loading points

C.4.3.4 Collector beam behaviour for loading in Y, high seismic option, test 1

Figure C.58 shows the wall and beam rotations when the core is loaded in the North-South direction. The beam rotations are very small compared to the wall rotations and are likely to be imposed only by the out-of-plane rotation of the North and South walls. The graph also shows 16 loading points for the first 1.5% drift loading cycle.

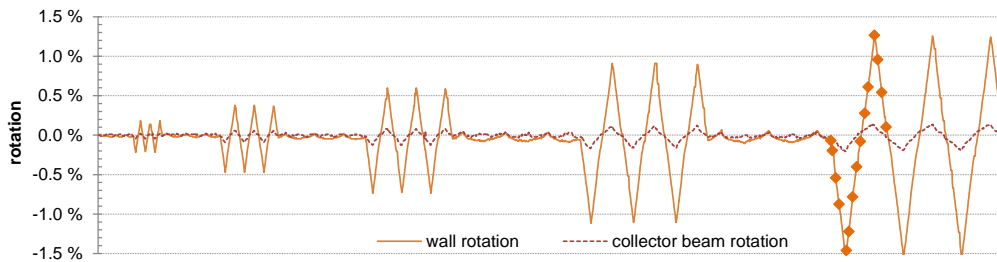


Figure C.58 Wall and collector beam rotations for the high seismic option in the North-South direction; 16 loading points for the 1.5% drift cycle are marked

Figure C.59 shows the ram forces and wall rotation of the selected 16 loading points.

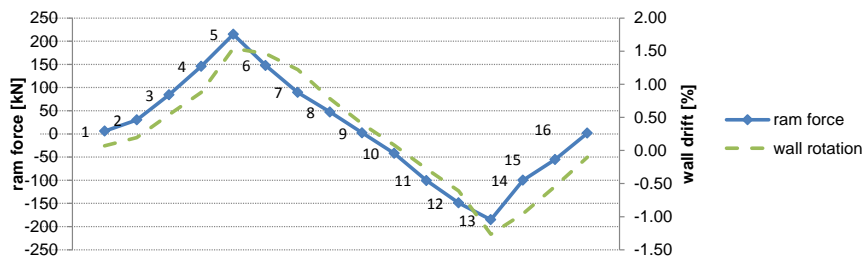


Figure C.59 Ram forces and respective wall rotations for the high seismic option in the North-South direction for the 16 loading points

Figure C.60 shows the deformation of the collector beams for the 16 loading points. In the North-South loading direction, the beams remain almost always straight. The uplifting force of the ram when pushing on the beam has less effect in the high seismic option. The remaining deformations of the beams are imposed by the out-of-plane rotations of the walls orthogonal to the loading direction.

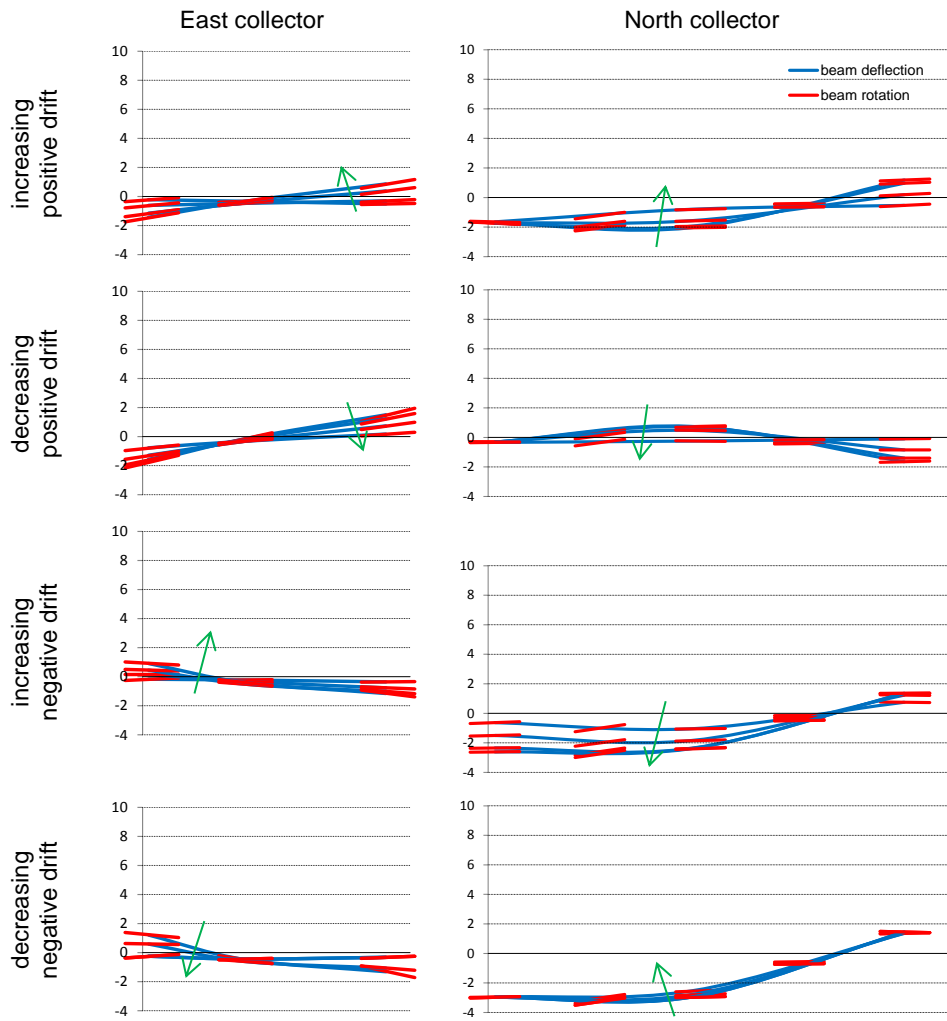


Figure C.60 Collector beam deflections and rotations along the single (left) and the coupled (right) walls for the high seismic option in the North-South direction for the 16 loading points

D Appendix – Derivation of the stiffness formulae for wall-beam assemblies

D.1 DERIVATION OF THE STIFFNESS RELATIONSHIP BETWEEN A ROCKING WALL AND A COLLECTOR BEAM

Figure D.1 shows that the pushover of a rocking wall connected to collector beams is governed by the moment rotation behaviour at the interface between the wall and the foundation, the bending flexibility of the collector beam and the translational and rotational stiffnesses of the connection.

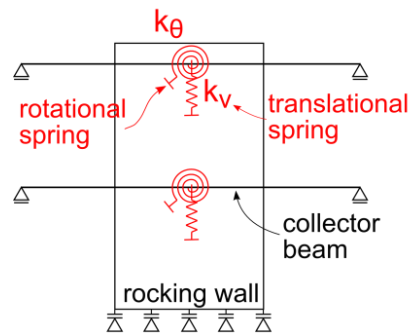


Figure D.1 Statical model of a rocking wall connected to collector beams

To analytically study the interaction between the wall and the beam, the stiffness of the beam-connection assembly is herein derived. Once the rotational and translational stiffnesses of this system are known, the forces and moments created by the imposed wall uplift and rotation can be determined. To derive the system stiffness, the stiffnesses of the beam and of the connection under imposed vertical and rotational displacements need to be derived and combined. The translational and rotational stiffnesses for a connection with metallic fasteners are derived in section D.3.3.

D.1.1 Beam stiffness

Figure D.2 shows the deflected shape and rotations of a beam with an imposed force P and moment M respectively, applied at a distance l_1 from the support. The rotation and deflection of the beam at the position, where the force and moment are applied, can be calculated with the equations provided in Table D.1. The beam rotational and deflection stiffnesses k_b of the

beam are also shown. The term in parenthesis describes the type of imposed action (P for force and M for moment) and the respective deformation (ϑ for rotation and v for deflection).

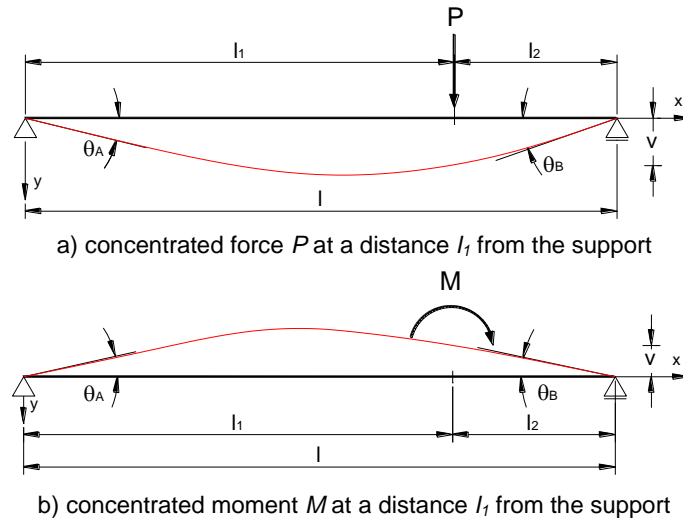


Figure D.2 Beam deflections and rotations due to a discrete force and discrete moment

Table D.1 Deflections and rotations and relative stiffnesses for a beam under a concentrated force P and moment M at a distance l_1 from the support

Beam rotation/deflection	Stiffness
$\theta_{beam(P)} = \frac{P}{k_{b(P,\theta)}} = \frac{Pl_2(l^2 - l_1^2 - 3l_2^2)}{6EI}$	$k_{b(P,\theta)} = \frac{6EI}{l_2(l^2 - l_1^2 - 3l_2^2)}$
$\theta_{beam(M)} = \frac{M}{k_{b(M,\theta)}} = \frac{P(3l_1l - 3l_1^2 - l^2)}{3EI}$	$k_{b(M,\theta)} = \frac{3EI}{(3l_1l - 3l_1^2 - l^2)}$
$v_{beam(P)} = \frac{P}{k_{b(P,v)}} = \frac{Pl_1l_2(l^2 - l_1^2 - l_2^2)}{6EI}$	$k_{b(P,v)} = \frac{6EI}{l_1l_2(l^2 - l_1^2 - l_2^2)}$
$v_{beam(M)} = \frac{M}{k_{b(M,v)}} = \frac{Ml_1l_2(2l_1 - l)}{3EI}$	$k_{b(M,v)} = \frac{3EI}{l_1l_2(2l_1 - l)}$

For a force application at mid-span, the rotation is zero because of symmetry, resulting in an infinite stiffness $k_{b(P,\theta)}$. Similarly, if the moment is applied at mid-span, the beam undergoes a deflection in double curvature, resulting in a zero deflection at mid-span. The beam deflection stiffness under an external moment $k_{b(M,v)}$ is therefore infinite.

D.1.2 System stiffness

To obtain the system stiffness, the beam stiffnesses derived above need to be combined with the connection stiffness. Since an imposed force at a distance l_1 creates both deflection and rotation at the point of application, both the translational and rotational stiffness of the connection need to be considered. Similarly, an imposed moment can create deflections when

applied away from the mid-span, activating both connection stiffnesses. Table D.2 summarized the different statical systems and the notations used for the derivation of the system stiffness. The term in parenthesis can be read as the deriving action (force P or moment M) for the type of imposed deformation (deflection v or rotation ϑ)

Table D.2 Stiffness denomination of a beam element loaded by a force P and moment M under different restraining conditions

Statical system	Stiffness denomination	Notation
	$k_{beam}(P,v)$ $k_{beam}(P,\theta)$	$k_{b(P,v)}$ $k_{b(P,\theta)}$
	$k_{beam + vertical\ connection}(P,v)$ $k_{beam + vertical\ connection}(P,\theta)$	$k_{b+v.c.}(P,v)$ $k_{b+v.c.}(P,\theta)$
	$k_{beam + rotational\ connection}(P,v)$ $k_{beam + rotational\ connection}(P,\theta)$	$k_{b+r.c.}(P,v)$ $k_{b+r.c.}(P,\theta)$
	$k_{beam + vertical\ and\ rotational\ connection}(P,v)$ $k_{beam + vertical\ and\ rotational\ connection}(P,\theta)$	$k_{b+v.&r.c.}(P,v)$ $k_{b+v.&r.c.}(P,\theta)$
	$k_{beam}(M,v)$ $k_{beam}(M,\theta)$	$k_{b(M,v)}$ $k_{b(M,\theta)}$
	$k_{beam + vertical\ connection}(M,v)$ $k_{beam + vertical\ connection}(M,\theta)$	$k_{b+v.c.}(M,v)$ $k_{b+v.c.}(M,\theta)$
	$k_{beam + rotational\ connection}(M,v)$ $k_{beam + rotational\ connection}(M,\theta)$	$k_{b+r.c.}(M,v)$ $k_{b+r.c.}(M,\theta)$
	$k_{beam + vertical\ and\ rotational\ connection}(M,v)$ $k_{beam + vertical\ and\ rotational\ connection}(M,\theta)$	$k_{b+r.&v.c.}(M,v)$ $k_{b+r.&v.c.}(M,\theta)$
	$k_{vertical\ connection}$	$k_{v.c.}$
	$k_{rotational\ connection}$	$k_{r.c.}$

The system stiffness for both the imposed deflection and rotation respectively are derived as a combination of the stiffnesses from Table D.2 in series.

D.1.2.1 Beam and translational spring system stiffness for an imposed deflection

First the stiffness of the beam combined with a translational stiffness under an imposed deflection is studied as shown in Figure D.3. The deflection compatibility of the system can be written as

$$v_{v.c.} = v_{imposed} - v_b \tag{D.1}$$

where

- $v_{v.c.}$ deformation of the translational spring;
- $v_{imposed}$ imposed deflection of the spring;
- v_b beam deflection.

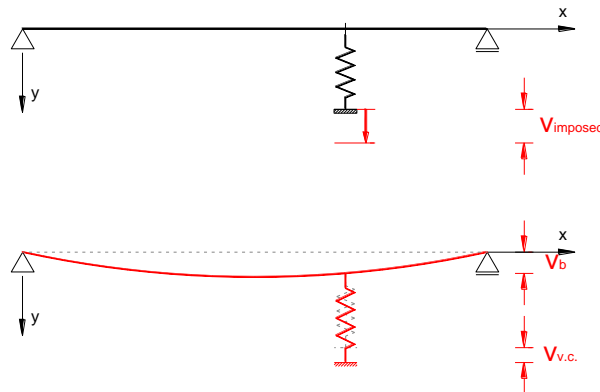


Figure D.3 Deflection of a beam restrained by a translational spring under an imposed deflection

Equation (D.1) can be rewritten in terms of force and relative stiffness as

$$\frac{P}{k_{v.c.}} = v_{imposed} - \frac{P}{k_{b(P,v)}} \tag{D.2}$$

This equation can be solved for P

$$P = v_{imposed} \left[\frac{1}{k_{b(P,v)}} + \frac{1}{k_{v.c.}} \right]^{-1} = v_{imposed} k_{b+v.c.(P,v)} \tag{D.3}$$

which allows us to write the deflection stiffness of a beam restrained by a translational spring under an imposed deflection

$$k_{b+v.c.(P,v)} = \left[\frac{1}{k_{b(P,v)}} + \frac{1}{k_{v.c.}} \right]^{-1} \tag{D.4}$$

D.1.2.2 Beam and rotational spring system stiffness for an imposed rotation

Similarly to above, the beam and rotational spring system stiffness needs to be determined.

The rotation compatibility of the system can be written as

$$\theta_{r.c.} = \theta_{imposed} - \theta_b \quad (D.5)$$

where

$\vartheta_{r.c.}$ rotation of the rotational spring;
 $\vartheta_{imposed}$ imposed rotation;
 ϑ_b beam rotation.

Equation (D.5) can be rewritten in terms of moment and relative stiffness as

$$\frac{M}{k_{r.c.}} = \theta_{imposed} - \frac{M}{k_{b(M,\theta)}}. \quad (D.6)$$

This equation can be solved for M

$$M = \theta_{imposed} \left[\frac{1}{k_{b(M,\theta)}} + \frac{1}{k_{r.c.}} \right]^{-1} = \theta_{imposed} k_{b+r.c.(M,\theta)}, \quad (D.7)$$

which allows us to write the deflection stiffness of a beam restrained by a translational spring under an imposed rotation

$$k_{b+r.c.(M,\theta)} = \left[\frac{1}{k_{b(M,\theta)}} + \frac{1}{k_{r.c.}} \right]^{-1}. \quad (D.8)$$

D.1.2.3 System stiffness for imposed rotations

To obtain the system stiffness for a beam restrained by a translational spring under an imposed rotation, the relation between the imposed rotation and the moment in the beam can be written as

$$M = k_{b+v.c.(M,\theta)} \theta = k_{b+v.c.(M,\theta)} [\theta_M + \theta_{v.c.}] = k_{b+v.c.(M,\theta)} \left[\frac{M}{k_{b(M,\theta)}} + \frac{P}{k_{b(P,\theta)}} \right], \quad (D.9)$$

where $\vartheta_{v.c.}$ is the rotation in the beam caused by the translational spring which is activated by the imposed rotation. The force in the spring can be calculated taking into consideration the deflection stiffness of the beam under an imposed moment and Equation (D.4)

$$P = v k_{b.+v.c.(P,v)} = \frac{M}{k_{b(M,v)}} k_{b.+v.c.(P,v)}. \quad (D.10)$$

By equating (D.10) into (D.9) we obtain

$$M = k_{b+v.c.(M,\theta)} \left(\frac{M}{k_{b(M,\theta)}} + \frac{M}{k_{b(M,v)}} \frac{k_{b.+v.c.(P,v)}}{k_{b(P,\theta)}} \right). \quad (D.11)$$

Further, the rotation stiffness of the system can be written as

$$k_{b+v.c.(M,\theta)} = \left[\frac{1}{k_{b(M,\theta)}} + \frac{k_{b+v.c.(P,v)}}{k_{b(M,v)}k_{b(P,\theta)}} \right]^{-1}. \quad (D.12)$$

The addition of the rotational spring to the system can be accounted for as

$$k_{b+v.&r.c.(M,\theta)} = \left[\frac{1}{k_{b+v.c.(M,\theta)}} + \frac{1}{k_{r.c.}} \right]^{-1}. \quad (D.13)$$

In the case where the translational and rotational springs are situated at the mid-span of the beam, Equations (D.12) and (D.13) can be simplified into

$$k_{b+v.c.(M,\theta)} = \left[\frac{1}{k_{b(M,\theta)}} + \frac{k_{b+v.c.(P,v)}}{\infty} \right]^{-1} = k_{b(M,\theta)} \quad (D.14)$$

and

$$k_{b+v.&r.c.(M,\theta)} = \left[\frac{1}{k_{b(M,\theta)}} + \frac{1}{k_{r.c.}} \right]^{-1}. \quad (D.15)$$

In the case the springs are situated away from the mid-span, the imposed rotation also activates the translational spring as stated above. The direct relation between the force in the spring and the imposed rotation can be written by combining Equations (D.10) and (D.13)

$$P = \frac{k_{b+v.&r.c.(M,\theta)}\theta}{k_{b(M,v)}} k_{b+v.c.(P,v)} = \theta \left[\frac{k_{b+v.&r.c.(M,\theta)}}{k_{b(M,v)}} k_{b+v.c.(P,v)} \right]; \quad (D.16)$$

and the stiffness can therefore be written as

$$k_{b+v.&r.c.(P,\theta)} = \left[\frac{k_{b+v.&r.c.(M,\theta)}}{k_{b(M,v)}} k_{b+v.c.(P,v)} \right]. \quad (D.17)$$

D.1.2.4 System stiffness for imposed deflections

To obtain the system stiffness for a beam restrained by a translational spring under an imposed deflection, the relation between the imposed deflection and the force in the beam can be written as

$$P = k_{b+r.c.(P,v)}v = k_{b+r.c.(P,v)}[v_P + v_{r.c.}] = k_{b+r.c.(P,v)} \left[\frac{P}{k_{b(P,v)}} + \frac{M}{k_{b(M,v)}} \right] \quad (D.18)$$

where $v_{r.c.}$ is the deflection in the beam caused by the rotational spring which is activated by the imposed deflection. The moment in the spring can be calculated taking into consideration the rotational stiffness of the beam under an imposed force and Equation (D.7)

$$M = \theta k_{b.+r.c.(M,\theta)} = \frac{P}{k_{b(P,\theta)}} k_{b.+r.c.(M,\theta)}. \quad (D.19)$$

By equating (D.19) into (D.18) we obtain

$$P = k_{b.+r.c.(P,v)} \left[\frac{P}{k_{b(P,v)}} + \frac{P}{k_{b(P,\theta)}} \frac{k_{b.+r.c.(M,\theta)}}{k_{b(M,v)}} \right] \quad (D.20)$$

and the deflection stiffness of the system can be written as

$$k_{b.+r.c.(P,v)} = \left[\frac{1}{k_{b(P,v)}} + \frac{k_{b.+r.c.(M,\theta)}}{k_{b(P,\theta)} k_{b(M,v)}} \right]^{-1}. \quad (D.21)$$

The addition of the translational spring to the system can be accounted for as

$$k_{b+v.&r.c.(P,v)} = \left[\frac{1}{k_{b+r.c.(P,v)}} + \frac{1}{k_{v.c.}} \right]^{-1}. \quad (D.22)$$

In the case were the translational and rotational springs are situated at the mid-span of the beam, Equations (D.21) and (D.22) can be simplified into

$$k_{b+r.c.(P,v)} = \left[\frac{1}{k_{b(P,v)}} + \frac{k_{b+r.c.(M,\theta)}}{\infty} \right]^{-1} = k_{b(P,v)} \quad (D.23)$$

and

$$k_{b+v.&r.c.(P,v)} = \left[\frac{1}{k_{b(P,v)}} + \frac{1}{k_{v.c.}} \right]^{-1}. \quad (D.24)$$

In the case the springs are situated away from the mid-span, the imposed deflection activates the rotational spring as stated above. The direct relation between the moment in the spring and the imposed deflection can be written by combing Equations (D.19) and (D.22)

$$M = \frac{k_{b+v.&r.c.(P,v)} v}{k_{b(P,\theta)}} k_{b.+r.c.(M,\theta)} = v \left[\frac{k_{b+v.&r.c.(P,v)} k_{b.+r.c.(M,\theta)}}{k_{b(P,\theta)}} \right]; \quad (D.25)$$

and the stiffness can therefore be written as

$$k_{b+v.&r.c.(M,v)} = \frac{k_{b+v.&r.c.(P,v)}}{k_{b(P,\theta)}} k_{b.+r.c.(M,\theta)}. \quad (D.26)$$

D.2 ADDITIONAL DEMAND IN THE WALL-TO-BEAM CONNECTION DUE TO DISPLACEMENT INCOMPATIBILITIES

The collector beam needs to transfer horizontal and, depending on the span direction of the floor, also gravity forces to the shear wall. Because of the rocking mechanism of the wall, the connection however also needs to transfer an additional moment and vertical force caused by the displacement incompatibilities. These additional actions depend on the rigidity of both the connection and the beam.

To rapidly determine the force in the fasteners for a bolted connection, a spreadsheet has been developed. Depending on the connection geometry, the translational and rotational stiffnesses of the fastener is determined based on the slip modulus of the single fastener. The slip modula K_{ser} or K_u for the serviceability or ultimate limit state respectively are determined according to Eurocode 5 (Eurocode 5 2008). If the hole in the timber to place the fasteners is oversized, part of the imposed displacement can be accommodated by the movement of the fastener. The collector beams are assumed to be connected to gravity columns by perfect hinges at the ends. The position of the connection along the beam can be chosen arbitrarily.

By inputting the expected uplift and rotation at the connection, the spreadsheet calculates the resulting vertical force and moment based on the various translational and rotational stiffnesses of the beam-connection system. These are then added to the external loads acting on the collector beam to calculate the maximum force in the fastener.

It has to be noted that the uplift and rotation in the wall as well as the horizontal force depend on the seismic behaviour of the structure and hence on the performance of the wall. Because perfect decoupling of the displacement between walls and beams are not possible, walls' stiffnesses can increase, changing their seismic behaviour, which again influences both the displacement demand and the horizontal forces. An iterative process will be necessary.

If the structure is designed as a low damage system, the fastener capacity should be determined by using elastic embedment strengths, the lower bound of the yield moment and without the contribution of the rope effect. If such information is not available, 2/3 of the ultimate capacity excluding any rope effect should be considered. In this way the connections will not be damaged for ULS events. In the case of a Maximum Credible Earthquake (MCE), the full capacity including the rope effect can be considered, as long as a ductile failure mode can be guaranteed.

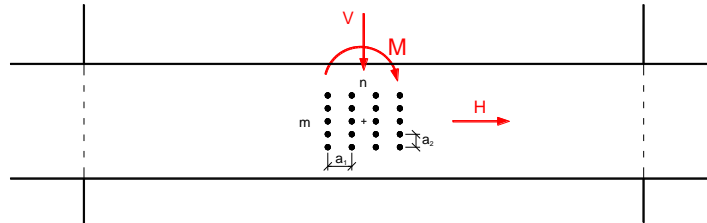
Next a sample spreadsheet for the calculation of the connection demand is reproduced.

Connection wall - collector beam

Beam-Wall connection for Scenario I (horizontal force only) - DBE

Connection geometry

(rectangular pattern)

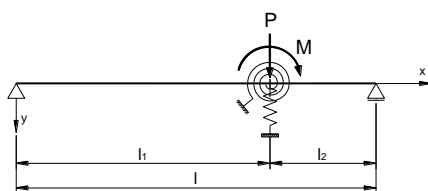


d =	16 mm	dowel diameter
m =	4	number of rows
a ₂ =	80 mm	distance of rows
n =	5	number of columns
a ₁ =	80 mm	distance of columns
n _{tot} =	20	total number of dowels

Collector beam

Material	LVL	$\rho_m =$ 597 kg/m ³
		E = 11,000 MPa

Geometry	b = 126 mm	I = 2.84.E+08 mm ⁴
	h = 300 mm	
	l ₁ = 4.00 m	
	l ₂ = 2.00 m	
	l = 6.00 m	



Positive forces and moments



Positive deformations and rotations

v positive in y direction
 θ positive if clockwise

Wall

Material	LVL	$\rho_m =$ 597 kg/m ³
-----------------	-----	----------------------------------

Rotation	$\theta_{imp} =$ 0.015 rad	imposed rotation (clockwise)
	$\Delta_d =$ 0.25 mm	oversized hole in timber (in each member)
	$\theta_{\Delta d} =$ 0.003 rad	accommodated rotation
	$\theta_{imp \text{ on beam}} =$ 0.013 rad	rotation in the connection

Deflection	$\Delta_{wall} =$ -7 mm	imposed uplift
	$\Delta_{\Delta d} =$ 0.5 mm	accommodated rotation
	$\Delta_{wall \text{ on beam}} =$ -6.5 mm	rotation in the connection

Connection stiffness

Slip modulus $K_{ser} = 10,147.37 \text{ N/mm}$ slip modulus per dowel per shear plane at SLS
 $K_u = 6,764.92 \text{ N/mm}$ slip modulus per dowel per shear plane at ULS

Limit state **SLS**

$n_{\text{shear plane}} = 2$ number shear planes

$k_{\text{rotational connection}} = 8,442.61 \text{ kNm/rad}$ rotational connection stiffness
 $k_{\text{vertical connection}} = 405.89 \text{ kN/mm}$ vertical connection stiffness

System stiffness

Beam stiffness

$k_{\text{beam (P,}\theta)} = -3,508.31 \text{ kN/rad}$ rotational stiffness of beam under imposed point load
 $k_{\text{beam (P,v)}} = 0.88 \text{ kN/mm}$ deflection stiffness of beam under imposed point load
 $k_{\text{beam (M,}\theta)} = 4,677.75 \text{ kNm/rad}$ rotational stiffness of beam under imposed moment
 $k_{\text{beam (M,v)}} = 3.51 \text{ kN/mm}$ deflection stiffness of beam under imposed moment

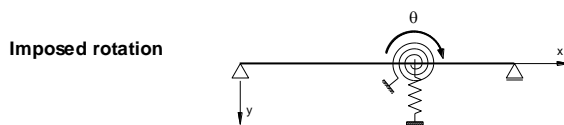
Beam with vertical stiffness

$k_{\text{beam + v vertical connection (P,v)}} = 0.88 \text{ kN/mm}$ deflection stiffness of beam with vertical connection
 $k_{\text{beam + v vertical connection (M,}\theta)} = 7,009.1 \text{ kNm/rad}$ rotational stiffness of beam with vertical connection

$k_{\text{beam + rotational connection (M,}\theta)} = 3,010.0 \text{ kNm/rad}$ rotational stiffness of beam with rotational connection
 $k_{\text{beam + rotational connection (P,v)}} = 1.12 \text{ kN/mm}$ deflection stiffness of beam with rotational connection

$k_{\text{beam + v vertical and rotational connection (M,}\theta)} = 3,829.7 \text{ kNm/rad}$ rotational stiffness of beam with vertical and rotational connection
 $k_{\text{beam + v vertical and rotational connection (P,v)}} = 1.11 \text{ kN/mm}$ deflection stiffness of beam with vertical and rotational connection

Wall - beam connection



$\theta_{\text{imp}} = 0.013 \text{ rad}$ imposed rotation on wall

$M_{\text{wall-beam connection}} = 47.87 \text{ kNm}$ moment in connection

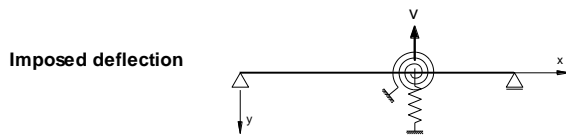
$P_{\text{vertical connection}} = -11.94 \text{ kN}$ associated force in vertical spring
 (upwards force in wall)

Deformations and internal forces

$v = -0.03 \text{ mm}$ beam deflection at the connection
 $\theta = 6.83 \text{ mrad}$ beam rotation at the connection

$M_{lx} = -15.99 \text{ kNm}$ moment on the right side of the connection
 $M_{rx} = 31.88 \text{ kNm}$ moment on the left side of the connection

$R_A = -4.00 \text{ kN}$ reaction at A
 $R_B = 15.94 \text{ kN}$ reaction at B



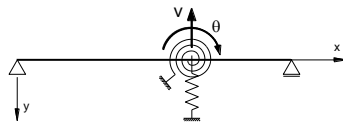
Imposed deflection

$V_{mp} =$	-6.5 mm	imposed deflection on wall
$P_{\text{wall-beam connection}} =$	7.24 kN	vertical force in connection (downwards force in wall)
$M_{\text{rotational connection}} =$	-6.21 kNm	associated moment in rotational spring

Deformations and internal forces

$v =$	-6.48 mm	beam deflection at the connection
$\theta =$	0.74 mrad	beam rotation at the connection
$M_{lx} =$	-5.51 kNm	moment on the right side of the connection
$M_{rx} =$	-11.72 kNm	moment on the left side of the connection
$R_A =$	-1.38 kN	reaction at A
$R_B =$	-5.86 kN	reaction at B

Total deformations and internal forces

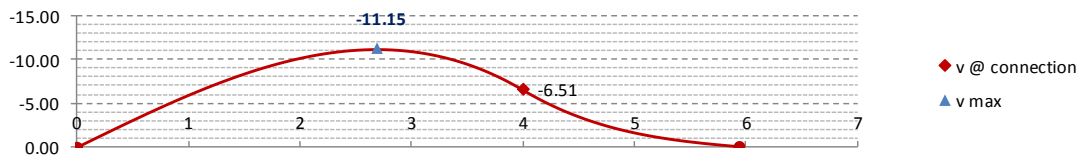


$P_{\text{wall-beam connection}} =$	-4.70 kN	vertical force in connection
$M_{\text{rotational connection}} =$	41.66 kNm	associated moment in rotational spring
$v =$	-6.51 mm	beam deflection at the connection
$\theta =$	7.57 mrad	beam rotation at the connection
$M_{lx} =$	-21.50 kNm	moment on the right side of the connection
$M_{rx} =$	20.16 kNm	moment on the left side of the connection
$R_A =$	-5.38 kN	reaction at A
$R_B =$	10.08 kN	reaction at B

Deformation checks

$v_{max} =$	-11.15 mm	maximum deflection
$x =$	2.70 m	point of maximum deflection

corresponds to $\frac{l}{538}$



Forces in connection

Additional actions (external)	H =	140.0 kN	horizontal force	
	V =	110.0 kN	vertical force	(downwards)
	M =	0.0 kNm	moment	
Imposed actions	Rotation:		Deflection:	
	$V_{\theta} =$	-11.94 kN	$V_v =$	7.24 kN
	$M_{\theta} =$	47.87 kNm	$M_v =$	-6.21 kNm
	Total forces and moments	$H_{tot} =$	140.0 kN	horizontal force
	$V_{tot} =$	105.30 kN	vertical force	(downwards force in wall)
	$M_{tot} =$	41.66 kNm	moment	

Maximum shear force in dowel

$$F_{max} = \sqrt{(F_h + F_{M,max,x})^2 + (F_v + F_{M,max,y})^2} = 28.55 \text{ kN}$$

$$\alpha = 48.22^\circ \quad \text{angle to the grain of collector beam}$$

If n_{ef} is considered, the fastener capacity including splitting has to be considered in the force component parallel to the grain

$F_{max, h} =$	19.02 kN	$n_{ef, h} =$	3.35	$\xi_h = n_{ef} h/n =$	0.67
$F_{max, v} =$	21.29 kN	$n_{ef, v} =$	2.74	$\xi_v = n_{ef} v/m =$	0.69

D.3 FASTENER DEMAND AND STIFFNESS OF BOLTED CONNECTIONS

D.3.1 Calculation of the fastener demand

Considering that all fasteners in the connection have the same stiffness and act as a rigid body, and assuming small rotations of the connected members, we know from geometry that

$$v_i = \frac{r_i}{r_{max}} v_{max}. \quad (D.27)$$

If a moment M is imposed onto the connection, it will undergo a rotation θ as shown in Figure D.4 and the fastener furthest away from the centroid will have a force F_{max} as follows:

$$F_{max} = K v_{max} = K r_{max} \theta \quad (D.28)$$

where

- K slip modulus of the fasteners;
- v displacement of the fastener;
- r radial distance between the fastener and the centroid;
- θ the rotation of the connection.

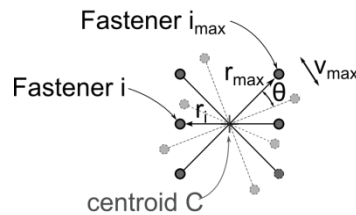


Figure D.4 Rotational behaviour of fasteners in a connection

The force in any fastener can be calculated as

$$F_i = K v_i = K \frac{r_i}{r_{max}} v_{max} = K \frac{r_i}{r_{max}} r_{max} \theta. \quad (D.29)$$

The moment taken by fastener i can be written as

$$M_i = F_i r_i = K \frac{r_i^2}{r_{max}} r_{max} \theta = F_{max} \frac{r_i^2}{r_{max}}. \quad (D.30)$$

The total moment of the connection is hence

$$M = F_{max} \frac{\sum_i r_i^2}{r_{max}}. \quad (D.31)$$

Finally, the maximum force in the fasteners can be written as a function of the imposed moment and the relative radii

$$F_{max} = M \frac{r_{max}}{\sum_i r_i^2} \quad (D.32)$$

which is independent from the single fastener stiffness, as it is assumed equal for all fasteners.

The polar moment of inertia I_p and its relation to the moment of inertia I_x and I_y of the connection can be written as

$$I_p = \sum_i r_i^2 = \sum_i x_i^2 + y_i^2 = I_x + I_y, \quad (D.33)$$

where

- x_i horizontal stiffness of fastener i from the centroid;
- y_i vertical stiffness of fastener i from the centroid.

Equation (D.32) can now be rewritten as

$$F_{M,max} = M \frac{r_{max}}{I_p}. \quad (D.34)$$

Similarly the components of F_{max} in respect to the two axis x and y become

$$F_{M,max,x} = M \frac{x_{max}}{I_p}, \quad F_{M,max,y} = M \frac{y_{max}}{I_p}, \quad (D.35)$$

with x_{max} and y_{max} being the coordinates of the fasteners with the biggest radial distance from the centroid.

D.3.2 Connection with moment and forces

If the connection is subjected to the horizontal and vertical forces H and V respectively, these will be resisted by each of the single fasteners as follows:

$$F_h = \frac{H}{n_{tot}}, \quad F_v = \frac{V}{n_{tot}} \quad (D.36)$$

where n_{tot} is the total number of fasteners.

The maximum force from the imposed moment and forces is given by the vector sum as follows

$$F_{max} = \sqrt{(F_h + F_{M,max,x})^2 + (F_v + F_{M,max,y})^2} \quad (D.37)$$

The inclination of the resultant force to the horizontal axis equals

$$\alpha = \arctan\left(\frac{F_v + F_{M,max,y}}{F_h + F_{M,max,x}}\right). \quad (D.38)$$

D.3.2.1 Connections with equally spaced fasteners

If the connection has equally spaced fasteners as shown in Figure D.5, the moment of inertias I_x^* and I_y^* in respect to the origin (conveniently placed at the lower left fastener) can be calculated as

$$\begin{aligned} I_x^* &= \sum_i^{m,n} x_{ij}^2 = m \sum_i^n x_i^2 = \\ &= m[0 + a_1^2 + 2^2 a_1^2 + \dots + (n-1)^2 a_1^2] = \\ &= m a_1^2 [0 + 1 + 2^2 + \dots + (n-1)^2] = \\ &= m a_1^2 \left[\frac{(n-1)^3}{3} + \frac{(n-1)^2}{2} + \frac{n-1}{6} \right]; \end{aligned} \quad (D.39)$$

$$\begin{aligned} I_y^* &= \sum_i^{m,n} y_{ij}^2 = n \sum_i^m y_i^2 = \\ &= n a_2^2 \left[\frac{(m-1)^3}{3} + \frac{(m-1)^2}{2} + \frac{m-1}{6} \right]. \end{aligned} \quad (D.40)$$

where:

- m number of fastener columns;
- n number of fastener rows;
- x_i x coordinate of fastener i ;
- y_i y coordinate of fastener i ;
- a_1 distance between fastener columns (distance in x direction);
- a_2 distance between fastener rows (distance in y direction).

The Huygens-Steiner theorem can be applied to calculate the moments of inertia in respect to the centroid of the connection

$$I_x = I_x^* - n_{tot} x_C^2; \quad (D.41)$$

$$I_y = I_y^* - n_{tot} y_C^2; \quad (D.42)$$

$$I_p = I_x + I_y = I_x^* + I_y^* - n_{tot} (x_C^2 + y_C^2); \quad (D.43)$$

where n_{tot} is the number of fastener and x_c and y_c are the coordinates of the centroid of the connection in respect to the origin.

Finally, the force components in respect to the two axes x and y can be written as

$$F_{M,max,x} = M \frac{x_c}{I_p}; \quad (D.44)$$

$$F_{M,max,y} = M \frac{y_c}{I_p}. \quad (D.45)$$

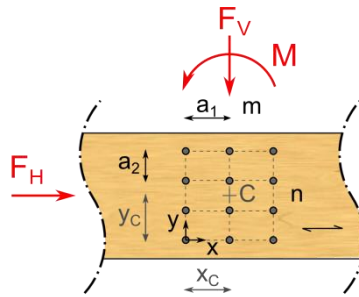


Figure D.5 Equally spaced rectangular pattern

D.3.2.2 Circular fastener pattern

In the case of a connection with circular pattern as shown in Figure D.6, the polar moment can be written as:

$$I_p = \sum_i r_i^2 = \sum_{(j)} n^{(j)} r^{(j)}; \quad (D.46)$$

where $n^{(j)}$ is the number of fasteners in circle (j) with a radius $r^{(j)}$.

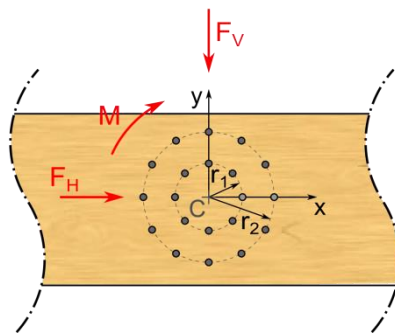


Figure D.6 Bolted connection with multiple fastener rings

In the case of a simple dowel ring and the presence of fasteners on the horizontal axis passing the centroid, equation (D.37) can be simplified to

$$F_{max} = \sqrt{(F_h)^2 + (F_v + F_M)^2}; \quad (D.47)$$

with an inclination of the resultant force to the horizontal axis equal to

$$\alpha = \arctan\left(\frac{F_v + F_M}{F_h}\right) \quad (\text{D.48})$$

where

$$F_M = \frac{M}{nr}. \quad (\text{D.49})$$

D.3.3 Connection stiffness

The lateral displacement stiffness k_v of a bolted connection is the sum of fasteners n_{tot} times the slip modulus of a singles fastener

$$k_v = n_{tot}K; \quad (\text{D.50})$$

where K is the slip modulus which can be K_{ser} or K_u depending on the limits state considered and which might need to be factored for long term effects (Eurocode 5 2008).

The relation between the lateral load and the fastener displacement can be written as:

$$F = k_v v. \quad (\text{D.51})$$

The rotational stiffness of a connection can be derived by rearranging equation (D.30):

$$\begin{aligned} M &= \sum_i M_i = \sum_i F_i r_i = \sum_i (K v_i) r_i = \sum_i \left(K \frac{r_i}{r_{max}} r_{max} \theta \right) r_i = \\ &= \sum_i (K r_i \theta) r_i = K \sum_i r_i^2 \theta; \end{aligned} \quad (\text{D.52})$$

the rotational stiffness k_θ therefore becomes

$$k_\theta = K \sum_i r_i^2 = K \sum_i x_i^2 + y_i^2 = K I_p. \quad (\text{D.53})$$

E Appendix – Design example

To demonstrate the application of the post-tensioned rocking frame and wall Pres-Lam systems, a case study building is presented in the STIC Guidelines for Post-Tensioned Timber Buildings (STIC 2013).

The case study building as shown in Figure E.1 has five storeys with four suspended floors and a lightweight timber penthouse on top of the fourth floor. The building has a footprint of 32 m times 18 m. Levels 1 to 3 are used as offices and level 4 has a lightweight timber penthouse with residential type loadings.

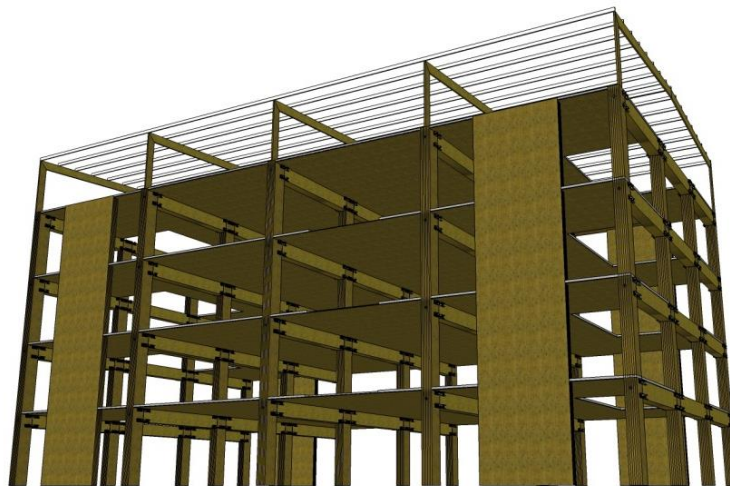


Figure E.1 3D view of the Case Study Building A – Seismic Design Worked Example Buildings (STIC 2013)

The design example shows the design of the post-tensioned frames for the seismic loads in the transversal direction and the post-tensioned walls in the longitudinal direction.

E.1 DIAPHRAGM DESIGN

The author of this thesis has carried out the diaphragm design for the building, considering a timber-concrete-composite (TCC) and an all timber floor with massive timber panels. Interested readers are referred to Part 2 of the STIC Guidelines for Post-Tensioned Timber Buildings (STIC 2013).

For both floor types, the diaphragm loads have been calculated based on the procedure proposed in Priestley et al. (2007) for the design of walls and frame columns. For the

determination of the diaphragm forced demand, overstrength and dynamic amplification due to higher mode effects were considered. For the concrete slabs, a strut-and-tie model shown in Figure E.2 as discussed in Chapter 3 is applied. The slab reinforcement was made of ductile mesh and standard reinforcement for the collector beams. Because of displacement incompatibilities with the frames, no shear was introduced to the beams close to the columns. In addition, unbonded rebars are placed over the potential crack line along the beam-column faces. This solution has not been tested yet and care should be take when choosing this design. Dowel action of the bars might require large deformations as discussed in Chapter 8 and lead to diaphragm damage.

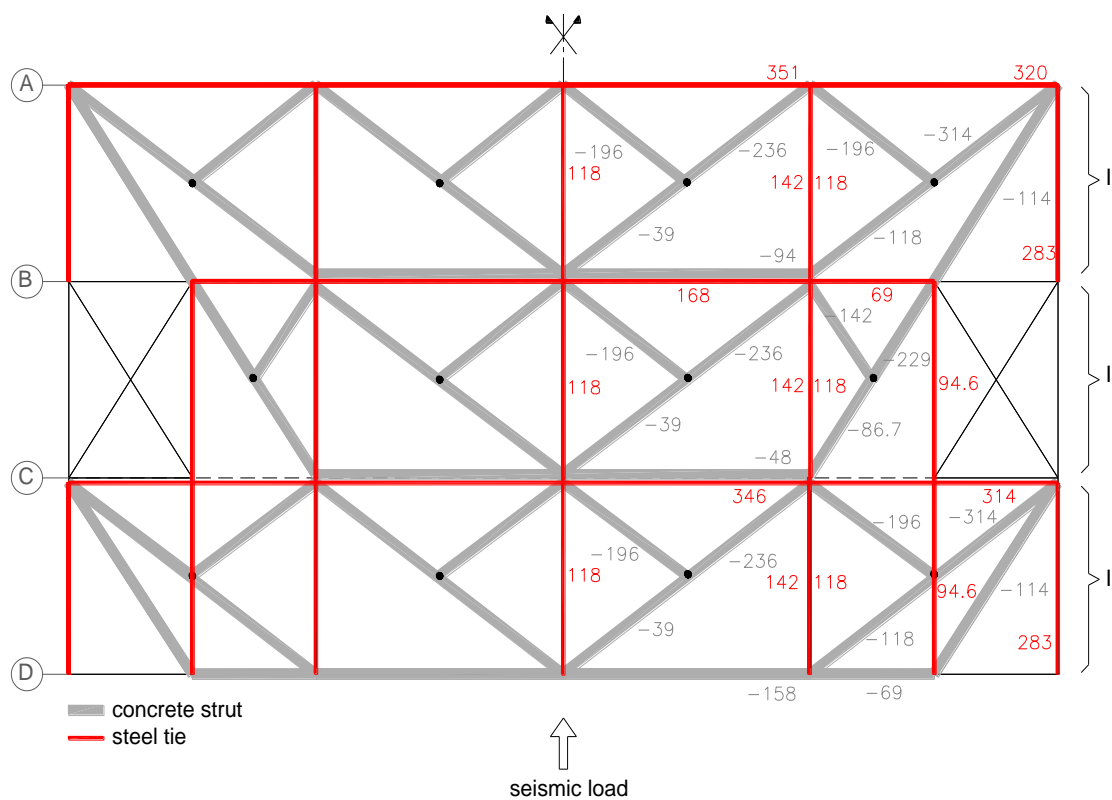


Figure E.2 Strut-and-tie analysis of the diaphragm loaded in frame direction (STIC 2013)

For the timber floor, the diaphragm forces are determined with the extended girder analogy as shown in Malone and Rice (2012). Figure E.3 shows exemplarily the collector and strut beam forces for the seismic load in the longitudinal direction. To accommodate the displacement incompatibilities induced by the frame elongation, a concentrated floor gap solution as presented in Chapter 9 has been adopted.

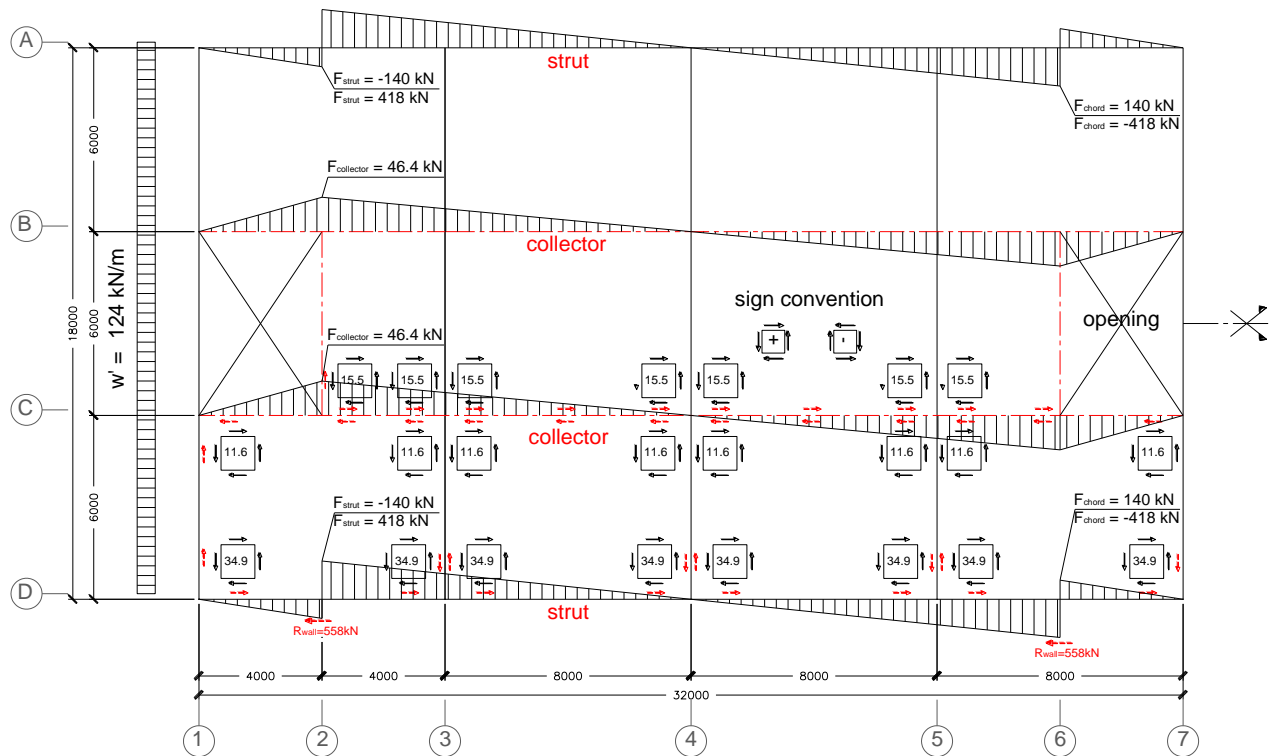


Figure E.3 Collector forces for the seismic action in the longitudinal direction (STIC 2013)

For both floor setups additional strategies to accommodate the displacement incompatibilities due to out-of plane frame and wall movements are given as well.

The case study design has been carried before the Equivalent Truss Method presented in Chapter 7 has been developed. Instead of manually calculating the unit shear forces in the panels and the relative collector and strut beam forces due to the diaphragm openings, a truss model could be applied to determine the demand in the individual diaphragm components.

E.2 ERRATA CORRIGE

The diaphragm forces in the frame direction, as calculated in sections 10.1 and 10.3.1 of the STIC Guideline, are incorrect and the following equation as proposed in Chapter 5 should be used instead

$$F_{diap} = (\phi^0 V_{E,top} + 0.2\mu V_{E,base}) 5 \quad (E.1)$$

where:

- ϕ^0 ... overstrength factor of the lateral load resisting system;
- $V_{E,top}$... shear demand and the top floor from the Direct Displacement Demand;
- $V_{E,base}$... shear demand at the base from the Direct Displacement Demand;
- μ ... ductility of the structure.